Neue lumineszente Lanthanoid-Architekturen

Dissertation

der Mathematisch-Naturwissenschaftlichen Fakultät

der Eberhard Karls Universität Tübingen

zur Erlangung des Grades eines

Doktors der Naturwissenschaften

(Dr. rer. nat.)

vorgelegt von

M. Sc. Carolin Dee

aus Köln

Tübingen

2020

Gedruckt mit Genehmigung der Mathematisch-Naturwissenschaftlichen Fakultät der Eberhard Karls Universität Tübingen.

Tag der mündlichen Qualifikation:	07.02.2020
Dekan:	Prof. Dr. Wolfgang Rosenstiel
1. Berichterstatter:	Prof. Dr. Michael Seitz
2. Berichterstatter:	Prof. Dr. Hermann A. Mayer

Preface

This work was carried out from March 2017 to January 2020 under the supervision of Prof. Dr. Michael Seitz at the Institute of Inorganic Chemistry, Eberhard Karls University Tübingen. Funding has been gratefully provided by the Deutsche Forschungsgemeinschaft (DFG).

The following thesis consists of a review on the chemistry of luminescent lanthanoid complexes, a summary of the main results, and a compilation of the scientific papers.

Parts of this thesis have been presented at several international and national conferences as oral and poster presentations.

1st Referee Prof. Dr. Michael Seitz

2nd Referee Prof. Dr. Hermann A. Mayer

Acknowledgements

Ein besonderer Dank gilt meinem Doktorvater Prof. Dr. Michael Seitz für die Möglichkeit diese Arbeit in seiner Gruppe anfertigen zu können, viele wertvolle Anregungen und Diskussionen und die große Unterstützung zu jeder Zeit.

Prof. Dr. Hermann A. Mayer danke ich für die Übernahme der Zweitbegutachtung.

Bei Prof. Dr. Katja Heinze (Universität Mainz), Prof. Dr. Carlos Platas-Iglesias (Universidade da Coruña), Dr. Francesco Zinna, Prof. Dr. Gennaro Pescitelli und Prof. Dr. Lorenzo Di Bari (Università di Pisa), Dr. Andrey Turshatov (Karlsruher Institut für Technologie) bedanke ich mich für erfolgreiche und spannende Kooperationen.

Bei Dr. Laura Büldt, Tobias Haas, Jens Kalmbach, Dr. Elisabeth Kreidt, Dr. Christian Kruck, Dr. Wolfgang Leis, Angelika Oswald und Markus Trautnitz bedanke ich mich für die abwechslungsreiche musikalische Unterstützung und eine schöne Zeit im Labor. Vielen Dank auch an den AK Kunz für gemeinsame Kaffee-Pausen und ständige Hilfsbereitschaft.

Bei Markus möchte ich mich für die letzten acht Jahre - vom allerersten Tag in der Uni bis zur Promotion - und unsere schöne Zeit in Tübingen und unterwegs bedanken.

Bei Wolfi möchte ich mich für unzählige Messungen, technischem Support und meist aufbauende Worte bedanken.

Anika, Ines, Janina, Julia, Kathinka und Regina danke ich für die lange Freundschaft und den Rückhalt aus der Stadt mit K.

Ich danke meiner ganzen Familie für die großartige Unterstützung, Liebe und die vielen schönen Besuche in Tübingen.

Basti danke ich sehr für seine Ruhe, Liebe und wunderbare Ablenkung von vielen Sorgen.

Meinen lieben Eltern

Contents

Abbreviations

BINAP	2,2′-bis(diphenylphosphino)-1,1′-binaphthyl
br	broad
bpy	2,2′-bipyridine
$bpyO_2$	2,2′-bipyridine-N,N′-dioxide
ca.	circa
CD	circular dichroism
COORNET	coordination network
CPL	circularly polarised luminescene
d	doublet
DFT	density functional theory
DHB	dihydroxybenzoic acid
DMF	dimethylformamide
DMSO	dimethylsulfoxide
DOTA	1,4,7,10-tetraazacyclododecane-N,N′,N′′,N′′′-tetraacetic acid
E	energy
EDX	energy dispersive X-ray spectroscopy
e.g.	exempli gratia (for example)
eq.	equivalent
ESI	Electrospray Ionization
et al.	et alii (and others)
FWHM	full width at half maximum
HPLC	high performance liquid chromatography
HSQC	heteronuclear single quantum coherence

IR	infrared
ISC	intersystem crossing
J	coupling constant
LMCT	ligand metal charge transfer
Ln	lanthanoid
MALDI	matrix assisted laser desorption ionization
MAS	magic angle spinning
mCPBA	meta-chloroperbenzoic acid
MLCT	metal ligand charge transfer
MS	mass spectrometry
NMR	nuclear magnetic resoncance
ppm	parts per million
q	quartet
rac	racemic
R_f	retention factor
rt	room temperature
s	singulet
S_0	singlet ground state
S_1	singlet first excited state
SEM	scanning electron microscopy
t	triplet
T_1	triplet first excited state
TBAF	tetrabutylammoniumfluoride
TBS	tert-butyldimethylsilyl
TD	time-dependent
TFA	trifluoroacetic acid
THF	tetrahydrofuran
TMS	tetramethylsilane
TLC	thin layer chromatography
UV	ultraviolet
vis	visible

Abstract

In the course of this work, new luminescent lanthanoid architectures were prepared and photophysically characterised. A main focus was the *ligand design* and the realisation of an extended, carboline-based cryptate, which allows europium luminescence upon excitation with visible light for future biological applications. Furthermore, a more flexible cryptate was developed and by variation of the cavity of the lanthanoid complex, their symmetry was analysed regarding the antenna properties.

For the investigation of *circularly polarised luminescence (CPL),* the chiral resolution of a variety of lanthanoid cryptates by chiral HPLC was successfully applied and the configurational stability of the enantiomers was experimentally confirmed. In addition, the new carboline-based cryptates facilitate the excitation of europium CPL with visible light. As an alternative to lanthanoid-based CPL emitters, a chromium(III) complex was chirally resolved and experimentally studied. A remarkable CPL activity was observed for such transition metal complexes.

Further studies on three dimensional coordination networks, based on 2,2′-bipyridine, facilitated the investigation of energy transfer processes between different lanthanoids in a rigid ligand environment.

Kurzzusammenfassung

Im Rahmen dieser Doktorarbeit wurden neue, lumineszente Lanthanoid-Architekturen synthetisiert und photophysikalisch charakterisiert. Ein besonderer Fokus lag auf dem *Ligandendesign* und der Realisierung eines erweiterten, Carbolin-basierten Cryptats. Im Hinblick auf biologische Anwendungen kann Europium in diesem Cryptat mit sichtbarem Licht zur Lumineszenz angeregt werden. Des Weiteren wurde ein flexibler Cryptat entwickelt und durch Variation der Kavität der Lanthanoidkomplexe wurde die Symmetrie und den Einfluss auf die Antenneneigenschaften untersucht.

Für Untersuchungen der *zirkular polarisierten Lumineszenz (CPL)* wurde zunächst die Enantiomerentrennung verschiedener Lanthanoid-Cryptate mittels chiraler HPLC erfolgreich angewendet sowie die enorme Konfigurationsstabilität der Enantiomere experimentell bestätigt. Mit dem neu entwickelten Carbolin-basierten Cryptat ist es zusätzlich möglich, Europium mit sichtbarem Licht effizient zur CPL anzuregen. Als Alternative zu den Lanthanoid-basierten CPL Emittern wurden die Enantiomere eines Chrom(III)-Komplexes getrennt und experimentell untersucht. Eine bemerkenswerte CPL Aktivität für solche Übergangsmetallkomplexe konnte beobachtet werden.

Weitere Studien zu dreidimensionalen Koordinationsnetzwerken, basierend auf 2,2′-Bipyridin, ermöglichen die Untersuchung von Energietransferprozessen zwischen verschiedenen Lanthanoiden in einer starren Liganden-Umgebung.

Publications, Contributions & Supervision

Publications (Peer Review)

The following publications are either directly related to the work of this PhD project or part of collaborations:

Paper 1 E. Kreidt, C. Dee, M. Seitz
Chiral Resolution of Lanthanoid Cryptates with Extreme Configurational Stability
Inorg. Chem. **2017**, *56*, 8752-8754.

Paper 2 C. Dee, D. Esteban-Gomez, C. Platas-Iglesias, M. Seitz
Long Wavelength Excitation of Europium Luminescence in Extended, Carboline-Based Cryptates
Inorg. Chem. **2018***, 57*, 7390-7401.

Paper 3 C. Kruck, P. Nazari, C. Dee, B. S. Richards, A. Turshatov, M. Seitz
Efficient Ytterbium Near-Infrared Luminophore Based on a Nondeuterated Ligand
Inorg. Chem. **2019**, *58*, 6959-6965.

Paper 4 C. Dee, F. Zinna, W. R. Kitzmann, G. Pescitelli, K. Heinze, L. Di Bari, M. Seitz
Strong Circularly Polarized Luminescence of an Octahedral Chromium(III) Complex
Chem. Commun. **2019***, 55*, 13078-13081.

Paper 5 C. Dee, F. Zinna, E. Kreidt, L. Arrico, A. Rodríguez-Rodríguez, C. Platas-Iglesias, L. Di Bari, M. Seitz

Circularly Polarized Luminescence of Europium in Enantiopure Carboline-based Cryptate Under Visible Light Excitation

Manuscript submitted

Paper 6 N. Kiseleva, P. Nazari, C. Dee, D. Busko, B. S. Richards, M. Seitz, I. A. Howard, A. Turshatov

Lanthanide Sensitisers for Large Anti-Stokes Shift NIR-to-VIS Triplet-Triplet Annihilation Photon Upconversion

Manuscript submitted

Publications (Non-Peer Review)

The following popular-scientific publication is related to the PhD project, especially to the project published in *Paper 2*:

C. Dee

Alles ist erleuchtet: Europium im Käfig

Faktor14 **2020**, *in press*.

The following popular-scientific publication is independent of the PhD project and is part of a collaboration with Prof. Dr. Klaus Roth and the Young Chemist's Network:

K. Roth, S. Streller, D. Appel, J. Ascherl, A. Baum, S. Bestgen, R.–C. Brachvogel, J. Buchsbaum, C. Dee, T. J. Feuerstein, E. A. Glitscher, A. - B. Grebhahn, J. Guschlbauer, S. Hecht, A. Heib, C. Heintz, G. Hierlmeier, R. Jordan, T. Klein, U. Koch, A. Kottmann, R. M. Kramer, M. M. Krejca, G. H. M. de Kruijff, H. Kühnle, R. O. Kusche, A. Lechner, K. Locke, P. Luger, A. Märker, J. Märker, S. Märker, M. Meissner, A. Metz, J. Moegling, G. Nagel, C. Neis, S. Ossinger, L. Pietsch, J. Pöppinghaus, G. Pöppinghaus, A. Roth, U. Schmitz, F. P. Schmitz, M. J. Schöwe, L. Schulz, E. Siemes, S. Sobottka, M. Stapf, D. J. Tindall, U. Vollgraf, C. Wulf, D. Zeller

Die ChiuZ-Spargelstudie: Vom wohl- oder übelriechenden Spargelurin

Chem. Unserer Zeit **2019**, *53*, 2-5.

Personal Contribution to Publications

***Paper 1*: Chiral Resolution of Lanthanoid Cryptates with Extreme Configurational Stability**

The method development of the chiral resolution (chiral HPLC) was planned by E. Kreidt and performed by both of us. The analytical, chiral resolution of several lanthanoid cryptates and preparative separation of the enantiomers of the **Lu-bpy$_3$O$_2$** was conducted by me. The configurational stability tests and CD measurements were performed by E. Kreidt.

***Paper 2*: Long-Wavelength Excitation of Europium Luminescence in Extended, Carboline-Based Cryptates**

All reactions and analyses described were planned and conducted by me including HPLC purification and subsequently structural examination of the lanthanoid complexes (NMR spectroscopic methods, IR). The characterisation of the photophysical properties (UV/Vis and luminescence spectroscopy) and the determination of important parameters (quantum yields, q-values, lifetimes, pH dependency) was performed by me. The DFT calculations and LIS analysis were performed by our collaborators D. Esteban-Gomez and C. Platas-Iglesias

***Paper 3*: Efficient Ytterbium Near-Infrared Luminophore Based on a Nondeuterated Ligand**

The preparation of the complexes and structural analysis was performed by C. Kruck. The photophysical measurements were conducted by P. Nazari. Supplementary luminescence measurements of the lanthanoid complexes were carried out by me.

***Paper 4:* Strong Circularly Polarised Luminescence of an Octahedral Chromium(III) Complex**

The method development of the chiral resolution (chiral HPLC) was planned and conducted by me. All preparative separations of the enantiomers and the analysis of the enantiopure material (NMR spectroscopy, analytical HPLC) was performed by me. The configurational stability tests together with their evaluation by analytical HPLC was carried out by me. W. R. Kitzmann performed the DFT calculations along possible racemization trajectories. The absolute configuration of the resolved enantiomer was elucidated via computational methods conducted by G. Pescitelli. F. Zinna and L. Di Bari carried out the CD and CPL measurements.

Paper 5: **Circularly Polarised Luminescence of Europium in Enantiopure Carboline-based Cryptate Under Visible Light Excitation**

The method development for the chiral resolution (chiral HPLC) and the preparative separation of the enantiomers of two carboline-based europium cryptates was performed by me. The examination of the enantiopure material with NMR spectroscopic methods and analytical HPLC was carried out by me. The configurational stability tests together with their evaluation by analytical HPLC was conducted by me. F. Zinna and L. Di Bari carried out the CD and CPL measurements. The absolute configuration of the resolved enantiomers was elucidated via computational methods conducted by C. Platas-Iglesias and A. Rodríguez-Rodríguez.

Paper 6: **Lanthanide Sensitisers for Large Anti-Stokes Shift NIR-to-VIS Triplet-Triplet Annihilation Photon Upconversion**

The Yb complex used for the upconversion measurements was provided by me.

Contributions to Conferences

2019 **Oral presentation** at the Wissenschaftsforum Chemie 2019 in Aachen (Germany, September 2019).
Title: Circular Polarized Luminescence of Enantiopure Carboline-Based Europium Cryptates under Visible Light Excitation

2019 **Poster Presentation** at the 23rd ISPPCC 2019 in Hongkong (Hongkong, July 2019).
Title: Circular Polarized Luminescence of Enantiopure Carboline-Based Europium Cryptates under Visible Light Excitation

2019 **Oral Presentation** at the Institute's Colloquium of the Institute of Inorganic Chemistry at the University of Tübingen (Germany, May 2019).
Title: New luminescent Lanthanoid-Architectures

2019 **Poster Presentation** at the 21st JCF Spring Symposium in Bremen (Germany, March 2019).
Title: Chiral Resolution of Carboline-based Europium Cryptates

2018 **Oral Presentation** at the 2nd Ligand Design Workshop in Köln (Germany, July 2018).
Title: Long Wavelength Excitation of Europium Luminescence in Extended, Carboline-based Cryptates

2018 **Poster Presentation** at the 20th JCF Spring Symposium in Konstanz (Germany, March 2018).
Title: Long Wavelength Excitation of Europium Luminescence in Extended, Carboline-based Cryptates

2018 **Oral presentation** at the 14th Coordination Chemistry Meeting in Heidelberg (Germany, March 2018).
Title: Long Wavelength Excitation of Europium Luminescence in Extended, Carboline-based Cryptates

2017 **Poster Presentation** at the 28th Tage der Seltenen Erden – Terrae Rarae in Tübingen (Germany, October 2017).
Title: New Lanthanoid Luminophores with Long Wavelength Excitation

2017 **Poster Presentation** at the 13th Coordination Chemistry Meeting in Potsdam (Germany, March 2017)
Title: New Lanthanoid Luminophores with Long Wavelength Excitation

Supervised Students

2019 Ralf Kern, Master Student
Title: Synthesis of New Lanthanoid Cryptates with Dipyridylamine Units

2018 Marc Edelmann, Master Student
Title: Synthesis of a New Lanthanoid Cryptate

1 Introduction

1.1 Lanthanoid Luminescence

Lanthanoids, the fifteen elements from lanthanum to lutetium with atomic numbers 57 – 71 (Figure 1), share very similar chemical behaviour and also exhibit fascinating photophysical properties. Together with scandium and yttrium, these elements are referred to as rare earths elements.[1] With their luminescence covering the whole spectral range from UV to near-IR, these metals are widely used in many optical applications (Figure 2).[2–6]

57 La	58 Ce	59 Pr	60 Nd	61 Pm	62 Sm	63 Eu	64 Gd	65 Tb	66 Dy	67 Ho	68 Er	69 Tm	70 Yb	71 Lu

Figure 1: The elements La-Lu in the 6th row of the periodic table of elements.

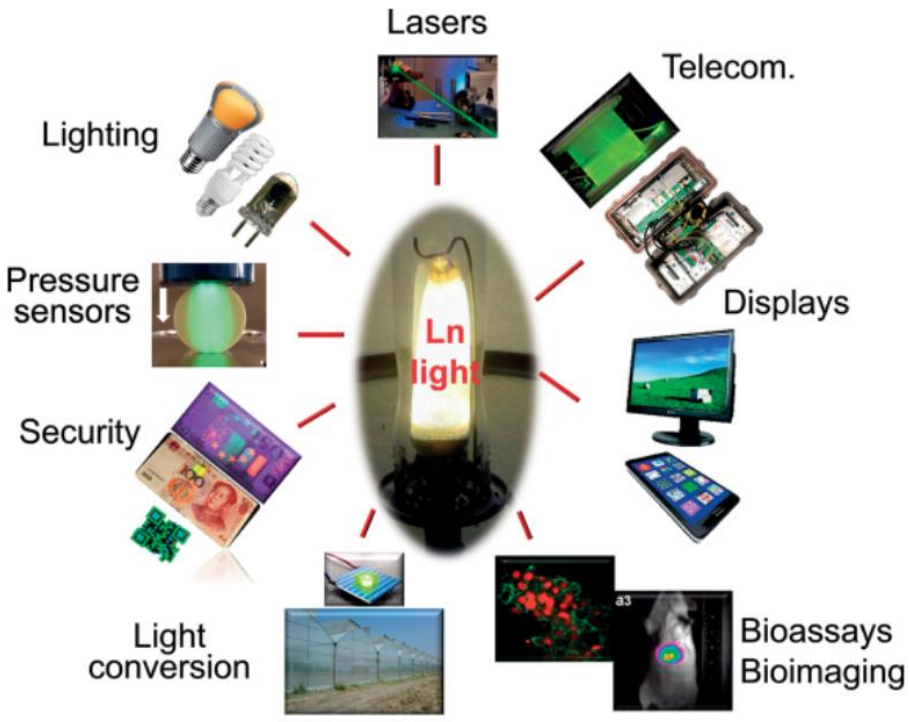

Figure 2: Several application fields of lanthanoid luminescence. Figure adopted from Bünzli.[2]

1.2 Photophysical Properties of Trivalent Lanthanoid Ions

Lanthanoids in the most stable oxidation state +III have an electron configuration of a completely filled xenon core ([Xe] = $1s^2 2s^2 2p^6 3s^2 3p^6 3p^{10} 4s^2 4p^6 4d^{10} 5s^2 5p^6$).[7] The additional electrons are located in the f-orbitals which are filled subsequently resulting in the electronic configuration [Xe]$4f^n$ (n = 0-14). Due to the fact that these spatially less extended f-orbitals are shielded by the filled 5s- and 5p-orbitals there is limited interaction between the f-electrons and the surrounding of the lanthanoid. Therefore, all lanthanoids behave chemically very similarly and some also show unique photophysical properties. The different electronic states of a lanthanoid are mainly caused by the repulsion between the electrons in the f-orbitals and the spin-orbit coupling. The Russell-Saunders term symbol of the form $^{2S+1}L_J$ gives a more detailed description of these states. Here, S is the total spin, 2S+1 is the spin multiplicity and L is the total orbital angular momentum. S and L are obtained as the sum of the spin s and the orbital angular momentum m_L of each involved electron. The values for L are given as capital letters (S, P, D, F, ... corresponding to L = 0, 1, 2, 3, …). While the interaction between the spins of the electrons and the angular momentum is rather insignificant for elements with small atomic numbers, this so-called spin-orbit coupling, is distinctly larger for lanthanoids. In the Russell-Saunders coupling scheme, the total angular momentum J is calculated from L and S according to J = L+S, L+S-1…, |L-S|. In the ligand environment the energy levels of the trivalent lanthanoid ion undergo crystal-field splitting leading to the so-called Stark levels.[8,9] Compared to transition metals where the larger splitting strongly depends on the symmetry of the ligand system, the symmetry also plays a role for the splitting observed for f-elements but is indeed much smaller and appears in the range of a few hundred wavenumbers.[8] This can also be explained by the efficient shielding of the f-electrons. Carnall and coworkers investigated the electronic energy levels of lanthanoid aquo ions.[10–13] These levels (Figure 3) can be discussed for several chemical surroundings independent of the chemical environment.

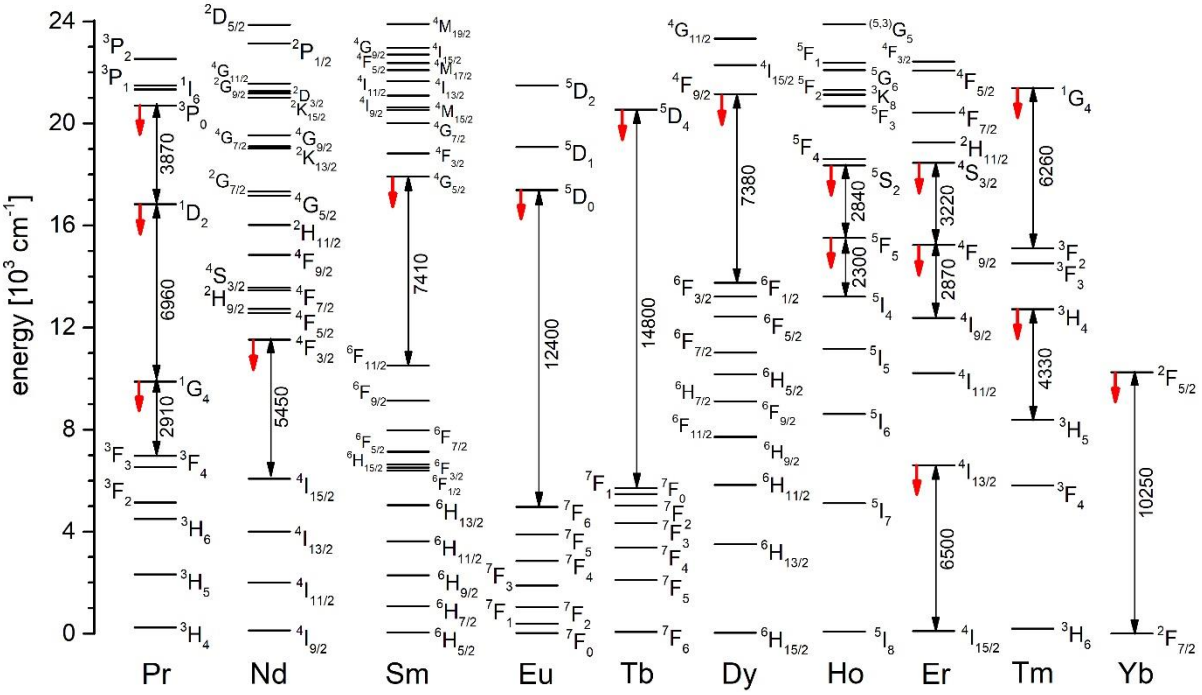

Figure 3: Partial energy level diagram for selected lanthanoid trivalent ions with the main emissive levels (red downward arrows) and the energy gaps (values in cm^{-1}, double headed arrows). Figure adopted from Seitz and coworkers.[14]

These electronic characteristics of the lanthanoids directly affect their typical properties:

- The shielding of the 4f-electrons prevents covalent interaction so that the *bonding is mainly ionic.*
- The small crystal field splitting corresponds to very low ligand field stabilisation energies, which directly induces the lack of preferred geometries for lanthanoid complexes. The resulting lanthanoid complexes are formed under *steric preferences.*
- Lanthanoid complexes are *kinetically labile,* they exhibit a low barrier of activation for ligand exchange, since there are no strong covalent bonds to break.
- The unique photophysical and magnetic properties are almost *independent* of *the chemical environment* of the lanthanoid.

The absorption of photonic energy may cause the subsequent emission of light which is called photoluminescence. The absorption of energy promotes an electron into an electronically excited state which may afterwards relax to the ground state again with emission of light. Different types of transitions are known for trivalent lanthanoid

complexes: f→d transitions, charge-transfer transitions (Ligand-Metal Charge Transfer, LMCT and Metal-Ligand Charge Transfer, MLCT), and f→f transitions. Since the first two types are rarely observed for lanthanoids, as these transitions are high in energy and mostly limited to a minority of lanthanoid ions, the most important transition is the intraconfigurational f→f transition.[15] This transition consists of mainly two types, the electric and the magnetic dipole transitions. With the help of the Laporte ($\Delta l = \pm 1$) and Spin ($\Delta S = 0$) selection rule the probability can be estimated. The f→f transitions are always Laporte-forbidden, however some are also spin-forbidden.

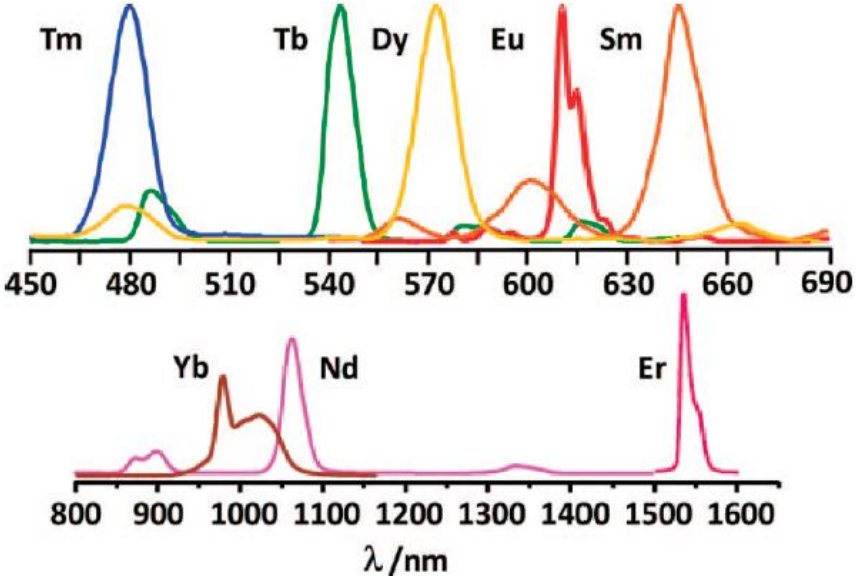

Figure 4: Characteristic emission bands of different lanthanoids in the visible and near-infrared region. Figure adopted from Bünzli.[16]

As a result, long-lived excited states and therefore long luminescence lifetimes (μs-ms) can be observed. Unfortunately, also low molar absorption coefficients (usually below 10 $M^{-1}cm^{-1}$) result from the forbidden nature of the transition. Again the f→f transition is independent of the chemical environment which leads to elementspecific luminescence of the lanthanoid ions (Figure 4).[16] Furthermore, there are only minor changes in the nuclear coordinates during the transitions, due to the shielding of the f-orbitals, which leads to sharp emission bands.[17]

In order to take advantage of the beneficial photophysical properties, such as sharp and elementspecific emission bands and long luminescence lifetimes, the problem of low molar absorption coefficients has to be solved.

1.3 The Role of the Ligand in Lanthanoid Coordination Compounds

Due to the small absorption coefficients of the trivalent lanthanoid ions, direct excitation with efficient luminescence is hard to achieve for all kind of applications. To tackle this drawback, either a powerful excitation source (e. g. laser) or indirect sensitisation of luminescence is required.

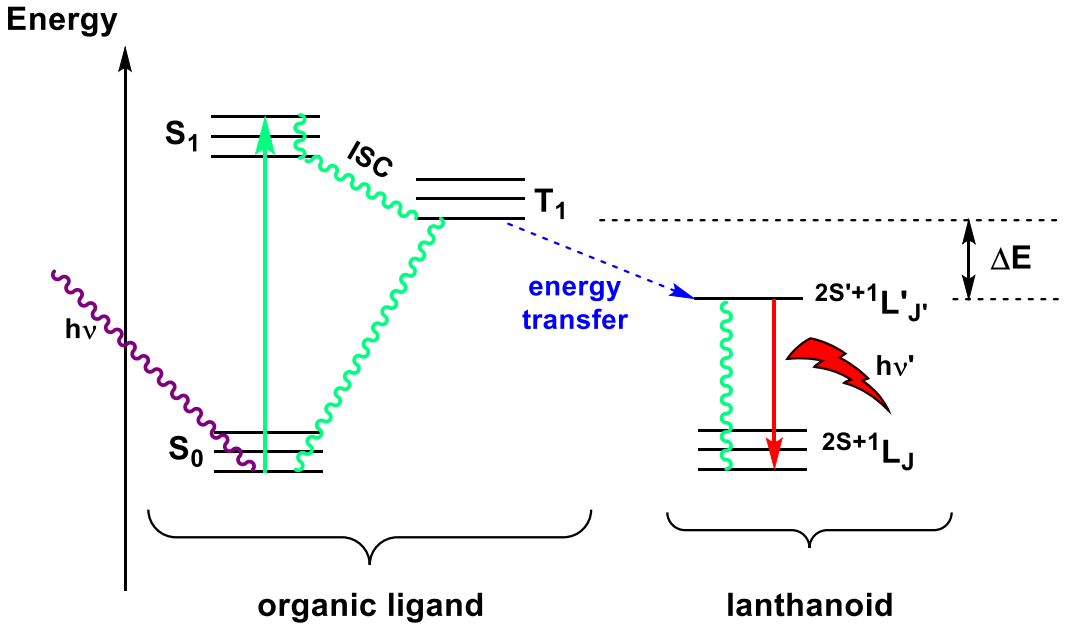

Figure 5: Jablonski diagram of the antenna effect: The electron in the ground state S_0 is excited to the S_1 state by absorption of light (green arrow). The long-lived triplet state is populated after an ISC process from where the energy is transferred (blue arrow) to excite the lanthanoid ion. The excited lanthanoid ion emits light (red arrow) and relaxes to the ground state. (green waved arrows: nonradiative deactivation).

The latter is also known as the antenna effect (Figure 5):[18,19] The lanthanoid is embedded in an organic ligand environment which can be excited to a higher electronic level with a certain excitation wavelength using a conventional light source. Via intersystem crossing (ISC) the triplet state of the ligand is populated and subsequently the energy is transferred to the lanthanoid's emissive excited states. Since the ISC from $T_1 \rightarrow S_1$ is a forbidden transition, the triplet lifetime is longer than the singlet lifetime which makes the energy transfer more probable. From this triplet level different processes are possible: With large energy gaps between the triplet state of the ligand and the energetically lower emissive excited state of the lanthanoid, lanthanoid luminescence can be observed. The excited lanthanoid ion emits light and relaxes to its ground state. Alternatively, with small energy gaps ($\Delta E \leq 2000\ cm^{-1}$) the probability

for back-ISC to the ligand increases due to thermal activation.[18] The excited triplet state can further become depopulated by phosphorescence or nonradiative deactivation *e.g.* through vibrational quenching or $^3O_2$.

1.4 Circularly Polarised Luminescence of Trivalent Metal Complexes

Chirality is an essential concept in the macroscopic world as well as on the molecular level. Therefore, it plays a crucial role in many fields of science and technology. A new emerging application arises with the growing research in circularly polarised luminescence (CPL).[20,21] With an improved signal-to-noise ratio compared to usual luminescence next to autofluorescence of biomolecules,[22] CPL is an emerging technique in the field of structural elucidation of biomolecules or imaging.[23–25] Furthermore, CPL emitters may be applied in innovative organic light emitting diodes.[26–28] The phenomenom of a CPL emitter preferentially emitting left- or right-handed circularly polarised light can be detected upon excitation with unpolarised light. Hence, insights about the chirality of the excited state can be gained and therefore this property is actually the emission analogue to circular dichroism (CD).[21,29] For both techniques, no effect can be detected in racemic mixtures, because left- and right-handed polarisation cancel each other out. Enantiopure or at least enantioenriched compounds are required to investigate the "chiral" properties and to quantify the respective signals. Examining the CPL activity, the luminescence dissymmetry factor g_{lum} is calculated as a quotient of the difference of the intensities of left and right circularly polarised light and the average of both intensities:

$$g_{lum} = \frac{I_L - I_R}{\frac{1}{2}(I_L + I_R)} = \frac{\Delta I}{I} \text{ with } 2 \leq g_{lum} \leq 2$$

Complete polarisation of the emitted light is expressed by $g_{lum} = \pm 2$ whereas a value of 0 occurs for unpolarised light. For all kinds of applications high values are essential. As a matter of fact, they can be found for electric dipole forbidden and magnetic dipole allowed transitions. For a given transition a→b the dissymmetry factor can also be given as:

$$g_{lum} = 4\,\frac{R_{ab}}{|D_{ab}|}$$

$$R_{ab} \sim |M_{ba}||P_{ab}| cos\tau_{ab} \qquad D_{ab} \sim |P_{ab}|^2$$

with R_{ab} as the transition's rotatory strength and D_{ab} as the oscillator strength. R_{ab} is given by the magnetic M_{ab} and electric P_{ab} transition dipole moments vectors as well as the angle τ_{ab} between both vectors. D_{ab} is proportional to the mean square of the electric transition dipole moment.[30] CPL is due to the dependence on the angle sensitive towards changes in the coordination geometry. For organic molecules typically $|g_{lum}|$ values in the range of 10^{-3}-10^{-2} are reported.[31,32] Enantiopure lanthanoid complexes with their electronic and photophysical properties are great candidates as efficient CPL emitters. Lanthanoid complexes outperform these values by far and reach dissymmetry factors of 0.1-1.[30,33,34] The world-record value of 1.38 could be found for the Eu^{3+} $^5D_0 \rightarrow {}^7F_1$ transition, which has a purely magnetic dipole character, in a campherato β-diketonate complex.[35,36] Next to this transition, the most commonly observed CPL signals of lanthanoids are measured for the Sm^{3+} ($^4G_{5/2} \rightarrow {}^6H_{5/2}$), Tb^{3+} ($^5D_4 \rightarrow {}^7F_5$) and Dy^{3+} ($^4F_{9/2} \rightarrow {}^6H_{11/2}$) transitions which is in line with Richardson's classification of the suitability of the lanthanoids for CPL activity.[37]

Especially for Eu^{3+} many complexes emitting CPL have been reported in the last years.[38–44] Figure 6 gives an example of a CPL emitter **1-Eu** incorporating Eu^{3+} which can be used in chiral contrast imaging techniques.[22]

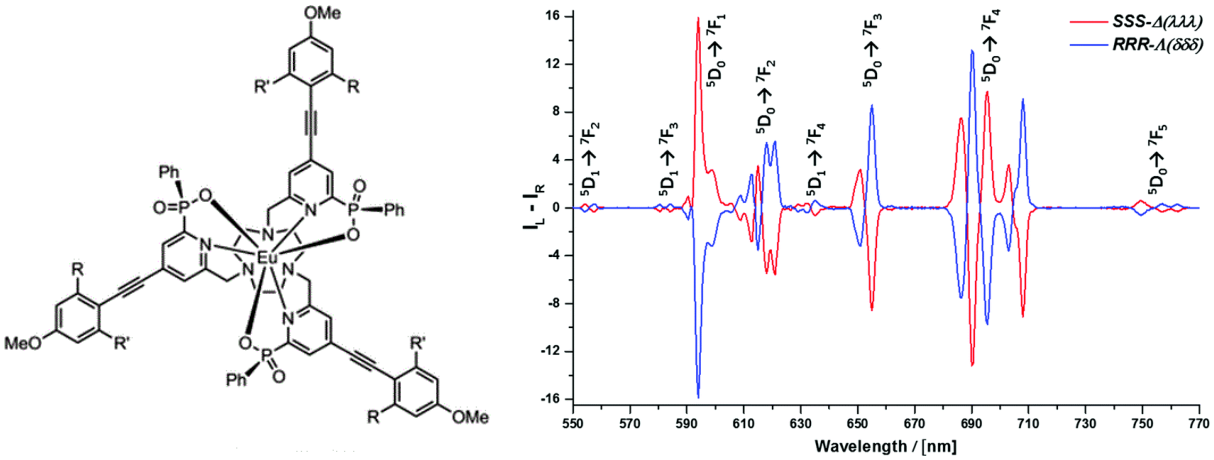

1-Eu

Figure 6: Circularly polarized luminescence of **1-Eu** complex applied in innovative techniques like chiral contrast imaging reported by Parker and coworkers.[22]

1.5 Cryptates

The ligand plays a crucial role for the preparation of highly luminescent lanthanoid complexes for different reasons as already described. Firstly, the ligand has to allow for efficient population of the excited state of the lanthanoid. Secondly, it also needs to suppress nonradiative deactivation processes either due to vibrational deactivation within the ligand or due to quenching solvent molecules in the vicinity. Furthermore, the analysed complexes must be stable in solution, especially for application as CPL emitters, complexes must be configurationally stable.

According to the nature of trivalent lanthanoids being hard Lewis acids, nitrogen and oxygen seem to be good choices as coordinating heteroatoms for lanthanoids. A group of ligands which has been extremely well studied is based on 1,4,7,10-tetraazacyclododecane-N,N′,N′′,N′′′-tetraacetic acid (**DOTA**, Figure 7). The corresponding lanthanoid complexes are very stable and unlikely to decomplex.[45,46] This system can easily be modified resulting in a multitude of ligands possessing different antenna properties. A common problem of lanthanoid complexes is the low configurational and conformational stability. **DOTA**-based ligands undergo rearrangement processes and therefore, a mixture of interconverting isomers is present while studying **DOTA** complexes in solution.[47]

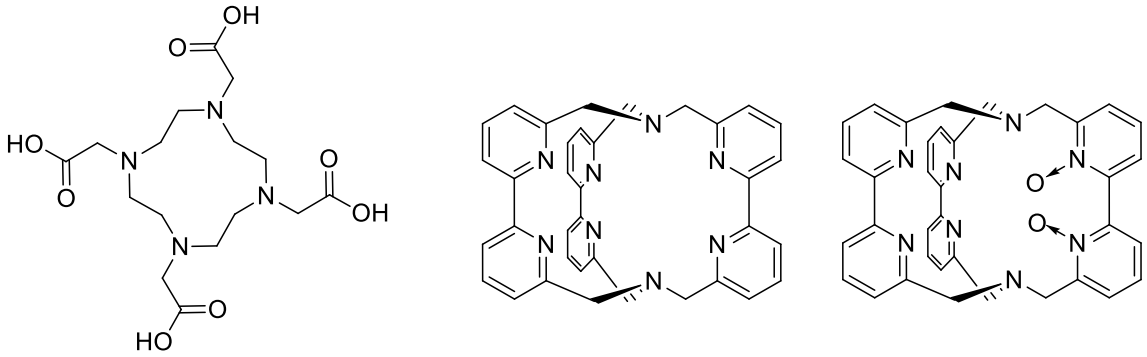

Figure 7: Molecule structures of important ligand systems for lanthanoids: **DOTA**, **bpy$_3$** and **bpy$_3$O$_2$**.

A ligand scaffold which offers great potential for the preparation of extremely well-defined complexes in solution is **bpy$_3$** (tris-(2,2′-bipyridine)).[48] The heterocycles allow for indirect sensitisation of lanthanoid luminescence in the corresponding complexes. However, for many applications in the field of structural elucidation of biomolecules or

regarding the phenomenon of CPL, lanthanoid complexes with extreme configurational and conformational stability in solution are required. By oxidizing one biaryl group to the corresponding 2,2′-bipyridine-*N,N*′-dioxide (**bpy$_3$O$_2$**, Figure 7), extremely rigid lanthanoid (Ln) complexes **2-Ln** can be prepared, originally introduced by Lehn.[49] This ligand scaffold was proven as an efficient antenna for a variety of trivalent lanthanoid ions with estimated excited triplet levels of E(T_1) ≈ 20400 cm^{-1}.[49,50]

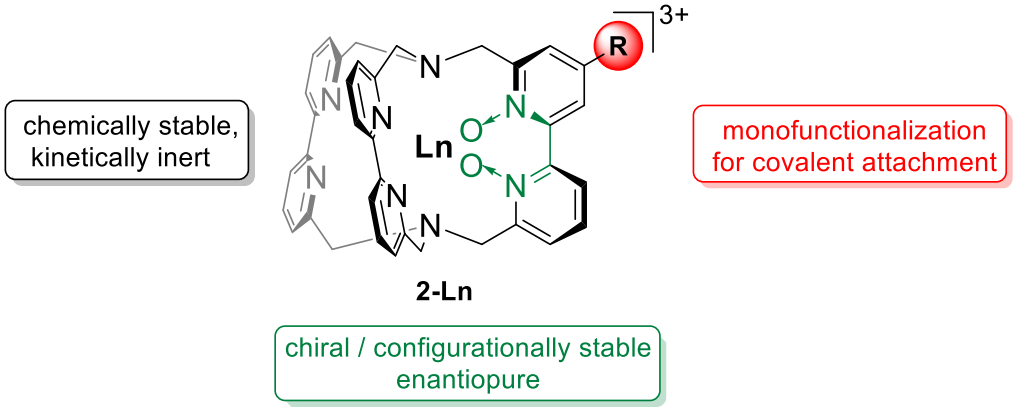

Figure 8: 2,2′-Bipyridine-*N,N*′-dioxide based cryptates **2-Ln** with several advantageous properties. Figure adopted from Seitz and coworkers.[51]

This cage-like ligand offers many advantageous properties (Figure 8): The three bipyridine units surround the lanthanoid in the center. Due to the sterically demanding *N*-oxides the pyridines are distorted. This leads to an overall sterical strain and a rigidified cryptate scaffold with C_2-symmetry. With its high rigidity this cage-like cryptate offers high kinetic stability even under harsh conditions. The purification can even be performed via HPLC using up to 1% TFA (pH ≈ 1) in the mobile phase without isomerisation. Furthermore, possible covalent attachments for applications are well established.[52] From a synthetic point of view, plenty of modifications of the cryptand scaffold have been undertaken in order to tune the rigidity, synthetic route or photophysical properties of the antenna. The derivatives have been prepared by replacing one **bpy** unit with different types of biaryl motifs *e. g.* isoquinoline and other nitrogen-based heterocycles (Figure 9).[48,53–55] Furthermore, first studies on biscarboline as a biaryl motif for the preparation of new cryptates have been conducted in order to extend the absorption band in the visible region.[56] Among the numerous advantages of lanthanoid cryptates **2-Ln** described above there is one important limitation concerning the excitation wavelength. Since the absorption maxima of the low-energy bands are below ≈ 350 nm,[49] short excitation wavelengths in the UV range are required. For the utilisation as luminophores in biological media,

longer excitation wavelengths are preferred. With visible light excitation of the luminescence various advantages emerge:

- less phototoxicity in living systems
- reduction of autofluorescence by preventing light absorption in biomolecules
- no need for expensive and uncommon quartz optics in luminescence microscopy
- possible use of laser excitation with widely used laser lines in confocal luminescence microscopy (e.g., argon-ion laser lines at λ_{exc} = 458 nm/476 nm; laser diode line at λ_{exc} = 405 nm)

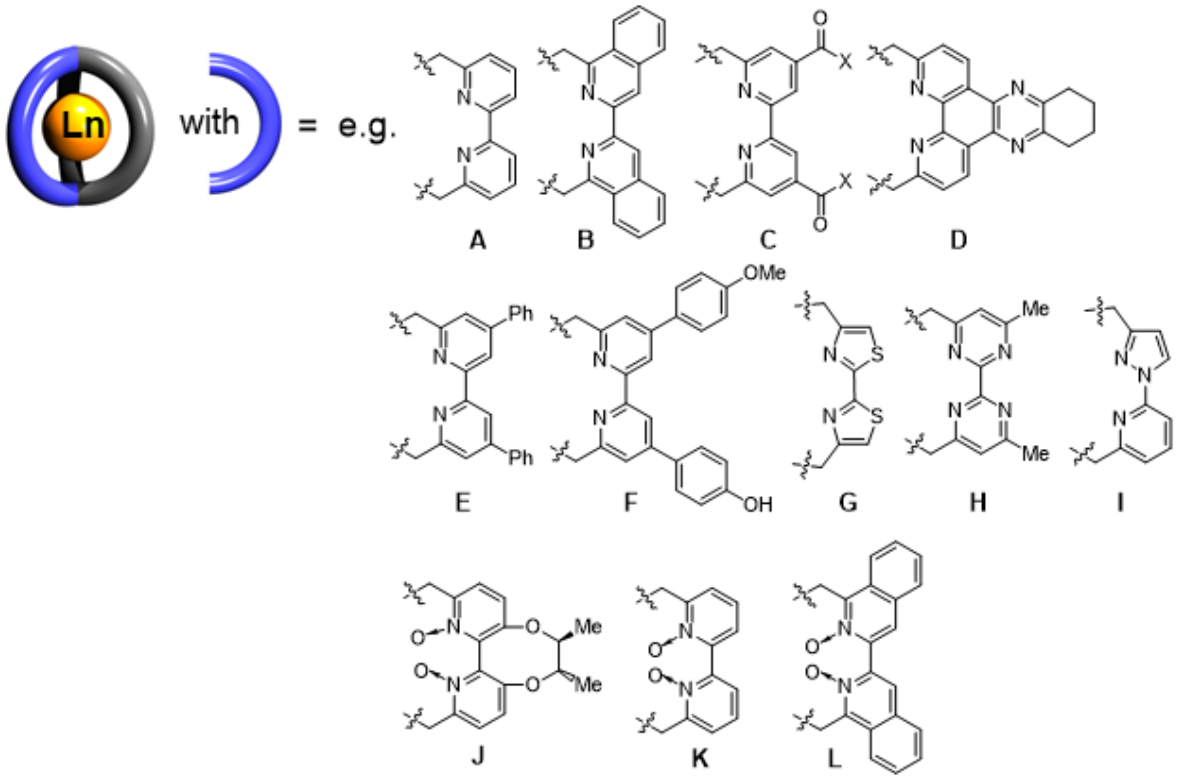

Figure 9: Examples of aromatic building blocks incorporating nitrogen-based heterocycles **A-L** for the realization of synthetic variation of **bpy$_3$**. Scheme adopted and modified from Seitz and coworkers.[51]

As an additional structural feature, these cryptates offer extreme configurational stability. Lanthanoid cryptates **2-Ln** represent examples for axial/helical chirality. The axis of axial chirality is perpendicular to the C_2-symmetry axis and runs through the C-C bond bridging the oxidised pyridine groups (Figure 10).[57] The cryptates are usually prepared as racemates in a macrocyclisation reaction of two racemic precursors, a nitrogen-fused macrocycle of two bipyridines **3** and the dibromide of the oxidised

bipyridine **4**. The excess of sodium carbonate results in the formation of a sodium encapsulated cryptate which can be further transformed into the corresponding lanthanoid complexes by cation exchange. However, there are also synthetic routes with a chiral derivative of the bipyridine-*N,N'*-dioxide unit **(*R,R*)-5** facilitating the preparation of enantiopure cryptates **6-Ln**. Here, one enantiopure bipyridine unit, derived from 2,3-butanediol, leads to a control of the orientation of the corresponding pyridine rings. The two methyl groups are strongly repulsed in the constructed eight-membered ring and they are therefore forced to fixed equatorial positions (Figure 11).[58]

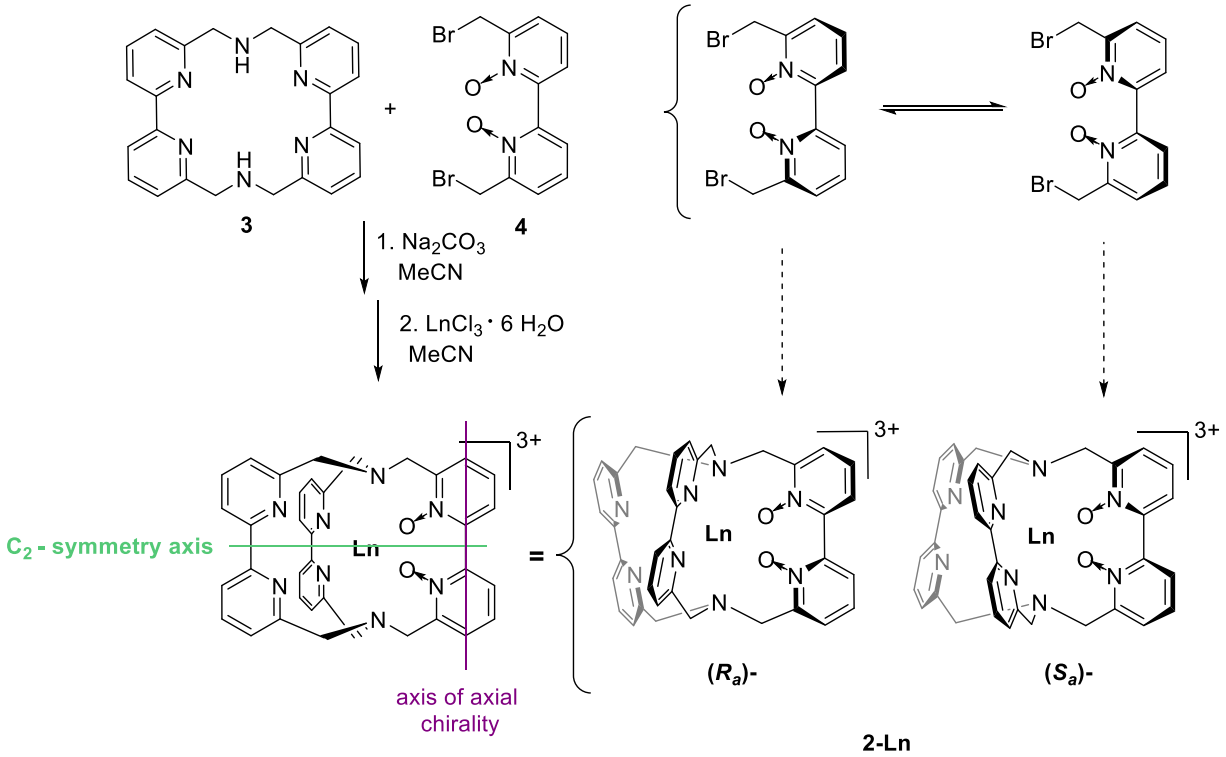

Figure 10: Preparation of the **2-Ln** cryptates in a macrocyclisation reaction and the resulting sterical distortion and the formation of the enantiomers **(R_a)-** and **(S_a)-2-Ln**.

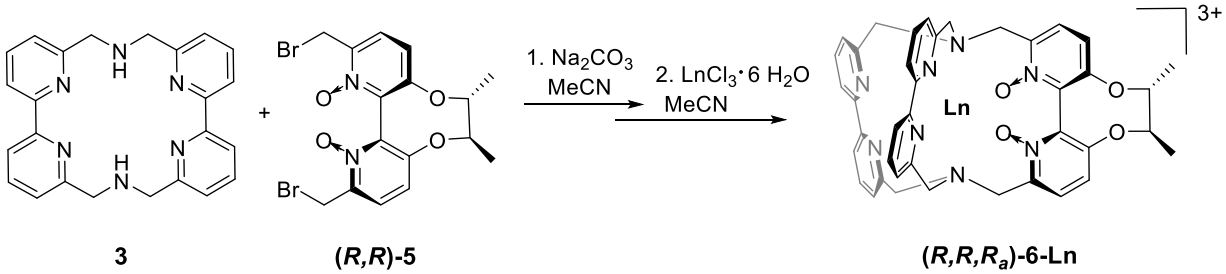

Figure 11: Synthesis of **(R,R,R_a)-6-Ln** cryptate in a macrocyclisation reaction with an enantiopure dibromide.

2 Objectives

Lanthanoid cryptates offer high potential for innovative applications. The main aim of this work is to design a new, extended cryptate which allows excitation of lanthanoid luminescence with visible light for the first time. Regarding the potential of lanthanoid complexes in the field of CPL, a method for the chiral resolution of these racemic cryptates has to be established in order to obtain enantiopure material for chiroptical studies, especially for application in bioimaging techniques.

Among these main topics, different side-projects concerning lanthanoid and chromium luminescence as well as energy transfer processes have been studied.

One of the main aims of this work is to overcome the excitation limit in the UV range by developing a new extended cryptate which shows red-shifted absorption bands for a possible long-wavelength excitation of lanthanoid luminescence. For a successful *ligand design* of this new cryptate, the following steps have to be accomplished:

- Preparation of a derivative of the ligand **bpy$_3$O$_2$** with an extended conjugated aromatic system and the corresponding lanthanoid cryptates
- Examination of the influence of the new ligand upon the structural and photophysical properties of the cryptate (e. g. red-shifted absorption band, triplet level)
- Characterisation of luminescence of the lanthanoid cryptates with focus on the long-wavelength excitation

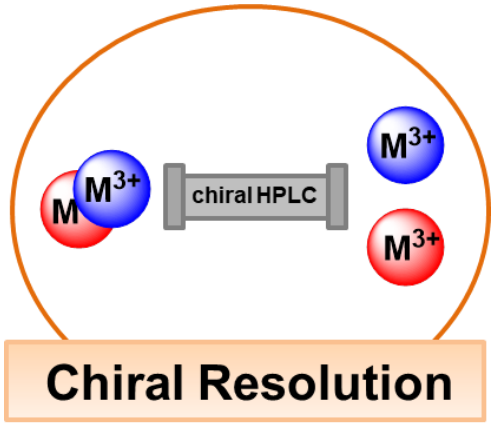

Chiral Resolution

In the course of this work more insights into the highly innovative phenomenon of *circularly polarised luminescence* (CPL) shall be given. In order to provide the enantiopure material, the following steps have to be accomplished:

- Method development for chiral resolution via chiral HPLC of lanthanoid cryptates prepared as racemic mixtures
- Investigation of the configurational stability of the enantiomers

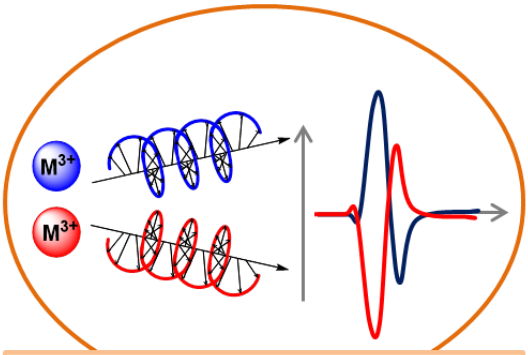

Circularly Polarised Luminescence

The realisation of lanthanoid CPL emitter is often hampered due to low complex stability. Rigidified, enantiopure lanthanoid cryptates are well suited for this purpose. In this work more insights in their CPL activity shall be given by accomplishing the following steps:

- Characterisation of the enantiopure samples with chiroptical methods like circular dichroism and circularly polarised luminescence especially under visible light excitation
- Determination of the absolute configuration by comparison of theoretical and experimental CD spectra

A side-project was the development of an enantiopure complex with an alternative, more earth-abundant trivalent metal with special interest in near-infrared CPL. Since Cr^{3+} shows similar chemical and electronic properties compared to trivalent lanthanoids, high dissymmetry factors can be expected. In order to provide a basis for a systematic study, the following steps have to be accomplished:

- Chiral resolution via chiral HPLC of the racemic chromium complex
- Theoretical and experimental studies on the configurational stability
- Characterisation of the enantiopure samples with chiroptical methods like circular dichroism and circularly polarised luminescence especially in the near-infrared spectral range

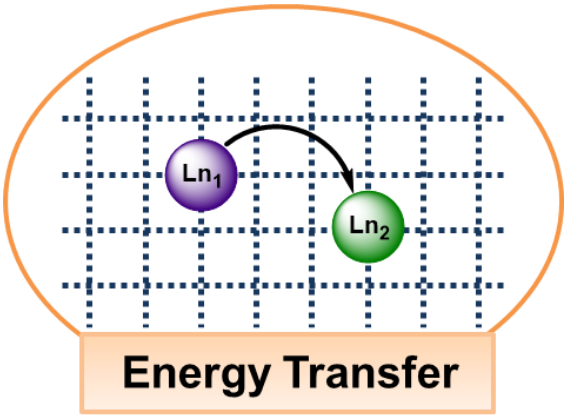

Another secondary aim of this work is the realisation of a three dimensional coordination network for the examination of *energy transfer* between different lanthanoids within this rigid system. The widely used ligand motif 2,2'-bipyridine, which is ubiquitously found in ligands for metal complexes, especially for lanthanoids, shall be synthetically expanded to form this network. In order to implement a lanthanoid coordination network, the following steps have to be accomplished:

- Expansion of the ligand with additional coordination sites for the preparation of lanthanoid coordination networks
- Structural characterisation for the analysis of the energy transfer processes
- Evaluation of the energy transfer processes by profound luminescence measurements

3 Results and Discussion

3.1 Visible Light Excitation of Europium Circularly Polarised Luminescence

3.1.1 Long-Wavelength Excitation in Carboline-Based Cryptates (*Paper 2*)

There are several ligand classes which have proven to facilitate long-wavelength excitation of lanthanoid luminescence.[59–63] Still, lanthanoid cryptates cannot be excited with visible light. A new ligand motif based on β-carboline was developed for the design of new lanthanoid cryptates. β-Carboline and its structural derivative harmane exhibit interesting photophysical properties such as absorption bands above 400 nm as well as triplet energy levels around 21700 cm^{-1}.[64] The energy gap between the triplett level and the excited $^5D_0$ state of Eu^{3+} (ca. 17200 cm^{-1}) is large enough to efficiently prevent energy back transfer.

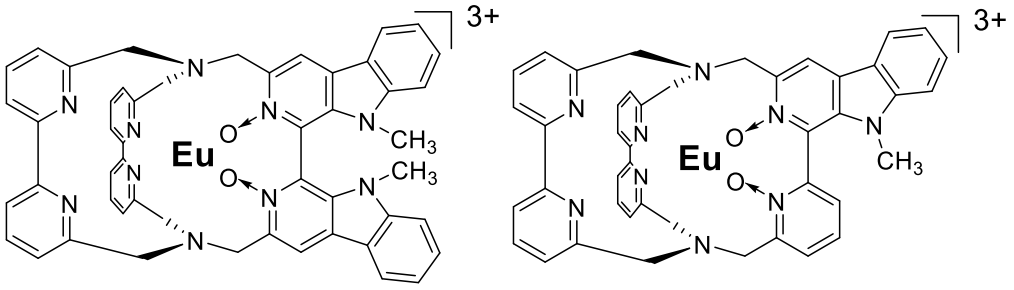

7-Eu **8-Eu**

Figure 12: New cryptates **7-Eu** and **8-Eu** incorporating one and two carboline units respectively.

Two different sodium cryptates were synthesised exhibiting one and two carboline units, respectively. The europium cryptates **7-Eu** and **8-Eu** (Figure 12) were obtained after a metal exchange reaction with the corresponding europium chloride salt followed by purification via HPLC yielding two major fractions for both cryptates. The first fraction gives a single set of resonances in the ^{1}H NMR spectrum consistent with a C_2 symmetry. The second fraction shows a very similar ^{1}H NMR spectrum but with small splittings of signals and C_1 symmetry. Concerning the latter, together with the

information gained from MALDI mass spectrometry (water molecule in the inner coordination sphere) and IR spectroscopy (strong N-O stretching bands) this fraction can tentatively be assigned to the corresponding carboline cryptate with only one N-oxide unit. For detailed structural studies of the biscarboline cryptate with two N-oxide units, DFT calculations for the geometry were performed. The resulting distances and angles are in the usual range for similar complexes. The inner-sphere water ligand is slightly elongated (d = 2.543 Å) than expected for Eu-OH_2 bonds.[65] Also the torsion angle around the atropisomeric axis of the biscarboline unit is slightly larger (60.5°) than the one found in related systems (52.8° around the 3,3′-biisoquinoline 2,2′-dioxide moiety).[66] However, the overall steric strain seems to allow stable complexes.

The ^{1}H paramagnetic lanthanoid induced shift analysis was performed to gain insights in the structure in solution. According to the recorded ^{1}H NMR spectrum there are 18 paramagnetically-shifted signals in the range of 29.3 to -14.6 ppm. The diamagnetic contributions were found by comparison of the chemical shifts measured for the diamagnetic lutetium cryptate. As the paramagnetic shifts are composed of contact and pseudocontact contributions, both influences have to be considered to find a reasonable agreement between calculated and experimental chemical shifts with small deviations less than 4.8 ppm.

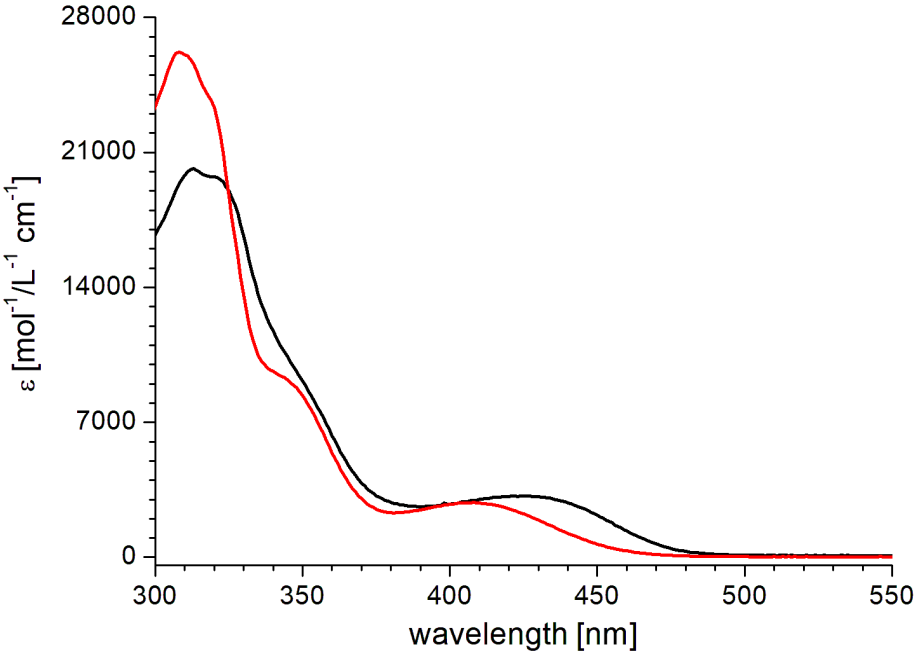

Figure 13: UV-vis absorption spectra of the europium cryptates **7-Eu** (black) and **8-Eu** (red) in H_2O. Figure adopted from Seitz and coworkers.[51]

Compared to **2-Eu** cryptates both carboline cryptates show next to the common UV/vis absorption bands up to 370 nm, a new additional band with $\lambda_{abs,max} \approx 410$ nm for **8-Eu** and even $\lambda_{abs,max} \approx 422$ nm for **7-Eu** (Figure 13). The bathochromic shift depends on the number of carboline units, due to the extended aromatic system. According to previous studies[64] on the photophysics of β-carbolines, which also absorb strongly beyond 400 nm, these results are as expected.

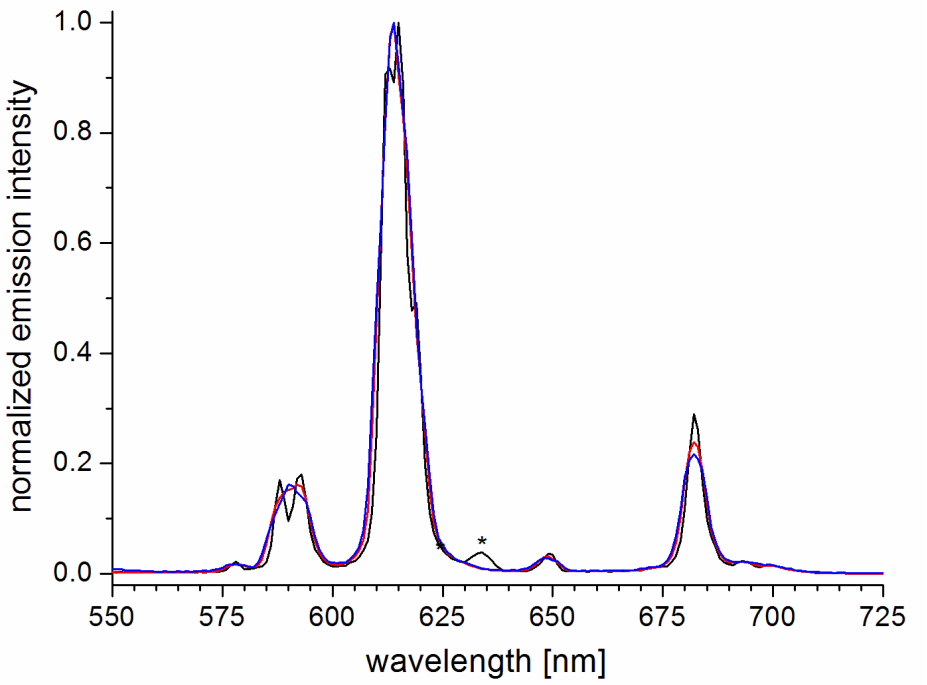

Figure 14: Normalized steady-state emission spectra of **7-Eu** in H_2O (c ≈ 10 µM, * second order excitation peak) after excitation at different wavelengths (black: λ_{exc} = 317 nm, bandwidth 2.0 nm; red: λ_{exc} = 425 nm, bandwidth 4.0 nm; blue: λ_{exc} = 458 nm, bandwidth 5.0 nm). Figure adopted from Seitz and coworkers.[51]

The emission spectra do not change with excitation wavelength and the europium cryptates even show luminescence after long-wavelength excitation with λ_{exc} = 458 nm (Figure 14). Regarding the luminescence properties, the number of carbolines does not seem to have an impact. Luminescence lifetimes are about 0.5 ms and the quantum yields are 3 % for both cryptates in water. These results are useful for applications and in line with luminescence efficiencies reported for similar cryptates.[48,49,67]

Beyond that, the luminescence shows a strong pH dependence according to the luminescence lifetimes. A saturation curve can be recorded measuring from lower pH to higher pH with increasing lifetimes from 50 µs below pH = 5 to 500 µs and 600 µs

at pH = 12 for **8-Eu** and **7-Eu**, respectively. The inflection points lie in the physiologically interesting pH range between pH = 7-9. This kind of pH dependence was never found for **2-Eu** and comes from the successful incorporation of basic carboline moieties.

The newly developed carboline cryptates provide a solution for the excitation limit of europium luminescence in cryptates. The luminescence efficiencies are in a medium range compared to other literature examples, but the low energy excitation with visible light can be very useful in applications were UV light has to be prevented.

C. Dee, D. Esteban-Gomez, C. Platas-Iglesias, M. Seitz

Long Wavelength Excitation of Europium Luminescence in Extended, Carboline-Based Cryptates

Inorganic Chemistry **2018**, *57*, 7390 - 7401.

3.1.2 Chiral Resolution of Lanthanoid Cryptates with Extreme Configurational Stability (*Paper 1*)

The cryptates **2-Ln** with the incorporated *N,N′*-dioxide moiety are well known for their high rigidity and stability.[49] A method for chiral resolution after racemic synthesis, is desired to prepare enantiopure lanthanoid cryptates for applications such as NMR shift reagents or CPL probes.

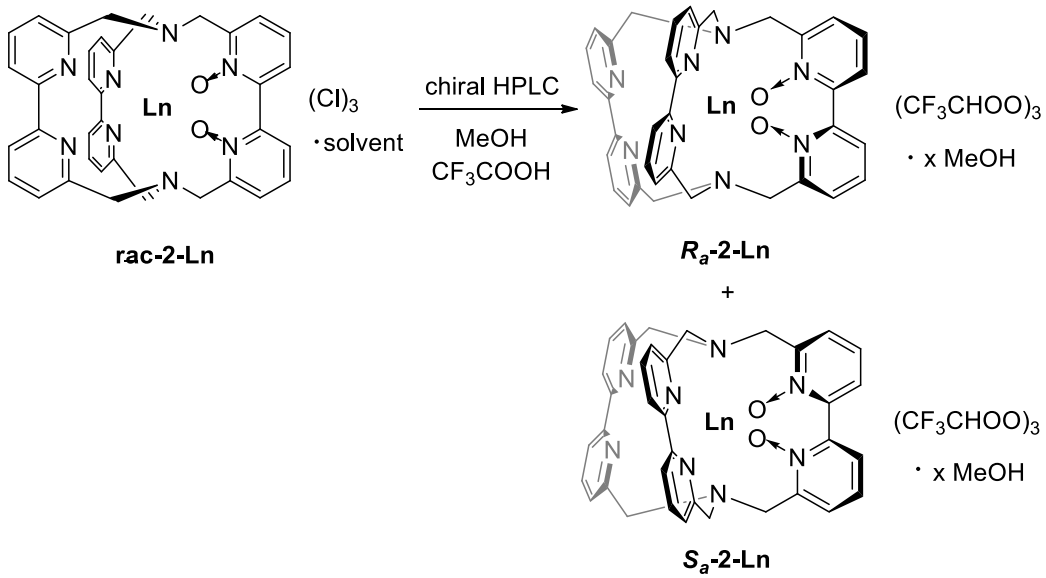

Figure 15: Chiral resolution of **rac-2-Ln**.

The lanthanoid cryptates **rac-2-Ln** (with Ln = Pr, Nd, Sm, Er, Lu) can be separated into the enantiomers *via* chiral HPLC under optimized conditions (Figure 15, stationary phase: CHIRALPAK IE; eluent: isocratic CH_3OH + 0.5 vol % CF_3COOH). In the HPLC trace of the racemate, the 50:50 ratio of the two peaks indicates the presence of both enantiomers. The first eluted component gives a sharp peak in the UV detection trace while the second is broadened through significant tailing (Figure 16). The real evidence for the resolved enantiopure cryptates can be given by three independent analytical methods: both resolved fractions showed no sign of the other enantiomer in the analytical HPLC traces, the ^1H NMR spectra in CD_3OD are identical and the ECD spectra in CH_3OH show perfect mirror-image behaviour.

Based on the fact that the enantiopure cryptates can be resolved *via* chiral HPLC their stability must be extremely high, since dilute CF_3COOH did not induce racemisation.

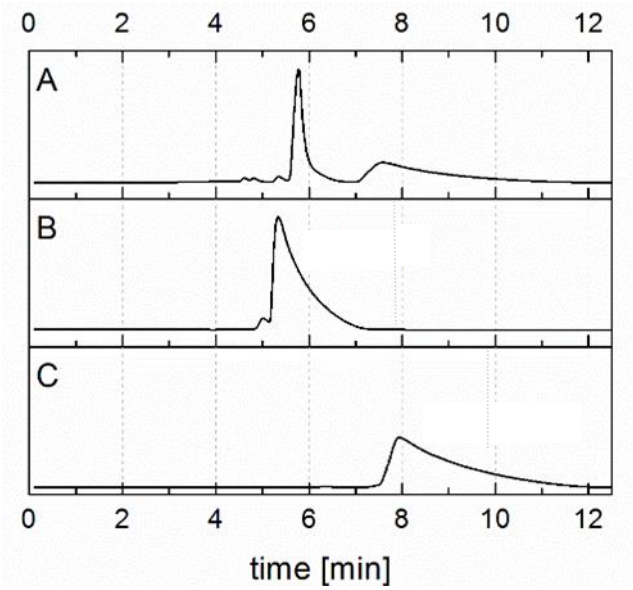

Figure 16: HPLC traces (CHIRALPAK IE, CH_3OH + 0.5 vol-% CF_3COOH, UV detection: 300 nm). (A): Preparative separation of **rac-2-Lu**. (B) and (C): Analytical HPLC traces of the resolved enantiomers from the preparative run in (A). Modified from Kreidt *et al*.[57]

In order to check the configurational stability of the resolved enantiomers systematically, rather harsh conditions were applied. Firstly, the tested enantiomer (first eluted fraction: Figure 16 B) was stirred in neat CF_3COOH at room temperature, which is a challenging condition in terms of decomplexation and configurational instability for most lanthanoid complexes. Secondly, the same enantiomer was heated under reflux in CH_3CN with 10 equivalents of $LuCl_3 \cdot 6\ H_2O$, which can induce self-exchange of the lutetium cations and therefore induce racemisation. In neither of these conditions we could detect any sign of racemization or instability after 5 days in the corresponding analytical HPLC traces.

With this new established method, it is possible to obtain enantiopure lanthanoid cryptates after the racemic synthesis for the first time. Together with the confirmed configurational stability new prospects arise concerning stable, enantiopure cryptates as CPL emitter.

E. Kreidt, C. Dee, M. Seitz
Chiral Resolution of Lanthanoid Cryptates with Extreme Configurational Stability
Inorganic Chemistry **2017**, *56*, 8752 − 8754.

3.1.3 Circularly Polarised Luminescence of Enantiopure Carboline-Based Europium Cryptates under Visible Light Excitation (*Paper 5*)

Enantiopure lanthanoid cryptates via chiral HPLC offer great potential for many applications in different fields of technology. In the field of bioimaging and bioanalytical techniques the excitation wavelength is often limited to the infrared and visible light region to avoid biological damage induced by high-energy ultraviolet radiation. The carboline-based cryptates **7-Eu** and **8-Eu** are ideal candidates as CPL emitter with interesting photophysical properties especially the sensitisation of europium emission with wavelengths well above 450 nm.[51] The racemic synthesis features many steps and therefore separation of the enantiomers via HPLC is desirable. We have shown before that the enantiomers of racemic **rac-2-Lu** can be separated by chiral HPLC[57]. Kreidt *et al.* have also reported that the enantioselectively prepared **6-Eu** exhibits remarkable CPL activity with dissymmetry values of $|g_{lum}| \leq 0.19$ (Figure 17).[68] Taking these beneficial aspects together, the separation of the enantiomers of **8-Eu** via chiral HPLC allows for the preparation of enantiopure CPL emitter which can be excited with visible light.

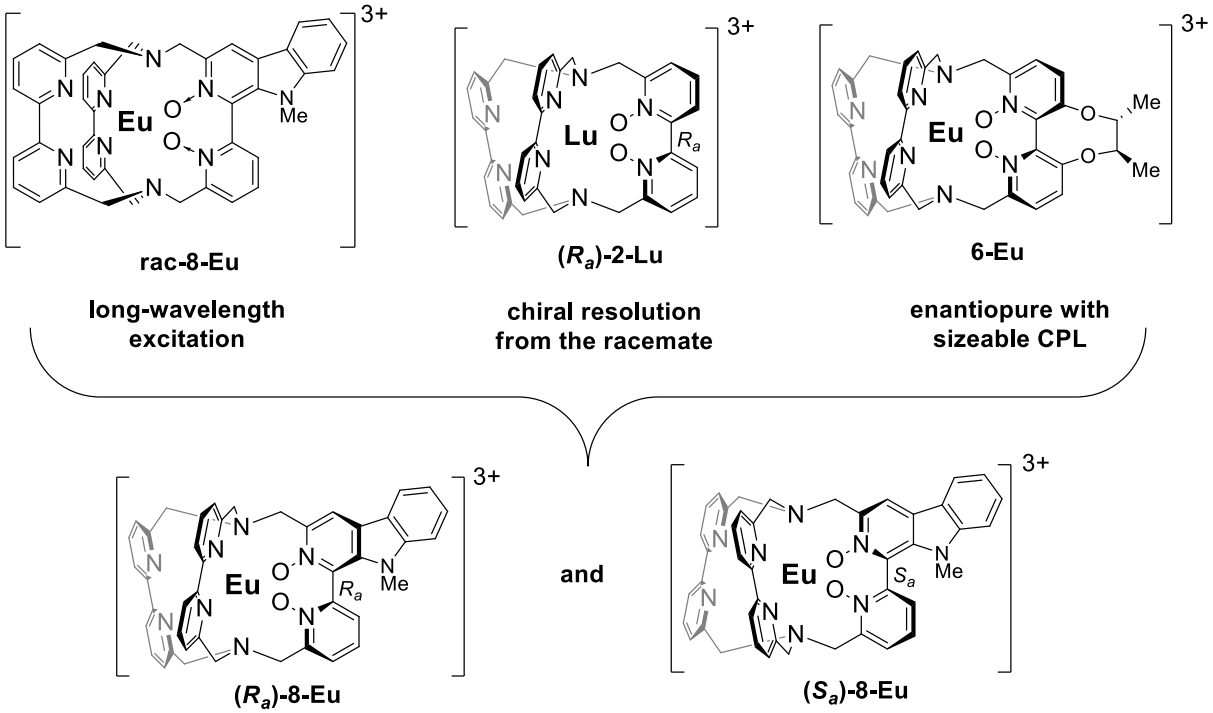

Figure 17: Combination of several beneficial aspects of known *2,2'*-bipyridine-*N,N'*-dioxide-based cryptates **rac-8-Eu**, **(*R*$_a$)-2-Lu**, and **6-Eu** into the new europium CPL emitters **(*R*$_a$)-8-Eu**

and **(S_a)-8-Eu** reported in this study. Figure adopted from Seitz and coworkers (*manuscript submitted*).

Both enantiomers of the carboline cryptate **8-Eu** were successfully resolved by adapting the chiral HPLC conditions of the separation of **rac-2-Ln** even though the separation was more complicated than for the parent cryptate. Again, identical ^{1}H NMR spectra for the enantiomers as well as mirror-imaged ECD spectra in CD_3OD were recorded as a proof of the both enantiomers. The configurational stability was tested in neat CF_3COOH, as for the **2-Ln** case before. After 5 days stirring at room temperature no chemical instability or racemization could be detected by analytical chiral HPLC.

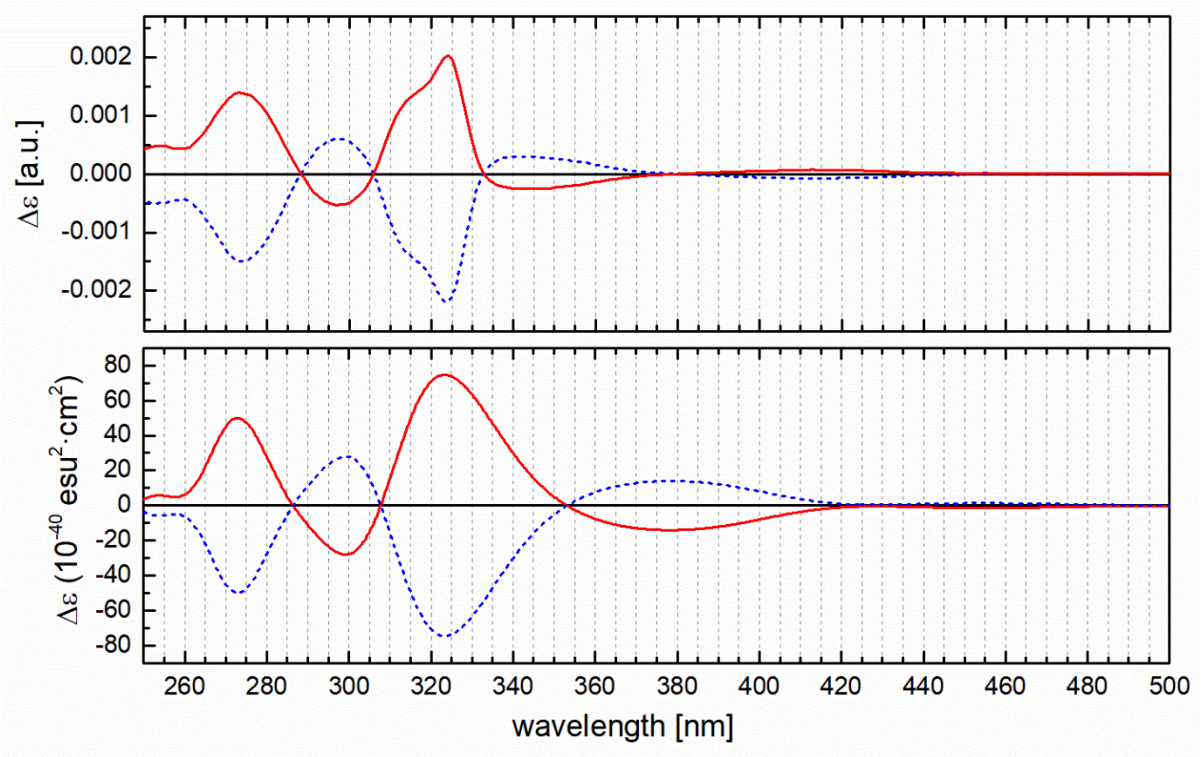

Figure 18: Experimental (top) and calculated (bottom) CD spectra of **(R_a)-8-Eu** (blue dashed line) and **(S_a)-8-Eu** (red solid line) in CD_3OD. Figure adopted from Seitz and coworkers (*manuscript submitted*).

The determination of the absolute configuration was performed by comparing the experimental and theoretical ECD spectra. The calculated spectra (Figure 18: bottom) are in good agreement with the measured ones (Figure 18: top) and here the first eluted enantiomer can be assigned to ***R_a*-8-Eu**, while the second corresponds to ***S_a*-8-Eu**. The CPL of the enantiomers was measured with excitation at 400 nm using a blue LED and shows two main CPL bands for the $^{5}D_0 \rightarrow {}^{7}F_1$ and the $^{5}D_0 \rightarrow {}^{7}F_2$ transition

(Figure 19: top). The resulting CPL spectra are identical in shape with opposite signs for each enantiomer. In addition, the $|g_{lum}|$ value of 0.25 was determined for the f-f transition $^5D_0 \rightarrow {}^7F_1$ (λ = 594 nm), which is an increase compared to **(*R,R,R*$_a$)-6-Eu** (0.19).[68]

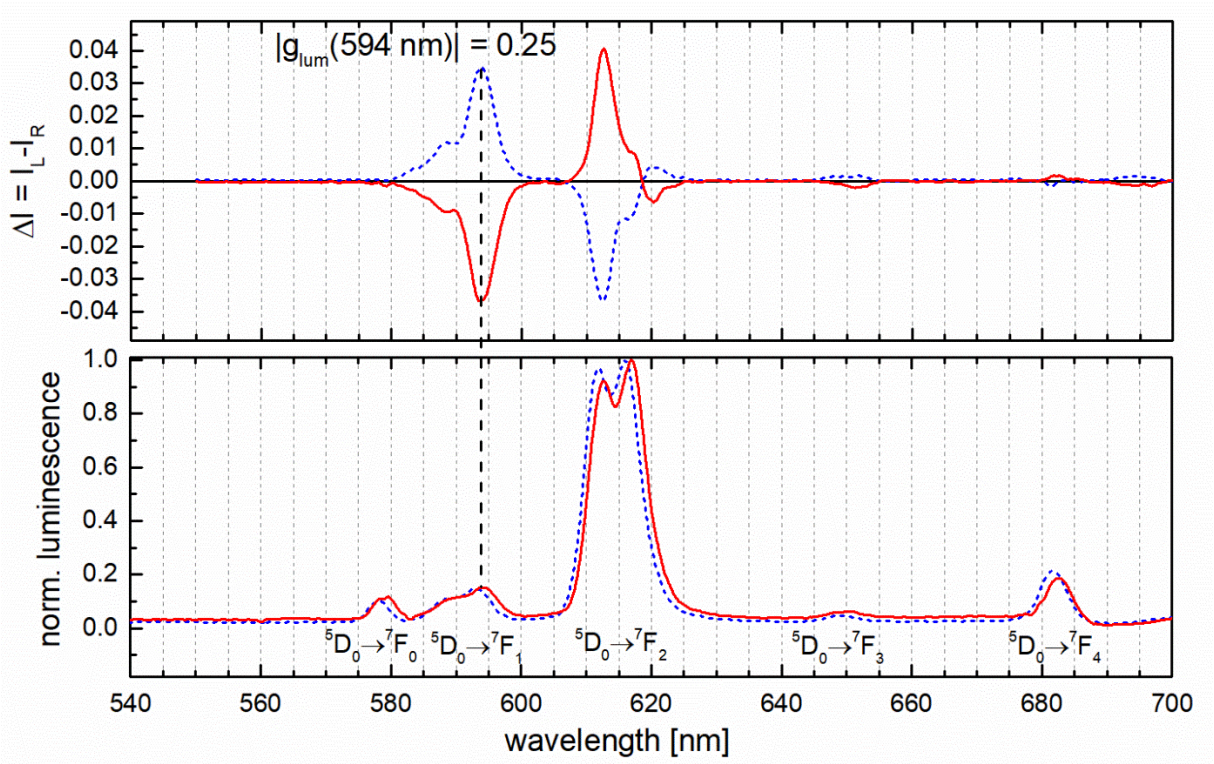

Figure 19: CPL (top) and normalized luminescence spectrum (bottom) of **(*R*$_a$)-8-Eu** (blue dashed line) and **(*S*$_a$)-8-Eu** (red solid line) in CD_3OD (λ_{exc} = 400 nm) - Highest g_{lum} value indicated for the emission band $^5D_0 \rightarrow {}^7F_1$ (594 nm). Figure adopted from Seitz and coworkers (*manuscript submitted*).

Overall, the enantiopure carboline cryptate shows great CPL activity under visible light excitation. Therefore, they are promising potential CPL probes for bioanalytical applications where extreme configurational stable compounds are essential and UV sensitisation can be avoided.

C. Dee, F. Zinna, E. Kreidt, L. Arrico, A. Rodriguez-Rodriguez, C. Platas-Iglesias, L. Di Bari, M. Seitz
Circularly Polarized Luminescence of Enantiopure Carboline-Based Europium Cryptates under Visible Light Excitation
Manuscript submitted

3.2 Circularly Polarised Luminescence of an Enantiopure Terbium Cryptate (*Unpublished Results*)

Next to the racemic preparation and subsequently chiral resolution *via* chiral HPLC of the cryptates mentioned above, there also exists an enantiopure synthesis.[58] Kreidt *et al.* reported the CPL activity of the corresponding **(*R,R,R*$_a$)-6-Ln** (Ln = Eu, Sm). The partially deuterated ligand scaffold allows for high g_{lum} values of +0.13 (Sm^{3+}, $^4G_{5/2} \rightarrow {}^6H_{5/2}$) and −0.19 ($Eu^{3+}$, $^5D_0 \rightarrow {}^7F_1$).[68] Among the purely magnetic dipole transititon $^5D_0 \rightarrow {}^7F_1$ of Eu^{3+}, Tb^{3+} exhibits electronic structures which also allow sizeable g_{lum} values. The nature of the $^5D_4 \rightarrow {}^7F_5$ transition of Tb is less promising for strong CPL, but with its generally high luminescence properties, many examples with high g_{lum} values have been reported.[69,70] Here, we report a CPL study of the enantiopure cryptate **D$_8$-(*R,R,R*$_a$)-6-Tb** (Figure 20).

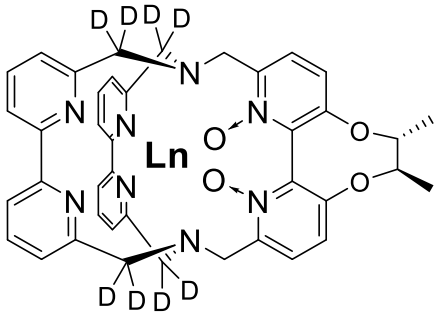

D$_8$-(*R,R,Ra*)-6-Ln
Ln = Lu, Tb

Figure 20: Enantiopure cryptate **D$_8$-(*R,R,R*$_a$)-6-Ln** prepared for this study.

The enantiopure synthesis of the ligand and the corresponding **D$_8$-(*R,R,R*$_a$)-6-Tb** and **D$_8$-(*R,R,R*$_a$)-6-Lu** cryptate was performed as described previously.[58,68] The purification of the complexes was done by semi-preparative reversed-phase HPLC. The analytical HPLC traces of the separated complexes show only one species (Figure A30-A31) which can be identified *via* ^{1}H NMR spectroscopy (Figure 21: **D$_8$-(*R,R,R*$_a$)-6-Tb**, Figure A1: **D$_8$-(*R,R,R*$_a$)-6-Lu**) and ESI mass spectrometry. The chemical shifts of the ^{13}C signals were obtained by ^{1}H-^{13}C correlated 2D spectra (HSQC, HMBC; Figure A2-A3). Impressively, all paramagnetically shifted ^{1}H signals of the terbium complex can be found, ranging from 200 to -100 ppm, showing C_2-symmetric behaviour of the complex (Figure 21).

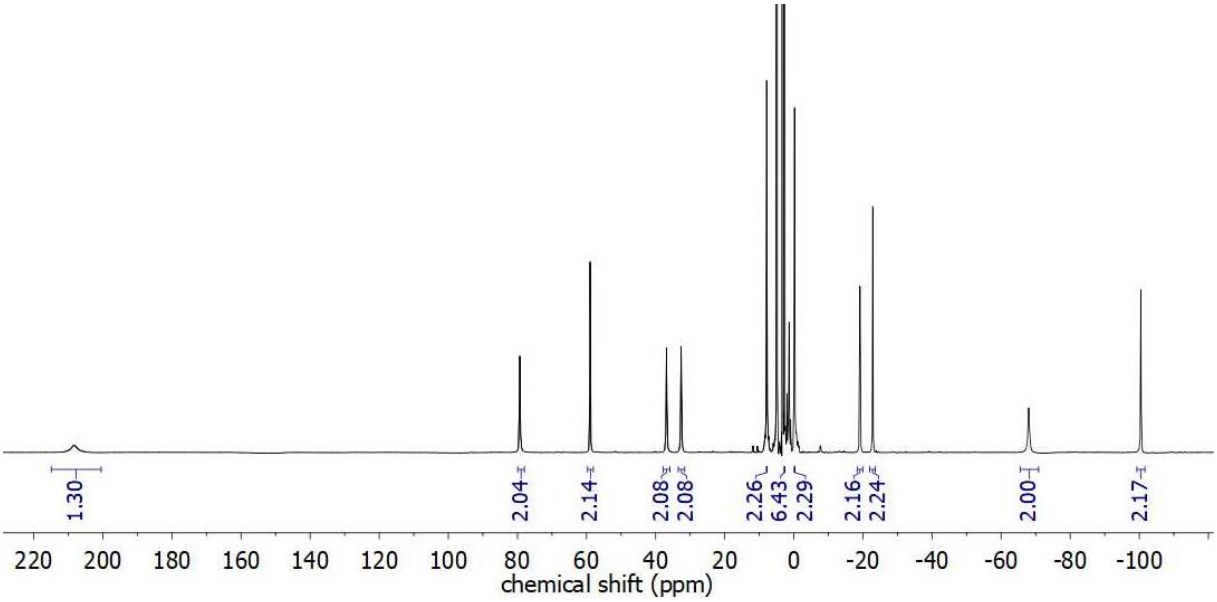

Figure 21. ^{1}H NMR (300 MHz, CD_3OD) spectrum of **D_8-(*R,R,R$_a$*)-6-Tb**.

D_8-(*R,R,R$_a$*)-6-Lu was used as a non-luminescent complex for the estimation of the triplet energy of the ligand. The zero-phonon transition $T_1 \rightarrow S_0$ was measured by low-temperature steady-state emission spectra (Figure 22). According to similar behaviour seen for the cryptates already described, the triplet energy can be estimated at approximately 446 nm which is corresponding to 22420 cm^{-1}. The gap between the triplet level of the ligand and the emissive Tb^{3+} $^5D_4$ level (20400 cm^{-1}) is a little bit small and may allows back energy transfer.

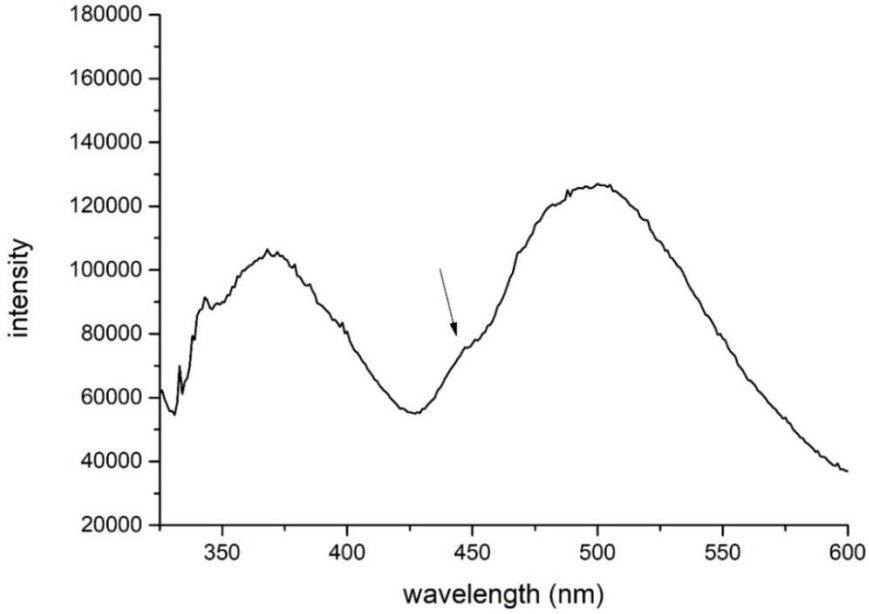

Figure 22: Low temperature emission spectra (λ_{exc} = 307 nm, T = 77 K) of the **D_8-(*R,R,R$_a$*)-6-Lu** (top) measured in a MeOH/EtOH glass matrix (1:1, v/v). The triplett energy was estimated at the arrow.

The partially deuterated cryptand scaffold is a moderately efficient antenna for Tb with appropriate measured luminescence data (Table 1) like quantum yields of 2.2 % in water against quinine as standard and luminescence lifetimes of roughly 1 ms in water. **D_8-(*R,R,R*$_a$)-6-Tb** in D_2O solution displayed relatively intense CPL bands associated with $^5D_4 \rightarrow {}^7F_J$ (J = 3-6) transitions (Figure 23), with $|g_{lum}|$ values of up to 0.03 (Table 2) which is in the common range for Tb^{3+} CPL emitter.[69–71]

Table 1. Luminescence data of **D_8-(*R,R,R*$_a$)-6-Tb**.

Φ^a	τ_{obs} in H_2O (µs)[b]	τ_{obs} in D_2O (µs)[b]
2.2 %	64.5 (30%) 297 (34%) 926 (36%)	436 (26%) 1921 (74%)

[a]absolute quantum yield in water measured against quinine (1M H_2SO_4), [b]luminescence lifetimes (λ_{exc} = 317 nm, λ_{em} = 540 nm ($^5D_0 \rightarrow {}^7F_2$).

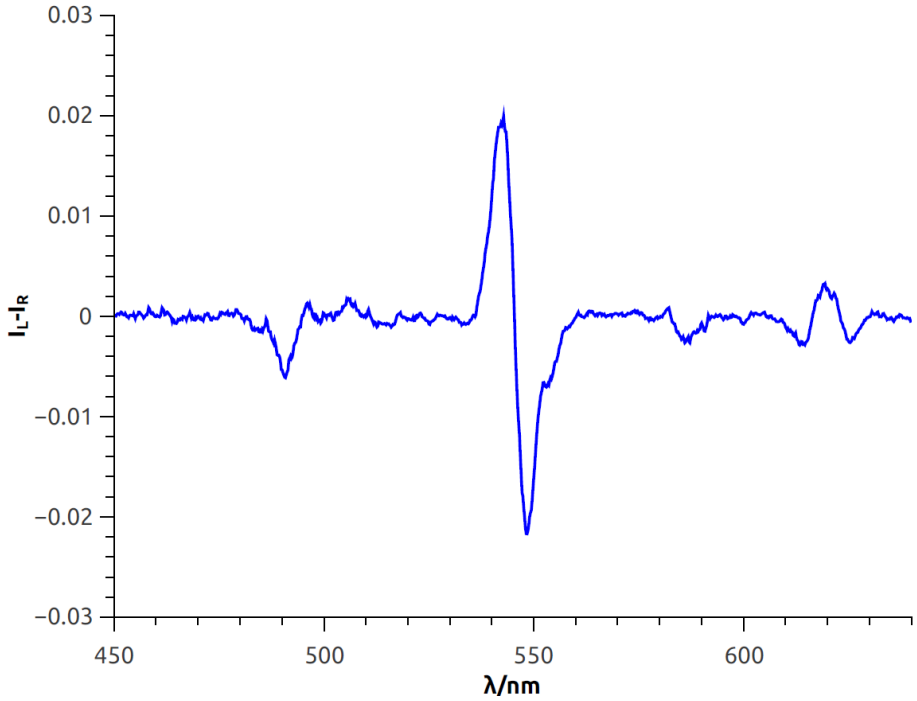

Figure 23: CPL spectrum of **D_8-(*R,R,R*$_a$)-6-Tb** (3 mM D_2O solution, λ_{exc} = 254 nm).

Table 2. Measured g_{lum} values for **D_8-(*R,R,R_a*)-6-Tb** in D_2O.

Transition	Wavelength (nm)	g_{lum}
$^5D_4 \rightarrow {}^7F_6$	490	-0.015
$^5D_4 \rightarrow {}^7F_5$	543	+0.020
	548	-0.03
$^5D_4 \rightarrow {}^7F_4$	586	-0.019
$^5D_4 \rightarrow {}^7F_3$	620	+0.02

The deuterated cryptand scaffold was very promising after the great results reported for the corresponding Sm and Eu cryptates. Although the energy gap between the triplet level and the emitting Tb state is relatively small, distinct CPL can be measured with moderate dissymmetry factors.

3.3 Strong Circularly Polarised Luminescence of an Octahedral Chromium(III) Complex (*Paper 4*)

In search of high values of the dissymmetry factor g_{lum}, which is important for various applications, compounds with luminescence bands, which are electric dipole forbidden and magnetic dipole allowed, are required. The best candidates are enantiopure lanthanoid complexes.[29,30] Naturally, it is desirable to find alternative CPL emitter based on more abundant elements. The CPL-active lanthanoid transitions occur to a large part in the visible spectral range (Eu^{3+}, Tb^{3+}). Unfortunately, emitter for the near-IR region are missing. A very promising alternative solution is Cr^{3+} with its phosphorescent, spin-flip-transitions $^2E/^2T_1 \rightarrow {}^4A_2$ resembling the lanthanoid transitions especially the strongly electric dipole forbidden and magnetic dipole allowed character as well as the excited and ground states in the weak coupling limit. To date, CPL studies of Cr^{3+} are scarcely reported except for solid state and low-temperature cases.[72–74] The problem with molecular chromium complexes has been their low quantum efficiencies at room temperature in solution. Heinze and coworkers developed the molecular ruby **$[Cr(ddpd)_2]^{3+}$** (**9-Cr**, ddpd = N,N'-dimethyl-N,N'-dipyridine-2-ylpyridine-2,6-diamine) with impressive phosphorescence quantum yields of up to 30% for the deuterated ligand in deoxygenated, deuterated solutions at room temperature.[75–77] Due to the strongly twisted ddpd ligands with homochiral helicities (M,M or P,P) the complex is chiral with D_2 symmetry (Figure 24).

To gain insight into its configurational stability, DFT calculations along possible racemisation trajectories were performed. As a result, racemization is only possible following a dissociative or associative pathway with varied coordination number. Feasible intermediates are high in energy or inaccessible suggesting significant configurational stability.

The racemic material can be resolved by chiral HPLC (stationary phase: CHIRALPAK IC; eluent: isocratic $CH_2Cl_2/CH_3OH/NEt_3/CF_3COOH$ 90:10:0.3:0.5) (Figure 24). The HPLC trace of the racemate shows the 50:50 ratio of the two peaks, which are unfortunately not baseline separated. It was only possible to provide enantiopure material of the second fraction (100% ee) while the first fraction only gave an enantiomeric excess of 80%. However, the corresponding mirror-image CD spectra in deoxygenated D_2O indicate the presence of both enantiomers.

The configurational stability of the enantiopure material was confirmed by stirring the enantiopure material in H_2O at room temperature with no sign of any racemization over a period of 48 h.

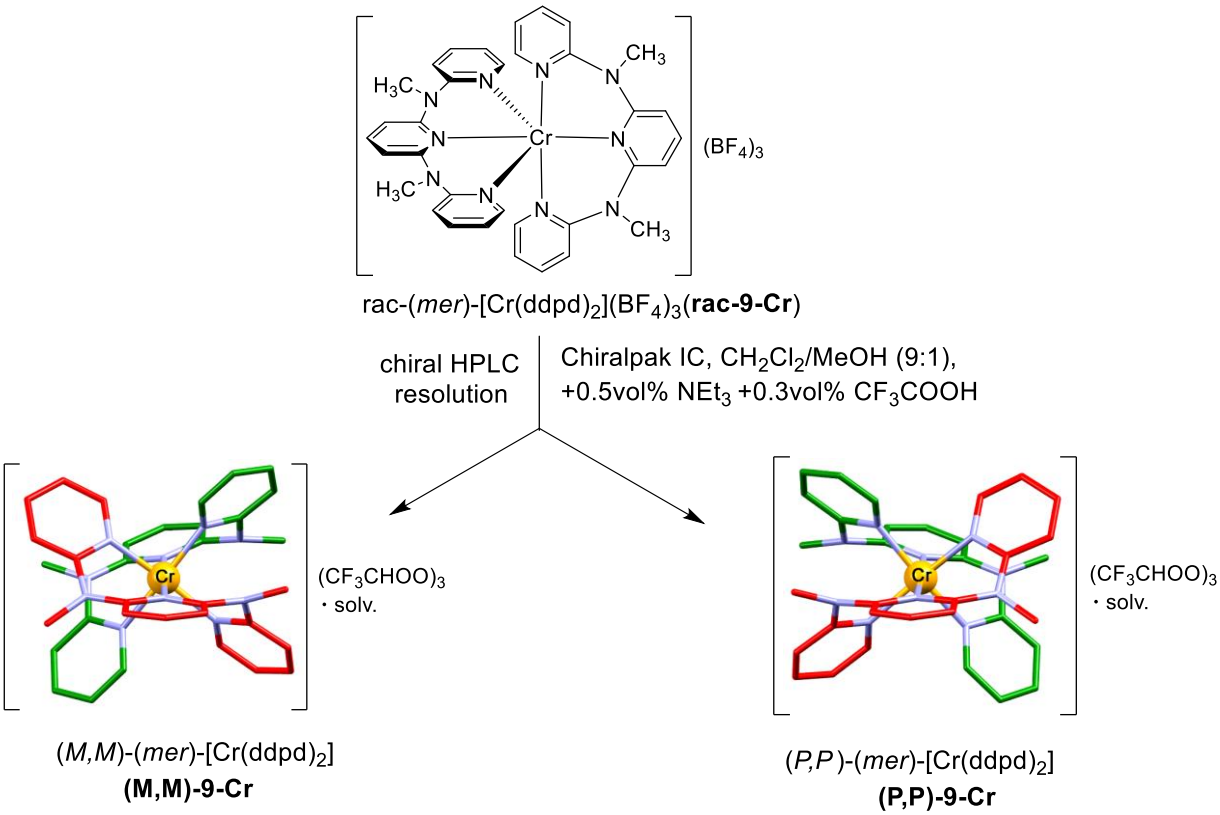

Figure 24: Schematic representation of the racemic, meridional **$[Cr(ddpd)_2]^{3+}$** complex into the **(M,M)-9-Cr** and **(P,P)-9-Cr** enantiomers. Figure adopted from Seitz and coworkers.[78]

Comparing the experimental and calculated (TD-DFT, CASSCF(7,12)-NEVPT2) CD spectra the absolute stereoconfiguration could be assigned. The resemblance of the calculated spectral shape with the measured CD spectra of the second fraction clearly assigns the second as **(M,M)** and therewith the first fraction as **(P,P)**.

The CPL of the enantiopure **(M,M)-9-Cr** were measured in deoxygenated D_2O and a high value for g_{lum} = -0.093 at 775 nm was obtained (Figure 25). Recently, Piguet *et al.* also measured a high CPL activity for a similar, enantiopure chromium complex **$[Cr(dqp)_2]^{3+}$** (dqp = 2,6-di(quinolin-8-yl)pyridine) with large dissymmetry factors of up to $|g_{lum}|$ = 0.2.[79] Both values are outstanding for a 3d-metal complex and are in the same range as many lanthanoid-based complexes.

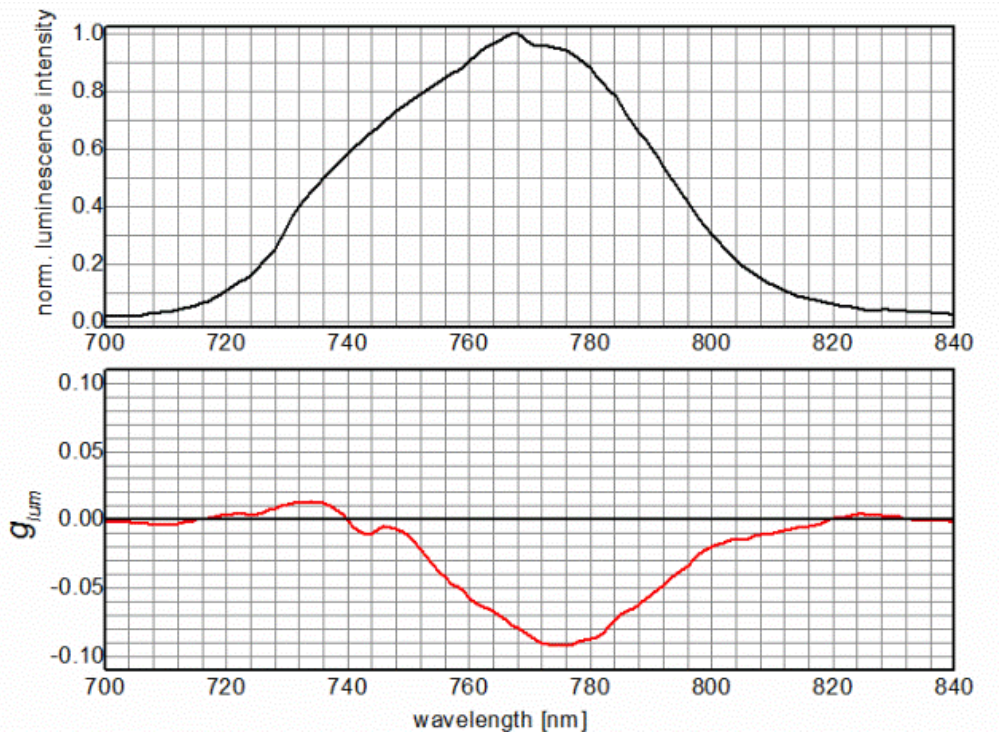

Figure 25: Steady-state emission (top, black) and CPL spectra (bottom, red) of the near-IR luminescence band $^2E_g/^2T_{1g} \rightarrow {}^4A_{2g}$ of **(M,M)-9-Cr** in solution at room temperature (deoxygenated D_2O, c = 10 µM, λ_{exc} = 365 nm). Figure adopted from Seitz and coworkers.[78]

Taking all into account, with the excellent luminescence properties of **$[Cr(ddpd)_2]^{3+}$** and its high stability the enantiopure material is perfectly suited as a very efficient NIR-CPL emitter based on an earth-abundant element for application in chiral optoelectronics.

C. Dee, F. Zinna, W. R. Kitzmann, G. Pescitelli, K. Heinze, L. Di Bari, M. Seitz
Strong Circularly Polarized Luminescence of an Octahedral Chromium(III) Complex
Chemical Communications **2019**, *55*, 13078 - 13081.

3.4 Energy Transfer Studies in Lanthanoid-Based Systems

3.4.1 Lanthanide Sensitisers for Large Anti-Stokes Shift NIR-to-VIS Triplet-Triplet Annihilation Photon Upconversion (*Paper 6*)

Upconversion (UC) describes the transformation of two low-energy photons to a single high-energy photon.[80] This process can be induced by two-photon absorption or among other mechanisms, follow the triplet-triplet annihilation (TTA) mechanism (Figure 26).[81] The main advantage of TTA is the low intensity which is required (0.01-10 W/cm^2)[80] compared to other UC processes (GW/cm^2).[82] In a more detailed description, TTA includes two energy transfer steps and the participation of excited states of two species, a sensitiser and an emitter. Firstly, the energy is transferred from the sensitiser to the triplet state of the emitter. Secondly, the TTA process between two emitter molecules takes place.[81,83] With organic molecules being sensitiser and emitter molecules, the ability for TTA-UC system upconverting NIR light was limited. A first approach in this direction was made by Wu et al. with the use of PbS nanocrystals as the sensitiser paired with rubrene as the emitter. At first, PbS absorbed NIR light, then, the energy was transferred from the excited state to the triplet state of rubrene followed by emission in the visible region. One drawback of this TTA-UC system was the reabsorption of the upconverted light by PbS.[84]

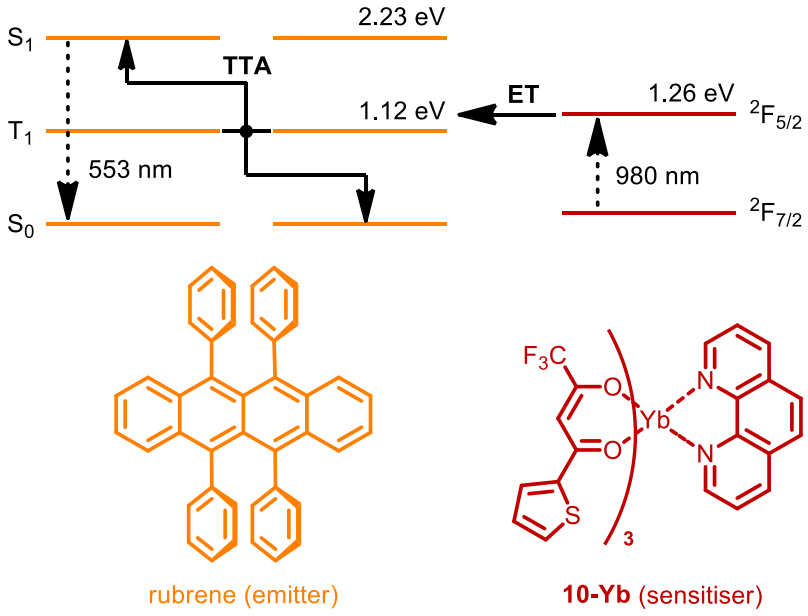

Figure 26: Scheme of TTA-UC with **10-Yb** (sensitiser) and rubrene (emitter): chemical structures of chromophores used for IR-to-yellow UC.

In this study, an improved system consisting of the molecular complex **10-Yb** as the sensitiser and rubrene with TTA-UC from the NIR (978 nm) to the visible (559 nm) is reported. The corresponding anti-Stokes shift is very large with ΔE_{AS} = 0.95 eV. **10-Yb** is a well-suited sensitiser due to its stability in solution, solubility in non-polar/ moderately polar organic solvents and luminescence properties (Φ = 1.1 % and τ = 10 μs in toluene after UV excitation).[50,85] The energy transfer was analysed in deuterated THF and efficiencies of 1.5 % were obtained.

Although this proof-of-concept system shows rather low upconversion efficiency, lanthanoid-based complexes as sensitiser in TTA UC processes offer high potential especially regarding applications with NIR to visible photon upconversion.

N. Kiseleva, P. Nazari, C. Dee, D. Busko, B. S. Richards, M. Seitz, I. A. Howard, A. Turshatov

Lanthanide Sensitisers for Large Anti-Stokes Shift NIR-to-VIS Triplet-Triplet Annihilation Photon Upconversion

Manuscript Submitted

3.4.2 Efficient Ytterbium Near-Infrared Luminophore Based on a Nondeuterated Ligand (*Paper 3*)

Molecular near-infrared emitter complexes are often degraded by vibrational deactivation of metal-centered states. Due to multiphonon relaxation, the energy is transferred from the lanthanoid to oscillator overtones in molecules in its vicinity.[14] Mainly, solvent molecules in the inner-sphere (O-H anharmonic oscillator) and multidentate ligands (C-H stretching vibrations) lead to inefficiency of the near-infrared luminescence. To overcome these drawbacks, concerning the antenna ligand, the C-H oscillators are avoided by deuteration of the ligand.[86,87] However, complexes are preferred which can be prepared in a simple way without synthetic effort. Molecular ytterbium complexes without deuterated ligands exhibit low quantum yields in solution below 1%, rarely exceeding 4%.[88–90]

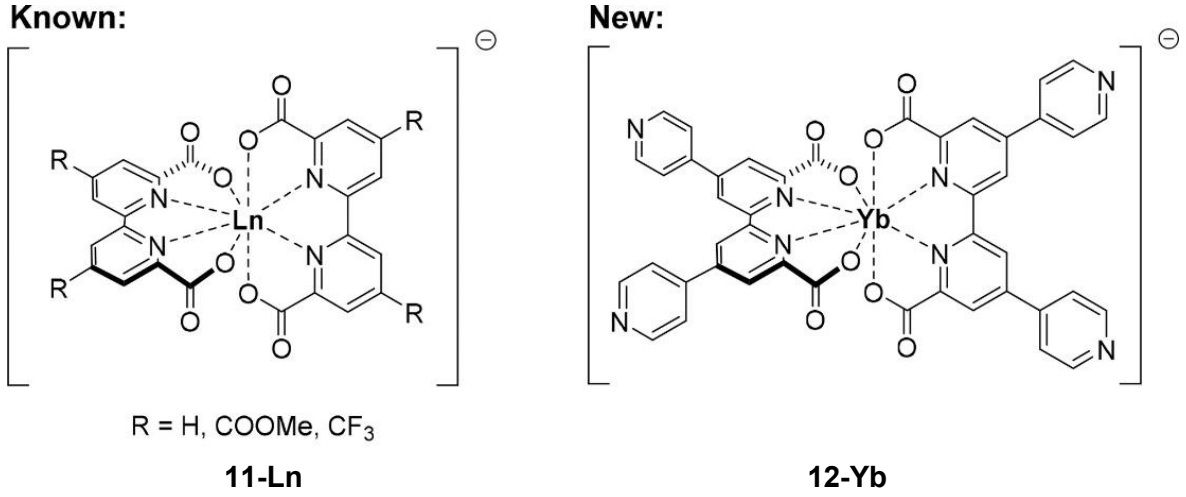

11-Ln **12-Yb**

Figure 27: Antenna motifs based on 2,2′-bipyridine-6,6′-dicarboxylic acid (left: **11-Ln**) and new Yb complex **12-Yb** reported here (right).

The structural motif 2,2'-bipyridine-6,6'-dicarboxylate (Figure 27: left) has been widely used as a ligand in different metal complexes. The excellent antenna is suitable for many lanthanoid complexes **11-Ln** (Ln = Sm, Eu, Tb, Dy, Ho, Er, Tm, Yb), especially for the near-infrared emitting lanthanoids after deuteration of the pyridines.[91–93] This antenna motif was expanded with appended pyridyl groups (Figure 27: right). In fact, this ligand was prepared in order to form coordination networks. The ligand acts as a linker between different lanthanoid centers. Therefore, three coordination sites arise: the 2,2′-bipyridine-6,6′-dicarboxylic acid pocket as well as the nitrogen atoms in the appended pyridyl groups. Unfortunately, the latter did not bind lanthanoid ions as theoretically considered and only molecular complexes with two ligands and one

lanthanoid have formed. The corresponding ytterbium complex **12-Yb** (Figure 27: right) can be efficiently sensitised and shows absolute luminescence quantum yields of 3% in CD_3OD (λ_{exc} = 300 nm) which is a high value rarely observed for non-halogenated/non-deuterated complexes.

C. Kruck, P. Nazari, C. Dee, B. S. Richards, A. Turshatov, M. Seitz
Efficient Ytterbium Near-Infrared Luminophore Based on a Nondeuterated Ligand
Inorganic Chemistry **2019**, *58*, 6959 - 6965.

3.4.3 A New Eu/Tb-Coordination Network as an Optical Cryogenic Thermometer based on a 2,2'-Bipyridine Tetracarboxylate Ligand (*In Preparation*)

Energy transfer between excited states and their chemical environment is an elementary process in Nature, *e.g.* the energy transfer in photosynthesis. Some molecules can be used as antenna chromophores, which can absorb light and transfer the energy to a reaction center. For this purpose pigment-protein complexes have been developed by Nature to yield high efficiencies above 95%.[94] Investigations on energy transfer is not trivial since precise structural as well as electronic properties have to be considered. Molecular and flexible systems are complicated to examine in this respect. The abbreviation COORNETs stands for metal organic **coor**dination **net**work**s**. This compound class provides key features (Figure 28) for the analysis of energy transfer processes:[95,96]

- Rigid ligands (linker) between metal centers control the geometry
- periodical arrangements possible
    - Energy transfer can be studied at close and far distances

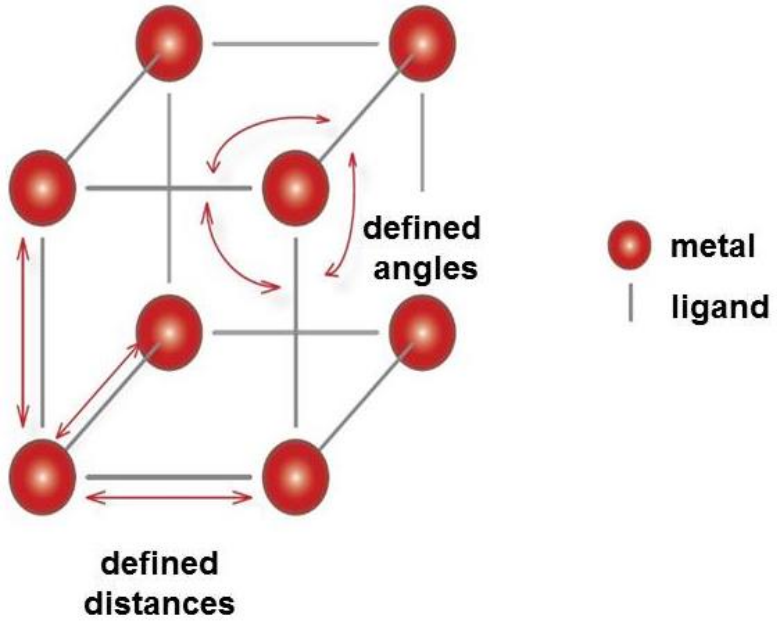

Figure 28. Schematic representation of a COORNET with defined distances and angles in the known geometry.

In several studies, the energy transfer between metals, ligands and guest molecules was examined which was important in the field of sensing and photovoltaic.[97] The

process of energy transfer between metal centers however is rarely studied. Lin et al. reported a Ru-Os energy transfer in tris(bipyridine)-based COORNETs with a statistical doping with Os instead of Ru.[98] Lanthanoids offer enormous potential for COORNETs because of their fascinating photophysical properties, but have rarely been studied in this field by now.[99]

One important example of energy transfer between lanthanoids has been shown in cryogenic nanothermometers. By varying the temperature changes of luminescence intensity and lifetime occurs immediately. At low temperature, the ligand is excited and via ISC the corresponding T_1 level is populated (Figure 29). Both energy transfers to the emitting states of Eu ($^5D_0$) and Tb ($^5D_4$) occur and the luminescence can be detected with high intensities for both lanthanoids. Increasing the temperature leads to a thermally activated back energy transfer from the $^5D_4$ level of Tb to the T_1 level of the ligand and therefore a decreased Tb luminescence intensity can be observed. The energy gap between the $^5D_0$ level of Eu and the triplet level of the ligand is usually large enough to prevent this back energy transfer. This kind of temperature sensor can be used in a wide range of areas including metallurgy, aerospace and manufacturing.[100–102]

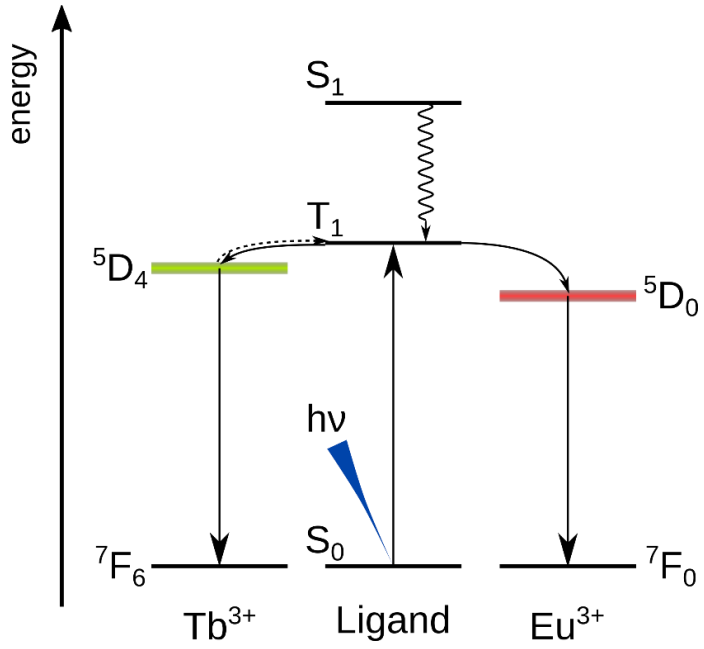

Figure 29. Schematic energy diagram of the energy transfer processes in a Eu/Tb-based thermometer: At low temperature, energy transfer from the ligand's T_1 level to the emitting levels of the lanthanoids occur via the antenna effect. Thermally activated back energy transfer from $^5D_4$ level to the T_1 and subsequently transfer to $^5D_0$ leads to a decreased Tb luminescence intensity and an increased Eu luminescence intensity.

In contrast to the common cryogenic temperature sensors and control elements which have a large size and must be in physical contact with the object monitored, luminescence-based thermometers overcome these drawbacks.[103,104] They provide high spatial resolution, extreme sensitivity and the advantage of being a self-calibrating device. In the past, numerous luminescent thermometers have been developed ranging from nanoparticles,[105] molecular lanthanoid coordination compounds[106] to lanthanide metal-organic frameworks.[107]

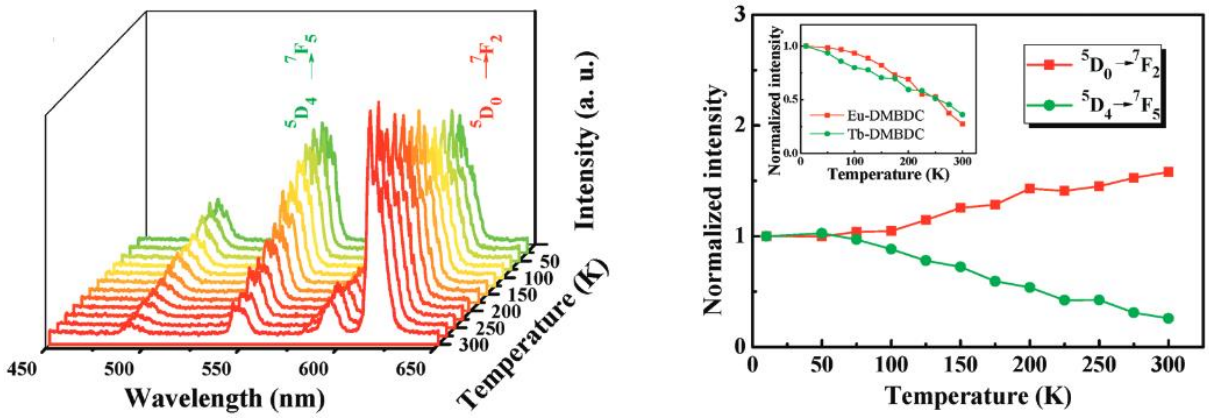

Figure 30. Emission spectra of $Eu_{0.0069}Tb_{0.9931}$-DMBDC recorded between 10 and 300 K (left, λ_{exc}=355 nm) and temperature dependence of integrated intensities of the $^5D_4 \rightarrow {}^7F_5$ and $^5D_0 \rightarrow {}^7F_2$ transitions. Figure adopted from Qian and coworkers.[107]

Qian and coworkers reported the first luminescent Tb^{3+}/Eu^{3+} metal-organic framework thermometer (based on 2,5-dimethoxy-1,4-benzendicarboxylate) with the emission ratio of the two lanthanoids as the thermometric parameter. As can be seen in Figure 30, the luminescence of Tb^{3+} decreases significantly by increasing the temperature while the intensity of Eu^{3+} luminescence is only slightly decreasing by decreased temperature. This thermometer is suitable for operating range of 50-200 K (Figure 30) and has a maximum relative sensitivity of 1.15 % K^{-1} at 200 K.[107] Since then, many other Tb/Eu-thermometers have been published showing sensitivity in the range of 10-300 K.[108–111] The development of higher sensitivity as well as the design of systems with effective control of the energy transfer processes (ligand-to-Ln^{3+}, Tb^{3+}-to-Eu^{3+}) is very challenging.

The aim of this project was the elaboration of a lanthanoid-based COORNET. In collaboration with A. Turshatov, Karlsruhe, photophysical experiments shall help to get a deeper understanding on the energy transfer processes. In a former study, Kruck *et al*. developed the new complex **12-Yb** based on the ligand 2,2'-bipyridine-6,6'-

dicarboxylate with appended pyridyl groups in 4- and 4'-position. On these grounds, the shown ligand should be prepared with additional coordination sites to act as a linker in a three dimensional polymer structure (Figure 31).

The synthesis started with a Kröhnke reaction of the diketone **13**[112] and the pyridinium salt **14**[113] yielding the bipyridine **15** (Figure 31). The tetracarboxylic acid **16** was prepared by cleavage of the esters and simultaneous oxidation of the furanyl groups with $KMnO_4$.[114] The targeted coordination network **17-Eu/Tb** with triethylammonium as counter cation was obtained by reacting one equivalent of **16** with one equivalent of a statistical mixture of $EuCl_3 \cdot 6\ H_2O$ and $TbCl_3 \cdot 6\ H_2O$ in the presence of a slight excess of NEt_3 in methanolic solution. As a diamagnetic control **17-Lu/Lu** was prepared in the same manner. It should be mentioned that these coordination networks are challenging to crystallise du to their insolubility. The shown structure in Figure 31 is only a reasonable guess how the ligands are arranged.

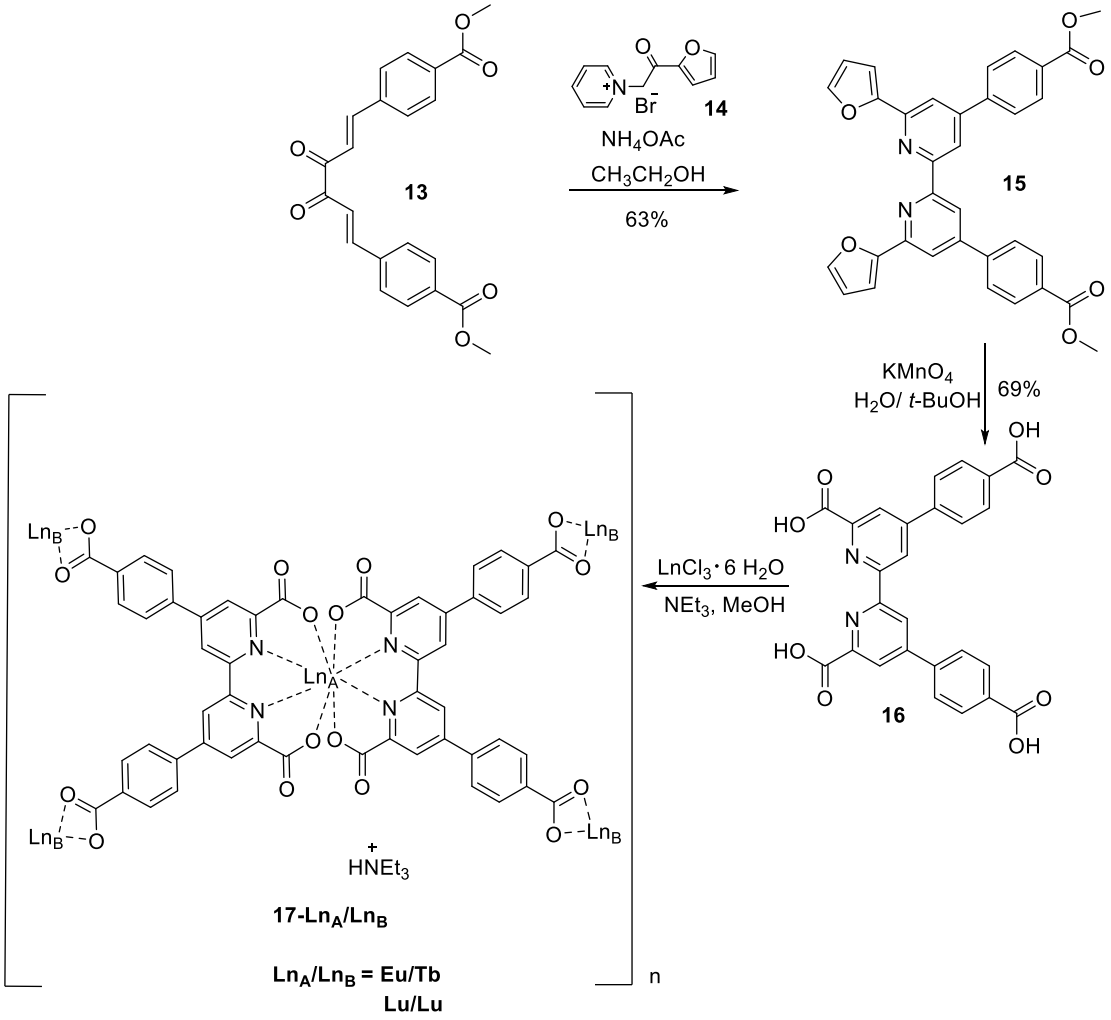

Figure 31. Synthesis of the coordination networks **17-Ln_A/Ln_B**.

The ^{1}H NMR spectrum of **16** shows only very broad peaks when measuring in $(CD_3)_2SO$ (Figure A7). The solubility of the tetracarboxylic acid is diminished and for the complexes almost gone. For comparison of the ligand and the coordination networks also the solid state ^{1}H NMR spectrum of the tetracarboxylic acid was measured (Figure 32: left, black). The signal of the aromatic protons can be found as a broad peak in the range of ≈ 0-10 ppm. Next to it is a smaller broad peak of the acid protons downfield shifted up to ≈ 15 ppm. Around 1 ppm is a small water signal. The ^{1}H NMR spectrum of the solid sample of **17-Lu/Lu** as a diamagnetic reference compound (Figure 32: left, red) in addition shows the signals of the three equivalent ethyl groups of the counterion triethylammonium.

The integration of the signals was performed after the Lorentz fitting of the deconvoluted spectra (Figure 32: right). The integral ratios between the two sets of signals account to 2:1 for aromatic ligand protons and triethylammonium respectively (Table 3). For triethylammonium the integral of the CH_3 group was taken into account because the signal of the CH_2 group probably covers the water signal and is not reliable for the analysis. In order to check the distribution of the lanthanoids SEM images of the coordination networks were obtained (Figure 33). The surface seems to be relatively plain. According to the EDX analysis, Eu and Tb are present in equal parts of the coordination network **17-Eu/Tb** (atomic%: Eu = 1.88, Tb = 1.68). The elemental analysis proves the composition of the coordination networks. The result fits perfectly with the overall ratio 2:2:1 (ligand / Ln / $HNEt_3$), additional 4 water molecules and a $LuCl_3$ for **17-Lu/Lu** and 12 water molecules for **17-Eu/Tb** respectively.

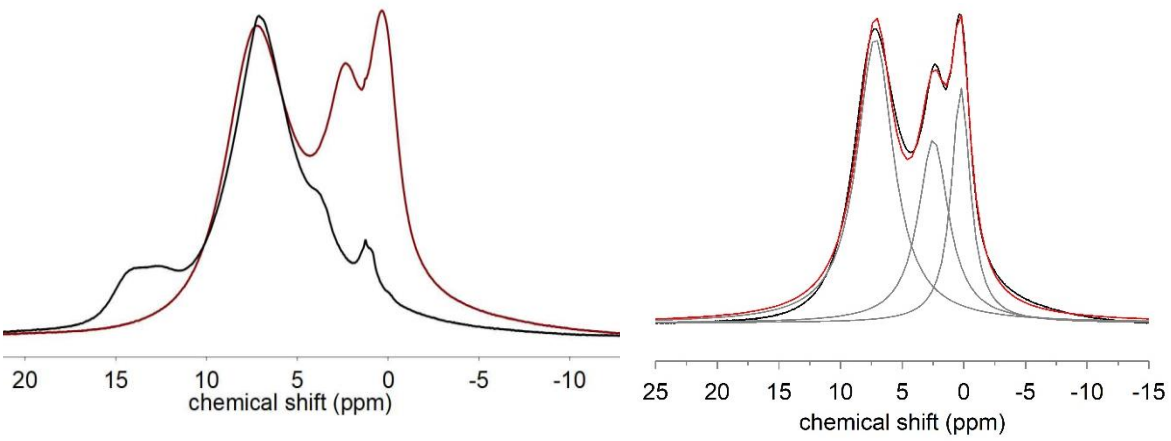

Figure 32: ^{1}H NMR (500 MHz) spectrum in solid state of the tetracarboxylic acid **16** (left: black), **17-Lu/Lu** (left: red) and the Lorentz fitted peaks (right: grey, cumulative function in red) in the ^{1}H NMR (500 MHz) spectrum in solid state of **17-Lu/Lu** (right: black).

Table 3: Results of the Lorentzian peak fitting.

peak	peak area	number of protons	area of 1 H	Ratio
aromatic protons	3577	12 H	298	~2 (1.8)
CH_3	1515	9 H	168	1

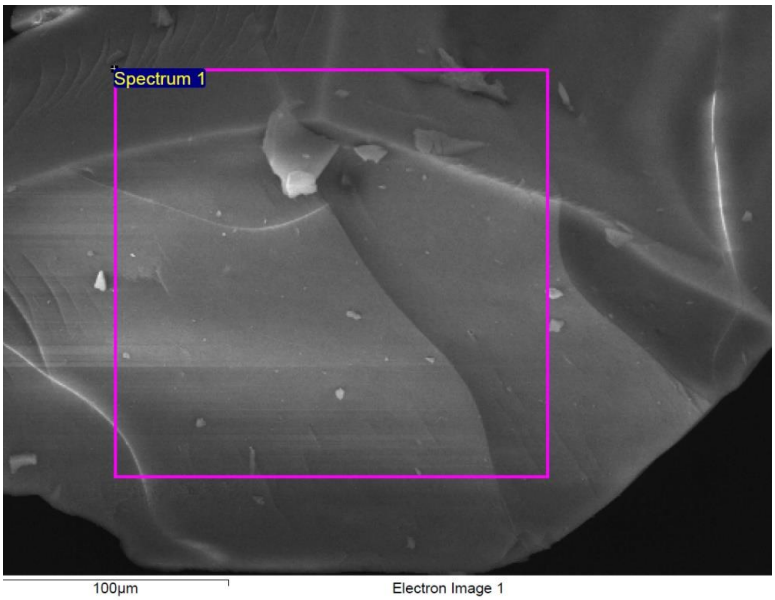

Figure 33: SEM / EDX image of **17-Eu/Tb** (atomic%: Eu = 1.88, Tb = 1.68).

The analysis of the energy transfer in this coordination network was performed by A. Turshatov, Karlsruhe. First results show a certain temperature dependence for this energy transfer between europium and terbium. The emissive energy levels of Eu^{3+} ($^5D_0 \rightarrow {}^7F_2$) and Tb^{3+} ($^5D_4 \rightarrow {}^7F_5$) are bridged via the triplet state of the organic ligand. Since the energy gap between the ligand triplet state and the Eu^{3+} ($^5D_0 \rightarrow {}^7F_2$) level is relatively large, the intensity is rarely dependent of the temperature. In contrast, the energy gap between the ligand triplet state and the Tb level is much smaller. That is why the luminescene of Tb^{3+} ($^5D_4 \rightarrow {}^7F_5$) is strongly quenched at room temperature via back-energy transfer to the ligand triplet state. By decreasing the temperature the Tb^{3+} ($^5D_4 \rightarrow {}^7F_5$) luminescence gets stronger due to less back-energy transfer.

A new three-dimensional coordination network was prepared via a relatively short synthetic route. While the exact structure elucidation still has to be undertaken, the temperature-dependent luminescence ratio of Eu^{3+}/Tb^{3+} points to a possible application as a temperature probe.

C. Dee, P. Nazari, A. Turshatov, B. S. Richards, M. Seitz

A New Eu/Tb Coordination Network as an Optical Cryogenic Thermometer Based on a 2,2'-Bipyridine Tetracarboxylate Ligand

Manuscript in Preparation

3.5 Highly Flexible Cryptates based on Dipyridylamine Ligands (*Unpublished Results*)

The cryptand **bpy$_3$** has been modified quite elaborately to obtain new properties of the corresponding cryptates as already described. The extension of the conjugated aromatic system as in carboline-based cryptates **7-Eu** and **8-Eu** shifts the absorption maximum of the complex to lower energies. A different modification of the original **bpy$_3$** cryptate, containing one, two and three new dipyridylamino groups (Figure 34), may also affect the absorption properties. Additionally, the size of the cavity may change. The introduction of space-consuming *N*-oxides in **bpy$_3$O$_2$** decreases the size of the cavity for the central metal atom. In order to expand the cavity, the cryptand scaffold may be enlarged by inserting an alkylamino group between the pyridine rings.

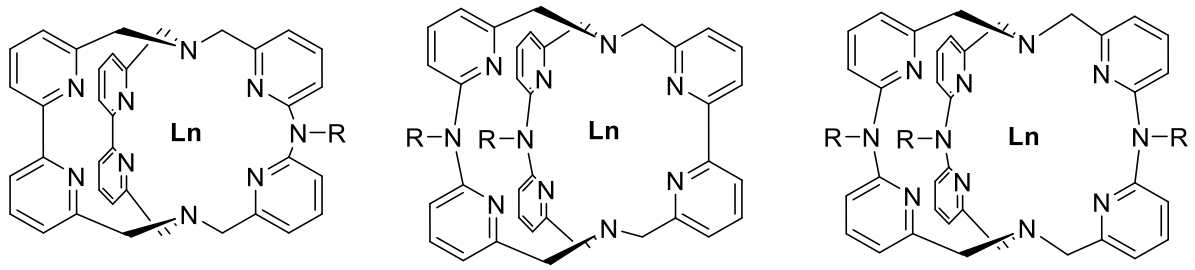

18-Ln **19-Ln** **20-Ln**

Figure 34: The new extended cryptands **18-Ln**, **19-Ln** and **20-Ln** containing one, two and three dipyridylamine units, respectively.

At first sight, this insert seems to lead to an enlarged cavity in the new dipyridylamine based cryptand **20-Ln** with an increased flexibility compared to other cryptands. However, the size of the cavity depends on how likely this cryptand will distort and may also be smaller than for the original cryptand. Additionally, interesting properties arise for the new corresponding lanthanoid complexes. Firstly, at the bridging amine, functionalization chemistry can be performed for *e.g.* binding to biomolecules. Secondly, the symmetry can differ from other C_2 symmetric cryptates due to a resulting C_3 axis in the case of **20-Ln**.

The synthesis of the analogous building blocks for the cryptand syntheses, the dibromide **26** and a diamine **27**/diamine-macrocycle **3**, starts with a Buchwald-Hartwig reaction of the TBS protected pyridine precursors **21** and **22** (Figure 35). The crude coupling product **23** was purified by column chromatrography to obtain it pure in good yields of 63%. The amine **23** is methylated with methyliodide and NaH. This reaction

does not proceed to completeness and the precursor remains in the ^{1}H NMR spectrum as well as the unprotected product **25** (Figure A12). No further separation was conducted since the following step is the deprotection to the corresponding diol **25**. The complete deprotection was achieved by stirring with TBAF in THF. Bromination with PBr_3 gives a high yield of 75% of pure product **26** without any purification step.

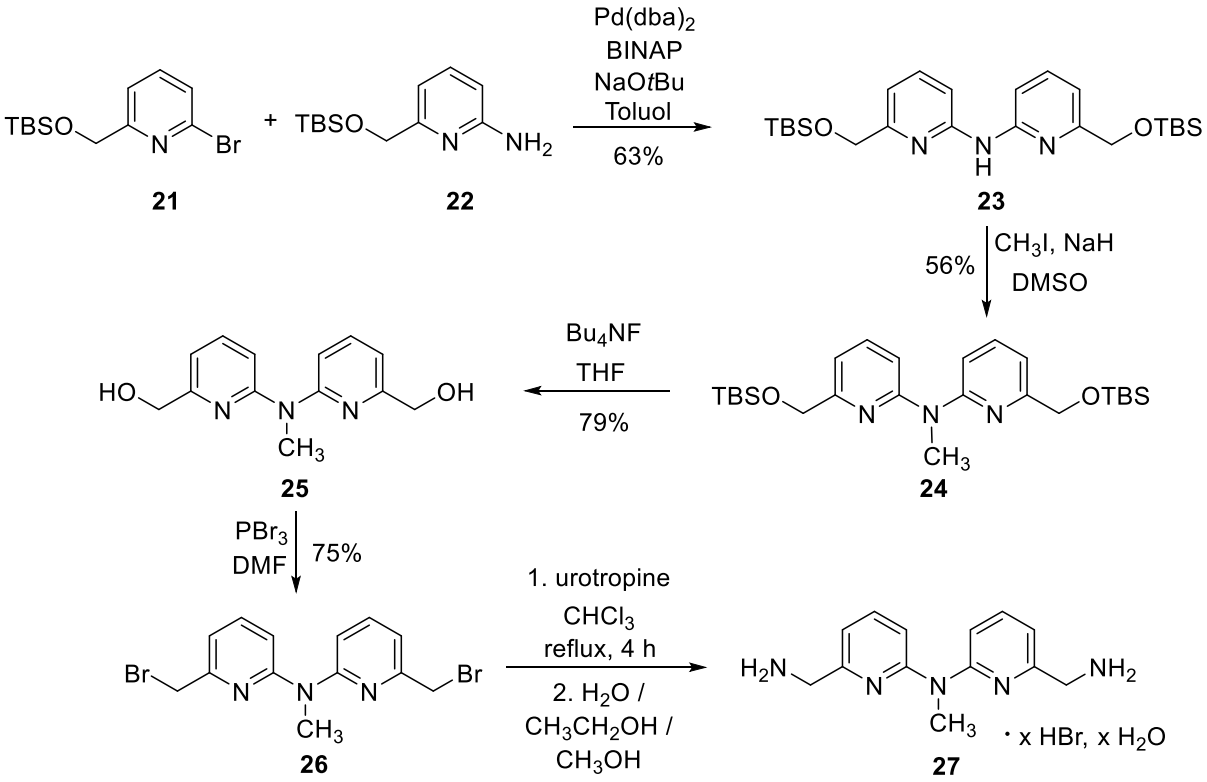

Figure 35: Synthesis route to diamine **27**.

The dibromide **26** was subjected to two macrobicyclization reactions with macrocycle **3**[115] resulting in the formation of the corresponding sodium cryptate **18-Na** and subsequently with bipyridinediamine **28**[116] resulting in the formation of sodium cryptate **19-Na** (Figure 36). The yields are decreasing with the number of dipyridylamine units from 28% for **18-Na** to 11% for **19-Na**. For the latter the reaction was conducted with sodium as well as with potassium as templating metal ion. Due to the enlarged cryptand scaffold potassium may be the more suitable ion for the cryptate formation. Both ^{1}H NMR spectra are well defined and show C_2 symmetric behaviour (Figure A19, A21). The structure of **19-Na** was further verified by ^{1}H-^{13}C correlated 2D spectra (HSQC, HMBC) which were also the source of the ^{13}C chemical shifts (Figure A23-A24). Especially in the range of the benzylic positions,

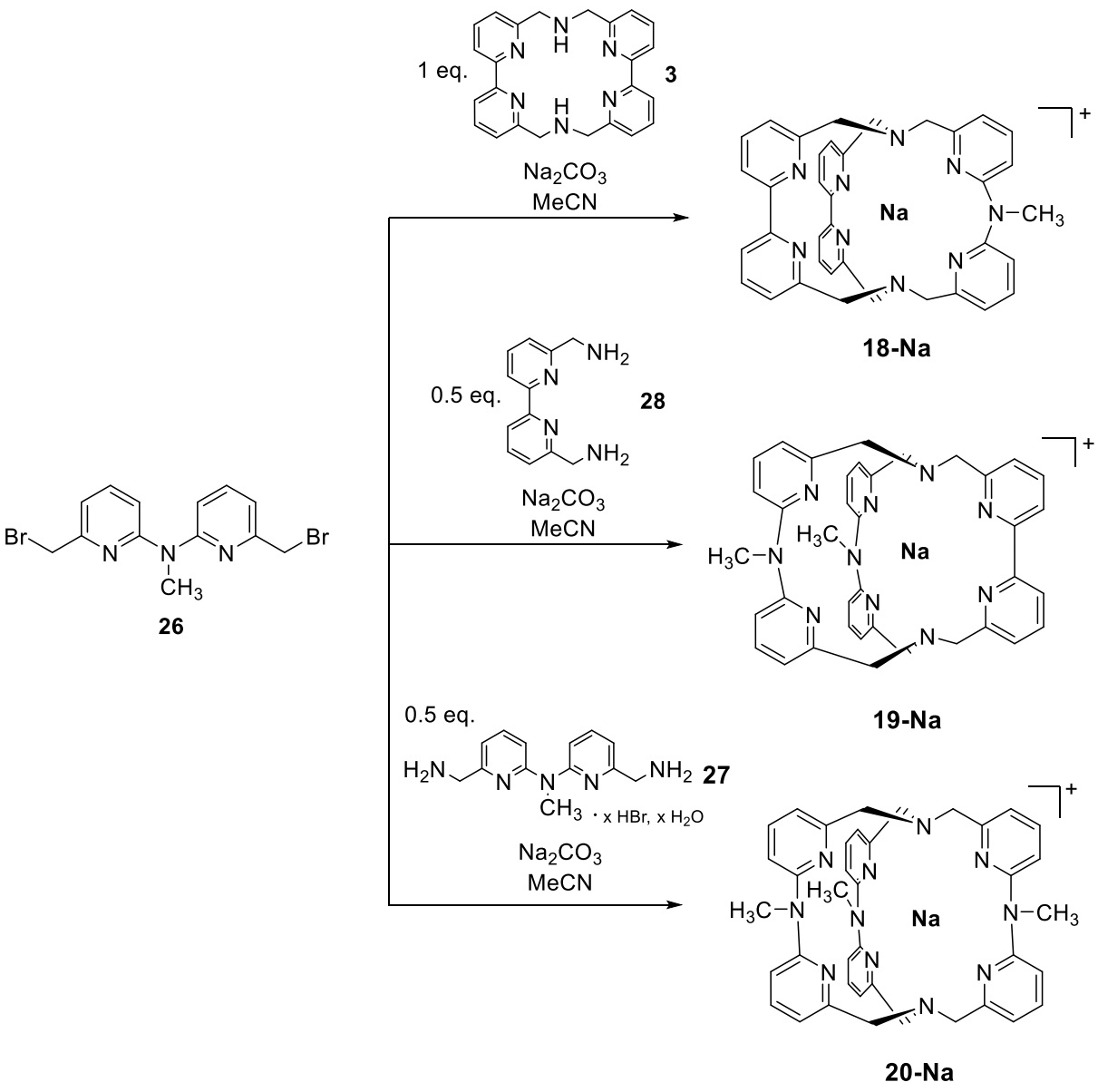

Figure 36: The formation of the **18-Na**, **19-Na** and **20-Na** (proven by ESI mass spectrometry) in macrocyclisation reactions.

the doublets are partially superimposed. For the exact analysis, chemical shifts and coupling constants were obtained from 2D HSQC NMR spectra. However, no change in the yields could be observed. Both sodium cryptates were transformed to the corresponding lanthanoid cryptates **18-Ln** and **19-Ln** (Ln = Lu, Eu) according to previous procedures of metal exchange reactions of the cryptates (Figure 37).[51,52] The ^{1}H NMR spectra of **18-Lu** and **18-Eu** in CD_3OD show many multiplets and broad signals (Figure A26, A28). In contrast, the corresponding ^{1}H NMR spectra of **19-Lu** and **19-Eu** display well defined sharp signals and a C_2 complex symmetry (Figure A27, A29). The cryptates with one dipyridylamine unit seems to be more dynamic on the NMR time scale than the cryptates with two dipyridylamine units.

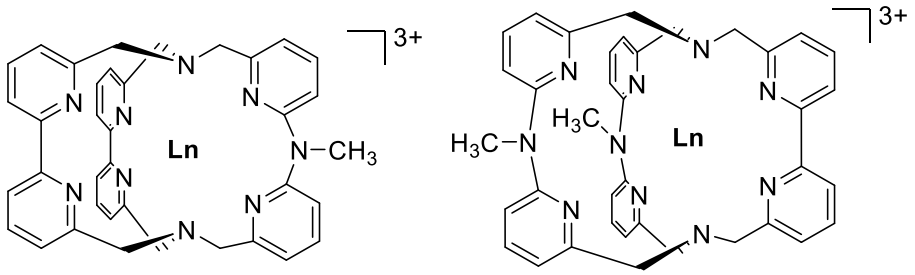

18-Ln
Ln = Lu, Eu

19-Ln
Ln = Lu, Eu

Figure 37: New lanthanoid cryptates **18-Ln** and **19-Ln**.

For the formation of **20-Na** (Figure 36) the corresponding diamine **27** as a building block for the macrobicyclization reaction is required. This precursor can be synthesised by the reaction of dibromide **26** with urotropine and subsequent aqueous workup (Figure 35). Unlike the reaction of bipyridine, here the dipyridylamine behaves differently. According to Wang *et al.* the bipyridine product **28** can be recrystallized.[116] Due to different solubility properties no suitable conditions could be found up to now. With several washing procedures at different pH values the free amine could be obtained: At high pH the free amine is soluble in CH_2Cl_2 while at low pH values the HBr adduct can be separated in the aqueous phase. Unfortunately, some unknown impurities remain according to the ^{1}H NMR spectrum (Figure A18). In spite of that the obtained product **27** was used in a macrobicyclisation reaction together with dibromide **26** in a 1:2 ratio. After twofold column chromatography a pure product was obtained which has a clear spot on the thin layer chromatogram. The ^{1}H NMR spectrum shows many signals which is not surprising for such a flexible system (Figure A25). In the ESI mass spectrum peaks occur referring to the desired protonated and twofold protonated cryptand scaffold without sodium. These findings suggest the successful reaction outcome.

The new cryptands **18-Eu** and **19-Eu** show very similar UV-vis absorption bands with a maximum at 303 nm (Figure 38). This absorption behaviour is in line with previous studies of many other **bpy** cryptates.[49,50,52] This enlarged cryptate shows no red-shifted absorption bands as seen for carboline-based cryptates. With the introduction of carboline groups the aromatic system was extended while here, the inserted amines do not affect the absorption properties.

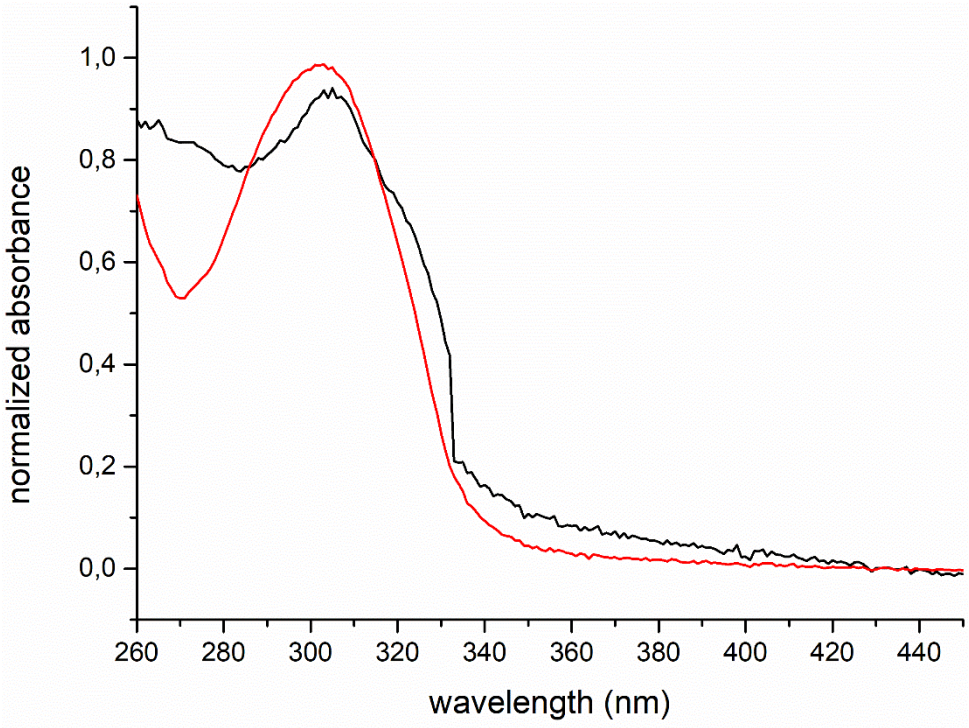

Figure 38: Normalized UV-vis absorption spectra of **18-Eu** (black) and **19-Eu** (red) in H_2O.

The lutetium cryptates **18-Lu** and **19-Lu** have been synthesized as non-emissive complexes for the measurement of their zero phonon transition $T_1 \rightarrow S_0$ (Figure 39). The transition energy of **18-Lu** is slightly smaller than the one obtained for **19-Lu**.

Table 4: Estimated triplet energies of **18-Lu** and **19-Lu**.

complex	E (T_1) in cm^{-1}
18-Lu	21800
19-Lu	22300

19-Lu shows a broad band around 500 nm with a small shoulder around 370 nm. In the spectrum of **18-Lu**, the latter is more intense than the band around 500 nm. Assigning the first to singlet and the second to triplet emission, there is rarely singlet emission for the cryptate with two dipyridylamine units observed which gives a hint for a fast ISC process between the S_1 and T_1 level of the ligand. This also leads to a strong population of the T_1 level which can also affect the energy transfer to the lanthanoid. The energy gap between the T_1 level for **18-Lu** and the emitting $^5D_0$ level (17500 cm^{-1}) of Eu^{3+} is 4300 cm^{-1} which leads to a possible energy transfer of the antenna to the lanthanoid. Considering Tb^{3+} the gap between T_1 and the emitting $^5D_4$ level (20400 cm^{-1}) would be ca. 1400 cm^{-1} which is rather small and thermally activated energy back transfer can occur. Regarding **19-Lu** the triplet level seems to be more

suitbale for the excitation of Tb (ΔE = 1900 cm^{-1}). The emission spectrum of **18-Eu** (Figure 40: top) indicates a high symmetry due to the poorly observable $^7F_0$ band. The emission spectrum of **19-Eu** (Figure 40: bottom) shows a strong $^7F_0$ emission band which indicates a complex with low symmetry. With two dipyridylamine units the cryptate is much more flexible than the complex with one dipyridylamine unit and two **bpy**. Due to the fact that the $^7F_1$ band is split in three parts and the $^7F_2$ in several bands the symmetry of the complex according to Binnemans findings has to be C_1, C_2, C_s or C_{2v}.[117]

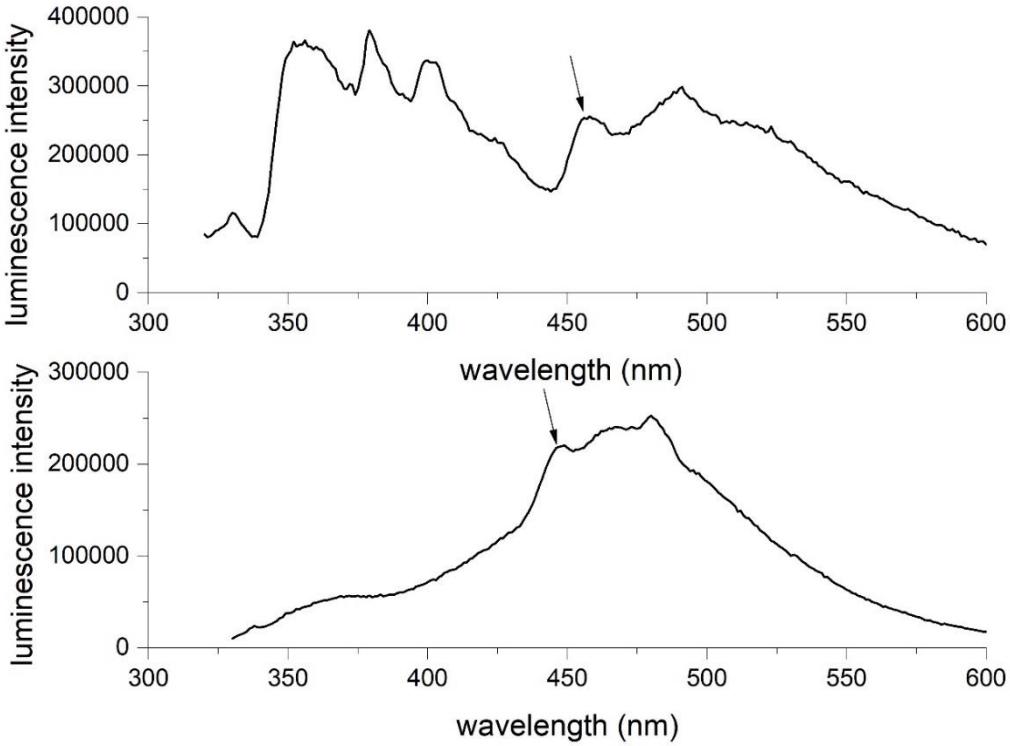

Figure 39: Low temperature emission spectra (λ_{exc} = 307 nm, T = 77 K) of the **18-Lu** (top) and **19-Lu** (bottom) measured in a MeOH/EtOH glass matrix (1:1, v/v). The triplett energies were estimated at the arrows.

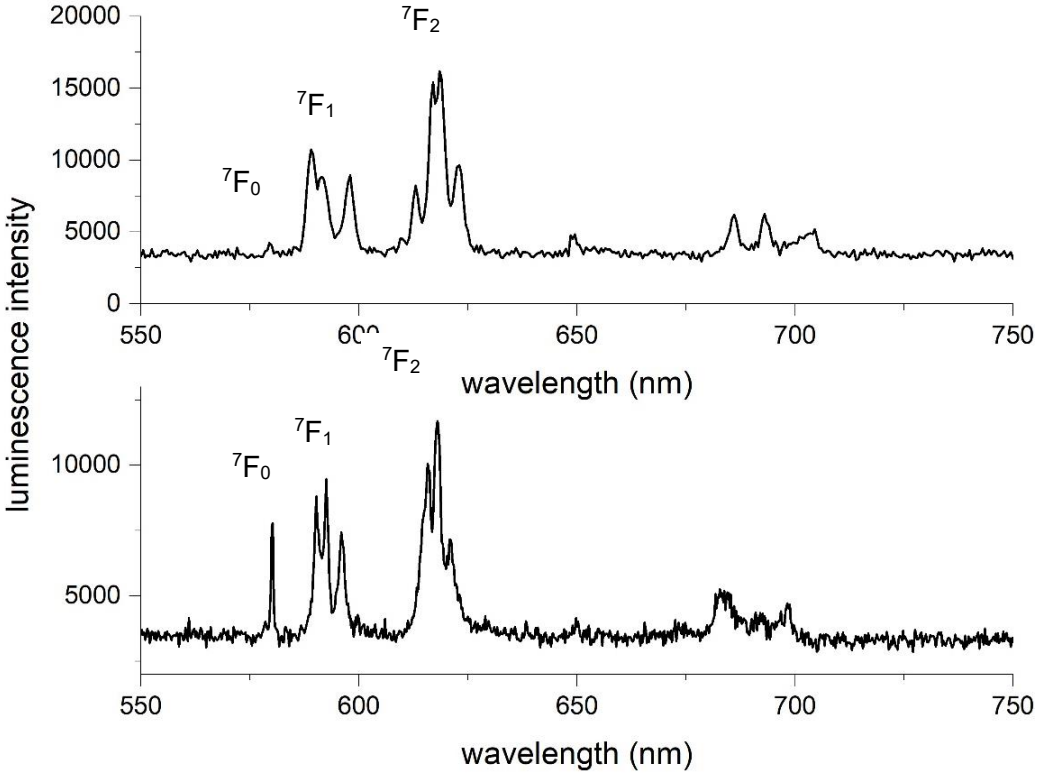

Figure 40: Steady-state emission spectra (λ_{exc}= 310 nm, longpass filter 380 nm) of the cryptates **18-Eu** (top) and **19-Eu** (bottom) in H_2O (c ≈ 10 µM).

The lifetimes of both europium cryptates have been measured in H_2O and D_2O in order to determine the number of the inner-sphere coordinating water molecules q according to the following equation:

$$q = A\left(\frac{1}{\tau_{H_2O}} - \frac{1}{\tau_{D_2O}} - B\right) \; with \; A = 1.2\,ms; B = 0.25\,ms \; for \; Eu$$

In the case of Eu, the correction values are A = 1.2 ms and B = 0.25 ms according to the Beeby *et al*.[118] The results are remarkable in respect of the almost four times higher luminescene lifetime of **19-Eu** in water compared to **18-Eu** (Table 5). Due to less vibrational quenching processes, the lifetimes increase for both complexes in D_2O. The calculated q values differ a lot from 4.5 to 0.6 with increasing number of dipyridylamine units. The dipyridylamine units give the cryptate more flexibility to arrange itself in a more distorted fashion, which inhibits water molecules binding to the central metal atom. **18-Eu** with two bpy units is much more rigid in its structure, but the one dpa unit seems to create a cryptate which is not efficiently coordinating central metal atom so that many water molecules have the chance to bind in the inner coordination sphere. Computational work in this direction is part of ongoing research.

Table 5: Luminescence lifetimes τ_{obs} of **18-Eu** and **19-Eu** in H_2O and D_2O and the calculated q values.

Compound	τ_{obs} in H_2O (ms)	τ_{obs} in D_2O (ms)	q
18-Eu	0.22	1.76	4.5
19-Eu	0.78	1.98	0.6

The first lanthanoid cryptates incorporating one and two new dipyridylamine units could be successfully prepared. The sodium cryptate with three dipyridylamine units could be detected in the ESI mass spectrum. Further preparation of lanthanoid cryptates and the analysis of their photophysical properties have to be undertaken.

4 Conclusion

In the course of this work, several scientific goals could be achieved:

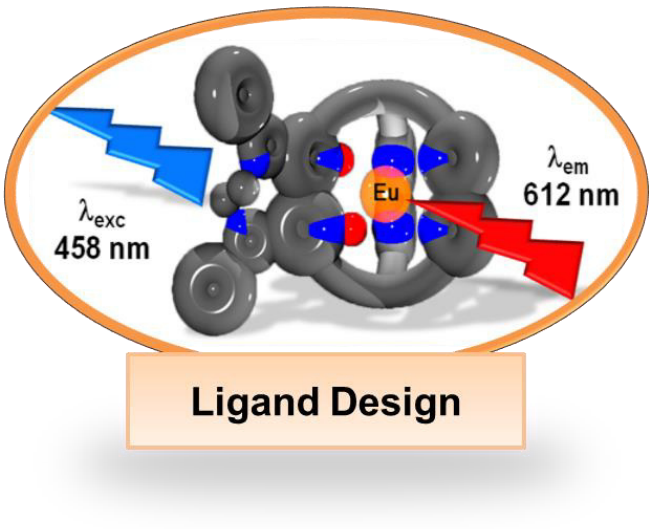

Long-Wavelength Excitation in Carboline-Based Cryptates

- Preparation of an extended β-carboline-based cryptand scaffold for development of two different types of tris(biaryl)-*N,N'*-dioxide europium cryptates
- Long-wavelength excitation possible due to the red-shifted absorption bands (especially at the argon-ion laser line 458 nm)
- Beneficial luminescence properties in water with luminescence lifetimes $\tau \approx 0.5$ ms and absolute quantum yields of up to 3.3 %
- pH-dependent luminescence in the physiologically relevant range pH ≈ 7-9

For the first time, long-wavelength excitation of europium luminescence is possible in tris(biaryl) cryptates. Together with the advantageous luminescence properties these cryptates are great candidates for biological applications.

Chiral Resolution of Lanthanoid Cryptates with Extreme Configurational Stability

- Preparation of enantiopure samples of **Ln-bpy$_3$O$_2$** cryptates by chiral HPLC
- Demonstration of their extreme configurational stability by stability studies

Chiral resolution of lanthanoid cryptates was achieved for the first time. The extreme configurational stability is rare among lanthanoid chelates.

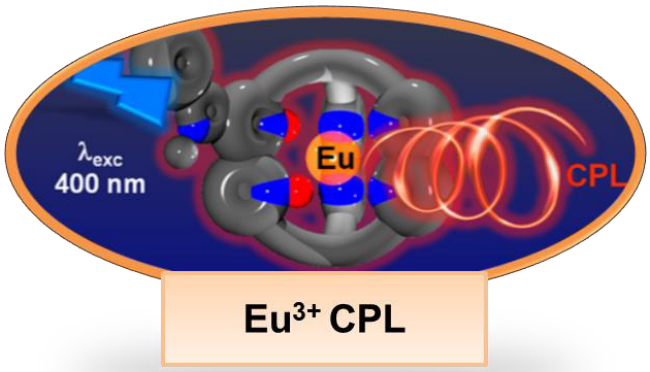

Circularly Polarised Luminescence of Carboline-Based Cryptates under Visible Light Excitation

- Separation of the enantiomers of carboline cryptates via chiral HPLC and demonstration of their configurational stability
- Assignment of the absolute configuration by comparing experimental and theoretical CD spectra
- Strong CPL with $|g_{lum}| = 0.25$ under visible light excitation

The highest dissymmetry factor for europium CPL in cryptates could be obtained with visible light excitation.

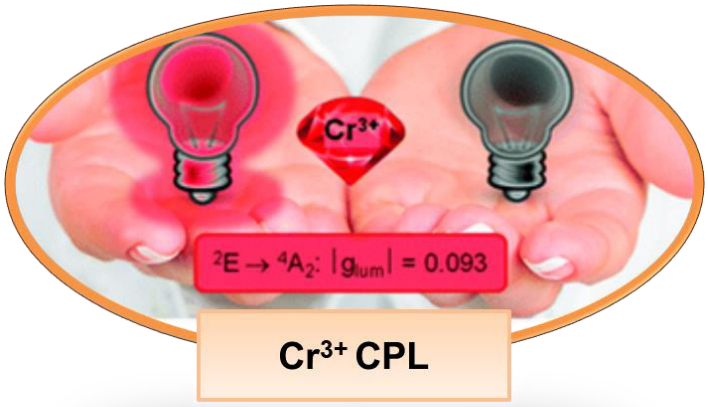

Strong Circularly Polarised Luminescence of an Octahedral Chromium(III) Complex

- Enantiopure, configurational stable chromium complex via chiral HPLC
- Assignment of the absolute configuration by comparing experimental and theoretical CD spectra
- Analysis of racemisation process via computational methods
- Strong CPL with $|g_{lum}| = 0.093$ among the highest reported for chromium in the literature

A more earth-abundant alternative to lanthanoid-based CPL emitter was developed and paves the way for future studies concerning chromium CPL for NIR optoelectronical applications.

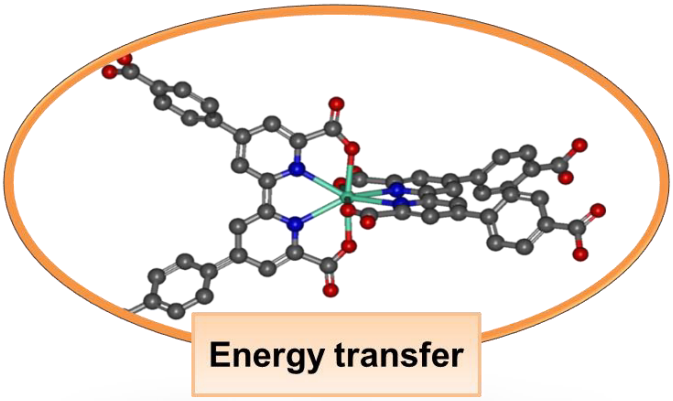

Energy Transfer Studies in Lanthanoid-based Systems

- Proof-of-concept TTA-UC from the NIR to the visible with a molecular Yb complex as sensitiser and rubrene as emitter

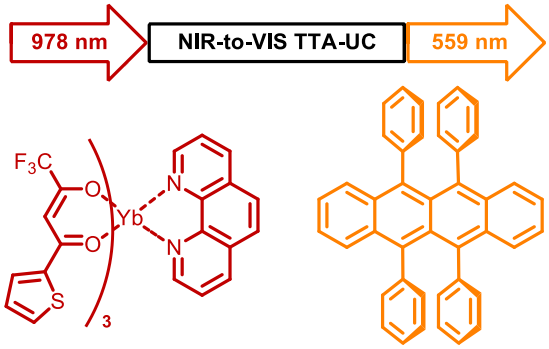

- Preliminary investigation of a new tetradentate ligand based on the 2,2'-bipyridine-6,6'-dicarboxylic acid scaffold and the corresponding ytterbium complex showing high absolute quantum yield of 3 %

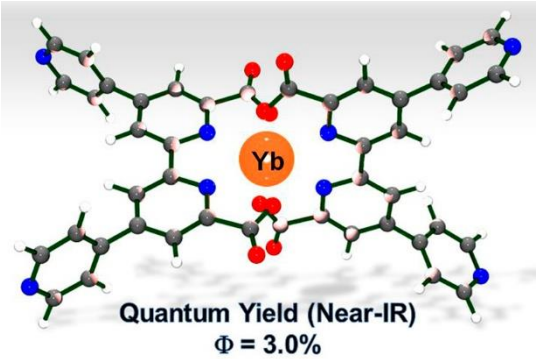

- Successful approach for the preparation of a linker based on this ligand for the incorporation of lanthanoids in a coordination network
- Tb/Eu COORNET displays temperature dependent luminescence which is an interesting property for application as cryogenic, luminescent thermometers

5 Experimental Part

5.1 General

All chemicals were purchased from commercial suppliers and used as received unless stated otherwise. Deuterated solvents had deuterium contents > 99.8%D. Toluene was dried using a MBraun SPS-800 solvent purification system. MeOH was dried by a standard procedure using Mg. Air-sensitive reactions were performed under a dry, dioxygen-free atmosphere of Ar using Schlenk technique. Column-chromatography was performed with silica gel 60 (Merck, 0.063 - 0.200 mm). Analytical thin layer chromatography (TLC) was done on silica gel 60 F 254 plates (Merck, coated on aluminium sheets).

NMR

NMR spectra were measured on a Bruker AVII+300 (^{1}H: 300 MHz, ^{13}C: 75 MHz, ^{19}F: 283 MHz), Bruker AVII+400 (^{1}H: 400 MHz, ^{13}C: 101 MHz), Bruker AVII+500 (^{1}H: 500 MHz, ^{13}C: 125 MHz) and a Bruker AVII+700 (^{13}C: 177 MHz). The chemical shifts (δ) are reported in ppm relative to TMS and the residual solvent signals were used as internal reference. Solid state H-1 MAS and C-13 CP/MAS NMR spectra were obtained on a Bruker AVII+500 standard bore spectrometer using a 2.5 mm MAS broad band probe head. Powdered samples were placed in a 2.5 mm o.d. zirconia rotor and MAS NMR spectra were obtained at spinning rates of 15 kHz. Chemical shifts are referenced to external 1% TMS in $CDCl_3$. All NMR spectra were analysed using MestReNova (Mestrelab Research) and/or Origin (OriginLab). Observed multiplicities are specified as: singlet (s), doublet (d), triplet (t), quartet (q), and multiplet (m). Further abbreviations: br = broad.

Mass spectrometry

ESI mass spectrometry was measured using Bruker Daltonics Esquire 3000plus. MALDI mass spectrometry was performed using Bruker Autoflex and 2,5-

dihydroxybenzoic acid (DHB) as matrix material. Isotopic patterns were only reported when the overall intensity of the signal was sufficiently high.

Elemental Analysis

Elemental Analysis was performed on a VarioMicro V1.9.2. analysis system.

SEM / EDX

The SEM/EDX images were measured with a Philips XL30 FEG. The sample was sputtered with gold prior to the measurements.

HPLC

Preparative reversed-phase HPLC (RP-18e, 250 x 100 mm - 10 µm, flowrate: 3 mL / min, UV detection: 300 nm) was conducted to obtain pure complexes. To confirm the purity of the complexes, samples were taken up in a minimum of CH_3CN/H_2O (1:1, v/v), filtered (0.45 mm nylon membrane filters) and subjected to analytical reversed-phase HPLC (RP-18e,125 x 4 mm – 5 µm, flowrate: 1 mL / min, UV detection: 300 nm) with H_2O (degassed,+1% TFA, v/v) as mobile phase A, CH_3CN (degassed, HPLCgrade) as mobile phase B, and the following gradient: 0 min: 85% A/15% B; 5 min: 85% A/15% B; 19 min: 45% A/55% B; 25 min: 45% A/55% B; 40 min: 85% A/15% B; 50 min: 85% A/15% B.

All chiral HPLC runs of the racemic or enantiopure cryptates were performed on a Knauer Azura HPLC system (UV detection at λ = 300 nm), equipped with a CHIRALPAK IE column (Daicel, particle size: 5 µm, internal diameter: 4.6 mm, column length: 150 mm, flow rate: 1.0 mL/min) for analytical runs and an analogous CHIRALPAK IE column (Daicel, particle size: 5 µm, internal diameter: 10.0 mm, column length: 150 mm, flow rate: 4 mL/min) for preparative runs. In both cases, the mobile phase was HPLC-grade MeOH with additional 0.5 vol.-% CF_3COOH. All samples were prepared using HPLC-grade MeOH and filtered with a membrane filter (nylon, 0.45 µm pore size, 13 mm diameter) in a stainless steel filter holder prior to injection. For the separation of the racemic cryptates, samples with a concentration of 3 mg/mL were used, which was found to be the optimal compromise between separation and time efficiency. The solution was subjected to chiral HPLC in portions of 100 µL. The collected fractions of the respective enantiomers were combined and the solvents were removed in vacuo at room temperature. After drying, samples of the

enantiomers were redissolved in MeOH (HPLC-grade), filtered (see above) and injected to verify the enantiopurity.

Notes: The separation efficiency and the relative and absolute retention of the two enantiomers are dependent on the concentration of the analyte. Special care has to be taken that only freshly prepared MeOH/CF_3COOH mobile phases are used. The range of the fractions which were collected varies with the quality of the separation to obtain pure separated enantiomers.

Photophysical Measurements

UV/VIS spectra were measured on a Jasco V-770 spectrophotometer using quartz cuvettes (1 cm pathlength) at room temperature.

Steady state emission spectra were acquired on a Horiba Fluorolog-3 DF spectrofluorimeter using quartz cuvettes (1 cm pathlength) at room temperature or in a solid matrix of CH_3OH/CH_3CH_2OH (1:1, v/v) in an NMR tube at 77 K. The excitation light source was a 450 W xenon lamp. Emission was monitored at 90° using a Hamamatsu R2658P PMT (UV/vis/NIR, 200 nm < λ_{em} < 1010 nm). Spectral selection was achieved by double grating monochromators (excitation: 1200 grooves/nm, blazed at 300 nm, visible emission: 1200 grooves/nm, blazed at 500 nm). Luminescence decay profiles were determined with the same instrumental setup as described above for the steady state experiments. The light source for the recording of the decay profiles was a 70 W xenon lamp (pulse width ca. 2 µs FWHM). Lifetime data analysis (deconvolution, statistical parameters, etc.) was performed using the software package DAS from Horiba. Lifetimes τ_{obs} were determined by fitting the middle and tail portions of the decays. Estimated uncertainties in τ_{obs} are ±10%.

Quantum yields were determined in aqueous solution using quinine sulfate (in 1 M sulfuric acid) (Φ_r = 54.6%)[23] as the quantum yield standard after excitation at λ_{exc} = 317 nm. They were measured by the optically dilute method using the following equation:

$$\Phi_x = \Phi_r \cdot (Grad_x / Grad_r) \cdot (n_x/n_r)^2$$

where n is the refractive index (H_2O = 1.333) and Grad is the linearly fitted slope from the plot of the integrated luminescence intensity versus the absorbance at the excitation wavelength. The subscripts ‘x’ and ‘r’ refer to the sample and reference, respectively. The estimated uncertainties in Φ_x are ± 15%.

5.2 Enantiopure Cryptates

D_8-(*R,R,R$_a$*)-6-Lu

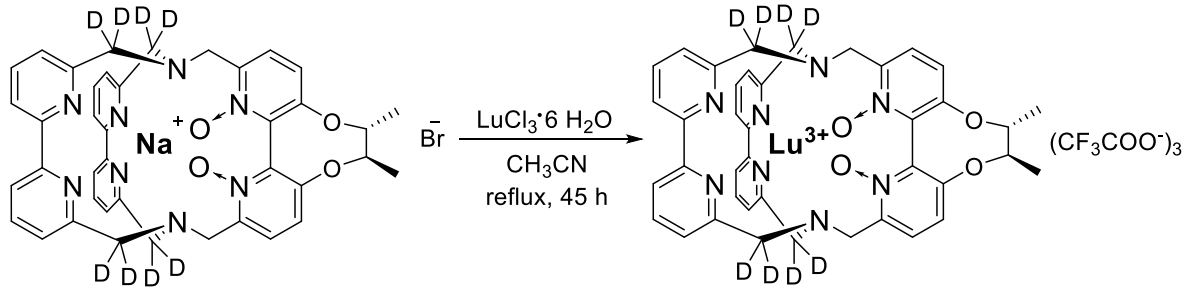

D_8-(*R,R,Ra*)-6-Na

Chemical Formula: $C_{40}H_{28}D_8BrN_8NaO_4$
Molecular Weight: 803,72

D_8-(*R,R,Ra*)-6-Lu

Chemical Formula: $C_{46}H_{28}D_8F_9LuN_8O_{10}$
Molecular Weight: 1214,84

The sodium cryptate **D_8-(*R,R,R$_a$*)-6-Na**[58] (3.0 mg, 3.7 μmol, 1.0 eq.) was dissolved in CH_3CN (3 mL) and $LuCl_3$ • 6 H_2O (2.2 mg, 5.6 μmol, 1.5 eq.) was added. The reaction mixture was refluxed for 45 h. The solvent was removed and the residue was taken up in a minimum of H_2O/CH_3CN (v/v 1:1) and subjected to preparative reversed-phase HPLC. The fractions containing the pure lanthanoid complex were combined (retention time: t_r = 13.5 min) and evaporated to dryness. The complex was isolated as a colourless solid (2.8 mg).

^{1}H NMR (400 MHz, CD_3OD) δ = 8.48 (dd, *J* = 8.2, 1.1 Hz, 2H), 8.40 (dd, *J* = 8.3, 0.9 Hz, 2H), 8.13-8.27 (m, 8H), 7.70 (dd, *J* = 7.8, 1.1 Hz, 2H), 7.65 (dd, *J* = 7.7, 0.9 Hz, 2H), 4.73 (d, *J* = 12.7 Hz, 2H), 4.28 (dd, *J* = 4.2, 2.0 Hz, 2H), 3.90 (d, *J* = 12.9 Hz, 2H), 1.48-1.54 (m, 6H) ppm.

^{13}C NMR (176.8 MHz, CD_3OD) δ = 18.1, 56.1, 59.1, 60.4, 87.8, 122.5, 123.1, 125.9, 126.8, 131.2, 131.9, 141.9, 142.6, 137.7, 146.5, 153.5, 155.5, 156.5, 158.6, 159.3 ppm.

^{19}F NMR (283 MHz, CD_3OD) δ = -77.17 (br), -76.87 (s) ppm.

ESI pos. mode *m/z* (%) = 460.1 (100, $[M-3CF_3COO+CH_3CH_2O]^{2+}$).

D_8-(*R,R,R$_a$*)-6-Tb

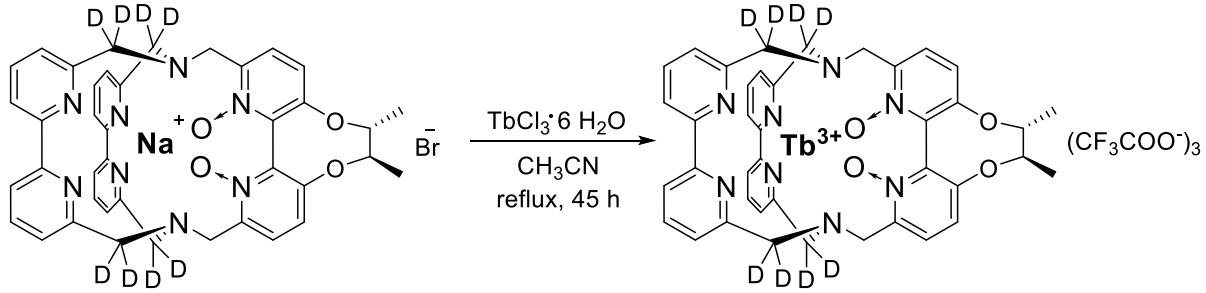

D_8-(*R,R,Ra*)-6-Na

Chemical Formula: $C_{40}H_{28}D_8BrN_8NaO_4$
Molecular Weight: 803,72

D_8-(*R,R,Ra*)-6-Tb

Chemical Formula: $C_{46}H_{28}D_8F_9N_8O_{10}Tb$
Molecular Weight: 1198,80

The sodium cryptate **D_8-(*R,R,R$_a$*)-6-Na**[58] (10.0 mg, 12.4 μmol, 1.0 eq.) was dissolved in CH_3CN (5 mL) and $TbCl_3$ • 6 H_2O (7.5 mg, 5.6 μmol, 1.5 eq.) was added. The reaction mixture was refluxed for 45 h. The solvent was removed and the residue was taken up in a minimum of H_2O/CH_3CN (v/v 1:1) and subjected to preparative reversed-phase HPLC. The fractions containing the pure lanthanoid complex were combined (retention time: t_r = 13.5 min) and evaporated to dryness. The complex was isolated as a light yellow solid (7.5 mg).

^{1}H NMR (300 MHz, CD_3OD) δ = 208.31 (br, 2H), 79.30 (s, 2H), 58.95 (s, 2H), 36.85 (s, 2H), 32.62 (s, 2H), 7.84 (s, 2H), 2.70 (s, 6H), -0.20 (s, 2H), -19.15 (s, 2H), -22.86 (s, 2H), -68.01 (s, 2H), -100.45 (s, 2H) ppm.

^{19}F NMR (283 MHz, CD_3OD) δ = -77.46 (br), -76.85 (s) ppm.

ESI pos. mode *m/z* (%) = 486.1 (100, $[M-2CF_3COO]^{2+}$).

5.3 Coordination Networks

Bipyridine 15

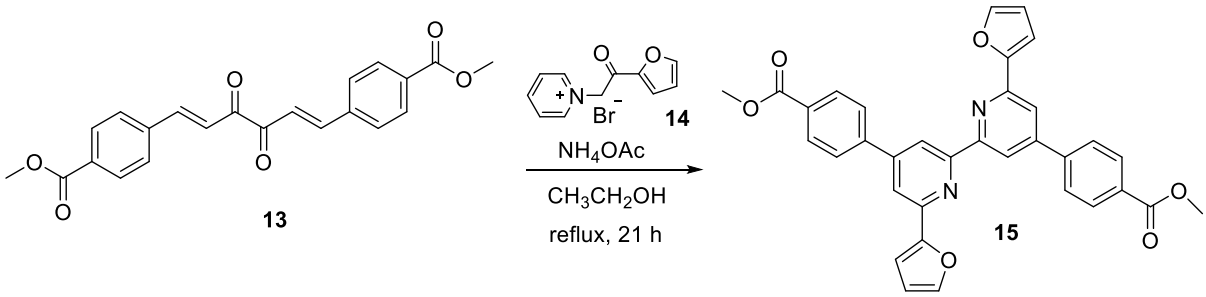

Chemical Formula: $C_{22}H_{18}O_6$
Molecular Weight: 378,38

Chemical Formula: $C_{34}H_{24}N_2O_6$
Molecular Weight: 556,57

Diketone **13**[112] (250 mg, 0.66 mmol, 1.0 eq.), pyridinium salt **14**[113] (350 mg, 1.31 mmol, 2.0 equivs.) and NH_4OAc (1.31 g, 17.03 mmol, 26 equivs.) were suspended in EtOH (25 mL) according to established literature procedures for Kröhnke reactions[1] and refluxed for 21 h. The mixture was allowed to cool to room temperature. The precipitate was collected on a Büchner funnel, washed with EtOH and dried under reduced pressure to give title compound **15** as a light beige solid (230 mg, 0.41 mmol, 63 %).

^{1}H NMR (400 MHz, $CDCl_3$) δ = 8.72 (d, *J* = 1.6 Hz, 2H), 8.23 (d, *J* = 8.3 Hz, 4H), 8.02 (d, *J* = 1.7 Hz, 2H), 7.93 (d, *J* = 8.3 Hz, 4H), 7.61 (br s, 2H), 7.35 (d, *J* = 3.4 Hz, 2H), 6.61 (dd, *J* = 3.3, 1.8 Hz, 2H), 3.99 (s, 6H) ppm.

MS (ESI pos. mode) *m/z* (%) = 557.0 (100, $[M+H]^+$), 634.1 (46, $[M+H+NH_4OAc]^+$).

Elemental analysis: Anal. Calcd for $C_{34}H_{24}N_2O_6 \cdot 2.5\ H_2O$ (M_r = 601.61): C, 67.88; H, 4.86; N, 4.66. Found: C, 67.38; H, 4.76; N, 5.03.

Tetracarboxylic acid 16

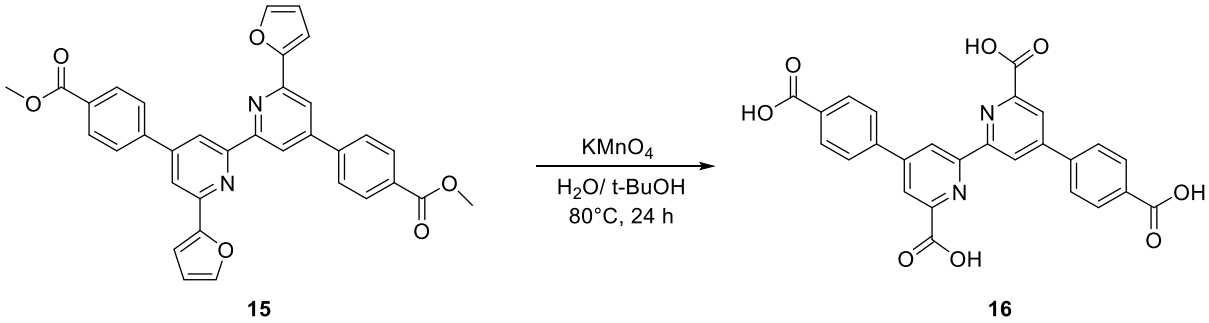

15

Chemical Formula: $C_{34}H_{24}N_2O_6$
Molecular Weight: 556,57

16

Chemical Formula: $C_{26}H_{16}N_2O_8$
Molecular Weight: 484,42

A mixture of bipyridine **15** (1.00 g, 1.8 mmol, 1.0 equiv.), tert-butyl alcohol (200 mL) and water (40 mL) was heated to 80° C and $KMnO_4$ (3.70 g, 23.4 mmol, 13 equivs.) was added in analogy to a literature procedure.[114] After stirring for 24 h the suspension was filtered over celite on a Buchner funnel while hot to remove MnO_2 and the solid was washed with a mixture of 20 mL t-butyl alcohol / 80 mL water. Solvents were evaporated until a minimum of water remained. The aqueous solution was acidified with 2 N HCl and the precipitate was collected on a Büchner funnel, washed with water and dried in vacuo to give title compound **16** as a light beige solid (600 mg, 1.3 mol, 72 %).

MS (ESI neg. mode) *m/z* (%) = 483.0 (100, $[M-H]^-$).

Elemental Analysis: Anal. Calcd for $C_{26}H_{16}N_2O_8 \cdot 3.5\ H_2O$ (M_r = 547.48): C, 57.04; H, 4.23; N, 5.12. Found: C, 57.19; H, 3.71; N, 5.07.

General procedure for 17-Ln_A/Ln_B

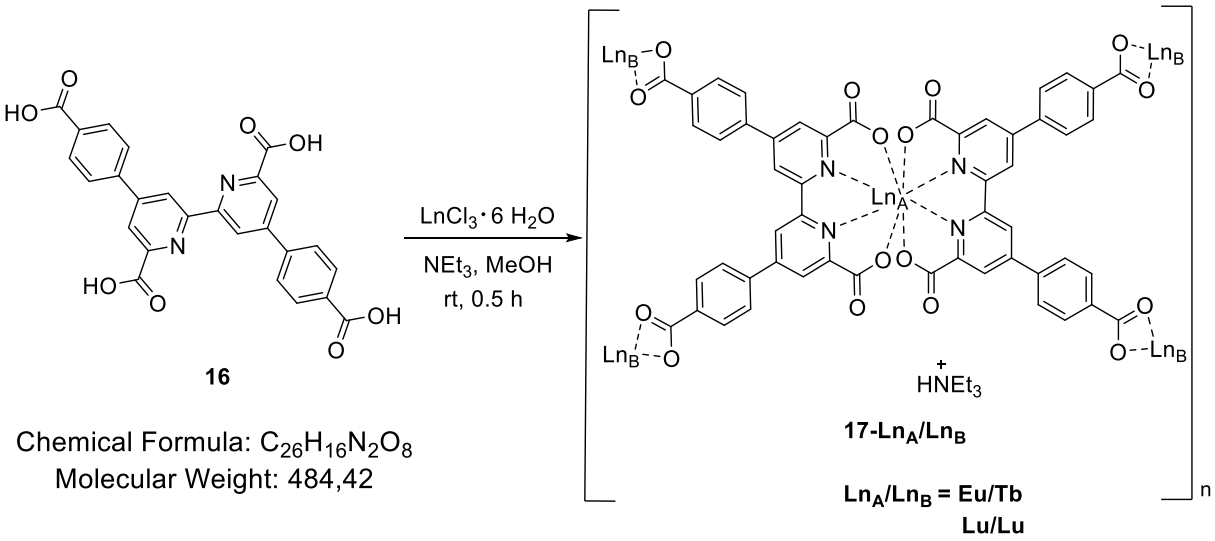

16

Chemical Formula: $C_{26}H_{16}N_2O_8$
Molecular Weight: 484,42

17-Ln_A/Ln_B

Ln_A/Ln_B = Eu/Tb
Lu/Lu

Tetracarboxylic acid **16** (50 mg, 0.10 mmol, 1.0 eq.) was suspended in dry MeOH (10 mL) and a solution of the mixture of the lanthanoid salts $LnCl_3 \cdot 6\ H_2O$ (Ln_A, Ln_B: 0.05 mmol, 0.5 equiv. each) in dry MeOH (2 mL) was added. After 10 minutes of stirring, triethylamine (0.1 g, 0.14 mL, 1.0 mmol, 10.0 eq.) was added and the mixture was stirred for 30 minutes at room temperature. The residue was filtered on a Büchner funnel with a Nylon membrane filter and washed with ice-cold MeOH, dried in vacuo to give the complexes as insoluble light orange solids.

17-Eu/Tb: 57.7 mg

Elemental analysis: Anal. Calcd for $C_{52}H_{25}N_4O_{16}EuTb \cdot HNEt_3 \cdot 12\ H_2O$ (M_r = 1591.06): C, 43.78; H, 4.12; N, 4.40. Found: C, 43.40; H, 3.76; N, 4.47.

17-Lu/Lu: 50.2 mg

Elemental analysis: Anal. Calcd for $C_{52}H_{25}N_4O_{16}Lu_2 \cdot HNEt_3 \cdot 4\ H_2O \cdot LuCl_3$ (M_r = 1767.30): C, 39.42; H, 2,79; N, 3.96. Found: C, 39.73; H, 3.04; N, 3.77.

5.4 Dipyridylamine-based Cryptates

Dipyridylamine 23

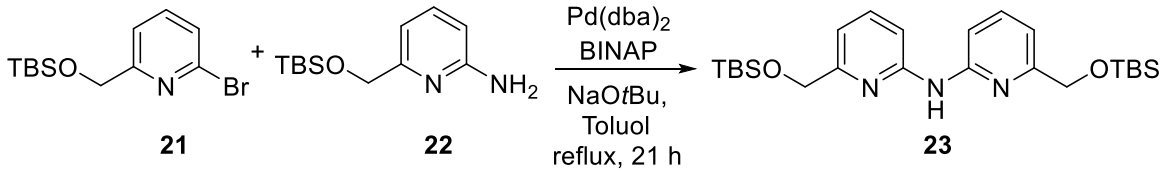

21 **22** **23**

Chemical Formula: $C_{12}H_{20}BrNOSi$
Molecular Weight: 302,29

Chemical Formula: $C_{12}H_{22}N_2OSi$
Molecular Weight: 238,41

Chemical Formula: $C_{24}H_{41}N_3O_2Si_2$
Molecular Weight: 459,78

Under Ar, both TBS-protected educts **21** (3.51 g, 11.6 mmol, 1.0 equiv.) and **22** (2.77 g, 11.6 mmol, 1.0 equiv.) were suspended in dry toluene (40 mL) together with $Pd_2(dba)_3$ (0.43 g, 0.47 mmol, 0.04 equiv.), *rac*-BINAP (0.37 g, 0.58 mmol, 0.05 equiv.) and ^{t}BuONa (1.67 g, 17.4 mmol, 1.5 equiv.) and refluxed for 21 h. The dark red mixture was then allowed to warm to room temperature and filtered. The filtrate was concentrated under reduced pressure and the solid residue was subjected to column chromatography (SiO_2, gradient: CH_2Cl_2/MeOH 100:1 → 50:1, detection: UV) yielding the product **23** as an orange solid (3.37 g, 7.33 mmol, 63%).

^{1}H NMR (400 MHz, $CDCl_3$) δ = 7.57-7.64 (m, 2H), 7.40 (d, *J* = 8.1 Hz, 2H), 7.21 (br, 1H), 7.04 (dd, *J* = 7.4, 0.8 Hz, 2H), 4.74 (s, 4H), 0.97 (s, 18H), 0.13 (s, 12H) ppm.

^{13}C NMR (101 MHz, $CDCl_3$) δ = 159.8, 153.1, 138.5, 112.5, 109.8, 66.1, 26.1, 18.6, - 5.2 ppm.

MS (ESI pos. mode): *m/z* (%) = 460.3 ($[M+H]^+$, 100).

Elemental analysis: Anal. Calcd for $C_{24}H_{41}N_3O_2Si_2$ (Mr = 459.8): C, 62.70; H, 8.99; N, 9.14. Found: C, 62.44; H, 8.56; N, 9.51.

R_f = 0.31 (SiO_2, CH_2Cl_2/MeOH 50:1, detection: UV).

Dipyridylmethylamine 24

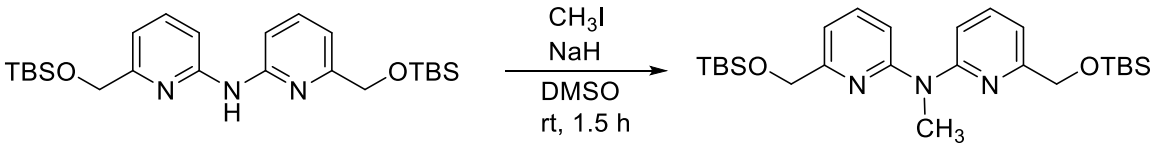

23

Chemical Formula: $C_{24}H_{41}N_3O_2Si_2$
Molecular Weight: 459,78

24

Chemical Formula: $C_{25}H_{43}N_3O_2Si_2$
Molecular Weight: 473,81

Dipyridylamine **23** (3.37 g, 7.33 mmol, 1.0 equiv.) and KOH (2.06 g, 36.7 mmol, 5.0 equivs.) were dissolved in DMSO (65 mL). The suspension was stirred at room temperature for 30 minutes. Methyliodide (0.55 mL, 8.81 mmol, 1.2 equiv.) was added dropwise and the mixture was stirred for additional 90 minutes at room temperature. The reaction mixture was quenched with water (65 mL), extracted with Et_2O (4 x 65 mL) and the combined organic layers were dried ($MgSO_4$). After concentration under reduced pressure the product was obtained without any further purification as an orange oil (2.06 g, 4.35 mmol, 56%).

^{1}H NMR (300 MHz, $CDCl_3$) δ = 7.55 – 7.48 (m, 2H), 7.04 (dd, *J* = 7.4, 0.8 Hz, 2H), 7.00 (dd, *J* = 8.3, 0.7 Hz, 2H), 4.74 (s, 4H), 3.58 (s, 3H), 0.97 (s, 18H), 0.13 (s, 12H) ppm.

^{13}C NMR (101 MHz, $CDCl_3$) δ = 160.1, 157.1, 137.7, 112.8, 112.4, 66.3, 36.0, 26.1, 18.5, -5.2 ppm.

MS (ESI pos. mode): *m/z* (%) = 460.2 ([**23**+H]$^+$, 88), 474.3 ([M+H]$^+$, 100).

Elemental analysis: Anal. Calcd for $C_{25}H_{43}N_3O_2Si_2$ (Mr = 473.8): C, 63.37; H, 9.15; N, 8.87. Found: C, 63.94; H, 8.73; N 9.26.

Diol 25

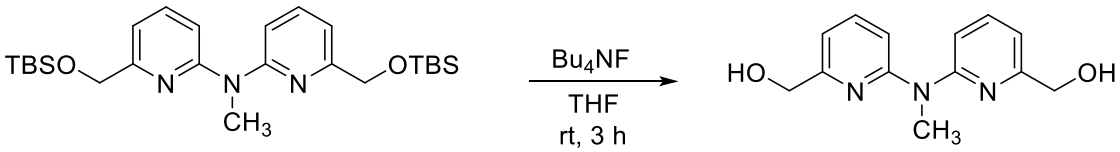

24
Chemical Formula: $C_{25}H_{43}N_3O_2Si_2$
Molecular Weight: 473,81

25
Chemical Formula: $C_{13}H_{15}N_3O_2$
Molecular Weight: 245,28

To a solution of dipyridylmethylamine **24** (2.06 g, 4.35 mmol, 1.0 equiv.) in THF (60 mL) a solution of 1M Bu_4NF (20.1 mL, 20.1 mmol, 4.4 equivs.) in THF was added and the mixture was stirred for 3 h at room temperature. After filtration the precipitate was washed with THF (100 mL). The filtrate was concentrated under reduced pressure, then water (50 mL) was added and the aqueous phase was extracted with EtOAc (3 x 60 mL). The combined organic layers were dried ($MgSO_4$) and the solvent was removed. The residue was subjected to column chromatography (SiO_2, CH_2Cl_2/MeOH 9:1, detection: UV) yielding the product as a yellow solid (846 mg, 3.45 mmol, 79%).

^{1}H NMR (300 MHz, $CDCl_3$) δ = 7.55 (dd, *J* = 8.2, 7.4 Hz, 2H), 7.05 (dd, *J* = 8.3, 0.7 Hz, 2H), 6.80 (dd, *J* = 7.4, 0.7 Hz, 2H), 4.68 (s, 4H), 3.79 (br s, 2H), 3.63 (s, 3H) ppm.

^{13}C NMR (75 MHz, $CDCl_3$) δ = 157.6, 156.7, 138.1, 113.4, 112.6, 63.9, 36.1 ppm.

MS (ESI pos. mode) *m/z* (%) = 245.9 ($[M+H]^+$, 100).

R_f = 0.50 (SiO_2, CH_2Cl_2/MeOH 9:1, detection: UV).

Dibromide 26

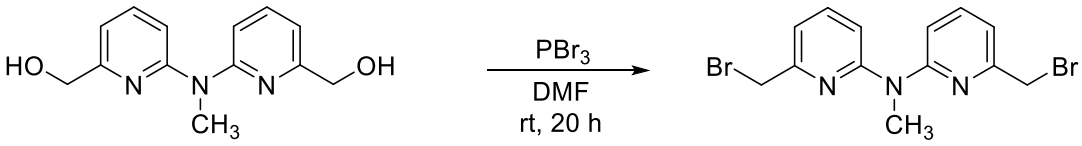

25

Chemical Formula: $C_{13}H_{15}N_3O_2$
Molecular Weight: 245,28

26

Chemical Formula: $C_{13}H_{13}Br_2N_3$
Molecular Weight: 371,08

Under Ar, diol **25** (500 mg, 2.0 mmol, 1.0 equiv.) was dissolved in dry DMF (15 mL), cooled to 0 °C and PBr_3 (0.97 mL, 10.2 mmol, 5.0 equiv.) was added slowly. The suspension was stirred for 15 minutes, then was allowed to warm to room temperature and stirred for 20 h. Volatiles were removed under reduced pressure and water (40 mL) was added cautiously under ice-cooling. The pH was adjusted to ca. 6 with saturated aqueous $NaHCO_3$ solution. The aqueous phase was extracted with $CHCl_3$ (4 x 50 mL). The combined organic layers were dried ($MgSO_4$) and the solvent was removed. The precipitate was dissolved in CH_2Cl_2 (50 mL) and washed with water (3 x 30 mL). The organic phase was dried ($MgSO_4$) again and the solvent was removed under reduced pressure. The product **26** was obtained as a light brown solid (560 mg, 1.5 mmol, 75%).

^{1}H NMR (400 MHz, $CDCl_3$) δ = 7.54 (dd, *J* = 8.4, 7.4 Hz, 2H), 7.17 (d, *J* = 8.4 Hz, 2H), 6.99 (d, *J* = 7.4 Hz, 2H), 4.47 (s, 4H), 3.64 (s, 3H) ppm.

^{13}C NMR (101 MHz, $CDCl_3$) δ = 157.1, 155.1, 138.1, 116.4, 113.7, 36.0, 34.5 ppm.

MS (ESI pos. mode) *m/z* (%) = 371.9 ($[M+H]^+$, 100, Br_2 isotope pattern).

Elemental analysis: Anal. Calcd for $C_{13}N_3H_{13}Br_2$ (Mr = 371.1): C, 42.08; H, 3.53; N, 11.32. Found: C, 42.78; H, 3.56; N 11.45.

Diamine 27

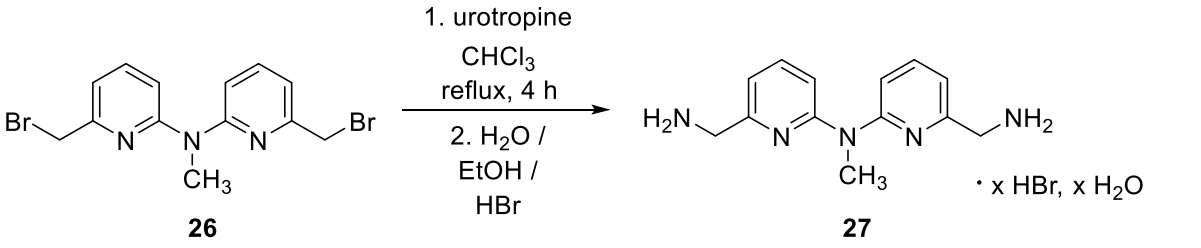

26

Chemical Formula: $C_{13}H_{13}Br_2N_3$
Molecular Weight: 371,08

27

Chemical Formula: $C_{13}H_{17}N_5$ x HBr, x H_2O
Molecular Weight: 243,31

To a solution of dibromide **26** (200 mg, 0.54 mmol, 1.0 eq.) in $CHCl_3$ was added a solution of urotropine (163 mg, 1.16 mmol, 2.16 eq.) in $CHCl_3$ (10 mL) dropwise. The reaction mixture was stirred at 70° C for 4 h and was then allowed to cool to room temperature overnight. The clear solution is separated from the yellow oil which is washed with $CHCl_3$ (2 x 5 mL). The solvent was removed under reduced pressure and the residue was solved in H_2O (1.50 mL), EtOH (6.47 mL) and 48% aqueous HBr (1.08 mL). The reaction mixture was refluxed for 1.5 h and was then allowed to cool to room temperature. The pH was adjusted to 14 with NaOH and the product was extracted with CH_2Cl_2 (3 x 15 mL). The combined organic phases were washed with H_2O (15 mL) and saturated aqueous NaCl solution (15 mL), dried ($MgSO_4$) and the solvent was removed under reduced pressure. The remaining oil was suspended in H_2O (10 mL), the pH was adjusted to 1 and it was extracted with CH_2Cl_2 (3 x 10 mL). The pH of the aqueous phase was then adjusted to 14 with NaOH whereupon a yellow precipitate occured. The product was extracted with CH_2Cl_2 (3 x 10 mL), dried ($MgSO_4$). The orange oil was suspended in H_2O, acidified with 48% HBr and the solvent was removed under reduced pressure yielding a brown oil.

^{1}H NMR (400 MHz, $(CD_3)_2SO$) δ = 8.22 (br s, 4H), 7.69 (t, *J* = 7.9 Hz, 2H), 7.23 (d, *J* = 8.3 Hz, 2H), 7.00 (d, *J* = 7.4 Hz, 2H), 4.11 (s, 4H), 3.58 (s, 3H) ppm.

MS (ESI pos. mode) *m/z* (%) = 244.1 (100, $[M+H]^+$), 254.1 (42).

18-Na

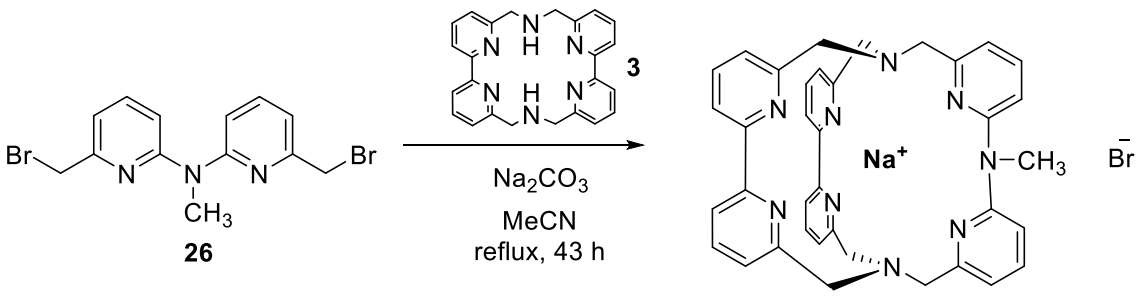

Chemical Formula: $C_{13}H_{13}Br_2N_3$
Molecular Weight: 371,08

Chemical Formula: $C_{37}H_{33}BrN_9Na$
Molecular Weight: 706,63

Under Ar, dibromide **26** (28.2 mg, 76.0 μmol, 1.0 equiv.) and the macrocycle **3**[115] (30.0 mg, 76 μmol, 1.0 equiv.) were suspended in MeCN (HPLC grade, 12 mL). After 5 minutes stirring at room temperature, Na_2CO_3 (80.6 mg, 760 μmol, 10.0 equivs.) was added and the reaction mixture was refluxed for 43 h. Then, the suspension was allowed to cool to room temperature, filtered and the residue was washed with MeCN (3 x 10 mL). The solvent was removed under reduced pressure and the residue was subjected to two column chromatographies (SiO_2, CH_2Cl_2/MeOH 9:1; CH_2Cl_2/MeOH 15:1, detection: UV) yielding the product **18-Na** as a colourless solid (15.1 mg, 21.4 μmol, 28%).

^{1}H NMR (400 MHz, CD_3OD) δ = 8.04 (d, *J* = 7.3 Hz, 4H), 7.87-7.93 (m, 4H), 7.36 (d, *J* = 6.8 Hz, 4H), 7.18 (dd, *J* = 8.1, 7.4 Hz, 2H), 6.76 (d, *J* = 7.4 Hz, 2H), 6.28 (d, *J* = 6.7 Hz, 2H), 4.22 (d, *J* = 14.5 Hz, 4H), 3.86 (d, *J* = 14.4 Hz, 4H), 3.61 (s, 4H), 3.24 (s, 3H) ppm.

^{13}C NMR (101 MHz, CD_3OD) δ = 161.7, 160.0, 159.3, 155.7, 139.4, 139.3, 124.8, 121.1, 117.6, 114.9, 61.5, 60.2, 38.5 ppm.

MS (ESI pos. mode) *m/z* (%) = 302.5 ($[M\text{-}Br+H]^{2+}$, 18), 626.3 ($[M\text{-}Br^-]^+$, 100), 642.2 ($[M\text{-}Na\text{-}Br+K]^+$, 68).

R_f = 0.29 (SiO_2, CH_2Cl_2/MeOH 9:1, detection: UV).

19-Na

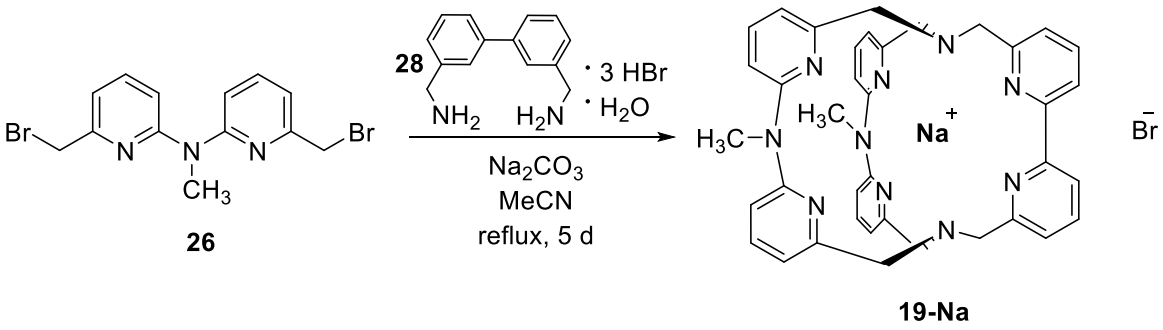

Chemical Formula: $C_{13}H_{13}Br_2N_3$
Molecular Weight: 371,08

Chemical Formula: $C_{38}H_{36}BrN_{10}Na$
Molecular Weight: 735,67

Under Ar, dibromide **26** (56 mg, 150 μmol, 1.0 equiv.) and bpy(NH_2)$_2$ (• 3 HBr; H_2O) **28** (36 mg, 76 μmol, 0.5 equiv.) was suspended in MeCN (HPLC grade, 250 mL). After 5 minutes stirring at room temperature, Na_2CO_3 (80.6 mg, 760 μmol, 5.0 equivs.) was added and the reaction mixture was refluxed for 5 days. Then, the suspension was allowed to warm to room temperature, filtered the solvent was removed under reduced pressure. The residue was subjected to column chromatographiy (SiO_2, CH_2Cl_2/MeOH 9:1, detection: UV) yielding the product **19-Na** as a colourless solid (11.9 mg, 16.1 μmol, 11%).

^{1}H NMR (400 MHz, CD_3OD) δ = 7.93 (d, *J* = 7.3 Hz,1H), 7.88-7.92 (m, 1H), 7.70-7.74 (m, 2H), 7.55-7.62 (m, 2H), 7.45 (d, *J* = 7.5 Hz, 2H), 7.40-7.44 (m, 1H), 7.19-7.24 (m, 1H), 6.98 (d, *J* = 7.4 Hz, 2H), 6.81 (d, *J* = 8.2 Hz, 2H), 6.80 (d, *J* = 8.4 Hz, 2H), 6.65 (d, *J* = 7.4 Hz, 2H), 4.06 (s, 2H), 3.98 (s, 2H), 3.97 (d, *J* = 13.4 Hz, 2H), 3.75 (d, *J* = 13.5 Hz, 2H), 3.64 (d, *J* = 13.3 Hz, 2H), 3.59 (d, *J* = 13.4 Hz, 2H), 3.28 (s, 3H), 3.13 (s, 3H) ppm.

^{13}C NMR (101 MHz, CD_3OD) δ = 161.3, 160.9, 160.3, 160.2, 159.3, 157.8, 156.9, 156.4, 140.2, 139.5, 139.5, 138.9, 126.1, 124.1, 122.4, 120.9, 120.2, 119.1, 116.2, 114.3, 63.9, 63.8, 62.7, 61.6, 39.5, 38.3 ppm.

MS (ESI pos. mode) *m/z* (%) = 317.1 ([M-Br+H]$^{2+}$, 100), 633.3 ([M+H-Na-Br]$^+$, 15).

R_f = 0.18 (SiO_2, CH_2Cl_2/MeOH 9:1, detection: UV).

20-Na

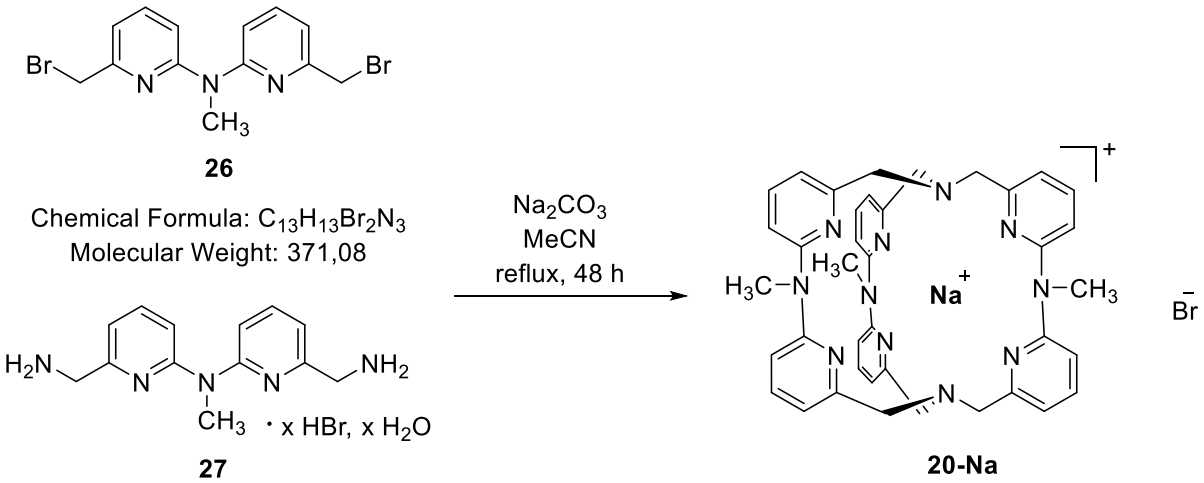

Under Ar, dibromide **26** (50 mg, 0.135 mmol, 1.0 eq.) and diamine **27** (33.8 mg, 0.067 mmol, 0.5 eq.) were suspended in MeCN (HPLC grade, 250 mL). Na_2CO_3 (71.6 mg, 0.675 mmol, 5 eq.) was added and the reaction mixture was refluxed for 48 h. The precipitate was filtered off after the mixture was allowed to cool to room temperature. The solvent was removed and the residue was subjected to column chromatography (SiO_2, CH_2Cl_2/MeOH 9:1 → 5:1, detection: UV) yielding the product **20-Na** as a yellow solid (15 mg, 0.016 mmol, 24%).

MS (ESI pos. Mode) *m/z* (%) = 662.3 (22, $[M\text{-}Na+H]^+$), 331.7 (100, $[M\text{-}Na+2H]^{2+}$).

General Procedure for Preparation of Lanthanoid Cryptates 18-Ln and 19-Ln

Under Ar, **18-Na/19-Na** (1.0 eq.) and $LnCl_3 \cdot 6\ H_2O$ (1.7 eq.) were suspended in MeCN (HPLC grade) and refluxed for 20 h. The reaction mixture was cooled to room temperature and filtered. The solvent was removed under reduced pressure and the residue was solved in a minimum of MeOH. After slow addition of Et_2O, a white precipitate forms. The suspension is stored at 4° C for 5 h and then the solid was filtered through a Buchner funnel over a nylon membrane filter (0.45 μm). The complexes were obtained as colourless solids.

18-Lu

MS (MALDI) *m/z* (%) = 813.1 ([M + Cl^- + e^-], 100), 840.5 (73), 931.1 (M + deprotonated DHB + e^-], 55), 958.6 (60).

18-Eu

MS (MALDI) *m/z* (%) = 909.2 ([M + deprotonated DHB]$^{2+}$, Eu istope pattern, 100).

19-Lu

^{1}H NMR (500 MHz, CD_3OD) δ = 8.33 (d, *J* = 8.0 Hz, 2H), 7.93-7.87 (m, 6H), 7.43 (d, *J* = 7.4 Hz, 4H), 7.09 (d, *J* = 8.2 Hz, 4H), 7.01 (d, *J* = 7.9 Hz, 2H), 5.79 (d, *J* = 13.6 Hz, 4H), 4.03 (d, *J* = 13.7 Hz, 4H), 3.91 (s, 4H), 2.57 (s, 6H) ppm.

MS (MALDI) *m/z* (%) = 960.2 ([M + deprotonated DHB + e^-], 100).

19-Eu

^{1}H NMR (300 MHz, CD_3OD) δ = 11.18 (br s, 4H), 9.40 (br s, 4H), 7.47 (s, 6H), 5.22 (d, *J* = 7.2 Hz, 4H), 5.04-5.16 (m, 2H), 3.37-3.53 (m, 2H), -0.94 (br s, 2H), -6.82 (br s, 4H), -16.70 (br s, 4H), -19.04 (br s, 4H) ppm.

MS (MALDI) *m/z* (%) = 938.1 ([M + deprotonated DHB]$^{2+}$, Eu istope pattern, 100)

6 Bibliography

[1] C. Huang, Z. Bian, in *Rare Earth Coord. Chem.* (Ed.: C. Huang), John Wiley & Sons, Ltd, Chichester, UK, **2010**, pp. 1–39.

[2] J.-C. G. Bünzli, *Eur. J. Inorg. Chem.* **2017**, 5058–5063.

[3] J. M. Zwier, H. Bazin, L. Lamarque, G. Mathis, *Inorg. Chem.* **2014**, *53*, 1854–1866.

[4] J. Andres, A.-S. Chauvin, in *Encycl. Inorg. Bioinorg. Chem.* (Ed.: R.A. Scott), John Wiley & Sons, Ltd, Chichester, UK, **2012**, pp. 111–134.

[5] L. Armelao, S. Quici, F. Barigelletti, G. Accorsi, G. Bottaro, M. Cavazzini, E. Tondello, *Coord. Chem. Rev.* **2010**, *254*, 487–505.

[6] S. V. Eliseeva, J.-C. G. Bünzli, *Chem Soc Rev* **2010**, *39*, 189–227.

[7] R. E. Connick, *J. Chem. Soc.* **1949**, 235–241.

[8] J.-C. G. Bünzli, S. V. Eliseeva, in *Compr. Inorg. Chem. II*, Elsevier, **2013**, pp. 339–398.

[9] J.-C. G. Bünzli, S. V. Eliseeva, in *Lanthan. Lumin.* (Eds.: P. Hänninen, H. Härmä), Springer Berlin, **2010**, pp. 1–45.

[10] W. T. Carnall, P. R. Fields, K. Rajnak, *J. Chem. Phys.* **1968**, *49*, 4447–4449.

[11] W. T. Carnall, P. R. Fields, K. Rajnak, *J. Chem. Phys.* **1968**, *49*, 4450–4455.

[12] W. T. Carnall, P. R. Fields, K. Rajnak, *J. Chem. Phys.* **1968**, *49*, 4424–4442.

[13] W. T. Carnall, P. R. Fields, K. Rajnak, *J. Chem. Phys.* **1968**, *49*, 4443–4446.

[14] E. Kreidt, C. Kruck, M. Seitz, in *Handb. Phys. Chem. Rare Earths*, Elsevier, **2018**, pp. 35–79.

[15] J.-C. G. Bünzli, *Coord. Chem. Rev.* **2015**, *293*, 19–47.

[16] J.-C. G. Bünzli, *Chem. Rev.* **2010**, *110*, 2729–2755.

[17] J.-C. G. Bünzli, C. Piguet, *Chem. Soc. Rev.* **2005**, *34*, 1048–1077.

[18] B. Alpha, R. Ballardini, V. Balzani, J.-M. Lehn, S. Perathoner, N. Sabbatini, *Photochem. Photobiol.* **1990**, *52*, 299–306.

[19] A. K. R. Junker, L. R. Hill, A. L. Thompson, S. Faulkner, T. J. Sørensen, *Dalton Trans.* **2018**, *47*, 4794–4803.

[20] G. Longhi, E. Castiglioni, J. Koshoubu, G. Mazzeo, S. Abbate, *Chirality* **2016**, *28*, 696–707.

[21] J. P. Riehl, F. S. Richardson, *Chem. Rev.* **1986**, *86*, 1–16.

[22] A. T. Frawley, R. Pal, D. Parker, *Chem. Commun.* **2016**, *52*, 13349–13352.

[23] K. Staszak, K. Wieszczycka, V. Marturano, B. Tylkowski, *Coord. Chem. Rev.* **2019**, *397*, 76–90.

[24] A. T. Frawley, H. V. Linford, M. Starck, R. Pal, D. Parker, *Chem. Sci.* **2018**, *9*, 1042–1049.

[25] J.-C. G. Bünzli, *J. Lumin.* **2016**, *170*, 866–878.

[26] F. Zinna, M. Pasini, F. Galeotti, C. Botta, L. Di Bari, U. Giovanella, *Adv. Funct. Mater.* **2017**, *27*, 1603719.

[27] F. Zinna, U. Giovanella, L. D. Bari, *Adv. Mater.* **2015**, *27*, 1791–1795.

[28] J. R. Brandt, X. Wang, Y. Yang, A. J. Campbell, M. J. Fuchter, *J. Am. Chem. Soc.* **2016**, *138*, 9743–9746.

[29] F. Zinna, L. Di Bari, *Chirality* **2015**, *27*, 1–13.

[30] R. Carr, N. H. Evans, D. Parker, *Chem. Soc. Rev.* **2012**, *41*, 7673–7686.

[31] J. Kumar, T. Nakashima, T. Kawai, *J. Phys. Chem. Lett.* **2015**, *6*, 3445–3452.

[32] E. M. Sánchez-Carnerero, A. R. Agarrabeitia, F. Moreno, B. L. Maroto, G. Muller, M. J. Ortiz, S. de la Moya, *Chem. - Eur. J.* **2015**, *21*, 13488–13500.

[33] H. G. Brittain, *J. Coord. Chem.* **1989**, *20*, 331–347.

[34] G. Muller, *Dalton Trans.* **2009**, 9692–9707.

[35] J. L. Lunkley, D. Shirotani, K. Yamanari, S. Kaizaki, G. Muller, *Inorg. Chem.* **2011**, *50*, 12724–12732.

[36] J. L. Lunkley, D. Shirotani, K. Yamanari, S. Kaizaki, G. Muller, *J. Am. Chem. Soc.* **2008**, *130*, 13814–13815.

[37] F. S. Richardson, *Inorg. Chem.* **1980**, *19*, 2806–2812.

[38] L. Dai, J. Zhang, Y. Chen, L. E. Mackenzie, R. Pal, G.-L. Law, *Inorg. Chem.* **2019**, *58*, 12506–12510.

[39] M. Starck, L. E. MacKenzie, A. S. Batsanov, D. Parker, R. Pal, *Chem. Commun.* **2019**, *55*, 14115–14118.

[40] O. Kotova, S. Comby, K. Pandurangan, F. Stomeo, J. E. O'Brien, M. Feeney, R. D. Peacock, C. P. McCoy, T. Gunnlaugsson, *Dalton Trans.* **2018**, *47*, 12308–12317.

[41] K. Matsumoto, K. Suzuki, T. Tsukuda, T. Tsubomura, *Inorg. Chem.* **2010**, *49*, 4717–4719.

[42] B. Casanovas, F. Zinna, L. Di Bari, M. S. El Fallah, M. Font-Bardía, R. Vicente, *Dalton Trans.* **2017**, *46*, 6349–6357.

[43] Y. Kono, N. Hara, M. Shizuma, M. Fujiki, Y. Imai, *Dalton Trans.* **2017**, *46*, 5170–5174.

[44] S. D. Bonsall, M. Houcheime, D. A. Straus, G. Muller, *Chem. Commun.* **2007**, 3676–3678.

[45] M. F. Loncin, J. F. Desreux, E. Merciny, *Inorg. Chem.* **1986**, *25*, 2646–2648.

[46] W. P. Cacheris, S. K. Nickle, A. D. Sherry, *Inorg. Chem.* **1987**, *26*, 958–960.

[47] A. C. L. Opina, M. Strickland, Y.-S. Lee, N. Tjandra, R. A. Byrd, R. E. Swenson, O. Vasalatiy, *Dalton Trans.* **2016**, *45*, 4673–4687.

[48] J.-C. Rodriguz-Ubis, B. Alpha, D. Plancherel, J.-M. Lehn, *Helv. Chim. Acta* **1984**, *67*, 2264–2269.

[49] J.-M. Lehn, C. O. Roth, *Helv. Chim. Acta* **1991**, *74*, 572–578.

[50] C. Doffek, M. Seitz, *Angew. Chem. Int. Ed.* **2015**, *54*, 9719–9721.

[51] C. Dee, D. Esteban-Gómez, C. Platas-Iglesias, M. Seitz, *Inorg. Chem.* **2018**, *57*, 7390–7401.

[52] E. Kreidt, C. Bischof, C. Platas-Iglesias, M. Seitz, *Inorg. Chem.* **2016**, *55*, 5549–5557.

[53] J.-M. Lehn, J.-B. R. De Vains, *Helv. Chim. Acta* **1992**, *75*, 1221–1236.

[54] V. Balzani, E. Berghmans, J.-M. Lehn, N. Sabbatini, R. Terörde, R. Ziessel, *Helv. Chim. Acta* **1990**, *73*, 2083–2089.

[55] A. Beeby, B. P. Burton-Pye, S. Faulkner, G. R. Motson, J. C. Jeffery, J. A. McCleverty, M. D. Ward, *J. Chem. Soc. Dalton Trans.* **2002**, 1923–1928.

[56] C. Dee, Neue Lanthanoid-Luminophore mit langwelliger Anregung, Master Thesis, Universität Tübingen, **2016**.

[57] E. Kreidt, C. Dee, M. Seitz, *Inorg. Chem.* **2017**, *56*, 8752–8754.

[58] T. Güden-Silber, C. Doffek, C. Platas-Iglesias, M. Seitz, *Dalton Trans* **2014**, *43*, 4238–4241.

[59] E. S. Andreiadis, R. Demadrille, D. Imbert, J. Pécaut, M. Mazzanti, *Chem. - Eur. J.* **2009**, *15*, 9458–9476.

[60] A. Dadabhoy, S. Faulkner, P. G. Sammes, *J. Chem. Soc. Perkin Trans. 2* **2002**, 348–357.

[61] E. Deiters, B. Song, A.-S. Chauvin, C. D. B. Vandevyver, F. Gumy, J.-C. G. Bünzli, *Chem. - Eur. J.* **2009**, *15*, 885–900.

[62] C. Yang, L.-M. Fu, Y. Wang, J.-P. Zhang, W.-T. Wong, X.-C. Ai, Y.-F. Qiao, B.-S. Zou, L.-L. Gui, *Angew. Chem. Int. Ed.* **2004**, *43*, 5010–5013.

[63] J. D. Routledge, M. W. Jones, S. Faulkner, M. Tropiano, *Inorg. Chem.* **2015**, *54*, 3337–3345.

[64] A. P. Varela, H. D. Burrows, P. Douglas, M. da Graça Miguel, *J. Photochem. Photobiol. Chem.* **2001**, *146*, 29–36.

[65] M. Seitz, N. Alzakhem, *J. Chem. Inf. Model.* **2010**, *50*, 217–220.

[66] C. O. Paul-Roth, J.-M. Lehn, J. Guilhem, C. Pascard, *Helv. Chim. Acta* **1995**, *78*, 1895–1903.

[67] L. Prodi, M. Maestri, V. Balzani, J.-M. Lehn, C. Roth, *Chem. Phys. Lett.* **1991**, *180*, 45–50.

[68] E. Kreidt, L. Arrico, F. Zinna, L. Di Bari, M. Seitz, *Chem. - Eur. J.* **2018**, *24*, 13556–13564.

[69] A. P. S. Samuel, J. L. Lunkley, G. Muller, K. N. Raymond, *Eur. J. Inorg. Chem.* **2010**, *2010*, 3343–3347.

[70] M. Seitz, K. Do, A. J. Ingram, E. G. Moore, G. Muller, K. N. Raymond, *Inorg. Chem.* **2009**, *48*, 8469–8479.

[71] M. Leonzio, A. Melchior, G. Faura, M. Tolazzi, F. Zinna, L. Di Bari, F. Piccinelli, *Inorg. Chem.* **2017**, *56*, 4413–4421.

[72] C. A. Emeis, L. J. Oosterhoff, *Chem. Phys. Lett.* **1967**, *1*, 129–132.

[73] R. D. Peacock, B. Stewart, *J. Chem. Soc. Chem. Commun.* **1982**, 295–296.

[74] G. L. Hilmes, H. G. Brittain, F. S. Richardson, *Inorg. Chem.* **1977**, *16*, 528–533.

[75] C. Wang, S. Otto, M. Dorn, E. Kreidt, J. Lebon, L. Sršan, P. Di Martino-Fumo, M. Gerhards, U. Resch-Genger, M. Seitz, et al., *Angew. Chem. Int. Ed.* **2018**, *57*, 1112–1116.

[76] S. Otto, M. Dorn, C. Förster, M. Bauer, M. Seitz, K. Heinze, *Coord. Chem. Rev.* **2018**, *359*, 102–111.

[77] S. Otto, M. Grabolle, C. Förster, C. Kreitner, U. Resch-Genger, K. Heinze, *Angew. Chem. Int. Ed.* **2015**, *54*, 11572–11576.

[78] C. Dee, F. Zinna, W. R. Kitzmann, G. Pescitelli, K. Heinze, L. Di Bari, M. Seitz, *Chem. Commun.* **2019**, *55*, 13078–13081.

[79] J.-R. Jiménez, B. Doistau, C. M. Cruz, C. Besnard, J. M. Cuerva, A. G. Campaña, C. Piguet, *J. Am. Chem. Soc.* **2019**, *141*, 13244–13252.

[80] J. Zhou, Q. Liu, W. Feng, Y. Sun, F. Li, *Chem. Rev.* **2015**, *115*, 395–465.

[81] T. N. Singh-Rachford, F. N. Castellano, *Coord. Chem. Rev.* **2010**, *254*, 2560–2573.

[82] M. Ingaramo, A. G. York, P. Wawrzusin, O. Milberg, A. Hong, R. Weigert, H. Shroff, G. H. Patterson, *Proc. Natl. Acad. Sci.* **2014**, *111*, 5254–5259.

[83] A. Monguzzi, R. Tubino, S. Hoseinkhani, M. Campione, F. Meinardi, *Phys. Chem. Chem. Phys.* **2012**, *14*, 4322–4332.

[84] M. Wu, D. N. Congreve, M. W. B. Wilson, J. Jean, N. Geva, M. Welborn, T. Van Voorhis, V. Bulović, M. G. Bawendi, M. A. Baldo, *Nat. Photonics* **2016**, *10*, 31–34.

[85] S. B. Meshkova, Z. M. Topilova, D. V. Bolshoy, S. V. Beltyukova, M. P. Tsvirko, V. Ya. Venchikov, *Acta Phys. Pol. A* **1999**, *95*, 983–990.

[86] C. Bischof, J. Wahsner, J. Scholten, S. Trosien, M. Seitz, *J. Am. Chem. Soc.* **2010**, *132*, 14334–14335.

[87] W. Browne, *Coord. Chem. Rev.* **2001**, *219–221*, 761–787.

[88] J. Zhang, S. Petoud, *Chem. - Eur. J.* **2008**, *14*, 1264–1272.

[89] N. Wartenberg, O. Raccurt, E. Bourgeat-Lami, D. Imbert, M. Mazzanti, *Chem. - Eur. J.* **2013**, *19*, 3477–3482.

[90] N. M. Shavaleev, R. Scopelliti, F. Gumy, J.-C. G. Bünzli, *Inorg. Chem.* **2009**, *48*, 7937–7946.

[91] J. Wahsner, M. Seitz, *Inorg. Chem.* **2015**, *54*, 10841–10848.

[92] C. Doffek, J. Wahsner, E. Kreidt, M. Seitz, *Inorg. Chem.* **2014**, *53*, 3263–3265.

[93] T. Güden-Silber, K. Klein, M. Seitz, *Dalton Trans.* **2013**, *42*, 13882–13888.

[94] Y.-C. Cheng, G. R. Fleming, *Annu. Rev. Phys. Chem.* **2009**, *60*, 241–262.

[95] T. R. Cook, Y.-R. Zheng, P. J. Stang, *Chem. Rev.* **2013**, *113*, 734–777.

[96] M. Li, D. Li, M. O'Keeffe, O. M. Yaghi, *Chem. Rev.* **2014**, *114*, 1343–1370.

[97] X. Zhang, W. Wang, Z. Hu, G. Wang, K. Uvdal, *Coord. Chem. Rev.* **2015**, *284*, 206–235.

[98] C. A. Kent, B. P. Mehl, L. Ma, J. M. Papanikolas, T. J. Meyer, W. Lin, *J. Am. Chem. Soc.* **2010**, *132*, 12767–12769.

[99] L. V. Meyer, F. Schönfeld, K. Müller-Buschbaum, *Chem. Commun.* **2014**, *50*, 8093–8108.

[100] X. Wang, O. S. Wolfbeis, R. J. Meier, *Chem. Soc. Rev.* **2013**, *42*, 7834–7869.

[101] C. D. S. Brites, P. P. Lima, N. J. O. Silva, A. Millán, V. S. Amaral, F. Palacio, L. D. Carlos, *Adv. Mater.* **2010**, *22*, 4499–4504.

[102] J. Feng, K. Tian, D. Hu, S. Wang, S. Li, Y. Zeng, Y. Li, G. Yang, *Angew. Chem. Int. Ed.* **2011**, *50*, 8072–8076.

[103] Y. Cui, F. Zhu, B. Chen, G. Qian, *Chem. Commun.* **2015**, *51*, 7420–7431.

[104] J. Rocha, C. D. S. Brites, L. D. Carlos, *Chem. - Eur. J.* **2016**, *22*, 14782–14795.

[105] C. D. S. Brites, P. P. Lima, N. J. O. Silva, A. Millán, V. S. Amaral, F. Palacio, L. D. Carlos, *Nanoscale* **2012**, *4*, 4799–4829.

[106] M. Ren, C. D. S. Brites, S.-S. Bao, R. A. S. Ferreira, L.-M. Zheng, L. D. Carlos, *J. Mater. Chem. C* **2015**, *3*, 8480–8484.

[107] Y. Cui, H. Xu, Y. Yue, Z. Guo, J. Yu, Z. Chen, J. Gao, Y. Yang, G. Qian, B. Chen, *J. Am. Chem. Soc.* **2012**, *134*, 3979–3982.

[108] D. Ananias, C. D. S. Brites, L. D. Carlos, J. Rocha, *Eur. J. Inorg. Chem.* **2016**, *2016*, 1967–1971.

[109] Z. Wang, D. Ananias, A. Carné-Sánchez, C. D. S. Brites, I. Imaz, D. Maspoch, J. Rocha, L. D. Carlos, *Adv. Funct. Mater.* **2015**, *25*, 2824–2830.

[110] Y. Zhou, B. Yan, F. Lei, *Chem Commun* **2014**, *50*, 15235–15238.

[111] X. Liu, S. Akerboom, M. de Jong, I. Mutikainen, S. Tanase, A. Meijerink, E. Bouwman, *Inorg. Chem.* **2015**, *54*, 11323–11329.

[112] T. Renouard, M. Grätzel, *Tetrahedron* **2001**, *57*, 8145–8150.

[113] T. Fujimori, P. Wirsching, K. D. Janda, *J. Comb. Chem.* **2003**, *5*, 625–631.

[114] D. D. Weller, G. R. Luellen, D. L. Weller, *J. Org. Chem.* **1982**, *47*, 4803–4806.

[115] G. R. Newkome, S. Pappalardo, V. K. Gupta, F. R. Fronczek, *J. Org. Chem.* **1983**, *48*, 4848–4851.

[116] Z. Wang, J. Reibenspies, R. J. Motekaitis, A. E. Martell, *J Chem Soc Dalton Trans* **1995**, 1511–1518.

[117] K. Binnemans, *Coord. Chem. Rev.* **2015**, *295*, 1–45.

[118] A. Beeby, I. M. Clarkson, R. S. Dickins, S. Faulkner, D. Parker, L. Royle, A. S. de Sousa, J. A. G. Williams, M. Woods, *J. Chem. Soc. Perkin Trans. 2* **1999**, 493–504.

A Appendix

A.1 NMR spectra

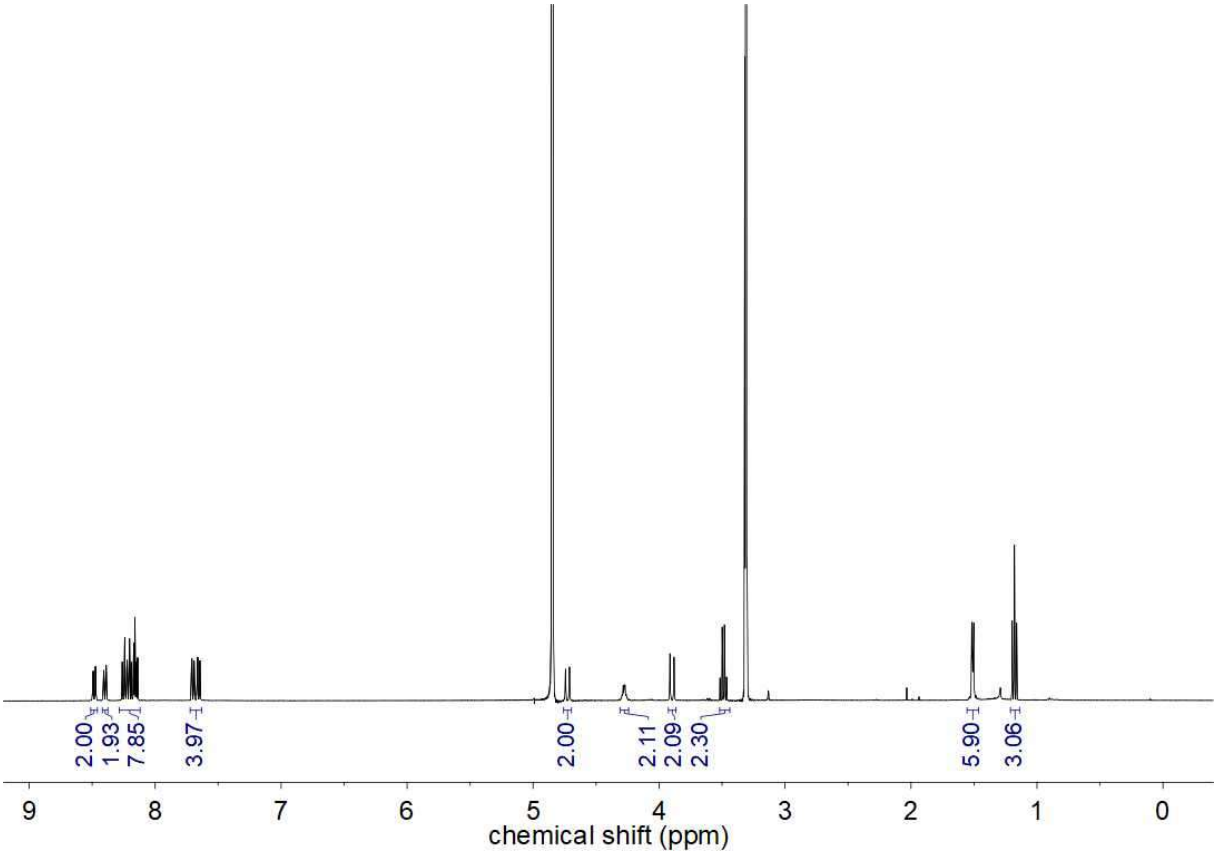

Figure A1. ^{1}H NMR (400 MHz, CD_3OD) spectrum of **D_8-(*R,R,R_a*)-6-Lu**.

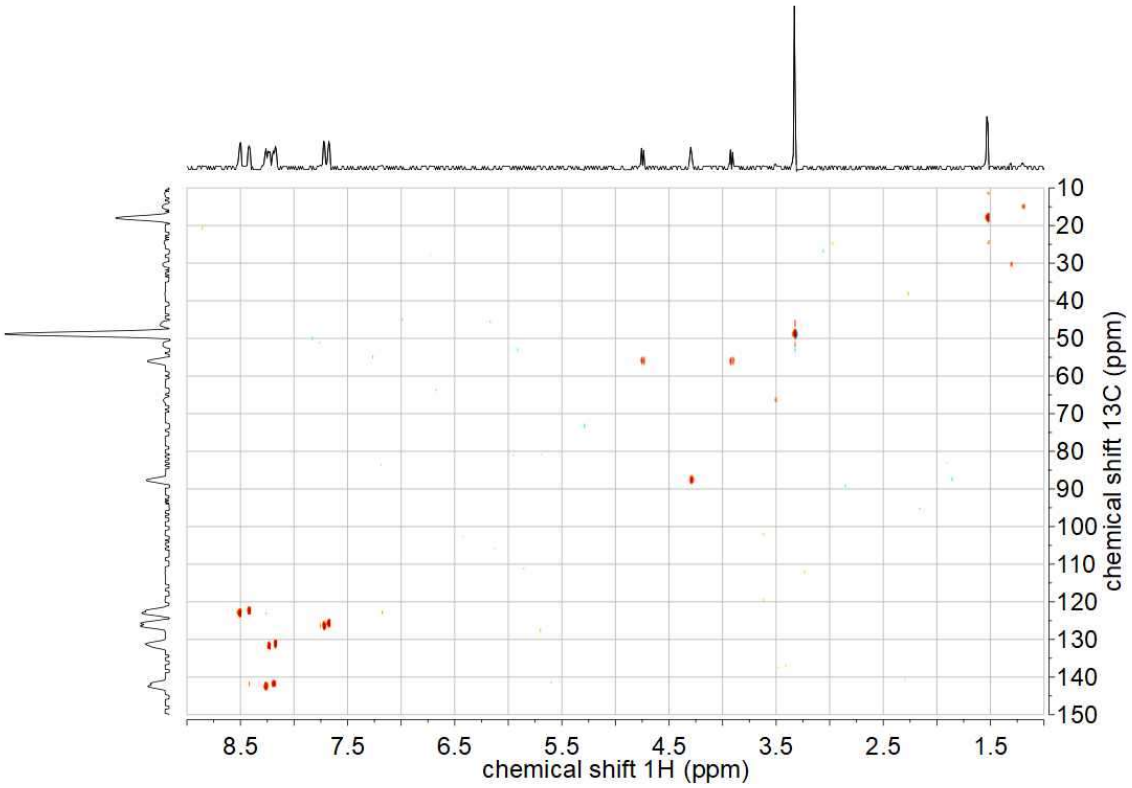

Figure A2. ^{1}H-^{13}C HSQC (^{1}H: 700 MHz, CD_3OD) spectrum of **D_8-(*R,R,R$_a$*)-6-Lu**. Projections obtained from the 2D spectrum (no high-resolution 1D spectrum).

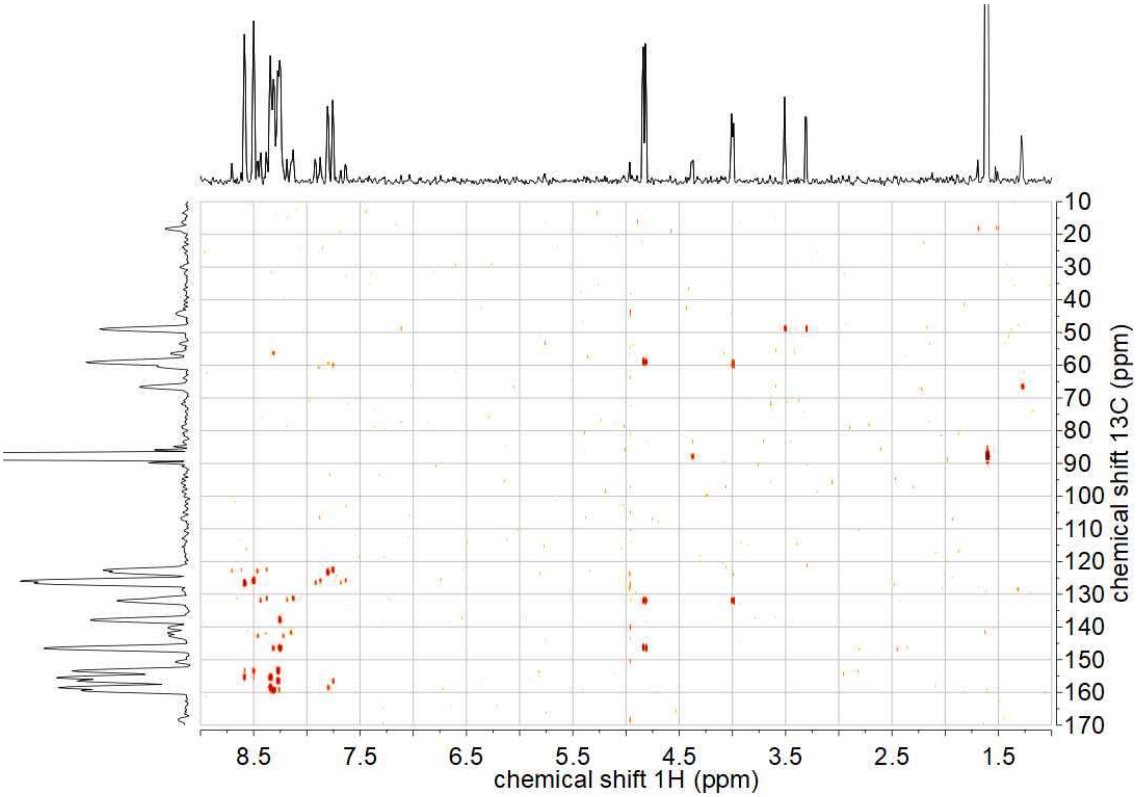

Figure A3. ^{1}H-^{13}C HMBC (^{1}H: 700 MHz, CD_3OD) spectrum of **D_8-(*R,R,R$_a$*)-6-Lu**. Projections obtained from the 2D spectrum (no high-resolution 1D spectrum).

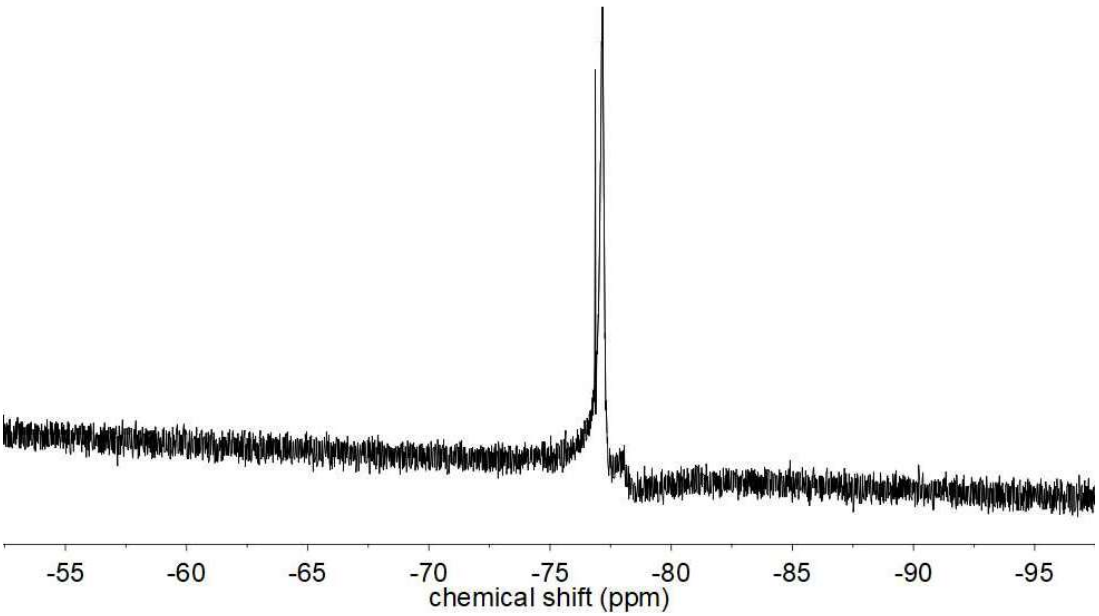

Figure A4. ^{19}F NMR (283 MHz, CD_3OD) spectrum of **D_8-(*R,R,R$_a$*)-6-Lu**.

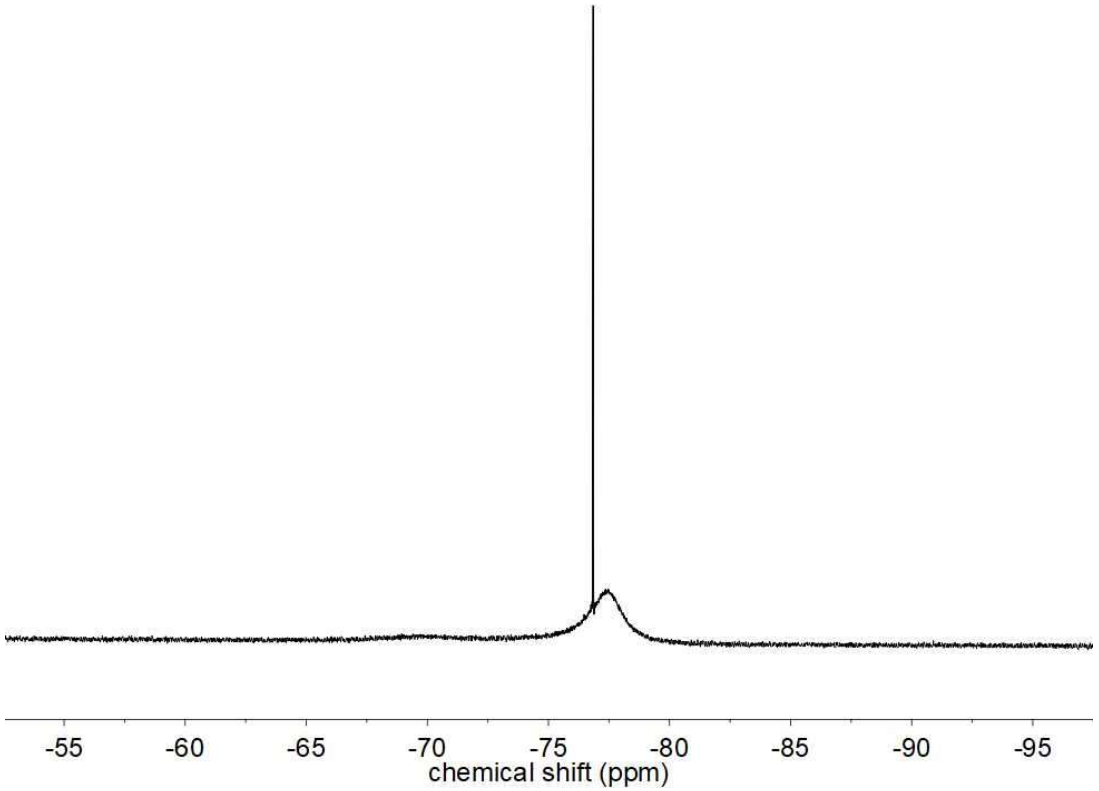

Figure A5. ^{19}F NMR (283 MHz, CD_3OD) spectrum of **D_8-(*R,R,R$_a$*)-6-Tb**.

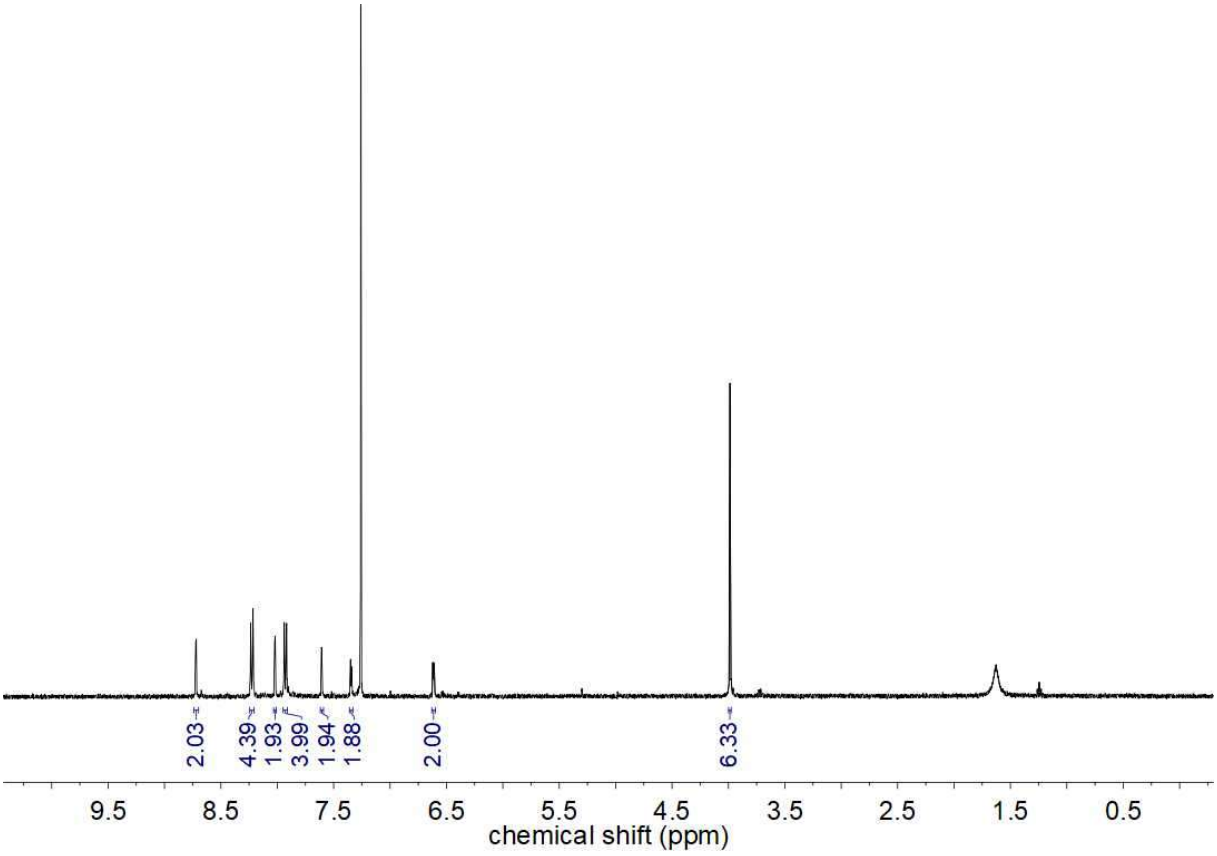

Figure A6: ^{1}H NMR spectrum (400 MHz, $CDCl_3$) of bipyridine **15**.

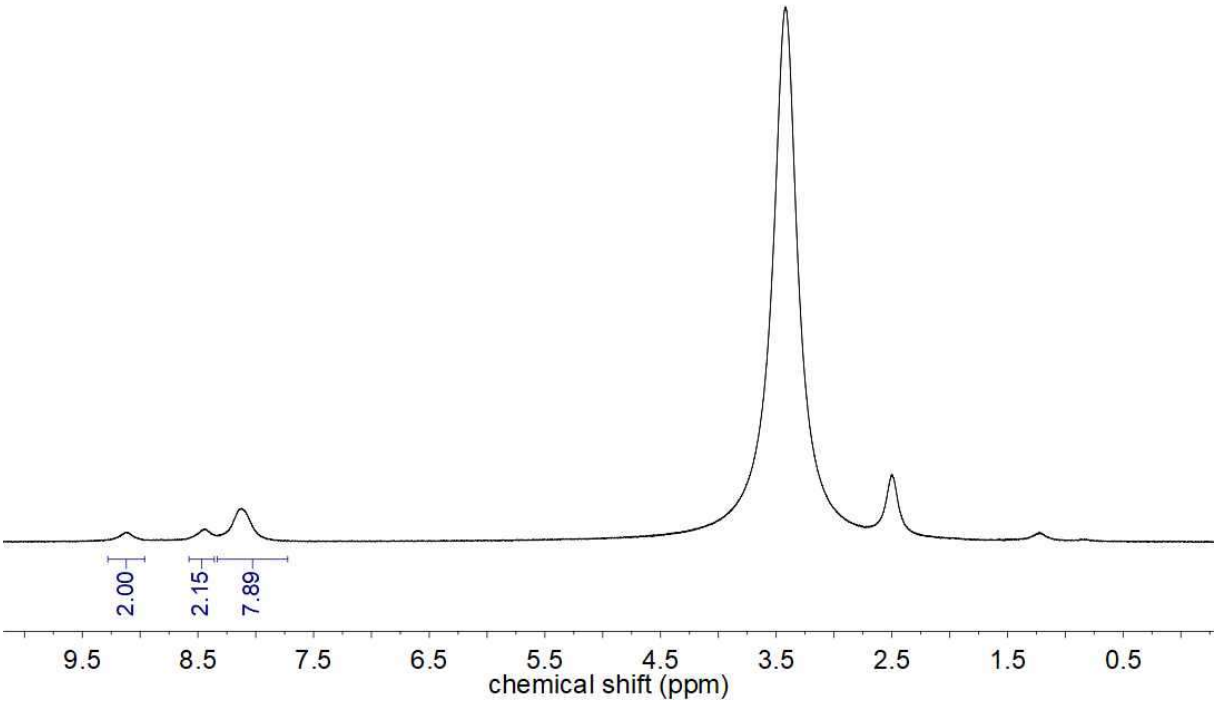

Figure A7: ^{1}H NMR ($(CD_3)_2SO$, 400 MHz) spectrum of tetracarboxylic acid **16.**

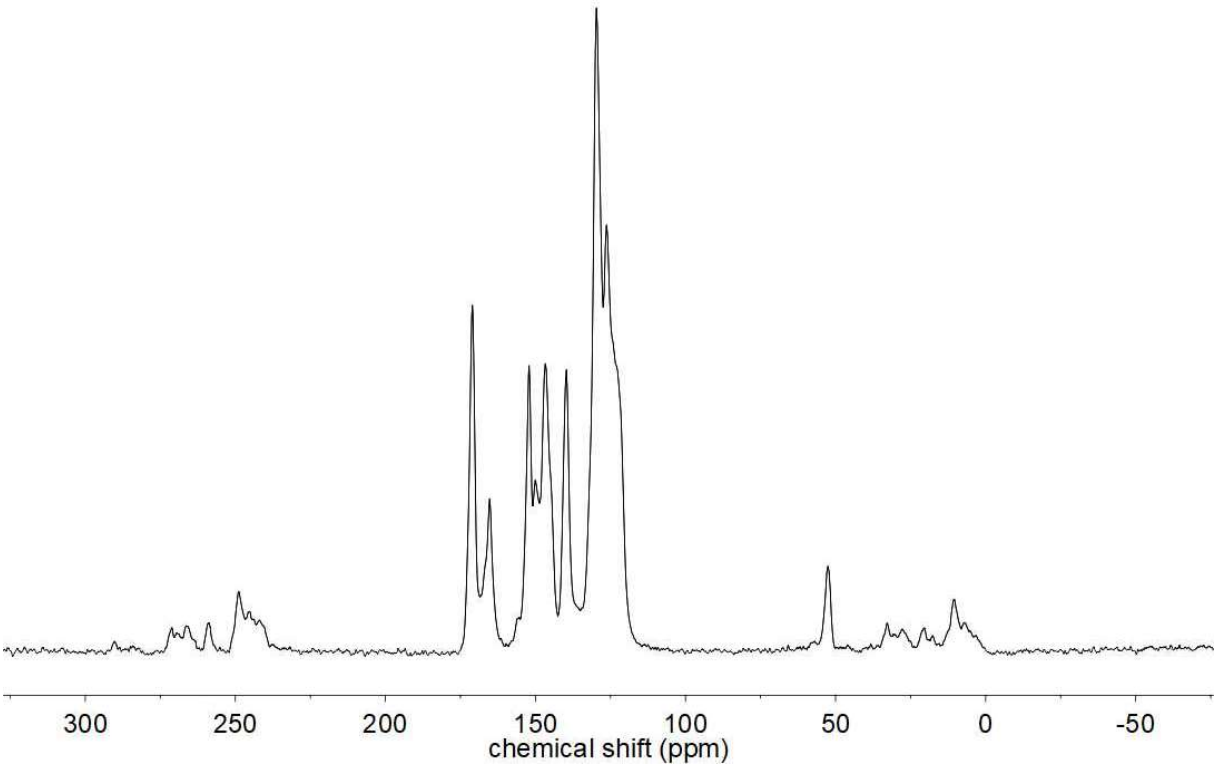

Figure A8: ^{13}C NMR (125 MHz) spectrum in solid state of tetracarboxylic acid **16**.

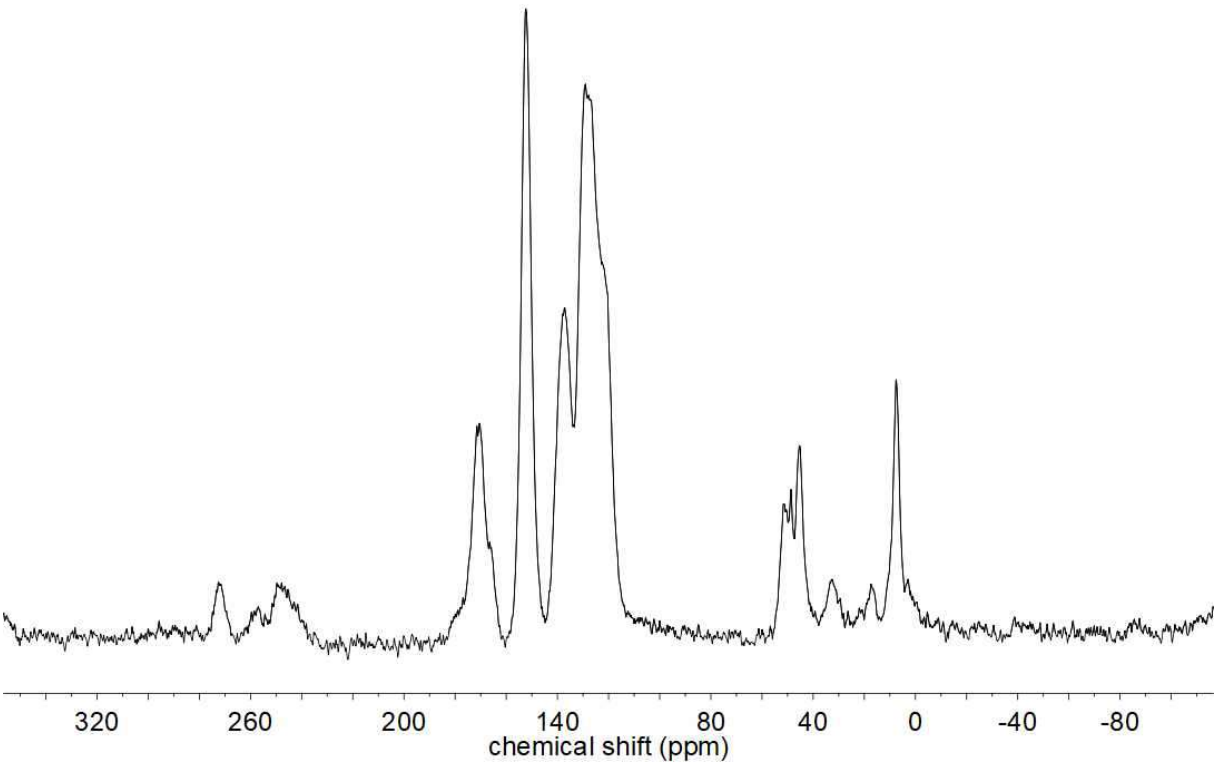

Figure A9: ^{13}C NMR (125 MHz) spectrum in solid state of **17-Lu/Lu**.

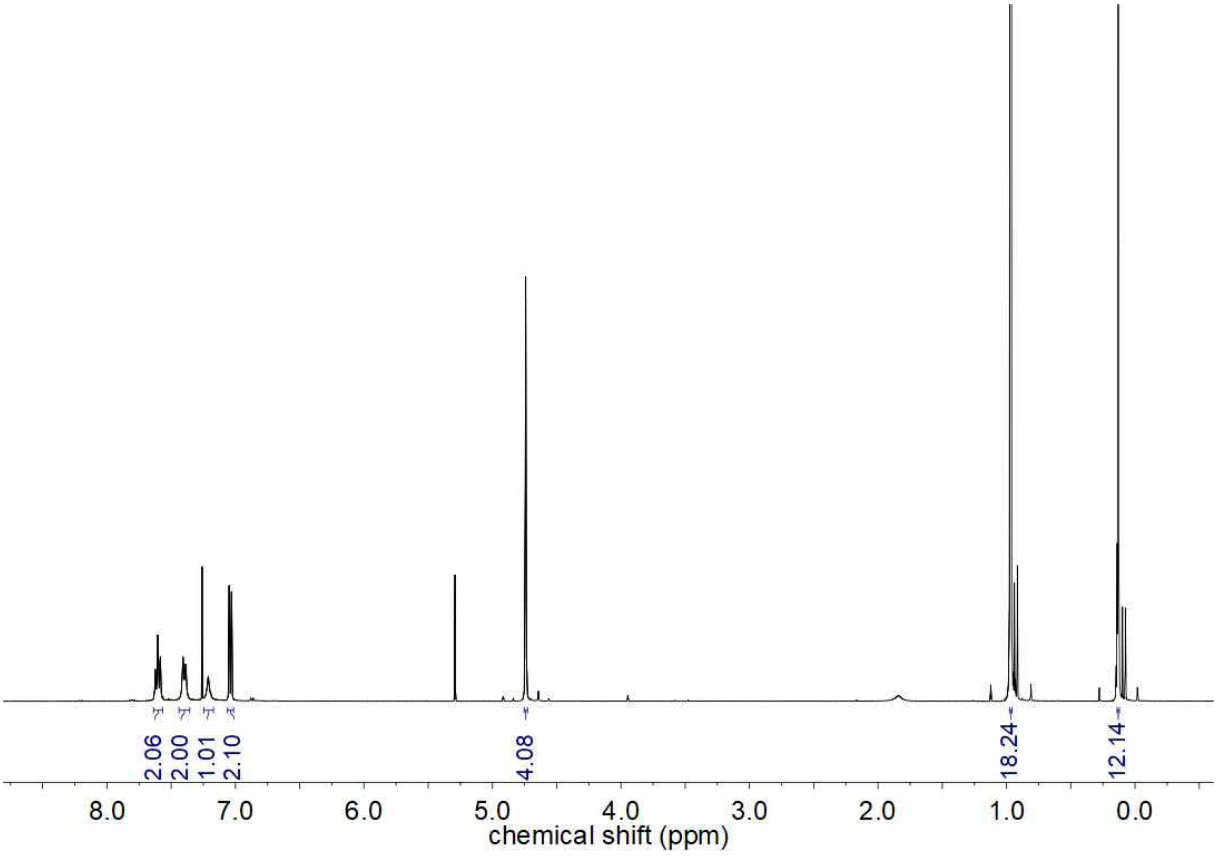

Figure A10: ^{1}H NMR spectrum (400 MHz, $CDCl_3$) of dipyridylamine **23**.

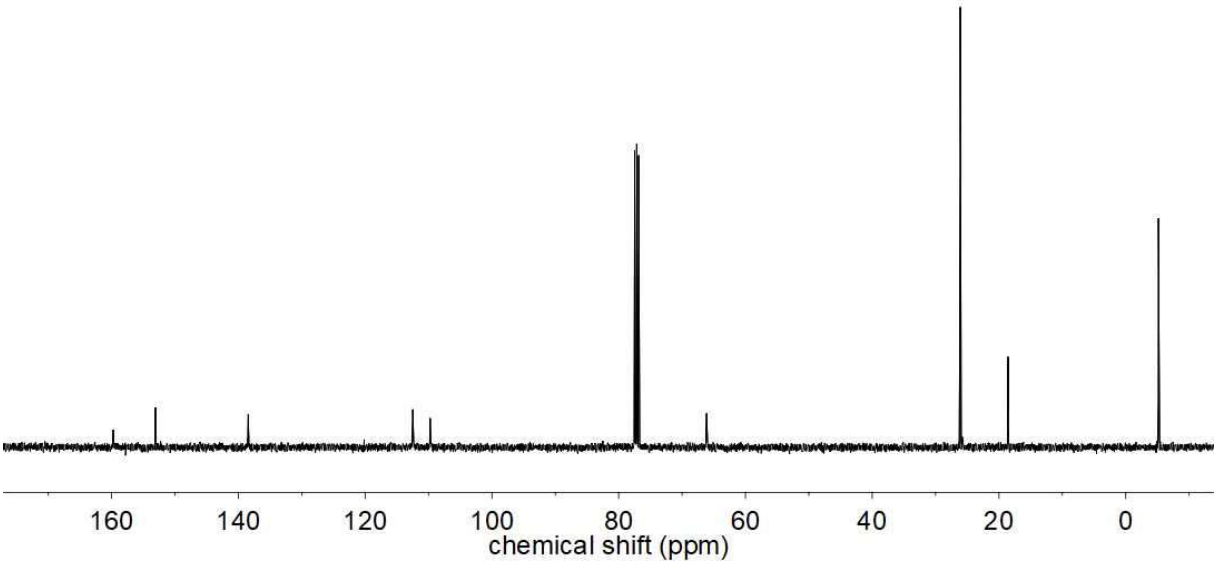

Figure A11: ^{13}C NMR spectrum (101 MHz, $CDCl_3$) of dipyridylamine **23**.

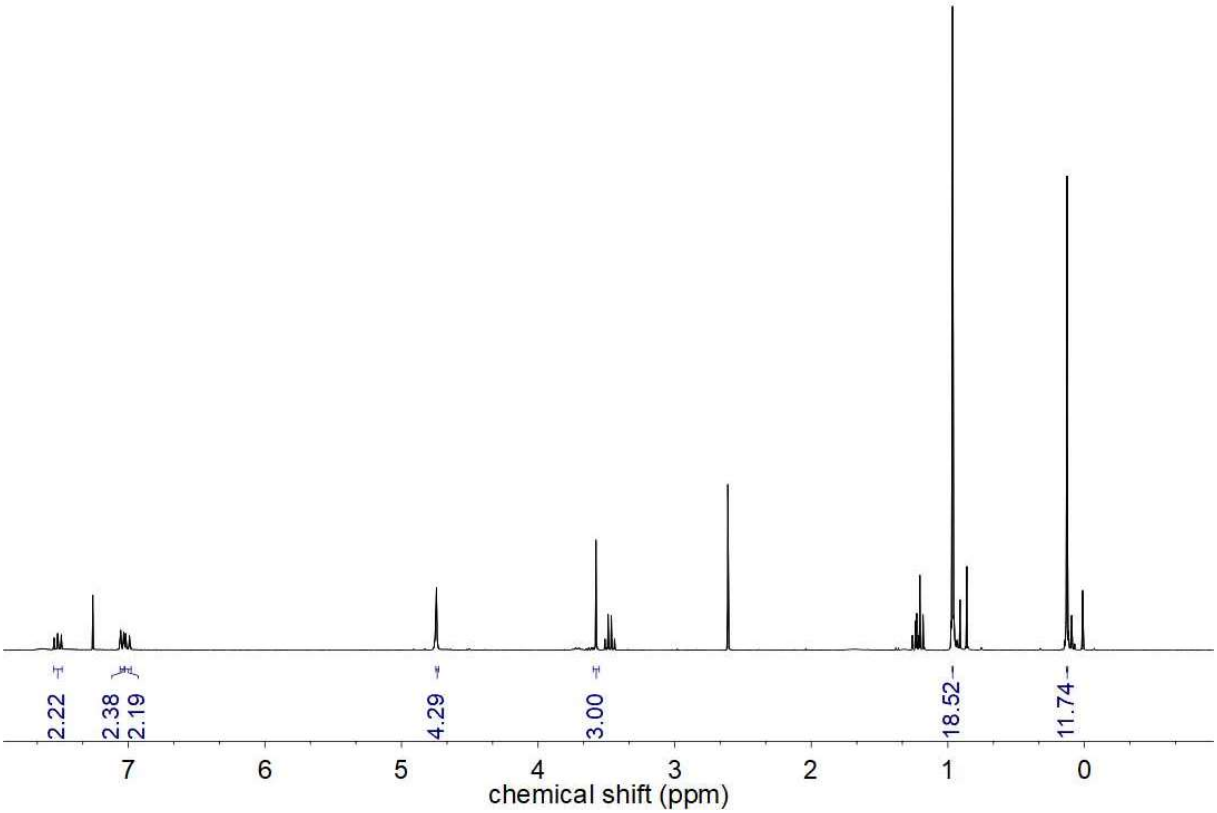

Figure A12: ^{1}H NMR spectrum (300 MHz, $CDCl_3$) of dipyridylmethylamine **24**.

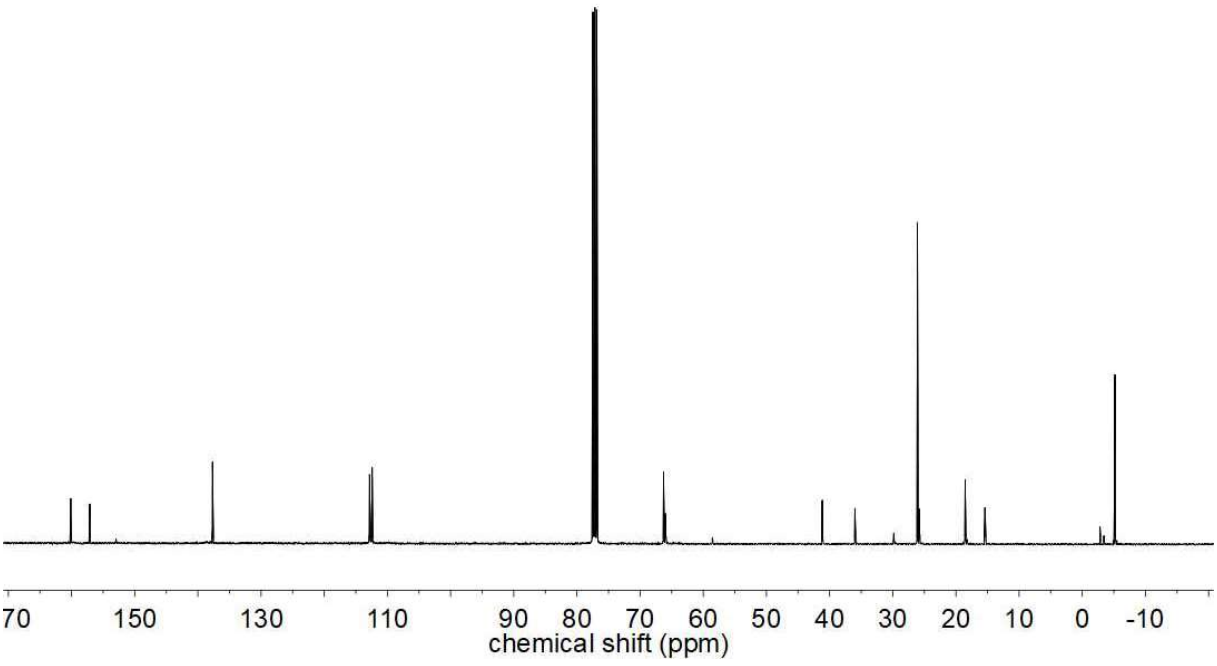

Figure A13: ^{13}C NMR spectrum (101 MHz, $CDCl_3$) of dipyridylmethylamine **24**.

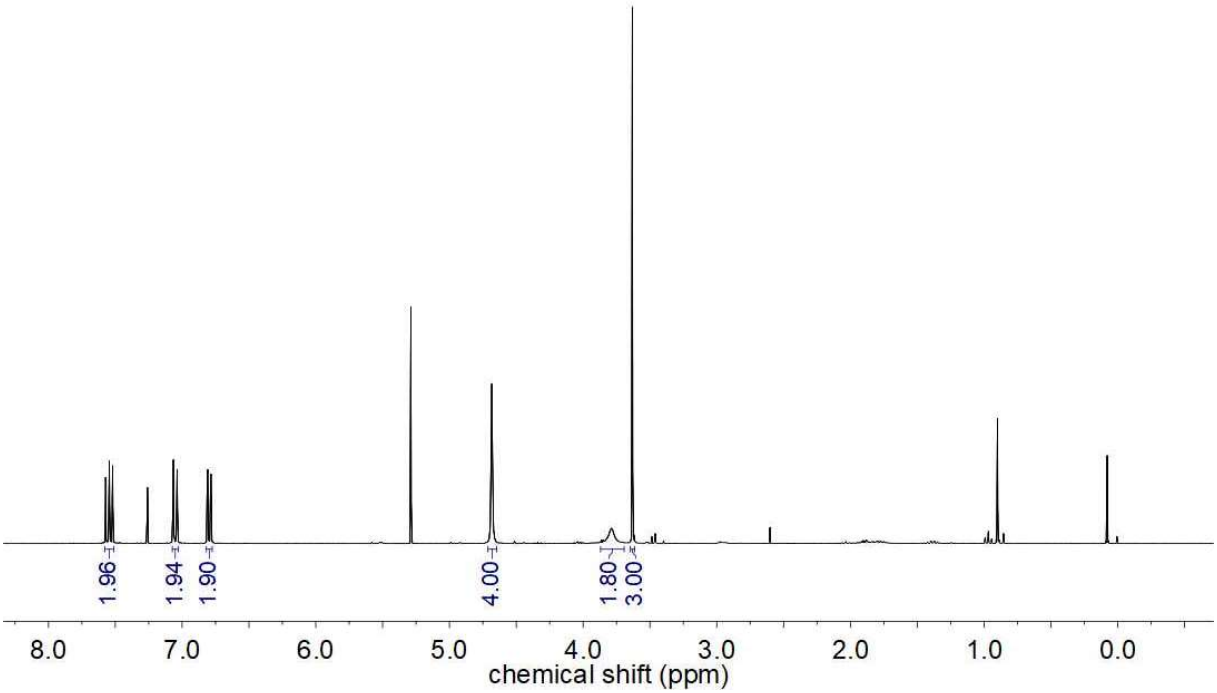

Figure A14: ^{1}H NMR spectrum (300 MHz, $CDCl_3$) of diol **25**.

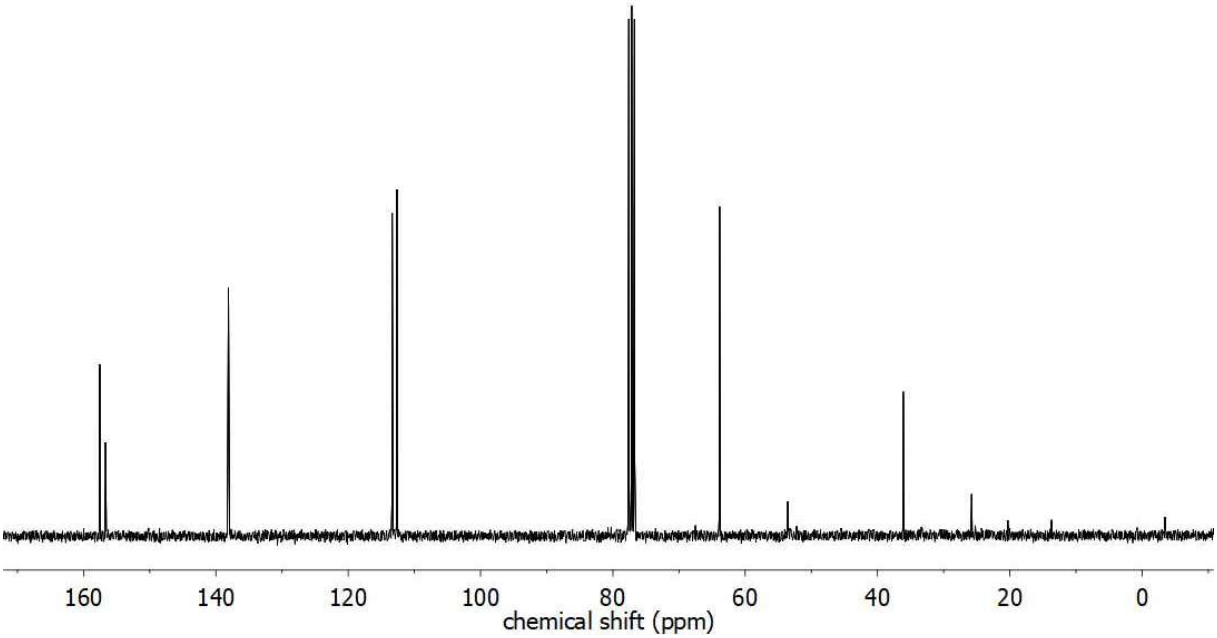

Figure A15: ^{13}C NMR spectrum (75 MHz, $CDCl_3$) of diol **25**.

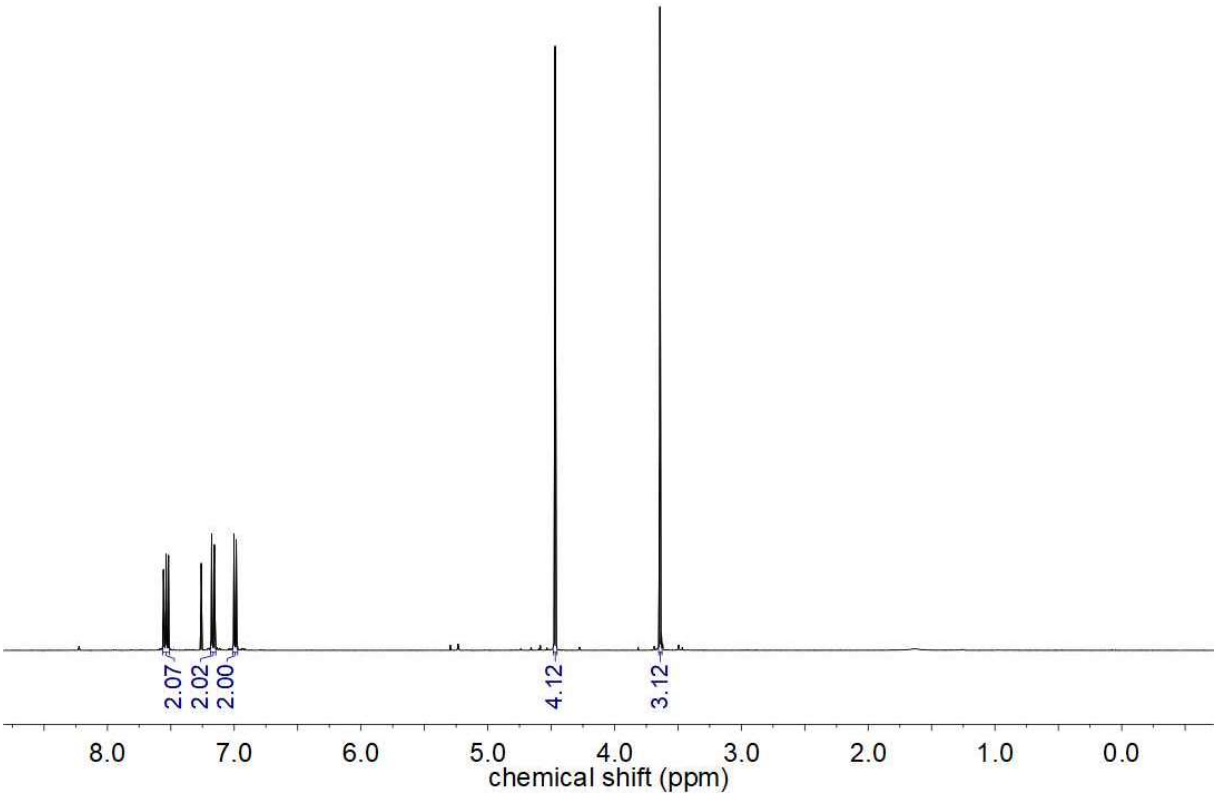

Figure A16: ^{1}H NMR spectrum (400 MHz, $CDCl_3$) of dibromide **26**.

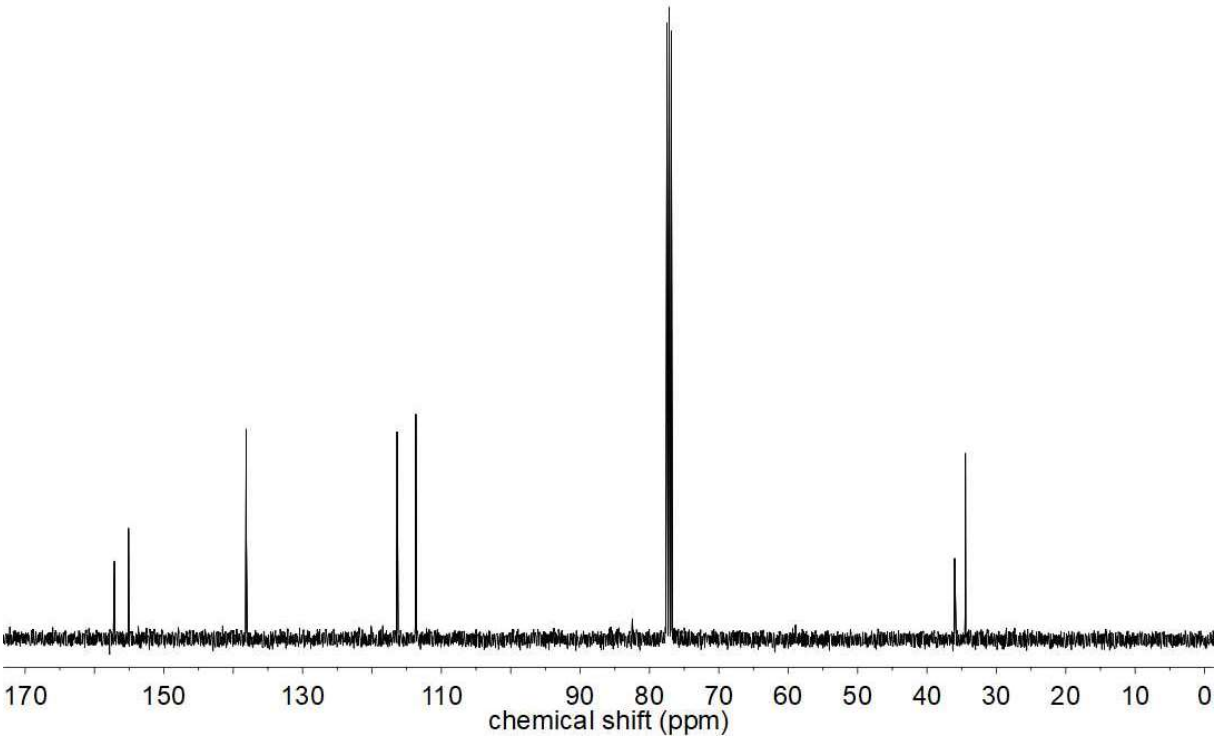

Figure A17: ^{13}C NMR spectrum (101 MHz, $CDCl_3$) of dibromide **26**.

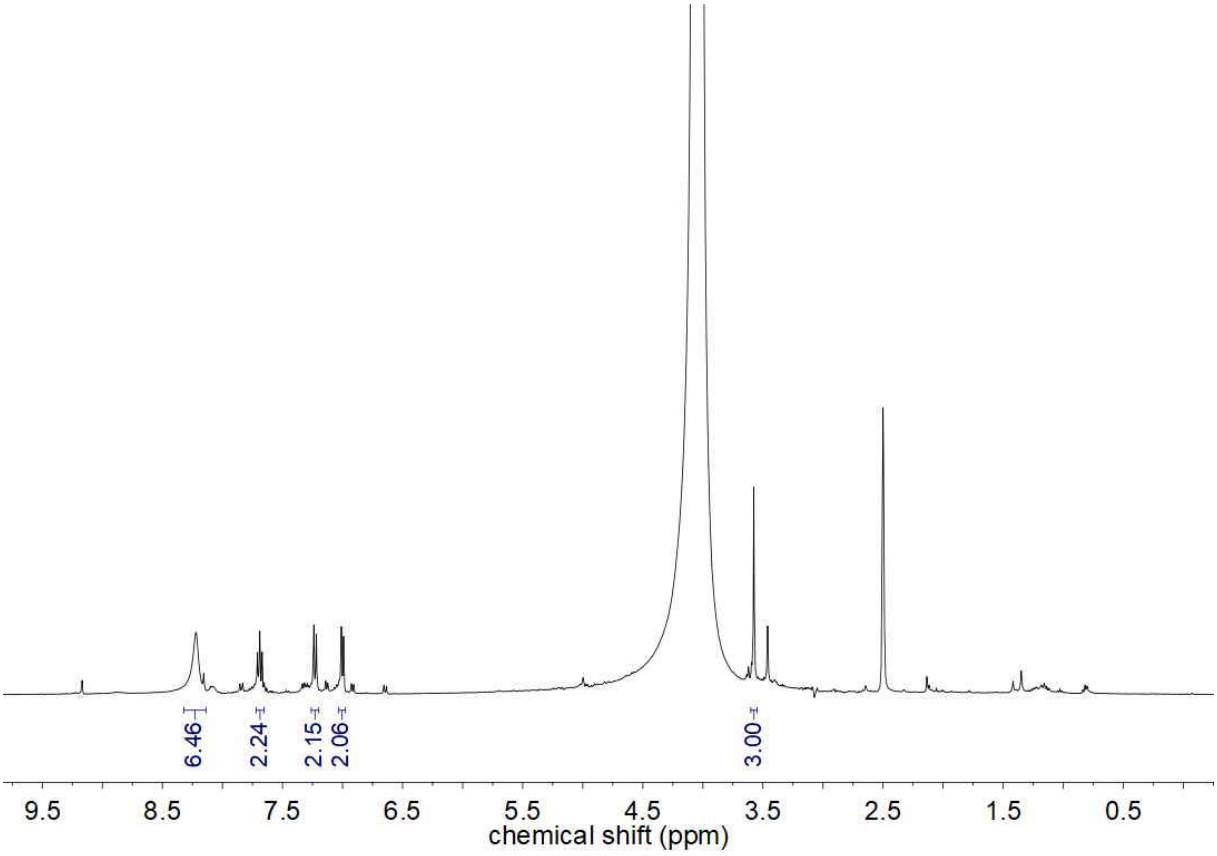

Figure A18: ^{1}H NMR spectrum (400 MHz, $(CD_3)_2SO$) of diamine **27**.

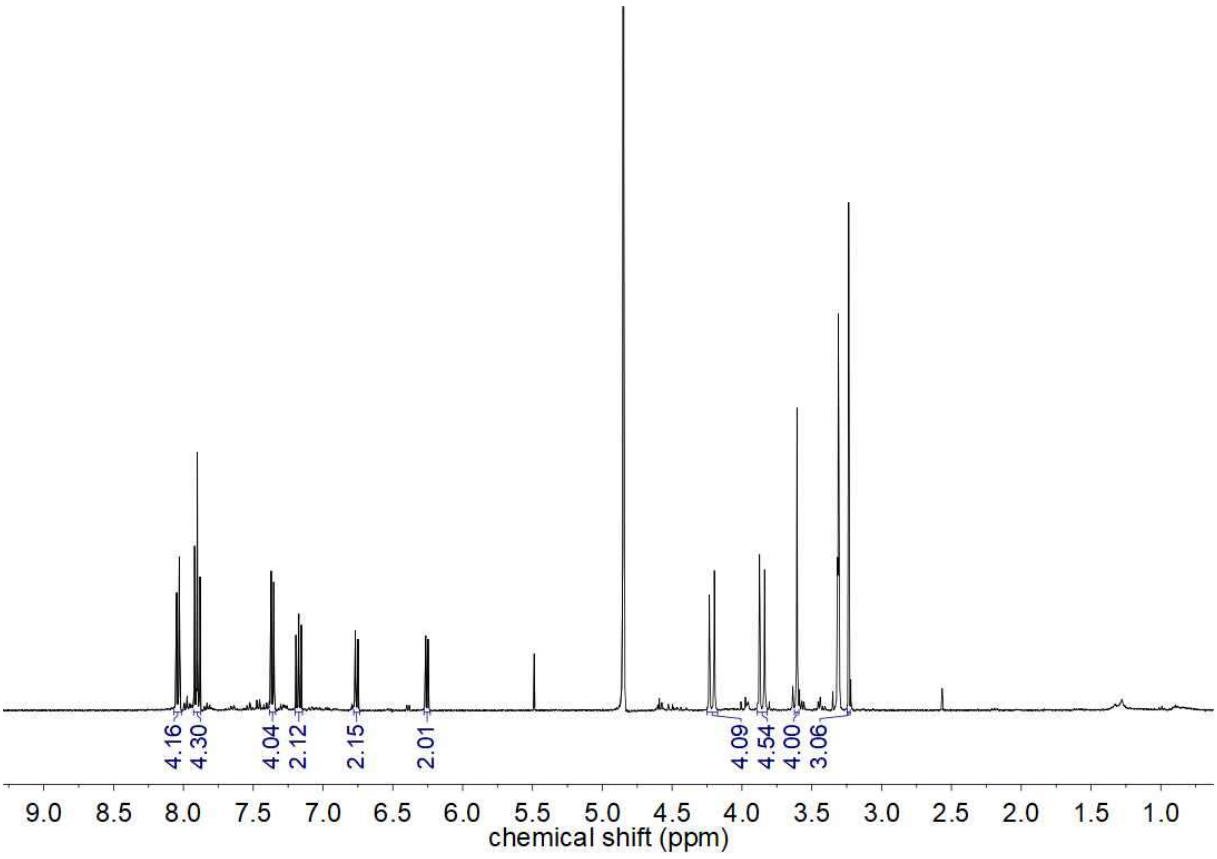

Figure A19: ^{1}H NMR spectrum (400 MHz, CD_3OD) of **18-Na**.

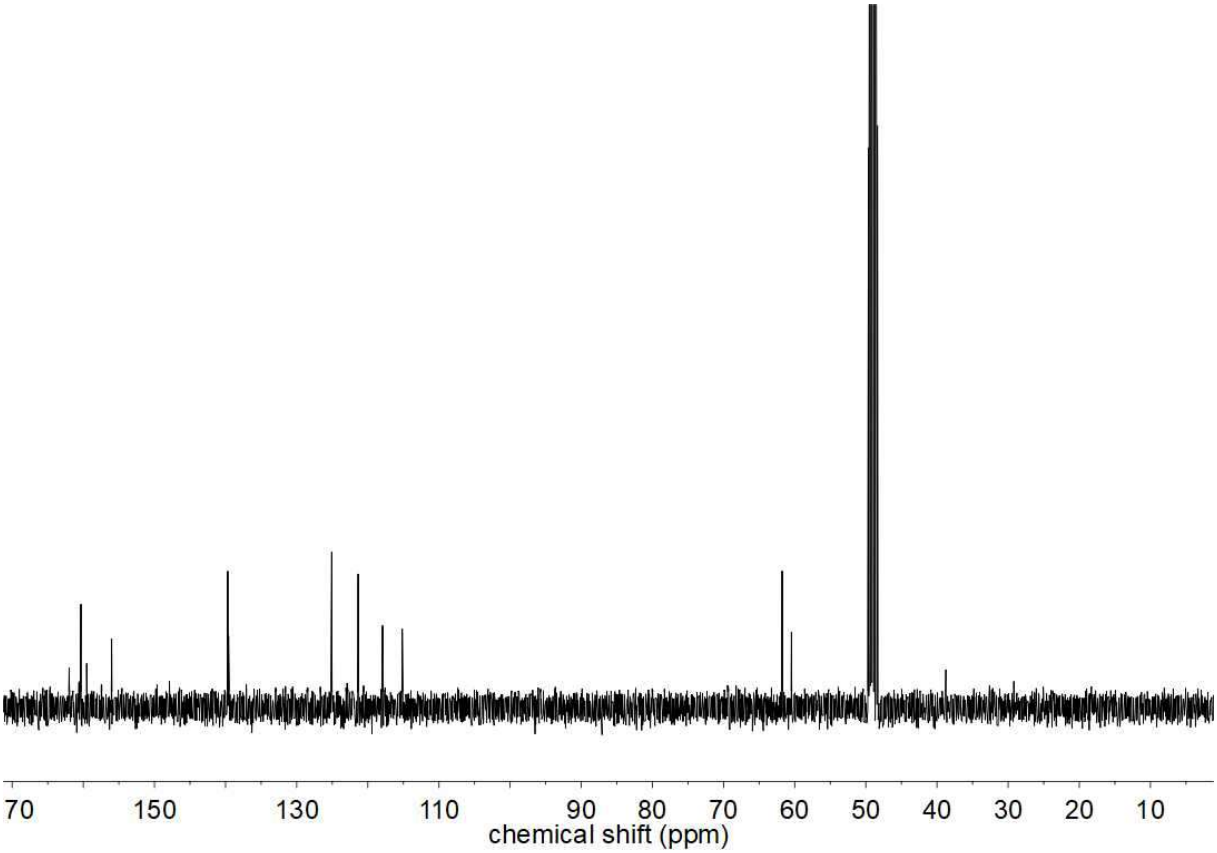

Figure A20: ^{13}C NMR spectrum (101 MHz, $CDCl_3$) of **18-Na**.

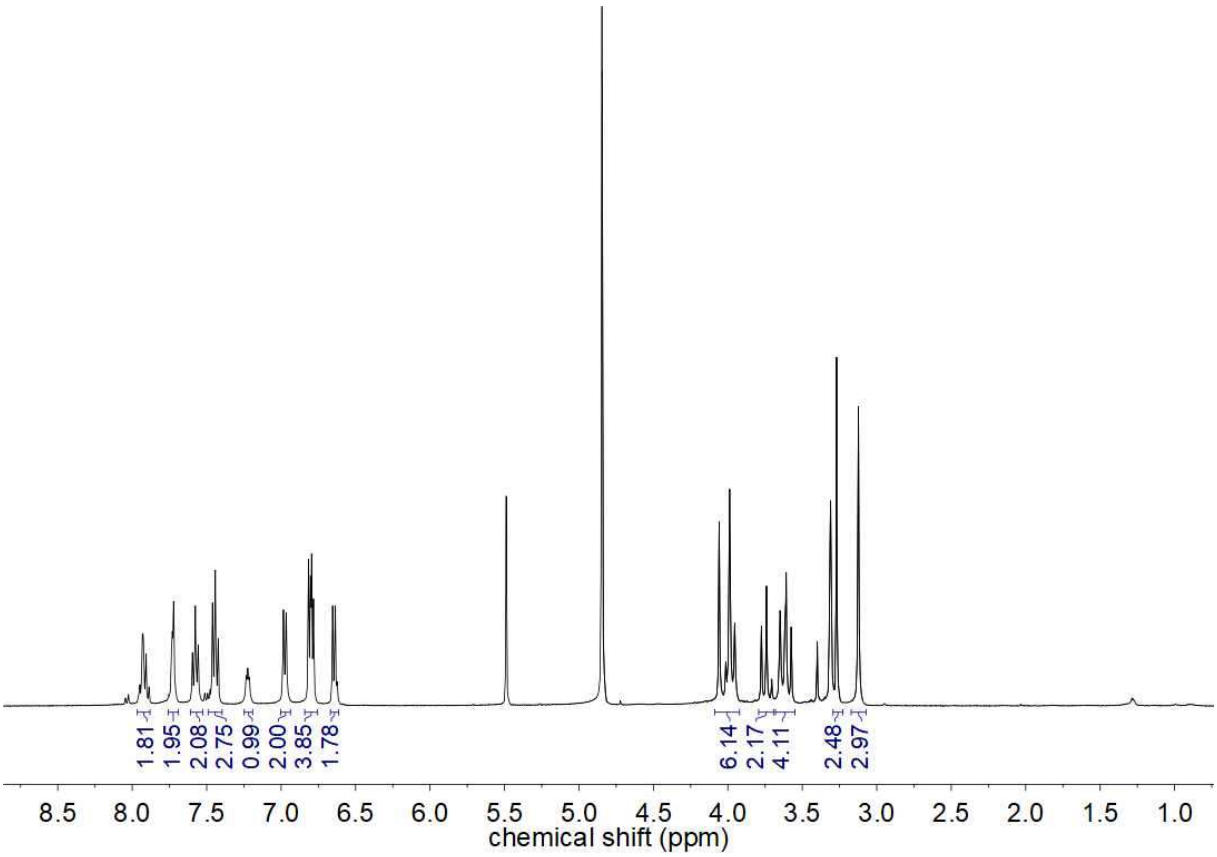

Figure A21: ^{1}H NMR spectrum (400 MHz, CD_3OD) of **19-Na**.

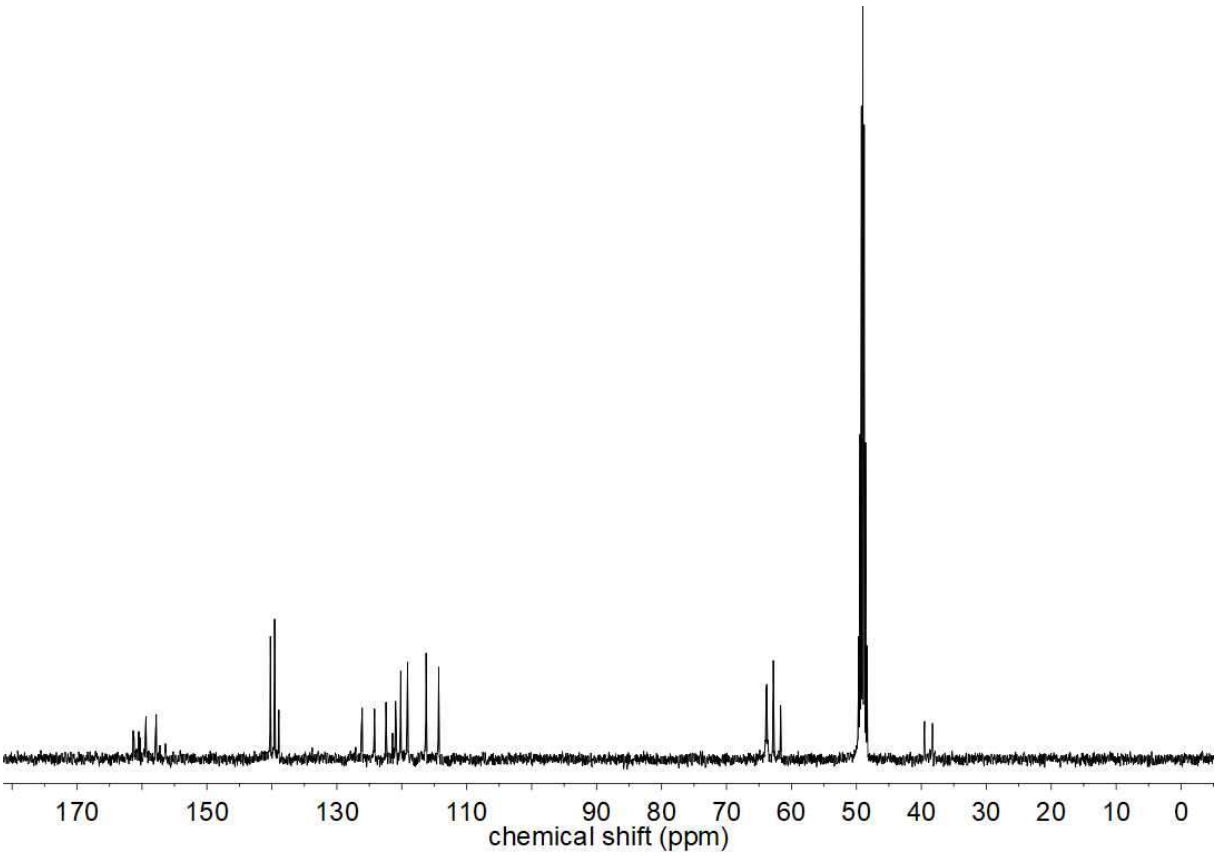

Figure A22: ^{13}C NMR spectrum (101 MHz, CD_3OD) of **19-Na**.

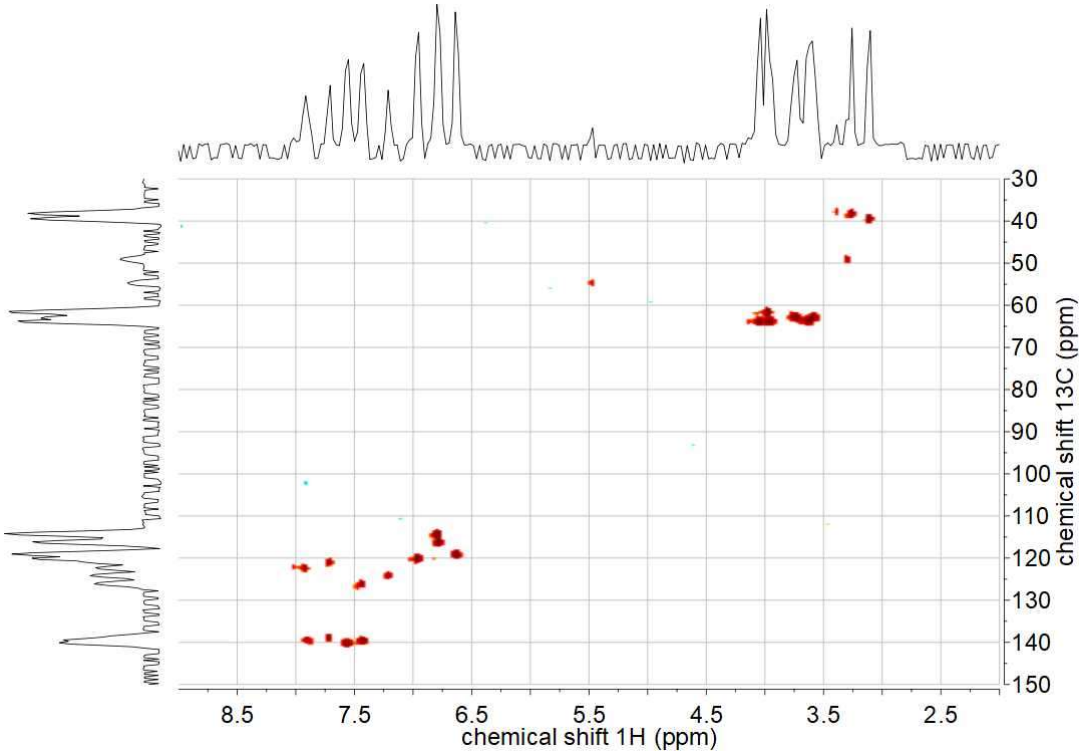

Figure A23: ^{1}H-^{13}C HSQC (^{1}H: 400 MHz, CD_3OD) spectrum of **19-Na**. Projections obtained from the 2D spectrum (no high-resolution 1D spectrum).

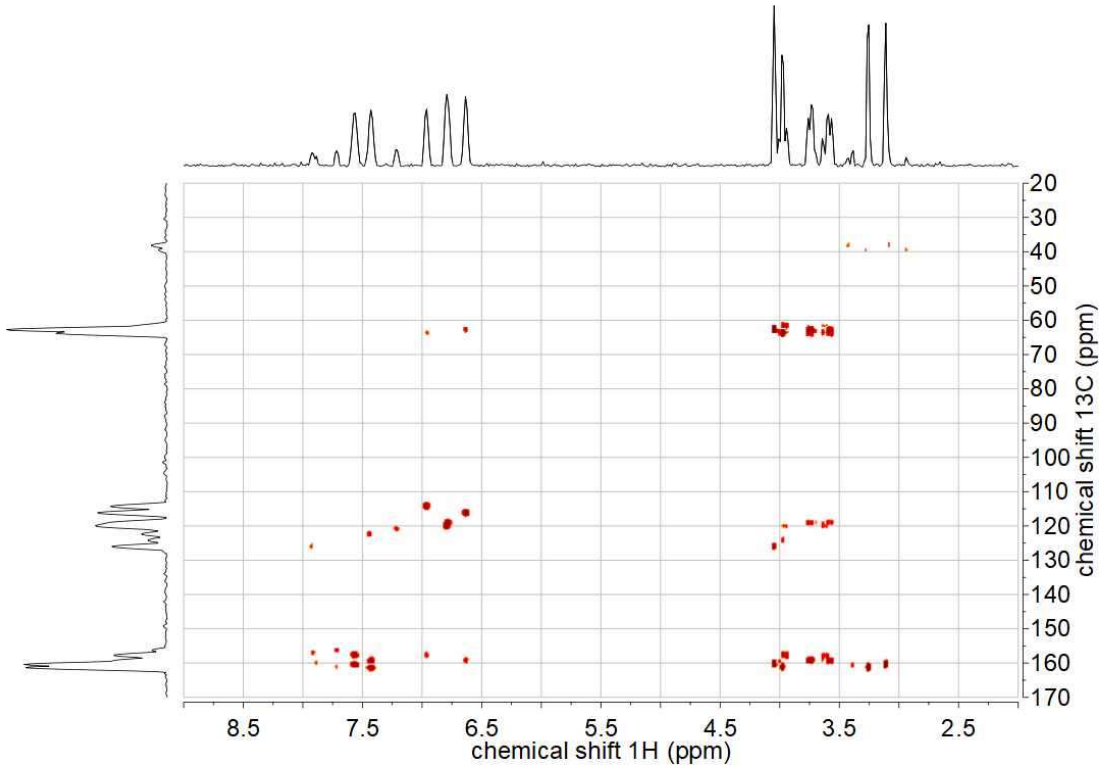

Figure A24: ^{1}H-^{13}C HMBC (^{1}H: 400 MHz, CD_3OD) spectrum of **19-Na**. Projections obtained from the 2D spectrum (no high-resolution 1D spectrum).

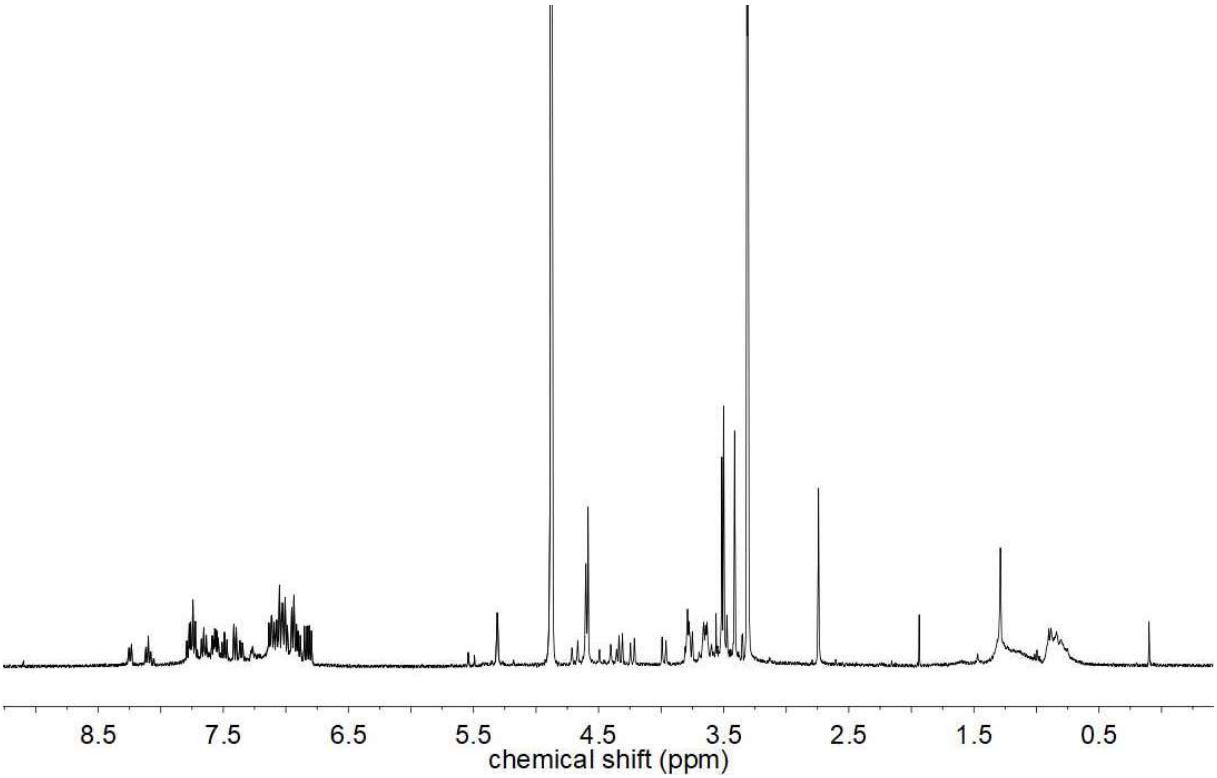

Figure A25: ^{1}H NMR spectrum (400 MHz, CD_3OD) of **20-Na**.

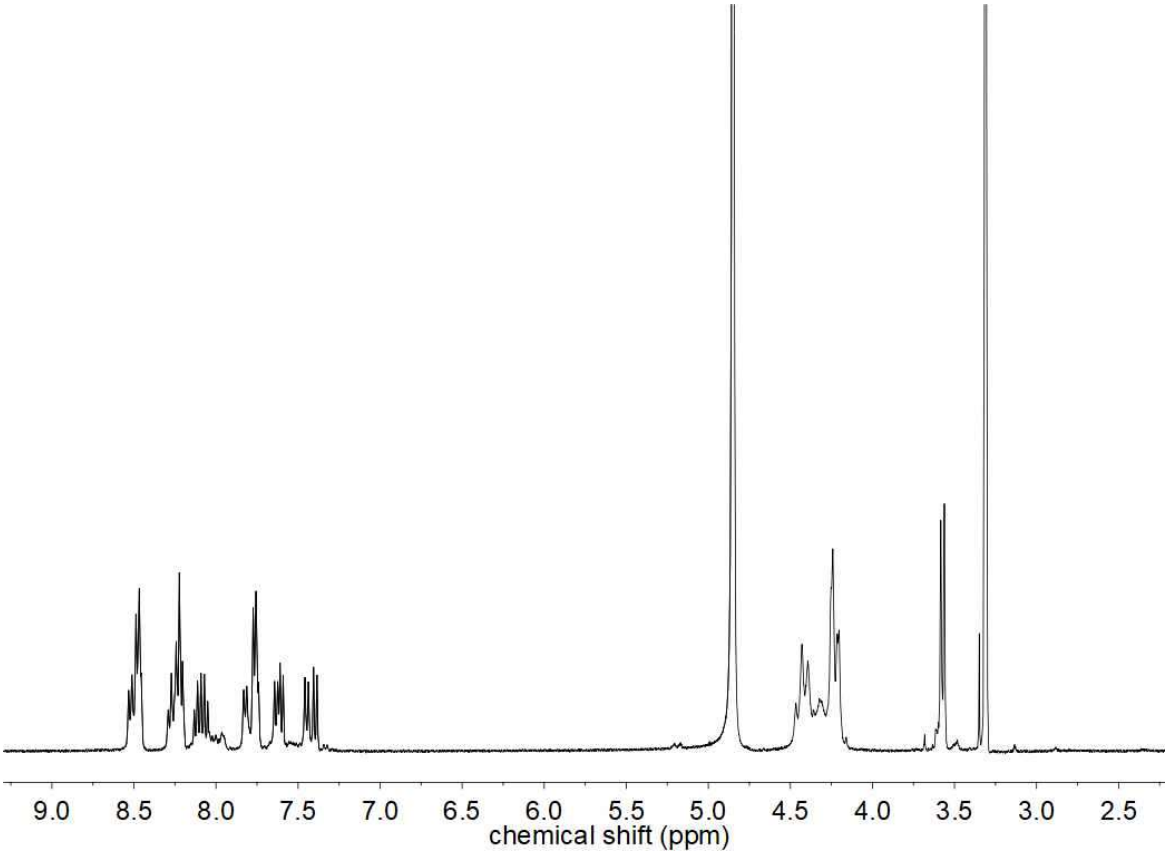

Figure A26: ^{1}H NMR spectrum (400 MHz, CD_3OD) of **18-Lu**.

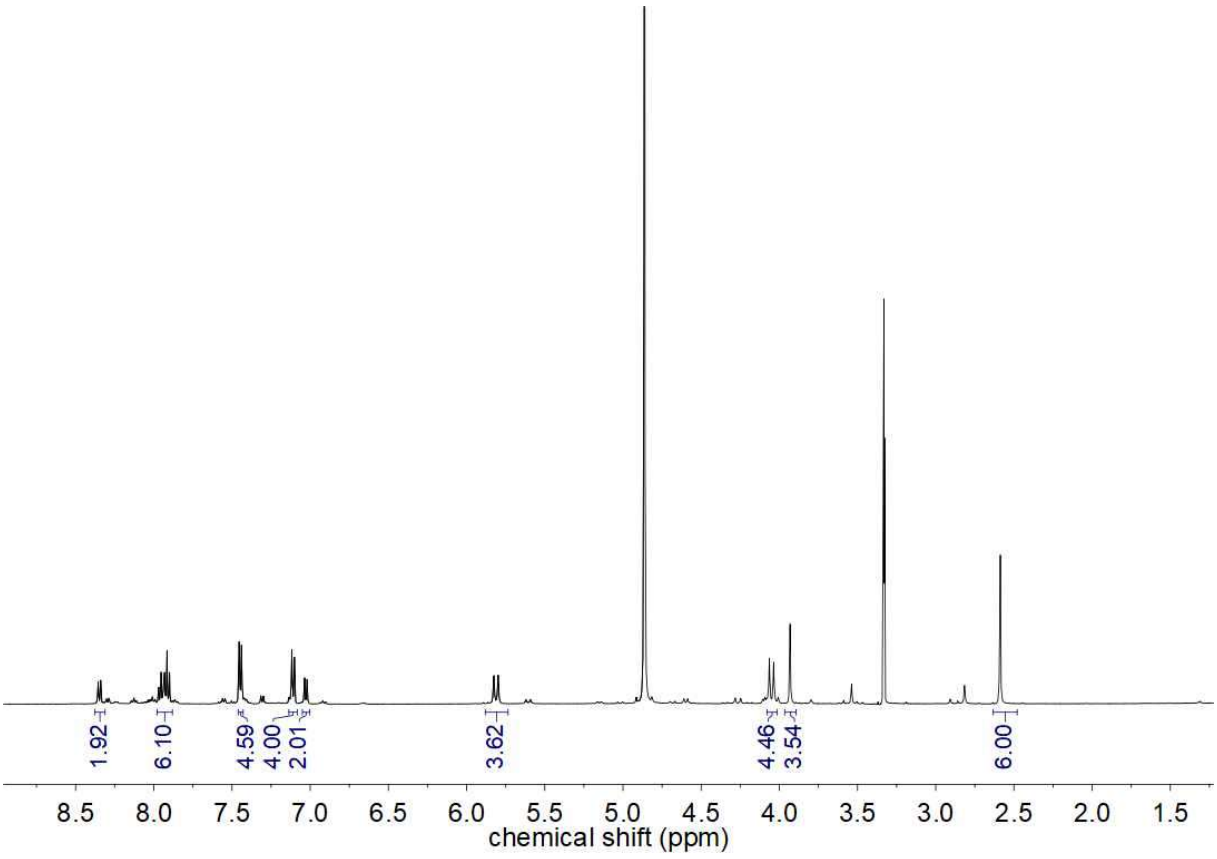

Figure A27: ^{1}H NMR spectrum (500 MHz, CD_3OD) of **19-Lu**.

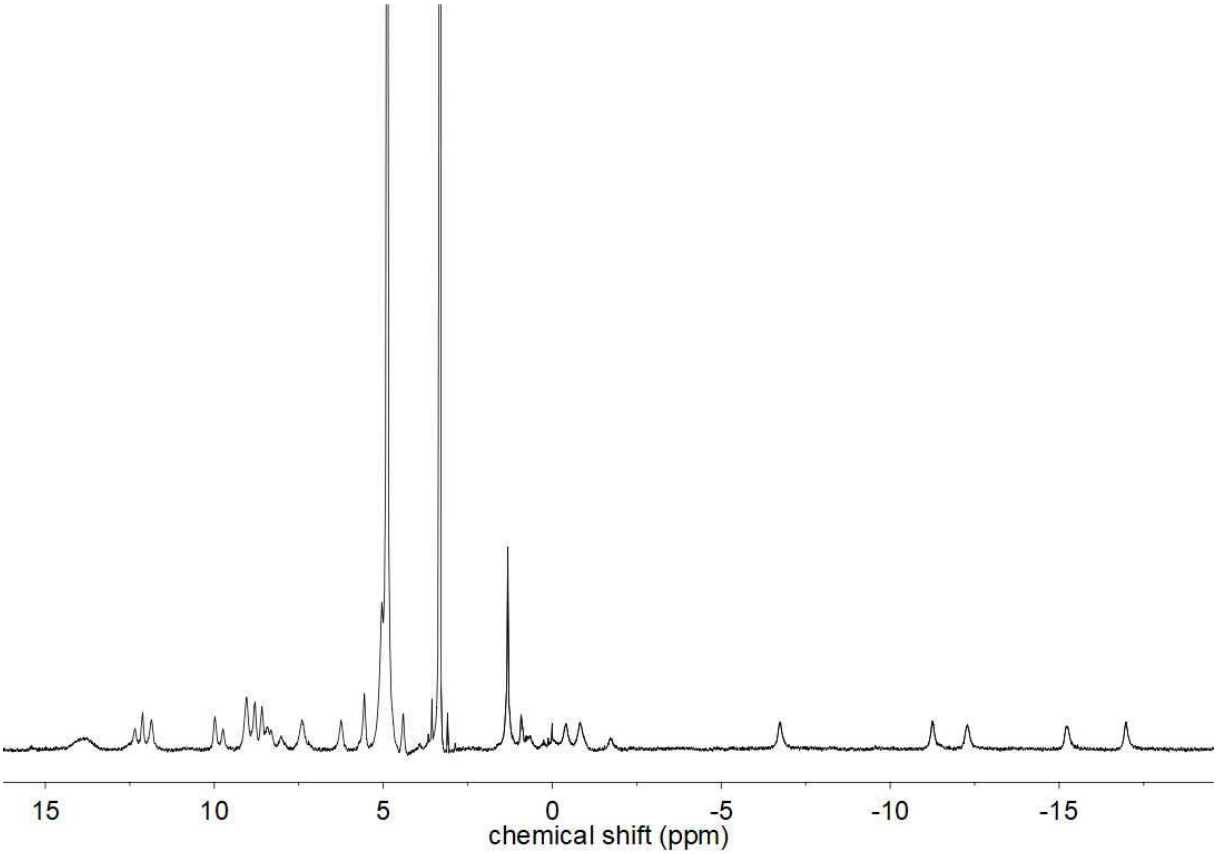

Figure A28: ^{1}H NMR spectrum (500 MHz, CD_3OD) of **18-Eu**.

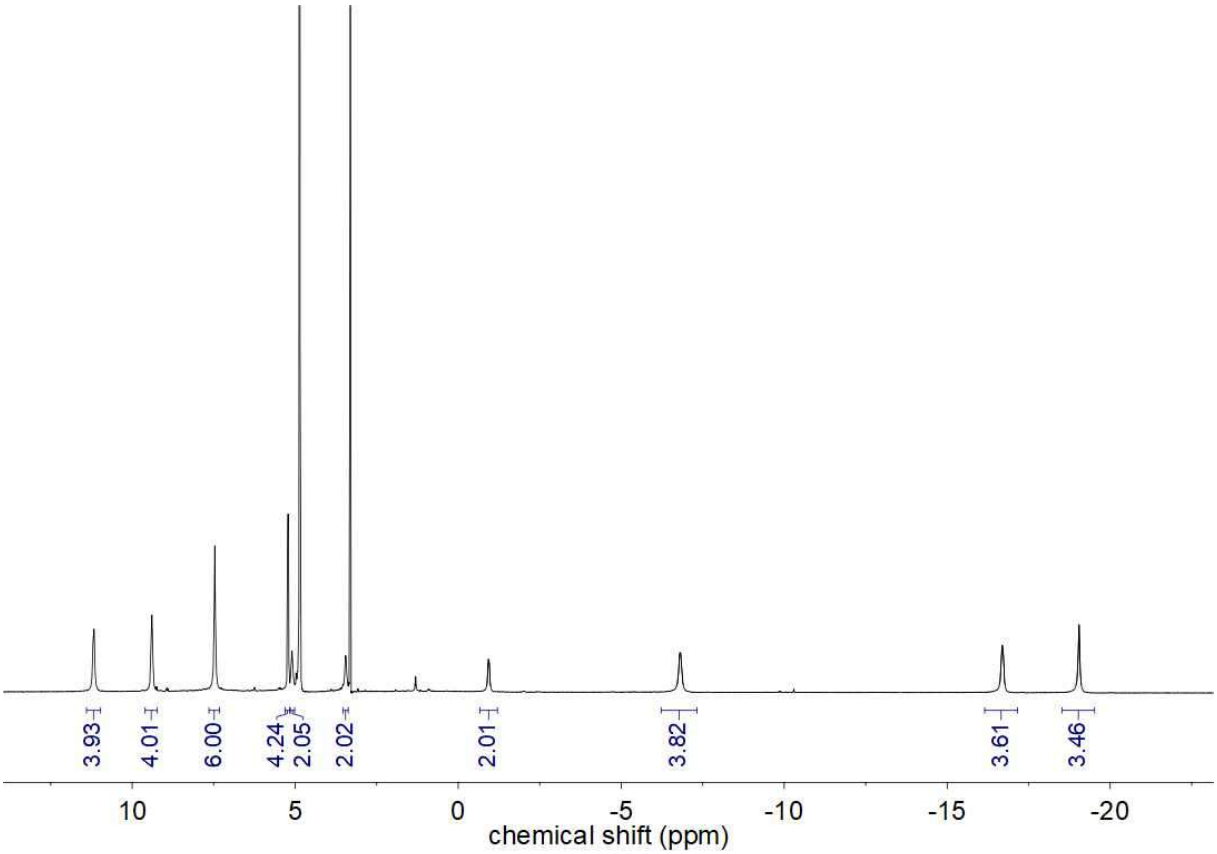

Figure A29: ^{1}H NMR spectrum (300 MHz, CD_3OD) of **19-Eu**.

A.2 HPLC traces

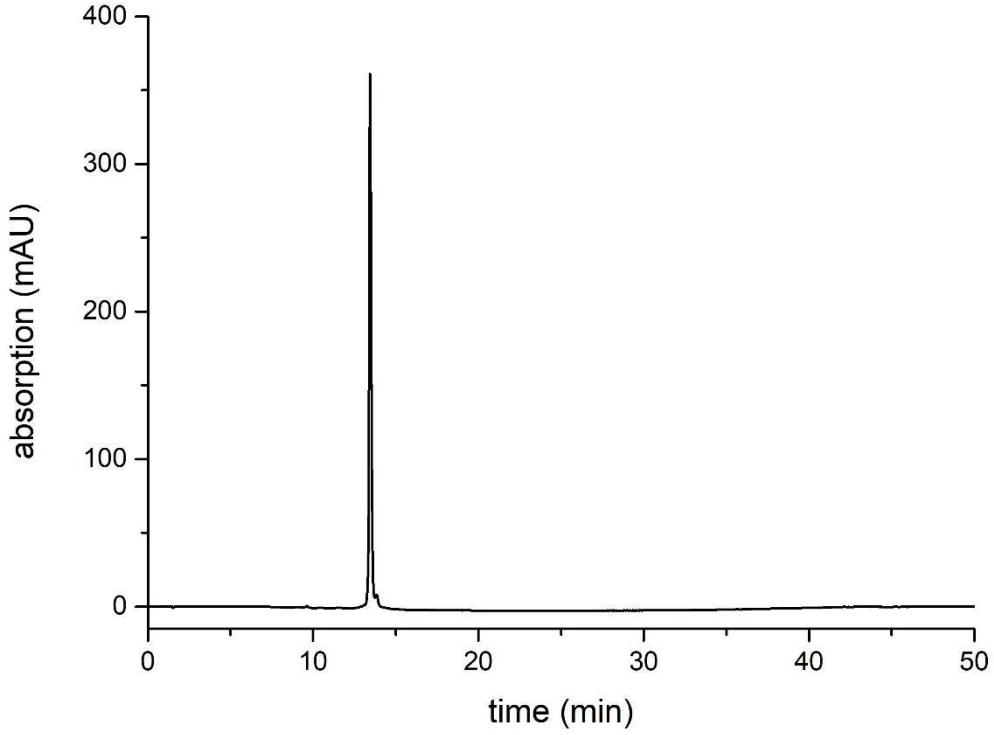

Figure A30. Analytical HPLC chromatogram of **D_8-(*R,R,R$_a$*)-6-Lu**.

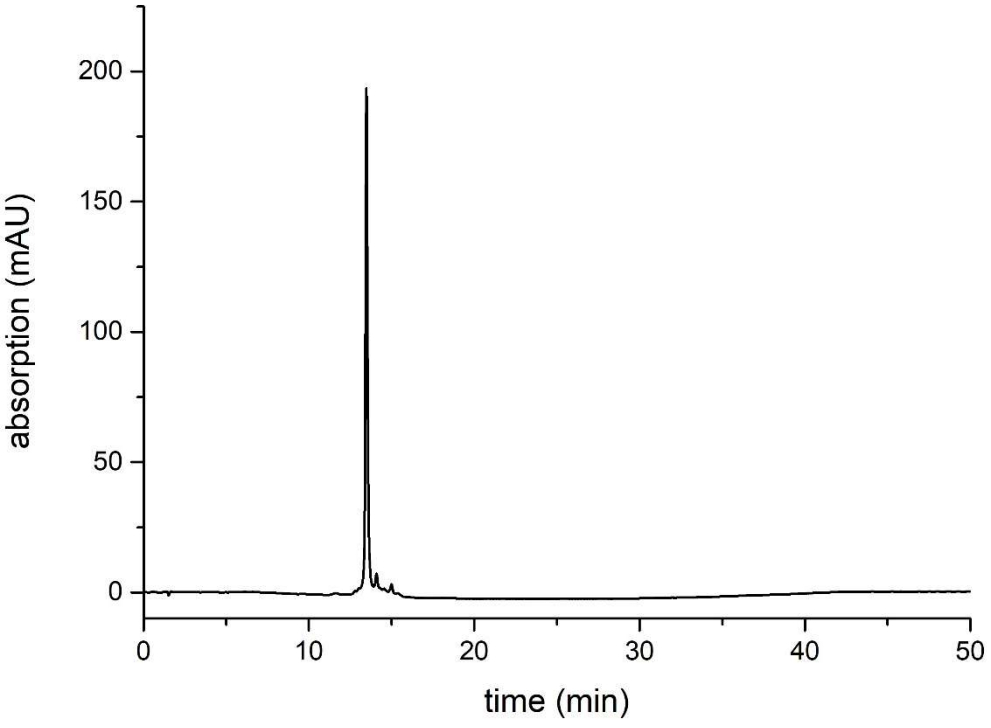

Figure A31. Analytical HPLC chromatogram of **D_8-(*R,R,R$_a$*)-6-Tb**.

Inorganic Chemistry

Communication

pubs.acs.org/IC

Chiral Resolution of Lanthanoid Cryptates with Extreme Configurational Stability

Elisabeth Kreidt,[†] Carolin Dee,[†] and Michael Seitz*[,†]

[†]Institute of Inorganic Chemistry, University of Tübingen, Auf der Morgenstelle 18, 72076 Tübingen, Germany

Supporting Information

ABSTRACT: Chiral resolution is achieved for racemic tris(2,2′-bipyridine)-based lanthanoid cryptates by chiral HPLC. The resolved complexes exhibit very rare configurational stability under extreme conditions.

Chirality is one of the most fundamental aspects of chemistry. In this context, enantiopure metal complexes have long been recognized to play a crucial role in a wide variety of areas, most prominently in the recent past as catalysts in asymmetric catalysis. The archetypes of this class of compounds are octahedral tris(bidentate) complexes such as $[Ru(bpy)_3]^{n+}$, which in many instances can be chirally resolved and often show remarkable configurational stability in enantiopure form.[1] In contrast, lanthanoid complexes, due to their inherent kinetic lability and generally rather fluxional coordination sphere, rarely show similarly advantageous properties and usually only form configurationally stable complexes with enantiopure ligands.[2] For example, the chiral europium complex anion $[Eu(dpa)_3]^{3-}$ (with dpa ≡ dipicolinate) shows very fast exchange between its Δ and Λ enantiomers with a half-life on the order of a few tens of milliseconds in aqueous solution at ambient temperature.[3] Despite the great potential that enantiopure lanthanoid complexes have for unique applications such as paramagnetic NMR shift reagents[4] or circularly polarized luminescence (CPL) probes,[5] there is currently only one practically useful ligand platform based on 1,4,7-triazacyclononane that provides lanthanoid complexes which can be chirally resolved and which show sufficient configurational stability after resolution.[6] It has so far proven very difficult to develop other ligands for lanthanoid chelation with the same advantageous properties. Here, we report the chiral resolution of tris(2,2′-bipyridine)-based lanthanoid cryptates as a different class of universally applicable rare earth chelators and their remarkable chemical and configurational stability under rather harsh conditions.

Rigidified bipyridine cryptands such as (±)-**1**-Ln (Scheme 1, left) have proven to be excellent ligands for lanthanoids, providing kinetically inert complexes with outstanding photophysical and interesting magnetic properties.[7] Due to the helical arrangement of the overall cryptate architecture and the axial chirality of the 2,2′-bipyridine-*N*,*N*′-dioxide units, these cryptates are chiral but have so far almost exclusively been synthesized and used as racemates.

Cryptates of this type are also accessible as single enantiomers using enantiomerically pure cryptands,[8] but the much more desirable and practically straightforward chiral resolution to obtain both enantiomers of the corresponding cryptates with racemic or achiral cryptands has not been achieved so far. In order to test the latter possibility, we subjected a series of previously realized cryptates (±)-**1**-Ln (with Ln = Pr, Nd, Sm, Er, Lu)[7c,d] to chiral HPLC. Under optimized HPLC conditions (stationary phase, CHIRALPAK IE; eluent, isocratic CH_3OH + 0.5 vol % CF_3COOH), the racemates could be sufficiently resolved for all lanthanoids investigated along the series. As a representative example, Figure 1 shows the HPLC traces for the racemate (±)-**1**-Lu, as well as the isolated enantiomers **1**-Lu-ent1 (first fraction) and **1**-Lu-ent2 (second fraction) after the preparative resolution (see Figure S1 in the Supporting Information for the HPLC traces for all other lanthanoids). The HPLC trace of the racemate shows the two peaks assigned to the enantiomers in the expected 50:50 ratio. The recovery of the pure enantiomers from the racemate was quite good with 72% for **1**-Lu-ent1 and 88% for **1**-Lu-ent2 (see the Supporting Information for details). Both of these resolved fractions showed no sign of the other enantiomer in the HPLC traces, identical ^1H NMR spectra (Figure S1 in the Supporting Information) in CD_3OD, and perfect mirror-image CD spectra in CH_3OH (Figure 2). Taken together, this constitutes conclusive evidence that the two fractions contain the corresponding enantiomers and that the enantiopurity of each form is very high. At the moment, we cannot assign the absolute configurations of the two enantiomers, but efforts in this direction are underway.

In order to test the configurational stability of the resolved enantiomers, **1**-Lu-ent1 was subjected to two rather harsh environments, and the progress over time was monitored by chiral HPLC (Figure 3). On the one hand, we evaluated

Scheme 1. Chiral Resolution of the Racemic Cryptates 1-Ln

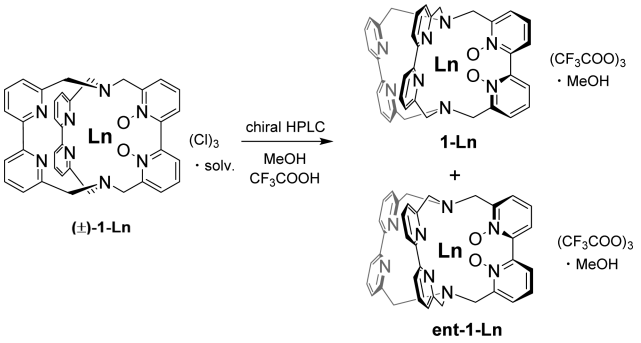

Received: June 7, 2017
Published: July 12, 2017

DOI: 10.1021/acs.inorgchem.7b01407
Inorg. Chem. 2017, 56, 8752−8754

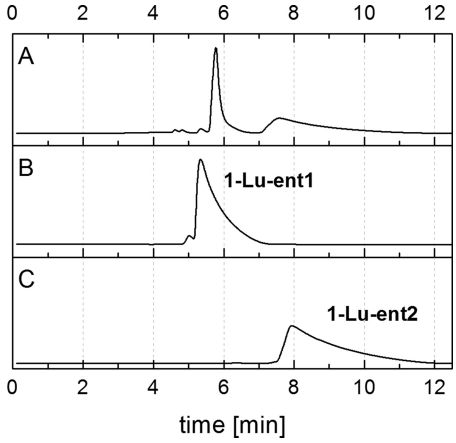

Figure 1. HPLC traces (CHIRALPAK IE, CH_3OH + 0.5 vol % CF_3COOH, UV detection: 300 nm). (A) Preparative separation of racemic (±)-**1**-Lu. (B and C) Analytical HPLC of the purified enantiomers **1**-Lu-ent1 (B) and **1**-Lu-ent2 (C) from the preparative run in A.

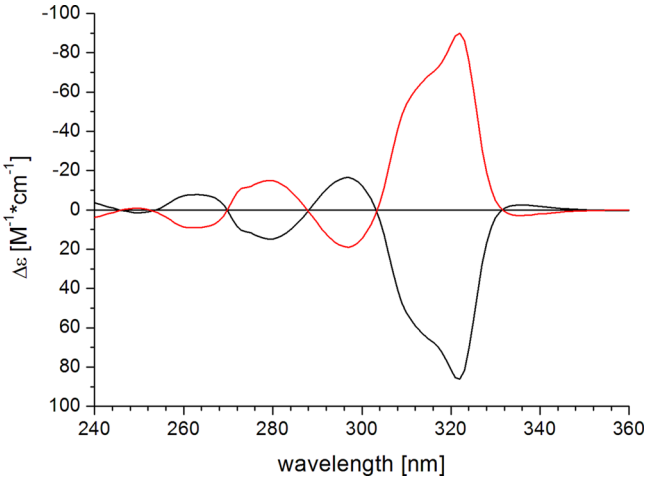

Figure 2. CD spectra of both enantiomers: **1**-Lu-ent1 (black) and **1**-Lu-ent2 (red) in CH_3OH ($c \approx 0.4$ mM).

potential racemization reactions in solutions of this enantiomer in neat CF_3COOH at room temperature, conditions which usually favor rapid decomplexation and/or configurational instability in most other lanthanoid chelates. Second, we also heated **1**-Lu-ent1 in CH_3CN under reflux with 10 equiv of externally added $LuCl_3{\cdot}6H_2O$ and monitored the potential self-exchange of the lutetium cations which would lead to the appearance of the second enantiomer **1**-Lu-ent2. In neither of these experiments could we detect any chemical instability or any sign of the other enantiomer after 5 days.

In conclusion, we could show that the lanthanoid cryptates (±)-**1**-Ln can be separated into pure enantiomers by chiral HPLC and that the resolved, enantiopure complexes show very high configurational stability. This extraordinary and very rare ability to preserve the absolute stereochemical information under extremely challenging conditions makes these enantiopure cryptates very interesting lanthanoid chelates. We expect that this will open up entirely new prospects for applications where enantiopurity is a key requirement, for example for the development of new CPL probes in the near-IR wavelength range, a spectral region where we have already shown the great worth of these cryptates.[7b−d]

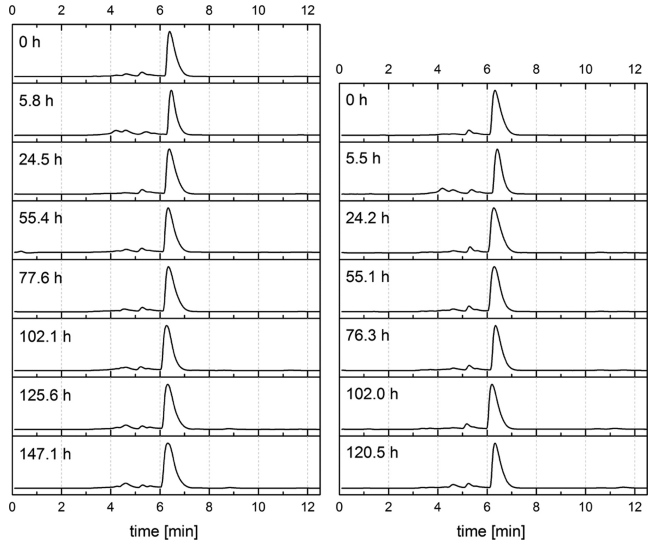

Figure 3. Configurational stability tests by chiral HPLC of **1**-Lu-ent1 under the following conditions: Left, neat CF_3COOH, room temperature; Right, 10 equiv $LuCl_3{\cdot}6H_2O$ in CH_3CN, reflux.

■ ASSOCIATED CONTENT

Supporting Information

The Supporting Information is available free of charge on the ACS Publications website at DOI: 10.1021/acs.inorgchem.7b01407.

Experimental details for chiral HPLC measurements, the configurational stability studies, and CD spectroscopy; chiral HPLC traces of the racemates (±)-**1**-Ln (Ln = Pr, Nd, Sm, Er); and NMR spectra of **1**-Lu-ent1 and **1**-Lu-ent2 (PDF)

■ AUTHOR INFORMATION

Corresponding Author

*E-mail: michael.seitz@uni-tuebingen.de.

ORCID

Michael Seitz: 0000-0002-9313-2779

Notes

The authors declare no competing financial interest.

■ ACKNOWLEDGMENTS

We gratefully acknowledge financial support from the German Research Foundation (DFG, research grant SE 1448/6-1) and the German National Academic Foundation (predoctoral fellowship for E.K.). We thank Mrs. Joana Tavares Macedo (Interfaculty Institute for Biochemistry, University of Tübingen) for help with the CD measurements.

■ REFERENCES

(1) *Stereochemistry of Coordination Compounds*; von Zelewsky, A., Ed.; John Wiley & Sons Ltd.: Chichester, 1996.

(2) Reviews: (a) Aspinall, H. C. Chiral Lanthanide Complexes: Coordination Chemistry and Applications. *Chem. Rev.* **2002**, *102*, 1807−1850. (b) Di Bari, L.; Salvadori, P. Solution structure of chiral lanthanide complexes. *Coord. Chem. Rev.* **2005**, *249*, 2854−2879. Selected examples: (c) Ranganathan, S. R.; Raju, N.; Fan, H.; Zhang, X.; Tweedle, M. F.; Desreux, J. F.; Jacques, V. Polymethylated DOTA Ligands. 2. Synthesis of Rigidified Lanthanide Chelates and Studies on the Effect of Alkyl Substitution on Conformational Mobility and Relaxivity. *Inorg. Chem.* **2002**, *41*, 6856−6866. (d) Mamula, O.; Lama,

DOI: 10.1021/acs.inorgchem.7b01407
Inorg. Chem. 2017, 56, 8752−8754

M.; Telfer, S. G.; Nakamura, A.; Kuroda, R.; Stoeckli-Evans, H.; Scopelitti, R. A Trinuclear Eu^{III} Array within a Diastereoselectively Self-Assembled Helix Formed by Chiral Bipyridine-Carboxylate Ligands. *Angew. Chem.* **2005**, *117*, 2583−2587. (e) Seitz, M.; Moore, E. G.; Ingram, A. J.; Muller, G.; Raymond, K. N. Enantiopure, Octadentate Ligands as Sensitizers for Europium and Terbium Circularly Polarized Luminescence in Aqueous Solution. *J. Am. Chem. Soc.* **2007**, *129*, 15468−15470. (f) Lama, M.; Mamula, O.; Kottas, G. S.; Rizzo, F.; De Cola, L.; Nakamura, A.; Kuroda, R.; Stoeckli-Evans, H. Lanthanide Class of a Trinuclear Enantiopure Helical Architecture Containing Chiral Ligands: Synthesis, Structure, and Properties. *Chem. - Eur. J.* **2007**, *13*, 7358−7373. (g) Montgomery, C. P.; Murray, B. S.; New, E. J.; Pal, R.; Parker, D. Cell-Penetrating Metal Complex Optical Probes: Targeted and Responsive Systems Based on Lanthanide Luminescence. *Acc. Chem. Res.* **2009**, *42*, 925−937. (h) Harada, T.; Nakano, Y.; Fujiki, M.; Naito, M.; Kawai, T.; Hasegawa, Y. Circularly Polarized Luminescence of Eu(III) Complexes with Point- and Axis-Chiral Ligands Dependent on Coordination Structures. *Inorg. Chem.* **2009**, *48*, 11242−11250.

(3) Metcalf, D. H.; Snyder, S. W.; Demas, J. N.; Richardson, F. S. Excited-state racemization kinetics and chiroptical activity of a labile metal complex in aqueous solution. Time-resolved circularly polarized luminescence study of $Eu(dpa)_3^{3-}$ in H_2O and D_2O. *J. Am. Chem. Soc.* **1990**, *112*, 469−479.

(4) Wenzel, T. J.; Wilcox, J. D. Chiral Reagents for the Determination of Enantiomeric Excess and Absolute Configuration Using NMR Spectroscopy. *Chirality* **2003**, *15*, 256−270.

(5) (a) Muller, G. Luminescent chiral lanthanide(III) complexes as potential molecular probes. *Dalton Trans.* **2009**, 9692−6707. (b) Zinna, F.; Di Bari, L. Lanthanide Circularly Polarized Luminescence: Bases and Applications. *Chirality* **2015**, *27*, 1−13.

(6) (a) Frawley, A. T.; Pal, R.; Parker, D. Very bright, enantiopure europium(III) complexes allow time-gated chiral contrast imaging. *Chem. Commun.* **2016**, *52*, 13349−13352. (b) Evans, N. H.; Carr, R.; Delbianco, M.; Pal, R.; Yufit, D. S.; Parker, D. Complete stereocontrol in the synthesis of macrocyclic lanthanide complexes: direct formation of enantiopure systems for circularly polarised luminescence applications. *Dalton Trans.* **2013**, *42*, 15610−15616. (c) Walton, J. W.; Di Bari, L.; Parker, D.; Pescitelli, G.; Puschmann, H.; Yufit, D. S. Structure, resolution and chiroptical analysis of stable lanthanide complexes of a pyridylphenylphosphinate triazacyclononane ligand. *Chem. Commun.* **2011**, *47*, 12289−12291.

(7) (a) Lehn, J.-M.; Roth, C. O. 56. Synthesis and Properties of Sodium and Europium(III) Cryptates Incorporating the 2,2′-Bipyridine 1,1′-Dioxide and 3,3′-Biisoquinoline 2,2′-Dioxide Units. *Helv. Chim. Acta* **1991**, *74*, 572−578. (b) Doffek, C.; Alzakhem, N.; Molon, M.; Seitz, M. Rigid, Perdeuterated Lanthanoid Cryptates: Extraordinarily Bright Near-IR Luminophores. *Inorg. Chem.* **2012**, *51*, 4539−4545. (c) Doffek, C.; Wahsner, J.; Kreidt, E.; Seitz, M. Breakdown of the Energy Gap Law in Molecular Lanthanoid Luminescence: The Smallest Energy Gap Is Not Universally Relevant for Nonradiative Deactivation. *Inorg. Chem.* **2014**, *53*, 3263−3265. (d) Doffek, C.; Alzakhem, N.; Bischof, C.; Wahsner, J.; Güden-Silber, T.; Lügger, J.; Platas-Iglesias, C.; Seitz, M. Understanding the Quenching Effects of Aromatic C−H- and C−D-Oscillators in Near-IR Lanthanoid Luminescence. *J. Am. Chem. Soc.* **2012**, *134*, 16413−16423.

(8) Güden-Silber, T.; Doffek, C.; Platas-Iglesias, C.; Seitz, M. The first enantiopure lanthanoid cryptate. *Dalton Trans.* **2014**, *43*, 4238−4241.

DOI: 10.1021/acs.inorgchem.7b01407
Inorg. Chem. 2017, 56, 8752−8754

Chiral Resolution of Lanthanoid Cryptates with Extreme Configurational Stability

Elisabeth Kreidt[a], Carolin Dee[a] and Michael Seitz[*a]

[a] Institute of Inorganic Chemistry, University of Tübingen, Auf der Morgenstelle 18, 72076 Tübingen, Germany.

Email: michael.seitz@uni-tuebingen.de

Supporting Information

Table of Contents Page

1. Materials and Methods

NMR spectra were recorded on a Bruker AVII+400 spectrometer (^{1}H: 400 MHz) using CD_3OD (≥ 99.8% D) as the solvent. The racemic lanthanoid cryptates were synthesized as described previously from the corresponding sodium cryptates using $LnCl_3 \cdot x\ H_2O$ (x = 7 for Ln = Pr, x = 6 for Ln = Nd, Sm, Er, or Lu).[1]

2. Chiral HPLC

All chiral HPLC runs of **(±)-1-Ln** (with Ln = Pr, Nd, Sm, Er, Lu) were performed on a Knauer Azura HPLC system (UV detection at λ = 300 nm), equipped with a CHIRALPAK IE column (Daicel, particle size: 5 µm, internal diameter: 4.6 mm, column length: 150 mm) using MeOH with additional 0.5 vol.-% CF_3COOH as mobile phase with a flow of 1.0 mL/min. All samples were prepared using HPLC-grade MeOH and filtered with a membrane filter (nylon, 0.45 µm pore size, 13 mm diameter) in a stainless steel filter holder prior to injection. The obtained HPLC traces for **(±)-1-Ln** with Ln = Pr, Nd, Sm, Er are shown in Figure S1 and for **(±)-1-Lu** in Figure 1 in the manuscript.

Notes: The separation efficiency and the relative and absolute retention of the two enantiomers is dependent on the concentration of the analyte. Special care has to be taken that only freshly prepared MeOH/CF_3COOH mobile phases are used.

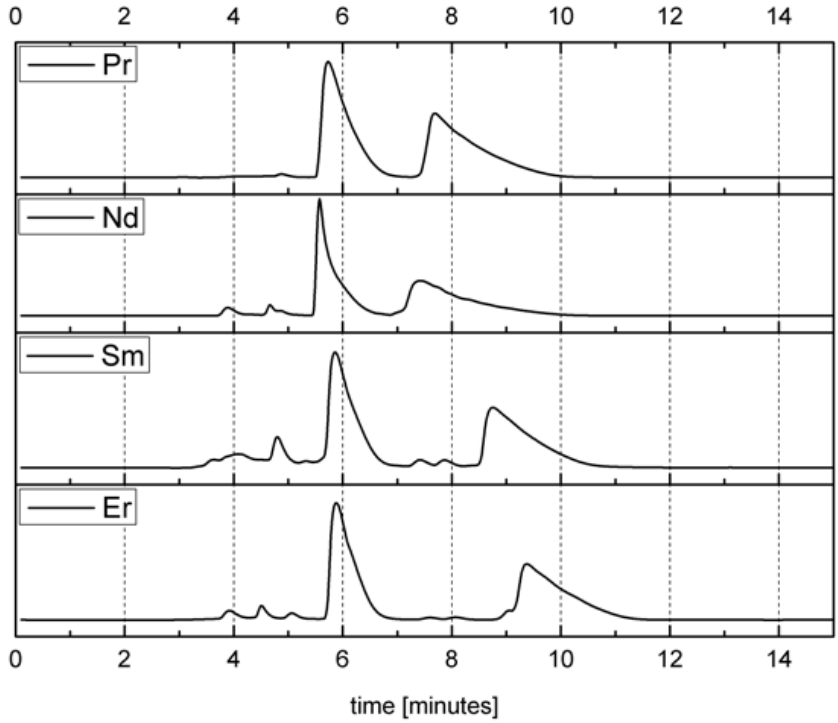

Figure S1. Normalized chiral HPLC traces of the racemates **(±)-1-Ln** (Ln = Pr, Nd, Sm, Er).

Preparative chiral resolution of 1-Lu:

Racemic **1-Lu**[1a] (8.0 mg, 6.4 µmol, 2.0 equivs.) was dissolved in MeOH (2.7 mL, HPLC-grade) and filtered through a membrane filter (vide infra). The filter was washed with additional 0.5 mL of MeOH (HPLC-grade), to yield a total volume of 3.2 mL and a concentration of 2.5 mg/mL, which was found to be the optimal compromise between separation and time efficiency. The solution was subjected to chiral HPLC in portions of 100 µL. The collected fractions of the respective enantiomers were combined and the solvents were removed in vacuo at room temperature. After drying, samples of the enantiomers were redissolved in MeOH (HPLC-grade), filtered and injected to verify the enantiopurity (see main article). After this HPLC purification with MeOH/CF_3COOH (0.5 vol.-%) as mobile phase, a molecular composition of $[C_{36}H_{30}N_8O_2Ln]$ $(O_2C_2F_3)_3 \cdot CH_3OH$ was assumed, resulting in a molar mass of M = 1152.74 g/mol in the case of Lu.

1-Lu-ent1: 2.7 mg (2.3 µmol, 72% yield) of a colorless solid

^{1}H NMR (400 MHz, CD_3OD): δ = 8.48 (d, *J* = 7.9 Hz, 2 H), 8.42-8.36 (m, 4 H), 8.28-8.14 (m, 8 H), 7.70 (d, *J* = 7.7 Hz, 2 H), 7.66 (d, *J* = 7.8 Hz, 2 H), 4.82 (d, *J* = 12.7 Hz, 2 H), 4.81 (d, *J* = 15.8 Hz, 2 H), 4.14 (d, *J* = 15.3 Hz, 2 H), 4.10 (d, *J* = 15.2 Hz, 2 H), 3.95 (d, *J* = 12.9 Hz, 2 H), 3.70 (d, *J* = 15.7 Hz, 2 H) ppm.

1-Lu-ent2: 3.2 mg (2.8 µmol, 88% yield) of a colorless solid

^{1}H NMR (400 MHz, CD_3OD): δ = 8.48 (d, *J* = 8.1 Hz, 2 H), 8.42-8.35 (m, 4 H), 8.27-8.14 (m, 8 H), 7.70 (d, *J* = 7.8 Hz, 2 H), 7.66 (d, *J* = 7.8 Hz, 2 H), 4.82 (d, *J* = 12.9 Hz, 2 H), 4.81 (d, *J* = 15.9 Hz, 2 H), 4.14 (d, *J* = 15.1 Hz, 2 H), 4.10 (d, *J* = 15.1 Hz, 2 H), 3.95 (d, *J* = 12.8 Hz, 2 H), 3.70 (d, *J* = 15.8 Hz, 2 H) ppm.

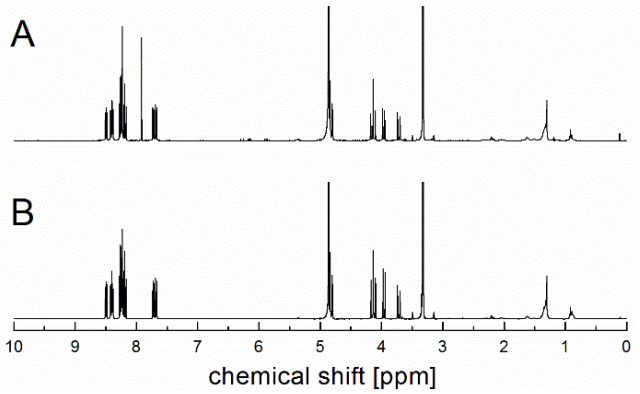

Figure S2. ^{1}H NMR spectra (400 MHz, CD_3OD) of **1-Lu-ent1** (A) and **1-Lu-ent2** (B).

Configurational stability studies:

A) Neat CF_3COOH, room temperature

1-Lu-ent1 (0.25 mg) was dissolved in CF_3COOH (3.3 mL) and the solution was stirred at room temperature for seven days. In total eight samples of 200 µL were taken at different times (see Figure 4 in the manuscript).

B) 10 eq. $LuCl_3 \cdot 6\ H_2O$, reflux

1-Lu-ent1 (0.25 mg, 0.22 µmol, 1.0 equiv.) and $LuCl_3 \cdot 6\ H_2O$ (0.84 mg, 2.2 µmol, 10 equivs.) were dissolved in CH_3CN (3.3 mL, HPLC-grade) and heated under reflux for six days. In total seven samples of 200 µL were taken at different times (see Figure 4 in the manuscript). To prevent the mixture from running dry, several additional portions of CH_3CN were added at

different times (24.2 h: 0.4 mL; 51.3 h: 2.5 mL; 57.8 h: 1.5 mL; 76.3: 0.8 mL; 102 h: 1.8 mL; 120 h, 1.9 mL).

For both studies (A and B), the samples were treated as follows:
The solvents were concentrated under a stream of air and the residues were taken up in MeOH (100 µL). The solutions were filtered through a membrane filter (nylon, 0.45 µm pore size), the filter was washed with additional MeOH (0.3 mL) and the combined methanolic filtrates were concentrated. For chiral HPLC analysis, the dry samples were redissolved in MeOH (100 µL) directly before the HPLC run.

3. Circular Dichroism Spectroscopy

CD spectra were collected on a Jasco J-720 spectropolarimeter, using a bandwidth of 1.0 nm, a response time of 2 seconds and a scan speed of 50 mm/min. Samples of the enantiomers (**1-Lu-ent1**: 0.21 mg, **1-Lu-ent2**: 0.19 mg) were dissolved in MeOH (400 µL each), yielding solutions with concentrations of c = 0.46 mmol/L (**1-Lu-ent1**) and c = 0.41 mmol/L (**1-Lu-ent2**), respectively. The solutions were measured in rectangular quartz cuvettes (Suprasil, d = 1 mm path length).

4. References

[1] a) Pr, Nd, and Er, Lu: Doffek, C.; Alzakhem, N.; Bischof, C.; Wahsner, J.; Güden-Silber, T.; Lügger, J.; Platas-Iglesias, C.; Seitz, M.; *J. Am. Chem. Soc.*, **2012**, *134*, 16413; b) Sm: Doffek, C.; Wahsner, J.; Kreidt, E.; Seitz, M.; *Inorg. Chem.*, **2014**, *53*, 3263; c) Doffek, C.; Seitz, M.; *Angew. Chem. Int Ed.* **2015**, *54*, 9719

Inorganic Chemistry
Article
Cite This: Inorg. Chem. 2018, 57, 7390−7401
pubs.acs.org/IC

Long Wavelength Excitation of Europium Luminescence in Extended, Carboline-Based Cryptates

Carolin Dee,[†] David Esteban-Gómez,[‡] Carlos Platas-Iglesias,*[,‡] and Michael Seitz*[,†]

[†]Institute of Inorganic Chemistry, University of Tübingen, Auf der Morgenstelle 18, 72076 Tübingen, Germany
[‡]Centro de Investigacións Científicas Avanzadas (CICA) and Departamento de Química, Universidade da Coruña, Campus da Zapateira-Rúa da Fraga 10, 15008 A Coruña, Spain

Supporting Information

ABSTRACT: Two new β-carboline-based tris(biaryl) europium cryptates are introduced. The extended antenna moiety incorporated into the cryptand frameworks enables the sensitization of europium emission with excitation wavelengths well above 450 nm. In aqueous solution, the cryptates show great complex stability, luminescence lifetimes around 0.5 ms, and absolute quantum yields of ca. 3%. In addition, the europium luminescence shows a well-defined pH-dependence in the physiologically interesting pH range 7−9.

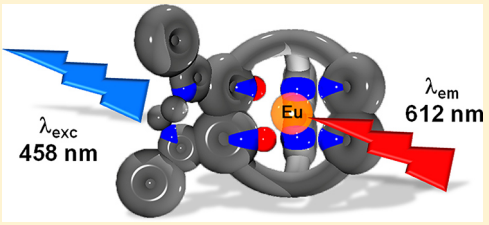

INTRODUCTION

Lanthanoid luminescence in molecular coordination compounds has found a wide array of fascinating applications over the last few decades such as luminescence sensors and probes, counterfeiting tags, or solar energy conversion.[1] Due to the difficulty to populate lanthanoid excited states via direct, parity-forbidden f−f-absorption, luminescence is usually sensitized by an appropriate organic "antenna" ligand with suitable electronic states that can feed energy into the emitting metal states. One of the first successful systems for this purpose was the class of tris(biaryl)-based cryptates **1** developed by Lehn et al. (Figure 1).[2]

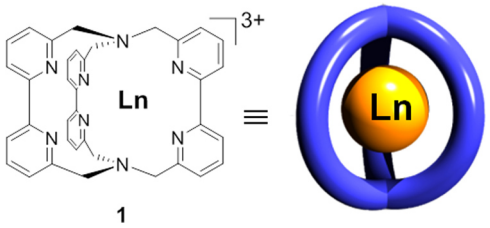

1

Figure 1. Tris(bipyridine) lanthanoid cryptate **1** and schematic representation of its macrobicyclic topology.

The cryptates **1** have proven their worth in numerous time-resolved luminescence assays in the context of drug discovery and related diagnostic biomedical applications.[3] From a chemical perspective, the macrobicyclic cryptand scaffold has been varied quite extensively by the replacement of the 2,2′-bipyridine moieties with other biaryl motifs such as isoquinolines, pyridine-*N*-oxide, or other common nitrogen-based heterocycles (Figure 2).[4,5]

In general, the described cryptates have a number of very advantageous properties for the development of luminescence probes, e.g., high kinetic inertness and efficient light absorption

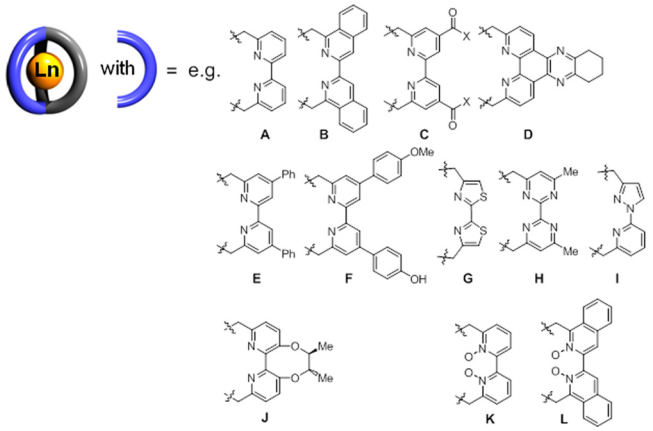

Figure 2. Representative examples of aromatic building blocks **A**−**L** for cryptate construction reported in the literature.[4,5]

by the antenna moieties.[3] One drawback so far, however, is the need for rather short excitation wavelengths with absorption maxima of the low-energy bands usually below $\lambda_{max} \approx 320$ nm and rarely exceeding $\lambda_{max} \approx 350$ nm. For the use of luminophores in biological media, a longer excitation wavelength would be highly beneficial as it causes less phototoxicity in living systems, limits autofluorescence in biological samples by preventing light absorption in biomolecules, does not require expensive and uncommon quartz optics in luminescence microscopy, and increases the possibility for laser excitation with widely used laser lines required in confocal luminescence microscopy (e.g., with the argon-ion laser lines at $\lambda_{exc} = 458$ nm/476 nm or a laser diode line at $\lambda_{exc} = 405$ nm). While several other ligand classes for lanthanoid chelation have

Received: April 15, 2018
Published: June 5, 2018

DOI: 10.1021/acs.inorgchem.8b01031
Inorg. Chem. 2018, 57, 7390−7401

already been shown to enable long-wavelength excitation, cryptates are unfortunately still lacking in this respect.[6]

Here, we introduce a new ligand motif for lanthanoid sensitization based on β-carboline that is capable of sensitizing europium luminescence after long-wavelength excitation with $\lambda_{exc} < 476$ nm. We report the synthesis of the new cryptand chelators, the preparation and characterization of the corresponding europium complexes, as well as a comprehensive study of the photophysical properties.

RESULTS AND DISCUSSION

Cryptate Design – General Strategy. In order to tackle the long-wavelength excitation problem for cryptate luminophores outlined in the introduction, we chose the tris(bipyridine)-based cryptate scaffold **2** (Figure 3) featuring

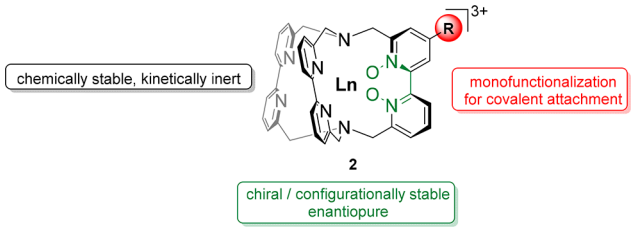

Figure 3. 2,2′-Bipyridine-*N*,*N*′-dioxide-based cryptate **2** with a number of attractive features.[4d,e,5a−f]

two pyridine-*N*-oxide moieties[4d,e] instead of the original design exemplified in **1** without *N*-oxides. Cryptates **2** inherit all the general advantages of the original cryptates **1** (Figure 1) but display additional attractive structural features such as exquisite conformational rigidity,[5e] extreme configurationally stable chirality with the possibility for chiral HPLC resolution,[5f] and known, straightforward monofunctionalization chemistry.[5e]

As new sensitizer motif, we chose the β-carboline scaffold, which is naturally occurring in numerous fluorescent harmala alkaloids such as harmane or harmine (Figure 4), and that

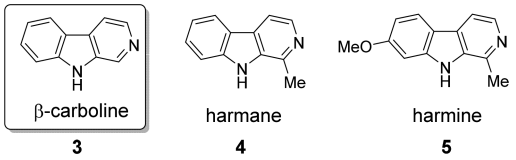

Figure 4. β-Carboline, the photoactive building block for naturally occurring alkaloids such as harmane or harmine.

provides a useful pyridine-like substructure in analogy to the usual binding units in cryptates **1**. The corresponding protonated species of the β-carbolines have interesting photophysical properties and are known to show absorption bands well above 400 nm, as well as triplet energies of ca. 21 700 cm^{-1} (~460 nm).[7] Therefore, the carboline-centered triplet levels should in principle be good antennae for lanthanoids with emitting levels considerably lower in energy such as Eu^{3+} ($^5D_0$ at ca. 17 200 cm^{-1}) but inefficient for the sensitization of lanthanoids with high-lying emitting states such as Tb^{3+} ($^5D_4$ at ca. 20 500 cm^{-1}). In coordination chemistry, β-carboline-based ligands have sporadically been used in the past in combination with transition metals for applications such as luminescent probes or antiproliferative agents,[8] but lanthanoid complexes with carboline-based chelators have not been reported so far.

For the purposes of this study, we chose the cryptates **6-Eu** and **7-Eu** with either two or one β-carboline unit as target structures (Figure 5).

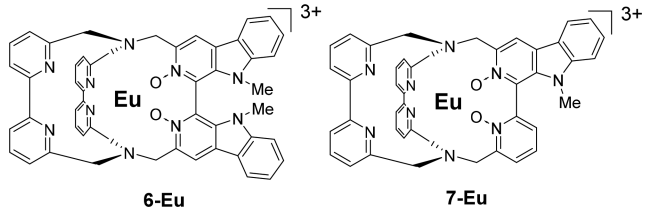

Figure 5. New β-carboline-based cryptates **6-Eu** and **7-Eu**.

Cryptate Synthesis/Structure Elucidation. The synthesis of the sodium cryptates **6-Na** started from the literature-known bis(carboline) dialcohol **8** (Scheme 1).[9]

Scheme 1. Synthesis of the Cryptates [D_x]-6-Na

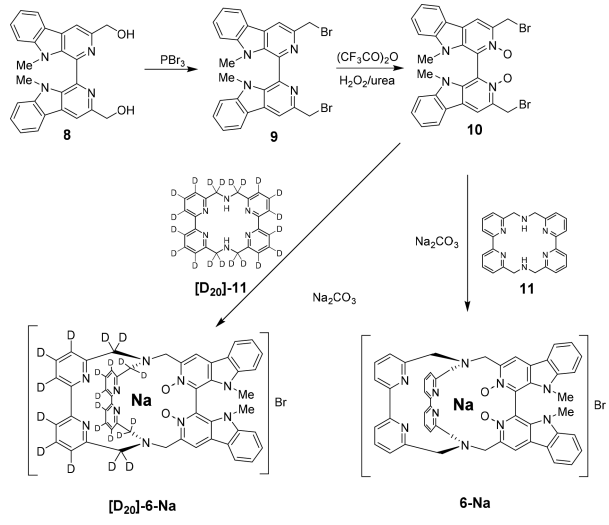

Bromination with PBr_3 followed by oxidation[10] yielded the *N*,*N*′-dioxide **10**. This building block was subjected to the typical macrobicyclization reaction using macrocycle **11**[10] resulting in the formation of the corresponding sodium cryptate **6-Na**. In order to aid the ^1H NMR spectral assignment later on, we also prepared the corresponding deuterated cryptate [D_{20}]-**6-Na** by using the known, perdeuterated macrocycle [D_{20}]-**11**.[5a] In a similar fashion, the mixed pyridine-carboline sodium cryptates **7-Na** were prepared (Scheme 2). The diester **15** was obtained by the Pictet–Spengler reaction of L-tryptophane methyl ester (**12**) with 6-formyl-2-picolinic acid methyl ester (**13**),[12] followed by oxidative aromatization of the diastereomeric mixture **14** using trichloroisocyanuric acid (TCCA) and methylation of the N–H moiety at the β-carboline. Reduction of both ester functions in **15** with $LiAlH_4$ and subsequent bromination/*N*-oxidation[10] gave benzylic dibromide *N*,*N*′-dioxide **18**. Macrocyclization under standard conditions with macrocycle **11**[11] yielded sodium cryptate **7-Na**.

All sodium cryptates ([D_x]-**6-Na** and **7-Na**) could be converted to the europium cryptates by metal exchange with $EuCl_3 \cdot 6H_2O$ (Scheme 3) in CH_3CN. HPLC purification of the obtained crude cryptate mixtures for the europium species surprisingly yielded two major fractions for all cases (see Figures S1–S9). Importantly, however, the two isolated

DOI: 10.1021/acs.inorgchem.8b01031
Inorg. Chem. 2018, 57, 7390−7401

Scheme 2. Synthesis of the Cryptate 7-Na

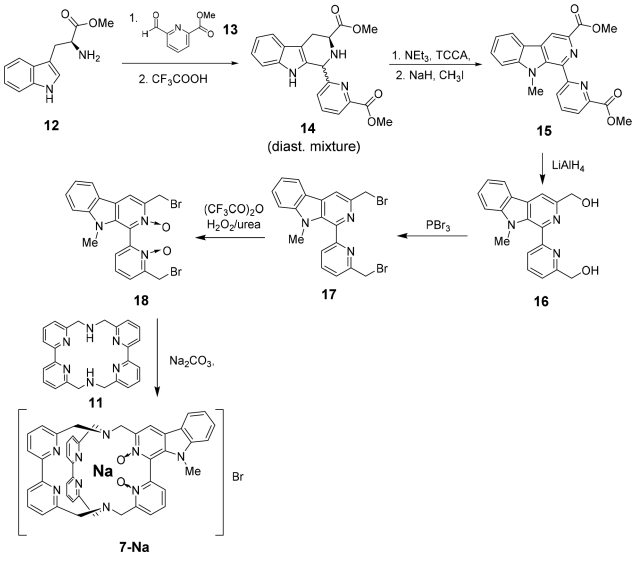

Scheme 3. Synthesis of the Lanthanoid Cryptates [D$_x$]-6-Eu and 7-Eu

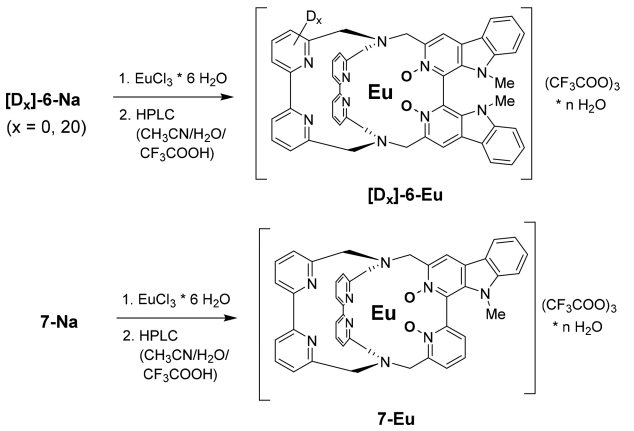

europium complexes were stable at ambient temperature in solution as evidenced by the very clean analytical HPLC traces after the preparative HPLC separations, suggesting that the observation of two fractions was not due to degradation under the relatively harsh HPLC conditions. For **6-Eu**, the ^{1}H NMR spectrum of the first eluting fraction in CD_3OD showed a single, well-behaved set of resonances consistent with C_2 symmetry. In contrast, the second fraction, labeled **6-Eu′**, exhibited a very similar chemical shift pattern compared to **6-Eu** but with small splittings of previously identical protons, effectively decreasing the symmetry of **6-Eu′** to C_1 (Figure 6B). The phenomenon that the formation of these two very similar species is also seen for the europium cryptates **7-Eu** and **7-Eu′** (see HPLC in Figures S7−S9 and ^{1}H NMR spectra in Figures S33−34) raised questions as to the identity of the two different species. The comparison of the ^{1}H NMR spectra of **6-Eu′** (Figure S21) and its deuterated isotopologue [**D$_{20}$**]-**6-Eu′** (Figure S23) allowed the unambiguous assignment of the four broad singlets around ca. −9.2 ppm and around ca. −14.5 ppm to the benzylic methylene groups of the bis(carboline) unit. Due to the helical arrangement of these cryptates, the geminal hydrogen atoms of the methylene groups are not equivalent and usually show distinctly different chemical shifts. While in

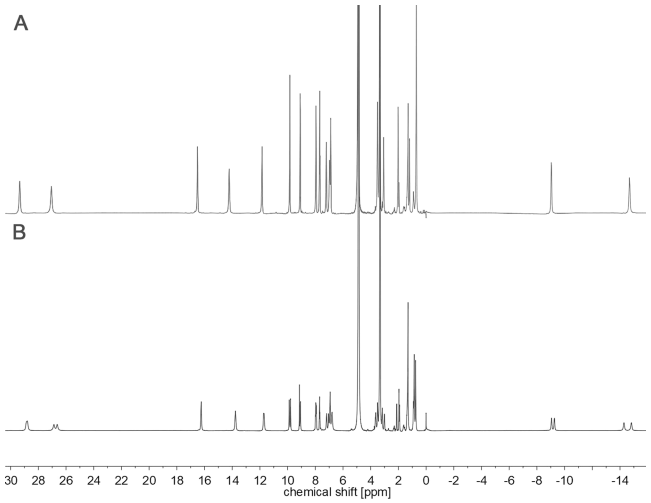

Figure 6. ^{1}H NMR (400 MHz, CD_3OD) spectra of **6-Eu** (A) and **6-Eu′** (B, see text).

the more symmetric cryptate **6-Eu** only two resonances are observed, in **6-Eu′** these signals split into four separate resonances, and the splitting of the previously symmetry-related protons is the most pronounced among all signal groups observed. This gave a first indication that the unknown structural difference leading to the two cryptate fractions **6-Eu** and **6-Eu′** is very likely stemming from the bis(carboline) moiety (vide infra).

Unfortunately, cryptates of this kind are notoriously challenging to crystallize, and we were not successful in obtaining single crystals for structure elucidation purposes by X-ray crystallography. Mass spectrometry, in general, also proved to be difficult due to the high charge of the cryptate cations. The method of choice, that at least permitted meaningful measurements, proved to be MALDI-MS with 2,5-dihydroxybenzoic acid (DHB) as matrix. Under these highly reducing conditions, the europium centers in the cryptates studied (**6-Eu**/**6-Eu′** and **7-Eu**/**7-Eu′**) were reduced to the corresponding Eu(II) species, a common occurrence for similar compounds featuring lanthanoids with accessible divalent oxidation states (e.g., Eu, Yb).[5c,g] In addition, different degrees of reductive oxygen loss of the *N*-oxide moieties were observed (see Figures S10−S13). Nevertheless, the mass spectra clearly proved the two fractions to be europium cryptates related to target structures shown in Figure 5. For **6-Eu′** and **7-Eu′**, the spectra also indicated water molecules in the inner coordination sphere around the metal center, a detail not seen for **6-Eu** and **7-Eu** (Figures S10−S13). IR spectra of **6-Eu** and **6-Eu′** unambiguously revealed the presence of *N*-oxide units in both species with the expectedly strong N−O stretching bands around 1240 cm^{-1} (Figure S14). Taken together, we assign the first HPLC fractions **6-Eu** and **7-Eu** as the *N*,*N*′-dioxide cryptates envisioned at the outset. The remaining second fractions correspondingly are related but C_1-symmetric cryptates **6-Eu′** and **7-Eu′**. The exact structures of these unexpected species are currently uncertain but could be connected to the presence of only one *N*-oxide unit instead of two as seen for **6-Eu** and **7-Eu**. Work in this direction is currently underway.

In order to get further proof of the identity of **6-Eu**, we performed additional computational work using density functional theory (DFT) calculations.[13] On the grounds of

DOI: 10.1021/acs.inorgchem.8b01031
Inorg. Chem. 2018, 57, 7390−7401

our previous experience,[14] we used the hybrid meta-GGA TPSSh functional together with a large-core quasirelativistic effective core potential (ECP) and the associated (7s6p5d)/[5s4p3d]-GTO basis set for Eu,[15] and the standard 6-31G(d,p) basis set for ligand atoms. Bulk solvent effects (methanol) were considered with the integral equation formalism of the polarized continuum model (IEFPCM).[16]

The cation of **6-Eu** was modeled as the *N*,*N*′-dioxide shown in Figure 5 with an additional inner-sphere water ligand in the space between the two bipyridine moieties. Figure 7 shows the

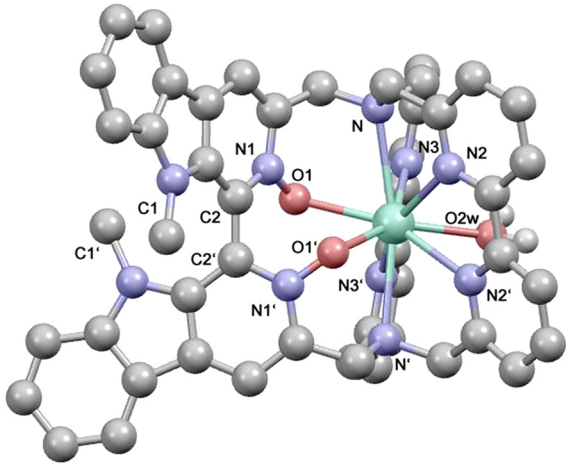

Figure 7. Calculated geometry (TPSSh/LCRECP/6-31G(d,p) for the cation of **6-Eu**. Hydrogen atoms are omitted for clarity, except for the ones at the inner-sphere water molecule.

results for the geometry optimizations. The inner-sphere water molecule in **6-Eu** occupies a coordination site at a distance d_{Eu-O2w} = 2.543 Å from the metal center (Table 1). This is a

Table 1. Selected Distances, Angles, and Dihedral Angles in the Calculated Structure of 6-Eu (see Figure 7 for Atom Labeling)

geometric parameter	
Eu−O2w [Å]	2.543
Eu−O1 [Å]	2.413
Eu−O1′ [Å]	2.414
Eu−N [Å]	2.746
Eu−N′ [Å]	2.733
Eu−N2 [Å]	2.688
Eu−N2′ [Å]	2.663
Eu−N3 [Å]	2.658
Eu−N3′ [Å]	2.669
C1−C1′ [Å]	3.764
O1−Eu−O1′ [deg]	67.5
N1−C2−C2′−N1′ [deg]	60.5

little longer than the normal range for Eu−OH_2 bond lengths (usually 2.35 Å < d_{Eu-O} < 2.50 Å) in molecular complexes.[17] The dihedral angles N1−C2−C2′−N1′, representing the torsion angle around the atropisomeric axis in the bis-(carboline) unit, with a value of 60.5° are slightly larger than the one found (52.8°) around the 3,3′-biisoquinoline 2,2′-dioxide moiety in the related europium cryptate with the cryptand [bpy.bpy.biqiO_2].[18] Nevertheless, the steric strain on the cryptate structure exerted by the interaction of the two spatially rather close *N*-methyl groups (Figure 7: C1 and C1′) still seems to be unproblematic with distances of $d_{C1-C1'}$ = 3.764 Å, which is larger than in related systems (e.g., in yttrium complexes with 3,3′-dimethyl-2,2′-biphenolate ligands:[19] $d_{C-C'}$ = 3.33 Å) and which permits favorable van-der-Waal interactions.[20]

The structure of **6-Eu** in solution was further studied by analyzing the ^{1}H paramagnetic lanthanoid induced shifts (LIS). The ^{1}H NMR spectrum of **6-Eu** (Figure 6A) presents 18 paramagnetically shifted signals in the range 29.3 to −14.6 ppm. The assignment of the proton signals was achieved by line width analysis and comparison to the spectra of **2-Eu** (R = H) and [$\mathbf{D_{20}}$]**-6-Eu**. The diamagnetic contributions were estimated from the chemical shifts observed for the diamagnetic analogue **2-Lu** (R = H).[5c] The ^{1}H NMR paramagnetic shifts observed for lanthanoid complexes are the result of both contact and pseudocontact contributions. Ligand field effects remove the spherical symmetry around the lanthanide ion, causing magnetic susceptibility anisotropy, and thus a pseudocontact contribution through dipolar interaction between the proton and electron magnetic moments. The pseudocontact shift (δ^{PC}) can be conveniently expressed by the following equation:[21]

$$\delta^{PC} = \frac{1}{12\pi r^3}\left[\Delta\chi_{ax}\left(\frac{3z^2 - r^2}{r^2}\right) + \frac{3}{2}\Delta\chi_{rh}\left(\frac{x^2 - y^2}{r^2}\right)\right] \quad (1)$$

where $r = \sqrt{x^2 + y^2 + z^2}$ and x, y, and z are the Cartesian coordinates of the observed nucleus relative to the location of the paramagnetic ion placed at the origin, and $\Delta\chi_{ax}$ and $\Delta\chi_{rh}$ are the axial and rhombic parameters of the symmetric magnetic susceptibility tensor.

On the other hand, contact contributions (δ^{C}) are the result of through-bond delocalization of the electron spin density onto the observed nucleus, and in the case of the lanthanide ions can be given by eq 2:[22]

$$\delta^{C} = \langle S_z \rangle \frac{2\pi\mu_B}{3kT\gamma_I} A^{iso} \quad (2)$$

where $\langle S_z \rangle$ represents the reduced value of the average spin polarization, μ_B is the Bohr magneton, k the Boltzmann constant, γ_I the gyromagnetic ratio of the observed nucleus, and A^{iso} is the isotropic Fermi hyperfine coupling constant (in MHz).

It has been shown that both contact and pseudocontact mechanisms provide sizable contributions to the overall paramagnetic shifts in Eu^{3+} complexes.[23] The analysis of the ^{1}H NMR paramagnetic shifts of **2-Eu** was first carried out using the pseudocontact model, as expressed by eq 1. The Cartesian coordinates of ^{1}H nuclei were taken from the DFT optimized structure, so that five parameters were fitted to minimize the difference between the experimental and calculated shifts: $\Delta\chi_{ax}$, $\Delta\chi_{rh}$, and three Euler angles relating the coordinates from the arbitrary reference frame to the frame of the magnetic susceptibility tensor.[21] Neglecting contact shifts resulted in rather large deviations of the values obtained with eq 1 and the experimental paramagnetic shifts (up to 13.1 ppm, Figure S40, Supporting Information). Thus, we estimated the contact contributions of ^{1}H nuclei following the methodology reported earlier.[23,24] Briefly, this estimation of contact shifts requires the calculations of spin densities for the Gd^{3+} analogue using DFT. These calculations were conducted using the TPSSh functional and a small-core relativistic pseudopotential for Gd^{3+},[25] as the

DOI: 10.1021/acs.inorgchem.8b01031
Inorg. Chem. 2018, 57, 7390−7401

Table 2. Observed (δ^{obs}) and Calculated (δ^{calc}) ^{1}H NMR Shifts, Paramagnetic Shifts (δ^{para}), Hyperfine Coupling Constants (A^{iso}) and Contact (δ^{c}) and Pseudocontact (δ^{pc}) Contributions Calculated for 6-Eu[a]

	δ^{obs}	δ^{calc}	δ^{para}[b]	A^{iso}[c]	δ^{c}	δ^{pc}	$\delta^{pc,calc}$
H1o	−14.60	−15.27	18.59	−0.0270	4.79	13.80	14.47
H2o	−9.04	−4.21	13.77	−0.0590	10.46	3.31	−1.52
H3o	9.84	10.27	−1.48	0.0000	0.00	−1.48	−1.91
H6o	9.08	9.66	0.02	−0.0011	0.19	−0.17	−0.75
H7o	7.68	8.11	0.02	0.0004	−0.07	0.09	−0.34
H8o	7.94	7.43	−0.24	−0.0021	0.37	−0.61	−0.10
H9o	6.96	7.62	0.74	0.0008	−0.14	0.88	0.22
H10o	0.72	1.95	2.44	0.0002	−0.04	2.48	1.25
H1b	27.1	23.52	−22.90	0.0156	−2.76	−20.14	−16.60
H2b	6.88	7.05	−2.13	−0.0156	2.76	−4.89	−5.06
H3b	2.0	3.28	5.72	−0.0068	1.21	4.51	3.23
H4b	2.0	3.57	6.58	−0.0062	1.10	5.48	3.91
H5b	2.0	2.15	6.25	−0.0089	1.58	4.67	4.52
H6b	7.17	6.37	1.65	−0.0084	1.49	0.16	0.39
H7b	11.8	10.96	−4.13	−0.0042	0.75	−4.88	−3.23
H8b	16.5	14.27	−8.78	−0.0103	1.83	−10.61	−8.38
H9b	14.2	17.07	−9.98	−0.0104	1.84	−11.82	−14.69
H10b	29.30	29.78	−25.59	0.0202	−3.57	−22.02	−22.50

[a]Chemical shifts are given in ppm and A^{iso} values in MHz. See Figure 10 for labeling. [b]Paramagnetic shifts are defined as $\delta^{para} = \delta^{dia} - \delta^{obs}$, where δ^{dia} is the diamagnetic contribution. [c]Obtained with DFT calculations as explained in the text.

calculation of spin densities requires including the 4f electrons in the valence space (the EPR-III basis set[26] was used for the ligand atoms). These spin densities (A^{iso} values) are then used to estimate the contact contributions of the Eu^{3+} complex, which scale by a factor of 0.34 with respect to Gd^{3+} (the ratio of the corresponding $<S_z>$ values).[27]

The inclusion of contact contributions results in a very important improvement of the agreement between experimental and calculated shifts, with deviations < 4.8 ppm. Even so, the largest deviations are observed for those protons presenting the largest deviations when neglecting contact contributions (H2o, H1b, and H9b). This likely reflects some inaccuracies in the estimation of contact contributions. Nevertheless, the good agreement between the experimental and calculated paramagnetic shifts confirms that our DFT calculations provide a good description of the structure of **6-Eu** in solution (Table 2). The ^{1}H paramagnetic shifts of most nuclei are dominated by pseudocontact contributions, with the contact contribution being particularly important (~75%) for H2o protons. The calculated values of $\Delta\chi_{ax} = 0.61 \pm 0.27 \times 10^{-32}$ and $\Delta\chi_{rh} = 3.57 \pm 0.14$ m^3 indicate that the pseudocontact shifts are dominated by the rhombic contribution.

Photophysical Properties. As expected, the cryptates **6-Eu** and **7-Eu** show strong UV/vis absorption in aqueous solution (Figure 8). In addition to the usual bands below ca. 370 nm seen for bipyridine-based cryptates, new, long-wavelength bands are observed with maxima around $\lambda_{abs,max} \approx$ 410 nm for **7-Eu** and even more bathochromically shifted $\lambda_{abs,max} \approx$ 422 nm for **6-Eu** (Table 3). There is a clear dependence visible of the bathochromic shift on the number of β-carboline units, with the second carboline yielding an additional red-shift of $\Delta\lambda \approx$ 12 nm. The corresponding excitation spectra monitoring the europium emission band $^5D_0 \rightarrow {}^7F_2$ (λ_{em} = 610 nm, see Figure 9) mirrors almost perfectly the observed absorption features (Figure 8).

Especially for **6-Eu**, the long-wavelength absorption band extends far into the visible range and still has appreciable

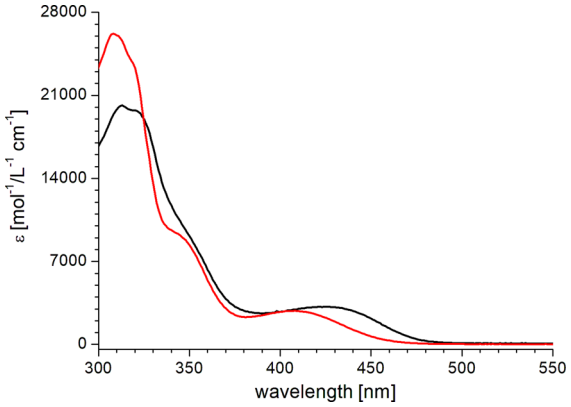

Figure 8. UV−vis absorption spectra of the europium cryptates **6-Eu** (black) and **7-Eu** (red) in H_2O.

intensity above 460 nm. This observation is completely in agreement with previous studies on the photophysics of simple β-carbolines such as protonated harmane which also shows absorption beyond 400 nm.[7] To the best of our knowledge, this finding extends the potential for excitation of lanthanoid luminescence in tris(biaryl)-based cryptates by at least 50 nm into the visible region compared to all previously reported examples indicated in Figure 2.[4,5] As far as the extent of the shift in the absorption is concerned, cryptates **6** are therefore among the most red-shifted sensitizers for all chelator classes developed for long-wavelength europium excitation.[6]

In order to get further insight into the energies of the relevant, ligand-centered states, we synthesized the corresponding lutetium cryptates **6-Lu** and **7-Lu** and measured their zero-phonon transition $T_1 \rightarrow S_0$ by low-temperature (77 K) steady-state emission spectra (Figure 11). Both spectra show two components to the emission, one minor band around 452 nm and a major band around ca. 525 nm (see Table 2). We assign the former to singlet emission and the latter to triplet emission, consistent with analogous behavior seen in model β-carbolines. For **7-Lu**, these assignments could also be supported by the

DOI: 10.1021/acs.inorgchem.8b01031
Inorg. Chem. 2018, 57, 7390−7401

Table 3. Luminescence Data for the Europium Cryptates 6-Eu and 7-Eu in Aqueous Solution ($c \approx 10\ \mu M$)

entry	compound	$\lambda_{abs,max}$ (long wavel) [nm]	E(T_1) [cm^{-1}][a]	τ_{H_2O} (τ_{D_2O}) [ms][b]	q[c]	τ_{rad} [ms][d]	$\Phi_{Ln}^{Ln} = \frac{\tau_{H_2O}}{\tau_{rad}}$ [%][e]	Φ_{Ln}^{L} [%][f]	$\eta_{sens} = \frac{\Phi_{Ln}^{L}}{\Phi_{Ln}^{Ln}}$[g]
1	**Eu-6**	422	19 000	0.54 (0.96)	0.67	3.6	15	3.3	0.22
2	**Eu-7**	407	19 200	0.45 (0.85)	0.95	4.2	11	2.7	0.25

[a]Zero-phonon transition energy $T_1 \rightarrow S_1$ measured on the corresponding lutetium cryptates in H_2O/glycerol at 77 K. [b]Luminescence lifetimes: λ_{exc} = 317 nm, λ_{em} = 610 nm ($^5D_0 \rightarrow {}^7F_2$). [c]$q$ = number of inner-sphere water molecules, see ref 30. [d]Radiative lifetime: calculated using the eq $1/\tau_{rad} = A_{MD,0}\cdot n^3\cdot(I_{tot}/I_{MD})$, see ref 32. [e]Intrinsic quantum yield, [f]Absolute quantum yield: measured using quinine sulfate (in 1 M H_2SO_4) as standard, see ref 31. [g]Sensitization efficiency.

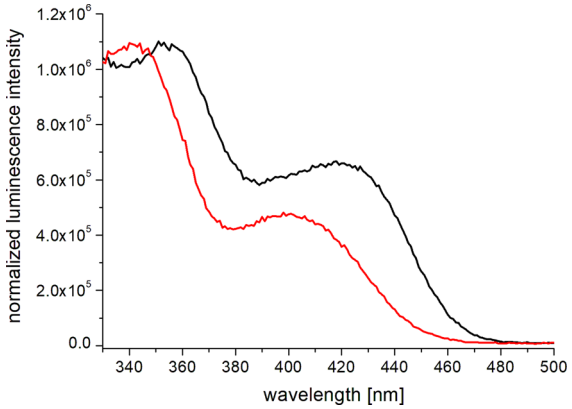

Figure 9. Excitation spectra (λ_{em} = 610 nm) of the europium cryptates **6-Eu** (black) and **7-Eu** (red) in H_2O.

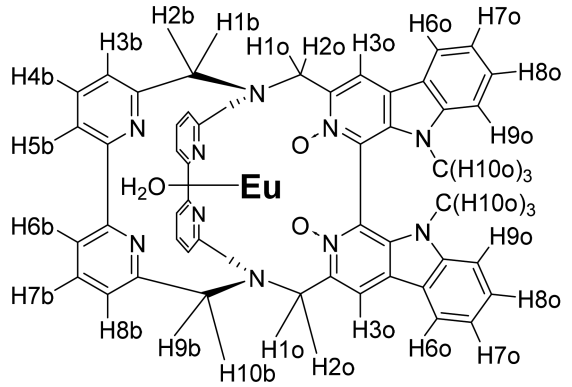

Figure 10. Labeling scheme used for lanthanoid induced shift analysis of the europium cryptate **6-Eu**.

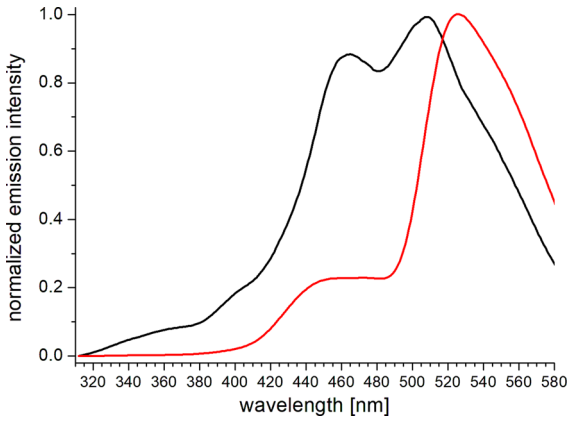

Figure 11. Low temperature emission spectra (λ_{exc} = 305 nm, T = 77 K) of the cryptates **6-Lu** (black) and **7-Lu** (red) measured in a H_2O/glycerol glass matrix (1:1, v/v).

very long luminescence lifetime in the millisecond range of the 525 nm band (λ_{exc} = 305 nm, λ_{em} = 525 nm: biexponential decay with τ_1 = 67 ms (62%) vs τ_2 = 25 ms (38%)) compared to the lifetime in the nanosecond-range of the short-wavelength band (λ_{exc} = 305 nm, λ_{em} = 475 nm: biexponential decay with τ_1 = 0.77 ns (24%) vs τ_2 = 5.6 ns (76%)). The observation of singlet emission is probably an indication that intersystem crossing from the excited singlet to the excited triplet state is not very efficient (vide infra). As has been observed before for similar *N*,*N*′-dioxide cryptates,[5a,c,e,g] the phosphorescence bands do not show vibronic structures which prevents the accurate determination of the zero-phonon triplet transition energies E(T_1). As a rough estimate of the lower boundaries of the triplet energies, the phosphorescence maxima can be taken which are at 19 000 cm^{-1} for **6-Lu** and 19 200 cm^{-1} for **7-Lu**. These values are well above the energy of the emitting $^5D_0$ state of europium (ca. 17 300 cm^{-1}),[28] but the gap E(T_1)-E($^5D_0$) < 2000 cm^{-1} is likely not large enough to comfortably rule out thermally activated energy backtransfer from the metal center to the ligand-centered triplet state (vide infra) potentially resulting in suboptimal luminescence efficiencies (vide infra).

The emission spectra of the europium cryptates **6-Eu** and **7-Eu** in aqueous solution after excitation in the UV (λ_{exc} = 317 nm) show the usual europium bands originating from the excited $^5D_0$ state. Owing to the great stability of the cryptates, the observed europium luminescence does not change in aqueous solution over several days and is not subject to degradation through europium decomplexation even at low concentrations (e.g., c < 10 μM). Comparing **6-Eu** with **7-Eu** shows the great similarity of the spectral features (Figure 12), with the exception of the emission band $^5D_0 \rightarrow {}^7F_0$ (ca. 579 nm), where considerably more intensity is seen for **7-Eu** (see

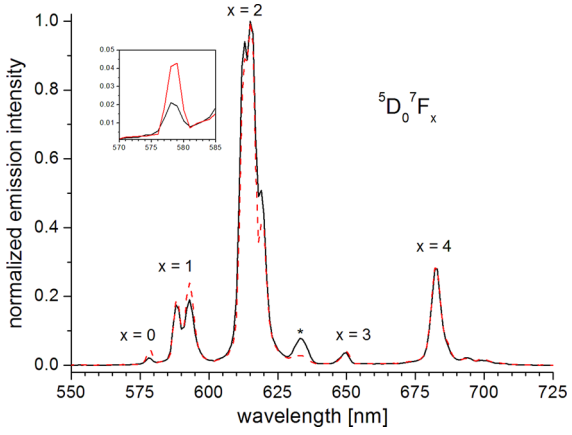

Figure 12. Normalized steady-state emission spectra (λ_{exc} = 317 nm, 2.0 nm bandwidth) of the cryptates **6-Eu** (black) and **7-Eu** (dashed red) in H_2O ($c \approx 10\ \mu M$, * second order excitation peak) – Inset: magnified $^5D_0 \rightarrow {}^7F_0$ transitions.

DOI: 10.1021/acs.inorgchem.8b01031
Inorg. Chem. 2018, 57, 7390–7401

inset in Figure 12). Since this transition is strictly forbidden by ΔJ selection rules and usually only seen for low symmetry environments around the europium centers, this observation likely reflects the symmetry reduction from C_2 for **6-Eu** to C_1 for **7-Eu**.[29]

The shape of the emission spectra for **6-Eu** also does not change significantly with excitation wavelength (Figure 13).

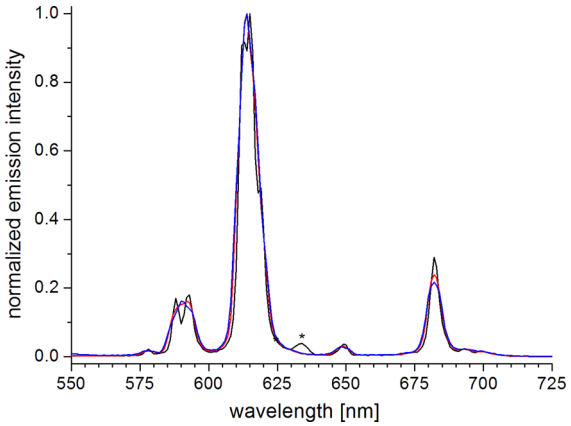

Figure 13. Normalized steady-state emission spectra of **6-Eu** in H_2O ($c \approx 10$ μM, * second order excitation peak) after excitation at different wavelengths (black: λ_{exc} = 317 nm, bandwidth 2.0 nm; red: λ_{exc} = 425 nm, bandwidth 4.0 nm; blue: λ_{exc} = 458 nm, bandwidth 5.0 nm).

The emission intensity naturally goes down with the decrease in extinction coefficients ε (see Figure 8), but the basic photophysical pathways seem to be maintained. Luminescence is still easily detectable after excitation at 458 nm, one of the prominent laser lines (argon-ion) used in confocal luminescence microscopy (Figure 13, blue spectrum).

Luminescence lifetimes τ for **6-Eu** and **7-Eu** were determined in aqueous solution at room temperature (see Figures S36–39). The cryptates show clean monoexponential lifetimes in H_2O ranging from τ = 0.45–0.54 ms (Table 3), with **7-Eu** having slightly shorter decay times compared to **6-Eu**. The same trend is also seen in D_2O (τ = 0.85–0.96 ms, monoexponential), with lifetimes roughly doubling compared to the values in H_2O. The absolute values for τ and the magnitude of the isotope effect upon solvent deuteration are very comparable to the ones previously observed for the unfunctionalized europium cryptate **2** (Figure 3 with R = H; H_2O: τ = 0.46 ms, D_2O: τ = 1.15 ms).[4d] With the measured lifetimes, the number of inner-sphere water molecules q were calculated using the empirical formula developed by Beeby et al.[30] For **6-Eu** and **7-Eu**, q values of 0.67 and 0.95 were obtained respectively (Table 2). For a detailed analysis of the luminescence efficiencies in aqueous solutions (Table 3), the radiative lifetimes τ_{rad} were calculated from the corrected steady-state emission spectra using the method described by Werts et al.,[32] and the absolute quantum yields Φ_{Ln}^{L} were measured against the luminescence standard quinine sulfate.[31] With these additional data, the photophysical parameters Φ_{Ln}^{Ln} (intrinsic quantum yield) and η_{sens} (sensitization efficiency) were calculated in the usual manner (Table 2).[1a] As seen for all other photophysical parameters before, all four cryptates show very similar data with only small deviations. As the bottom line result, the cryptate **6-Eu** achieve slightly higher absolute quantum yields of 3.3% compared to **7-Eu** (2.7%). Overall, these luminescence efficiencies are practically useful and in line with the results for other similar europium cryptates in aqueous solution (usually $\Phi_{Ln}^{L} \approx 1$–10%).[4,5] Among the reasons for the suboptimal efficiency are the low values for the sensitization efficiency $\eta_{sens} \approx 22$–25%, a direct consequence of the low energy of the triplet levels (vide supra) and a necessary trade-off for the possibility of long-wavelength excitation.

The luminescence of the cryptates shows a marked dependence on the pH of the solution. While the emission spectra generally remain the same, the luminescence efficiencies and luminescence lifetimes strongly increase going from lower to higher pH values. Figure 14 shows the corresponding plots

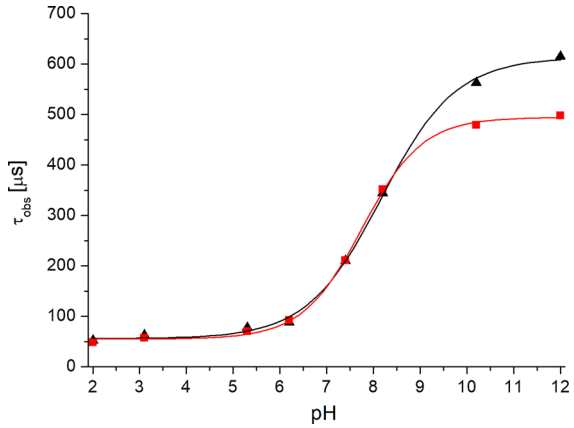

Figure 14. pH dependencies of the luminescence lifetimes ($c \approx 10$ μM, λ_{exc} = 317 nm, λ_{em} = 610 nm) of **6-Eu** (black) and **7-Eu** (red) in phosphate buffer (c = 25 mM) at ambient temperature.

for **6-Eu** and **7-Eu** in aqueous phosphate buffer. Both show clean sigmoidal behaviors with an approximately 10-fold increase from $\tau_{obs} \approx 50$ μs (below pH $\approx$ 5) to $\tau_{obs} \approx 500$ μs (**6-Eu**) and $\tau_{obs} \approx 600$ μs (**7-Eu**) above pH $\approx$ 10. The curves show inflection points at pH = 7.7 (**7-Eu**) and pH = 8.2 (**6-Eu**) which are in a physiologically interesting pH range. The europium cryptates are stable in the buffer solutions at all pH values over several days as indicated by the measurement of unchanging luminescence lifetimes over time. Almost identical results are obtained in aqueous Tris buffer in the applicable pH range (ca. 7.0–9.0). This phenomenon is not seen in the parent tris(bipyridine) cryptate **2** (Figure 3: R = H) which shows almost pH-independent luminescence. Similar pH-dependencies have been reported for a number of other molecular lanthanoid complex architectures[33] and could be very interesting for the development of pH-responsive probes based on the new cryptate scaffolds.

CONCLUSION

In conclusion, we have developed a new sensitizer moiety based on β-carboline and have synthesized two different types of tris(biaryl)-*N*,*N*′-dioxide europium cryptates with this structural motif. The reported cryptates are very stable in aqueous solution and can even be purified by HPLC methods. All europium cryptates show very beneficial red-shifted absorption bands, which allow photoexcitation of europium luminescence well above 400 nm and even at the wavelength of the important argon-ion laser line 458 nm, which could be very useful in the future, e.g., in the context of confocal microscopy. The new carboline-based cryptates exhibit very well-behaved europium photoluminescence in aqueous solution with practically useful

DOI: 10.1021/acs.inorgchem.8b01031
Inorg. Chem. 2018, 57, 7390–7401

luminescence lifetimes (monoexponential, $\tau \approx 0.5$ ms) and absolute quantum yields of up to 3.3%. In addition, the cryptates show well-defined, pH-dependent luminescence in the physiologically relevant range of pH ≈ 7−9. While the measured quantum yields cannot rival some of the more efficient systems in the literature, the possibility for extraordinarily long excitation wavelengths is very rare among lanthanoid complexes in general and will provide a very interesting solution for niche applications where UV excitation is neither desireable nor feasible.

EXPERIMENTAL SECTION

General. Chemicals were purchased from commercial suppliers and used as received unless stated otherwise. Deuterated solvents had deuterium contents >99.8%D. Solvents were dried by standard procedures (THF: solvent purification system MBraun; CH_2Cl_2: CaH_2) or purchased in dry form (DMF). Air-sensitive reactions were performed under a dry, dioxygen-free atmosphere of Ar using the Schlenk technique. Column chromatography was performed with silica gel 60 (Merck KGaA, 0.040−0.063 mm). Analytical thin layer chromatography (TLC) was done on silica gel 60 F254 plates (Merck, coated on aluminum sheets). Electrospray ionization (ESI) mass spectrometry was measured using Bruker Daltonics Esquire 3000plus. Matrix-assisted laser desorption ionization (MALDI) mass spectrometry was measured in 2,5-dihydroxybenzoic acid (DHB) as the matrix using Bruker Autoflex. NMR spectra were measured on an Avance II+400 (^{1}H: 400 MHz, ^{13}C: 101 MHz, ^{19}F: 376 MHz) and DRX-250 (^{1}H: 250 MHz, ^{13}C: 62.9 MHz). The chemical shifts (δ) are reported in ppm relative to TMS, and the residual solvent signals were used as internal reference.

Synthesis. *Dibromide* ***9***. Under Ar, diol **8**[9] (5.40 g, 13.0 mmol, 1.0 equiv) was dissolved in dry DMF (250 mL) and cooled to 0 °C, and PBr_3 (6.1 mL, 17.3 g, 65.0 mmol, 5.0 equivs) was added dropwise by syringe. The suspension was stirred at room temperature for 20 h, volatiles were removed under reduced pressure, and H_2O (250 mL) was added cautiously with ice-cooling. The pH was adjusted to ca. 6 with sat. aqueous $NaHCO_3$ solution, and the aqueous phase was extracted with $CHCl_3$ (4 × 150 mL). The combined organic layers were dried ($MgSO_4$), the solution was concentrated, and the brown solid residue was subjected to column chromatography (SiO_2, gradient: $CHCl_3$/MeOH 200:1 → 100:1, preloading onto SiO_2, detection: UV) yielding the product as an orange solid (1.15 g, 2.1 mmol, 16%).

^{1}H NMR (400 MHz, $CDCl_3$): δ = 8.16−8.30 (m, 4H), 7.63 (t, J = 7.2 Hz, 2H), 7.40 (d, J = 8.4 Hz, 2H), 7.35 (t, J = 7.5 Hz, 2H), 4.94 (br s, 2H), 4.90 (br s, 2H), 3.42 (s, 6H) ppm. ^{13}C NMR (101 MHz, $CDCl_3$) δ = 144.4, 143.1, 140.1, 135.3, 131.3, 129.0, 121.7, 120.8, 120.2, 115.0, 109.9, 36.0, 32.4 ppm. MS (ESI pos. mode): m/z (%) = 548.9 (100, $[M + H]^+$, Br_2 isotopic pattern). TLC: R_f = 0.31 (SiO_2, $CHCl_3$/MeOH 100:1, detection: UV).

N,N′-Dioxide ***10***. Under Ar and with ice-cooling, urea/H_2O_2 adduct (0.36 g, 3.7 mmol, 2.3 equiv) was added in portions to a suspension of dibromide **9** (900 mg, 1.6 mmol, 1.0 equiv) in dry CH_2Cl_2 (40 mL). $(CF_3CO)_2O$ (0.5 mL, 0.73 g, 3.7 mmol, 2.3 equiv) was added slowly, and the mixture was allowed to warm to room temperature and stirred overnight (23 h). A saturated solution of sodium thiosulfate pentahydrate (5 mL) and water (100 mL) was added, and the mixture was stirred for 15 min. The phases were separated, and the aqueous phase was extracted with CH_2Cl_2 (3 × 100 mL). The combined organic layers were dried ($MgSO_4$) and concentrated under reduced pressure. The crude product was purified by column chromatography (SiO_2, CH_2Cl_2/MeOH 50:1, detection: UV) yielding the title compound as a yellow solid (500 mg, 0.86 mmol, 54%).

^{1}H NMR (400 MHz, $CDCl_3$) δ = 8.15−8.28 (m, 2H), 8.01−8.12 (m, 2H), 7.49−7.57 (m, 2H), 7.28−7.36 (m, 4H), 5.66 (d, J = 14.6 Hz, 1H), 5.44 (d, J = 14.6 Hz, 1H), 5.19 (d, J = 10.4 Hz, 1H), 4.66 (d, J = 10.4 Hz, 1H), 3.17−3.33 (m, 6H) ppm. MS (ESI pos. mode): m/z (%) = 511.2 (100, Br_2-isotope pattern), 561.1 (59), 495.3 (44), 533.1 (44), 483.3 (29), 481.0 (29, $[M + H]^+$, Br_2 isotopic pattern). TLC: R_f = 0.25 (SiO_2, CH_2Cl_2/MeOH 25:1, detection: UV).

Sodium Cryptate ***6-Na***. Under Ar, the *N,N′*-dioxide **10** (300 mg, 520 μmol, 1.0 equiv) and the macrocycle **11**[11] (205 mg, 520 μmol, 1.0 equiv) were suspended in CH_3CN (300 mL, HPLC grade), and anhydrous Na_2CO_3 (548 mg, 5.2 mmol, 10.0 equiv) was added. The mixture was heated under reflux for 24 h, cooled to ambient temperature, and filtered. The filtrate was concentrated under reduced pressure and the resulting residue was subjected to column chromatography (SiO_2, CH_2Cl_2/MeOH 15:1 → 9:1, detection: UV) yielding the title compound as a yellow solid (40 mg, 48 μmol, 9%).

^{1}H NMR (250 MHz, CD_3OD) δ = 8.74 (s, 2H), 8.35 (d, J = 7.8 Hz, 2H), 7.86−7.94 (m, 8H), 7.61−7.69 (m, 2H), 7.43- 7.57 (m, 8H), 4.63 (d, J = 11.7 Hz, 2H), 3.95 (dd, J = 12.7, 9.1 Hz, 4H), 3.60 (dd, J = 15.6, 12.9 Hz, 6H), 3.20 (s, 6H) ppm. ^{13}C NMR (63 MHz, CD_3OD) δ = 160.3, 159.5, 158.6, 158.3, 145.5, 140.9, 139.4, 139.2, 138.8, 130.4, 128.2, 125.6, 125.5, 124.7, 123.2, 122.9, 122.6, 122.5, 121.9, 121.6, 111.4, 80.1, 62.1, 61.5, 30.9 ppm. MS (ESI pos. mode): m/z (%) = 835.4 (100, $[M]^+$), 903.3 (40), 869.3 (33). TLC: R_f = 0.15 (SiO_2, CH_2Cl_2/MeOH 15:1, detection: UV).

Sodium Cryptate ***[D$_{20}$]-6-Na***. Under Ar, the *N,N′*-dioxide **10** (8 mg, 14 μmol, 1.0 equiv) and the macrocycle [$\mathbf{D_{20}}$]-**11**[5a] (>99%D, 5.8 mg, 14 μmol, 1.0 equiv) were suspended in CH_3CN (15 mL, HPLC grade) and Na_2CO_3 (15 mg, 140 μmol, 10.0 equiv) was added. The mixture was heated under reflux for 21 h, cooled to ambient temperature, and filtered. The filtrate was concentrated under reduced pressure, and the resulting residue was subjected to column chromatography (SiO_2, $CHCl_3$/MeOH 10:1, detection: UV) to yield the title compound as a light yellow solid (4 mg, 4 μmol, 30%, >99% D).

^{1}H NMR (400 MHz, CD_3OD): δ = 8.75 (s, 1H), 8.74 (d, J = 1.4 Hz, 1H), 8.34 (d, J = 7.9 Hz, 2H), 7.62−7.67 (m, 2H), 7.53−7.56 (m, 2H), 7.41−7.47 (m, 2H), 4.64 (d, J = 2.6 Hz, 1H), 4.61 (d, J = 2.5 Hz, 1H), 3.64 (d, J = 4.2 Hz, 1H), 3.61 (d, J = 4.3 Hz, 1H), 3.20 (br s, 3H), 3.18 (br s, 3H) ppm. TLC: R_f = 0.18 (SiO_2, $CHCl_3$/MeOH 10:1, detection: UV).

Europium Cryptates ***6-Eu*** *and* ***6-Eu′***. The sodium cryptate **6-Na** (20 mg, 24 μmol, 1.0 equiv) and $EuCl_3 \cdot 6\ H_2O$ (15 mg, 41 μmol, 1.7 equiv) were suspended in CH_3CN (15 mL, HPLC grade), and the mixture was heated under reflux for 48 h. The solvent was removed in vacuo, and the remaining residue was taken up in a minimum of water and subjected to preparative reversed-phase HPLC (see the Supporting Information for details). Fractions containing pure lanthanoid complexes were combined (retention times: **6-Eu**, t_r = 17.4 min; **6-Eu′**, t_r = 18.4 min) and evaporated to dryness at room temperature. The complexes were isolated as yellow solids.

6-Eu. ^{1}H NMR (400 MHz, CD_3OD) δ = 29.35 (br s, 2H), 27.06 (br s, 2H), 16.51 (br s, 2H), 14.22 (br s, 2H), 11.84 (br s, 2H), 9.84 (br s, 2H), 9.09 (d, J = 8.0 Hz, 2H), 7.95 (t, J = 7.5 Hz, 2H), 7.68 (t, J = 7.7 Hz, 2H), 7.21 (br s, 2H), 6.97 (br s, 2H), 6.88 (d, J = 7.7 Hz, 2H), 3.51 (s, 2H), 3.06 (s, 2H), 2.01 (d, J = 7.4 Hz, 2H), 0.70 (br s, 6H), −9.04 (br s, 2H), −14.68 (br s, 2H) ppm. ^{19}F-NMR (377 MHz, CD_3OD) δ = −76.88 (s), −77.32 (br s) ppm. MS (MALDI, pos. mode): m/z (%) = 1086.2 (100, [M + deprotonated matrix DHB − 2 × O + e^-]$^+$, Eu isotopic pattern), 1102.2 (15, [M + deprotonated matrix DHB − O + e^-]$^+$, Eu isotopic pattern).

6-Eu′. ^{1}H NMR (400 MHz, CD_3OD) δ = 28.80 (br s, 2H), 26.88 (br s, 1H), 26.64 (br s, 1H), 16.24 (s, 2H), 13.77 (s, 2H), 11.72 (br, 2H), 9.88 (s, 1H), 9.79 (s, 1H), 9.14 (s, 1H), 9.08 (d, J = 7.9 Hz, 1H), 7.85−8.04 (m, 2H), 7.69 (t, J = 7.6 Hz, 1H), 6.68−7.28 (m, 7H), 3.63 (br, 1H), 3.50 (s, 1H), 3.16 (s, 1H), 3.02 (br s, 1H), 2.12 (d, J = 7.4 Hz, 1H), 1.96 (s) and 1.92 (d, J = 7.4 Hz, together 1H), 0.86 (s, 3H), 0.76 (s, 3H), −9.06 (br s, 1H), −9.27 (br s, 1H), −14.28 (br s, 1H), −14.82 (br s, 1H) ppm. ^{19}F-NMR (377 MHz, CD_3OD) δ = −76.88 (s), −77.32 (br s) ppm. MS (MALDI, pos. mode): m/z (%) = 1120.2 (100, [M + deprotonated matrix DHB + H_2O + e^-]$^+$, Eu isotopic pattern), 1136.2 (22, [M + deprotonated matrix DHB + O + H_2O + e^-]$^+$, Eu isotopic pattern), 1154.2 (15, [M + deprotonated matrix DHB + O + 2 H_2O + e^-]$^+$, Eu isotopic pattern).

DOI: 10.1021/acs.inorgchem.8b01031
Inorg. Chem. 2018, 57, 7390−7401

Europium Cryptates [D_{20}]-6-Eu and [D_{20}]-6-Eu′. The sodium cryptate [$\mathbf{D_{20}}$]-**6-Na** (4 mg, 5 μmol, 1.0 equiv) and $EuCl_3 \cdot 6\ H_2O$ (3 mg, 8.5 μmol, 1.7 equiv) were suspended in CH_3CN (5 mL, HPLC grade), and the mixture was heated under reflux for 42 h. The solvent was removed in vacuo, and the remaining residue was suspended in MeOH, covered with a layer of diethyl ether and stored at 4 °C overnight. The yellow precipitate was collected using a Büchner funnel (Nylon membrane filter, GE Healthcare Life Sciences, pore size 0.45 μm) and washed with diethyl ether. The remaining residue was taken up in a minimum of CH_3CN/H_2O (1:1, v/v) and subjected to preparative reversed-phase HPLC (see the Supporting Information for details). Fractions containing pure lanthanoid complexes were combined (retention times: [$\mathbf{D_{20}}$]-**6-Eu**, t_r = 17.2 min; [$\mathbf{D_{20}}$]-**6-Eu′**, t_r = 18.3 min) and evaporated to dryness at room temperature. The complexes were isolated as yellow solids.

[D$_{20}$]-6-Eu. ^{1}H NMR (400 MHz, CD_3OD): δ = 9.85 (s, 2H), 9.10 (d, *J* = 7.9 Hz, 2H), 7.96 (t, J = 7.6 Hz, 2H), 7.69 (t, *J* = 7.7 Hz, 2H), 6.93 (br, 2H), 0.77 (s, 6H), −9.15 (br s, 2H), −14.61 (br s, 2H) ppm. MS (MALDI, pos. mode): *m*/*z* (%) = 1106.4 (100, [M + deprotonated matrix DHB − 2 × O + e^-]$^+$, Eu isotopic pattern).

[D$_{20}$]-6-Eu′. ^{1}H NMR (400 MHz, CD_3OD): δ = 9.89 (br s, 1H), 9.80 (br s, 1H), 9.16 (br s, 1H), 9.09 (d, J = 8.0 Hz, 1H), 7.90−8.95 (m, 2H), 7.70 (t, J = 7.7 Hz, 1H), 6.95 (t, J = 7.5 Hz, 2H), 0.93 (br s, 3H), 0.82 (br s, 3H), −9.17 (br s, 1H), −9.38 (br s, 1H), −14.25 (br s, 1H), −14.78 (br s, 1H) ppm (1 H signal is missing). MS (MALDI, pos. mode): *m*/*z* (%) = 1140.3 (100, [M + deprotonated matrix DHB + H_2O + e^-]$^+$, Eu isotopic pattern).

Lutetium Cryptates ***6-Lu.*** The sodium cryptate **6-Na** (5 mg, 6 μmol, 1.0 equiv) and $LuCl_3 \cdot 6\ H_2O$ (4 mg, 10 μmol, 1.7 equivs) were suspended in CH_3CN (10 mL, HPLC grade), and the mixture was heated under reflux for 48 h. The solvent was removed in vacuo, and the remaining residue was suspended in MeOH, covered with a layer of diethyl ether, and stored at 4 °C overnight. The yellow precipitate was collected using a Büchner funnel (Nylon membrane filter, GE Healthcare Life Sciences, pore size 0.45 μm) and washed with diethyl ether. The complex was isolated as a yellow solid.

^{1}H NMR (400 MHz, CD_3OD) δ = 9.11 (s, 2H), 8.46−8.59 (m, 6H), 8.17−8.30 (m, 4H), 7.77−7.86 (m, 4H), 7.55−7.71 (m, 6H), 4.78 (d, *J* = 15.2 Hz, 2H), 4.23 (d, *J* = 15.3 Hz, 2H), 4.17 (d, *J* = 16.1 Hz, 2H), 4.10 (d, *J* = 12.4 Hz, 2H), 3.48−3.54 (m, 4H), 3.13−3.19 (m 6H) ppm. MS (MALDI, pos. mode): *m*/*z* (%) = 1142.4 (27), 1295.4 (100, [M + 2 × deprotonated matrix DHB + H_2O − O]$^+$, Lu isotopic pattern).

Tetrahydroharmane ***14*** *(Mixture of Diastereomers).* L-Tryptophan methyl ester **12** (2.64 g, 12.1 mmol, 1.0 equiv) was added to a stirred suspension of the aldehyde **13**[12] (2.00 g, 12.1 mmol, 1.0 equiv) in CH_2Cl_2 (400 mL) in the presence of molecular sieves (4 Å) and stirred at room temperature for 38 h. The mixture was then cooled to 0 °C, CF_3COOH (1.38 g, 0.95 mL, 12.1 mmol, 1.0 equiv) was added, and the reaction stirred at this temperature for 5 h. The reaction was quenched with sat. aqueous $NaHCO_3$ solution (75 mL) and was allowed to warm to room temperature. The phases were separated, and the combined organic layers were washed with aqueous NaCl solution (3 × 200 mL) and dried (Na_2SO_4), and the solvent was removed under reduced pressure. The resulting solid was purified by column chromatography (SiO_2, $CHCl_3$/MeOH 50:1, detection: UV) yielding the product as an orange solid (3.90 g, 10.7 mmol, 88%).

^{1}H NMR (400 MHz, $CDCl_3$) δ = 9.69 (br s, 1H), 7.94 (dd, *J* = 7.5, 1.2 Hz, 1H), 7.75 (t, *J* = 7.7 Hz, 1H), 7.69 (dd, *J* = 7.9, 1.1 Hz, 1H), 7.52 (d, *J* = 7.7 Hz, 1H), 7.34 (d, *J* = 7.8 Hz, 1H), 7.12−7.17 (m, 1H), 7.06−7.11 (m, 1H), 3.97 (dd, *J* = 6.6, 5.1 Hz, 1H), 3.90 (s, 3H), 3.55 (s, 3H), 3.21 (ddd, *J* = 15.2, 5.1, 1.3 Hz, 1H), 3.12 (ddd, *J* = 15.3, 6.7, 1.7 Hz, 1H), 2.80 (br s, 1H) ppm. ^{13}C NMR (MHz, $CDCl_3$) δ = 173.6, 165.1, 162.1, 146.6, 137.8, 136.3, 131.9, 126.6, 124.3, 123.5, 121.6, 119.0, 117.9, 111.0, 107.2, 54.9, 53.4, 52.5, 51.8, 24.6 ppm. MS (ESI pos. mode): *m*/*z* (%) = 366.2 (100, [M + H]$^+$). TLC: R_f = 0.11 (SiO_2, $CHCl_3$/MeOH 50:1, detection: UV).

Pyridine-Carboline Diester ***15.*** Under Ar, to a stirred solution of compound **14** (3.5 g, 9.6 mmol, 1.0 equiv) and triethylamine (1.94 g, 2.7 mL, 19.2 mmol, 2.0 equivs) in dry DMF (50 mL, peptide grade) at −10 °C, a solution of trichloroisocyanuric acid (TCCA, 2.47 g, 9.6 mmol, 1.0 equiv) in dry DMF (50 mL, peptide grade) was added by syringe over 20 min. After that, the mixture was stirred at 0 °C for 2 h and then filtered. The precipitate was washed with H_2O, CH_3OH, and CH_2Cl_2 in turn to give a pale yellow powder which cannot be dissolved. Under Ar, NaH (60% dispersion in mineral oil, 290 mg, 7.3 mmol, 1.25 equiv) was suspended in dry DMF (peptide grade) at -10 °C. The pale yellow powder was added, followed by methyl iodide (1.24 g, 0.54 mL, 8.7 mmol, 1.5 equiv) after 10 min. The mixture was stirred for 4 h at 0 °C and at room temperature overnight (15 h). The mixture was poured into ice water, and the precipitate was collected on a Büchner funnel, washed with H_2O, and dried under reduced pressure to give a white solid (2.1 g, 5.6 mmol, 96%).

^{1}H NMR (400 MHz, $CDCl_3$) δ = 8.94/8.88 (s, 1H), 8.40 (ddd, *J* = 7.8, 3.1, 1.1 Hz, 1H), 8.24−8.26 (m, 1H), 8.22−8.24 (m, 1H), 8.09 (td, *J* = 7.8, 1.4 Hz, 1H), 7.66 (ddd, *J* = 8.4, 7.1, 1.2 Hz, 1H), 7.52/7.50 (br s, 1H), 7.38 (ddd, *J* = 7.9, 7.1, 0.9 Hz, 1H), 4.04 (s, 3H), 4.00 (s, 3H), 3.73 (s, 3H) ppm. MS (ESI pos. mode): *m*/*z* (%) = 376.2 (100, [M + H]$^+$), 398.1 (37, [M + Na]$^+$).

Pyridine-Carboline Diol ***16.*** Under Ar, a solution of the diester **15** (2.00 g, 5.3 mmol, 1.0 equiv) in dry THF (50 mL) was added dropwise to a slurry of $LiAlH_4$ (0.30 g, 8.0 mmol, 1.5 equivs) in dry THF (30 mL) at 0 °C. When the addition was complete, the cooling bath was removed, and the mixture was stirred at ambient temperature for 0.5 h. The mixture was cooled to 0 °C and was carefully quenched with water (0.3 mL), 15% aqueous solution of NaOH (0.3 mL), and water (0.9 mL). After being stirred for 30 min, the mixture was diluted in EtOAc (50 mL), filtered through Celite, and concentrated under reduced pressure to give a yellow solid (1.00 g, 3.1 mmol, 59%).

^{1}H NMR (400 MHz, [D_6]-DMSO) δ = 8.33 (d, *J* = 7.6 Hz, 1H), 8.27 (s, 1H), 8.01 (t, *J* = 7.7 Hz, 1H), 7.79 (d, *J* = 6.8 Hz, 1H), 7.55−7.66 (m, 3H), 7.30 (ddd, *J* = 7.9, 6.2, 1.8 Hz, 1H), 5.54 (t, *J* = 5.8 Hz, 1H), 5.45 (t, *J* = 5.9 Hz, 1H), 4.77 (d, *J* = 5.6 Hz, 2H), 4.66 (d, *J* = 5.7 Hz, 2H), 3.50 (s, 3H) ppm. ^{13}C NMR (63 MHz, [D_6]-DMSO) δ = 160.5, 156.6, 150.0, 142.7, 141.3, 137.2, 133.6, 130.6, 128.5, 122.9, 121.5, 120.4, 119.6, 119.4, 111.0, 110.3, 64.5, 64.3, 33.2 ppm. MS (ESI pos. mode) *m*/*z* (%) = 320.3 (100, [M + H]$^+$), 342.2 (33, [M + Na]$^+$).

Pyridine-Carboline Dibromide ***17.*** Under Ar, compound **16** (1.00 g, 3.1 mmol, 1.0 equiv) was dissolved in dry DMF (50 mL, peptide grade) and cooled to 0 °C, and PBr_3 (1.5 mL, 4.24 g, 15.7 mmol, 5 equiv) was added dropwise by syringe. The suspension was stirred at room temperature for 23 h, volatiles were removed under reduced pressure, and H_2O (50 mL) was added cautiously with ice-cooling. The pH was adjusted to ca. 6 with sat. $NaHCO_3$ solution, and the aqueous phase was extracted with $CHCl_3$ (4 × 100 mL). The combined organic layers were dried ($MgSO_4$), the solution was concentrated, and the brown solid residue was subjected to column chromatography (SiO_2, gradient: $CHCl_3$/MeOH 200:1 → 100:1, preloading onto SiO_2, detection: UV) yielding the product as a yellow solid (0.50 g, 1.1 mmol, 36%).

^{1}H NMR (400 MHz, CD_2Cl_2) δ = 8.14−8.22 (m, 2H), 7.92−7.97 (m, 2H), 7.65 (ddd, J = 8.4, 7.1, 1.2 Hz, 1H), 7.53−7.57 (m, 1H), 7.51 (d, *J* = 8.4 Hz, 1H), 7.31−7.36 (m, 1H), 4.86 (s, 2H), 4.66 (s, 2H), 3.64 (s, 3H) ppm. MS (ESI pos. mode): *m*/*z* (%) = 446.0 (100, [M + H]$^+$ Br_2 isotopic pattern).TLC: R_f = 0.23 (SiO_2, CH_2Cl_2/MeOH 100:1, detection: UV).

Pyridine-Carboline N,N′-Dioxide ***18.*** Under Ar and with ice-cooling, urea/H_2O_2 adduct (200 mg, 2.1 mmol, 2.3 equivs) was added in portions to a suspension of dibromide **17** (400 mg, 0.9 mmol, 1.0 equiv) in dry CH_2Cl_2 (20 mL). Then, $(CF_3CO)_2O$ (0.3 mL, 440 mg, 2.1 mmol, 2.3 equiv) was added slowly. The mixture was allowed to warm to room temperature and stirred overnight (18 h). A saturated solution of sodium thiosulfate pentahydrate (2.5 mL) and water (50 mL) was added and the mixture was stirred for 30 min. The phases were separated and the aqueous phase was extracted with CH_2Cl_2 (3 × 100 mL). The combined organic layers were dried ($MgSO_4$) and concentrated under reduced pressure. The crude product was purified by column chromatography (SiO_2, CH_2Cl_2/MeOH 25:1, detection: UV) to give the product as a yellow solid (150 mg, 0.3 mmol, 35%).

DOI: 10.1021/acs.inorgchem.8b01031
Inorg. Chem. 2018, 57, 7390−7401

^{1}H NMR (400 MHz, CD_2Cl_2) δ = 8.20 (s, 1H), 8.03 (d, J = 2.0 Hz, 1H), 7.72 (dd, J = 7.8, 2.2 Hz, 1H), 7.62 (dd, J = 7.9, 2.2 Hz, 1H), 7.51 (dd, J = 8.8, 2.0 Hz, 1H), 7.44 (t, J = 7.8 Hz, 2H), 7.32 (d, J = 8.8 Hz, 1H), 4.95 (dd, J = 10.6, 7.1 Hz, 2H), 4.79 (d, J = 10.6 Hz, 1H), 4.56 (d, J = 10.6 Hz, 1H), 3.36 (s, 3H) ppm. MS (ESI pos. mode): m/z (%) = 511.9 (100, $[M + H]^+$), 477.9 (47, $[M + H]^+$, Br_2 isotopic pattern). TLC: R_f = 0.25 (SiO_2, CH_2Cl_2/MeOH 25:1, detection: UV).

Sodium Cryptate ***7-Na***. Under Ar, the *N*,*N*′-dioxide **17** (75 mg, 0.16 mmol, 1.0 equiv) and macrocycle **11**[11] (62 mg, 0.16 mmol, 1.0 equiv) were suspended in CH_3CN (150 mL, HPLC grade) and anhydrous Na_2CO_3 (170 mg, 1.6 mmol, 10 equiv) was added. The mixture was heated under reflux for 59 h, cooled to ambient temperature, and filtered. The filtrate was concentrated under reduced pressure, and the resulting residue was subjected to column chromatography (SiO_2, CH_2Cl_2/MeOH 15:1 → 9:1, detection: UV) to yield the title compound as a yellow solid (70 mg, 86 μmol, 54%).

^{1}H NMR (400 MHz, CD_2Cl_2) δ = 8.23−8.28 (m, 1H), 8.15 (d, J = 8.0 Hz) + 8.13 (d, J = 2.0 Hz) integrated together as 1H, 7.64−7.88 (m, 9H), 7.53−7.59 (m, 2H), 7.45−7.52 (m, 1H), 7.43 (d, J = 7.8 Hz, 3H), 7.39 (d, J = 8.3 Hz, 1H), 7.31−7.37 (m, 2H), 4.47 (dd, J = 11.7, 7.4 Hz, 1H), 4.40 (dd, J = 11.6, 4.7 Hz, 1H), 3.98 (dd, J = 12.7, 3.6 Hz, 1H), 3.93 (d, J = 5.1 Hz, 1H), 3.90 (d, J = 5.2 Hz, 1H), 3.80 (dd, J = 12.8, 7.9 Hz, 1H), 3.59 (d, J = 12.7 Hz, 1H). 3.36−3.50 (m, 8H) ppm. MS (ESI pos. mode): m/z (%) = 732.4 (100, $[M]^+$).

Europium Cryptates ***7-Eu*** *and* ***7-Eu′***. The sodium cryptate **7-Na** (10 mg, 12 μmol, 1.0 equiv) and $EuCl_3 \cdot 6\ H_2O$ (7.7 mg, 21 μmol, 1.7 equiv) were suspended in CH_3CN (15 mL, HPLC grade), and the mixture was heated under reflux for 43 h. The solvent was removed in vacuo, and the remaining residue was taken up in a minimum of water and subjected to preparative reversed-phase HPLC. Fractions containing pure lanthanoid complexes **7** were combined (retention times: **7-Eu**, t_r = 14.8 min; **7-Eu′**, t_r = 16.1 min) and evaporated to dryness at room temperature. The complexes were isolated as yellow solids.

7-Eu. ^{1}H NMR (400 MHz, CD_3OD) δ = 28.65 (d, J = 11.4 Hz, 1H), 28.56 (br s, 1H), 26.95 (br s, 1H), 26.13 (br s, 1H), 15.70 (d, J = 7.3 Hz, 1H), 15.61 (d, J = 7.5 Hz, 1H), 13.75 (d, J = 10.4 Hz, 1H), 12.73 (d, J = 11.0 Hz, 1H), 11.34 (t, J = 7.0 Hz, 1H), 11.27 (t, J = 7.2 Hz, 1H), 9.69 (d, J = 7.7 Hz, 1H), 9.26 (s, 1H), 9.22 (d, J = 7.5 Hz, 1H), 8.84 (d, J = 8.0 Hz, 1H), 7.95 (t, J = 7.6 Hz, 1H), 7.60 (t, J = 7.6 Hz, 1H), 7.21 (br, 1H), 7.14 (d, J = 8.1 Hz, 1 H), 7.10 (br, 1H), 6.81 (d, J = 7.0 Hz, 1H), 6.48 (d, J = 7.1 Hz, 1H), 5.19 (d, J = 6.9 Hz, 1H), 3.94 (t, J = 7.0 Hz, 1H), 3.76 (d, J = 7.0 Hz, 1H), 2.98 (d, J = 6.8 Hz, 1H), 2.14 (d, J = 7.5 Hz, 1H), 1.74 (s, 3H), 1.51 (d, J = 7.5 Hz, 1H), −8.07 (d, J = 11.0 Hz, 1H), −9.71 (d, J = 11.0 Hz, 1H), −12.22 (d, J = 9.0 Hz, 1H), −15.37 (br, 1H) ppm. (1H signal is missing). MS (MALDI pos. mode): m/z (%) = 983.2 (100, M + deprotonated matrix DHB + $e^-]^+$, Eu isotopic pattern).

7-Eu′. ^{1}H NMR (400 MHz, CD_3OD) δ = 28.15 (br, 2H), 26.40 (s, 1H), 25.90 (s, 1H), 15.42 (d, J = 6.6 Hz, 1H), 15.34 (d, J = 6.9 Hz, 1H), 13.26 (d, J = 10.9 Hz, 1H), 12.26 (d, J = 9.5 Hz, 1H), 11.16 (d, J = 8.1 Hz, 2H), 9.65 (d, J = 7.6 Hz, 1H), 9.30 (s, 1H), 9.26 (d, J = 7.5 Hz, 1H), 8.90 (s, 1H), 7.93 (d, J = 8.3 Hz, 1H), 7.18 (d, J = 8.5 Hz, 1H), 7.02 (br, 1H), 6.88 (br, 1H), 6.63 (d, J = 7.0 Hz, 1H), 6.44 (d, J = 7.0 Hz, 1H), 5.38 (d, J = 6.6 Hz, 1H), 3.91 (t, J = 6.9 Hz, 1H), 3.70 (d, J = 6.8 Hz, 1H), 3.52 (t, J = 6.7 Hz, 1H), 3.07 (d, J = 6.9 Hz, 1H), 2.04 (d, J = 7.5 Hz, 1H), 1.81 (s, 3H), 1.60 (d, J = 7.5 Hz, 1H), −8.32 (d, J = 10.6 Hz, 1H), −9.77 (d, J = 9.6 Hz, 1H), −12.40 (br, 1H), −15.01 (br, 1H) ppm. (1H signal is missing). MS (MALDI, pos. mode): m/z (%) = 1017.2 (100, [M + deprotonated matrix DHB + H_2O + $e^-]^+$, Eu isotopic pattern).

Lutetium Cryptates ***7-Lu***. The sodium cryptate **7-Na** (4 mg, 5 μmol, 1.0 equiv) and $LuCl_3 \cdot 6\ H_2O$ (3.3 mg, 8 μmol, 1.7 equiv) were suspended in CH_3CN (10 mL, HPLC grade), and the mixture was heated under reflux for 48 h. The solvent was removed in vacuo, and the remaining residue was suspended in MeOH, covered with a layer of diethyl ether, and stored at 4 °C overnight. The yellow precipitate was collected using a Büchner funnel (Nylon membrane filter, GE Healthcare Life Sciences, pore size 0.45 μm) and washed with diethyl ether. The complex was isolated as a yellow solid.

^{1}H NMR (400 MHz, CD_3OD) δ = 8.96 (d, J = 1.8 Hz, 1H), 8.60 (d, J = 8.1 Hz, 1H), 8.55 (d, J = 4.7 Hz, 1H), 8.53 (d, J = 4.1 Hz, 1H), 8.50 (br, 1H), 8.46 (d, J = 7.9 Hz, 1H), 8.38−8.43 (m, 2H), 8.34 (d, J = 7.7 Hz, 1H), 8.27−8.32 (m, 3H), 8.21 (td, J = 7.9, 2.1 Hz, 1H), 7.77−7.88 (m, 5H), 7.64 (d, J = 7.8 Hz, 1H), 7.55−7.59 (m, 1H), 4.68−4.76 (m, 3H), 4.30 (d, J = 15.8 Hz, 1H), 4.23 (d, J = 15.3 Hz, 2H), 4.13 (d, J = 15.9 Hz, 1H), 4.07 (d, J = 7.4 Hz, 1H), 4.04 (d, J = 7.6 Hz, 1H), 3.80 (d, J = 16.0 Hz, 1H), 3.67 (s, 3H), 3.43 (dd, J = 15.8, 6.2 Hz, 1H) ppm. (2H signals are missing). MS (MALDI, pos. mode): m/z (%) = 1032.8 (40), 1158.3 (40, [M + 2 × deprotonated matrix DHB − 2 × O]$^+$, Lu isotopic pattern).

Photophysics. UV/vis absorption spectra were recorded on a Jasco-V770 spectrophotometer using 1.0 cm quartz cuvettes. Steady state emission spectra were acquired on a Horiba Fluorolog-3 DF spectrofluorimeter using 1.0 cm quartz cuvettes at RT. CD_3OD and D_2O (NMR grade 99.8%D) were purchased from commercial suppliers and used as received without special drying procedures. The excitation light source was a 450 W continuous xenon lamp. Emission was monitored at 90° using a Hamamatsu R2658P PMT. Spectral selection was achieved by double-grating DFM/DFX monochromators (excitation: 1200 grooves/mm, blazed at 330 nm; emission: 1200 grooves/mm, blazed at 500 nm). Low temperature spectra were recorded on frozen glasses of solutions (H_2O/glycerol 1:1, v/v) using a dewar cuvette filled with liquid N_2 (T = 77 K). pH-dependent measurements were performed in 25 mM phosphate buffer (using $Na_xH_yPO_4$, x = 0−3).

Quantum yields were determined in aqueous solution using quinine sulfate (in 1 M sulfuric acid) (Φ_r = 54.6%)[23] as the quantum yield standard after excitation at λ_{exc} = 317 nm. They were measured by the optically dilute method using the following equation:

$$\Phi_x = \Phi_r \cdot (\mathrm{Grad}_x/\mathrm{Grad}_r) \times (n_x/n_r)^2$$

where n is the refractive index (H_2O = 1.333) and Grad is the linearly fitted slope from the plot of the integrated luminescence intensity versus the absorbance at the excitation wavelength. The subscripts "x" and "r" refer to the sample and reference, respectively. The estimated uncertainties in Φ_x are ±15%.

Luminescence lifetimes were determined with the same instrumental setup as described above for the steady-state experiments. The light source for these measurements was a 70 W xenon flash lamp (pulse width ca. 1.5 μs fwhm). Lifetime data analysis (deconvolution, statistical parameters, etc.) was performed using the software package DAS from Horiba. Lifetimes were either determined by fitting the middle and tail portions of the decays or by deconvolution of the decay profiles with the instrument response function, which was determined using a dilute aqueous dispersion of colloidal silica (Ludox AM-30). The estimated uncertainties in τ are ±10%.

■ ASSOCIATED CONTENT

Supporting Information

The Supporting Information is available free of charge on the ACS Publications website at DOI: 10.1021/acs.inorgchem.8b01031.

HPLC traces, MALDI mass spectra, additional NMR spectra, luminescence decay profiles, optimized Cartesian coordinates of **6-Eu**, and deviations of experimental and calculated LIS data (PDF)

■ AUTHOR INFORMATION

Corresponding Authors

*(M.S.) E-mail: michael.seitz@uni-tuebingen.de.

*(C.P-I.) E-mail: carlos.platas.iglesias@udc.es.

ORCID

David Esteban-Gómez: 0000-0001-6270-1660

Carlos Platas-Iglesias: 0000-0002-6989-9654

Michael Seitz: 0000-0002-9313-2779

DOI: 10.1021/acs.inorgchem.8b01031
Inorg. Chem. 2018, 57, 7390−7401

Notes

The authors declare no competing financial interest.

■ ACKNOWLEDGMENTS

Financial support is gratefully acknowledged from DFG (Research Grant SE 1448/6-1). Authors D. E.-G. and C. P.-I. thank Centro de Computación de Galicia (CESGA) for providing the computer facilities and Xunta de Galicia (ED431B 2017/59 and ED431D 2017/01) for generous financial support.

■ REFERENCES

(1) (a) Bünzli, J.-C. G.; Eliseeva, S. V.; Photophysics of Lanthanoid Coordination Compounds; In *Comprehensive Inorganic Chemistry II*, Reedijk, J.; Poeppelmeier, K.; Eds.; Elsevier: Amsterdam, 2013; *Vol. 8*, p 339. (b) Bünzli, J.-C. G. Lanthanide Luminescence: From a Mystery to Rationalization, Understanding, and Applications. In *Handbook on the Physics and Chemistry of Rare Earths*; Bünzli, J.-C. G.; Pecharsky, V. K., Eds.; Elsevier: Amsterdam, 2016, Vol. *50*, Chapter 287, p 141. (c) Bünzli, J.-C. G. Rising Stars in Science and Technology: Luminescent Lanthanide Materials. *Eur. J. Inorg. Chem.* **2017**, *2017*, 5058.

(2) (a) Alpha, B.; Lehn, J.-M.; Mathis, G. Energy Transfer Luminescence of Europium(III) and Terbium(III) Cryptates of Macrobicyclic Polypyridine Ligands. *Angew. Chem., Int. Ed. Engl.* **1987**, *26*, 266. (b) Alpha, B.; Balzani, V.; Lehn, J.-M.; Perathoner, S.; Sabbatini, N. Luminescence Probes: The Eu^{3+}- and Tb^{3+}-Cryptates of Polypyridine Macrobicyclic Ligands. *Angew. Chem., Int. Ed. Engl.* **1987**, *26*, 1266.

(3) Reviews Cryptates: (a) Bazin, H.; Preaudat, M.; Trinquet, E.; Mathis, G. Homogeneous time resolved fluorescence resonance energy transfer using rare earth cryptates as a tool for probing molecular interactions in biology. *Spectrochim. Acta, Part A* **2001**, *57*, 2197. (b) Zwier, J. M.; Bazin, H.; Lamarque, L.; Mathis, G. Luminescent Lanthanide Cryptates: from the Bench to the Bedside. *Inorg. Chem.* **2014**, *53*, 1854.

(4) Selected examples for tris(biaryl)-based cryptates: (a) Rodriguez-Ubis, J.-C.; Alpha, B.; Plancherel, D.; Lehn, J.-M. Synthesis of the Sodium Cryptates of Macrobicyclic Ligands Containing Bipyridine and Phenanthroline Groups. *Helv. Chim. Acta* **1984**, *67*, 2264. (b) Lehn, J.-M.; Regnouf de Vains, J.-B. Synthesis of Macrobicyclic Cryptates incorporating Bithiazole, Bisimidazole and Bipyrimidine Binding Subunits. *Tetrahedron Lett.* **1989**, *30*, 2209. (c) Lehn, J.-M.; Regnouf de Vains, J.-B. Synthesis and Properties of Macrobicyclic Cryptates Incorporating Five- and Six-Membered Biheteroaryl Units. *Helv. Chim. Acta* **1992**, *75*, 1221. (d) Prodi, L.; Maestri, M.; Balzani, V.; Lehn, J.-M.; Roth, C. Luminescence properties of cryptate europium (III) complexes incorporating heterocyclic N-oxide groups. *Chem. Phys. Lett.* **1991**, *180*, 45. (e) Lehn, J.-M.; Roth, C. O. Synthesis and Properties of Sodium and Europium(III) Cryptates Incorporating the 2,2′ Bipyridine 1,l′-Dioxide and 3,3′-Biisoquinoline 2,2′-Dioxide Units. *Helv. Chim. Acta* **1991**, *74*, 572. (f) Alpha, B.; Anklam, E.; Deschenaux, R.; Lehn, J.-M.; Pietraskiewiez, M. Synthesis and Characterisation of the Sodium and Lithium Cryptates of Macrobicyclic Ligands Incorporating Pyridine, Bipyridine, and Biisoquinoline Units. *Helv. Chim. Acta* **1988**, *71*, 1042. (g) Bodar-Houillon, F.; Heck, R.; Bohnenkamp, W.; Marsura, A. First example of dissymmetrical lanthanide cryptates: synthesis and steady state photophysical properties. *J. Lumin.* **2002**, *99*, 335. (h) Brunet, E.; Juanes, O.; Rodriguez-Blasco, M. A.; Vila-Nueva, S. P.; Garayalde, D.; Rodriguez-Ubis, J. C. Direct synthesis of new cryptates based on the *N,C*-pyrazolylpyridine motif. *Tetrahedron Lett.* **2005**, *46*, 7801. (i) Faulkner, S.; Beeby, A.; Carrie, M.-C.; Dadabhoy, A.; Kenwright, A. M.; Sammes, P. G. Time-resolved near-IR luminescence from ytterbium and neodymium complexes of the Lehn cryptand. *Inorg. Chem. Commun.* **2001**, *4*, 187. (j) Korovin, V.; Rusakova, N. V.; Popkov, A. Luminescence of ytterbium in complexes with cryptands containing bipyridine and biisoquinoline fragments. *J. Appl. Spectrosc.* **2002**, *69*, 89. (k) Havas, F.; Leygue, N.; Mestre, B.; Galaup, C.; Picard, C.; Danel, M. 6,6′-Dimethyl-2,2′-bipyridine-4-ester: A pivotal synthon for building tethered bipyridine ligands. *Tetrahedron* **2009**, *65*, 7673. (l) Havas, F.; Danel, M.; Galaup, C.; Tisnes, P.; Picard, C. A convenient synthesis of 6,6′-dimethyl-2,2′-bipyridine-4-ester and its application to the preparation of bifunctional lanthanide chelators. *Tetrahedron Lett.* **2007**, *48*, 999.

(5) (a) Doffek, C.; Alzakhem, N.; Molon, M.; Seitz, M. Rigid, Perdeuterated Lanthanoid Cryptates: Extraordinarily Bright Near-IR Luminophores. *Inorg. Chem.* **2012**, *51*, 4539. (b) Doffek, C.; Wahsner, J.; Kreidt, E.; Seitz, M. Breakdown of the Energy Gap Law in Molecular Lanthanoid Luminescence: The Smallest Energy Gap Is Not Universally Relevant for Nonradiative Deactivation. *Inorg. Chem.* **2014**, *53*, 3263. (c) Doffek, C.; Alzakhem, N.; Bischof, C.; Wahsner, J.; Güden-Silber, T.; Lügger, J.; Platas-Iglesias, C.; Seitz, M. Understanding the Quenching Effects of Aromatic C−H- and C−D-Oscillators in Near-IR Lanthanoid Luminescence. *J. Am. Chem. Soc.* **2012**, *134*, 16413. (d) Güden-Silber, T.; Doffek, C.; Platas-Iglesias, C.; Seitz, M. The first enantiopure lanthanoid cryptate. *Dalton Trans.* **2014**, *43*, 4238. (e) Kreidt, E.; Bischof, C.; Platas-Iglesias, C.; Seitz, M. Magnetic Anisotropy in Functionalized Bipyridyl Cryptates. *Inorg. Chem.* **2016**, *55*, 5549. (f) Kreidt, E.; Dee, C.; Seitz, M. Chiral Resolution of Lanthanoid Cryptates with Extreme Configurational Stability. *Inorg. Chem.* **2017**, *56*, 8752. (g) Doffek, C.; Seitz, M. The Radiative Lifetime in Near-IR Luminescent Ytterbium Cryptates - The Key to Extremely High Quantum Yields. *Angew. Chem., Int. Ed.* **2015**, *54*, 9719. (h) Alzakhem, N.; Bischof, C.; Seitz, M. The Dependence of the Photophysical Properties on the Number of 2,2-Bipyridine Units in a Series of Luminescent Europium and Terbium Cryptates. *Inorg. Chem.* **2012**, *51*, 9343. (i) Scholten, J.; Rosser, G. A.; Wahsner, J.; Alzakhem, N.; Bischof, C.; Stog, F.; Beeby, A.; Seitz, M. Anomalous Reversal of C−H and C−D Quenching Efficiencies in Luminescent Praseodymium Cryptates. *J. Am. Chem. Soc.* **2012**, *134*, 13915.

(6) Selected examples: (a) Andreiadis, E. S.; Demadrille, R.; Imbert, D.; Pecaut, J.; Mazzanti, M. Remarkable Tuning of the Coordination and Photophysical Properties of Lanthanide Ions in a Series of Tetrazole-Based Complexes. *Chem. - Eur. J.* **2009**, *15*, 9458. (b) Pal, R.; Parker, D. A single component ratiometric pH probe with long wavelength excitation of europium emission. *Chem. Commun.* **2007**, 474. (c) Dadabhoy, A.; Faulkner, S.; Sammes, P. G. Long wavelength sensitizers for europium(III) luminescence based on acridone derivatives. *J. Chem. Soc., Perkin Trans. 2* **2002**, 348. (d) Routledge, J. D.; Jones, M. W.; Faulkner, S.; Tropiano, M. Kinetically Stable Lanthanide Complexes Displaying Exceptionally High Quantum Yields upon Long-Wavelength Excitation: Synthesis, Photophysical Properties, and Solution Speciation. *Inorg. Chem.* **2015**, *54*, 3337. (e) Yang, C.; Fu, L.-M.; Wang, Y.; Zhang, J.-P.; Wong, W.-T.; Ai, X.-C.; Qiao, Y.-F.; Zou, B.-S.; Gui, L.-L. A highly luminescent europium complex showing visible-light-sensitized red emission: direct observation of the singlet pathway. *Angew. Chem., Int. Ed.* **2004**, *43*, 5010. (f) Dadabhoy, A.; Faulkner, S.; Sammes, P. G. Small singlet−triplet energy gap of acridone enables longer wavelength sensitisation of europium(III) luminescence. *J. Chem. Soc., Perkin Trans. 2* **2000**, 2359. (g) Deiters, E.; Song, B.; Chauvin, A.-S.; Vandevyver, C. D. B.; Gumy, F.; Bünzli, J.-C. G. Luminescent Bimetallic Lanthanide Bioprobes for Cellular Imaging with Excitation in the Visible-Light Range. *Chem. - Eur. J.* **2009**, *15*, 885. (h) Butler, S. J.; Delbianco, M.; Lamarque, L.; McMahon, B. K.; Neil, E. R.; Pal, R.; Parker, D.; Walton, J. W.; Zwier, J. M. EuroTracker dyes: design, synthesis, structure and photophysical properties of very bright europium complexes and their use in bioassays and cellular optical imaging. *Dalton Trans.* **2015**, *44*, 4791.

(7) (a) Becker, R. S.; Ferreira, L. F. V.; Elisei, F.; Machado, I.; Latterini, L. Comprehensive Photochemistry and Photophysics of Land- and Marine-based P-carbolines Employing Time resolved Emission and Flash Transient Spectroscopy. *Photochem. Photobiol.* **2005**, *81*, 1195. (b) Varela, A. P.; Burrows, H. D.; Douglas, P.; da Graca Miguel, M. Triplet state studies of *β*-carbolines. *J. Photochem. Photobiol., A* **2001**, *146*, 29. (c) Gonzalez, M. M.; Arnbjerg, J.; Denofrio, M. P.; Erra-Balsells, R.; Ogilby, P. R.; Cabrerizo, F. M. One-

DOI: 10.1021/acs.inorgchem.8b01031
Inorg. Chem. 2018, 57, 7390−7401

and Two-Photon Excitation of β-Carbolines in Aqueous Solution: pH-Dependent Spectroscopy, Photochemistry, and Photophysics. *J. Phys. Chem. A* **2009**, *113*, 6648. (d) Mesaros, M.; Tarzi, O. I.; Erra-Balsells, R.; Bilmes, G. M. The photophysics of some UV-MALDI matrices studied by using spectroscopic, photoacoustic and luminescence techniques. *Chem. Phys. Lett.* **2006**, *426*, 334.

(8) Selected examples: (a) He, L.; Tan, C.-P.; Ye, R. R.; Zhao, Y.-Z.; Liu, Y.-H.; Zhao, Q.; Ji, L.-N.; Mao, Z.-W. Theranostic Iridium(III) Complexes as One- and Two-Photon Phosphorescent Trackers to Monitor Autophagic Lysosomes. *Angew. Chem., Int. Ed.* **2014**, *53*, 12137. (b) Khan, A. K.; de Almeida, A.; Al-Farhan, K.; Alsalme, A.; Casini, A.; Ghazzali, M.; Reedijk, J. Transition-metal norharmane compounds as possible cytotoxic agents: New insights based on a coordination chemistry perspective. *J. Inorg. Biochem.* **2016**, *165*, 128.

(9) Bai, B.; Shen, L.; Ren, J.; Zhu, H. J. Chiral Biscarboline N,N′-Dioxide Derivatives: Highly Enantioselective Addition of Allyltrichlorosilane to Aldehydes. *Adv. Synth. Catal.* **2012**, *354*, 354.

(10) Caron, S.; Do, N. M.; Sieser, J. E. A practical, efficient, and rapid method for the oxidation of electron deficient pyridines using trifluoroacetic anhydride and hydrogen peroxide−urea complex. *Tetrahedron Lett.* **2000**, *41*, 2299.

(11) Newkome, G. R.; Pappalardo, S.; Gupta, V. K.; Fronczek, F. R. Synthesis and structural aspects of macrocyclic polyamines containing 2,2′-bipyridinyl units(s). *J. Org. Chem.* **1983**, *48*, 4848.

(12) (a) Dalle, K. E.; Daumann, L. J.; Schenk, G.; McGeary, R. P.; Hanton, L. R.; Gahan, L. R. Ligand modifications modulate the mechanism of binuclear phosphatase biomimetics. *Polyhedron* **2013**, *52*, 1336. (b) Platas-Iglesias, C.; Mato-Iglesias, M.; Djanashvili, K.; Muller, R. N.; Vander Elst, L.; Peters, J. A.; de Blas, A.; Rodríguez-Blas, T. Lanthanide Chelates Containing Pyridine Units with Potential Application as Contrast Agents in Magnetic Resonance Imaging. *Chem. - Eur. J.* **2004**, *10*, 3579−3590.

(13) Frisch, M. J.; Trucks, G. W.; Schlegel, H. B.; Scuseria, G. E.; Robb, M. A.; Cheeseman, J. R.; Scalmani, G.; Barone, V.; Mennucci, B.; Petersson, G. A.; Nakatsuji, H.; Caricato, M.; Li, X.; Hratchian, H. P.; Izmaylov, A. F.; Bloino, J.; Zheng, G.; Sonnenberg, J. L.; Hada, M.; Ehara, M.; Toyota, K.; Fukuda, R.; Hasegawa, J.; Ishida, M.; Nakajima, T.; Honda, Y.; Kitao, O.; Nakai, H.; Vreven, T.; Montgomery, J. A., Jr.; Peralta, J. E.; Ogliaro, F.; Bearpark, M.; Heyd, J. J.; Brothers, E.; Kudin, K. N.; Staroverov, V. N.; Kobayashi, R.; Normand, J.; Raghavachari, K.; Rendell, A.; Burant, J. C.; Iyengar, S. S.; Tomasi, J.; Cossi, M.; Rega, N.; Millam, J. M.; Klene, M.; Knox, J. E.; Cross, J. B.; Bakken, V.; Adamo, C.; Jaramillo, J.; Gomperts, R.; Stratmann, R. E.; Yazyev, O.; Austin, A. J.; Cammi, R.; Pomelli, C.; Ochterski, J. W.; Martin, R. L.; Morokuma, K.; Zakrzewski, V. G.; Voth, G. A.; Salvador, P.; Dannenberg, J. J.; Dapprich, S.; Daniels, A. D.; Farkas, Ö.; Foresman, J. B.; Ortiz, J. V.; Cioslowski, J.; Fox, D. J. *Gaussian 09*, Revision E.01, Gaussian, Inc.: Wallingford, CT, 2009.

(14) Regueiro-Figueroa, M.; Platas-Iglesias, C. Toward the Prediction of Water Exchange Rates in Magnetic Resonance Imaging Contrast Agents: A Density Functional Theory Study. *J. Phys. Chem. A* **2015**, *119*, 6436−6445.

(15) (a) Tao, J. M.; Perdew, J. P.; Staroverov, V. N.; Scuseria, G. E. Climbing the Density Functional Ladder: Nonempirical Meta-Generalized Gradient Approximation Designed for Molecules and Solids. *Phys. Rev. Lett.* **2003**, *91*, 146401. (b) Dolg, M.; Stoll, H.; Savin, A.; Preuss, H. Energy-adjusted Pseudopotentials for the Rare Earth Elements. *Theor. Chim. Acta* **1989**, *75*, 173−194.

(16) Tomasi, J.; Mennucci, B.; Cammi, R. Quantum Mechanical Continuum Solvation Models. *Chem. Rev. (Washington, DC, U. S.)* **2005**, *105*, 2999−3093.

(17) (a) Seitz, M.; Oliver, A. G.; Raymond, K. N. The Lanthanide Contraction Revisited. *J. Am. Chem. Soc.* **2007**, *129*, 11153. (b) Seitz, M.; Alzakhem, N. Computational Estimation of Lanthanoid-Water Bond Lengths by Semiempirical Methods. *J. Chem. Inf. Model.* **2010**, *50*, 217.

(18) Paul-Roth, C. O.; Lehn, J.-M.; Guilhem, J.; Pascard, C. Synthesis, Characterization, and Structural Properties of Luminescent Lanthanide Complexes. *Helv. Chim. Acta* **1995**, *78*, 1895.

(19) Gribkov, D. V.; Hultzsch, K. C.; Hampel, F. Synthesis and Characterization of New Biphenolate and Binaphtholate Rare-Earth-Metal Amido Complexes: Catalysts for Asymmetric Olefin Hydroamination/Cyclization. *Chem. - Eur. J.* **2003**, *9*, 4796.

(20) Baudry, J. van der Waals Interactions and Decrease of the Rotational Barrier of Methyl-Sized Rotators: A Theoretical Study. *J. Am. Chem. Soc.* **2006**, *128*, 11088.

(21) Peters, J. A.; Huskens, J.; Raber, D. J. Lanthanide Induced Shifts and Relaxation Rate Enhancements. *Prog. Nucl. Magn. Reson. Spectrosc.* **1996**, *28*, 283−350.

(22) Bertini, I.; Luchinat, C.; Parigi, G. Magnetic Susceptibility in Paramagnetic NMR. *Prog. Nucl. Magn. Reson. Spectrosc.* **2002**, *40*, 249.

(23) Castro, G.; Regueiro-Figueroa, M.; Esteban-Gómez, D.; Pérez-Lourido, P.; Platas-Iglesias, C.; Valencia, L. Magnetic Anisotropies in Rhombic Lanthanide(III) Complexes Do Not Conform to Bleaney's Theory. *Inorg. Chem.* **2016**, *55*, 3490.

(24) Rodríguez-Rodríguez, A.; Esteban-Gómez, D.; de Blas, A.; Rodríguez-Blas, T.; Botta, M.; Tripier, R.; Platas-Iglesias, C. Solution Structure of Ln(III) Complexes with Macrocyclic Ligands Through Theoretical Evaluation of ^{1}H NMR Contact Shifts. *Inorg. Chem.* **2012**, *51*, 13419.

(25) Dolg, M.; Stoll, H.; Preuss, H. Energy-adjusted Ab Initio Pseudopotentials for the Rare Earth Elements. *J. Chem. Phys.* **1989**, *90*, 1730.

(26) Rega, N.; Cossi, M.; Barone, V. Development and Validation of Reliable Quantum Mechanical Approaches for the Study of Free Radicals in Solution. *J. Chem. Phys.* **1996**, *105*, 11060.

(27) Bertini, I.; Luchinat, C. The Hyperfine Shift. *Coord. Chem. Rev.* **1996**, *150*, 29.

(28) Value for $Eu(EtSO_4)_3{\cdot}H_2O$ in 0.2 M aqueous $HClO_4$: Carnall, W. T.; Fields, P. R.; Rajnak, K. Electronic Energy Levels Of the Trivalent Lanthanide Aquo Ions. IV. Eu^{3+}. *J. Chem. Phys.* **1968**, *49*, 4450.

(29) Binnemans, K. Interpretation of europium(III) spectra. *Coord. Chem. Rev.* **2015**, *295*, 1.

(30) Beeby, A.; Clarkson, I. M.; Dickins, R. S.; Faulkner, S.; Parker, D.; Royle, L.; de Sousa, A. S.; Williams, J. A. G.; Woods, M. Non-radiative deactivation of the excited states of europium, terbium and ytterbium complexes by proximate energy-matched OH, NH and CH oscillators: an improved luminescence method for establishing solution hydration states. *J. Chem. Soc., Perkin Trans. 2* **1999**, 493.

(31) Melhuish, W. H. Quantum efficiencies of fluorescence of organic substances: Effect of solvent and concentration of fluorescent solute. *J. Phys. Chem.* **1961**, *65*, 229.

(32) Werts, M. H. V.; Jukes, R. T. F.; Verhoeven, J. W. The emission spectrum and the radiative lifetime of Eu^{3+} in luminescent lanthanide complexes. *Phys. Chem. Chem. Phys.* **2002**, *4*, 1542.

(33) (a) Meier, R. J.; Simbürger, J. M. B.; Soukka, T.; Schäferling, M. A FRET based pH probe with a broad working range applicable to referenced ratiometric dual wavelength and luminescence lifetime read out. *Chem. Commun.* **2015**, *51*, 6145. (b) Turel, M.; Čajlaković, M.; Austin, E.; Dakin, J. P.; Uray, G.; Lobnik, A. Direct UV-LED lifetime pH sensor based on a semi-permeable sol−gel membrane immobilized luminescent Eu^{3+} chelate complex. *Sens. Actuators, B* **2008**, *131*, 247. (c) Butler, S. J.; Pal, R.; McMahon, B. K.; Parker, D.; Walton, J. W. Bright Mono-aqua Europium Complexes Based on Triazacyclononane That Bind Anions Reversibly and Permeate Cells Efficiently. *Chem. - Eur. J.* **2013**, *19*, 9511. (d) Moore, J. D.; Lord, R. L.; Cisneros, G. A.; Allen, M. J. Concentration-Independent pH Detection with a Luminescent imetallic Eu(III)-Based Probe. *J. Am. Chem. Soc.* **2012**, *134*, 17372. (e) Giardiello, M.; Botta, M.; Lowe, M. P. pH-Responsive Lanthanide Complexes Based on Reversible Ligation of a Diphenylphosphinamide. *Inorg. Chem.* **2013**, *52*, 14264. (f) Routledge, J. D.; Jones, M. W.; Faulkner, S.; Tropiano, M. Kinetically Stable Lanthanide Complexes Displaying Exceptionally High Quantum Yields upon Long-Wavelength Excitation: Synthesis, Photophysical Properties, and Solution Speciation. *Inorg. Chem.* **2015**, *54*, 3337.

DOI: 10.1021/acs.inorgchem.8b01031
Inorg. Chem. 2018, 57, 7390−7401

Supporting Information

Long Wavelength Excitation of Europium Luminescence in Extended, Carboline-Based Cryptates

Carolin Dee,[†] David Esteban-Gómez,[‡] Carlos Platas-Iglesias,[*,‡] and Michael Seitz[*,†]

[†] Institute of Inorganic Chemistry, University of Tübingen, Auf der Morgenstelle 18, 72076 Tübingen, Germany

[‡] Centro de Investigacións Científicas Avanzadas (CICA) and Departamento de Química, Universidade da Coruña, Campus da Zapateira-Rúa da Fraga 10, 15008 A Coruña, Spain

Email: michael.seitz@uni-tuebingen.de
carlos.platas.iglesias@udc.es

Supporting Information

Table of Contents

1 Analytical and Preparative HPLC Traces

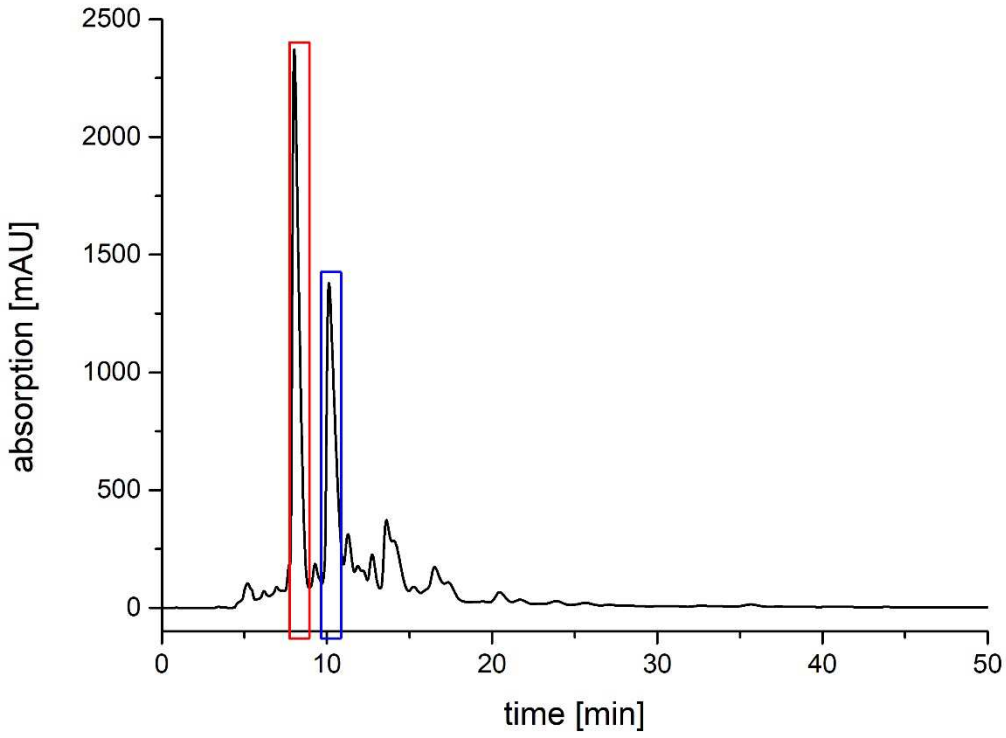

Figure S1. Preparative HPLC trace – Isolated fraction (red) → **6-Eu** and isolated fraction (blue) → **6-Eu'**.

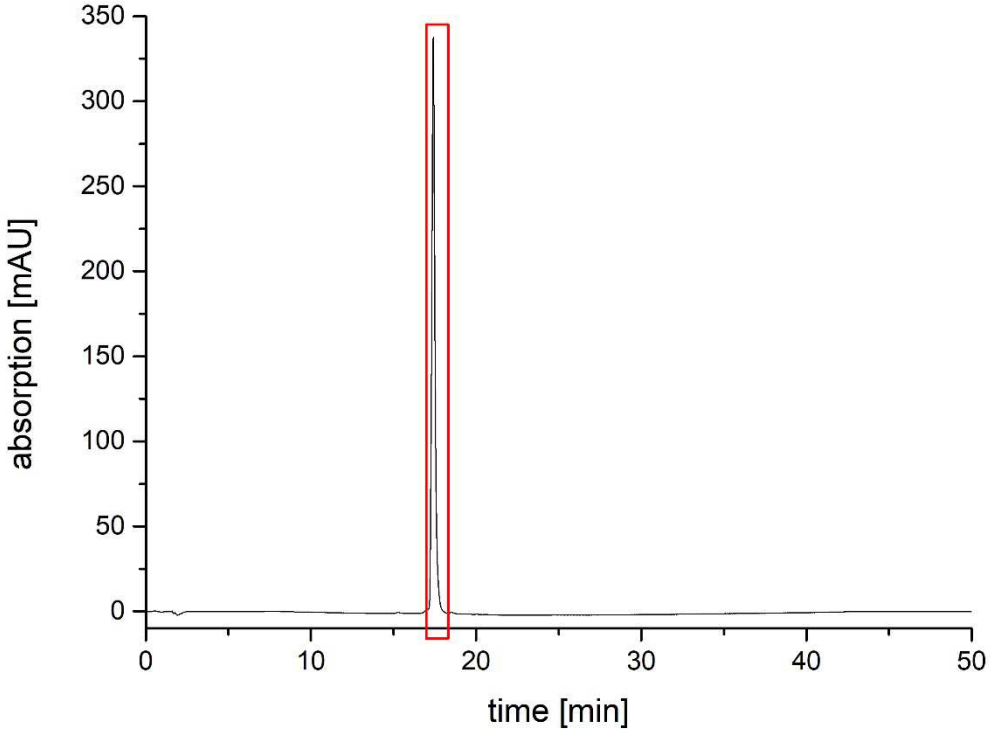

Figure S2. Analytical HPLC trace (after preparative HPLC) - Isolated fraction (red) → **6-Eu**.

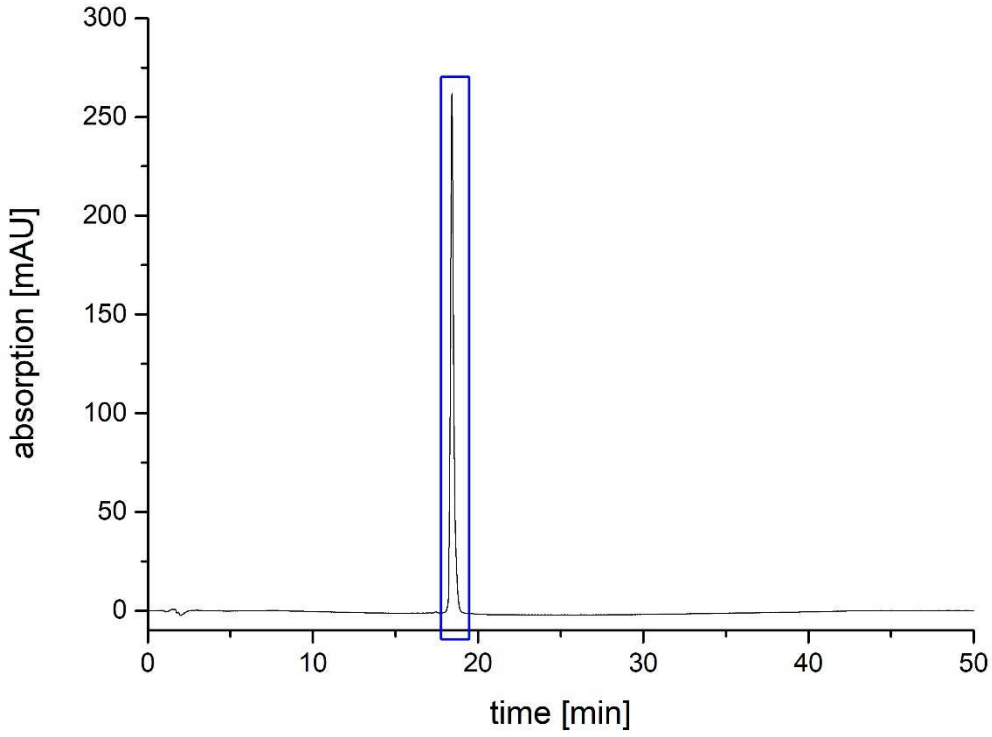

Figure S3. Analytical HPLC trace (after preparative HPLC) - Isolated fraction (blue) → **6-Eu'**.

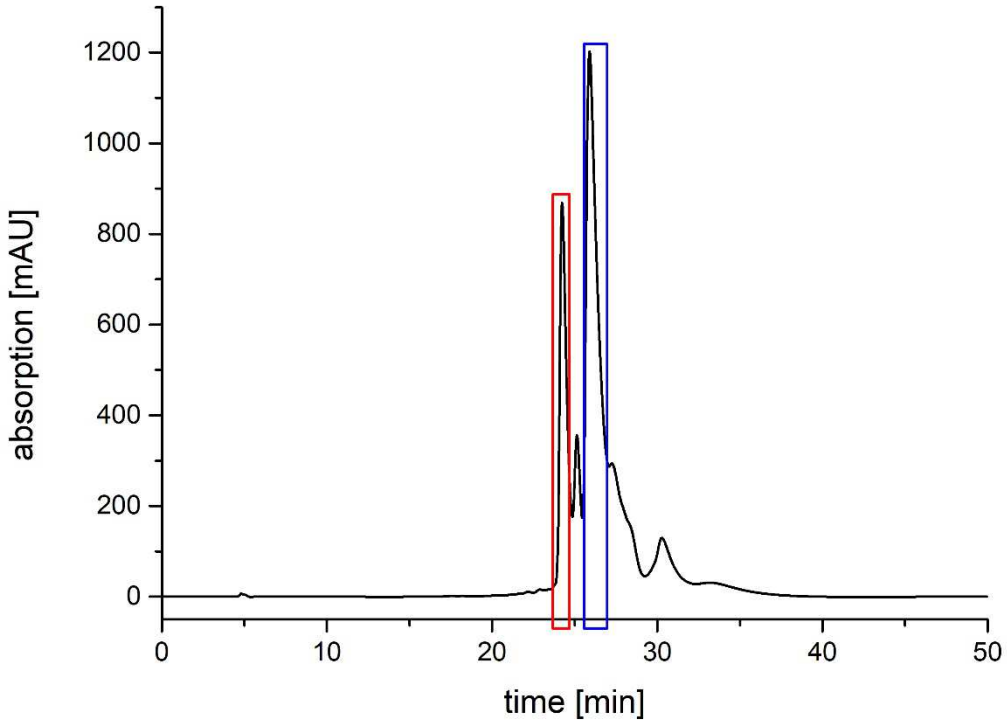

Figure S4. Preparative HPLC trace – Isolated fraction (red) → **[D_{20}]-6-Eu** and isolated fraction (blue) → **[D_{20}]-6-Eu'**.

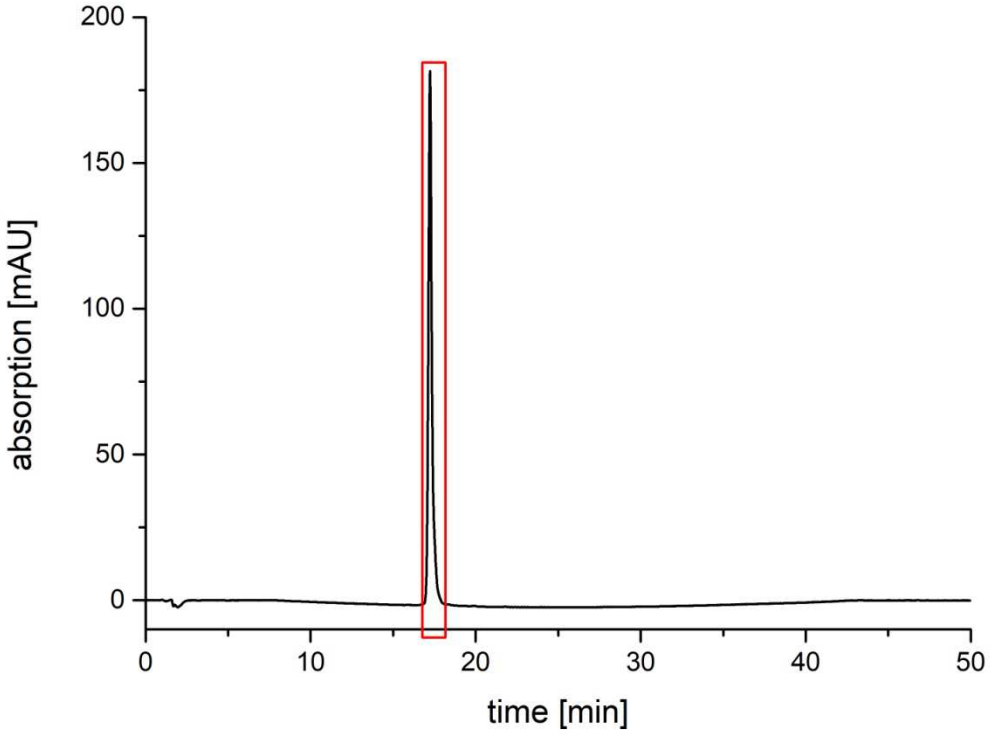

Figure S5. Analytical HPLC trace (after preparative HPLC) - Isolated fraction (red) → **[D_{20}]-6-Eu**.

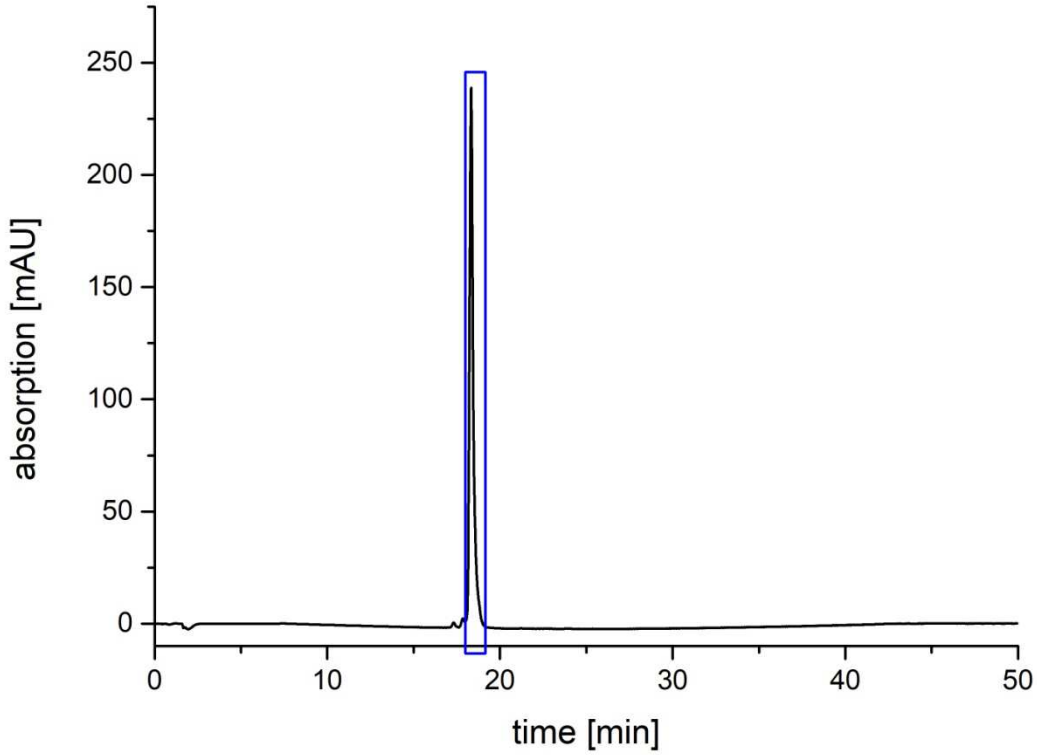

Figure S6. Analytical HPLC trace (after preparative HPLC) - Isolated fraction (blue) → **[D_{20}]-6-Eu'**.

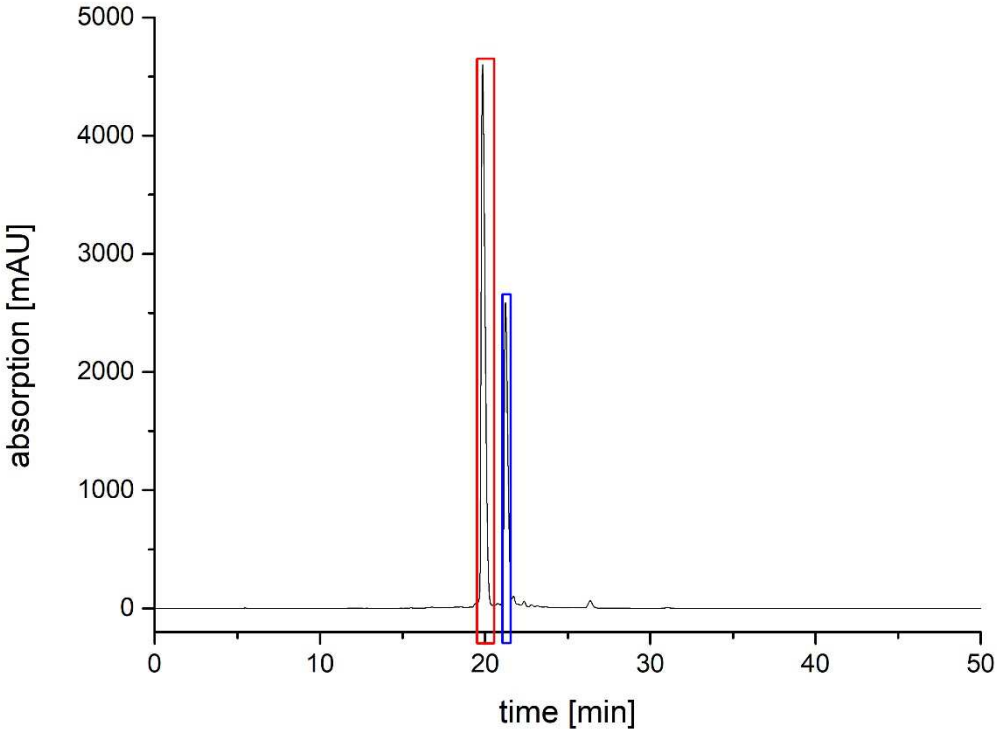

Figure S7. Preparative HPLC trace – Isolated fraction (red) → **7-Eu** and isolated fraction (blue) → **Eu-7'**.

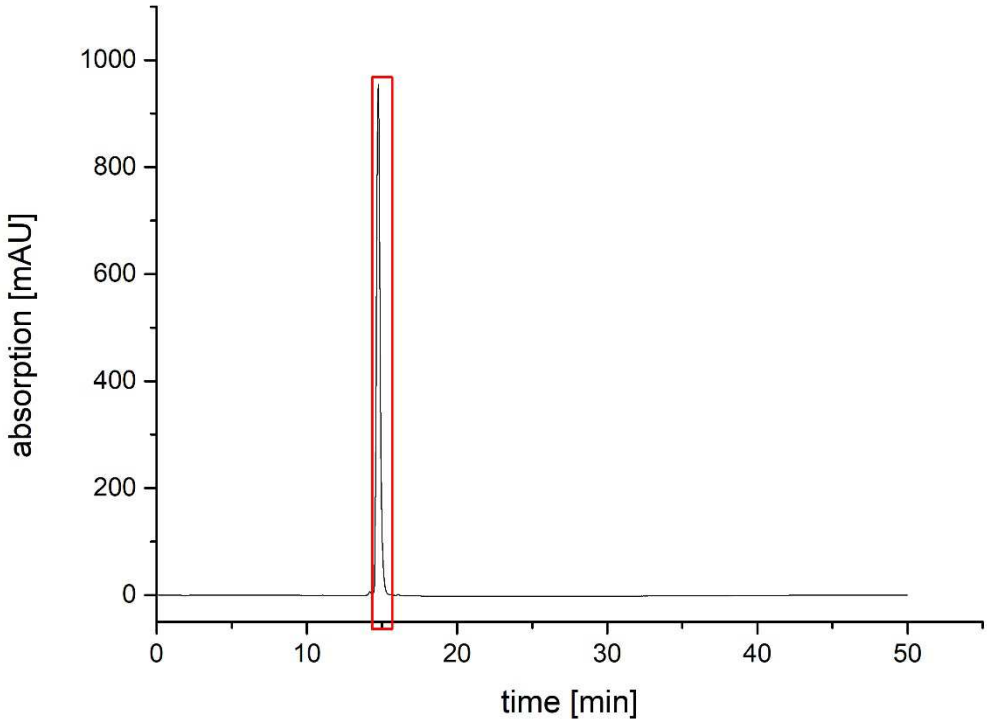

Figure S8. Analytical HPLC trace (after preparative HPLC) - Isolated fraction (red) → 7-**Eu**.

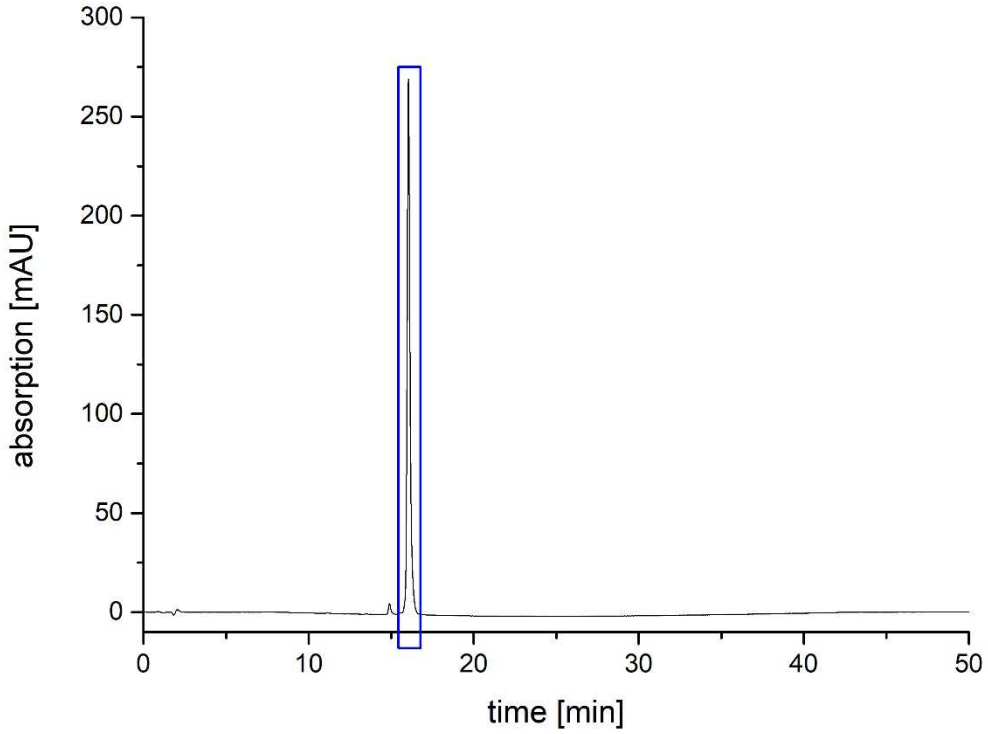

Figure S9. Analytical HPLC trace (after preparative HPLC) - Isolated fraction (blue) → **7-Eu'**.

2 MALDI Mass Spectra

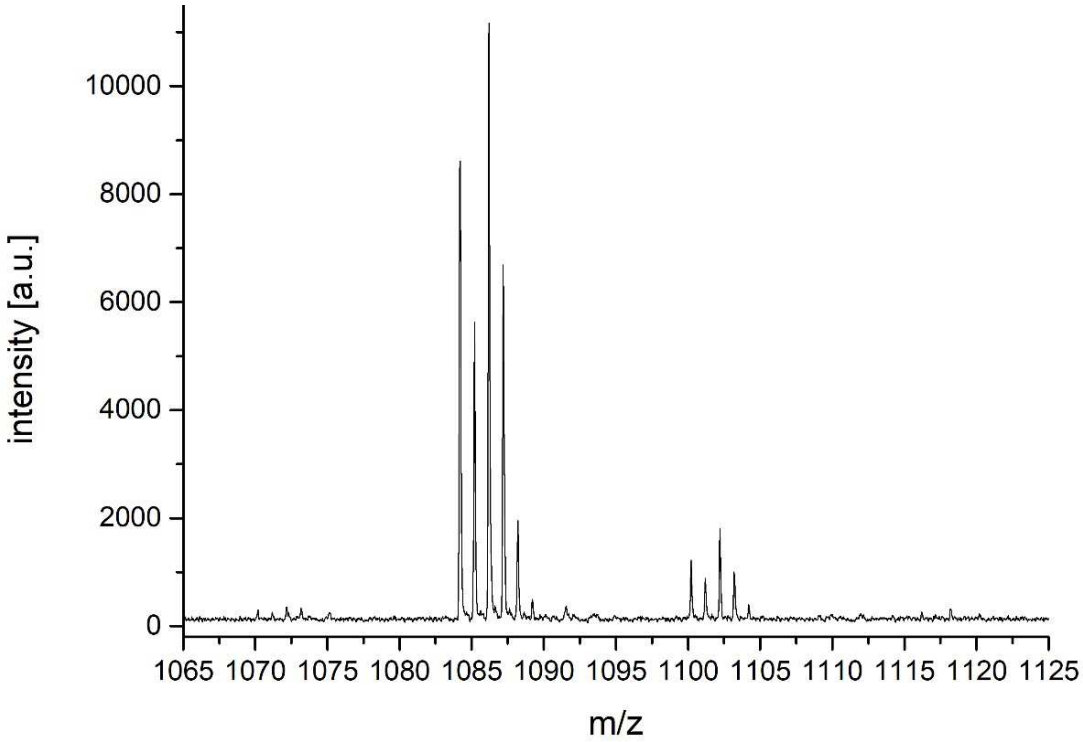

Figure S10. MALDI mass spectrum (DHB, pos. mode) → **6-Eu**: *m/z* (%) = 1086.2 (100, [M + deprotonated matrix DHB – 2 x O + e^-]$^+$, Eu isotopic pattern), 1102.2 (15, [M + deprotonated matrix DHB - O + e^-]$^+$, Eu isotopic pattern).

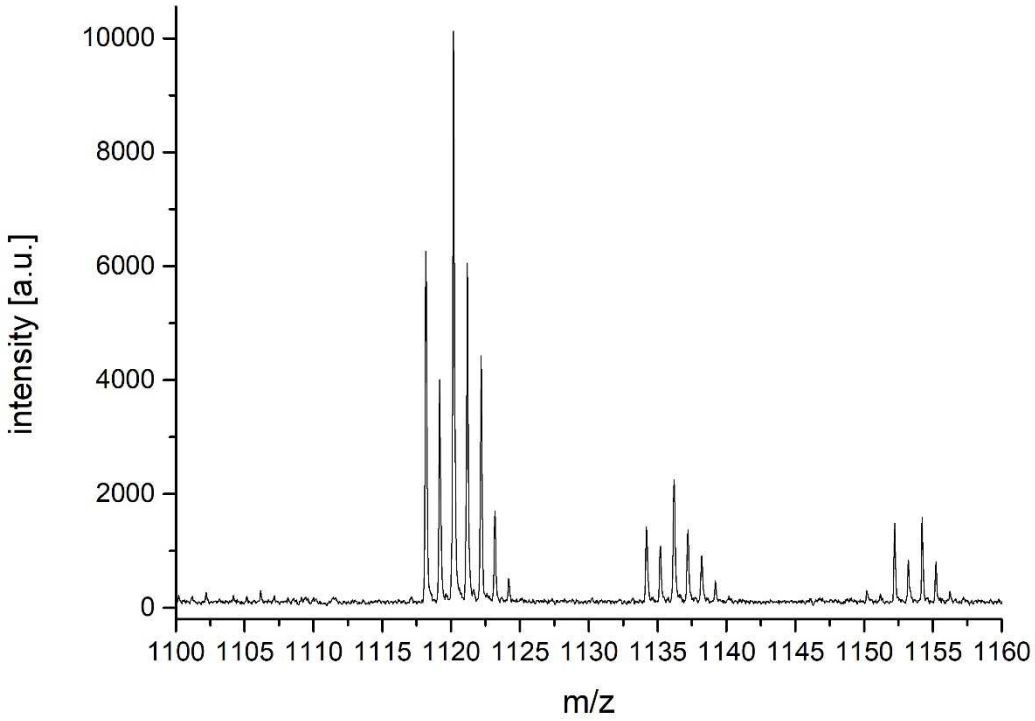

Figure S11. MALDI mass spectrum (DHB, pos. mode) → **6-Eu'**: *m/z* (%) = 1120.2 (100, [M + deprotonated matrix DHB + H_2O + e^-]$^+$, Eu isotopic pattern), 1136.2 (22, [M + deprotonated matrix DHB + O + H_2O + e^-]$^+$, Eu isotopic pattern), 1154.2 (15, [M + deprotonated matrix DHB + O + H_2O + e^-]$^+$, Eu isotopic pattern).

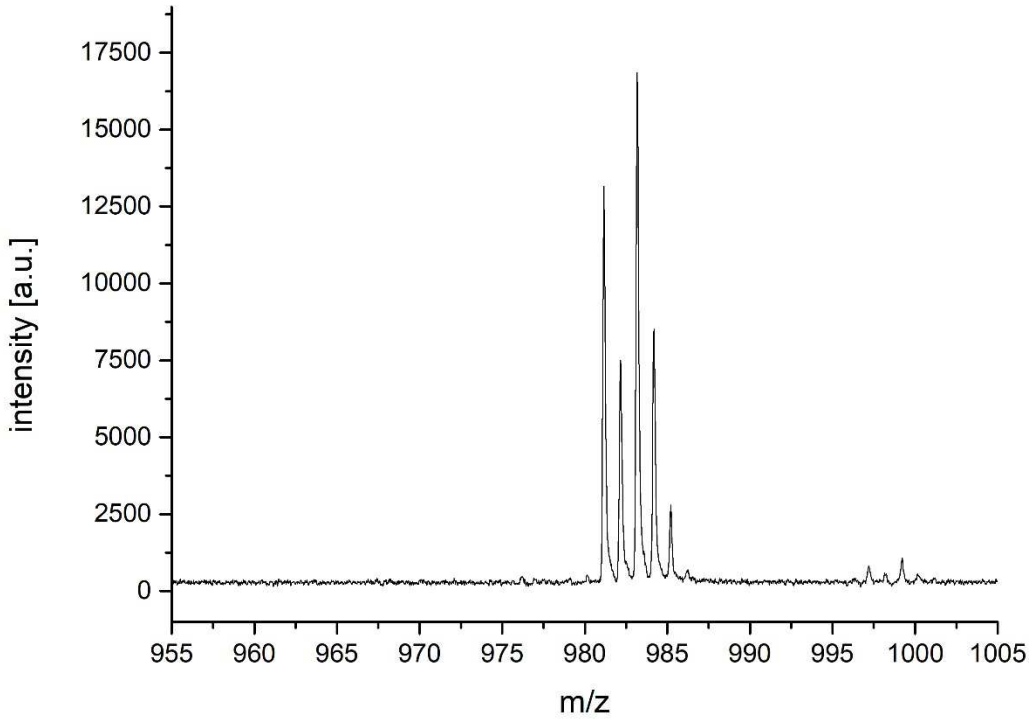

Figure S12. MALDI mass spectrum (DHB, pos. mode) → **7-Eu**: *m/z* (%) = 983.2 (100, M + deprotonated matrix DHB – O + e^-]$^+$, Eu isotopic pattern).

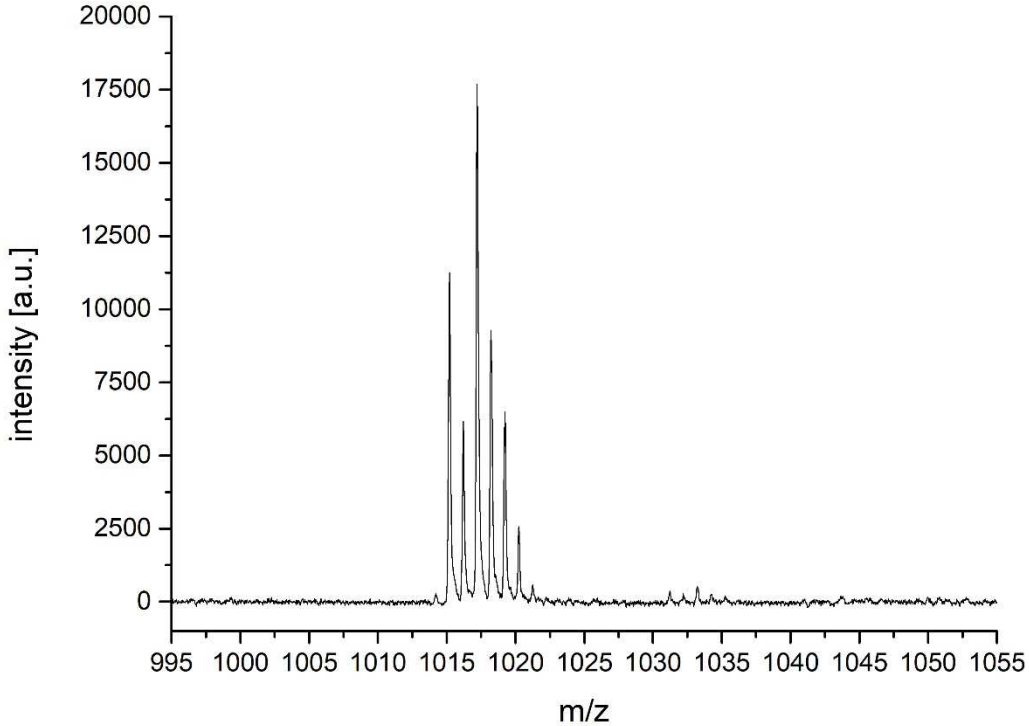

Figure S13. MALDI mass spectrum (DHB, pos. mode) → **7-Eu'**: *m/z* (%) = 1017.2 (100, [M + H_2O + deprotonated matrix DHB + e^-]$^+$, Eu isotopic pattern).

3 IR Spectra

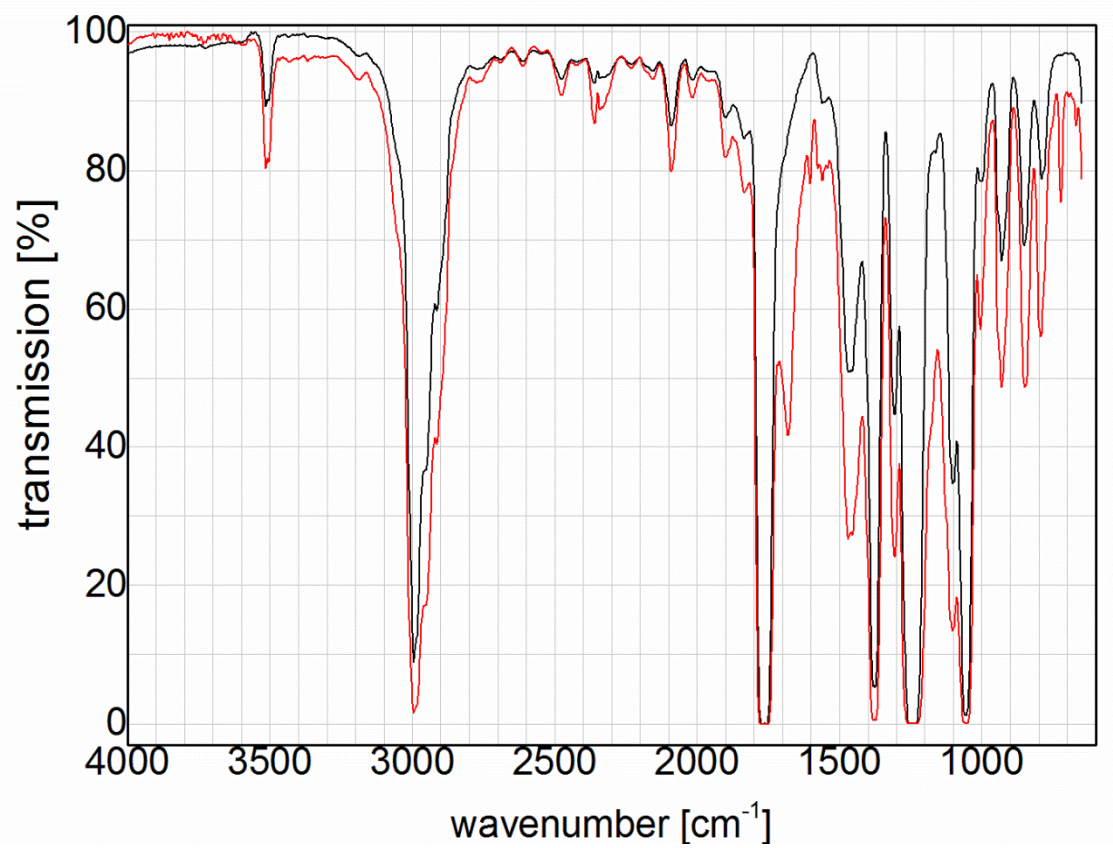

Figure S14. IR spectra (neat, ATR) of **6-Eu** (black) and **6-Eu'** (red).

4 NMR Spectra

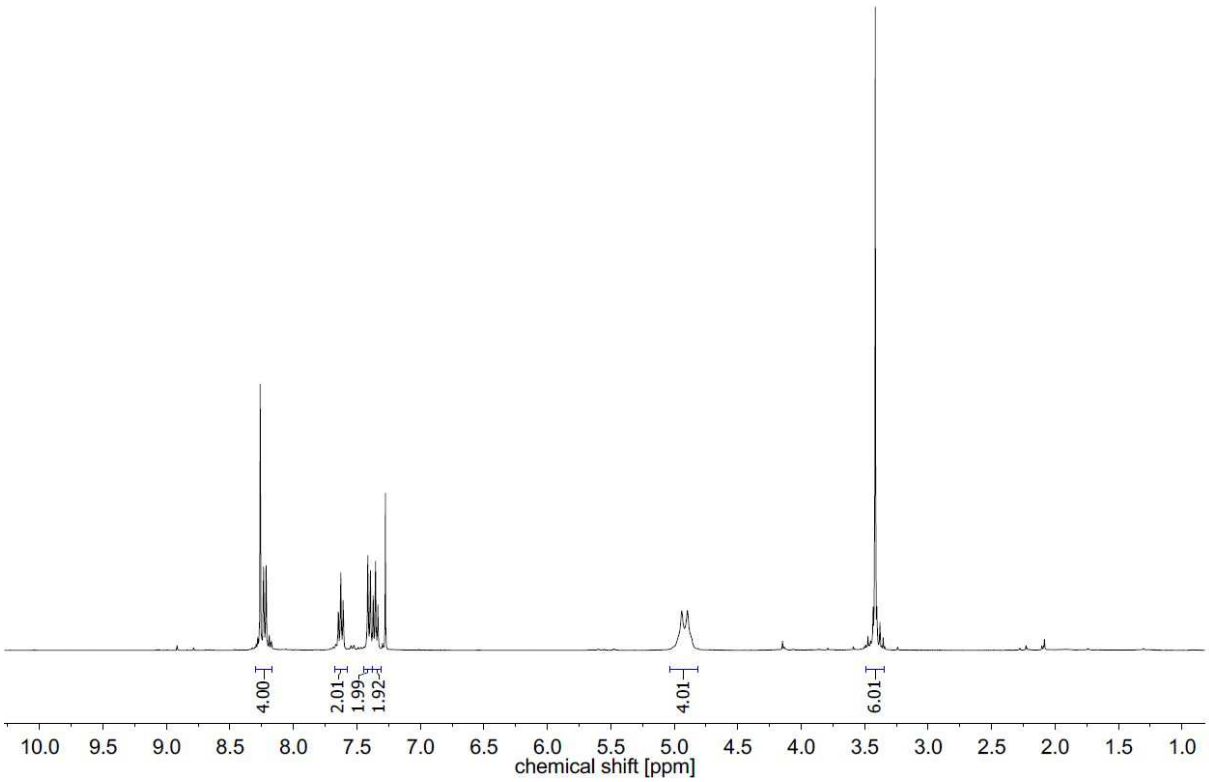

Figure S15. ^{1}H NMR ($CDCl_3$, 400 MHz) spectrum of dibromide **9**.

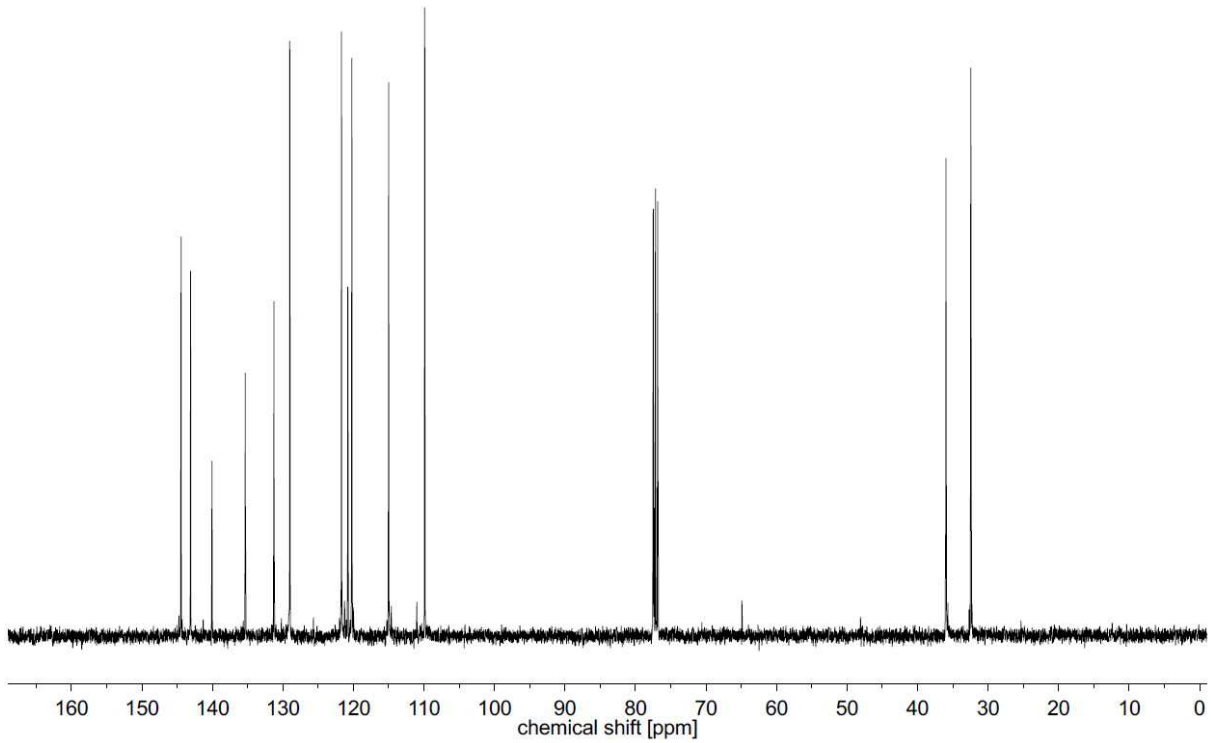

Figure S16. ^{13}C NMR ($CDCl_3$, 101 MHz) spectrum of dibromide **9**.

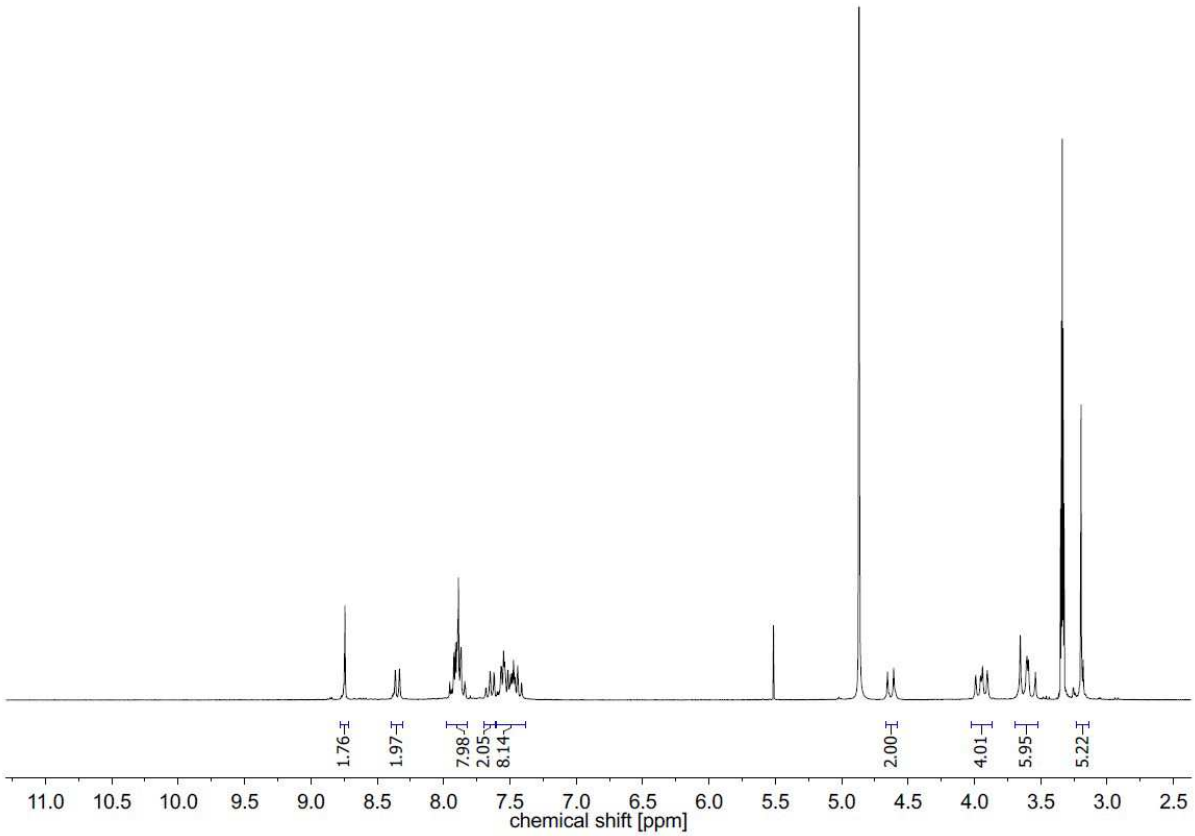

Figure S17. ^{1}H NMR (CD_3OD, 250 MHz) spectrum of sodium cryptate **6-Na**.

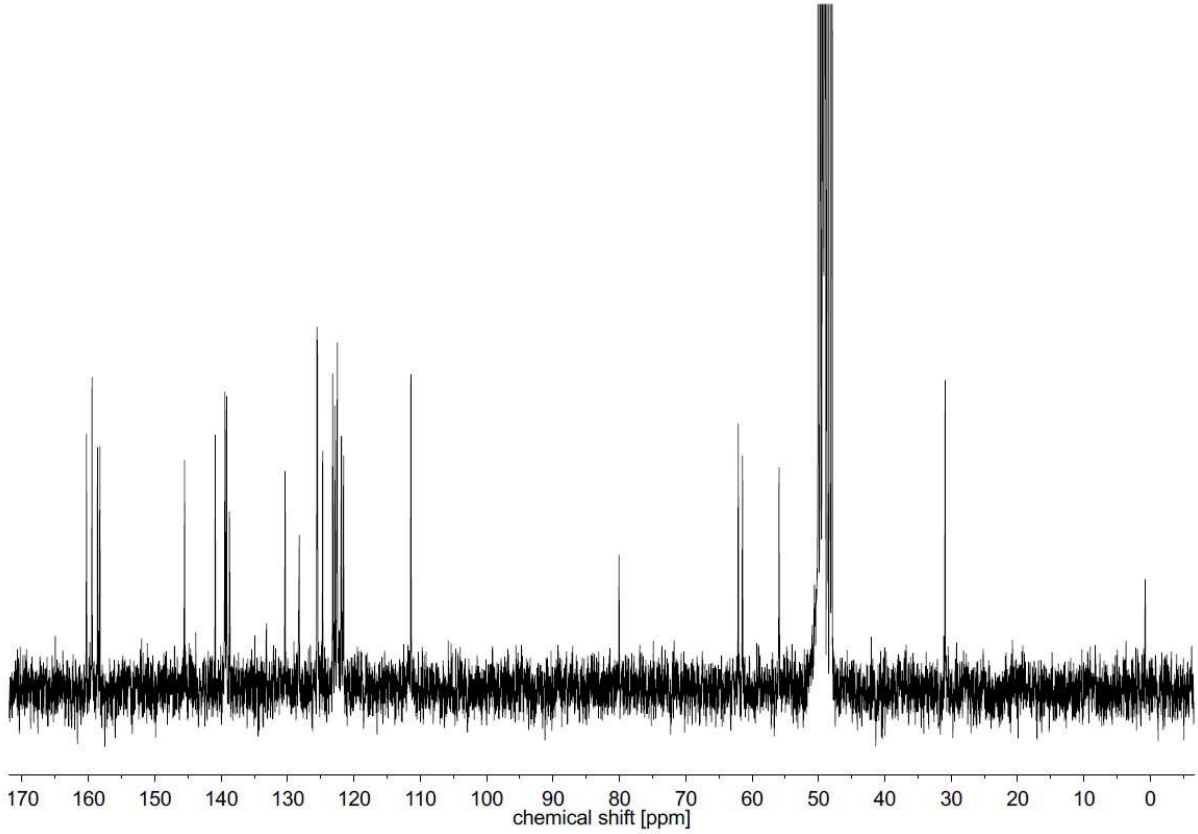

Figure S18. ^{13}C NMR (CD_3OD, 63 MHz) spectrum of sodium cryptate **6-Na**.

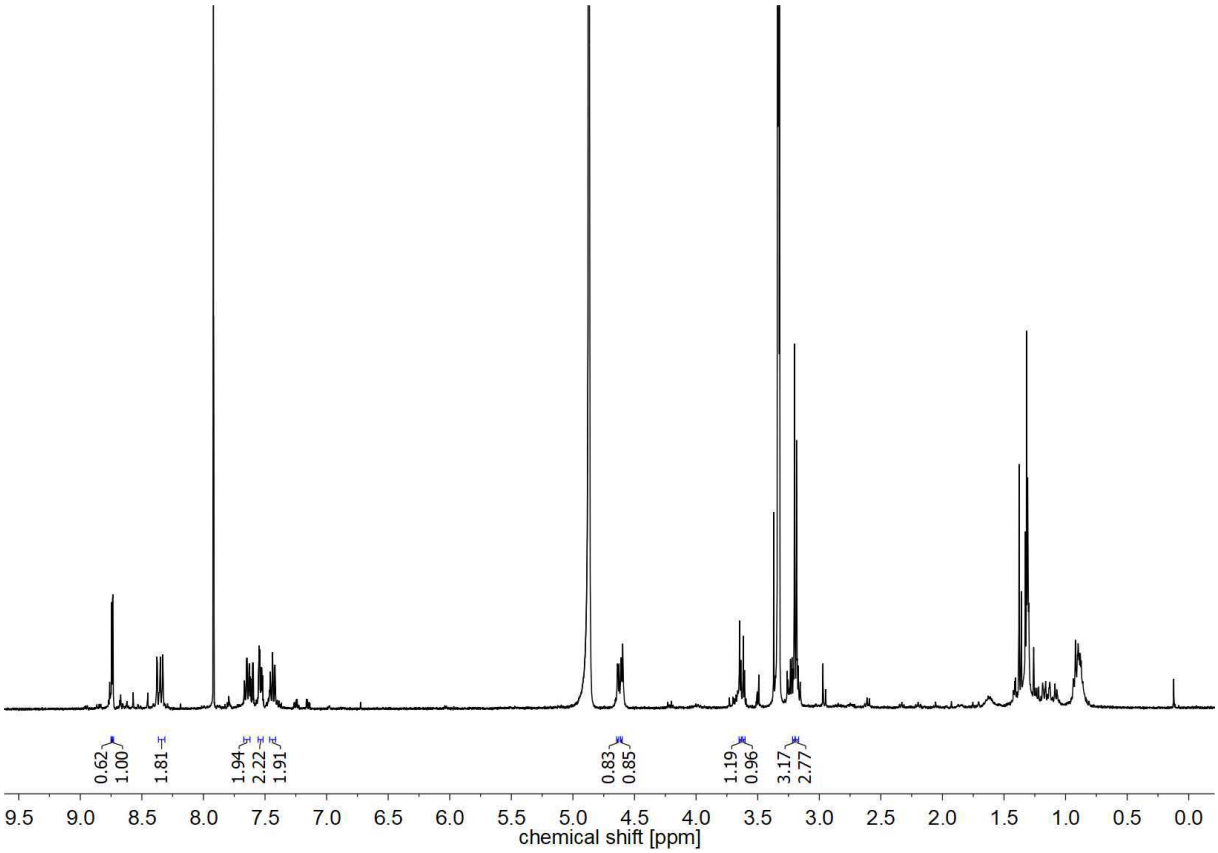

Figure S19. ^{1}H NMR (CD_3OD, 400 MHz) spectrum of sodium cryptate **[D_{20}]-6-Na**.

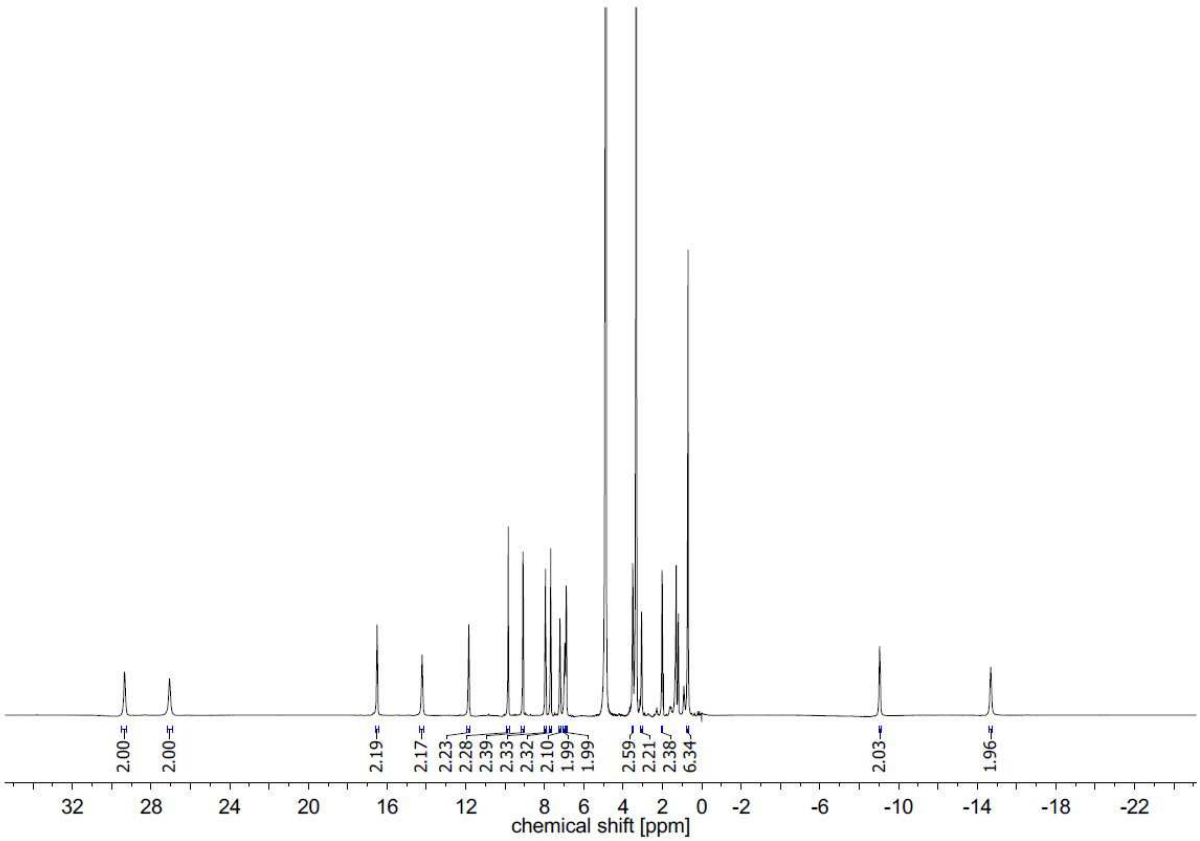

Figure S20. ^{1}H NMR (CD_3OD, 400 MHz) spectrum of cryptate **6-Eu**.

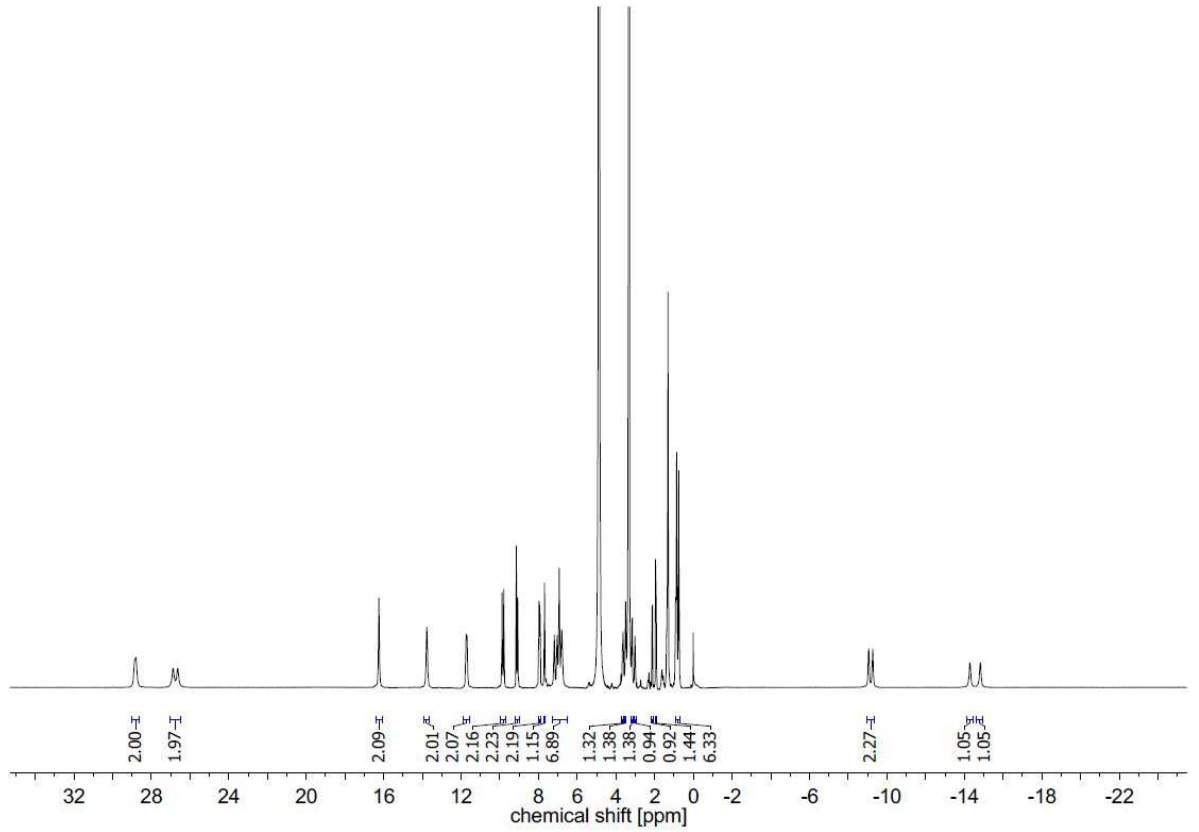

Figure S21. ^{1}H NMR (CD_3OD, 400 MHz) spectrum of cryptate **6-Eu'**.

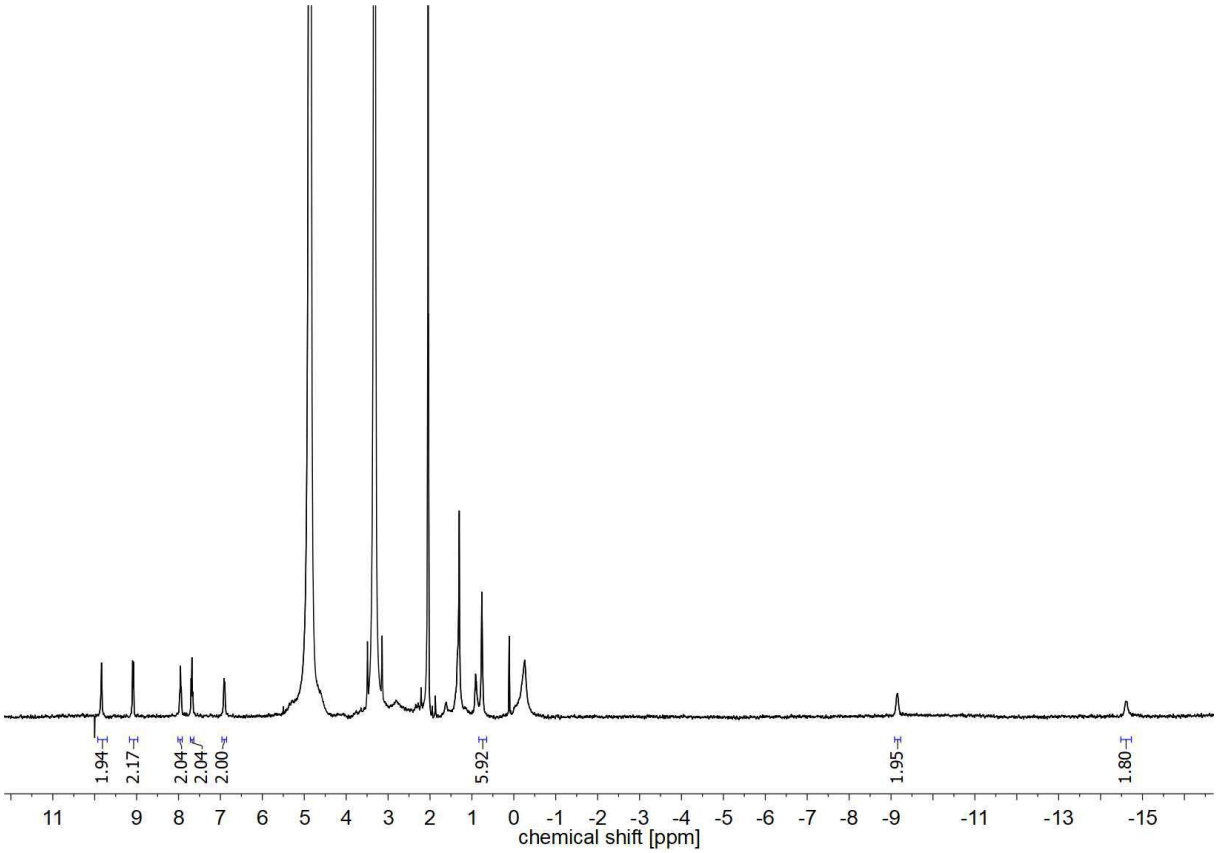

Figure S22. ^{1}H NMR (CD_3OD, 400 MHz) spectrum of cryptate **D_{20}-6-Eu**.

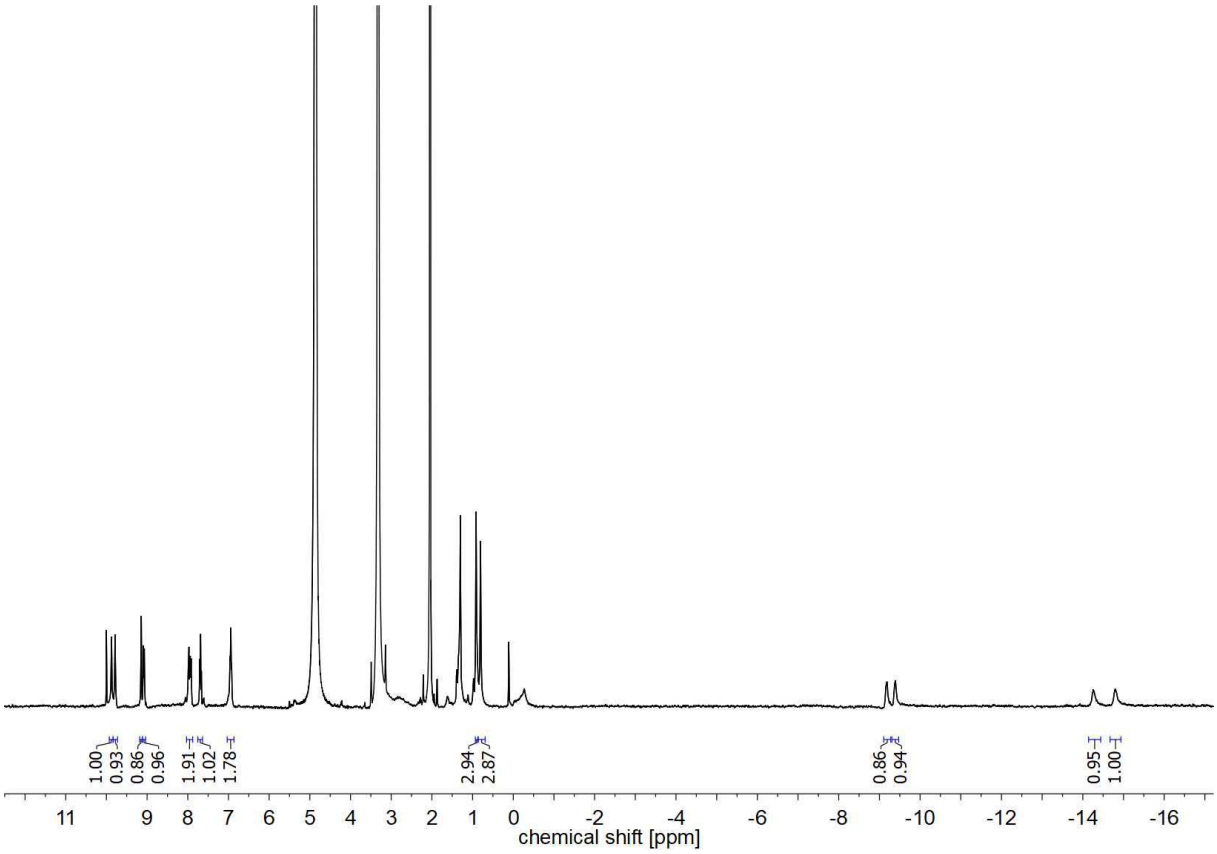

Figure S23. ^{1}H NMR (CD_3OD, 400 MHz) spectrum of cryptate **D_{20}-6-Eu'**.

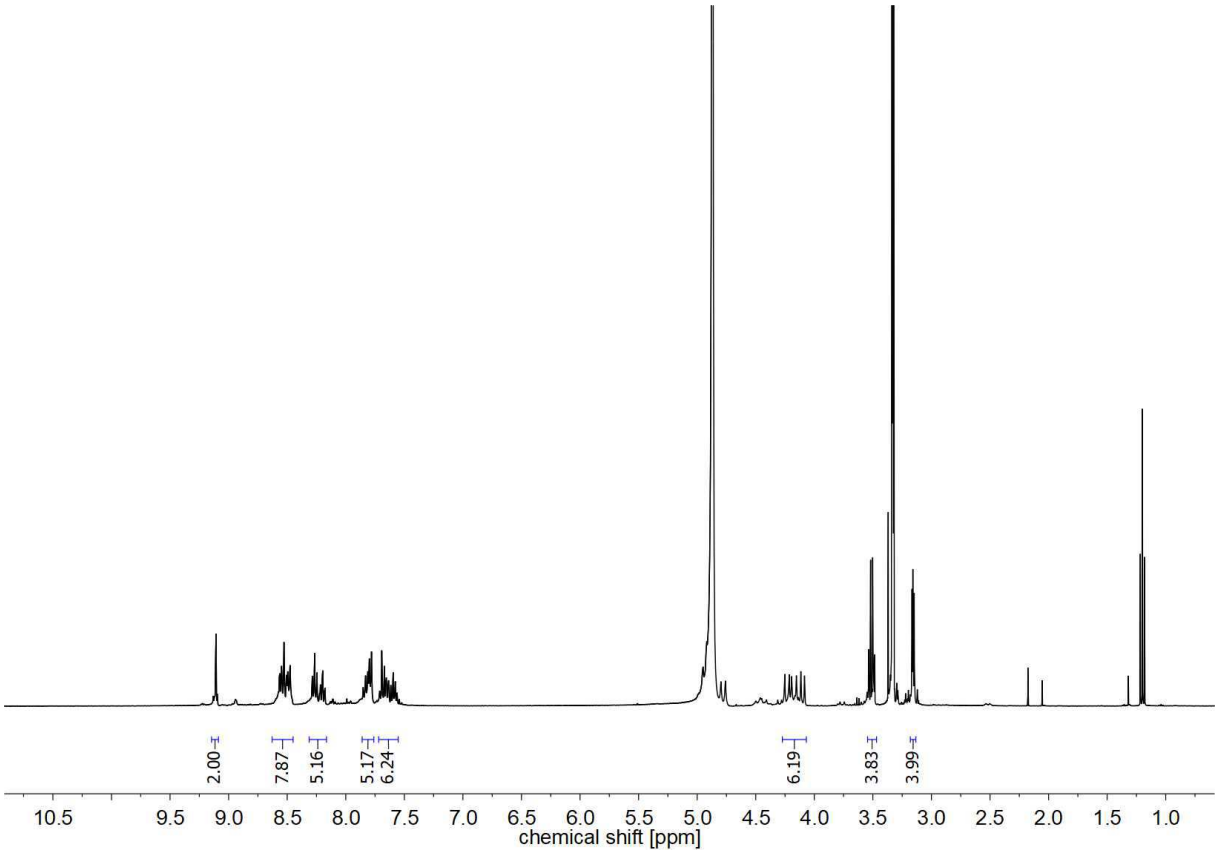

Figure S24. ^{1}H NMR (CD_3OD, 400 MHz) spectrum of cryptate **6-Lu**.

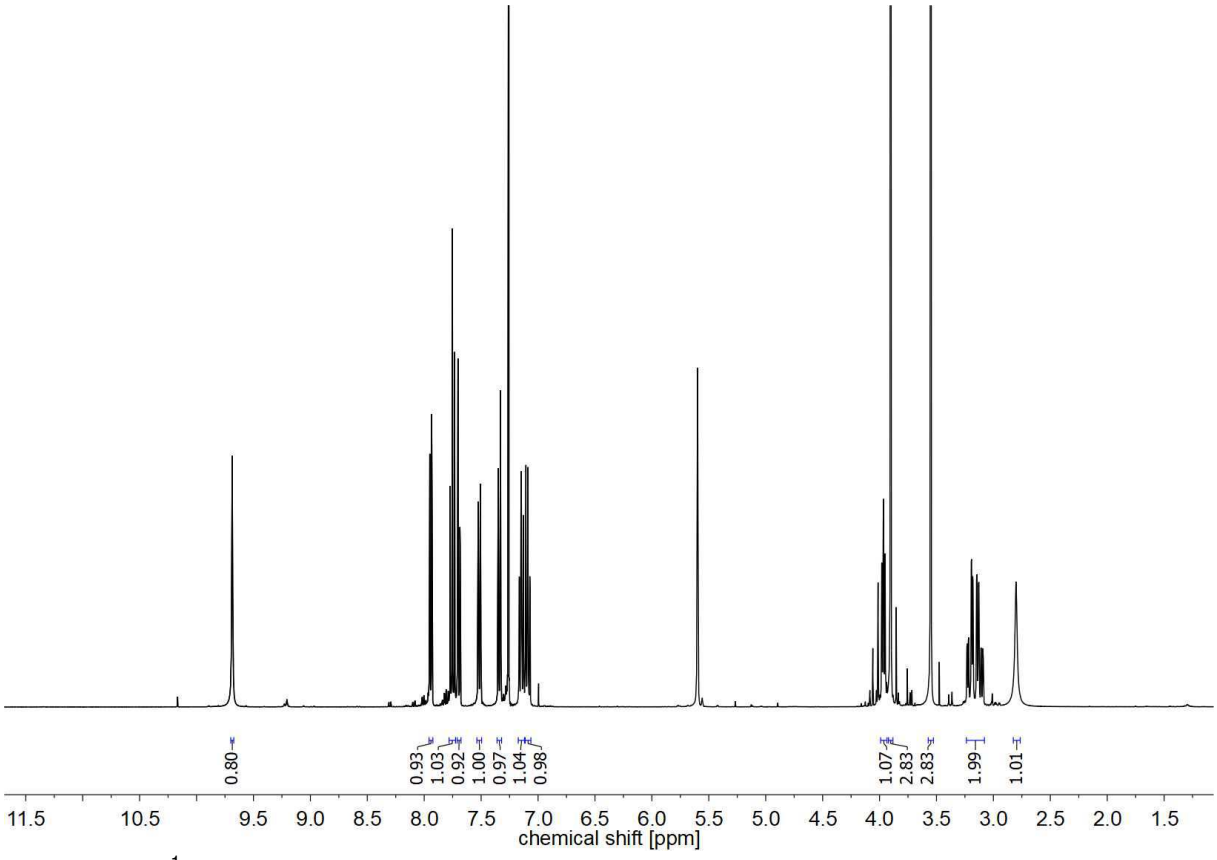

Figure S25. ^{1}H NMR ($CDCl_3$, 400 MHz) spectrum of Tetrahydroharmane **14**.

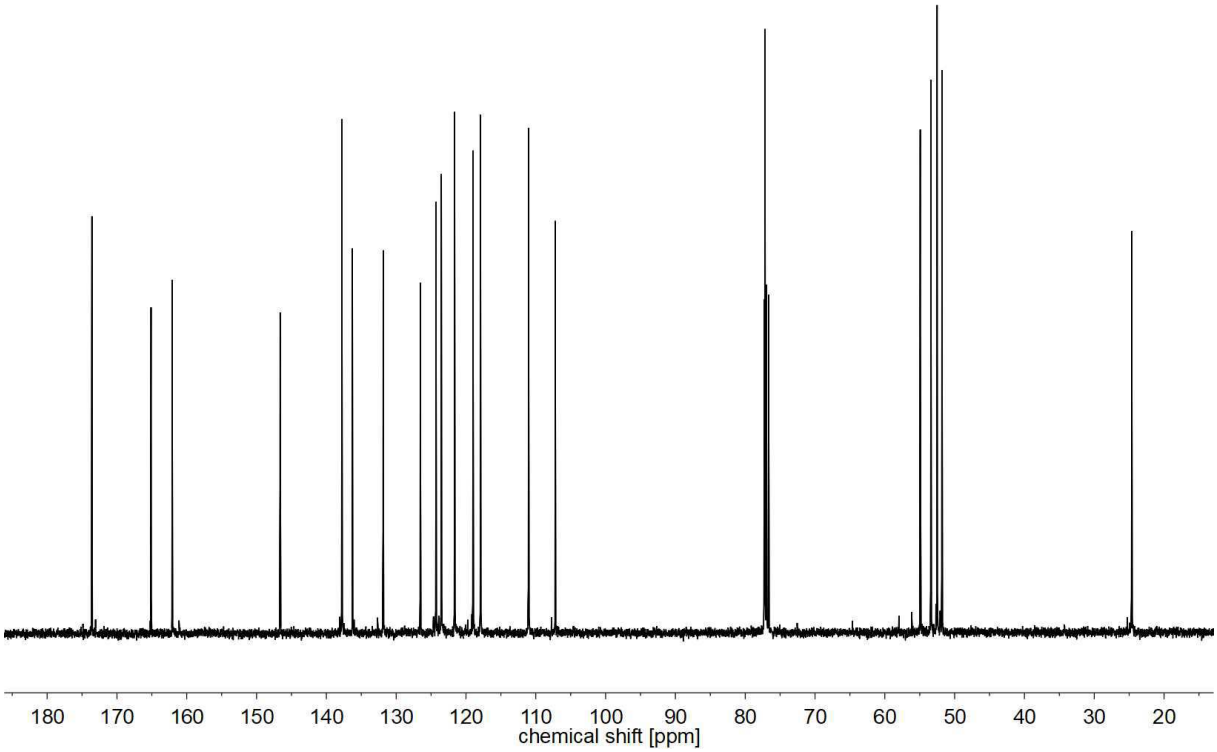

Figure S26. ^{13}C NMR ($CDCl_3$, 101 MHz) spectrum of Tetrahydroharmane **14**.

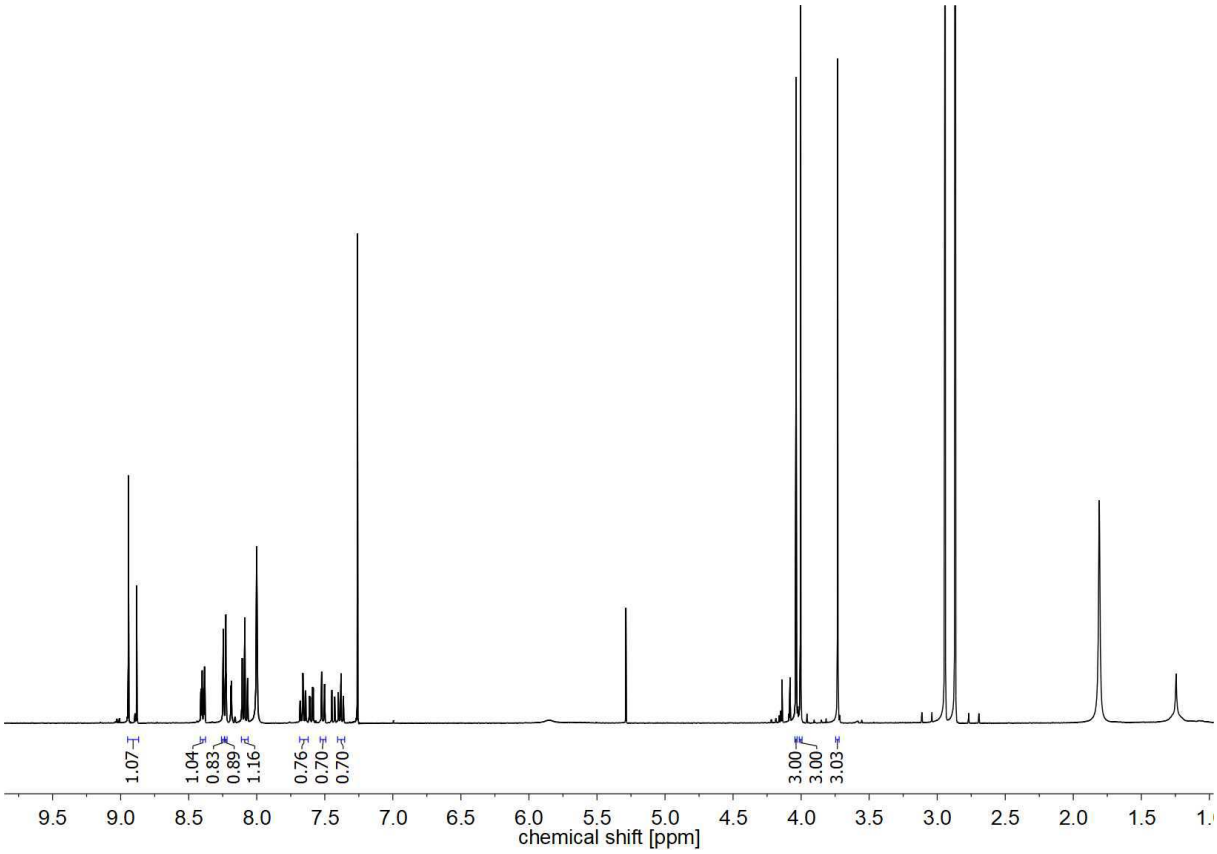

Figure S27. ^{1}H NMR ($CDCl_3$, 400 MHz) spectrum of pyridine-carboline diester **15**.

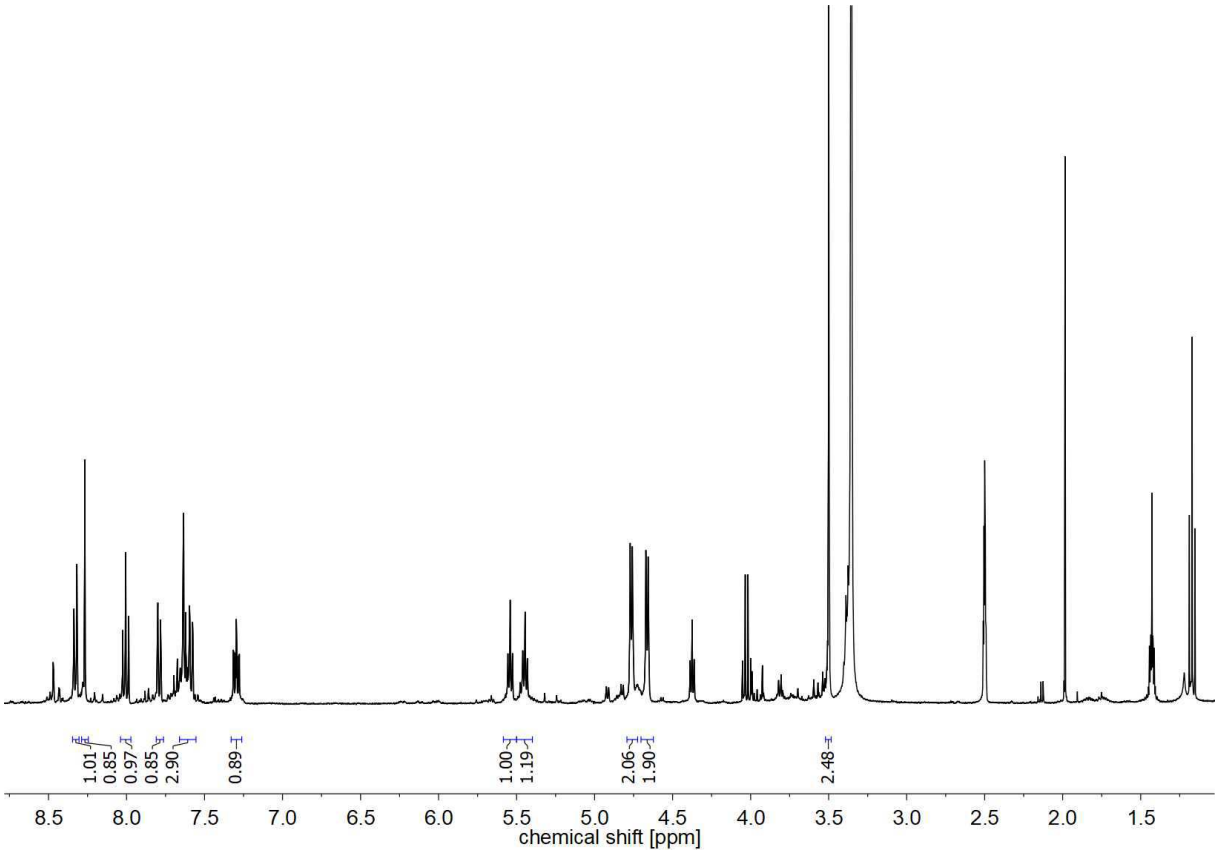

Figure S28. ^{1}H NMR ([D_6]-DMSO, 400 MHz) spectrum of pyridine-carboline diol **16**.

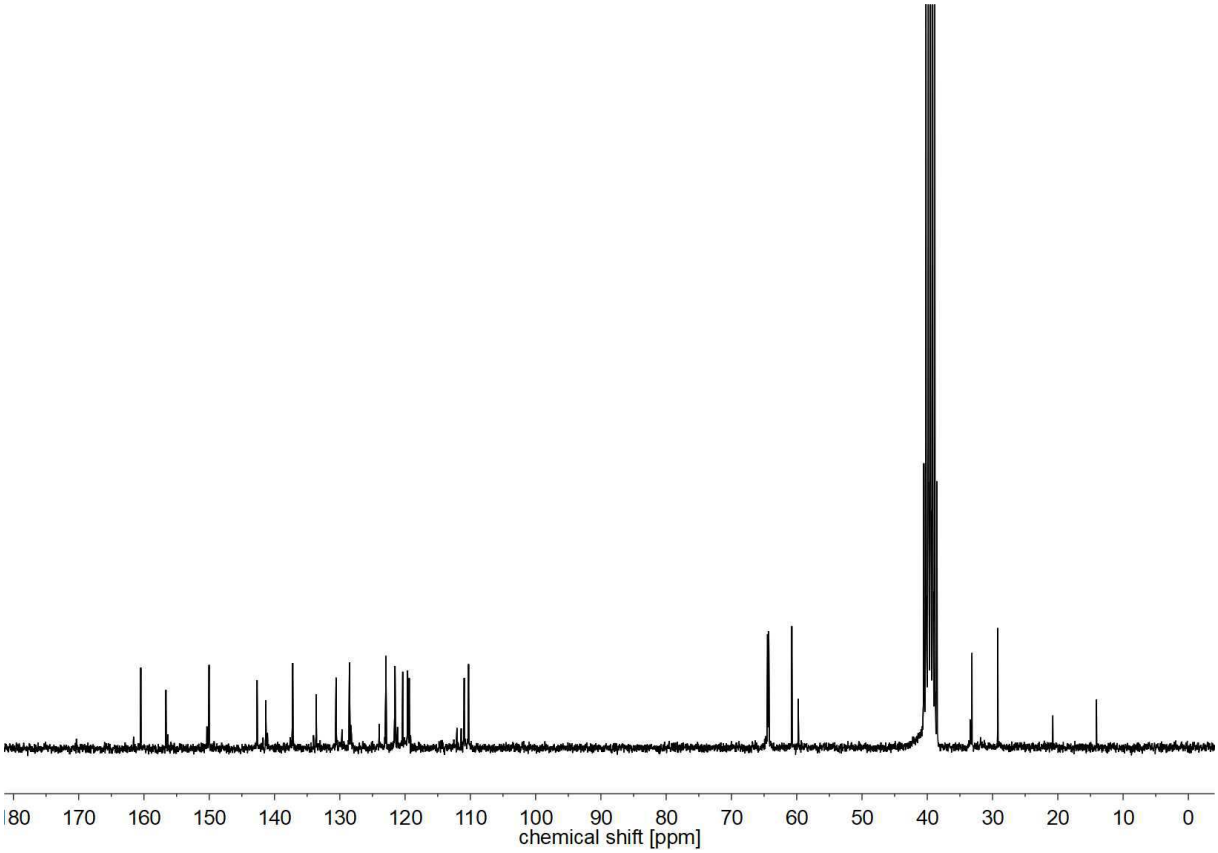

Figure S29. ^{13}C NMR ([D_6]-DMSO, 63 MHz) spectrum of pyridine-carboline diol **16**.

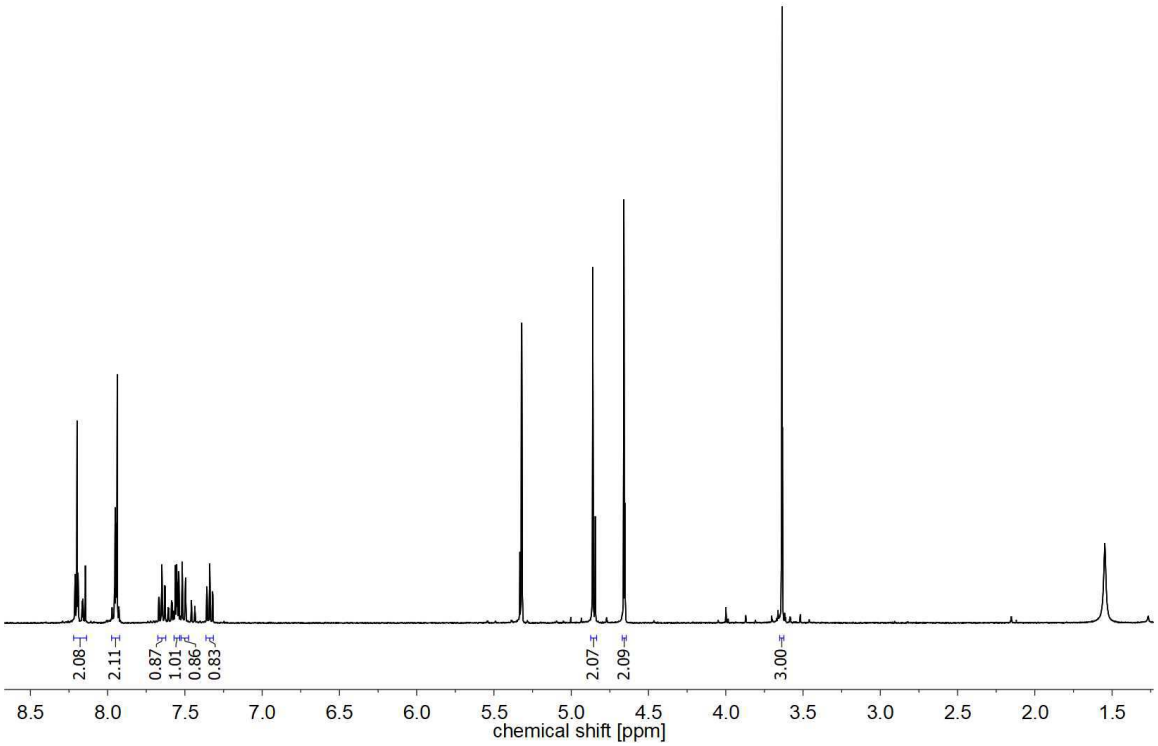

Figure S30. ^{1}H NMR (CD_2Cl_2, 400 MHz) spectrum of pyridine-carboline dibromide **17**.

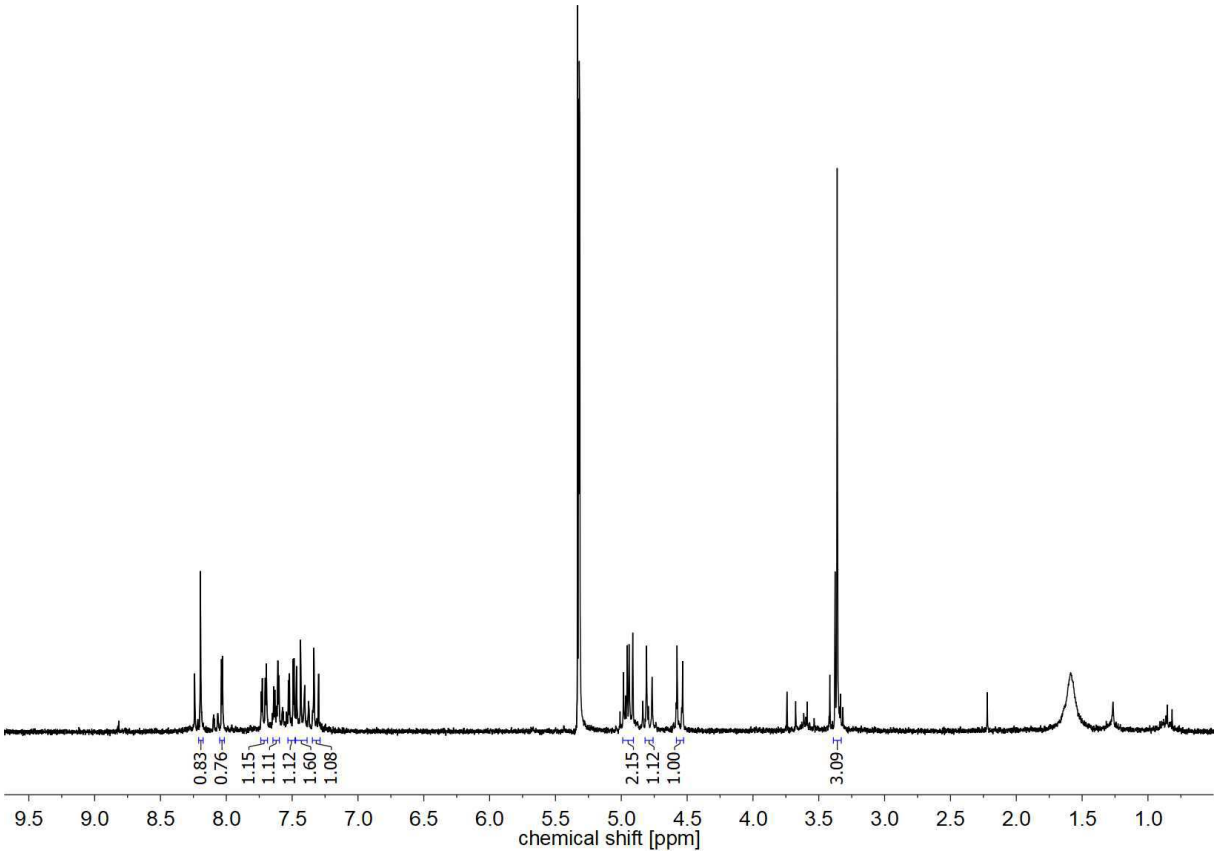

Figure S31. ^{1}H NMR (CD_2Cl_2, 400 MHz) spectrum of pyridine-carboline *N,N'*-dioxide **18**

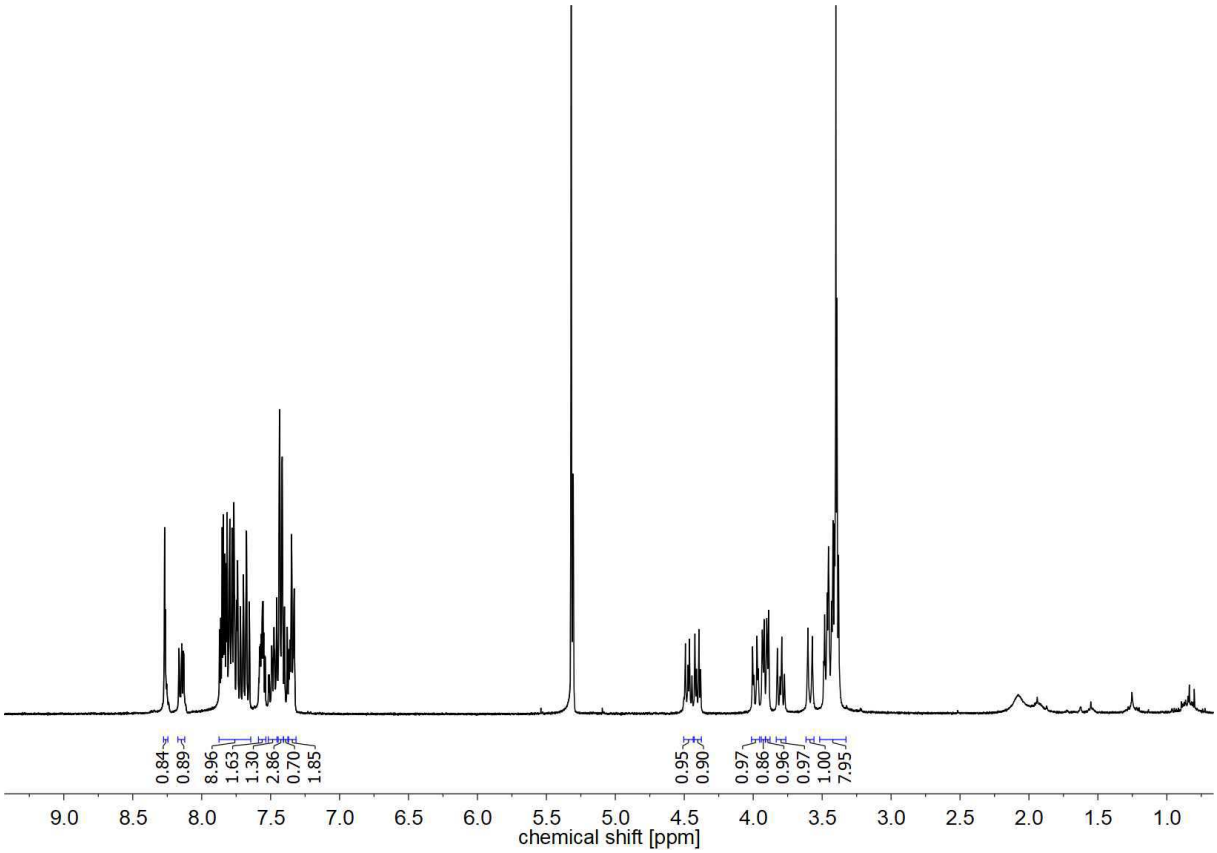

Figure S32. ^{1}H NMR (CD_2Cl_2, 400 MHz) spectrum of sodium cryptate **7-Na**.

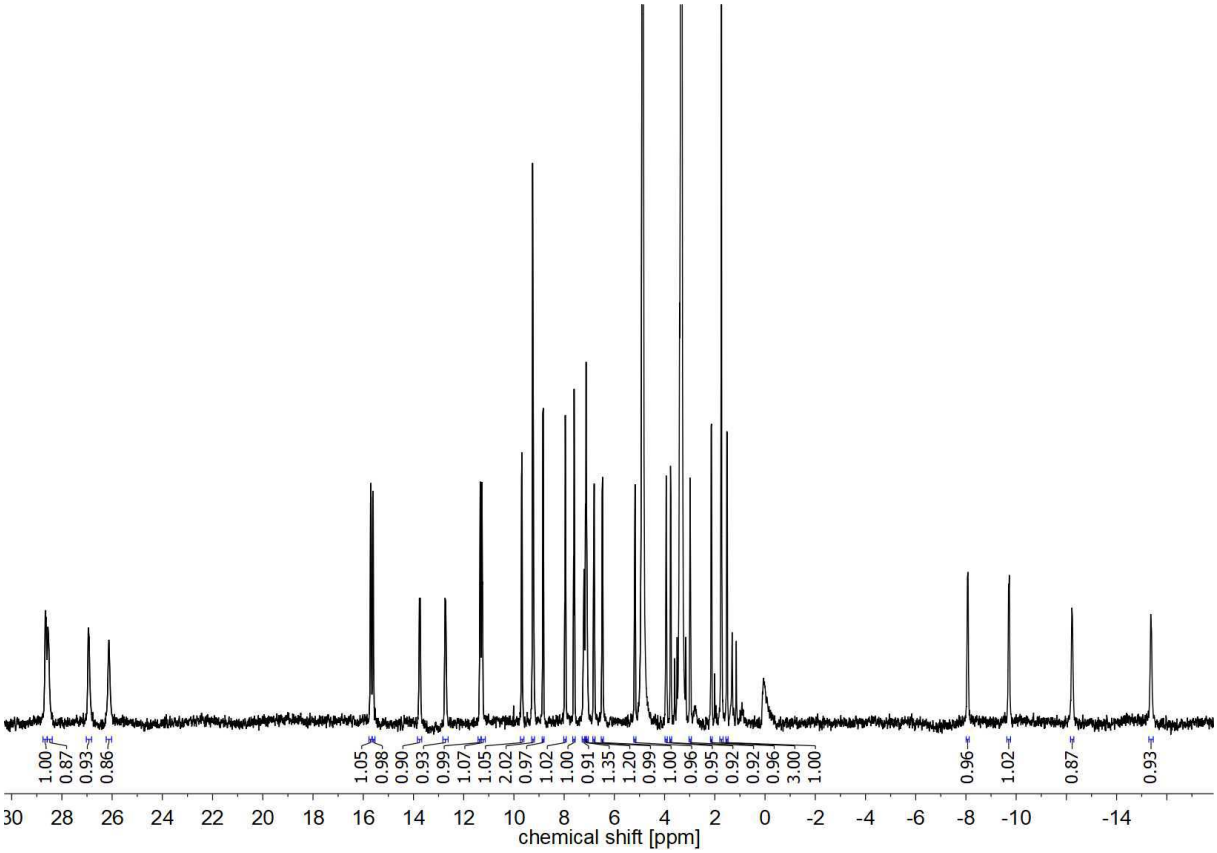

Figure S33. ^{1}H NMR (CD_3OD, 400 MHz) spectrum of cryptate **7-Eu**.

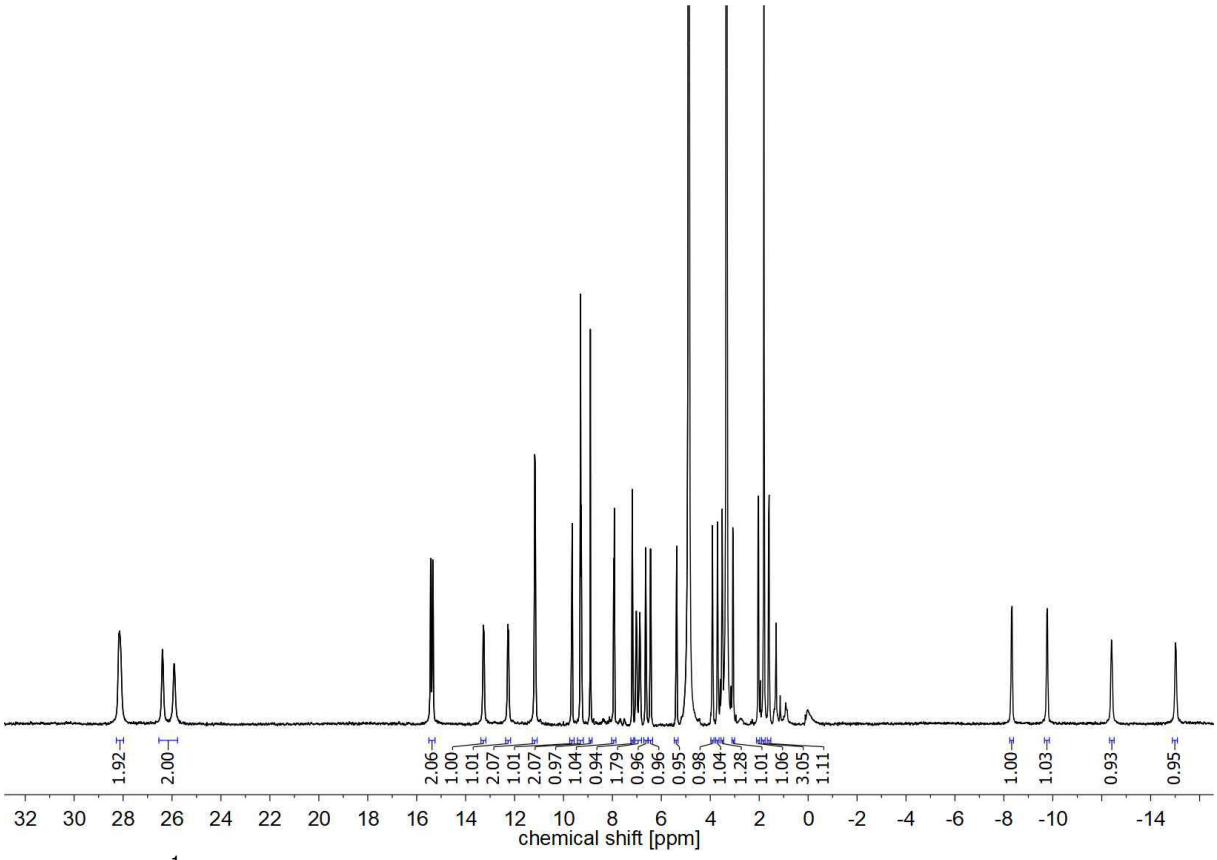

Figure S34. ^{1}H NMR (CD_3OD, 400 MHz) spectrum of cryptate **7-Eu'**.

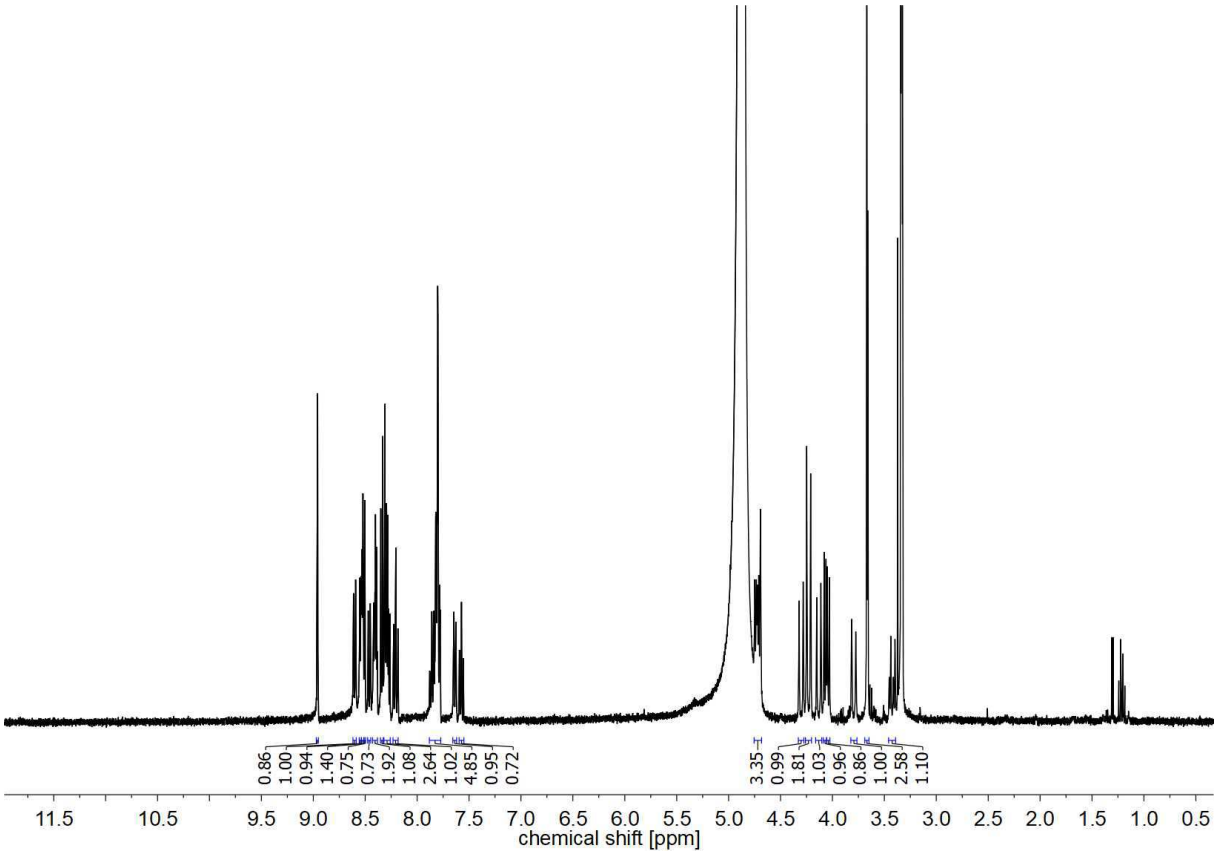

Figure S35. ^{1}H NMR (CD_3OD, 400 MHz) spectrum of cryptate **7-Lu**.

5 Luminescence Decay Profiles

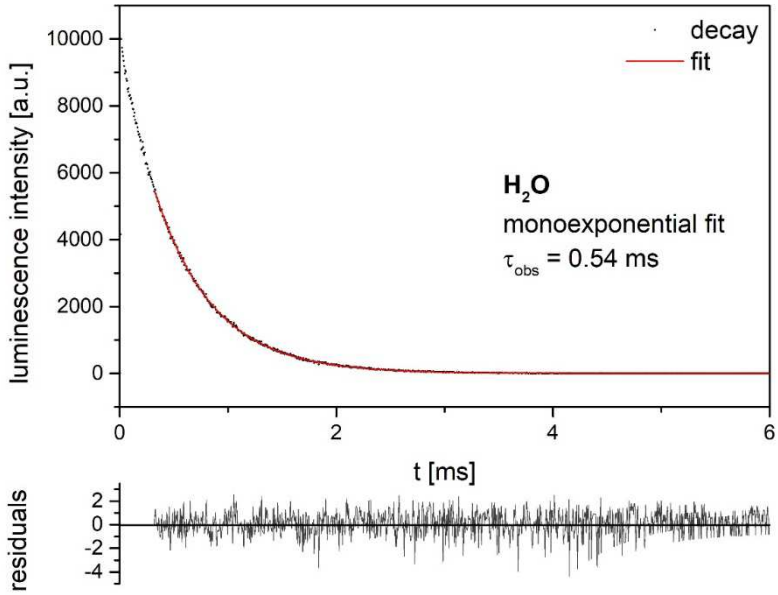

Figure S36. Luminescence decay profile of the transition $^5D_0 \rightarrow {}^7F_2$ (λ_{em} = 610 nm) in **6-Eu** (H_2O, λ_{exc} = 317 nm, monoexponential fit in red).

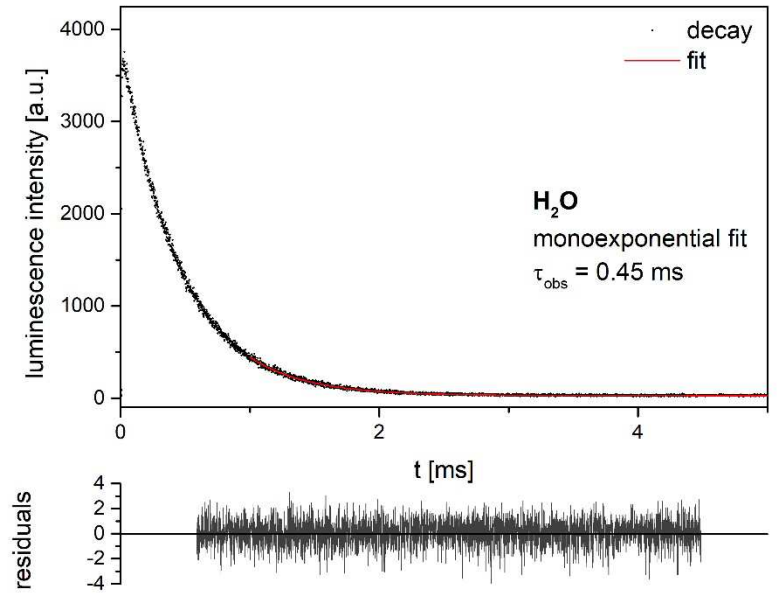

Figure S37. Luminescence decay profile of the transition $^5D_0 \rightarrow {}^7F_2$ (λ_{em} = 615 nm) in **7-Eu** (H_2O, λ_{exc} = 317 nm, monoexponential fit in red).

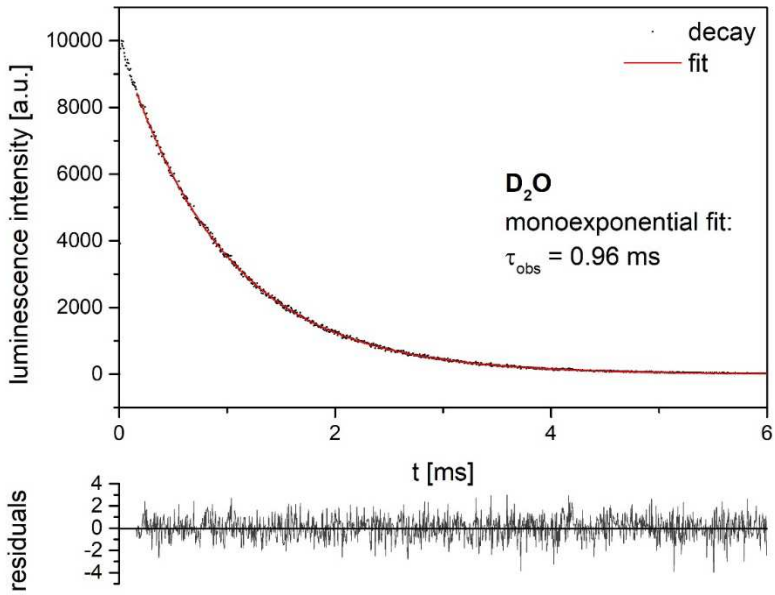

Figure S38. Luminescence decay profile of the transition $^5D_0 \rightarrow {}^7F_2$ (λ_{em} = 610 nm) in **6-Eu** (D_2O, λ_{exc} = 317 nm, monoexponential fit in red).

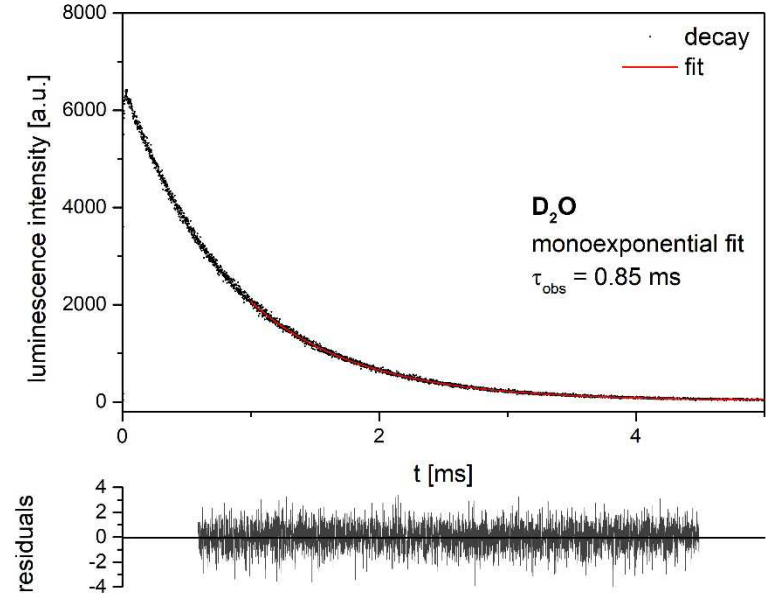

Figure S39. Luminescence decay profile of the transition $^5D_0 \rightarrow {}^7F_2$ (λ_{em} = 615 nm) in **7-Eu** (D_2O, λ_{exc} = 317 nm, monoexponential fit in red).

6 DFT Studies / Lanthanoid-Induced Shift Analysis

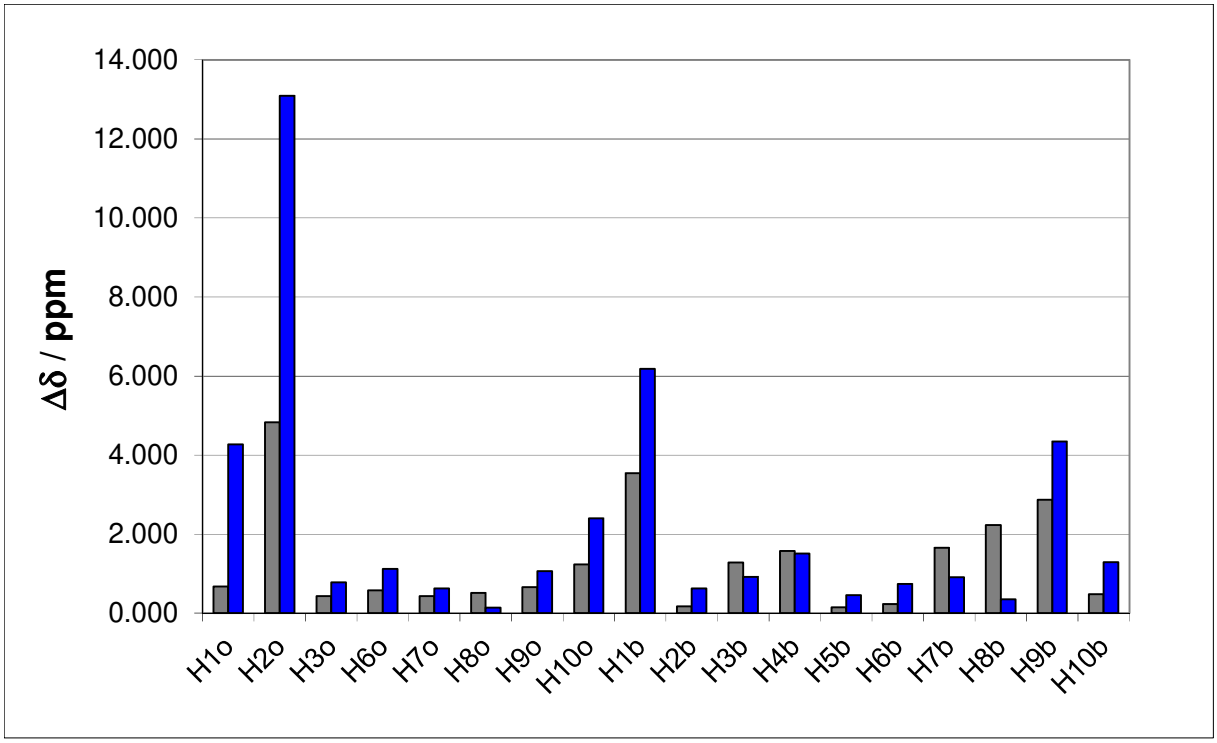

Figure S40. Absolute deviations ($\Delta\delta$) of experimental and calculated Eu^{3+}-induced ^{1}H NMR shifts in **6-Eu**. Grey: Contact contributions calculated at the TPSSh/RSC28/EPR-III level; Blue: neglecting contact contributions.

Table S1. Optimized Cartesian coordinates of **6-Eu** obtained with DFT calculations (TPSSh/LCRECP/6-31G(d,p).

Center Number	Atomic Number	Coordinates (Angstroms) X	Y	Z
1	7	-2.274238	-2.240106	1.414458
2	7	-2.868453	0.213868	2.409422
3	6	-2.951406	-2.193601	2.589232
4	6	-2.027289	-3.449375	0.867081
5	6	-3.187380	-0.853682	3.178211
6	6	-3.110991	1.452451	2.887874
7	6	-3.728186	-0.696761	4.462196
8	1	-3.949639	-1.555406	5.081498
9	6	-3.662300	1.680607	4.149585
10	1	-3.830709	2.694948	4.492322
11	7	-2.904434	-0.283073	-2.387453
12	6	-3.421571	-3.353823	3.217619
13	1	-3.981566	-3.296514	4.141092
14	6	-3.185718	-4.593567	2.631545
15	1	-3.555071	-5.500138	3.097848
16	6	-1.155142	-3.500279	-0.359675
17	1	-1.253705	-4.480038	-0.846369
18	1	-0.115782	-3.406414	-0.030610

19	6	-2.768485	2.596577	1.971516
20	1	-2.763150	3.541581	2.530570
21	1	-3.529622	2.677302	1.187214
22	6	-2.473220	-4.644524	1.438316
23	1	-2.261870	-5.587937	0.948336
24	6	-3.124427	-1.523405	-2.873399
25	6	-3.249291	0.783247	-3.148888
26	6	-3.970026	0.583527	4.950417
27	1	-4.385439	0.720808	5.942543
28	6	-3.682828	-1.754171	-4.131477
29	1	-3.831877	-2.769501	-4.480132
30	7	-2.331712	2.188989	-1.398525
31	6	-2.739772	-2.671000	-1.977003
32	1	-3.494916	-2.795417	-1.192167
33	1	-2.702932	-3.606099	-2.550996
34	6	-3.029934	2.127434	-2.560553
35	6	-3.537750	3.277403	-3.178474
36	1	-4.116769	3.208207	-4.089235
37	6	-4.019983	-0.659107	-4.922783
38	1	-4.440212	-0.798796	-5.912535
39	6	-3.797735	0.622584	-4.429321
40	1	-4.037131	1.480077	-5.043457
41	6	-2.097504	3.403342	-0.857998
42	6	-1.207651	3.469925	0.355033
43	1	-0.170908	3.395365	0.012766
44	1	-1.318602	4.446291	0.845773
45	8	0.238165	0.011789	-1.349169
46	8	0.248609	-0.017049	1.331294
47	7	-1.436751	-2.402564	-1.315053
48	7	-1.459432	2.365232	1.309790
49	6	-0.387099	2.352646	2.363983
50	1	-0.385402	3.302623	2.912338
51	1	-0.616777	1.542914	3.058582
52	6	-0.367962	-2.368418	-2.373711
53	1	-0.351621	-3.317010	-2.924154
54	1	-0.615339	-1.561583	-3.065607
55	6	-2.577896	4.588999	-1.421193
56	1	-2.374524	5.536835	-0.936432
57	6	-3.314354	4.522475	-2.598738
58	1	-3.711684	5.420756	-3.058011
59	6	2.222181	-0.652440	-0.324806
60	6	3.194187	-1.650277	-0.162136
61	6	0.974848	-2.145809	-1.755402
62	6	3.112859	-2.863398	-0.917023
63	6	1.977849	-3.103796	-1.687678
64	6	4.275633	-3.639692	-0.588785
65	6	4.996721	-2.883946	0.370103
66	1	1.833870	-4.045548	-2.204580
67	6	4.753786	-4.892445	-1.006404
68	6	6.195802	-3.349942	0.921096
69	6	5.944130	-5.359916	-0.461033
70	1	4.208609	-5.476795	-1.740482
71	6	6.651781	-4.594630	0.489565
72	1	6.760866	-2.772080	1.643604
73	1	6.338804	-6.322047	-0.770042
74	1	7.581523	-4.981440	0.894616

75	7	4.318839	-1.688659	0.632181
76	7	1.152785	-0.935070	-1.139153
77	6	4.706340	-0.761913	1.696266
78	1	5.363808	0.026403	1.321993
79	1	3.815298	-0.322821	2.142341
80	1	5.227756	-1.328545	2.467586
81	6	2.215932	0.677982	0.298589
82	6	3.176377	1.687417	0.137482
83	6	0.955511	2.151033	1.738809
84	6	3.081492	2.897227	0.896262
85	6	1.945309	3.122188	1.669654
86	6	4.235567	3.687390	0.571172
87	6	4.965448	2.942821	-0.389750
88	1	1.791213	4.060747	2.189399
89	6	4.700514	4.943038	0.995051
90	6	6.160443	3.423358	-0.937017
91	6	5.886929	5.424697	0.453616
92	1	4.148584	5.518465	1.731141
93	6	6.603410	4.670644	-0.499339
94	1	6.732521	2.854541	-1.661146
95	1	6.271639	6.389230	0.767678
96	1	7.529936	5.068397	-0.901118
97	7	1.147399	0.944254	1.119046
98	7	4.300733	1.741091	-0.656325
99	6	4.700934	0.818913	-1.719548
100	1	5.363376	0.035755	-1.343146
101	1	3.815613	0.372611	-2.170012
102	1	5.221008	1.390758	-2.487854
103	8	-4.278284	0.364625	0.031921
104	1	-4.844175	0.113423	0.777609
105	1	-4.823069	0.270703	-0.764216
106	64	-1.763618	-0.013052	-0.002414

E(RTPSSh) = -2739.7763213 Hartree
Zero-point correction = 0.846213
Thermal correction to Energy = 0.896797
Thermal correction to Enthalpy = 0.897741
Thermal correction to Gibbs Free Energy = 0.766721
Sum of electronic and zero-point Energies = -2738.930108
Sum of electronic and thermal Energies = -2738.879524
Sum of electronic and thermal Enthalpies = -2738.878580
Sum of electronic and thermal Free Energies = -2739.009601

Inorganic Chemistry
Cite This: Inorg. Chem. 2019, 58, 6959−6965
Article
pubs.acs.org/IC

Efficient Ytterbium Near-Infrared Luminophore Based on a Nondeuterated Ligand

Christian Kruck,[†] Pariya Nazari,[‡] Carolin Dee,[†] Bryce S. Richards,[‡] Andrey Turshatov,*[,‡] and Michael Seitz*[,†]

[†]Institute of Inorganic Chemistry, University of Tübingen, Auf der Morgenstelle 18, 72076 Tübingen, Germany
[‡]Institute of Microstructure Technology, Karlsruhe Institute of Technology, Hermann-von-Helmholtz-Platz 1, 76344 Eggenstein-Leopoldshafen, Germany

Supporting Information

ABSTRACT: A novel molecular ytterbium complex is reported with a new tetradentate ligand based on the 2,2′-bipyridine-6,6′-dicarboxylic acid scaffold. The photophysical properties are investigated, especially with respect to near-infrared luminescence. The ytterbium complex shows a rather high absolute luminescence quantum yield of Φ = 3.0% and a luminescence lifetime of τ_{obs} = 72 μs at room temperature in CD_3OD solution.

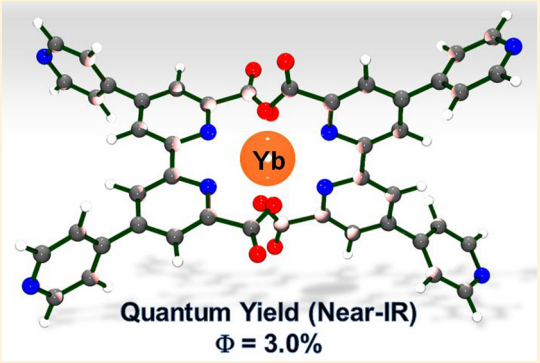

INTRODUCTION

Near-infrared lanthanoid(III) luminophores are highly interesting for technological applications such as biomedical imaging, optical telecommunication, spectral conversion materials, and many others.[1] The main challenge for the development of efficient, molecular, near-IR emitter complexes is the vibrational deactivation of metal-centered states by multiphonon relaxation (MR) where the energy is transferred from the lanthanoid to oscillator overtones in its vicinity.[2] The main culprits with respect to MR for trivalent lanthanoids are anharmonic, high-energy oscillators such as O−H (mainly in inner-sphere solvent molecules) and C−H stretching vibrations (e.g., found in the multidentate antenna chelators). The two main strategies to alleviate the problem caused by C−H moieties in the ligands are removing these oscillators by either deuteration[2,3] or halogenation.[4] Via this approach, considerable progress has been made in recent years, most notably, in the development of extremely efficient, molecular ytterbium(III) near-IR luminophores,[5] e.g., by the realization of absolute quantum yields in solution of up to 63% by Zhang and coworkers.[5a] For a number of reasons, Yb^{3+} will be very pivotal for future progress in advanced photonic applications of molecular lanthanoid complexes, among others exemplified by the discovery of Yb−Tb upconversion in solution over the past few years.[6] While the development of deuterated/halogenated near-IR ytterbium luminophores has made great progress, there is still a need for molecular emitters that are relatively simple to prepare, yet still able to exhibit acceptable luminescence efficiency. Usually, molecular ytterbium(III) complexes with nondeuterated and/or nonhalogenated ligand scaffolds show rather low quantum yields in solution of below 1%, and only a small number of such species exist which are more efficient emitters reaching ca. 4% in the best cases.[7] In an effort to develop new, nondeuterated ligand environments for Yb, we turned to derivatives of tetradentate 2,2′-bipyridine-6,6′-dicarboxylate ligands (Figure 1, structure **A**) which (i) can be employed with different functionalization patterns at the pyridine rings and (ii) form rather stable lanthanoid complexes with a wide range of different lanthanoids.[8] In addition, these chelators, while featuring aromatic C−H moieties, do not have high-energy C−H oscillators in close proximity to the metal

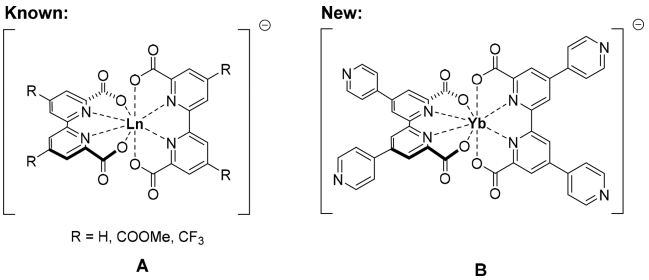

Figure 1. Previously reported lanthanoid motifs **A** based on 2,2′-bipyridine-6,6′-dicarboxylic acid (left) and new complex **B** (Ln = Yb) reported here (right).

Received: February 25, 2019
Published: May 3, 2019

DOI: 10.1021/acs.inorgchem.9b00548
Inorg. Chem. 2019, 58, 6959−6965

center and consequently show reduced MR for many near-IR emitting lanthanoids (e.g., for Tm,[8b] Dy,[8c] and Ho[8d]). Unfortunately, the ytterbium(III) complex **A** (Figure 1) with the simplest ligand (R = H), which is the obvious candidate for starting this endeavor, was previously reported to only exhibit limited near-IR efficiency, exemplified by the observed luminescence lifetime of τ_{obs} = 6.6 μs at room temperature, which indicates a quantum yield well below 1%.[8e]

Nevertheless, we chose this ligand scaffold for initial screening experiments by varying the substitution pattern in the 4- and 4′-positions of the bipyridine units, and we have identified complex **B** (Figure 1) with appended pyridyl groups as an ytterbium emitter possessing high luminescence efficiency. In this study, we introduce the synthesis of the new ligand, characterize the corresponding ytterbium chelate, and comprehensively investigate the relevant photophysics of this new luminophore.

RESULTS AND DISCUSSION

Synthesis. The synthesis of the new ligand H_2**7** used in structure **B** (Figure 1) started with the known bipyridine *N,N′*-dioxide **1** (Scheme 1).[10] Nitration to **2**, followed by

Scheme 1. Synthesis of Ligand $H_2$7

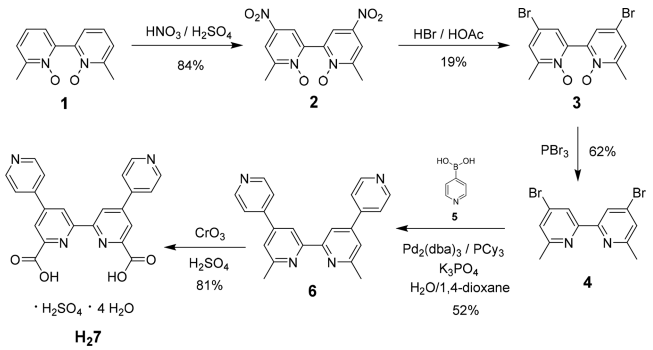

nucleophilic aromatic substitution of bromide for the nitro group using HBr in HOAc, yielded **3**, which in turn could be reduced to dibromo derivative **4**.[11] Standard Suzuki coupling of this intermediate with commercial pyridine-4-boronic acid (**5**) gave tetrapyridine **6** which was fully oxidized at the two benzylic methyl groups with CrO_3 in concentrated sulfuric acid to yield the sulfate salt of ligand H_2**7**. The targeted ytterbium complex **8-Yb** with triethylammonium as countercation was cleanly obtained by reacting 2 equiv of H_2**7** with $YbCl_3 \cdot 6H_2O$ in the presence of a slight excess of NEt_3 in methanolic solution (Scheme 2). As a diamagnetic and photoinactive control, the corresponding lutetium complex **8-Lu** was prepared in the same manner.

Scheme 2. Synthesis of the Lanthanoid Complexes 8-Ln

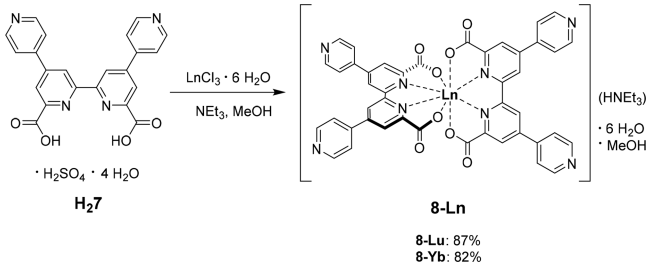

Structure Elucidation. ^{1}H NMR spectra of **8-Lu** and **8-Yb** in CD_3OD each show only four resonances for the aromatic protons of the ligand 7^{2-} as well as two signals for the three equivalent ethyl groups in triethylammonium (see Figures S2 and S3 in the Supporting Information). The integral ratios between the two sets of signals in each case amount to 2:1 (7^{2-}: $HNEt_3^+$). This reliably indicates the presence of the anticipated anionic lanthanoid complexes with the stoichiometry 2:1 (ligand/metal) exhibiting D_{2d} symmetry. Semi-empirical calculations (MOPAC2016: PM7/SPARKLE)[12−14] of the equilibrium geometry of the complex anion in **8-Yb** yield this structural element (Figure 2, see the Supporting Information for more details) with a point group symmetry close to D_{2d} (dihedral angle between the two planar ligand fragments ≈ 89°). The bonding distances Yb−X (X = N, O) are in a range very similar to those observed in related ytterbium complexes obtained by X-ray crystallography on single crystals of complexes **A** (Figure 1: R = H[8e] and R = COOMe[9a]). Importantly, the C−H oscillators, which are mostly responsible for MR in molecular complexes,[2] are rather far away as expected, with the closest ones being in the 5- and 5′-positions (r_{Yb-H} > 5.53 Å) of the central bipyridine unit.

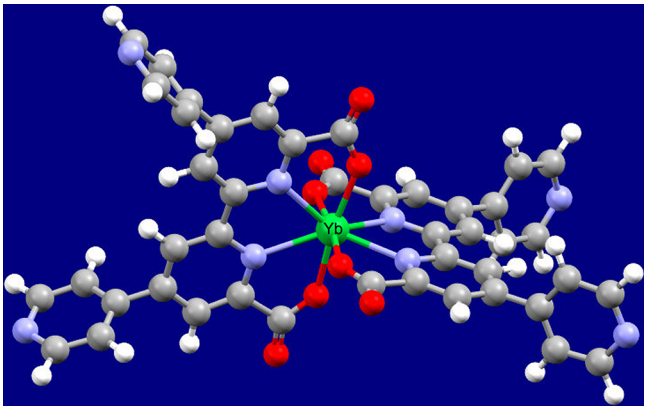

Figure 2. Calculated structure of **8-Yb** optimized by PM7[12]/SPARKLE[13] in MOPAC2016.[14] Representative geometric parameters around the metal center: av distance Yb−N 2.470 Å, av distance Yb−O 2.269 Å, dihedral angle between the two planar ligands (N1−N2−N3−N4) 89° (see the Supporting Information for more details).

Photophysics. Absorption and emission spectra in the visible region for **8-Lu** and **8-Yb** at room temperature were measured in CD_3OD (Figure 3). The absorption spectra for the two complexes are almost identical and exhibit a pronounced band between ca. 300 and 350 nm, which is typical for bipyridine-based lanthanoid complexes. After excitation at 280 nm, the emission spectrum for **8-Lu** features one fluorescence emission band ($S_1 \rightarrow S_0$) centered around ca. 360 nm (Figure 3) with quantum yield of 0.6% and no indication of additional room temperature phosphorescence at higher wavelengths. Interestingly, **8-Yb** also shows residual singlet emission, with roughly 20% relative intensity when compared to that of **8-Lu** (≡100%). Low-temperature (T = 77 K) emission spectra for **8-Lu** do, however, reveal the energetic position of the ligand-based triplet state T_1 (Figure 4). Spectral deconvolution of the structured band around 21 000 cm^{-1} yields a zero-phonon triplet energy of $E^{0\rightarrow0}(T_1) \approx 22\,600$ cm^{-1} which is slightly lower than that for the corresponding parent system **A** (Figure 1, R = H: $E^{0\rightarrow0}(T_1) \approx 23\,500$ cm^{-1}).[8b]

DOI: 10.1021/acs.inorgchem.9b00548
Inorg. Chem. 2019, 58, 6959−6965

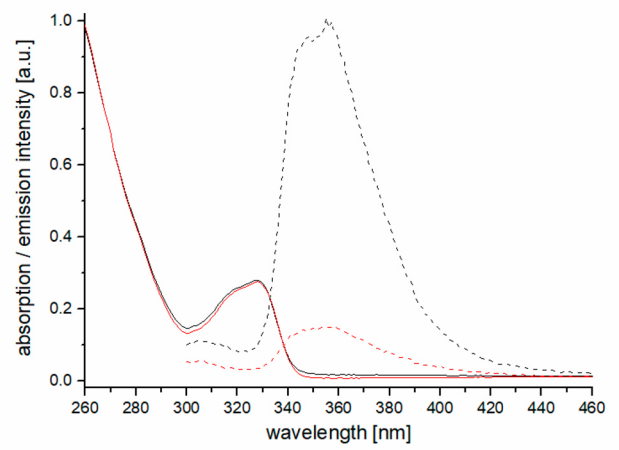

Figure 3. UV–vis absorption (solid lines) and singlet steady-state emission (dashed lines, λ_{exc} = 280 nm) spectra for **8-Lu** (black) and **8-Yb** (red) in CD_3OD (c = 10 μM) at room temperature (the relative scales of the emission spectra reflect the actual intensity differences).

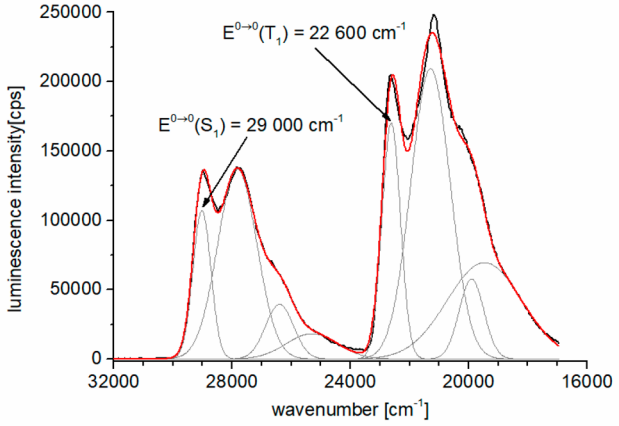

Figure 4. Low-temperature steady-state emission spectra (λ_{exc} = 305 nm, T = 77 K) for **8-Lu** in a glassy matrix (CD_3OD/C_2D_5OD, 1:1, v/v).

After excitation with UV light, the near-IR emission spectra of **8-Yb** originating from the transition $^2F_{5/2} \rightarrow {}^2F_{7/2}$ in CD_3OD at room temperature can easily be detected (Figure 5). Interestingly, direct f–f excitation at λ_{exc} = 940 nm of the same sample results in an emission spectrum that shows a broadly similar emission band but where emission from a higher ligand-field state (≈ 975 nm) is more prominent compared to the spectra after sensitized excitation via the ligand (Figure 5). The emission after ligand excitation exhibits a monoexponential luminescence lifetime τ_{obs} = 72 μs (Table 1), which is comparatively long for molecular species of this kind. The analogous spectra at T = 77 K in a glassy matrix of CD_3OD/C_2D_5OD are very similar to the room temperature signatures (Figure 5) with a slightly longer, monoexponential lifetime τ_{obs} = 96 μs. Surprisingly, near-IR luminescence of **8-Yb** is insensitive to molecular oxygen present in the solvent. Measurements performed in deoxygenated solutions revealed no difference in luminescence intensity as compared to the ones where dioxygen has not been removed. Thus, we assume that the triplet state of the ligand is not of primary importance for the photosensitization of Yb^{3+} or is very short-lived. Considering the large mismatch in the energy of ligand singlet

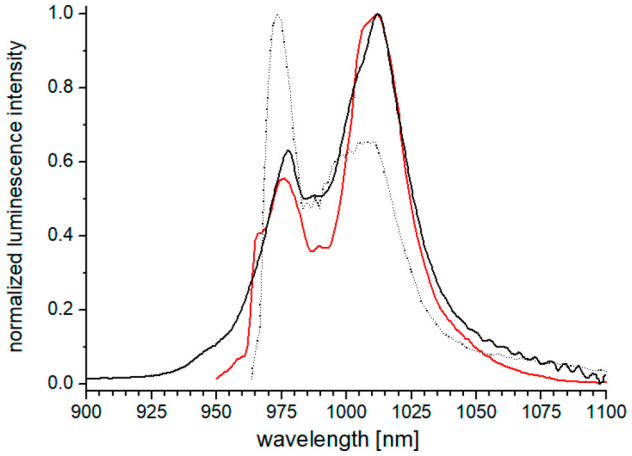

Figure 5. Steady-state emission spectra for the transition $^2F_{5/2} \rightarrow {}^2F_{7/2}$ in **8-Yb** at room temperature in CD_3OD (solid black, 298 K, λ_{exc} = 300 nm; dotted black, 298 K, λ_{exc} = 940 nm) and at low temperature in a glassy matrix (solid red, 77 K, λ_{exc} = 300 nm, CD_3OD/C_2D_5OD, 1:1, v/v).

and triplet states and the metal-centered $^2F_{5/2}$ level, it is not easy to imagine that near-IR luminescence is directly sensitized via singlet/triplet energy transfer from the ligand to the metal. An alternative explanation is photosensitization of Yb^{3+} via internal redox processes involving electron transfer as proposed in the past in other systems.[1c,15] The involvement of LMCT states in **8-Yb**, however, seems unlikely due to the observation of identical residual singlet emission of exactly the same magnitude in the corresponding erbium complex[16] and the rather electron-deficient nature of the ligands in our case. Therefore, a conclusive answer regarding the nature of the sensitization pathway remains unclear.

Gratifyingly, the measurement of the absolute quantum yield at room temperature in CD_3OD revealed a rather high value of Φ_{Ln}^{L} = 3.0% (Table 1), which compares well with other relatively efficient systems reported so far in the literature for nondeuterated, molecular ytterbium luminophores in solution. In order to get more insight into the sensitization process, we set out to determine a number of important parameters according to eq 1[1]

$$\Phi_{Ln}^{L} = \eta_{sens}\Phi_{Ln}^{Ln} = \eta_{sens}\frac{\tau_{obs}}{\tau_{rad}} \quad (1)$$

with η_{sens} as the sensitization efficiency, Φ_{Ln}^{Ln} as the intrinsic quantum yield, and τ_{rad} being the radiative (intrinsic) luminescence lifetime. Among the three unknown parameters so far (Φ_{Ln}^{Ln}, η_{sens}, τ_{rad}), the radiative lifetime τ_{rad} can be determined if the emissive transition in question terminates in the ground state.

This is the case for ytterbium, and τ_{rad} can be extracted from the molar extinction spectrum corresponding to the f–f transition $^2F_{5/2} \rightarrow {}^2F_{7/2}$ (eq 2):[17]

$$\frac{1}{\tau_{rad}} = 2303\frac{8\pi c n^2 \tilde{\nu}_m^{\,2}}{N_A}\frac{(2J_l + 1)}{(2J_u + 1)}\int \varepsilon(\tilde{\nu})\, d\tilde{\nu}$$

$$\text{with } \tilde{\nu}_m = \frac{\int \tilde{\nu}\varepsilon(\tilde{\nu})\, d\tilde{\nu}}{\int \varepsilon(\tilde{\nu})\, d\tilde{\nu}} \quad (2)$$

This equation includes the following parameters and constants: c speed of light (in cm s^{-1}), N_A Avogadro's constant, n

DOI: 10.1021/acs.inorgchem.9b00548
Inorg. Chem. 2019, 58, 6959–6965

Table 1. Luminescence Data for 8-Yb in CD_3OD

entry	compd	τ_{obs}^{298K} [a] [μs]	τ_{obs}^{77K} [a] [μs]	τ_{rad} [b] [ms]	$\Phi_{Ln}^{Ln} = \frac{\tau_{obs}^{298K}}{\tau_{rad}}$ [c] [%]	Φ_{Ln}^{L} [d] [%]	$\eta_{sens} = \frac{\Phi_{Ln}^{L}}{\Phi_{Ln}^{Ln}}$ [e] [%]
1	**8-Yb**	72	96	1.3	5.5	3.0	54%

[a]Luminescence lifetimes: λ_{exc} = 300 nm, λ_{em}(298 K) = 1012 nm, λ_{em}(77 K) = 1010 nm, estimated uncertainty ±10% for **8-Yb**. [b]Radiative lifetime: calculated using eq 2, estimated uncertainty ±20%. [c]Intrinsic quantum yield. [d]Absolute quantum yield, estimated uncertainty ±15%. [e]Sensitization efficiency.

refractive index, $\tilde{\nu}_m$ barycenter of the transition to the ground state (as defined above), $2J_l + 1$ degeneracy of the lower (ground) state, $2J_u + 1$ degeneracy of the upper (excited) state, and $\varepsilon(\tilde{\nu})$ molar extinction coefficient (in units of $[M^{-1}\ cm^{-1}]$) of the transition to the ground state vs the wavenumber. The analysis was performed on the basis of the measured extinction spectrum (Figure 6) yielding the value τ_{rad} = 1.3 ms for **8-Yb**

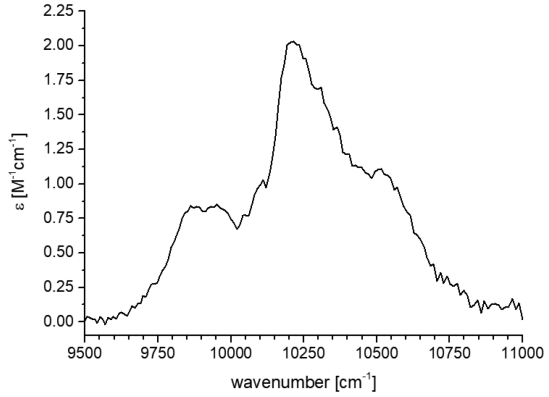

Figure 6. Quantitative absorption spectrum of the f–f transition $^2F_{7/2} \rightarrow {}^2F_{5/2}$ in **8-Yb** (c = 0.6 mM, path length d = 5 cm) in CD_3OD.

(see the Supporting Information for more details). This value is on the higher side of the usual range ($\tau_{rad} \approx 0.6–1.3$ ms)[18] in molecular complexes and very similar to the one found (τ_{rad} = 1.31 ms) in $Na_3[Yb(dpa)_3]$[19] (with dpa = pyridine-2,6-dicarboxylate) which is structurally very similar to **8-Yb**. The high value of τ_{rad} is a reflection of the relatively high symmetry (D_{2d}) of the inner coordination sphere around the metal center.

With the key parameter τ_{rad} in hand, the full evaluation according to eq 1 could be performed, giving an intrinsic quantum yield Φ_{Ln}^{Ln} = 5.5% and a sensitization efficiency η_{sens} = 54% for **8-Yb** (Table 1). The value for Φ_{Ln}^{Ln} is quite high for complexes of this type, while η_{sens} is rather low, reflected also by the previous observation of residual singlet emission (vide supra) in **8-Yb**.

CONCLUSION

In conclusion, we have identified a new chelator based on 2,2′-bipyridine-6,6′-dicarboxylate for the efficient sensitization of ytterbium near-IR luminescence. This antenna ligand allows the realization of rather high absolute luminescence quantum yields of 3% in solution, which is quite rare for a nondeuterated and/or nonhalogenated sensitizer of this kind.

EXPERIMENTAL SECTION

General. All commercially available chemicals for the synthetic and analytical work were purchased and used without any further purification steps. Isotopically labeled solvents ($CDCl_3$, CD_3OD, [d_6]-DMSO, CD_2Cl_2, CD_3CD_2OD) for NMR and optical spectroscopies had at least 99.8% isotope content. Unless indicated, reactions were carried out under an atmosphere of argon (dry, O_2-free) using standard Schlenk methodology. Preparative column chromatography was carried out using SiO_2 60 (Merck KGaA, 0.040–0.063 mm), whereas TLC was performed with silica gel 60 plates (Merck, coated on aluminum sheets, with fluorescence indicator F254). Mass spectrometry was performed using a Bruker Daltonics Esquire 3000plus instrument (ESI mode). NMR spectra were acquired on a Bruker instrument Avance II+400 (^1H 400 MHz, ^{13}C 101 MHz). All chemical shifts (δ) for the NMR spectra are given in parts per million (ppm) and relative to the usual standard (tetramethylsilane, TMS). The chemical shift range for each spectrum was calibrated using the residual solvent signals as internal reference.

Synthesis. *6,6′-Dimethyl-4,4′-dinitro-2,2′-bipyridine-N,N′-dioxide (**2**).*[11] 6,6′-Dimethyl-2,2′-bipyridine-*N,N*′-dioxide (**1**)[10] (5.60 g, 25.7 mmol, 1.0 equiv) was dissolved in concentrated sulfuric acid (50 mL). Concentrated nitric acid (17 mL) was added dropwise with a dropping funnel in the course of approximately 20 min, followed by continued stirring at 100 °C for 4 h. The resulting solution was allowed to attain room temperature and was poured onto crushed ice (200 g). After the ice melted, the pH was adjusted to ca. 9 by the dropwise addition of aqueous NaOH (10 wt % NaOH), resulting in precipitation of the product. It was collected, washed with ice cold water, and dried *in vacuo*. The product was obtained as a yellow solid (6.6 g, 84%). ^1H NMR ([d_6]-DMSO, 400 MHz): δ = 8.60 (s, 2 H), 8.53 (s, 2 H), 2.48 (s, 6 H) ppm.

*4,4′-Dibromo-6,6′-dimethyl-2,2′-bipyridine-N,N′-dioxide (**3**)*[11]. A flask was charged with 6,6′-dimethyl-4,4′-dinitro-2,2′-bipyridine-*N,N*′-dioxide (**2**) (6.60 g, 21.6 mmol, 1.0 equiv), and a solution of hydrogen bromide (33 wt % HBr in acetic acid, 150 mL) was added. The resulting mixture was stirred at 90 °C for 44 h and allowed to come to ambient temperature, and the pH was cautiously adjusted to approximatey 9 using a solution of sodium hydroxide (10 wt % NaOH in water). After extraction of the aqueous phase with CH_2Cl_2 (3 × 150 mL), the combined organic phases were dried ($MgSO_4$) and concentrated under reduced pressure. The crude title compound was purified by chromatography (SiO_2, CH_2Cl_2–MeOH, gradient 50:1 → 9:1), yielding the product as a light yellow solid (1.40 g, 19%). ^1H NMR ([d_6]-DMSO, 400 MHz): δ = 7.92 (s, 2 H), 7.84 (s, 2 H), 2.36 (s, 6 H) ppm. TLC: R_f = 0.23 (SiO_2, CH_2Cl_2/MeOH 9:1, detection UV). MS (ESI, pos mode): m/z (%) = 374.9 (100, $[M + H]^+$, Br_2 pattern).

*4,4′-Dibromo-6,6′-dimethyl-2,2′-bipyridine (**4**).* 4,4′-Dibromo-6,6′-dimethyl-2,2′-bipyridine-*N,N*′-dioxide (**3**) (2.18 g, 5.83 mmol, 1.0 equiv) was suspended in CH_3CN (200 mL, HPLC grade). PBr_3 (11.0 mL, 31.6 g, 117 mmol, 20 equiv) was added dropwise, and the red mixture was heated under reflux for 18 h. The green/brown suspension was poured onto crushed ice (ca. 150 g), and the pH was adjusted to ≈8 with saturated aqueous Na_2CO_3. The aqueous phase was extracted with $CHCl_3$ (1 × 200 mL, 2 × 100 mL). The combined organic phases were dried ($MgSO_4$) and concentrated under reduced pressure. The product was obtained as a light yellow solid (1.24 g, 62%) and was used without further purification for the next step. ^1H NMR ($CDCl_3$, 400 MHz): δ = 8.40 (s, 2 H), 7.36 (s, 2 H), 2.60 (s, 6 H) ppm.

DOI: 10.1021/acs.inorgchem.9b00548
Inorg. Chem. 2019, 58, 6959–6965

Dimethyl Tetrapyridine **6**. A two-neck Schlenk-flask equipped with a reflux condenser was charged with 4,4′-dibromo-6,6′-dimethyl-2,2′-bipyridine (**4**) (1.0 g, 2.9 mmol, 1.0 equiv), 4-pyridylboronic acid (**5**) (1.1 g, 8.8 mmol, 3.0 equiv), Pd_2dba_3 (107 mg, 117 μmol, 4.0 mol %), and K_3PO_4 (3.10 g, 14.6 mmol, 5.0 equiv). The apparatus was set under inert gas (argon), and 1,4-dioxane (degassed, 140 mL, 3 × freeze−pump−thaw) was added, followed by PCy_3 (66.0 mg, 285 μmol, 8.0 mol %) and deoxygenated H_2O (50 mL). The reaction mixture was heated under reflux for 48 h and allowed to attain ambient temperature. Water (20 mL) was added under atmospheric conditions, and the pH of the mixture was adjusted to ≈9 using saturated aqueous Na_2CO_3. The mixture was extracted with CH_2Cl_2 (3 × 70 mL). The combined organic phases were dried ($MgSO_4$), and the solvent was evaporated. The residue was purified by column chromatography (SiO_2, CH_2Cl_2/MeOH, gradient 50:1 → 25:1), yielding the title compound as a colorless solid (513 mg, 52%). ^{1}H NMR (CD_2Cl_2, 400 MHz): δ = 8.64 (dd, J = 4.5 Hz, 1.7 Hz, 4 H), 8.48 (s, 2 H), 7.76 (dd, J = 4.5 Hz, 1.7 Hz, 4 H), 7.54 (s, 2 H), 2.69 (s, 6 H) ppm. ^{13}C NMR (CD_2Cl_2, 100.6 MHz): δ = 159.6, 156.8, 151.1, 147.3, 146.5, 122.1, 121.6, 116.5, 25.0 ppm. MS (ESI, pos mode): m/z (%) = 339.1 (100, $[M + H]^+$), 361.1 (26, $[M + Na]^+$), 376.9 (21, $[M + K]^+$).

Bipyridinium Dicarboxylic Acid Sulfate H_2**7**. Dimethyl tetrapyridine **6** (641 mg, 1.90 mmol, 1.0 equiv) was slowly added as a solid to concentrated sulfuric acid (10 mL) while the mixture was stirred vigorously. The viscous solution was brought to an internal temperature of 65 °C before solid chromium(VI) oxide (0.83 g, 8.3 mmol, 4.4 equiv) was added at such a pace as to not let the reaction temperature (measured internally) rise beyond 70 °C. The green solution was stirred at 70 °C (internal temperature) for 3 h, allowed to cool to room temperature, and poured onto crushed ice (100 g). The resulting solution was stored in a refrigerator (4 °C) for 24 h. The precipitate was filtered over a Büchner funnel, washed with ice cold H_2O, and dried under reduced pressure. The product was obtained as a colorless solid (612 mg, 81%). ^{1}H NMR ([d_6]-DMSO, 400 MHz): δ = 9.18 (d, J = 1.6 Hz, 2 H) 8.97 (d, J = 6.2 Hz, 4 H), 8.59 (d, J = 1.6 Hz, 2 H), 8.30 (d, J = 6.1 Hz, 4 H) ppm. ^{13}C NMR ([d_6]-DMSO, 100.6 MHz): δ = 165.4, 155.2, 149.6 145.9, 145.3, 145.0, 124.6, 123.7, 122.6, 119.6 ppm. MS (ESI+): m/z (%) = 399.0 (100, $[M + H]^+$). Anal. Calcd for $C_{22}H_{14}N_4O_4{\cdot}H_2SO_4{\cdot}4H_2O$ (M_r = 568.51): C, 46.48; H, 4.26; N, 9.86; S, 5.64. Found: C, 46.38; H, 4.49; N, 9.69; S, 5.49.

Lanthanoid Complexes **8-Ln**. *General Procedure*. H_2**7** (2.0 equiv) and $LnCl_3{\cdot}6H_2O$ (1.0 equiv) were treated with anhydrous MeOH (80 μL per μmol of H_2**7**), followed by dry NEt_3 (10.0 equiv). The mixture was stirred at ambient temperature for 2 h, and the solid formed during this time was filtered over a Büchner funnel. It was subsequently washed with ice cold, anhydrous methanol and dried under reduced pressure.

Lutetium Complex **8-Lu**. The general procedure using H_2**7** (50.0 mg, 87.9 μmol), $LuCl_3{\cdot}6H_2O$ (18.0 mg, 44.0 μmol), and NEt_3 (61.3 μL, 439.7 μmol) yielded a light yellow solid (42.0 mg, 87%). ^{1}H NMR (CD_3OD, 400 MHz): δ = 9.40 (d, J = 1.5 Hz, 4 H), 8.78 (dd, J = 4.6 Hz, 1.6 Hz, 8 H), 8.52 (d, J = 1.2 Hz, 4 H), 8.10 (dd, J = 4.6 Hz, 1.6 Hz, 8 H), 3.14 (s br, 6 H), 1.28 (t, J = 6.9 Hz, 9 H) ppm. MS (ESI, neg mode): m/z (%) = 967.4 (100, $[M]^-$). Anal. Calcd for $[C_{44}H_{24}N_8O_8Lu]$ $(HNEt_3){\cdot}CH_3OH{\cdot}6H_2O$ (M_r = 1210.01): C, 50.62; H, 4.66; N, 10.42. Found: C, 50.48; H, 4.94; N, 10.40.

Ytterbium Complex **8-Yb**. The general procedure using H_2**7** (100.0 mg, 175.9 μmol), $YbCl_3{\cdot}6H_2O$ (34.3 mg, 88.0 μmol), and NEt_3 (122.6 μL, 879.5 μmol) yielded a colorless solid (79.0 mg, 82%). ^{1}H NMR (CD_3OD, 400 MHz): δ = 18.90 (s br, 4 H), 9.02 (s br, 16 H), 7.58 (s br, 4 H), 3.13 (s br, 6 H), 1.27 (s br, 9 H) ppm. MS (ESI, neg mode): m/z (%) = 966.3 (100, $[M]^-$, Yb pattern).

Photophysics. The NIR f−f absorption spectrum for **8-Yb** was measured using a spectrophotometer (Jasco V770) with long-path (5.0 cm) quartz cuvettes (see the Supporting Information).

Steady-state emission spectra at ambient temperature (298 K) were collected on a Cary Eclipse G9800A fluorimeter. The luminescence lifetime measurements were performed using a multichannel scaling card (Timeharp 260, PicoQuant) with modulation of the pulsed diode (M300L4: λ_{em} = 300 nm, Thorlabs) being achieved by a built-in function generator of the corresponding driver unit. Spectral selection was achieved using a double monochromator (DTMS300, Bentham), and the luminescence band at 1012 nm was detected via a photomultiplier tube (R928P, Hamamatsu, operated in a thermo-electrically cooled CoolOne PMT housing unit from Horiba). For the absolute quantum yield measurements, the beam from the diode (M300L4: λ_{em} = 300 nm, Thorlabs) was focused by a lens (focal length: 75 cm) into an integrating sphere (Labsphere, ⌀ 15 cm). The emitted light was transferred from the integrating sphere into the spectrometer (AvaSpec-ULS2048LTEC spectrometer, Avantes) with the help of an optical fiber (FP1000URT, Thorlabs, ⌀ 1 mm). A calibration lamp (HL-3plus-INT-CAL, Ocean Optics) was used to calibrate the entire system's optical response. The relative quantum yield of **8-Lu** was measured against the standard 9,10-diphenylanthracene[20] (Φ = 0.90 in cyclohexane).[21] Steady-state luminescence at 77 K (liquid N_2 cuvette) of **8-Lu** (CD_3OD/C_2D_5OD, 1:1, v/v) was collected with the help of a Horiba Fluorolog-3 DF fluorimeter (excitation, 450 W continuous xenon lamp; detection, Hamamatsu R2658P PMT) equipped with double-grating DFM/DFX monochromators (excitation, 1200 grooves/mm, blazed at 330 nm; emission, 1200 grooves/mm, blazed at 500 nm). The lifetime of **8-Yb** at the same temperature was determined with excitation from a pulsed xenon flash lamp (70 W, pulse width ca. 1.5 μs fwhm) by tail-fitting the decays using the DAS software package from Horiba.

■ ASSOCIATED CONTENT

Supporting Information

The Supporting Information is available free of charge on the ACS Publications website at DOI: 10.1021/acs.inorgchem.9b00548.

^{1}H NMR spectra for H_2**7**, **8-Lu**, and **8-Yb**; details for the geometry optimization of **8-Yb**; luminescence decay profiles for **8-Yb**; and details for the determination of τ_{rad} in **8-Yb** (PDF)

■ AUTHOR INFORMATION

Corresponding Authors

*E-mail: andrey.turshatov@kit.edu.

*E-mail: michael.seitz@uni-tuebingen.de.

ORCID

Bryce S. Richards: 0000-0001-5469-048X

Andrey Turshatov: 0000-0002-8004-098X

Michael Seitz: 0000-0002-9313-2779

Notes

The authors declare no competing financial interest.

■ ACKNOWLEDGMENTS

Financial support is gratefully acknowledged from DFG (Research Grants TU487/2-1 and SE1448/6-1) within the Priority Program SPP 1928: COORNET. P.N., B.S.R, and A.T. acknowledge the Helmholtz Energy Materials Foundry (HEMF).

■ REFERENCES

(1) (a) Bünzli, J.-C. G.; Eliseeva, S. V. Photophysics of Lanthanoid Coordination Compounds. In *Comprehensive Inorganic Chemistry II*; Reedijk, J., Poeppelmeier, K., Eds.; Elsevier: Amsterdam, 2013; Vol 8, pp 339−398. (b) Bünzli, J.-C. G.; Eliseeva, S. V. J. Lanthanide NIR luminescence for telecommunications, bioanalyses and solar energy conversion Rare Earths. *J. Rare Earths* **2010**, *28*, 824−842. (c) Comby, S.; Bünzli, J.-C. G. Lanthanide Near-Infrared Luminescence in Molecular Probes and Devices. In *Handbook on the Physics and Chemistry of Rare Earths*; Gschneidner, K. A., Jr.,

DOI: 10.1021/acs.inorgchem.9b00548
Inorg. Chem. 2019, 58, 6959−6965

Bünzli, J.-C. G., Pecharsky, V. K., Eds.; Elsevier: Amsterdam, 2007; Vol. 37, Chapter 235, pp 217−470. (d) Bünzli, C.-C. G On the design of highly luminescent lanthanide complexes. *Coord. Chem. Rev.* **2015**, *293*−*294*, 19−47.

(2) Kreidt, E.; Kruck, C.; Seitz, M. Nonradiative Deactivation of Lanthanoid Luminescence by Multiphonon Relaxation in Molecular Complexes. In *Handbook on the Physics and Chemistry of Rare Earths*; Bünzli, J.-C. G., Pecharsky, V. K., Eds.; Elsevier: Amsterdam, 2018; Vol *53*, Chapter 300, pp 35−79.

(3) (a) Browne, W. R.; Vos, J. G. The effect of deuteriation on the emission lifetime of inorganic compounds. *Coord. Chem. Rev.* **2001**, *219*−*221*, 761−787. (b) Yanagida, S.; Hasegawa, Y.; Murakoshi, K.; Wada, Y.; Nakashima, N.; Yamanaka, T. Strategies for enhancing photoluminescence of Nd^{3+} in liquid media. *Coord. Chem. Rev.* **1998**, *171*, 461−480. (c) Doffek, C.; Alzakhem, N.; Bischof, C.; Wahsner, J.; Güden-Silber, T.; Lügger, J.; Platas-Iglesias, C.; Seitz, M. Understanding the Quenching Effects of Aromatic C−H- and C−D-Oscillators in Near-IR Lanthanoid Luminescence. *J. Am. Chem. Soc.* **2012**, *134*, 16413−16423.

(4) Hernandez, I.; Gillin, W. P. Organic chromophores-based sensitization of NIR emitting lanthanides: toward highly efficient halogenated environments. In *Handbook on the Physics and Chemistry of Rare Earths*; Bünzli, J.-C. G., Pecharsky, V. K., Eds.; Elsevier: Amsterdam, 2015: Vol. *47*, Chapter 269, pp 1−100.

(5) Selected examples: (a) Hu, J.-Y.; Ning, Y.; Meng, Y.-S.; Zhang, J.; Wu, Z.-Y.; Gao, S.; Zhang, J.-L. Highly near-IR emissive ytterbium(III) complexes with unprecedented quantum yields. *Chem. Sci.* **2017**, *8*, 2702−2709. (b) Ning, Y.; Tang, J.; Liu, Y.-W.; Jing, J.; Sun, Y.; Zhang, J.-L. Highly luminescent, biocompatible ytterbium(III) complexes as near-infrared fluorophores for living cell imaging. *Chem. Sci.* **2018**, *9*, 3742−3753. (c) Doffek, C.; Alzakhem, N.; Molon, M.; Seitz, M. Rigid, Perdeuterated Lanthanoid Cryptates: Extraordinarily Bright Near-IR Luminophores. *Inorg. Chem.* **2012**, *51*, 4539−4545. (d) Doffek, C.; Seitz, M. The Radiative Lifetime in Near-IR Luminescent Ytterbium Cryptates - The Key to Extremely High Quantum Yields. *Angew. Chem., Int. Ed.* **2015**, *54*, 9719−9721. (e) Glover, P. B.; Bassett, A. P.; Nockemann, P.; Kariuki, B. M.; Van Deun, R.; Pikramenou, Z. Fully fluorinated imidodiphosphinate shells for visible- and NIR-emitting lanthanides: hitherto unexpected effects of sensitizer fluorination on lanthanide emission properties. *Chem. - Eur. J.* **2007**, *13*, 6308−6320. (f) Hernandez, I.; Zheng, Y.-X.; Motevalli, M.; Tan, R. H. C.; Gillin, W. P.; Wyatt, P. B. Efficient sensitized emission in Yb(III) pentachlorotropolonate complexes. *Chem. Commun.* **2013**, *49*, 1933−1935. (g) Foley, T. J.; Harrison, B. S.; Knefely, A. S.; Abboud, K. A.; Reynolds, J. R.; Schanze, K. S.; Boncella, J. M. Facile Preparation and Photophysics of Near-Infrared Luminescent Lanthanide(III) Monoporphyrinate Complexes. *Inorg. Chem.* **2003**, *42*, 5023−5032. (h) Zhang, T.; Zhu, X.; Cheng, C. C. W.; Kwok, W.-M.; Tam, H.-L.; Hao, J.; Kwong, D. W. J.; Wong, W.-K.; Wong, K.-L. Water-Soluble Mitochondria-Specific Ytterbium Complex withImpressive NIR Emission. *J. Am. Chem. Soc.* **2011**, *133*, 20120−20122.

(6) Charbonniere, L. J. Bringing upconversion down to the molecular scale. *Dalton Trans.* **2018**, *47*, 8566−8570.

(7) (a) Zhang, J.; Petoud, S. Azulene-Moiety-Based Ligand for the Efficient Sensitization of Four Near-Infrared Luminescent Lanthanide Cations: Nd^{3+}, Er^{3+}, Tm^{3+}, and Yb^{3+}. *Chem. - Eur. J.* **2008**, *14*, 1264−1272. (b) Wartenberg, N.; Raccurt, O.; Bourgeat-Lami, E.; Imbert, D.; Mazzanti, M. Multicolour Optical Coding from a Series of Luminescent Lanthanide Complexes with a Unique Antenna. *Chem. - Eur. J.* **2013**, *19*, 3477−3482. (c) Zhang, J.; Badger, P. D.; Geib, S. J.; Petoud, S. Sensitization of Near-Infrared-Emitting Lanthanide Cations in Solution by Tropolonate Ligands. *Angew. Chem., Int. Ed.* **2005**, *44*, 2508−2512. (d) Comby, S.; Imbert, D.; Chauvin, A.-S.; Bünzli, J.-C. G. Stable 8-Hydroxyquinolinate-Based Podates as Efficient Sensitizers of Lanthanide Near-Infrared Luminescence. *Inorg. Chem.* **2006**, *45*, 732. (e) Shavaleev, N. M.; Scopelliti, R.; Gumy, F.; Bünzli, J.-C. G. Surprisingly Bright Near-Infrared Luminescence and Short Radiative Lifetimes of Ytterbium in Hetero-Binuclear Yb−Na Chelates. *Inorg. Chem.* **2009**, *48*, 7937−7946.

(8) (a) Bünzli, J.-C. G.; Charbonniere, L. J.; Ziessel, R. F. Structural and photophysical properties of Ln^{III} complexes with 2,2'-bipyridine-6,6'-dicarboxylic acid: surprising formation of a H-bonded network of bimetallic entities. *J. Chem. Soc., Dalton Trans.* **2000**, 1917−1923. (b) Wahsner, J.; Seitz, M. Perdeuterated 2,2′-Bipyridine-6,6′-dicarboxylate: An Extremely Efficient Sensitizer for Thulium Luminescence in Solution. *Inorg. Chem.* **2013**, *52*, 13301−13303. (c) Doffek, C.; Wahsner, J.; Kreidt, E.; Seitz, M. Breakdown of the Energy Gap Law in Molecular Lanthanoid Luminescence: The Smallest Energy Gap Is Not Universally Relevant for Nonradiative Deactivation. *Inorg. Chem.* **2014**, *53*, 3263−3265. (d) Wahsner, J.; Seitz, M. Nonradiative Deactivation of Lanthanoid Excited States by Inner-Sphere Carboxylates. *Inorg. Chem.* **2015**, *54*, 10841−10848. (e) Li, Q.-W.; Liu, J.-L.; Jia, J.-H.; Leng, J.-D.; Lin, W.-Q.; Chen, Y.-C.; Tong, M.-L. Fluorescent single-ion magnets: molecular hybrid $(HNEt_3)[Dy_xYb_{1-x}(bpyda)_2]$ (x = 0.135−1). *Dalton Trans.* **2013**, *42*, 11262−11270. (f) Ren, Y.-L.; Wang, F.; Hu, H.-M.; Chang, Z.; Yang, M.-L.; Xue, G. Lanthanide coordination compounds with 2,2'-bipyridine-6,6'-dicarboxylate: Synthesis, crystal structure, luminescence and magnetic property. *Inorg. Chim. Acta* **2015**, *434*, 104−112. (g) Güden-Silber, T.; Klein, K.; Seitz, M. 4,4'-Bis(trifluoromethyl)-2,2'-bipyridine - a multipurpose ligand scaffold for lanthanoid-based luminescence/^{19}F NMR probes. *Dalton Trans.* **2013**, *42*, 13882−13888.

(9) Selected examples for coordination networks: (a) Kelly, N. R.; Goetz, S.; Batten, S. R.; Kruger, P. E. Coordination behaviour and network formation with 4,4',6,6'-tetracarboxy-2,2'-bipyridine and 4,4'-dicarboxy-2,2'-bipyridine ligands with rare and alkaline earth metals. *CrystEngComm* **2008**, *10*, 68−78. (b) Hu, M.; Wu, Z.; Yao, J.; Gu, X.; Su, H. Synthesis, structures and near-infrared luminescent properties of two novel temperature-dependant Er(III) coordination polymers based on 2,2'-bipyridine-3,3′,6,6'-tetracarboxylic acid. *Inorg. Chem. Commun.* **2013**, *36*, 31−34. (c) Ji, B.; Deng, D.; He, X.; Liu, B.; Miao, S.; Ma, N.; Wang, W.; Ji, L.; Liu, P.; Li, X. Syntheses, Structures, Luminescence, and Magnetic Properties of One-dimensional Lanthanide Coordination Polymers with a Rigid 2,2'-Bipyridine-3,3′,6,6'-tetracarboxylic Acid Ligand. *Inorg. Chem.* **2012**, *51*, 2170−2177.

(10) Newkome, G. R.; Puckett, W. E.; Kiefer, G. E.; Gupta, V. K.; Xia, Y.; Coreil, M.; Hackney, M. A. α-Methyl Functionalization of Electron-Poor Heterocycles: Chloromethyl Derivatives of 2,2'-Bipyridines. *J. Org. Chem.* **1982**, *47*, 4116−4120.

(11) Modified synthetic procedure adopted from the following: Mukkala, V.-M.; Kankare, J. J. New 2,2'-bipyridine derivatives and their luminescence properties with europium(II) and terbium(III) ions. *Helv. Chim. Acta* **1992**, *75*, 1578−1592.

(12) PM7: Stewart, J. J. P. Optimization of Parameters for Semiempirical Methods VI: More Modifications to the NDDO Approximations and Re-optimization of Parameters. *J. Mol. Model.* **2013**, *19*, 1−32.

(13) Dutra, J. D. L.; Filho, M. A. M.; Rocha, G. B.; Freire, R. O.; Simas, A. M.; Stewart, J. J. P. Sparkle/PM7 Lanthanide Parameters for the Modeling of Complexes and Materials. *J. Chem. Theory Comput.* **2013**, *9*, 3333−3341.

(14) Stewart, J. J. P. *MOPAC2016 (Version 17.173W)*; Stewart Computational Chemistry. Web: http://OpenMOPAC.net (last access: Jan 31, 2019).

(15) (a) Horrocks, W. D., Jr.; Bolender, J. P.; Smith, W. D.; Supkowski, R. M. Photosensitized Near Infrared Luminescence of Ytterbium(III) in Proteins and Complexes Occurs via an Internal Redox Process. *J. Am. Chem. Soc.* **1997**, *119*, 5972−5973. (b) Beeby, A.; Faulkner, S.; Williams, J. A. G. pH Dependence of the energy transfer mechanism in a phenanthridine-appended ytterbium complex. *J. Chem. Soc., Dalton Trans.* **2002**, 1918−1922.

(16) Unpublished results.

DOI: 10.1021/acs.inorgchem.9b00548
Inorg. Chem. 2019, 58, 6959−6965

(17) Werts, M. H. V.; Jukes, R. T. F.; Verhoeven, J. W. The emission spectrum and the radiative lifetime of Eu^{3+} in luminescent lanthanide complexes. *Phys. Chem. Chem. Phys.* **2002**, *4*, 1542−1548.
(18) Bünzli, J.-C. G.; Chauvin, A.-S.; Kim, H. K.; Deiters, E.; Eliseeva, S. V. Lanthanide luminescence efficiency in eight- and nine-coordinate complexes: Role of the radiative lifetime. *Coord. Chem. Rev.* **2010**, *254*, 2623.
(19) Aebischer, A.; Gumy, F.; Bünzli, J.-C. G. Intrinsic quantum yields and radiative lifetimes of lanthanide tris(dipicolinates). *Phys. Chem. Chem. Phys.* **2009**, *11*, 1346−1353.
(20) Würth, C.; Grabolle, M.; Pauli, J.; Spieles, M.; Resch-Genger, U. Relative and absolute determination of fluorescence quantum yields of transparent samples. *Nat. Protoc.* **2013**, *8*, 1535−1550.
(21) Brouwer, A. M. Standards for photoluminescence quantum yield measurements in solution. *Pure Appl. Chem.* **2011**, *83*, 2213−2228.

DOI: 10.1021/acs.inorgchem.9b00548
Inorg. Chem. 2019, 58, 6959−6965

Supporting Information

Efficient Ytterbium Near-Infrared Luminophore Based on a Nondeuterated Ligand

Christian Kruck, [†] Pariya Nazari, [‡] Carolin Dee,[†] Bryce S. Richards,[‡] Andrey Turshatov,[*,‡] and Michael Seitz[*,†]

[†] Institute of Inorganic Chemistry, University of Tübingen, Auf der Morgenstelle 18, 72076 Tübingen, Germany

[‡] Institute of Microstructure Technology, Karlsruhe Institute of Technology, Hermann-von-Helmholtz-Platz 1, 76344 Eggenstein-Leopoldshafen, Germany

Email: andrey.turshatov@kit.edu
michael.seitz@uni-tuebingen.de

Supporting Information

Table of Contents **Page**

1. ^{1}H NMR Spectra

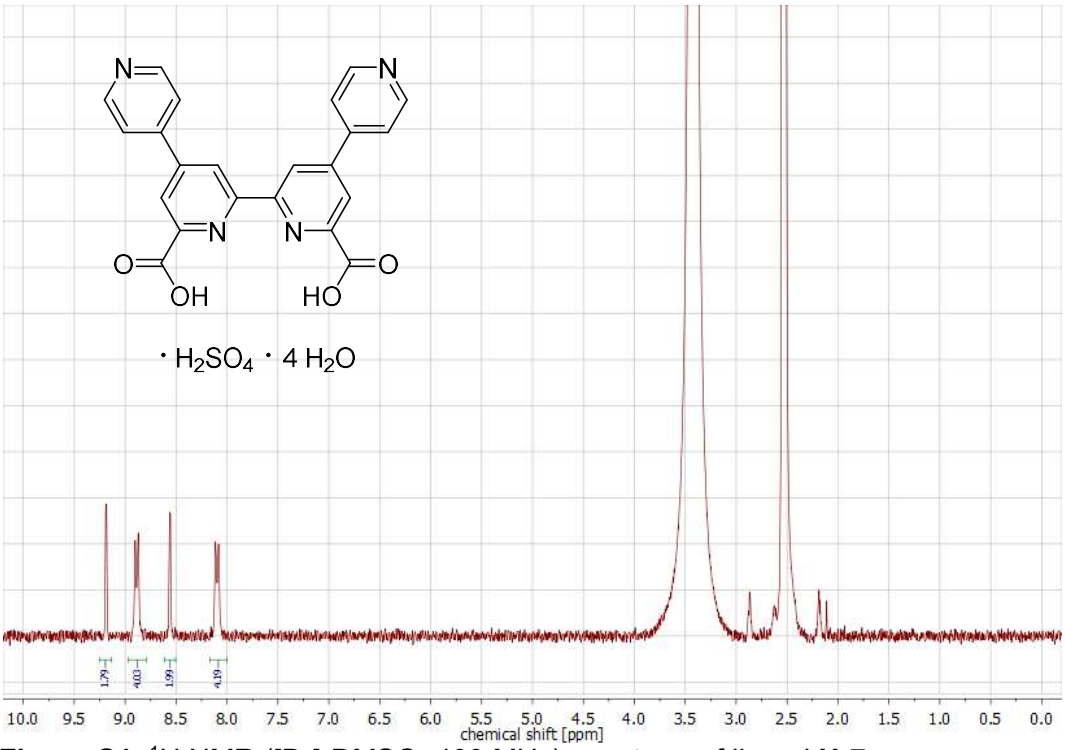

Figure S1. ^{1}H NMR ([D_6]-DMSO, 400 MHz) spectrum of ligand **$H_2$7**.

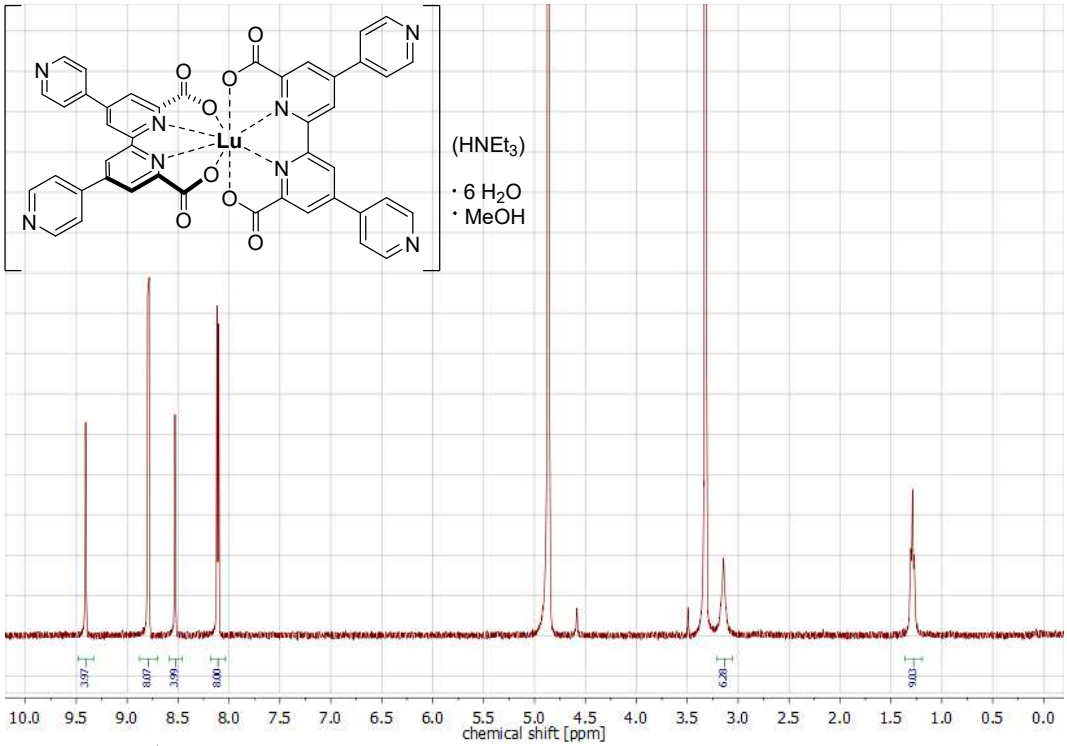

Figure S2. ^{1}H NMR (CD_3OD, 400 MHz) spectrum of lutetium complex **8-Lu**.

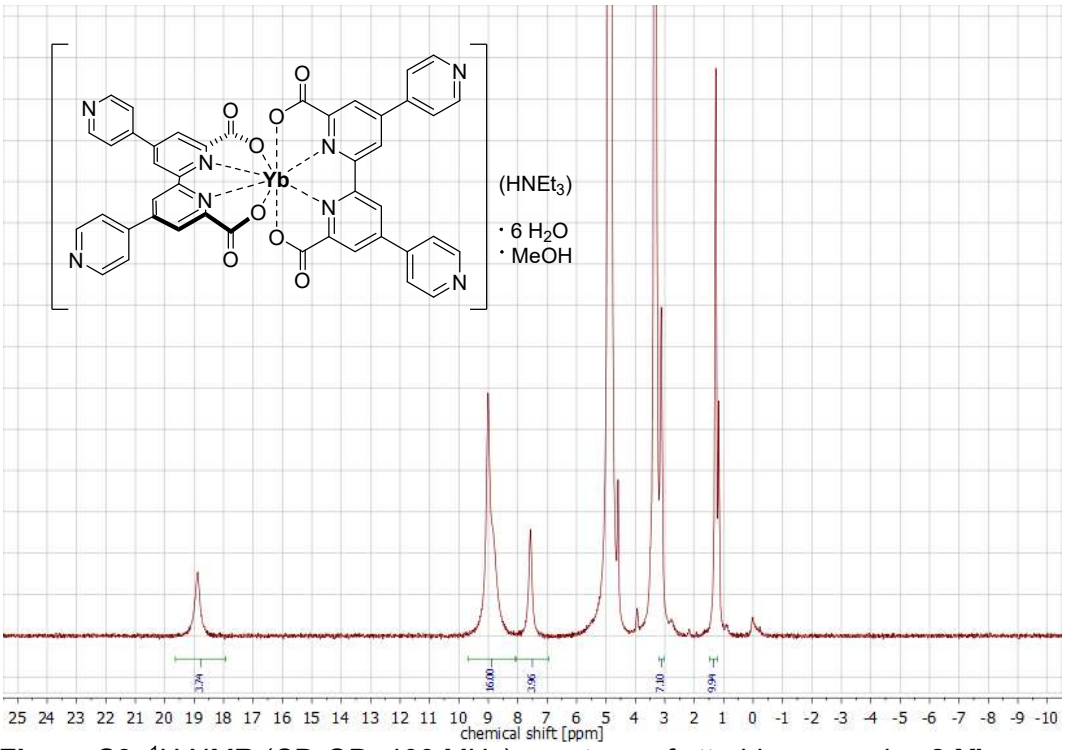

Figure S3. ^{1}H NMR (CD_3OD, 400 MHz) spectrum of ytterbium complex **8-Yb**.

2. Geometry Optimization of 8-Yb

The geometry optimization calculations were performed with the MOPAC 2016 package (version 17.173W)[1] using the semi-empirical PM7 method[2] with the SPARKLE extension for the ytterbium center.[3] The structures were optimized in Cartesian coordinates using the following keywords:

PM7 SPARKLE XYZ CHARGE=-1 GNORM=0.25 SCFCRT=1.D-10

The final cartesian coordinates in xyz format are as follows:

N	5.949200	8.333100	1.311900
N	4.333900	6.589800	2.458300
O	4.619100	9.543000	4.024600
N	7.785100	7.059100	5.322300
N	6.220000	9.123900	5.813700
C	7.126900	8.840200	6.814300
C	5.826700	8.985300	-1.447800
C	4.952100	8.041400	-0.899100
H	4.215700	7.556400	-1.535400
O	7.540900	9.315400	2.873600
C	7.982000	7.649300	6.554200
O	7.377900	6.063800	3.138000
O	3.596500	11.357800	4.944800
C	4.158300	6.727000	1.096300
C	4.384600	10.455400	4.893700
C	8.587900	5.977400	5.067800
O	3.096500	4.848300	5.297700
O	8.610900	10.686300	1.403300
C	5.043800	7.738600	0.456500
O	8.951200	4.420500	3.247800
C	8.322900	5.361600	3.646300
C	3.247400	5.976300	0.356700
H	3.154500	6.105900	-0.718400
C	5.473300	11.005300	7.196100
H	4.788200	11.849400	7.293200
C	6.414300	10.697700	8.169200
C	5.412800	10.204700	6.057700
C	3.509400	5.670700	3.055300
C	2.452700	5.029700	1.011300
O	4.707600	6.393700	4.855200
C	6.787400	9.244000	0.722300
C	9.524900	5.450400	5.953900
H	10.110600	4.578500	5.658500
C	9.671500	6.057800	7.193600
C	7.804300	9.868200	1.747100
C	8.892400	7.179100	7.496900
H	8.998200	7.661800	8.465300
C	7.251300	9.593100	7.978700
H	7.986400	9.337200	8.737900
C	6.766100	9.592900	-0.626200
H	7.477900	10.330600	-1.000800
C	3.749400	5.579000	4.606900
C	2.576300	4.882000	2.386400
H	1.974600	4.167600	2.951000
C	10.616700	5.539400	8.191400
C	11.896000	6.084900	8.305100
C	10.233300	4.502600	9.043700

C	12.753300	5.565100	9.282700
H	12.221400	6.891100	7.652100
C	11.156900	4.047900	9.992300
H	9.241900	4.059900	8.974800
N	12.393600	4.568300	10.112800
H	13.769100	5.951600	9.418100
H	10.913100	3.238300	10.688600
C	6.542700	11.512900	9.384500
C	5.697100	11.295000	10.472700
C	7.512100	12.514400	9.457300
C	5.848900	12.108000	11.603000
H	4.939000	10.515300	10.446100
C	7.589400	13.279900	10.626900
H	8.188900	12.700100	8.625800
N	6.773900	13.083400	11.681000
H	5.211500	11.987400	12.485200
H	8.323500	14.085100	10.738800
C	1.518200	4.199700	0.239000
C	0.220200	4.641800	-0.018600
C	1.927700	2.955400	-0.243500
C	-0.633700	3.804200	-0.747100
H	-0.123900	5.609600	0.337500
C	1.005800	2.186100	-0.963500
H	2.937000	2.590600	-0.064500
N	-0.252000	2.599200	-1.211300
H	-1.665200	4.094200	-0.972800
H	1.267200	1.199500	-1.361000
C	5.731000	9.318100	-2.875100
C	6.606400	8.743200	-3.796600
C	4.750300	10.206200	-3.320000
C	6.462500	9.082000	-5.147600
H	7.379300	8.047700	-3.476100
C	4.683600	10.489200	-4.689200
H	4.056200	10.668900	-2.621700
N	5.520300	9.937000	-5.588700
H	7.117900	8.660500	-5.917200
H	3.938100	11.180200	-5.097100
Yb	6.062700	7.818500	3.723600

3. Luminescence Decay Profiles

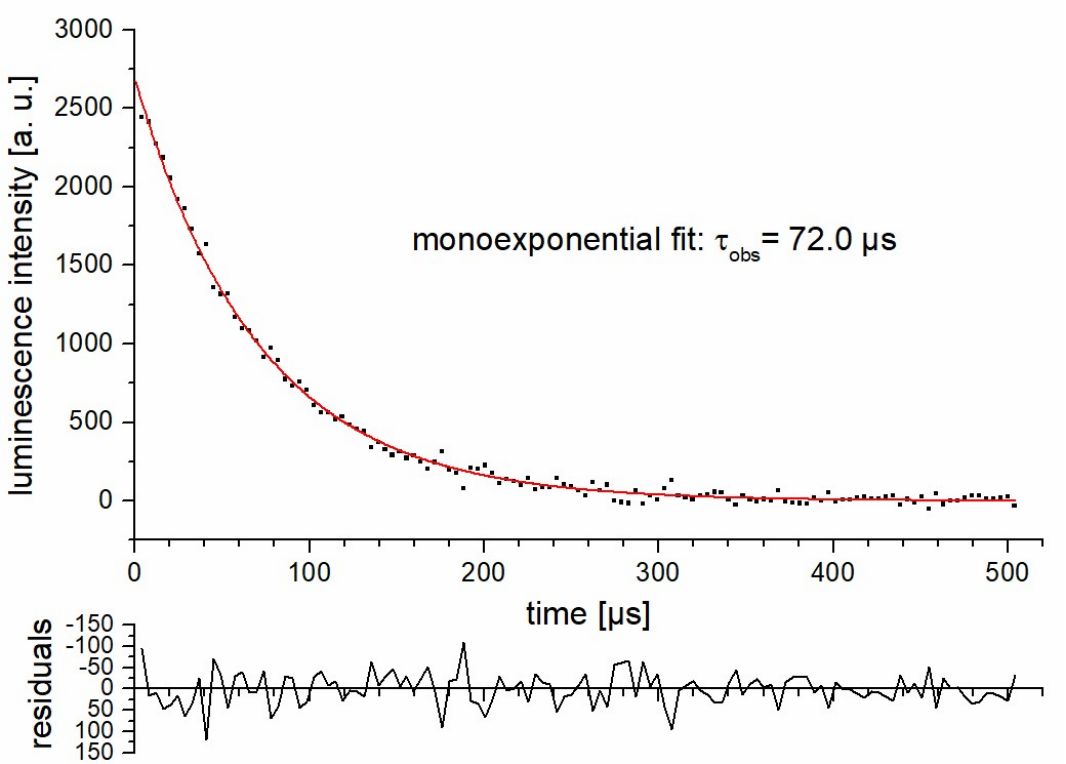

Figure S4. Luminescence decay profile of the transition $^2F_{5/2} \rightarrow {}^2F_{7/2}$ (λ_{em} = 1012 nm) in **8-Yb** (CD_3OD, λ_{exc} = 300 nm, monoexponential fit in red) at T = 298 K.

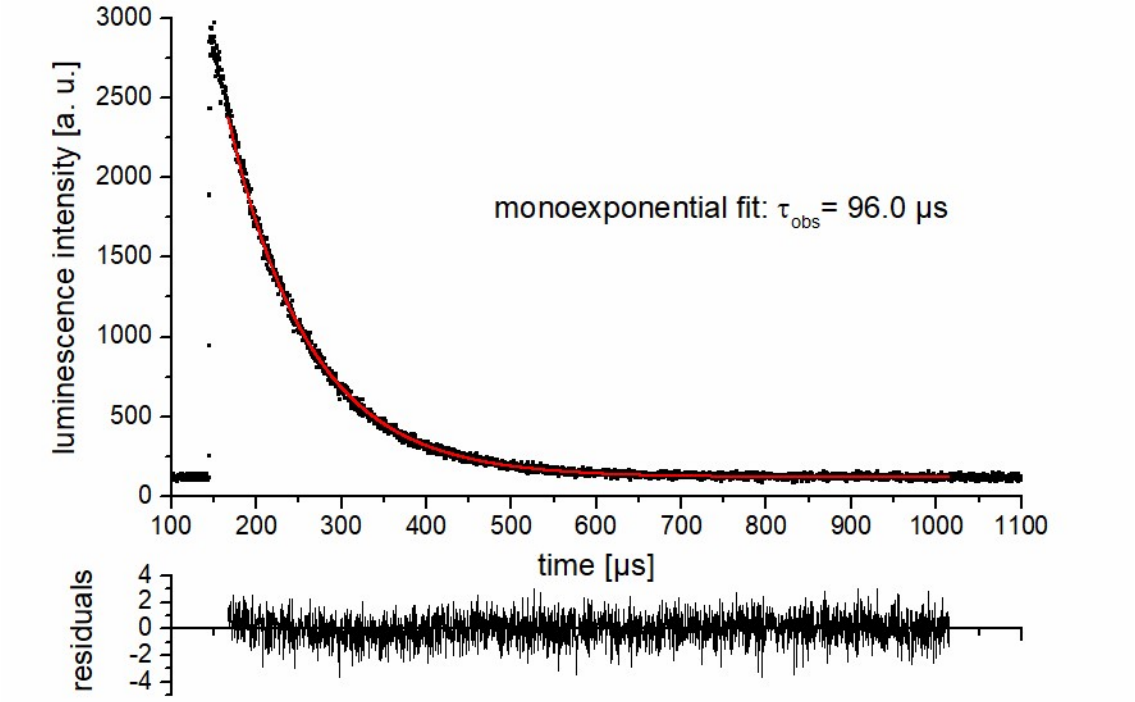

Figure S5. Luminescence decay profile of the transition $^2F_{5/2} \rightarrow {}^2F_{7/2}$ (λ_{em} = 1010 nm) in **8-Yb** (CD_3OD/C_2D_5OD 1:1 v/v, λ_{exc} = 300 nm, monoexponential fit in red) at 77 K.

4. Determination of τ_{rad} in 8-Yb

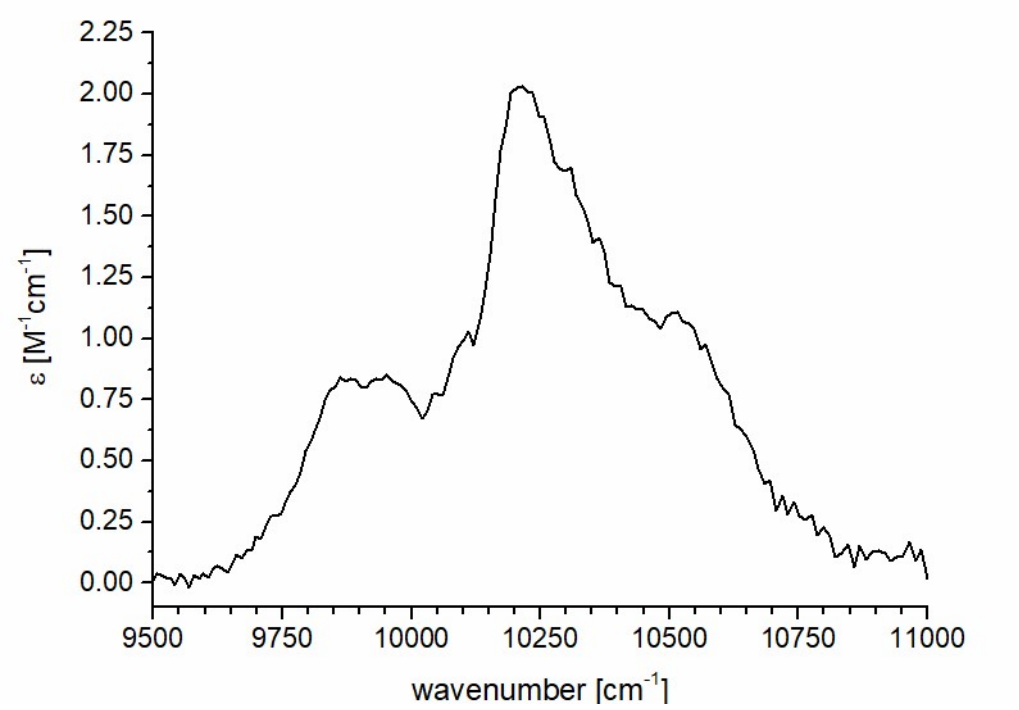

Figure S6. Quantitative absorption spectrum of the *f-f* transition $^2F_{7/2} \rightarrow {}^2F_{5/2}$ in **8-Yb** (c = 0.6 mM, path length d = 5 cm) in CD_3OD.

From the absorption spectrum (Figure S6), the radiative luminescence lifetime τ_{rad} of **8-Yb** was determined using the following equation:[4]

$$\frac{1}{\tau_{rad}} = 2303 \cdot \frac{8\pi c n^2 \cdot \tilde{\nu}_m{}^2}{N_A} \cdot \frac{(2J_l + 1)}{(2J_u + 1)} \cdot \int \varepsilon(\tilde{\nu}) d\tilde{\nu} \qquad \text{with } \tilde{\nu}_m = \frac{\int \tilde{\nu} \cdot \varepsilon(\tilde{\nu}) d\tilde{\nu}}{\int \varepsilon(\tilde{\nu}) d\tilde{\nu}}$$

with the following parameters and constants:

c	speed of light (in cm s^{-1}): c = 29979245800 cm s^{-1}
N_A	Avogardo's constant = 6.022 · 10^{23} mol^{-1}
n	refractive index (CD_3OD: n = 1.326)
$\tilde{\nu}_m$	barycenter of the transition ($^2F_{7/2} \rightarrow {}^2F_{5/2}$) as defined above
$2J_l+1$	degeneracy of the lower (ground) state (for Yb: J_l = 7/2)
$2J_u+1$	degeneracy of the upper (excited) state (for Yb: J_u = 5/2)
$\varepsilon(\tilde{\nu})$	molar extinction coefficient (in units of [$M^{-1}cm^{-1}$]) of the transition ($^2F_{7/2} \rightarrow {}^2F_{5/2}$) vs. the wavenumber $\tilde{\nu}$.

Integration of the absorption spectrum yielded the following:

$$\tilde{\nu}_m = \frac{\int \tilde{\nu} \cdot \varepsilon(\tilde{\nu}) d\tilde{\nu}}{\int \varepsilon(\tilde{\nu}) d\tilde{\nu}} = 10261 \text{ cm}^{-1} \quad \text{and} \quad \int \varepsilon(\tilde{\nu}) d\tilde{\nu} = 1077.77 \text{ M}^{-1} \text{ cm}^{-2}$$

Using all given data, the radiative lifetime for **8-Yb** evaluates to τ_{rad} = 1.3 ms.

5. References

1 MOPAC2016 (Version 17.173W), James J. P. Stewart, Stewart Computational Chemistry, Web: http://OpenMOPAC.net (last access: January 31, 2019).

2 PM7: Stewart, J. J. P.; Optimization of Parameters for Semiempirical Methods VI: More Modifications to the NDDO Approximations and Re-optimization of Parameters. *J. Mol. Mod.* **2013**, *19*, 1-32.

3 Dutra, J. D. L.; Filho, M. A. M.; Rocha, G. B.; Freire, R. O.; Simas, A. M.; Stewart, J. J. P.; Sparkle/PM7 Lanthanide Parameters for the Modeling of Complexes and Materials. *J. Chem. Theory Comput.* **2013**, *9*, 3333-3341.

4 Werts, M. H. V.; Jukes, R. T. F.; Verhoeven, J. W.; The emission spectrum and the radiative lifetime of Eu^{3+} in luminescent lanthanide complexes. *Phys. Chem. Chem. Phys.* **2002**, *4*, 1542-1548.

ChemComm

COMMUNICATION

View Article Online
View Journal | View Issue

Cite this: *Chem. Commun.*, 2019, **55**, 13078

Received 4th September 2019,
Accepted 7th October 2019

DOI: 10.1039/c9cc06909g

rsc.li/chemcomm

Strong circularly polarized luminescence of an octahedral chromium(III) complex†

Carolin Dee,[a] Francesco Zinna,[b] Winald R. Kitzmann,[c] Gennaro Pescitelli,[b] Katja Heinze,*[c] Lorenzo Di Bari*[b] and Michael Seitz*[a]

The chiral spin–flip luminophore $[Cr(ddpd)_2]^{3+}$ can be resolved into enantiopure material by chiral HPLC. The corresponding enantiomers show very high luminescence dissymmetry factors of up to $|g_{lum}| \approx 0.093$ in circularly polarized luminescence (CPL) measurements for the "ruby-like" phosphorescence transition $^2E/^2T_1 \rightarrow {}^4A_2$ in the near-IR region around $\lambda \approx 775$ nm.

The development of efficient luminophores capable of emitting "enantioenriched" light, *i.e.* the preferential emission of one form of either left- or right-circularly polarized luminescence (CPL), is a fascinating field in the photonic sciences due to many emerging applications (*e.g.* CPL bioanalytics, CP-OLEDs, *etc.*).[1,2] Naturally, the observation of CPL activity in isolated molecules is only possible for chiral, non-racemic compounds, ideally in enantiopure and configurationally stable systems. The extent of enantiomeric excess in the emitted, circularly polarized light is usually expressed as luminescence dissymmetry factor g_{lum} given as:

$$g_{lum}(\lambda) = 2\frac{I_L(\lambda) - I_R(\lambda)}{I_L(\lambda) + I_R(\lambda)}; \quad [-2 \leq g_{lum} \leq +2]$$

with I_L and I_R being the intensities of left- and right-circularly polarized light at a specific emission wavelength λ, respectively. For practical CPL applications, large values of g_{lum} are desirable, as well as high general photoluminescence quantum efficiencies Φ_{lum}, especially at the emissive transition chosen for CPL observation and sizeable molar extinction coefficients ε at the excitation wavelength λ_{exc}. High values of g_{lum} are especially expected for luminescence bands which are electric dipole forbidden and magnetic dipole allowed.[3] Therefore, while organic and most inorganic transition metal luminophores have a rich history in the photophysics of enantiopure compounds, the nature of the most prevalent luminescent transitions does not bode well for the achievement of high dissymmetry factors and typically, relatively small values of *ca.* $10^{-4} < g_{lum} < 10^{-2}$ are the norm.[1,4] On the other hand, the best candidates for the realization of sizeable g_{lum} factors are enantiopure complexes with trivalent lanthanoid cations where g_{lum} is routinely a few orders of magnitudes larger (*ca.* $10^{-2} < g_{lum} < 1$) than in other systems[2] and can reach values of up to 1.38 in solution.[5] Despite the suitability of lanthanoids for the development of efficient CPL emitters, it is highly desirable to have alternatives based on other, more abundant elements. In addition, the most prevalent CPL-active transitions of lanthanoids (mostly for Eu^{3+} and Tb^{3+}) do not cover various spectral ranges, for example the important near-IR wavelength region from approx. 700–900 nm. One of the most promising avenues for the development of alternative CPL-emitters is based on the photophysics of chromium(III) complexes, best known for the optical properties (*e.g.* color, luminescence) of ruby. Especially the phosphorescent, spin–flip-transitions analogous to the R1- and R2-ruby laser lines ($^2E/^2T_1 \rightarrow {}^4A_2$) have many properties that are reminiscent of the best CPL-active lanthanoid transitions (excited and ground states in the weak coupling limit, strongly electric-dipole forbidden, magnetically allowed).[6] Despite encouraging proof-of-concept CPL studies in the solid state and at low-temperature, previous work on Cr^{3+}–CPL starting as early as 1967 was hampered by the fact that generally, molecular chromium(III) complexes only showed very low quantum efficiencies at room temperature in solution and the potential for realistic CPL-applications was therefore rather low.[7] This situation has changed recently with the development of the molecular ruby $[Cr(ddpd)_2]^{3+}$ (Fig. 1)[8] which has extraordinarily high phosphorescence quantum yields Φ of up to 30% in deoxygenated solutions at room temperature, especially

[a] *Institute of Inorganic Chemistry, University of Tübingen, Auf der Morgenstelle 18, 72076 Tübingen, Germany. E-mail: michael.seitz@uni-tuebingen.de*
[b] *Dipartimento di Chimica e Chimica Industriale, Università di Pisa, Via Moruzzi 13, 56124 Pisa, Italy. E-mail: lorenzo.dibari@unipi.it*
[c] *Institute of Inorganic Chemistry and Analytical Chemistry, Johannes Gutenberg University of Mainz, Duesbergweg 10-14, 55128 Mainz, Germany. E-mail: katja.heinze@uni-mainz.de*

† Electronic supplementary information (ESI) available: Details of the chiral resolution, configurational stability, assignment of absolute configurations, CD spectroscopy, computational estimation of the racemization barriers. See DOI: 10.1039/c9cc06909g

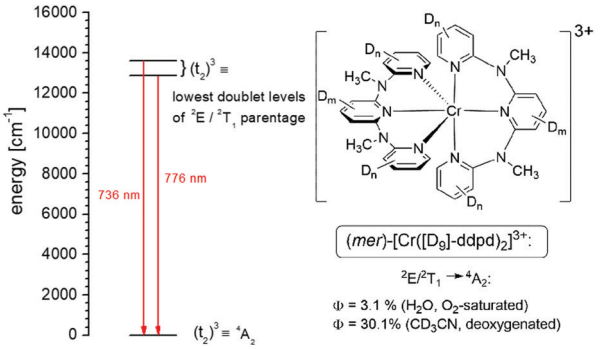

Fig. 1 Energy level diagram for the metal-centered states in the chromium complex $[Cr(ddpd)_2]^{3+}$ showing the "ruby-like" spin–flip emission $^2E/^2T_1 \rightarrow {}^4A_2$ with very favorable general luminescence properties such as high quantum yields Φ, especially in the deuterated version shown.[8]

after reducing multiphonon quenching through deuteration of the ligands and the solvent (see Fig. 1). In a seminal work in the area of CPL luminophores, Piguet *et al.*[9] could show recently that a similar, enantiopure chromium(III) complex is indeed capable of combining sizeable general phosphorescence quantum yields (Φ = 5.2% in deoxygenated H_2O at room temperature) with unprecedentedly high values for the luminescence dissymmetry factors of up to $|g_{lum}| = 0.2$. In this communication, we show that the successful luminophore $[Cr(ddpd)_2]^{3+}$, which previously was employed in its racemic form, can also be resolved into enantiopure material and that the enantiomers exhibit very high g_{lum} values for a 3d-metal complex.

Despite its simplified depiction in Fig. 1, the complex $[Cr(ddpd)_2]^{3+}$ is not achiral with D_{2d} symmetry as would be expected for a homoleptic, meridionally coordinated metal center with planar tridentate chelators such as tpy (= 2,2′:6′,2″-terpyridine). Instead, the previously determined structure of racemic material in the solid state[8b] shows strongly twisted ddpd ligands with homochiral helicities (*M*,*M* or *P*,*P*), which effectively lowers the local symmetry to D_2, making the complex chiral (Scheme 1). Since the chirality of the complexes only relies on the conformations of the rather flexible ddpd ligands, it was not clear at the outset if these presumably rather "soft" stereogenic elements would be suitable to

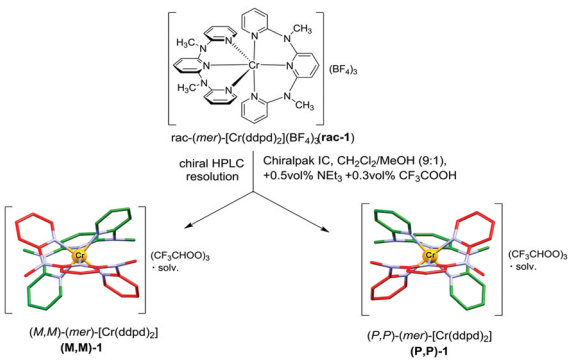

Scheme 1 Chiral resolution of the racemic, meridional chromium(III) complex $[Cr(ddpd)_2]^{3+}$ into the (*M*,*M*)- and (*P*,*P*)-enantiomers (schematic representations, red and green colors used for carbon atoms in different ddpd units in order to clarify the helicity of each ligand).

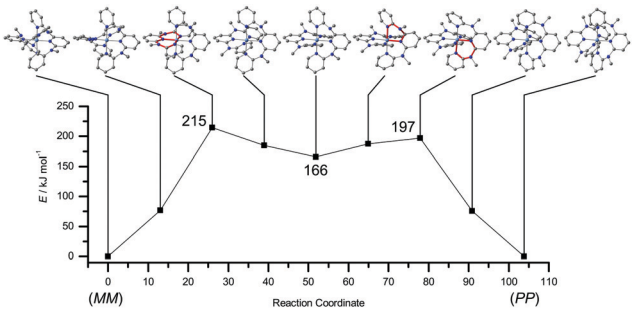

Fig. 2 DFT calculations of the trajectory for the stepwise racemization of six-coordinate $[Cr(ddpd)_2]^{3+}$ (hydrogen atoms omitted; inverting chelate rings marked in red; see the ESI,† for details).

endow the complex with enough configurational stability in order to be able to obtain pure enantiomers and to prevent their rapid racemization once resolved.

In order to evaluate this question, we performed DFT calculations along possible racemization trajectories (Fig. 2, see ESI,† for details). The highest energy species along a trajectory with all N donors remaining coordinated was calculated at 215 kJ mol^{-1} higher in energy than the ground state (D_2-symmetric enantiomers). These results suggest that racemization of **(M,M)-1** or **(P,P)-1** without a change in coordination number is rather unlikely and a dissociative or associative pathway might be followed instead (if racemization occurs at all). Pathways with 5- or 7-coordinate intermediates $[Cr(ddpd)(k^2N\text{-}ddpd)]^{3+}$ or $[Cr(ddpd)_2(H_2O)]^{3+}$ are either high in energy (calculated free dissociation enthalpy of 132 kJ mol^{-1}) or inaccessible (H_2O coordination to Cr proved unfeasible). This suggests considerable configurational stability of $[Cr(ddpd)_2]^{3+}$. The practical resolution of the two enantiomers proved to be surprisingly difficult and to date we were only successful by employing chiral HPLC using highly optimized conditions (see ESI,† for details). The racemic material **rac-1** clearly shows two peaks with a peak area ratio very close to 50 : 50 (Fig. 3A) which, despite considerable efforts, could not be baseline-separated completely. For separations on a larger scale necessary for the spectroscopic work, it proved impossible to cleanly obtain the first fraction without contamination by the second fraction and consequently gave only an enantiomeric excess of 80%. In contrast, sampling only the middle and tail portions of the second fraction provided enantiopure material (100% ee). Nevertheless, CD spectra of both fractions in deoxygenated D_2O showed a mirror-image pattern indicative of their enantiomeric relationship (see Fig. S2 in the ESI†).

The counterions for the tricationic chromium complex enantiomers after chiral HPLC resolution were assumed to be trifluoroacetates due to the large excess of the trifluoroacetic acid additive used in the HPLC eluents. ^{19}F NMR spectra of the compounds confirmed this by showing resonances around *ca.* −78 ppm, which can unambiguously be assigned to free trifluoroacetate (see ESI†).[10] The configurational stability under the experimental conditions was assessed by stirring enantiopure material in H_2O at room temperature. The enantiopurity of the dissolved complex was monitored over 48 h by taking samples at certain intervals and determining the enantiomeric

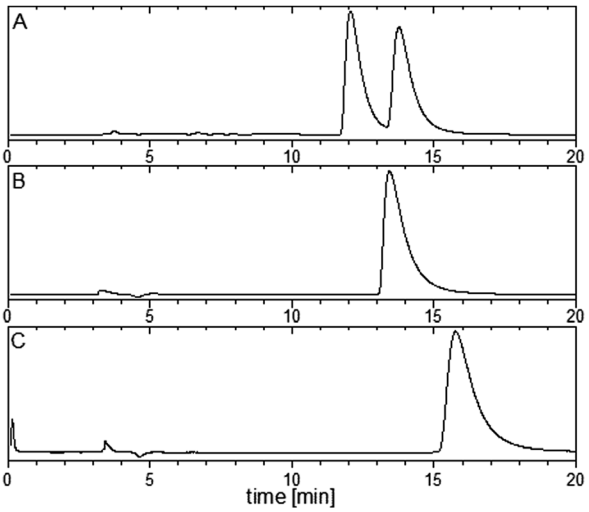

Fig. 3 Chiral HPLC traces (Chiralpak IC, CH_2Cl_2/MeOH/NEt_3/CF_3COOH 90 : 10 : 0.3 : 0.5, UV detection at 300 nm) for the preparative resolution of **rac-1** (A) and the corresponding analytical runs after the separation (B: **(P,P)-1** and C: **(M,M)-1**; see text for assignment of the configurations).

excess by chiral HPLC. Over the course of this timeframe, no deterioration of the enantiomeric excess through racemization was detectable. Similarly, enantiomerically resolved material was configurationally stable in the solid state over extended periods (several weeks) of storage at room temperature. The absolute configuration of the resolved enantiomers **(M,M)-1** and **(P,P)-1** was elucidated *via* computational methods (TD-DFT, CASSCF(7,12)-NEVPT2[11]) by calculating the CD spectrum of **(M,M)-1** (see ESI† for details). The good agreement of the TD-DFT derived spectral shape in the region of the ligand-centered UV-transitions (*ca.* $\lambda < 350$ nm) with the experimental CD spectrum of the second HPLC fraction permits the assignment of the first HPLC fraction as **(P,P)-1** and the second as **(M,M)-1** (see Fig. 3). The metal centered transitions >400 nm display an overall positive rotatory strength according to CASSCF-NEVPT calculations on **(M,M)-1** confirming the assignment based on TD-DFT (see ESI†). Finally, the CPL properties

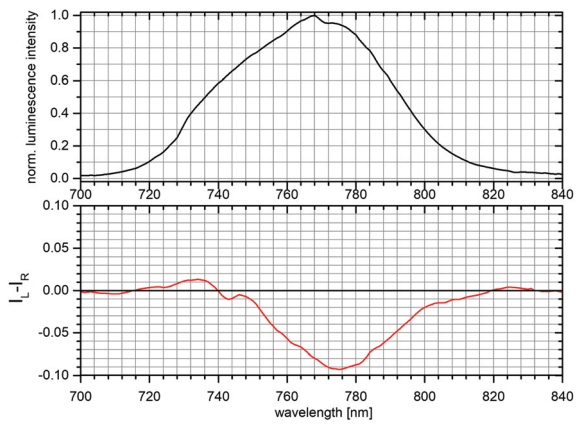

Fig. 4 Steady-state emission (top, black) and CPL spectra (bottom, red) of the near-IR luminescence band $^2E/^2T_1 \rightarrow {}^4A_2$ of **(M,M)-1** in solution at room temperature (deoxygenated D_2O, c = 10 μM, λ_{exc} = 365 nm).

of the phosphorescent near-IR emission bands ($\lambda_{em} \approx$ 738/775 nm) were measured for the enantiopure complex **(M,M)-1** in deoxygenated D_2O (see Fig. 4 and Fig. S3 in the ESI†). The CPL measurement confirmed a large maximum value for $g_{lum} = -0.093$ at 775 nm (and a positive g_{lum} for the weaker high-energy transition), which is less than the value recently obtained by Piguet[9] ($|g_{lum}| < 0.2$) but which still represents a very large dissymmetry factor for a 3d-metal complex and which is on a par with many lanthanoid-based CPL emitters.[2] Together with the superior general luminescence properties of $[Cr(ddpd)_2]^{3+}$ (*e.g.* phosphorescence quantum yields up to 30% in solution) and high stability (configurational, thermal, photochemical), its resolved enantiomers are excellent candidates for the development of very efficient NIR-CPL luminophores based on the earth-abundant and cheap element chromium. Moreover, thanks to their ruby-like emission, optically active chromium(III) compounds could be advantageously used in the field of chiral optoelectronics and photonics.

Financial support from the German Research Foundation (DFG, Priority Program SPP 2102 ''Light-controlled reactivity of metal complexes'', grant no. HE 2778/15-1, SE 1448/8-1) is gratefully acknowledged. Parts of this research were conducted using the supercomputer Mogon and advisory services offered by Johannes Gutenberg University of Mainz (https://hpc.uni-mainz.de), which is a member of the AHRP and the Gauss Alliance.

Conflicts of interest

There are no conflicts to declare.

Notes and references

1 (*a*) J. P. Riehl and G. Muller in *Comprehensive Chiroptical Spectroscopy*, ed. N. Berova, P. L. Polavarapu, K. Nakanishi, R. W. Woody, John Wiley & Sons, Hoboken, 2012, vol. 1, p. 65; (*b*) J. Kumar, T. Naashima and T. Kawai, *J. Phys. Chem. Lett.*, 2015, **6**, 3445; (*c*) H. Tanaka, Y. Inoue and T. Mori, *ChemPhotoChem*, 2018, **2**, 386; (*d*) G. Longhi, E. Castiglioni, J. Koshoubu, G. Mazzeo and S. Abbate, *Chirality*, 2016, **28**, 696; (*e*) J. P. Riehl and F. S. Richardson, *Chem. Rev.*, 1986, **86**, 1.
2 (*a*) F. Zinna and L. Di Bari, *Chirality*, 2015, **27**, 1; (*b*) G. Muller in *Luminescence of Lanthanide Ions in Coordination Compounds and Nanomaterials*, ed. A. de Bettencourt-Dias, John Wiley & Sons, Hoboken, 2014, p. 77; (*c*) R. Carr, N. H. Evans and D. Parker, *Chem. Soc. Rev.*, 2012, **41**, 7673; (*d*) F. Zinna, U. Giovanella and L. Di Bari, *Adv. Mater.*, 2015, **27**, 1791; (*e*) J. R. Brandt, X. Wang, Y. Yang, A. J. Campbell and M. J. Fuchter, *J. Am. Chem. Soc.*, 2016, **138**, 9743; (*f*) F. Zinna, M. Pasini, F. Galeotti, C. Botta, L. Di Bari and U. Giovanella, *Adv. Funct. Mater.*, 2017, **27**, 1603719.
3 F. S. Richardson, *Inorg. Chem.*, 1980, **19**, 2806.
4 (*a*) J. OuYang and J. Crassous, *Coord. Chem. Rev.*, 2018, **376**, 533; (*b*) J. Kumar, T. Nakashima and T. Kawai, *J. Phys. Chem. Lett.*, 2015, **6**, 3445; (*c*) E. M. Sanchez-Carnerero, A. R. Agarrabeitia, F. Moreno, B. L. Maroto, G. Muller, M. J. Ortiz and S. de la Moya, *Chem. – Eur. J.*, 2015, **21**, 13488.
5 (*a*) J. L. Lunkley, D. Shirotani, K. Yamanari, S. Kaizaki and G. Muller, *J. Am. Chem. Soc.*, 2008, **130**, 13814; (*b*) J. L. Lunkley, D. Shirotani, K. Yamanari, S. Kaizaki and G. Muller, *Inorg. Chem.*, 2011, **50**, 12724; (*c*) S. Di Pietro and L. Di Bari, *Inorg. Chem.*, 2012, **51**, 12007.
6 (*a*) L. A. Büldt and O. S. Wenger, *Chem. Sci.*, 2017, **8**, 7359; (*b*) D. Zare, B. Doistau, H. Nozary, C. Besnard, L. Guénée, Y. Suffren, A.-L. Pelé, A. Hauser and C. Piguet, *Dalton Trans.*, 2017, **46**, 8992; (*c*) P. S. Wagenknecht and P. C. Ford, *Coord. Chem. Rev.*, 2011, **255**, 591; (*d*) S. Otto, M. Dorn, C. Förster, M. Bauer, M. Seitz and K. Heinze, *Coord. Chem. Rev.*, 2018, **359**, 102.

7 (*a*) G. L. Hilmes, H. G. Brittain and F. S. Richardson, *Inorg. Chem.*, 1977, **16**, 528; (*b*) T. Tsubomura, M. Morita and I. Ohkouchi, *J. Lumin.*, 1988, **40–41**, 268; (*c*) M. Morita, K. Eguchi, M. Shishikura, H. Nishikawa and M. Inoue, *J. Lumin.*, 1984, **31–32**, 558; (*d*) T. Tsubomura, I. Ohkouchi and M. Morita, *Bull. Chem. Soc. Jpn.*, 1991, **64**, 2341; (*e*) R. D. Peacock and B. Stewart, *J. Chem. Soc., Chem. Commun.*, 1982, 295; (*f*) C. Emeis and L. Oosterhoff, *Chem. Phys. Lett.*, 1967, **1**, 129.

8 (*a*) C. Wang, S. Otto, M. Dorn, E. Kreidt, J. Lebon, L. Srsan, P. Di Martino-Fumo, M. Gerhards, U. Resch-Genger, M. Seitz and K. Heinze, *Angew. Chem., Int. Ed.*, 2018, **57**, 1112; (*b*) S. Otto, M. Grabolle, C. Förster, C. Kreitner, U. Resch-Genger and K. Heinze, *Angew. Chem., Int. Ed.*, 2015, **54**, 11572.

9 J.-R. Jiménez, B. Doistau, C. M. Cruz, C. Besnard, J. M. Cuerva, A. G. Campaña and C. Piguet, *J. Am. Chem. Soc.*, 2019, **141**, 13244.

10 J. W. Emsley and L. Phillips, *Prog. Nucl. Magn. Reson. Spectrosc.*, 1971, **7**, 1.

11 S. Otto, J. Harris, K. Heinze and C. Reber, *Angew. Chem., Int. Ed.*, 2018, **57**, 11069.

Electronic Supplementary Material (ESI) for ChemComm.

Strong Circularly Polarized Luminescence of an Octahedral Chromium(III) Complex

Carolin Dee,[a] Francesco Zinna,[b] Winald R. Kitzmann,[c] Gennaro Pescitelli,[b] Katja Heinze,*[c] Lorenzo Di Bari*[b] and Michael Seitz*[a]

[a] Institute of Inorganic Chemistry, University of Tübingen, Auf der Morgenstelle 18, 72076 Tübingen, Germany
[b] Dipartimento di Chimica e Chimica Industriale, Università di Pisa, Via Moruzzi 13, 56124 Pisa, Italy.
[c] Institute of Inorganic Chemistry and Analytical Chemistry, Johannes Gutenberg University of Mainz, Duesbergweg 10-14, 55128 Mainz, Germany
Email: katja.heinze@uni-mainz.de, lorenzo.dibari@unipi.it, michael.seitz@uni-tuebingen.de

Supplementary Information

Table of Contents

1. Materials and Methods

NMR spectra were recorded on a Bruker AVII+400 spectrometer (^{1}H: 400 MHz, ^{19}F: 377 MHz) using CD_3OD (≥ 99.8% D) as the solvent. The racemic Cr complex $[Cr(ddpd)_2](BF_4)_3$ was synthesized as described previously.[1] NMR-grade D_2O (>99.8%D) was used for the photophysical measurements.

2. Chiral HPLC / Configurational Stability Test

All chiral HPLC runs of the $[Cr(ddpd)_2](X)_3$ complexes (**rac-1** or enantioenriched samples) were performed on a Knauer Azura HPLC system (UV detection at λ = 300 nm), equipped with a CHIRALPAK IC column (Daicel, particle size: 5 µm, internal diameter: 4.6 mm, column length: 250 mm) using CH_2Cl_2/MeOH (90:10) with additional 0.5 vol.-% NEt_3 and 0.3 vol.-% CF_3COOH as mobile phase with a flow of 1.0 mL/min. All samples were filtered through a membrane filter (nylon, 0.45 µm pore size, 13 mm diameter) in a stainless steel filter holder prior to injection.

Racemic $[Cr(ddpd)_2](BF_4)_3$ (6.0 mg) was dissolved in CH_2Cl_2/MeOH (90:10, v/v, 5.5 mL) and filtered through a membrane filter (vide infra). The filter was washed with additional 0.5 mL of the solvent mixture, to yield a concentration of ca. 1 mg/mL. The solution was subjected to chiral HPLC in portions of 100 µL. The collected fractions of the respective enantiomers were combined and the solvents were removed in vacuo at room temperature. After drying in vacuo, samples of the enantiomers were redissolved in the HPLC solvent mixture, filtered, and injected to verify the enantiopurity. After the HPLC purification, the enantiopure complexes contain additional triethylammonium trifluoroacetate ($HNEt_3CF_3COO$). This raw material was washed repeatedly with CH_2Cl_2 which slowly removes the slightly soluble impurity triethylammonium trifluoroacetate. This procedure yields material with only a minimum presence of the salt.

The counterions after chiral HPLC resolution was confirmed to be trifluoroacetate by mass spectrometry (ESI-MS, neg. mode: m/z(%) = 113.11 {31%, $[CF_3COO]^-$}, 226.96 {100%, $[2CF_3COO + H]^-$}) and by ^{19}F NMR spectroscopy[2] (Figure S1):

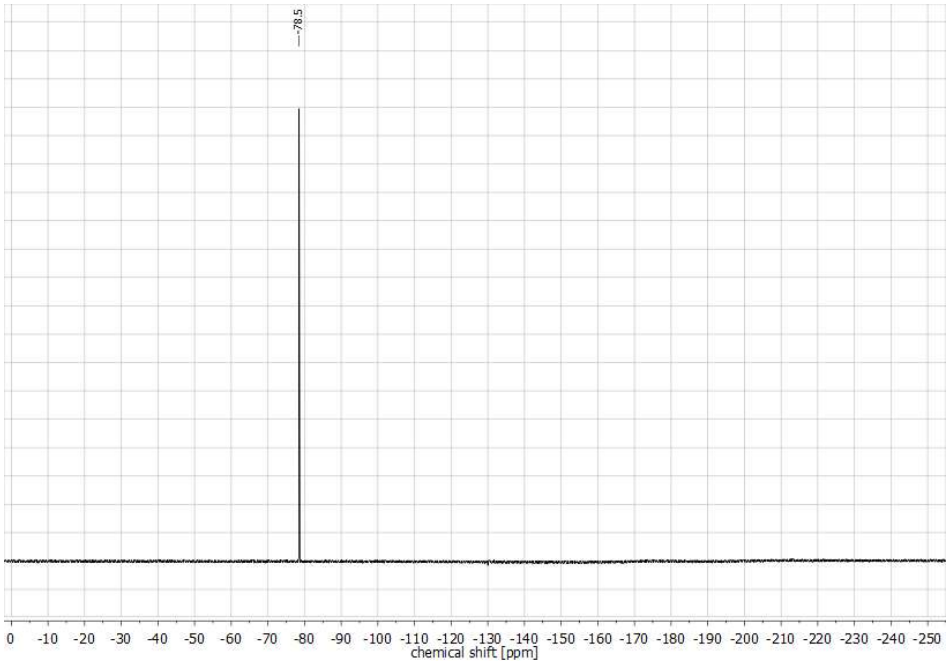

Figure S1. ^{19}F NMR spectrum (377 MHz, CD_3OD) of **(*M,M*)-1**.

Configurational stability test in solution

An enantiomerically pure sample of **(*M,M*)-1** (0.3 mg) was stirred at room temperature in H_2O (1.0 mL, HPLC grade). During the course of 48 h, samples of 100 µl were taken at certain intervals (1h, 3h, 24 h, 48 h). These samples were immediately concentrated under a stream of air and the residues were taken up in CH_2Cl_2/MeOH (90:10, 100 µL). The solutions were filtered through a membrane filter (nylon, 0.45 µm pore size), the filter was washed with additional solvent mixture (100 µL), and the combined filtrates were concentrated. For chiral HPLC analysis, the dry samples were redissolved in CH_2Cl_2/MeOH (90:10, 100 µL) directly before the run.

3. ECD and CPL measurements

The ECD spectra (Figure S2) were recorded with a Jasco J-715 spectropolarimeter (4 accumulations) on 10 µM solutions in deoxygenated D_2O. CPL spectra were measured with a home-made spectrofluoropolarimeter[3] in the configuration described before.[4] The spectra were acquired on 10 µM solutions in deoxygenated D_2O under 365 nm irradiation, with 4 sec integration time and 4 accumulations. The spectra were baseline corrected by subtracting the trace of the solvent.

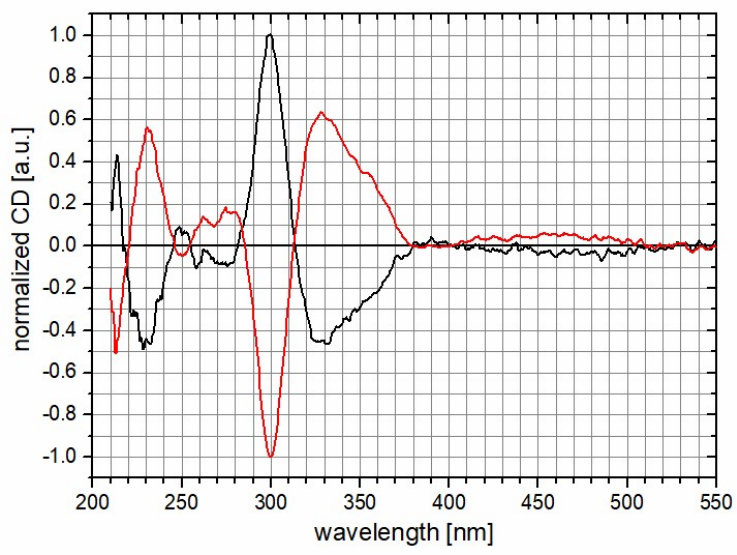

Figure S2. Normalized CD spectra (deoxygenated D_2O, c = 10 µM) of the first chiral HPLC fraction (black) and the second fraction (red) – Mirror-image relationship indicating the enantiomeric nature of both fractions.

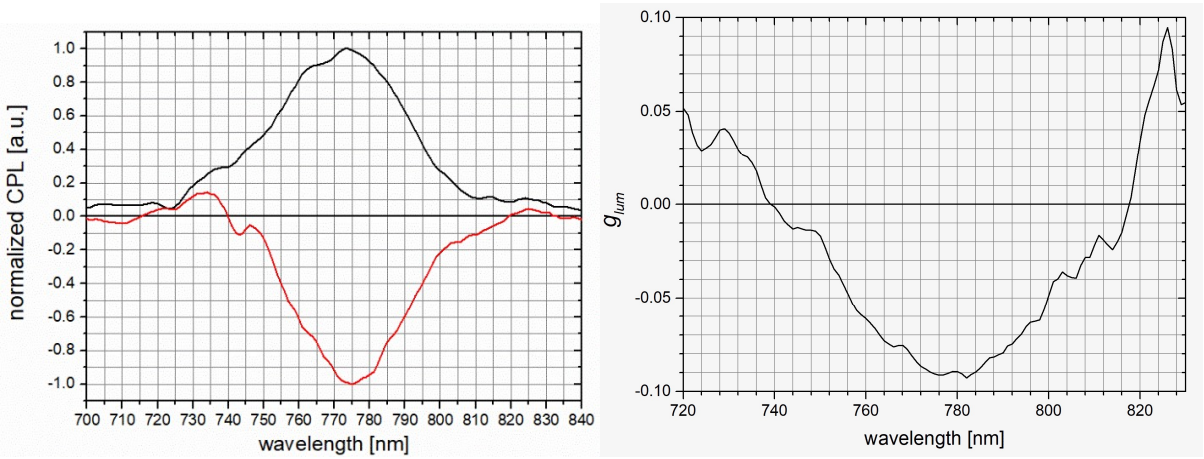

Figure S3. Left: Normalized CPL spectra (deoxygenated D_2O, c = 10 µM) of the first chiral HPLC fraction (black) and the second fraction (red) – Right: Plot of g_{lum} vs. the wavelength for (***M,M*-1**).

4. Calculation of the Energy Barriers for Racemization Pathways

Racemization of (*M,M*)- or (*P,P*)-$[Cr(ddpd)_2]^{3+}$ can occur without changing the coordination number via inverting the boat conformations of the four six-membered chelate rings. Using DFT optimizations with constrained dihedral angles in the chelate rings, geometries of $[Cr(ddpd)_2]^{3+}$ with one half-chair, one flattened ring and with fully flattened ligands were optimized with free enthalpy differences of 31, 141 and 337 kJ/mol, respectively. These numbers show that the planarization of only one chelate ring is very unfavorable (Figure S4). Since completely flattened ligands might be avoided in the actual mechanism, a reaction path from (*M,M*)- to (*P,P*)-$[Cr(ddpd)_2]^{3+}$ was calculated using the nudged elastic band (NEB) method. The NEB method indeed favors a stepwise minimum energy path (Figure 2 in the manuscript). The inversion of both chelate rings of the first ligand is followed by the planarization and subsequent inversion of the first chelate ring on the second ddpd ligand. Finally, the last six-membered chelate-ring inverts.

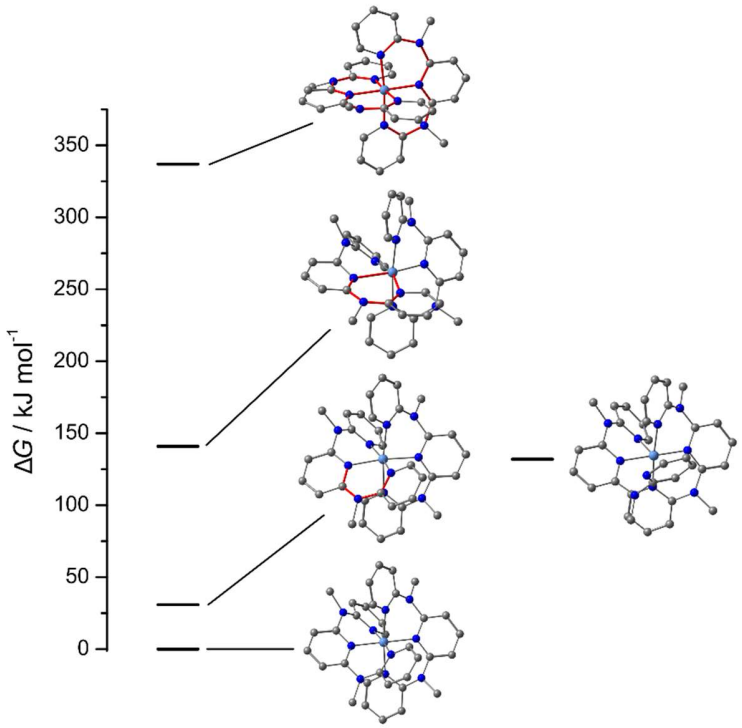

Figure S4. Optimized geometries of $[Cr(ddpd)_2]^{3+}$ with constrained chelate rings indicated in red (left) and of $[Cr(ddpd)(\kappa^2N\text{-ddpd})]^{3+}$ (right).

To investigate a conceivable dissociative pathway, the geometry of $[Cr(ddpd)(\kappa^2N\text{-ddpd})]^{3+}$ was optimized using DFT (Figure S4, right). This yielded a free enthalpy difference of 132 kJ/mol. It

was not possible to obtain the optimized geometry of 7-coordinate $[Cr(ddpd)_2(H_2O)]^{3+}$. Instead, the calculation yielded 6-coordinate $[Cr(ddpd)(k^2N\text{-}ddpd)(H_2O)]^{3+}$ with the dissociated pyridyl residue forming a hydrogen bond with the water ligand.

DFT calculations were carried out using the ORCA program package (version 4.1.1)[5] using the B3LYP functional.[6-8] Tight convergence criteria were chosen for geometry optimizations and frequency calculations (Keywords TightSCF and TightOpt, convergence criteria for the SCF part: energy change 1.0×10^{-8} E_h, 1-El. energy change 1.0×10^{-5} E_h, orbital gradient 1.0×10^{-5}, orbital rotation angle 1.0×10^{-5}, DIIS Error 5.0×10^{-7}; for geometry optimizations: energy change: 1.0×10^{-6} E_h, max. gradient 1.0×10^{-4} E_h a_0^{-1}, RMS gradient 3.0×10^{-5} E_h a_0^{-1}, max. displacement 1.0×10^{-3} a_0, RMS displacement 6.0×10^{-4} a_0). All calculations make use of the resolution of identity (Split-RI-J) approach for the Coulomb term in combination with the chain-of-spheres approximation for the exchange term (COSX).[9,10] The ZORA relativistic approximation was used to describe relativistic effects in all calculations.[11] To account for solvent effects, a conductor-like screening model (CPCM) modeling acetonitrile was used in all calculations.[12] Atom-pairwise dispersion correction was performed with the Becke-Johnson damping scheme (D3BJ).[13,14] For the geometries of the ground state and with (partly) planarized ligands geometry optimizations were performed using Ahlrichs' split valence triple-ξ basis set def2-TZVPP which comprises polarization functions for all non-hydrogen atoms.[15,16] Dihedral angles were fixed to 0° for the calculations of the structures with (partly) planarized ligands. For ground state geometries the presence of energy minima was checked by numerical frequency calculations. Explicit counter ions and/or solvent molecules were not taken into account. NEB calculations were performed using Ahlrichs' split valence polarization basis set def2-SVP basis with ground state geometries optimized using the same basis set.[13,14] Seven intermediate images were calculated with initial path generation via the image dependent pair potential (IDPP) method[17] and optimized using the Limited-memory Broyden-Fletcher-Goldfarb-Shanno (L-BFGS) algorithm.[18] Tolerance for the maximum component of the atomic force perpendicular to the path was 5.0×10^{-4} Eh a_0^{-1} with a root-mean-square of 2.0×10^{-4} Eh a_0^{-1}. The spring constant was set to 1.0×10^{-1} Eh a_0^{-2}.
CASSCF(7,12)-NEVPT2 calculations for metal-centered excited states were performed as previously described.[19]

5. Assignment of Absolute Configuration

To assign the absolute configuration of the enantiomers of $[Cr(ddpd)_2]^{3+}$ and the elution order of its enantioseparation, experimental electronic circular dichroism (ECD) spectra were compared with those calculated by means of density functional theory (DFT).[20,21] The X-ray geometry of **rac-1** served as starting point to produce a DFT-optimized geometry (M06/def2-SVP) with (*M,M*)-chirality and D_2-symmetry, shown in Figure S5. Excited state calculations were then run with the time-dependent DFT method (TD-DFT). After a minimal screening of functionals and basis sets,[22] final calculations were run at the CAM-B3LYP/def2-TZVP level of theory using a PCM solvent model for water. The comparison between experimental and calculated UV/ECD spectra is shown in Figure S6. The agreement is excellent between the ECD spectrum calculated for the (*M,M*)-enantiomer and the experimental trace recorded for the second eluted isomer. As it frequently happens with open-shell transition metal complexes with multi-chromophoric ligands, there is a very high densities of states in the short-wavelength region (see vertical bars in Figure S6).[23,24] Moreover, a clear distinction between metal-centered and ligand-centered transitions is challenging by TD-DFT methods. To extract the metal-centered transitions, CASSCF(7,12)-NEVPT2 calculations were performed additionally.[19]

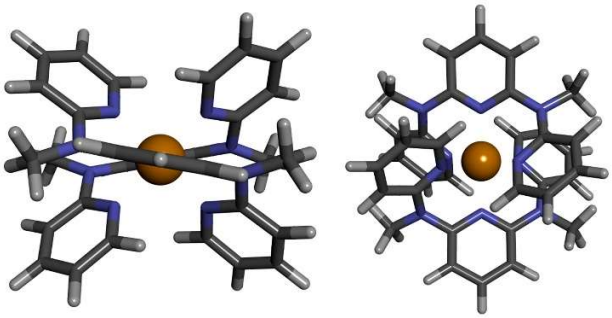

Figure S5. DFT-optimized structure of the cationic metal complex in **(*M,M*)-1** with D_2 symmetry seen along two different C_2 axes.

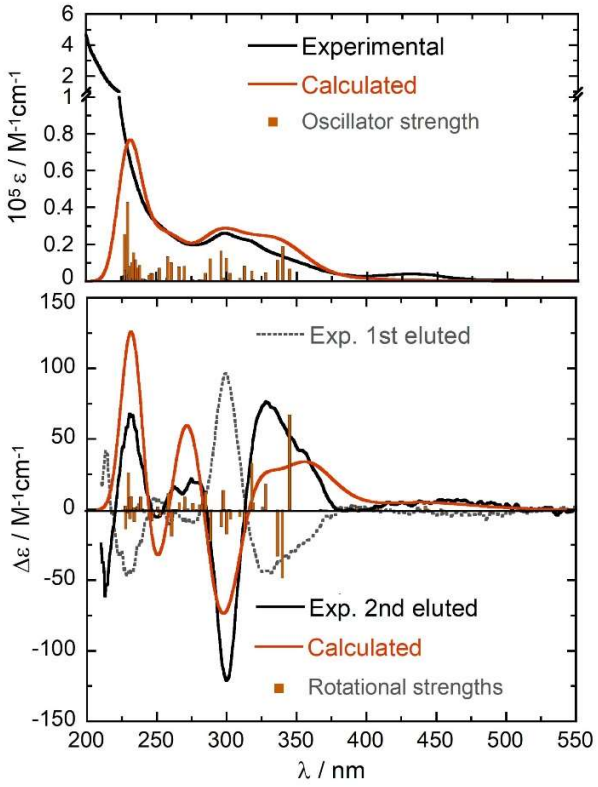

Figure S6. Comparison between the experimental and calculated UV/vis absorption (top) and ECD (bottom) spectra measured in D_2O at 10^{-5} M concentration, and TD-DFT-calculated spectra on **(*M,M*)-1** at the CAM-B3LYP/def2-TZVP/PCM//M06/def2-SVP level. Calculated spectra were plotted using an exponential bandwidth of 0.35 eV and red-shifted by 33 nm.

DFT/TD-DFT calculations for the assignment of absolute configurations were run with the Gaussian16 package,[25] using default grids and convergence criteria. The starting geometry was extracted from the published X-ray structure of a racemic form of $[Cr(ddpd)_2]^{3+}$ and had (*M,M*)-configuration.[1] The tricationic metal complex was optimized at the M06/def2-SVP level in vacuo. TD-DFT calculations were run using B3LYP and CAM-B3LYP functionals, def2-SVP or def2-TZVP basis set on all atoms, either in vacuo or including IEF-PCM solvent model for water. All calculations were run for $[Cr(ddpd)_2]^{3+}$ in its quartet state using unrestricted wavefunctions; ground and excited states were checked for wavefunction stability and spin contamination. Up to 100 excited states (roots) were considered. UV/vis absorption and ECD spectra were plotted using the software SpecDis.[26,27]

The absorption bands at wavelengths > 400 nm (the metal-centered quartet transitions) were reproduced by CASSCF(7,12)-NEVPT2 calculations on **(M,M)-1**.[19] The calculated overall positive CD intensity for **(M,M)-1** at wavelengths > 400 nm confirm the TD-DFT based

assignment of the second fraction as **(M,M)-1** (434 nm: R^*T = –4.5x10^{40} cgs; 429 nm: R^*T = –3.4x10^{40} cgs; 411 nm: R^*T = -12.5x10^{40} cgs).

6. Cartesian Coordinates for Calculated Species

Cartesian Coordinates (in Å) for the optimized geometries of constrained chelate rings (Figure S3), NEB calculations (Figure 2 in the manuscript) and the five-coordinate complex [Cr(ddpd)(k^{2}N-ddpd)]$^{3+}$ (Figure S4):

[Cr(ddpd)$_2$]$^{3+}$ with one half-chair:

24	10.634778000	12.457922000	5.063104000
7	9.012260000	13.664918000	5.635481000
6	8.988788000	14.323422000	6.815651000
1	9.906857000	14.353730000	7.376477000
7	8.023550000	13.061364000	3.620616000
6	7.853464000	14.915969000	7.309190000
1	7.881250000	15.410296000	8.267528000
7	10.311847000	13.164149000	2.860345000
6	6.686841000	14.848172000	6.549204000
1	5.770218000	15.294113000	6.908482000
7	11.723999000	14.155526000	5.605300000
6	6.719747000	14.238368000	5.312428000
1	5.843488000	14.222993000	4.686366000
7	12.770385000	12.976580000	7.355545000
6	7.916525000	13.673981000	4.862550000
7	10.675374000	11.883625000	7.024539000
6	6.792570000	12.456893000	3.085861000
1	6.081305000	13.188704000	2.702507000
1	6.320176000	11.890852000	3.885604000
1	7.063798000	11.774641000	2.286610000
6	8.992063000	13.436078000	2.647376000
6	8.519165000	13.916158000	1.446198000
1	7.485388000	14.199501000	1.340121000
6	9.381664000	13.931210000	0.360928000
1	9.036715000	14.255496000	-0.610361000

6	11.581457000	15.272372000	4.858994000
1	10.768409000	15.273750000	4.151787000
6	12.420948000	16.351434000	4.972497000
1	12.268261000	17.219349000	4.350055000
6	13.450647000	16.286541000	5.909878000
1	14.129938000	17.117066000	6.040228000
6	13.582005000	15.166956000	6.704374000
1	14.343604000	15.126253000	7.464158000
6	12.682566000	14.106280000	6.546050000
6	14.046400000	12.747368000	8.051935000
1	14.852787000	12.904238000	7.341405000
1	14.072411000	11.715946000	8.387468000
1	14.181768000	13.407238000	8.908358000
6	11.648433000	12.312220000	7.872617000
6	11.567818000	12.078455000	9.236330000
1	12.334931000	12.451694000	9.893339000
6	10.470498000	11.401125000	9.737729000
1	10.387762000	11.209123000	10.797944000
7	12.407366000	11.904387000	4.161282000
6	13.030561000	11.135963000	5.116522000
1	12.480530000	10.972363000	6.022358000
7	12.381619000	12.484167000	1.842861000
6	14.250428000	10.537432000	4.990494000
1	14.661751000	9.977766000	5.815737000
6	14.885378000	10.632590000	3.756944000
1	15.835661000	10.152799000	3.573021000
6	14.242446000	11.290358000	2.741931000
1	14.677081000	11.266910000	1.761090000
6	13.002396000	11.933904000	2.950504000
6	13.299545000	12.846543000	0.724082000
1	13.326499000	12.060477000	-0.027337000
1	14.291229000	13.022435000	1.117535000
1	12.974913000	13.774340000	0.276488000
6	11.122849000	13.063139000	1.786942000

6	10.655760000	13.447958000	0.513660000
1	11.265631000	13.316654000	-0.359127000
7	9.724951000	10.676627000	4.641404000
7	8.547356000	10.860690000	6.667809000
6	9.964005000	10.054126000	3.466213000
1	10.776119000	10.438644000	2.873739000
6	9.209638000	8.998397000	3.021854000
1	9.435634000	8.541129000	2.071347000
6	8.158960000	8.557380000	3.823543000
1	7.537966000	7.730830000	3.509103000
6	7.928233000	9.164088000	5.042300000
1	7.145750000	8.804330000	5.688828000
6	8.745514000	10.224855000	5.443607000
6	7.204427000	10.764324000	7.259408000
1	6.474333000	10.866185000	6.461947000
1	7.073526000	11.587815000	7.954754000
1	7.037441000	9.821929000	7.780421000
6	9.589483000	11.232808000	7.522374000
6	9.475457000	10.971381000	8.881844000
1	8.628884000	10.423993000	9.259006000

$[Cr(ddpd)_2]^{3+}$ with one flattened ring:

24	10.634778000	12.457922000	5.063104000
7	9.012260000	13.664918000	5.635481000
6	8.988788000	14.323422000	6.815651000
1	9.906857000	14.353730000	7.376477000
7	8.023550000	13.061364000	3.620616000
6	7.853464000	14.915969000	7.309190000
1	7.881250000	15.410296000	8.267528000
7	10.311847000	13.164149000	2.860345000
6	6.686841000	14.848172000	6.549204000
1	5.770218000	15.294113000	6.908482000
7	11.723999000	14.155526000	5.605300000
6	6.719747000	14.238368000	5.312428000

1	5.843488000	14.222993000	4.686366000
7	12.770385000	12.976580000	7.355545000
6	7.916525000	13.673981000	4.862550000
7	10.675374000	11.883625000	7.024539000
6	6.792570000	12.456893000	3.085861000
1	6.081305000	13.188704000	2.702507000
1	6.320176000	11.890852000	3.885604000
1	7.063798000	11.774641000	2.286610000
6	8.992063000	13.436078000	2.647376000
6	8.519165000	13.916158000	1.446198000
1	7.485388000	14.199501000	1.340121000
6	9.381664000	13.931210000	0.360928000
1	9.036715000	14.255496000	-0.610361000
6	11.581457000	15.272372000	4.858994000
1	10.768409000	15.273750000	4.151787000
6	12.420948000	16.351434000	4.972497000
1	12.268261000	17.219349000	4.350055000
6	13.450647000	16.286541000	5.909878000
1	14.129938000	17.117066000	6.040228000
6	13.582005000	15.166956000	6.704374000
1	14.343604000	15.126253000	7.464158000
6	12.682566000	14.106280000	6.546050000
6	14.046400000	12.747368000	8.051935000
1	14.852787000	12.904238000	7.341405000
1	14.072411000	11.715946000	8.387468000
1	14.181768000	13.407238000	8.908358000
6	11.648433000	12.312220000	7.872617000
6	11.567818000	12.078455000	9.236330000
1	12.334931000	12.451694000	9.893339000
6	10.470498000	11.401125000	9.737729000
1	10.387762000	11.209123000	10.797944000
7	12.407366000	11.904387000	4.161282000
6	13.030561000	11.135963000	5.116522000
1	12.480530000	10.972363000	6.022358000

7	12.381619000	12.484167000	1.842861000
6	14.250428000	10.537432000	4.990494000
1	14.661751000	9.977766000	5.815737000
6	14.885378000	10.632590000	3.756944000
1	15.835661000	10.152799000	3.573021000
6	14.242446000	11.290358000	2.741931000
1	14.677081000	11.266910000	1.761090000
6	13.002396000	11.933904000	2.950504000
6	13.299545000	12.846543000	0.724082000
1	13.326499000	12.060477000	-0.027337000
1	14.291229000	13.022435000	1.117535000
1	12.974913000	13.774340000	0.276488000
6	11.122849000	13.063139000	1.786942000
6	10.655760000	13.447958000	0.513660000
1	11.265631000	13.316654000	-0.359127000
7	9.724951000	10.676627000	4.641404000
7	8.547356000	10.860690000	6.667809000
6	9.964005000	10.054126000	3.466213000
1	10.776119000	10.438644000	2.873739000
6	9.209638000	8.998397000	3.021854000
1	9.435634000	8.541129000	2.071347000
6	8.158960000	8.557380000	3.823543000
1	7.537966000	7.730830000	3.509103000
6	7.928233000	9.164088000	5.042300000
1	7.145750000	8.804330000	5.688828000
6	8.745514000	10.224855000	5.443607000
6	7.204427000	10.764324000	7.259408000
1	6.474333000	10.866185000	6.461947000
1	7.073526000	11.587815000	7.954754000
1	7.037441000	9.821929000	7.780421000
6	9.589483000	11.232808000	7.522374000
6	9.475457000	10.971381000	8.881844000
1	8.628884000	10.423993000	9.259006000

$[Cr(ddpd)_2]^{3+}$ with fully planarized ligands:

24	0.194337000	0.103937000	0.639206000
7	-0.246153000	-0.156350000	2.672886000
7	0.618343000	0.357652000	-1.398737000
7	-1.593250000	-0.844703000	0.023159000
7	2.016210000	1.081091000	1.029588000
7	-0.825627000	1.943944000	0.773424000
7	1.224679000	-1.732966000	0.738023000
6	-1.418095000	-0.746003000	3.086621000
6	-1.639387000	-1.038176000	4.435719000
6	-0.823148000	-0.509479000	5.399402000
6	0.283946000	0.196679000	5.002836000
6	0.632985000	0.256544000	3.651253000
1	-2.460280000	-1.663427000	4.727119000
1	0.887652000	0.687481000	5.740332000
6	-1.823493000	-1.023373000	-1.309588000
6	-2.911174000	-1.657256000	-1.844718000
6	-3.837952000	-2.209046000	-0.969525000
6	-3.634075000	-2.048509000	0.374641000
6	-2.530619000	-1.314578000	0.865212000
1	-4.685310000	-2.776341000	-1.326408000
1	-1.089384000	-0.642435000	-1.980832000
1	-3.005250000	-1.740268000	-2.916610000
1	-4.304479000	-2.528924000	1.061799000
6	2.513331000	1.286023000	2.261256000
6	3.673381000	2.073600000	2.439943000
6	4.373011000	2.557502000	1.365628000
6	3.900248000	2.277711000	0.089770000
6	2.734373000	1.572940000	-0.019611000
1	5.255210000	3.161256000	1.521234000
1	3.994858000	2.342284000	3.428528000
1	4.396387000	2.622383000	-0.803956000
1	2.345873000	1.396239000	-0.996089000
6	0.142642000	1.444224000	-2.100378000

6	0.289967000	1.522571000	-3.487468000
6	1.168744000	0.691192000	-4.132288000
6	1.765335000	-0.312754000	-3.415013000
6	1.364149000	-0.563522000	-2.099068000
1	-0.249774000	2.256602000	-4.051746000
1	2.510365000	-0.927090000	-3.881523000
6	-1.309495000	2.347989000	1.983583000
6	-2.068055000	3.466358000	2.193043000
6	-2.424879000	4.226165000	1.085317000
6	-1.929575000	3.860448000	-0.137339000
6	-1.058557000	2.755484000	-0.272533000
1	-3.088248000	5.074535000	1.169951000
1	-1.072200000	1.740289000	2.826155000
1	-2.398160000	3.706954000	3.191723000
1	-2.241996000	4.404691000	-1.008109000
6	1.861797000	-2.301377000	-0.300935000
6	2.679712000	-3.437683000	-0.105416000
6	2.773719000	-4.042941000	1.119068000
6	2.049249000	-3.503221000	2.174848000
6	1.313815000	-2.375028000	1.938278000
1	3.412684000	-4.903672000	1.252240000
1	3.277932000	-3.810911000	-0.914473000
1	2.060579000	-3.929821000	3.165914000
1	0.759711000	-1.961549000	2.749538000
7	-0.603340000	2.495703000	-1.561162000
6	-0.469229000	3.765601000	-2.362512000
1	-0.393997000	4.602914000	-1.682995000
1	0.449819000	3.733689000	-2.930679000
1	-1.314899000	3.903995000	-3.030909000
7	1.903071000	-1.740922000	-1.572922000
6	2.100194000	-2.799458000	-2.631260000
1	3.136906000	-2.848222000	-2.954414000
1	1.788721000	-3.755406000	-2.233364000
1	1.462050000	-2.581458000	-3.475882000

7	-2.416820000	-1.252510000	2.249372000
7	1.856759000	0.897996000	3.425948000
6	-3.772441000	-1.252288000	2.912106000
1	-4.507846000	-0.898993000	2.201860000
1	-4.039971000	-2.244449000	3.265339000
1	-3.768696000	-0.557684000	3.740022000
6	2.835074000	0.671047000	4.550497000
1	3.811123000	0.468602000	4.129956000
1	2.884380000	1.532285000	5.211657000
1	2.541895000	-0.205284000	5.111028000
1	-1.046693000	-0.648688000	6.447246000
1	1.388717000	0.828658000	-5.181000000

NEB #1:

24	-0.000085000	0.000888000	0.000253000
7	-0.091023000	-2.052760000	-0.086249000
6	0.884859000	-2.745412000	-0.715287000
1	1.569522000	-2.167731000	-1.316003000
7	-2.053586000	-1.988559000	1.210512000
6	1.027682000	-4.103621000	-0.588001000
1	1.834570000	-4.611595000	-1.094810000
7	-2.034199000	-0.000496000	-0.095014000
6	0.113162000	-4.788757000	0.210524000
1	0.191126000	-5.859726000	0.339944000
7	0.191078000	0.000730000	-2.048492000
6	-0.917198000	-4.099316000	0.815357000
1	-1.659811000	-4.628061000	1.389924000
7	2.084339000	1.382703000	-1.840314000
6	-1.013260000	-2.713917000	0.635101000
7	2.034201000	0.000888000	0.095121000
6	-2.748954000	-2.603010000	2.350455000
1	-3.457787000	-3.374198000	2.046916000
1	-2.003352000	-3.036342000	3.012078000
1	-3.276702000	-1.822135000	2.890063000

6	-2.741265000	-0.981898000	0.517110000
6	-4.129131000	-0.996776000	0.477268000
1	-4.680242000	-1.792662000	0.950207000
6	-4.787647000	-0.004343000	-0.226778000
1	-5.867933000	-0.005771000	-0.278452000
6	-0.720389000	-0.644303000	-2.810685000
1	-1.402524000	-1.297362000	-2.289596000
6	-0.804839000	-0.470693000	-4.168658000
1	-1.562409000	-0.992885000	-4.733790000
6	0.103455000	0.393239000	-4.778645000
1	0.070643000	0.559943000	-5.846784000
6	1.070820000	1.016322000	-4.017874000
1	1.810652000	1.642911000	-4.488205000
6	1.108687000	0.788073000	-2.636729000
6	2.752816000	2.576395000	-2.377955000
1	1.997895000	3.219069000	-2.823507000
1	3.216004000	3.109347000	-1.552780000
1	3.511485000	2.335932000	-3.123538000
6	2.756371000	0.683018000	-0.827381000
6	4.143650000	0.708206000	-0.775871000
1	4.707954000	1.236641000	-1.526175000
6	4.788086000	-0.002297000	0.221174000
1	5.868473000	-0.003467000	0.270665000
7	-0.101451000	2.054480000	0.078163000
6	0.811060000	2.747861000	0.795175000
1	1.437790000	2.170547000	1.456366000
7	-1.934740000	1.988628000	-1.395804000
6	0.963433000	4.106340000	0.682394000
1	1.719495000	4.614691000	1.262000000
6	0.125404000	4.791020000	-0.196391000
1	0.213854000	5.862124000	-0.317499000
6	-0.844054000	4.100825000	-0.894041000
1	-1.531124000	4.629019000	-1.534482000
6	-0.954095000	2.715103000	-0.724783000

6	-2.520893000	2.602876000	-2.595770000
1	-3.258181000	3.371081000	-2.359871000
1	-1.717448000	3.040026000	-3.182950000
1	-2.991999000	1.821051000	-3.184119000
6	-2.682154000	0.979352000	-0.771655000
6	-4.067538000	0.990093000	-0.864528000
1	-4.572760000	1.785304000	-1.386928000
7	-0.000085000	0.000888000	2.057842000
7	1.904605000	-1.380694000	2.027339000
6	-0.978914000	0.645323000	2.731730000
1	-1.609491000	1.298395000	2.149429000
6	-1.189844000	0.471230000	4.075831000
1	-1.997146000	0.993153000	4.567620000
6	-0.342265000	-0.392603000	4.767781000
1	-0.475188000	-0.560001000	5.828001000
6	0.692439000	-1.014952000	4.100703000
1	1.385517000	-1.641683000	4.637599000
6	0.858960000	-0.786050000	2.729244000
6	2.519009000	-2.575039000	2.624769000
1	1.725247000	-3.216521000	2.998739000
1	3.055729000	-3.108540000	1.845933000
1	3.205183000	-2.335618000	3.437753000
6	2.667406000	-0.682739000	1.079844000
6	4.053615000	-0.711065000	1.155133000
1	4.545432000	-1.240114000	1.954334000

NEB #2:

24	0.000155000	0.001794000	-0.004132000
7	0.026286000	-2.085673000	-0.238049000
6	1.096243000	-2.670703000	-0.835707000
1	1.891774000	-2.016887000	-1.169825000
7	-2.115204000	-2.251242000	0.773056000
6	1.205271000	-4.035369000	-1.020321000
1	2.092850000	-4.449524000	-1.492427000

7	-2.082294000	-0.007366000	-0.096421000
6	0.141562000	-4.842206000	-0.598478000
1	0.166986000	-5.919165000	-0.753320000
7	0.037142000	0.018060000	-2.119496000
6	-0.966911000	-4.252093000	-0.007878000
1	-1.815182000	-4.862513000	0.280610000
7	2.265054000	0.861554000	-2.156993000
6	-1.005112000	-2.853799000	0.166531000
7	2.104100000	-0.003401000	0.099589000
6	-2.905193000	-3.121321000	1.661438000
1	-3.570224000	-3.797351000	1.108566000
1	-2.216327000	-3.713417000	2.267541000
1	-3.502672000	-2.495115000	2.327106000
6	-2.780670000	-1.127886000	0.259489000
6	-4.175669000	-1.168541000	0.156569000
1	-4.714703000	-2.084302000	0.367475000
6	-4.861150000	-0.026016000	-0.235092000
1	-5.947584000	-0.034460000	-0.294175000
6	-1.056146000	-0.424363000	-2.794423000
1	-1.926735000	-0.677273000	-2.206656000
6	-1.099006000	-0.561279000	-4.167556000
1	-2.018248000	-0.887617000	-4.646817000
6	0.072741000	-0.309590000	-4.889760000
1	0.110044000	-0.465851000	-5.965922000
6	1.202866000	0.118426000	-4.210455000
1	2.129057000	0.278071000	-4.750848000
6	1.153446000	0.316242000	-2.813730000
6	3.133168000	1.693967000	-3.013319000
1	2.498838000	2.291135000	-3.670195000
1	3.712873000	2.370068000	-2.382608000
1	3.818815000	1.095461000	-3.626990000
6	2.856476000	0.369297000	-0.983726000
6	4.255858000	0.297236000	-0.952935000
1	4.835771000	0.493206000	-1.846110000

6	4.896633000	-0.032444000	0.231603000
1	5.983591000	-0.045470000	0.283601000
7	0.005808000	2.089502000	0.218200000
6	1.028331000	2.682458000	0.886760000
1	1.807947000	2.034338000	1.265706000
7	-2.059132000	2.242746000	-0.949483000
6	1.107965000	4.046893000	1.088940000
1	1.959218000	4.467503000	1.618541000
6	0.061347000	4.843378000	0.609122000
1	0.060753000	5.918930000	0.775519000
6	-0.997656000	4.244747000	-0.058775000
1	-1.831160000	4.848227000	-0.400013000
6	-1.005246000	2.848271000	-0.250652000
6	-2.778034000	3.119364000	-1.890270000
1	-3.491275000	3.783465000	-1.385070000
1	-2.045792000	3.723586000	-2.429847000
1	-3.313910000	2.498606000	-2.611080000
6	-2.756211000	1.107007000	-0.512844000
6	-4.155424000	1.127424000	-0.550633000
1	-4.684026000	2.035779000	-0.812966000
7	-0.174112000	0.003333000	2.106641000
7	2.032938000	-0.856935000	2.364465000
6	-1.324372000	0.455268000	2.671777000
1	-2.136057000	0.702659000	2.003286000
6	-1.496817000	0.604713000	4.033323000
1	-2.456018000	0.937535000	4.421440000
6	-0.400529000	0.355726000	4.865961000
1	-0.466349000	0.520095000	5.939582000
6	0.787602000	-0.080902000	4.299436000
1	1.659058000	-0.238427000	4.924873000
6	0.869378000	-0.293084000	2.906588000
6	2.799042000	-1.697009000	3.305267000
1	2.093856000	-2.274369000	3.904958000
1	3.421291000	-2.390232000	2.736777000

1	3.436316000	-1.104871000	3.974410000
6	2.742298000	-0.386540000	1.250140000
6	4.140183000	-0.345605000	1.349629000
1	4.630218000	-0.555862000	2.291486000

NEB #3:

24	0.032777000	-0.005506000	-0.005640000
7	0.135490000	-2.085428000	-0.357432000
6	1.305511000	-2.666196000	-0.732429000
1	2.187828000	-2.049313000	-0.732143000
7	-2.149429000	-2.385790000	0.249844000
6	1.435747000	-3.997865000	-1.076402000
1	2.414561000	-4.388019000	-1.341970000
7	-2.068771000	-0.004481000	-0.102766000
6	0.285378000	-4.790660000	-1.093103000
1	0.322268000	-5.830309000	-1.410400000
7	-0.001115000	0.193761000	-2.091156000
6	-0.915148000	-4.220218000	-0.702784000
1	-1.827863000	-4.804478000	-0.721321000
7	2.378510000	0.142651000	-2.330466000
6	-0.959106000	-2.872647000	-0.293795000
7	2.138992000	-0.005112000	0.101184000
6	-2.986583000	-3.391910000	0.935268000
1	-3.613383000	-3.968290000	0.244338000
1	-2.329315000	-4.074550000	1.477809000
1	-3.627511000	-2.879080000	1.655820000
6	-2.773118000	-1.177861000	-0.062892000
6	-4.164682000	-1.206363000	-0.216270000
1	-4.682137000	-2.155200000	-0.284233000
6	-4.873967000	-0.016106000	-0.248726000
1	-5.960421000	-0.020644000	-0.306431000
6	-1.184925000	0.249987000	-2.757175000
1	-2.041021000	0.591122000	-2.206878000
6	-1.353440000	-0.100707000	-4.081016000

1	-2.331209000	0.007273000	-4.542977000
6	-0.255023000	-0.638518000	-4.757306000
1	-0.350063000	-1.029195000	-5.767712000
6	0.971904000	-0.649031000	-4.115307000
1	1.844185000	-1.047514000	-4.620132000
6	1.096441000	-0.128664000	-2.808067000
6	3.344519000	0.478749000	-3.408043000
1	2.789806000	0.865440000	-4.260960000
1	4.016515000	1.262513000	-3.056440000
1	3.928082000	-0.394832000	-3.723960000
6	2.908883000	0.038710000	-1.045866000
6	4.309688000	-0.050651000	-0.990339000
1	4.896700000	-0.118846000	-1.891986000
6	4.954721000	-0.048693000	0.228534000
1	6.041245000	-0.065245000	0.279117000
7	0.096252000	2.074982000	0.347389000
6	1.228695000	2.657434000	0.822071000
1	2.115973000	2.048617000	0.863072000
7	-2.133003000	2.378402000	-0.443990000
6	1.314835000	3.979285000	1.215354000
1	2.266239000	4.372773000	1.562525000
6	0.155076000	4.757409000	1.173716000
1	0.153984000	5.786140000	1.526397000
6	-1.003175000	4.188235000	0.670512000
1	-1.920177000	4.764300000	0.630353000
6	-0.997830000	2.854845000	0.216535000
6	-2.903506000	3.399946000	-1.183470000
1	-3.594910000	3.959726000	-0.542053000
1	-2.198322000	4.095465000	-1.643436000
1	-3.471507000	2.906550000	-1.975528000
6	-2.775128000	1.163465000	-0.213015000
6	-4.175735000	1.179755000	-0.206877000
1	-4.704854000	2.124347000	-0.192382000
7	-0.197758000	-0.201455000	2.070794000

7	2.146913000	-0.122357000	2.543710000
6	-1.439643000	-0.256843000	2.622362000
1	-2.235494000	-0.622442000	2.001303000
6	-1.738323000	0.126107000	3.914002000
1	-2.754012000	0.015546000	4.283791000
6	-0.717160000	0.701255000	4.675566000
1	-0.913989000	1.120456000	5.659573000
6	0.565704000	0.710232000	4.154318000
1	1.381096000	1.134107000	4.728547000
6	0.822150000	0.151098000	2.882779000
6	3.002328000	-0.420596000	3.721330000
1	2.365143000	-0.755640000	4.537337000
1	3.685678000	-1.233411000	3.474091000
1	3.572076000	0.459286000	4.044413000
6	2.798724000	-0.064632000	1.314039000
6	4.202375000	-0.024263000	1.383969000
1	4.709761000	0.029592000	2.333512000

NEB #4:

24	0.039588000	0.004986000	-0.005317000
7	0.145396000	-2.086943000	-0.310670000
6	1.347273000	-2.692151000	-0.503749000
1	2.226333000	-2.121150000	-0.263895000
7	-2.196971000	-2.405408000	0.025278000
6	1.501279000	-3.996728000	-0.932113000
1	2.501098000	-4.403409000	-1.059677000
7	-2.099240000	0.004037000	-0.110648000
6	0.351506000	-4.743258000	-1.199531000
1	0.414381000	-5.756163000	-1.589667000
7	0.115096000	0.309567000	-2.072088000
6	-0.882105000	-4.170100000	-0.934208000
1	-1.795617000	-4.729793000	-1.103956000
7	2.329711000	-0.515862000	-2.272898000
6	-0.959336000	-2.853190000	-0.442011000

7	2.102298000	0.005306000	0.092148000
6	-3.044638000	-3.458567000	0.627803000
1	-3.651489000	-3.996080000	-0.109119000
1	-2.395853000	-4.169113000	1.143804000
1	-3.705220000	-2.996259000	1.364806000
6	-2.805439000	-1.169105000	-0.188252000
6	-4.195918000	-1.192068000	-0.356079000
1	-4.704029000	-2.135058000	-0.513238000
6	-4.914944000	-0.010935000	-0.288513000
1	-6.000350000	-0.016581000	-0.360625000
6	-1.015069000	0.751533000	-2.684921000
1	-1.746063000	1.224529000	-2.056212000
6	-1.264411000	0.622189000	-4.034173000
1	-2.209620000	0.965280000	-4.444986000
6	-0.269125000	0.039952000	-4.825947000
1	-0.414481000	-0.110008000	-5.893563000
6	0.933241000	-0.315792000	-4.240358000
1	1.729615000	-0.698610000	-4.863435000
6	1.115030000	-0.165505000	-2.844991000
6	3.273933000	-1.225352000	-3.160893000
1	2.722706000	-1.955737000	-3.750368000
1	3.797280000	-0.532925000	-3.830739000
1	4.001137000	-1.761943000	-2.555775000
6	2.861304000	-0.099093000	-1.047823000
6	4.253879000	0.050756000	-1.000927000
1	4.821662000	0.132818000	-1.918801000
6	4.900308000	-0.003222000	0.223453000
1	5.987079000	-0.007941000	0.274910000
7	0.098298000	2.093747000	0.317434000
6	1.273741000	2.700965000	0.627988000
1	2.174606000	2.142687000	0.441428000
7	-2.205340000	2.413459000	-0.228325000
6	1.376828000	3.993149000	1.107848000
1	2.357726000	4.406542000	1.326644000

6	0.199687000	4.718210000	1.308298000
1	0.217645000	5.717978000	1.735256000
6	-1.001194000	4.144141000	0.921558000
1	-1.931858000	4.690565000	1.029851000
6	-1.021409000	2.847475000	0.375108000
6	-2.986383000	3.485939000	-0.886636000
1	-3.676867000	3.994837000	-0.204288000
1	-2.286554000	4.216000000	-1.298486000
1	-3.554309000	3.050766000	-1.712383000
6	-2.822327000	1.169870000	-0.114823000
6	-4.223983000	1.177205000	-0.126563000
1	-4.758537000	2.113961000	-0.033297000
7	-0.090508000	-0.292323000	2.060919000
7	2.106619000	0.515033000	2.469742000
6	-1.277153000	-0.719152000	2.569571000
1	-1.964958000	-1.166139000	1.876415000
6	-1.639041000	-0.604658000	3.894574000
1	-2.621722000	-0.936543000	4.216458000
6	-0.707286000	-0.051946000	4.778925000
1	-0.941468000	0.082797000	5.832666000
6	0.544254000	0.294769000	4.302018000
1	1.289840000	0.657728000	4.995745000
6	0.843631000	0.162335000	2.925115000
6	2.967720000	1.221158000	3.442243000
1	2.366219000	1.946089000	3.988388000
1	3.436808000	0.526104000	4.148555000
1	3.741150000	1.763938000	2.903368000
6	2.751306000	0.103991000	1.297790000
6	4.141579000	-0.054082000	1.381409000
1	4.622021000	-0.143498000	2.347450000

NEB #5:

24	-0.000119000	-0.017389000	-0.007602000
7	0.061697000	-2.109661000	-0.237910000

6	1.196488000	-2.725336000	-0.657547000
1	2.061873000	-2.107171000	-0.808256000
7	-2.164787000	-2.315602000	0.554159000
6	1.304480000	-4.086939000	-0.866785000
1	2.253815000	-4.505288000	-1.190570000
7	-2.097207000	-0.006112000	-0.105421000
6	0.172356000	-4.881134000	-0.663060000
1	0.192790000	-5.951294000	-0.856575000
7	0.018339000	0.207549000	-2.104004000
6	-0.990207000	-4.274337000	-0.216269000
1	-1.890982000	-4.857796000	-0.061123000
7	2.342853000	-0.293136000	-2.286015000
6	-1.014141000	-2.885395000	0.011778000
7	2.131704000	-0.027686000	0.095437000
6	-2.971947000	-3.189263000	1.425447000
1	-3.613977000	-3.880497000	0.866328000
1	-2.293081000	-3.762267000	2.062235000
1	-3.599225000	-2.562712000	2.063753000
6	-2.797348000	-1.171373000	0.064567000
6	-4.179089000	-1.239431000	-0.124033000
1	-4.683182000	-2.197014000	-0.070472000
6	-4.895865000	-0.071653000	-0.342814000
1	-5.978933000	-0.096915000	-0.442886000
6	-1.125751000	0.479556000	-2.782368000
1	-2.053357000	0.252225000	-2.285720000
6	-1.162508000	0.963476000	-4.077301000
1	-2.122177000	1.151485000	-4.552320000
6	0.051046000	1.210477000	-4.724639000
1	0.081984000	1.652028000	-5.718190000
6	1.224440000	0.844544000	-4.082285000
1	2.185332000	0.977240000	-4.567998000
6	1.177282000	0.290087000	-2.791634000
6	3.175086000	-0.983707000	-3.294731000
1	3.867204000	-0.310805000	-3.814617000

1	2.510873000	-1.438260000	-4.033104000
1	3.737331000	-1.779792000	-2.799192000
6	2.907515000	-0.083986000	-1.034579000
6	4.306395000	-0.032536000	-0.984681000
1	4.875551000	0.002741000	-1.904558000
6	4.950673000	-0.040311000	0.239927000
1	6.036623000	-0.043916000	0.297207000
7	0.029803000	2.072859000	0.208708000
6	1.152572000	2.680331000	0.671304000
1	2.018966000	2.060017000	0.808462000
7	-2.164636000	2.323856000	-0.690217000
6	1.252581000	4.033964000	0.929190000
1	2.195123000	4.445154000	1.280890000
6	0.119210000	4.828342000	0.736696000
1	0.129278000	5.891641000	0.966404000
6	-1.028622000	4.232014000	0.240275000
1	-1.925243000	4.820269000	0.082392000
6	-1.040751000	2.853636000	-0.052147000
6	-2.902491000	3.259135000	-1.561517000
1	-3.611651000	3.884795000	-1.007638000
1	-2.179645000	3.898196000	-2.071336000
1	-3.447687000	2.687931000	-2.315581000
6	-2.807754000	1.133407000	-0.369423000
6	-4.208750000	1.128121000	-0.425243000
1	-4.746234000	2.060018000	-0.545010000
7	-0.193585000	-0.216069000	2.085343000
7	2.102985000	0.280811000	2.480786000
6	-1.403117000	-0.450626000	2.655998000
1	-2.271765000	-0.244183000	2.056169000
6	-1.575716000	-0.874178000	3.961330000
1	-2.579803000	-1.036310000	4.345965000
6	-0.437254000	-1.095691000	4.739900000
1	-0.512119000	-1.491689000	5.750195000
6	0.799364000	-0.767346000	4.203933000

1	1.705778000	-0.882347000	4.789351000
6	0.888666000	-0.273855000	2.890540000
6	2.829071000	1.027739000	3.529799000
1	3.462944000	0.387482000	4.154167000
1	2.093763000	1.518678000	4.171418000
1	3.440566000	1.797583000	3.051070000
6	2.787941000	0.031838000	1.298294000
6	4.183524000	-0.038055000	1.391985000
1	4.654842000	-0.070162000	2.365970000

NEB #6:

24	-0.034485000	-0.014860000	0.027437000
7	-0.030470000	-2.076273000	-0.306279000
6	1.054003000	-2.660895000	-0.874154000
1	1.711690000	-2.011383000	-1.432825000
7	-2.162279000	-2.285072000	0.624939000
6	1.328926000	-4.008253000	-0.762258000
1	2.215386000	-4.420241000	-1.235629000
7	-2.107239000	0.016850000	-0.090977000
6	0.447255000	-4.799144000	-0.010814000
1	0.647304000	-5.857384000	0.142220000
7	-0.003321000	0.242100000	-2.085777000
6	-0.710058000	-4.233839000	0.501273000
1	-1.434400000	-4.850319000	1.020847000
7	2.362806000	-0.001233000	-2.289062000
6	-0.958476000	-2.862879000	0.280645000
7	2.111461000	-0.053096000	0.117375000
6	-3.087829000	-3.065443000	1.461422000
1	-3.543600000	-3.903162000	0.919277000
1	-2.542919000	-3.449462000	2.327817000
1	-3.873874000	-2.400356000	1.820938000
6	-2.736082000	-1.204093000	-0.079774000
6	-3.998021000	-1.391374000	-0.624243000
1	-4.429121000	-2.385799000	-0.667511000

6	-4.691003000	-0.280318000	-1.101705000
1	-5.664339000	-0.394855000	-1.570942000
6	-1.162061000	0.369789000	-2.782808000
1	-2.055667000	-0.011674000	-2.320430000
6	-1.247967000	0.904030000	-4.053888000
1	-2.214407000	0.962676000	-4.546164000
6	-0.075811000	1.373483000	-4.651101000
1	-0.093451000	1.867005000	-5.619483000
6	1.126918000	1.150707000	-3.998422000
1	2.063610000	1.448509000	-4.455794000
6	1.143772000	0.508212000	-2.746194000
6	3.241093000	-0.504410000	-3.373285000
1	3.832803000	-1.337398000	-2.987878000
1	2.610056000	-0.877587000	-4.182059000
1	3.913172000	0.266331000	-3.766403000
6	2.897331000	0.010093000	-1.005323000
6	4.299331000	0.016555000	-0.932395000
1	4.886369000	0.172173000	-1.826880000
6	4.925893000	-0.193807000	0.281401000
1	6.009901000	-0.250909000	0.343670000
7	-0.034797000	2.047473000	0.264276000
6	1.128116000	2.628182000	0.660139000
1	1.822803000	1.993392000	1.185739000
7	-2.319085000	2.409630000	-0.362130000
6	1.447715000	3.949798000	0.426395000
1	2.394766000	4.346910000	0.778176000
6	0.543715000	4.714255000	-0.318556000
1	0.786269000	5.728400000	-0.627840000
6	-0.685980000	4.163712000	-0.641750000
1	-1.409974000	4.752333000	-1.191714000
6	-0.997755000	2.840512000	-0.256595000
6	-3.332435000	3.491308000	-0.316374000
1	-2.915909000	4.331470000	0.237755000
1	-3.631371000	3.824176000	-1.316128000

1	-4.202993000	3.134673000	0.234664000
6	-2.823010000	1.118062000	-0.457815000
6	-4.131179000	0.974951000	-0.969225000
1	-4.670780000	1.839739000	-1.326336000
7	-0.234891000	-0.258962000	2.103213000
7	2.091018000	0.032568000	2.536534000
6	-1.470789000	-0.398613000	2.650700000
1	-2.306233000	-0.121483000	2.030580000
6	-1.697748000	-0.827949000	3.944301000
1	-2.717274000	-0.912037000	4.309716000
6	-0.594130000	-1.165408000	4.730702000
1	-0.717591000	-1.575777000	5.730037000
6	0.673816000	-0.940520000	4.217477000
1	1.553905000	-1.157392000	4.811586000
6	0.828760000	-0.425881000	2.916734000
6	2.891032000	0.602657000	3.644766000
1	3.571104000	1.352268000	3.233998000
1	2.210312000	1.097686000	4.340491000
1	3.472357000	-0.152640000	4.185496000
6	2.757328000	-0.150880000	1.325415000
6	4.144763000	-0.313897000	1.417105000
1	4.603945000	-0.495710000	2.379661000

NEB #7:

24	-0.019576000	-0.044455000	-0.060631000
7	0.000444000	-2.123900000	-0.320824000
6	1.202565000	-2.744778000	-0.465349000
1	1.959945000	-2.198978000	-0.998767000
7	-2.340120000	-2.471877000	-0.075810000
6	1.482059000	-4.010071000	0.005511000
1	2.457566000	-4.451544000	-0.177497000
7	-2.113883000	-0.056896000	-0.131269000
6	0.494985000	-4.648006000	0.766220000
1	0.692183000	-5.592409000	1.268470000

7	0.037554000	0.327001000	-2.130050000
6	-0.762719000	-4.072764000	0.842368000
1	-1.545862000	-4.566472000	1.404895000
7	2.305014000	-0.398269000	-2.315206000
6	-1.026150000	-2.859041000	0.165343000
7	2.082449000	-0.089418000	0.065443000
6	-3.328663000	-3.575026000	-0.077585000
1	-2.811594000	-4.525147000	-0.015076000
1	-4.024969000	-3.476801000	0.760754000
1	-3.878128000	-3.594203000	-1.016829000
6	-2.836226000	-1.203085000	-0.375541000
6	-4.172547000	-1.126485000	-0.810586000
1	-4.738891000	-2.015784000	-1.030907000
6	-4.789132000	0.100360000	-0.954287000
1	-5.805938000	0.158447000	-1.334288000
6	-1.072423000	0.793170000	-2.757701000
1	-1.986787000	0.826449000	-2.189177000
6	-1.100990000	1.203689000	-4.076272000
1	-2.037057000	1.542068000	-4.511454000
6	0.096909000	1.192412000	-4.794825000
1	0.143879000	1.560945000	-5.816676000
6	1.236189000	0.706208000	-4.174591000
1	2.181275000	0.702328000	-4.703780000
6	1.175579000	0.233236000	-2.849074000
6	3.176485000	-1.058265000	-3.308568000
1	3.759885000	-1.832321000	-2.805368000
1	2.542223000	-1.533520000	-4.059253000
1	3.861167000	-0.359906000	-3.805344000
6	2.866367000	-0.161216000	-1.057569000
6	4.260237000	-0.071480000	-0.989971000
1	4.846671000	-0.041472000	-1.899286000
6	4.883775000	-0.026239000	0.248236000
1	5.969107000	-0.006712000	0.321068000
7	0.147406000	2.054845000	0.097376000

6	1.357708000	2.662122000	-0.027287000
1	2.233261000	2.038367000	0.020356000
7	-2.209716000	2.315444000	0.367429000
6	1.528816000	4.018349000	-0.219233000
1	2.534046000	4.425088000	-0.285812000
6	0.388819000	4.811795000	-0.371030000
1	0.465525000	5.869578000	-0.612818000
6	-0.852890000	4.215449000	-0.229931000
1	-1.755015000	4.799894000	-0.369071000
6	-0.951885000	2.838625000	0.062737000
6	-3.166973000	3.293772000	0.926995000
1	-2.622662000	3.957827000	1.601521000
1	-3.661383000	3.898050000	0.156114000
1	-3.924658000	2.755977000	1.499767000
6	-2.787671000	1.140295000	-0.131088000
6	-4.106245000	1.246193000	-0.582469000
1	-4.584062000	2.213404000	-0.662606000
7	-0.239768000	-0.366738000	2.018168000
7	1.990907000	0.356615000	2.430787000
6	-1.424589000	-0.775440000	2.546036000
1	-2.273362000	-0.800400000	1.883998000
6	-1.603635000	-1.122157000	3.871995000
1	-2.589004000	-1.419995000	4.219944000
6	-0.491202000	-1.101470000	4.717053000
1	-0.565003000	-1.423068000	5.753551000
6	0.717932000	-0.661537000	4.203333000
1	1.601331000	-0.637589000	4.830772000
6	0.809228000	-0.251937000	2.858940000
6	2.706142000	1.131206000	3.465806000
1	3.322695000	1.887195000	2.974562000
1	1.964882000	1.637743000	4.088261000
1	3.343610000	0.505511000	4.101629000
6	2.706596000	0.054318000	1.275088000
6	4.102884000	0.005847000	1.390565000

1	4.565081000	0.017045000	2.369666000

NEB #8:

24	0.003573000	-0.016832000	-0.027468000
7	0.063272000	-2.125565000	-0.069508000
6	1.183687000	-2.751683000	0.374933000
1	2.039587000	-2.130759000	0.585298000
7	-2.164118000	-2.295173000	-0.925016000
6	1.276337000	-4.114269000	0.572484000
1	2.218265000	-4.550655000	0.893796000
7	-2.102266000	-0.021340000	-0.100981000
6	0.121289000	-4.878614000	0.390983000
1	0.119829000	-5.944841000	0.604510000
7	0.094779000	0.230039000	-2.109024000
6	-1.034433000	-4.250372000	-0.044957000
1	-1.944671000	-4.825021000	-0.157444000
7	2.222523000	-0.827568000	-2.171038000
6	-1.032499000	-2.867679000	-0.325509000
7	2.087403000	0.014460000	0.079029000
6	-2.961383000	-3.242478000	-1.732926000
1	-2.281817000	-3.947127000	-2.213276000
1	-3.685136000	-3.796586000	-1.121787000
1	-3.491900000	-2.692126000	-2.510526000
6	-2.800232000	-1.103721000	-0.565878000
6	-4.197591000	-1.052017000	-0.702872000
1	-4.756391000	-1.927585000	-1.001543000
6	-4.868472000	0.128067000	-0.440422000
1	-5.943083000	0.188785000	-0.590710000
6	-0.925683000	0.863306000	-2.742068000
1	-1.746806000	1.206438000	-2.126372000
6	-0.951073000	1.076260000	-4.106338000
1	-1.802454000	1.575460000	-4.561173000

6	0.149434000	0.646742000	-4.856568000
1	0.192695000	0.823907000	-5.928740000
6	1.207188000	0.018950000	-4.215778000
1	2.081482000	-0.277868000	-4.782406000
6	1.161589000	-0.183256000	-2.822218000
6	3.033356000	-1.724772000	-3.014136000
1	3.577530000	-2.417889000	-2.369588000
1	2.360449000	-2.300596000	-3.653023000
1	3.748753000	-1.178750000	-3.642037000
6	2.838521000	-0.353206000	-1.002862000
6	4.235828000	-0.307976000	-0.955666000
1	4.821960000	-0.531409000	-1.838373000
6	4.865129000	0.042790000	0.231475000
1	5.950978000	0.052760000	0.292533000
7	0.065736000	2.101774000	-0.005374000
6	1.175346000	2.734045000	-0.467265000
1	1.999684000	2.112484000	-0.785925000
7	-2.138376000	2.198056000	0.867444000
6	1.290614000	4.107717000	-0.543196000
1	2.215671000	4.553842000	-0.899016000
6	0.181579000	4.879826000	-0.181866000
1	0.204793000	5.963227000	-0.273698000
6	-0.967164000	4.244532000	0.263853000
1	-1.849039000	4.828464000	0.498982000
6	-0.999984000	2.838327000	0.363778000
6	-2.988784000	3.027489000	1.741989000
1	-2.343904000	3.595649000	2.415446000
1	-3.619637000	3.725976000	1.177886000
1	-3.626536000	2.371407000	2.337187000
6	-2.787546000	1.114645000	0.244087000
6	-4.162627000	1.226478000	0.029200000
1	-4.673983000	2.160218000	0.223415000
7	-0.114431000	-0.268662000	2.057283000
7	1.961044000	0.853797000	2.331537000

6	-1.183826000	-0.913555000	2.590170000
1	-1.933104000	-1.275834000	1.899790000
6	-1.351401000	-1.107774000	3.946950000
1	-2.236834000	-1.617910000	4.316982000
6	-0.347900000	-0.643450000	4.804273000
1	-0.420302000	-0.801095000	5.878220000
6	0.760371000	-0.003592000	4.268279000
1	1.563598000	0.319662000	4.919463000
6	0.858518000	0.180776000	2.874442000
6	2.652358000	1.778645000	3.245828000
1	3.239222000	2.483080000	2.653383000
1	1.901645000	2.337941000	3.808312000
1	3.315332000	1.257737000	3.948191000
6	2.707617000	0.399960000	1.233972000
6	4.102904000	0.383546000	1.339582000
1	4.583921000	0.622341000	2.279603000

NEB #9:

24	-0.000063000	0.000898000	-0.000217000
7	-0.094015000	-2.054296000	-0.023984000
6	0.820932000	-2.779434000	0.657817000
1	1.445687000	-2.233707000	1.347168000
7	-1.928109000	-1.921579000	-1.492264000
6	0.977984000	-4.130034000	0.477428000
1	1.735575000	-4.664290000	1.031131000
7	-2.034245000	-0.000423000	-0.094029000
6	0.142935000	-4.772783000	-0.435243000
1	0.234961000	-5.836238000	-0.609585000
7	0.190601000	0.102451000	-2.046433000
6	-0.828492000	-4.051921000	-1.098178000
1	-1.513479000	-4.549922000	-1.764480000
7	2.087367000	-1.283409000	-1.907801000
6	-0.943953000	-2.676885000	-0.859438000
7	2.034258000	0.000820000	0.093942000

6	-2.513472000	-2.477389000	-2.720669000
1	-1.708796000	-2.879284000	-3.330935000
1	-3.245649000	-3.260958000	-2.522555000
1	-2.990699000	-1.669601000	-3.267655000
6	-2.679341000	-0.948759000	-0.816729000
6	-4.064891000	-0.962338000	-0.906443000
1	-4.568017000	-1.732619000	-1.467118000
6	-4.788042000	-0.004322000	-0.218322000
1	-5.868458000	-0.005770000	-0.267105000
6	-0.723014000	0.781649000	-2.775489000
1	-1.406302000	1.406660000	-2.222602000
6	-0.808095000	0.674601000	-4.140300000
1	-1.567523000	1.222048000	-4.678415000
6	0.101893000	-0.156011000	-4.792526000
1	0.068163000	-0.270568000	-5.867466000
6	1.071727000	-0.812947000	-4.063973000
1	1.812977000	-1.414035000	-4.564615000
6	1.109930000	-0.652401000	-2.673365000
6	2.757167000	-2.448248000	-2.503948000
1	3.220605000	-3.020792000	-1.706016000
1	2.002917000	-3.068630000	-2.981066000
1	3.515187000	-2.170602000	-3.237038000
6	2.757518000	-0.634854000	-0.860409000
6	4.144801000	-0.662676000	-0.808231000
1	4.709745000	-1.152785000	-1.583556000
6	4.787972000	-0.002587000	0.223608000
1	5.868296000	-0.003842000	0.274444000
7	-0.098385000	2.056067000	0.014275000
6	0.875084000	2.781851000	-0.579995000
1	1.561680000	2.236408000	-1.207952000
7	-2.060215000	1.921840000	1.306970000
6	1.013300000	4.132749000	-0.386666000
1	1.818674000	4.667314000	-0.867918000
6	0.095908000	4.775182000	0.443405000

1	0.170352000	5.838793000	0.624908000
6	-0.932474000	4.053667000	1.013302000
1	-1.677116000	4.551217000	1.612609000
6	-1.023244000	2.678249000	0.766384000
6	-2.756418000	2.477486000	2.476310000
1	-2.011826000	2.883242000	3.156270000
1	-3.470400000	3.258121000	2.211314000
1	-3.278261000	1.668681000	2.979164000
6	-2.744312000	0.946349000	0.567197000
6	-4.132362000	0.955737000	0.531715000
1	-4.685600000	1.725377000	1.043662000
7	0.000431000	-0.100820000	2.054912000
7	1.901729000	1.285307000	2.091530000
6	-0.976292000	-0.780550000	2.696596000
1	-1.605736000	-1.405497000	2.082946000
6	-1.186603000	-0.673977000	4.047809000
1	-1.992107000	-1.221648000	4.513846000
6	-0.340684000	0.156668000	4.781231000
1	-0.472707000	0.270529000	5.848654000
6	0.691615000	0.814275000	4.145058000
1	1.383274000	1.415154000	4.712272000
6	0.857815000	0.654380000	2.763788000
6	2.514828000	2.449441000	2.747062000
1	3.051291000	3.021384000	1.995673000
1	1.720429000	3.071107000	3.151920000
1	3.201681000	2.170699000	3.546955000
6	2.666300000	0.634897000	1.111932000
6	4.052325000	0.659347000	1.190498000
1	4.543487000	1.148785000	2.015027000

[Cr(ddpd)(κ^2*N*-ddpd)]$^{3+}$:

24	10.575316000	13.219758000	5.444876000
7	9.220212000	14.762761000	5.390157000
6	9.283273000	15.709474000	6.356467000

1	10.150087000	15.685090000	6.995260000
7	8.176461000	13.847927000	3.481868000
6	8.302071000	16.648586000	6.539339000
1	8.392949000	17.371182000	7.335150000
7	10.462683000	13.169813000	3.403808000
6	7.205398000	16.632045000	5.680085000
1	6.407240000	17.351928000	5.791786000
7	12.048815000	14.581253000	5.458148000
6	7.156265000	15.709211000	4.656661000
1	6.338948000	15.720568000	3.956603000
7	13.006406000	13.587617000	7.362994000
6	8.196116000	14.785657000	4.515384000
7	10.662239000	13.214466000	7.499392000
6	6.874511000	13.588752000	2.838441000
1	6.585524000	14.380065000	2.148012000
1	6.124521000	13.493856000	3.617991000
1	6.938883000	12.647745000	2.302495000
6	9.322191000	13.509302000	2.745747000
6	9.260582000	13.513674000	1.359953000
1	8.355615000	13.807409000	0.857230000
6	10.392226000	13.188544000	0.636273000
1	10.364015000	13.193733000	-0.443937000
6	12.088153000	15.497462000	4.458418000
1	11.186191000	15.619465000	3.883774000
6	13.215683000	16.215393000	4.165872000
1	13.206837000	16.921170000	3.350464000
6	14.356459000	15.993509000	4.938185000
1	15.273101000	16.525051000	4.726354000
6	14.306116000	15.117285000	5.999437000
1	15.164310000	14.987612000	6.635296000
6	13.115502000	14.429016000	6.272061000
6	14.249115000	13.157131000	8.023011000
1	14.955376000	12.850784000	7.256497000
1	14.022792000	12.299703000	8.648061000

1	14.691056000	13.945184000	8.632460000
6	11.826603000	13.500241000	8.124646000
6	11.877589000	13.693169000	9.496360000
1	12.810314000	13.932566000	9.978012000
6	10.700580000	13.624996000	10.224853000
1	10.718484000	13.804201000	11.290519000
7	11.886052000	11.646787000	5.346574000
6	11.943383000	10.738103000	6.348745000
1	11.162092000	10.787138000	7.085504000
7	12.764419000	12.553811000	3.354761000
6	12.956274000	9.823745000	6.469374000
1	12.960744000	9.133470000	7.298420000
6	13.964130000	9.827998000	5.507002000
1	14.782842000	9.124979000	5.563613000
6	13.902166000	10.725262000	4.462388000
1	14.653200000	10.711065000	3.691328000
6	12.836740000	11.630271000	4.392884000
6	14.019521000	12.855486000	2.645789000
1	14.295945000	12.081518000	1.930607000
1	14.807487000	12.963889000	3.385144000
1	13.899161000	13.800306000	2.126328000
6	11.573672000	12.856574000	2.685439000
6	11.561146000	12.864331000	1.297222000
1	12.442459000	12.586171000	0.745964000
7	8.796380000	10.294477000	7.505101000
7	8.411884000	12.625492000	7.525155000
6	8.972676000	9.151339000	6.838390000
1	9.100185000	8.261078000	7.440872000
6	9.013496000	9.071229000	5.444998000
1	9.178490000	8.119840000	4.961749000
6	8.822385000	10.227041000	4.713206000
1	8.824058000	10.211241000	3.632354000
6	8.602258000	11.422602000	5.405207000
1	8.279979000	12.309550000	4.880093000

6	8.611536000	11.402789000	6.794056000
6	7.093843000	12.719608000	8.166048000
1	6.344597000	12.463533000	7.421857000
1	6.928875000	13.742152000	8.496018000
1	6.997735000	12.038272000	9.013741000
6	9.522676000	13.059206000	8.233240000
6	9.508013000	13.310528000	9.597654000
1	8.596922000	13.197415000	10.161198000

7. References

1 S. Otto, M. Grabolle, C. Förster, C. Kreitner, U. Resch-Genger and K. Heinze, *Angew. Chem. Int. Ed.*, 2015, **54**, 11572.
2 J. W. Emsley and L. Phillips, *Prog. Nucl. Magn. Reson. Spectrosc.,* 1971, **7**, 1.
3 F. Zinna, T. Bruhn, C. A. Guido, J. Ahrens, M. Bröring, L. Di Bari and G. Pescitelli, *Chem. Eur. J.*, 2016, **22**, 16089.
4 F. Zinna, L. Arrico and L. Di Bari, *Chem. Commun.*, 2019, **55**, 6607.
5 F. Neese, *WIREs Comput. Mol. Sci.*, 2012, **2**, 73.
6 A. D. Becke, *J. Chem. Phys.*, 1993, **98**, 5648.
7 C. Lee, W. Yang and R. G. Parr, *Phys. Rev. B*, 1988, **37**, 785.
8 B. Miehlich, A. Savin, H. Stoll and H. Preuss, *Chem. Phys. Lett.*, 1989, **157**, 200.
9 F. Neese, F. Wennmohs, A. Hansen and U. Becker, *Chem. Phys.*, 2009, **356**, 98.
10 R. Izsák and F. Neese, *J. Chem. Phys.*, 2011, **135**, 144105.
11 D. A. Pantazis, X.-Y. Chen, C. R. Landis and F. Neese, *J. Chem. Theory Comput.*, 2008, **4**, 908.
12 S. Sinnecker, A. Rajendran, A. Klamt, M. Diedenhofen and F. Neese, *J. Phys. Chem. A*, 2006, **110**, 2235.
13 S. Grimme, J. Antony, S. Ehrlich and H. Krieg, *J. Chem. Phys.*, 2010, **132**, 154104.
14 S. Grimme, S. Ehrlich and L. Goerigk, *J. Comput. Chem.*, 2011, **32**, 1456.
15 F. Weigend and R. Ahlrichs, *Phys. Chem. Chem. Phys.*, 2005, **7**, 3297.
16 F. Weigend, *Phys. Chem. Chem. Phys.*, 2006, **8**, 1057.
17 S. Smidstrup, A. Pedersen, K. Stokbro and H. Jónsson, *J. Chem. Phys.*, 2014, **140**, 214106.
18 J. Nocedal, *Math. Comp.*, 1980, **35**, 773.
19 S. Otto, J. P. Harris, K. Heinze and C. Reber, *Angew. Chem. Int. Ed.*, 2018, **57**, 11069.
20 J. Autschbach in *Comprehensive Inorganic Chemistry II*, 2nd ed. (Eds. J. Reedijk, K. Poeppelmeier), Elsevier, Amsterdam, 2013; pp. 407.
21 M. Srebro-Hooper and J. Autschbach, *Annu. Rev. Phys. Chem.*, 2017, **68**, 399.
22 G. Pescitelli and T. Bruhn, *Chirality*, 2016, **28**, 466.
23 M. Enamullah, A. Uddin, G. Pescitelli, R. Berardozzi, G. Makhloufi, V. Vasylyeva, A. C. Chamayou and C. Janiak, *Dalton Trans.*, 2014, **43**, 3313.
24 G. Pescitelli, S. Lüdeke, A.-C. Chamayou, M. Marolt, V. Justus, M. Górecki, L. Arrico, L. Di Bari, M. A. Islam, I. Gruber, M. Enamullah and C. Janiak, *Inorg. Chem.*, 2018, **57**, 13397.
25 Gaussian 16 (Revision A.03): M. J. Frisch, G. W. Trucks, H. B. Schlegel, G. E. Scuseria, M. A. Robb, J. R. Cheeseman, G. Scalmani, V. Barone, G. A. Petersson, H. Nakatsuji, X. Li, M. Caricato, A. V. Marenich, J. Bloino, B. G. Janesko, R. Gomperts, B. Mennucci, H. P. Hratchian, J. V. Ortiz, A. F. Izmaylov, J. L. Sonnenberg, D. Williams-Young, F. Ding, F. Lipparini, F. Egidi, J. Goings, B. Peng, A. Petrone, T. Henderson, D. Ranasinghe, V. G. Zakrzewski, J. Gao, N. Rega, G. Zheng, W. Liang, M. Hada, M. Ehara, K. Toyota, R. Fukuda, J. Hasegawa, M. Ishida, T. Nakajima, Y. Honda, O. Kitao, H. Nakai, T. Vreven, K. Throssell, J. A. Montgomery, Jr., J. E. Peralta, F. Ogliaro, M. J. Bearpark, J. J. Heyd, E. N. Brothers, K. N. Kudin, V. N. Staroverov, T. A. Keith, R. Kobayashi, J. Normand, K.

Raghavachari, A. P. Rendell, J. C. Burant, S. S. Iyengar, J. Tomasi, M. Cossi, J. M. Millam, M. Klene, C. Adamo, R. Cammi, J. W. Ochterski, R. L. Martin, K. Morokuma, O. Farkas, J. B. Foresman and D. J. Fox, Gaussian, Inc., Wallingford CT, 2016.
26 T. Bruhn, A. Schaumlöffel, Y. Hemberger and G. Bringmann, *Chirality*, 2013, **25**, 243.
27 T. Bruhn, A. Schaumlöffel, Y. Hemberger and G. Pescitelli, SpecDis (version 1.71), Berlin, Germany, 2017; Web: https://specdis-software.jimdo.com (last access: August 11, 2019).

Circularly Polarized Luminescence of Enantiopure Carboline-Based Europium Cryptates under Visible Light Excitation

Carolin Dee,[a] Francesco Zinna,[b] Elisabeth Kreidt,[a] Lorenzo Arrico,[b] Aurora Rodríguez-Rodríguez,[c] Carlos Platas-Iglesias,[c,*] Lorenzo Di Bari,[b,*] Michael Seitz[a,*]

[a] University of Tübingen, Institute of Inorganic Chemistry, Auf der Morgenstelle 18, 72076 Tübingen, Germany, E-mail: michael.seitz@uni-tuebingen.de

[b] Dipartimento di Chimica e Chimica Industriale, Università di Pisa, Via Moruzzi 13, 56124 Pisa, Italy, E-mail: dibari@unipi.it

[c] Centro de Investigacións Científicas Avanzadas (CICA) and Departamento de Química, Universidade da Coruña, Campus da Zapateira-Rúa da Fraga 10, 15008 A Coruña, Spain, E-mail: carlos.platas.iglesias@udc.es

Abstract

The enantiomers of carboline-based cryptates were successfully resolved by chiral HPLC. These complexes show high configurational stability under harsh condition and their absolute configuration was determined comparing theoretical and experimental electronic circular dichroism spectra. The enantiopure cryptates exhibit strong circularly polarized luminescence with a maximum dissymmetry factor g_{lum} = 0.25 for the f-f transition $^5D_0 \rightarrow {}^7F_1$ (λ = 594 nm) under visible light excitation at λ_{exc} = 400 nm.

Keywords

Molecular lanthanoid complexes
Lanthanoid luminescence
Chirality
Circularly polarized luminescence (CPL)
Carboline
Cryptates

1. Introduction

Circularly polarized luminescence (CPL)[1-3] based on molecular lanthanoid(III) complexes[4-8] is one of the emerging topics in photophysics, particularly driven by the renewed interest in the various areas such as bioimaging[9-12] and for the development of organic light emitting diodes (OLEDs).[13-15] CPL is for luminescence what circular dichroism (CD) is for the absorption of light, namely the differential emission (CPL) or absorption (CD) of right and left circularly polarized light (i.e. two "enantiomeric" forms of light). The quantitative expression for the "enantioenrichment" in the emitted CPL is the so-called luminescence dissymmetry factor g_{lum} (depending on the wavelength λ) which is defined as:

$$g_{lum}(\lambda) = 2\frac{I_L(\lambda) - I_R(\lambda)}{I_L(\lambda) + I_R(\lambda)}; \qquad [-2 < g_{lum} < +2]$$

with I_L and I_R as the intensities of left- and right-circularly polarized light, respectively.

Taking into account the spectroscopic selection rules governing CPL,[16] one can expect the largest values for g_{lum} for electronic transitions which are electric dipole forbidden but magnetic dipole allowed. Purely organic CPL emitters do not easily satisfy these conditions and therefore only give relatively small values for g_{lum} in the range of ca. 10^{-4} to 10^{-2}.[17-18] Recently, it has been shown that the phosphorescence band $^2E/^2T \rightarrow {}^4A$ in octahedral chromium(III) complexes can give considerable dissymmetry factors of up to $|g_{lum}| = 0.2$.[19-20] The best candidates for this purpose, however, are trivalent lanthanoids and the corresponding *f-f* emission bands are highly suitable for the generation of high g_{lum} values[2] (typically $g_{lum} > 10^{-1}$), with the best system reaching $g_{lum} = 1.38$ in solution.[21-23] One of the most popular lanthanoids in this context is europium which has multiple emission bands in the yellow to red region of the visible spectrum. Especially the $^5D_0 \rightarrow {}^7F_1$ band, which is parity- and spin-forbidden but magnetic-dipole allowed, can be expected to exhibit sizeable g_{lum} values. This circumstance has been used in many successful europium complexes over the last years.[21-37] For many important applications (e.g. confocal luminescence microscopy), a severe drawback of many known europium luminophores is the short excitation wavelength (e.g. $\lambda_{exc} < 320$ nm) usually required, because this can lead to problems associated with photodamage to the samples (e.g. phototoxicity in living cells) or to the necessity for expensive and uncommon quartz components in the

optical devices used. This issue has been solved for europium luminophores with long-wavelength excitation only in a relatively small number of cases[38-44] and is even less common for europium CPL emitters.[25,33,34] In this context, we have recently introduced *2,2'*-bipyridine-*N,N'*-dioxide-based lanthanoid cryptates initially developed by Lehn[45-46] that have provided partial solutions to the aspects mentioned above (Figure 1). In particular, we have developed racemic europium cryptates **rac-1-Eu**[47] based on carboline antenna moieties with the possibility for long-wavelength excitation well above 400 nm, we have demonstrated for the lutetium cryptate **(*R*$_a$)-2-Lu**[48] that cryptates of this type can be resolved by chiral HPLC methods from the corresponding racemates, and that the europium cryptate **(*R,R,R*$_a$)-3-Eu**,[49-50] which can be prepared enantioselectively, shows considerable europium CPL activity with dissymmetry values of $|g_{lum}| \leq 0.19$.

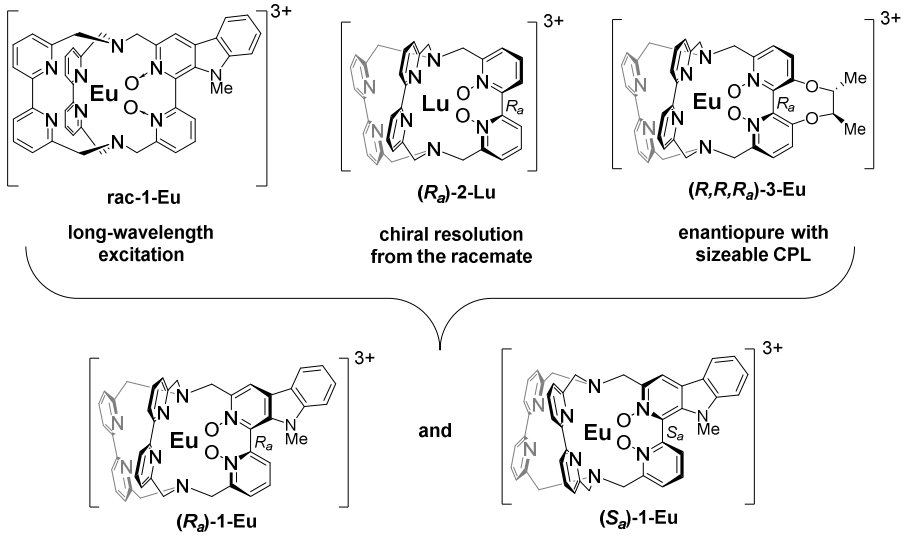

Figure 1. Combination of several beneficial aspects of known *2,2'*-bipyridine-*N,N'*-dioxide-based cryptates **rac-1-Eu**,[47] **(*R*$_a$)-2-Lu**,[48] and **(*R,R,R*$_a$)-3-Eu**[49-50] into the new europium CPL emitters **(*R*$_a$)-1-Eu** and **(*S*$_a$)-1-Eu** reported in this study.

In the present study, we report that these aspects can also be combined into the europium CPL emitters **(*R*$_a$)-1-Eu** and **(*S*$_a$)-1-Eu**. We will show that these new enantiopure complexes can be cleanly obtained by chiral HPLC and that they provide very high configurational stability under challenging conditions. In addition, we will elucidate the absolute configuration of the two enantiomers by computational analysis of the CD spectra. Finally, we will demonstrate that these species provide very high CPL activity in methanolic solution.

2 Results and Discussions

2.1 Synthesis / Chiral Resolution

In order to obtain the target complexes **(R_a)-1-Eu** and **(S_a)-1-Eu**, the chiral resolution started from the previously reported racemic material **rac-1-Eu** (Scheme 1).[47]

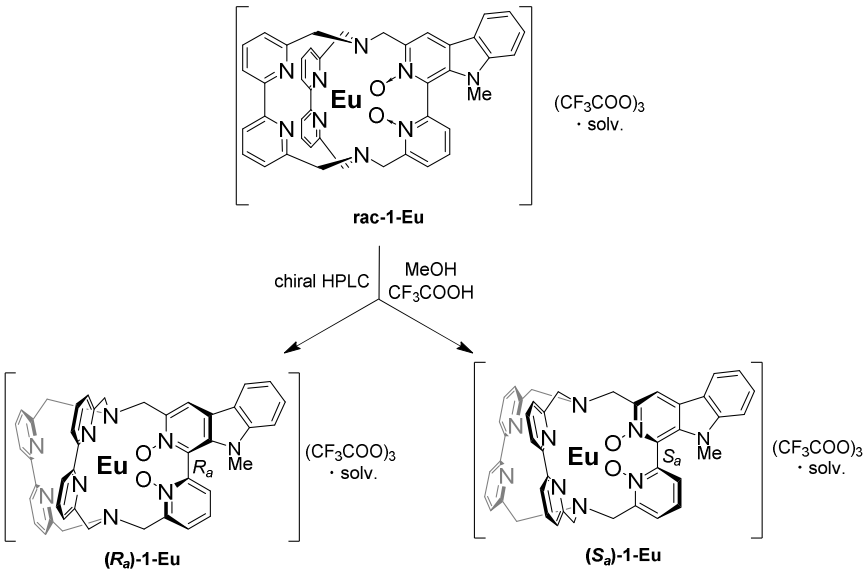

Scheme 1. Chiral resolution of the racemic carboline cryptate **rac-1-Eu**.

The resolution by chiral HPLC proved to be much more difficult than the one optimized for the related cryptate **(R_a)-2-Lu**.[48] Screening of several different conditions did not provide baseline-separated HPLC peaks (Figure 2) for the two enantiomeric complexes even when using the most optimized protocol (stationary phase: CHIRALPAK IE, eluent: isocratic CH_3OH + 0.5 vol.-% CF_3COOH). Careful collection of the fractions in the preparative HPLC separations, however, gave enantiopure materials and the chiral, analytical HPLC traces for the preparatively resolved enantiomers **(R_a)-1-Eu** and **(S_a)-1-Eu** showed no contamination with the other enantiomer (Figure 2, B and C). The chemical purity of the separated enantiomers was confirmed by ^{1}H NMR spectra in CD_3OD (Figure 3) yielding in each case well-resolved sets of resonances consistent with one single species in solution. As expected, the NMR spectra of both enantiomers are virtually identical with each other and also with the racemic starting material.

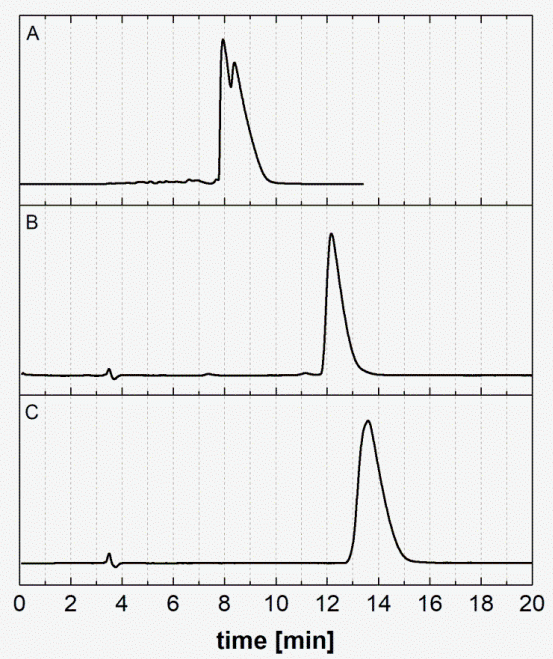

Figure 2. HPLC traces for the chiral HPLC runs (CHIRALPAK IE, MeOH + 0.5 vol.% CF_3COOH) of **rac-1-Eu** (A), **(*R*$_a$)-1-Eu** (B), and **(*S*$_a$)-1-Eu** (C) – For the assignment of the absolute stereochemistry see the text (Remark: The differences in retention times in A vs. B and C is due to the use of a preparative column in A and a smaller, analytical column of the same type in B and C).

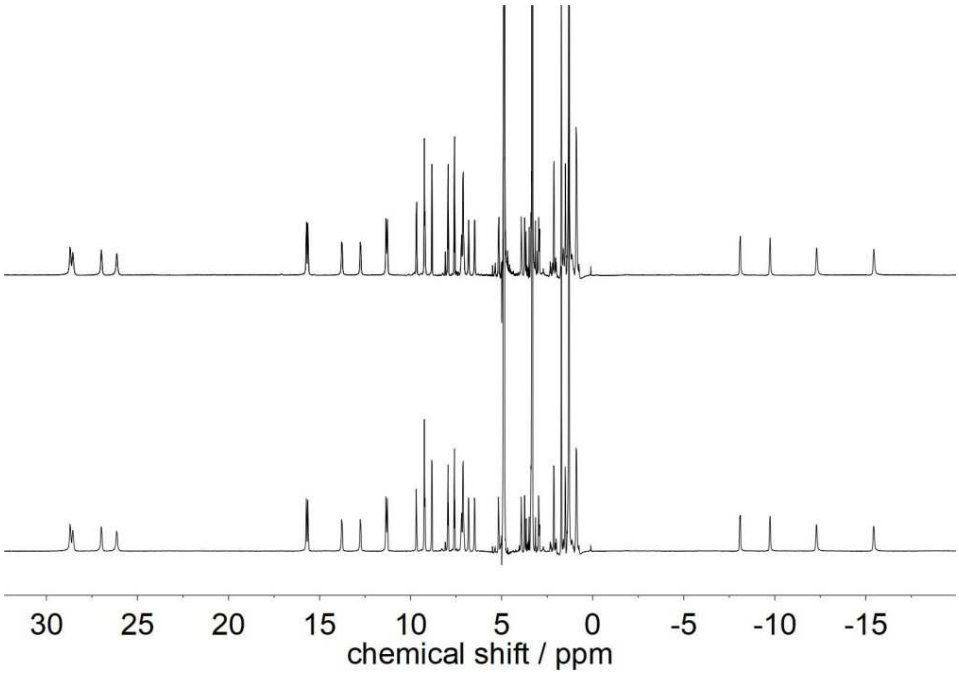

Figure 3. ^{1}H NMR spectra (400 MHz, CD_3OD) of **(*R*$_a$)-1-Eu** (bottom) and **(*S*$_a$)-1-Eu** (top).

2.2 Configurational Stability

The configurational stability of the resolved enantiomers was tested with **(*R*$_a$)-1-Eu** under conditions usually leading to decomplexation of lanthanoid chelates. For this purpose, solutions of **(*R*$_a$)-1-Eu** were prepared in neat CF_3COOH and stirred at room temperature. After 5 days, no chemical decomposition or any sign of racemization could be detected by chiral HPLC (Figure 4). In this respect, the enantiopure carboline cryptates behave very similarly to the related parent cryptate **(*R*$_a$)-2-Lu**.[48]

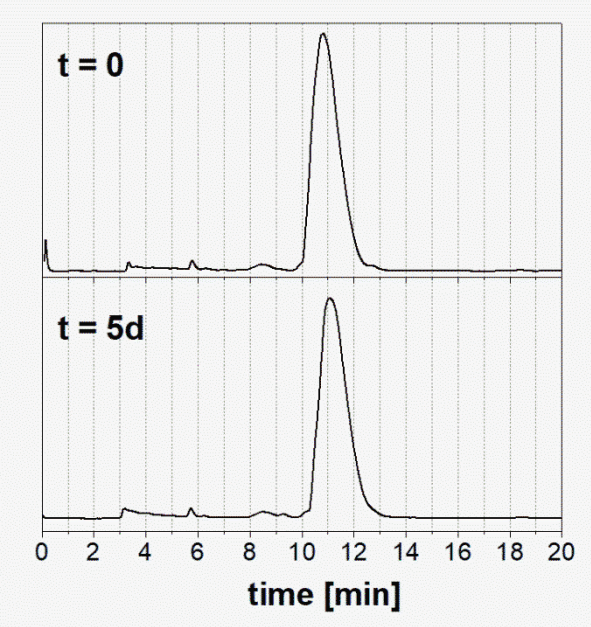

Figure 4. Configurational stability tests for enantiopure **(*R*$_a$)-1-Eu** in neat CF_3COOH – Chiral HPLC traces at the start of the experiment (top) and after five days (bottom) showing no deterioration of enantiopurity and/or chemical decomposition.

UV/vis Absorption and Electronic Circular Dichroism (ECD) Spectra

All photophysical studies were performed in CD_3OD solutions in order to have a consistent set of data and in order to achieve maximum signal intensities in the luminescence and CPL measurements (see below). The recorded UV/vis absorption spectra of the enantiopure carboline cryptates **(*R*$_a$)-1-Eu** and **(*S*$_a$)-1-Eu** are indistinguishable from each other and, similar to the parent racemate **rac-1-Eu**, show the desired long-wavelength absorption bands centered around ca. 350 nm and ca. 400 nm (Figure 5, bottom). These spectral features are also reflected in the corresponding ECD spectra (Figure 5, top). The pattern observed for **(*R*$_a$)-1-Eu** and **(*S*$_a$)-1-Eu** are mirror-images of each other and exhibit several strong CD bands below 340 nm, as well as two bands above 340 nm.

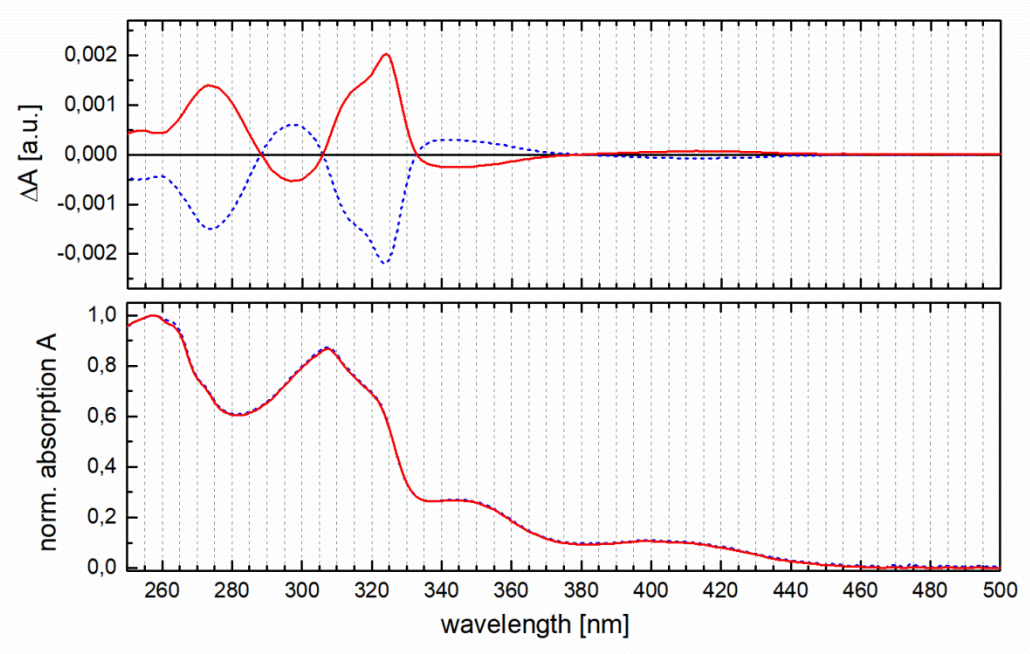

Figure 5. UV/vis absorption (bottom) and CD (top) spectra of **(*R*$_a$)-1-Eu** (dashed line) and **(*S*$_a$)-1-Eu** (solid line) in CD_3OD.

2.3 Structural Elucidation

The assignment of the absolute stereochemistry to the different enantiomers was achieved by comparing experimental and theoretical (TDDFT) ECD spectra. The geometries of the europium complexes were optimized by DFT methods including solvent effects in MeOH (see the section Materials and Methods for details). The cryptates were modelled with one inner-sphere methanol molecule because in the previous studies on the racemic parent compound **rac-1-Eu** one inner-sphere water molecule (q = 1) was found in aqueous solution via luminescence lifetime measurements in H_2O and D_2O.[47] The obtained geometries are shown in Figure 6 and do not display any unusual structural features compared to other, related lanthanoid cryptates. The calculated ECD spectra based on the ground state geometries are generally in good agreement with the experimental spectra in CD_3OD (Figure 7) and allowed the assignment of the stereochemical descriptor R_a for the first eluted HPLC peak (see Figure 2) and consequently S_a for the second.

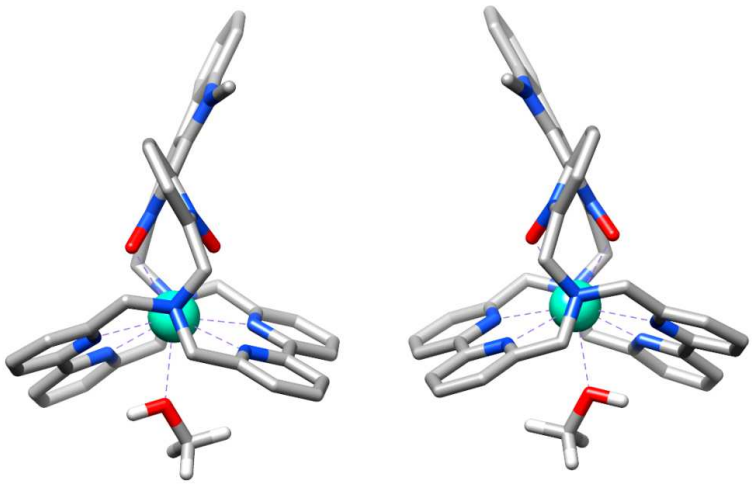

Figure 6. Geometry-optimized ground state structures (DFT) for **(*S*$_a$)-1-Eu** (left) and **(*R*$_a$)-1-Eu** (right) with one inner-sphere methanol molecule each (see the section Materials and Methods for details).

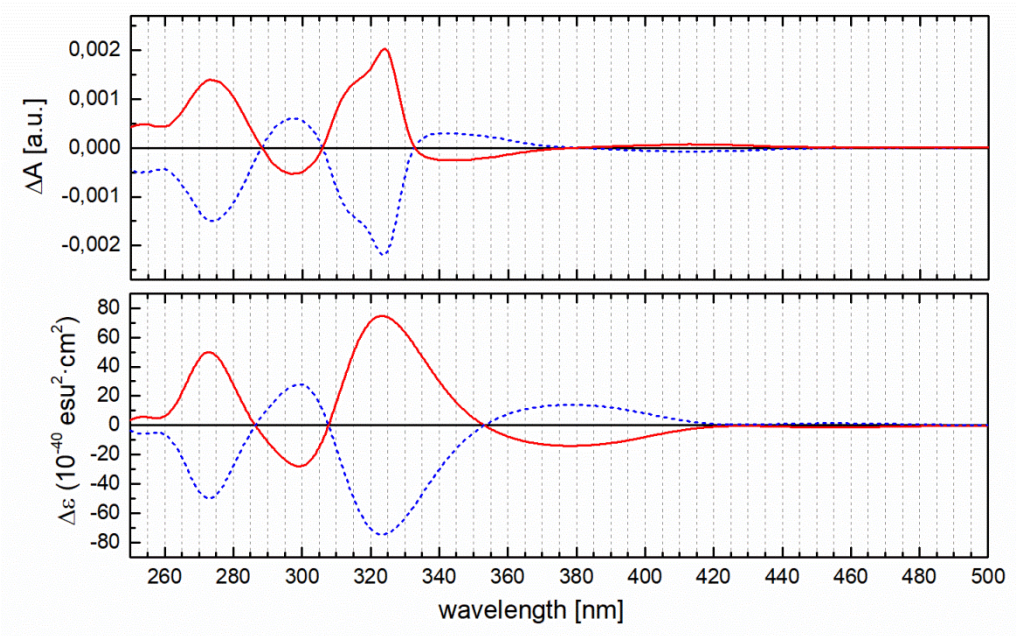

Figure 7. Experimental (top) and calculated (bottom) CD spectra of **(*R*$_a$)-1-Eu** (dashed line) and **(*S*$_a$)-1-Eu** (solid line) in CD_3OD.

2.4 Luminescence and CPL Spectra

The luminescence and CPL spectra of **(*R*$_a$)-1-Eu** and **(*S*$_a$)-1-Eu** were measured in CD_3OD. As outlined in the introduction, the extended carboline-based π-system of the cryptates permits the sensitization of europium luminescence at rather long excitation wavelengths (see the UV/vis absorption spectra in Figure 5). Therefore,

excitation could very conveniently be achieved here using a cost-effective blue LED with a peak output around ca. 400 nm. The luminescence spectra of both enantiomers are virtually identical (Figure 8, bottom) and show the usual europium emission bands $^5D_0 \rightarrow ^7F_J$ (with J = 0,1,2,3,4). Overall, the spectra are also very similar to the emission bands of the racemic material.[47] The CPL spectra of **(*R*$_a$)-1-Eu** and **(*S*$_a$)-1-Eu** are mirror-images of each other and show two major CPL bands with clearly visible substructures for $^5D_0 \rightarrow ^7F_1$ ($\lambda \approx 590$ nm) and the hypersensitive band $^5D_0 \rightarrow ^7F_2$ ($\lambda \approx 615$ nm) with opposite signs for the two enantiomers (Figure 8). As expected from the selection rules governing CPL transitions,[16] the magnetic-dipole transition $^5D_0 \rightarrow ^7F_1$ shows the strongest CPL activity with dissymmetry factors as high as $|g_{lum}| = 0.25$. This magnitude of g_{lum} is a clear improvement relative to the previously reported, enantiopure europium cryptate **(*R,R,R*$_a$)-3-Eu** ($|g_{lum}| \leq 0.19$)[49] and also compares well with other, highly CPL-active europium luminophores reported in the literature.[24-37]

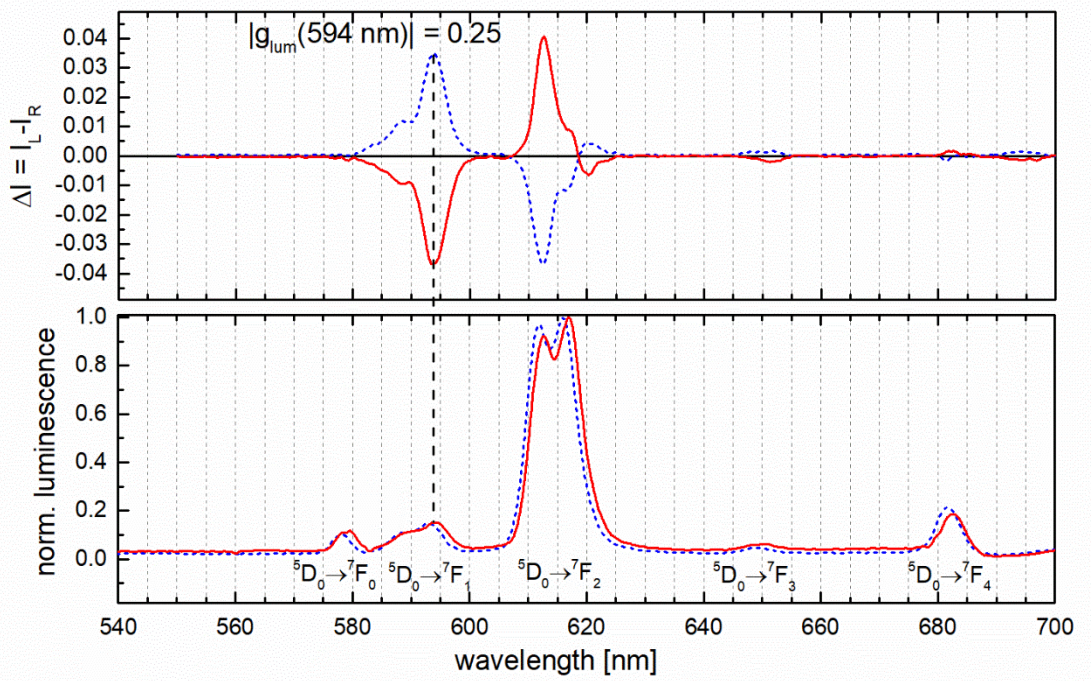

Figure 8. CPL (top) and normalized luminescence spectrum (bottom) of **(*R*$_a$)-1-Eu** (dashed line) and **(*S*$_a$)-1-Eu** (solid line) in CD_3OD (λ_{exc} = 400 nm) – Highest g_{lum} value indicated for the emission band $^5D_0 \rightarrow ^7F_1$ (594 nm).

3. Conclusions

With the cryptates **(R_a)-1-Eu** and **(S_a)-1-Eu** based on carboline-antennae, we have realized new and promising europium CPL emitters. These new molecular materials can conveniently be prepared in both enantiomeric forms by chiral resolution using chromatographic techniques, show excellent configurational stability in solution, advantageously can be excited in the long-wavelength region up to λ_{exc} = 400 nm, and finally exhibit sizeable CPL activities as expressed by high g_{lum} values of up to 0.25.

4. Materials and Methods

NMR spectra were recorded on a Bruker AVII+400 spectrometer (^{1}H: 400.1 MHz) using CD_3OD (≥ 99.8% D) as the solvent. The racemic lanthanoid cryptates were synthesized as described previously.[47]

Enantiopure Cryptates / Chiral Resolution of rac-1-Eu

All chiral HPLC runs of the racemic or enantiopure europium cryptates were performed on a Knauer Azura HPLC system (UV detection at λ = 300 nm), equipped with a CHIRALPAK IE column (Daicel, particle size: 5 μm, internal diameter: 4.6 mm, column length: 150 mm, flow rate: 1.0 mL/min) for analytical runs and an analogous CHIRALPAK IE column (Daicel, particle size: 5 μm, internal diameter: 10.0 mm, column length: 150 mm, flow rate: 4 mL/min) for preparative runs. In both cases, the mobile phase was HPLC-grade MeOH with additional 0.5 vol.-% CF_3COOH. All samples were prepared using HPLC-grade MeOH and filtered with a membrane filter (nylon, 0.45 μm pore size, 13 mm diameter) in a stainless steel filter holder prior to injection. For the separation of the racemic cryptates, samples with a concentration of 3 mg/mL were used, which was found to be the optimal compromise between separation and time efficiency. The solution was subjected to chiral HPLC in portions of 100 μL. The collected fractions of the respective enantiomers were combined and the solvents were removed in vacuo at room temperature. After drying, samples of the enantiomers were redissolved in MeOH (HPLC-grade), filtered (see above) and injected to verify the enantiopurity.

Notes: The separation efficiency and the relative and absolute retention of the two enantiomers are dependent on the concentration of the analyte. Special care has to be taken that only freshly prepared MeOH/CF_3COOH mobile phases are used. The

range of the fractions which were collected varies with the quality of the separation to obtain pure separated enantiomers.

(R_a)-1-Eu

^{1}H NMR (400 MHz, CD_3OD): δ = 28.71 (br s, 1 H), 28.55 (br s, 1 H), 26.99 (br s, 1 H), 26.14 (br s, 1 H), 15.72 (d, *J* = 6.8 Hz, 1 H), 15.63 (d, *J* = 6.9 Hz, 1 H), 13.77 (d, *J* = 10.2 Hz, 1 H), 12.75 (d, *J* = 10.1 Hz, 1 H), 11.35 (br, 1 H), 11.28 (br, 1 H), 9.68 (d, *J* = 7.5 Hz, 1 H), 9.24 (s, 1 H), 9.20 (d, *J* = 7.1 Hz, 1 H), 8.83 (d, *J* = 8.0 Hz, 1 H), 7.94 (t, *J* = 7.6 Hz, 1 H), 7.59 (t, *J* = 7.7 Hz, 1 H), 7.20 (br, 1 H), 7.12 (d, *J* = 8.0 Hz, 1 H), 7.07 (br, 1 H), 6.82 (d, *J* = 6.6 Hz, 1 H), 6.48 (d, *J* = 6.6 Hz, 1 H), 5.16 (d, *J* = 6.6 Hz, 1 H), 3.92 (t, *J* = 6.5 Hz, 1 H), 3.74 (d, *J* = 6.5 Hz, 1 H), 2.96 (d, *J* = 6.6 Hz, 1 H), 2.13 (d, *J* = 7.5 Hz, 1 H), 1.72 (s, 3 H), 1.50 (d, *J* = 7.6 Hz, 1 H), -8.10 (d, *J* = 10.3 Hz, 1 H), -9.74 (d, *J* = 9.8 Hz, 1 H), -12.29 (d, *J* = 8.8 Hz, 1 H), -15.44 (br, 1 H) ppm.

(S_a)-1-Eu

^{1}H NMR (400 MHz, CD_3OD): δ = 28.70 (br s, 1 H), 28.55 (br s, 1 H), 26.99 (br s, 1 H), 26.14 (br s, 1 H), 15.72 (d, *J* = 6.3 Hz, 1 H), 15.63 (d, *J* = 6.2 Hz, 1 H), 13.77 (d, *J* = 10.2 Hz, 1 H), 12.75 (d, *J* = 9.0 Hz, 1 H), 11.35 (br, 1 H), 11.28 (br, 1 H), 9.68 (d, *J* = 7.6 Hz, 1 H), 9.25 (s, 1 H), 9.21 (s, 1 H), 8.83 (d, *J* = 8.0 Hz, 1 H), 7.94 (t, *J* = 7.7 Hz, 1 H), 7.59 (t, *J* = 7.7 Hz, 1 H), 7.20 (br, 1 H), 7.12 (d, *J* = 8.1 Hz, 1 H), 7.08 (br, 1 H), 6.82 (d, *J* = 6.0 Hz, 1 H), 6.48 (d, *J* = 6.3 Hz, 1 H), 5.16 (d, *J* = 6.5 Hz, 1 H), 3.92 (br, 1 H), 3.73 (d, *J* = 6.4 Hz, 1 H), 2.95 (d, *J* = 6.4 Hz, 1 H), 2.13 (d, *J* = 7.6 Hz, 1 H), 1.72 (s, 3H), 1.51 (d, *J* = 7.6 Hz, 1 H), -8.11 (br, 1 H), -9.75 (br, 1 H), -12.31 (br, 1 H), -15.43 (br, 1 H) ppm.

ECD and CPL Spectroscopy

The ECD spectra were recorded with a Jasco J-715 spectropolarimeter on 0.8 mM solutions in CD_3OD. The spectra were baseline corrected by subtracting the trace of the solvent. CPL spectra were measured with a home-made spectrofluoropolarimeter.[15] The spectra were acquired on the same solutions in CD_3OD under 400 nm irradiation from a LED source, with 4 sec integration time and 4 accumulations.

Computational Studies

Geometry optimizations of the complexes **(R_a)-1-Eu** and **(S_a)-1-Eu** were performed within the framework of DFT with the hybrid meta-GGA functional TPSSh[52] and the

Gaussian09 program package.[53] Following previous studies,[54] the basis set used for structure optimizations comprised the large-core quasi-relativistic effective core potential (LCRECP) of Dolg for Eu, which includes the 46+4f^6 electrons of Eu^{3+} in the core, and the (7s6p5d)/[5s4p3d]-GTO valence basis set to describe the valence space.[55] The standard 6-31G(d,p) basis set was used for all ligand atoms. Geometry optimizations were followed by frequency analysis to confirm the nature of the calculated structures as true energy minima. Time-dependent density functional theory (TDDFT)[56-58] was used for the calculation of the 100 lowest energy singlet-singlet electronic transitions. It has been shown that, while TDDFT calculations are relatively insensitive to the size of the basis set, the inclusion of diffuse functions improves significantly the quality of the results.[59-60] Given the relatively high computational cost of the TDDFT calculations involving up to 100 excited states, we used the 6-31+G(d) basis set to compute ECD spectra. The experimental and calculated spectra were compared using Gaussian convolution with GaussView 6.0.[61] The half-width at half-maximum was adjusted to best mimic the experimental spectra, and finally set to 0.15 eV for the enantiomeric europium complexes. This value is within the common range used for the computational simulation of ECD spectra (0.1 – 0.3 eV).[62] Since all calculations included the $4f^6$ electrons of Eu in the core, they were conducted in a pseudo-singlet configuration. Bulk solvent effects (methanol) were considered throughout by using the integral equation formalism variant of the polarizable continuum model (IEFPCM),[63] employing the universal force field radii (UFF)[64] scaled by a factor of 1.1, to define the solute cavities. All calculations were performed using the default SCF energy convergence threshold (10^{-8} a. u.), while the integration grid was set to 99 radial shells and 590 angular points using the ultrafinegrid command in g09.

Acknowledgements

This work was financially supported by the German Research Foundation (DFG, research grant SE1448/7-1 for M. S.), the German Academic Scholarship Foundation (Studienstiftung des deutsches Volkes, predoctoral fellowship for E. K.), C. P.-I. and A. R.-R. thank Centro de Supercomputación de Galicia (CESGA) for providing access to supercomputing facilities.

References

[1] Riehl J P, Muller G. Circularly Polarized Luminescence Spectroscopy and Emission-Detected Circular Dichroism. In *Comprehensive Chiroptical Spectroscopy*, *Vol. 1*. Edited by Berova N, Polavarapu P L, Nakanishi K, Woody R W. Hoboken: John Wiley Sons, 2012. 65.

[2] Longhi G, Castiglioni E, Koshoubu J, Mazzeo G, Abbate S. Circularly Polarized Luminescence: A Review of Experimental and Theoretical Aspects. Chirality, 2016, 28: 696.

[3] Riehl J P, Richardson F S. Circularly Polarized Luminescence Spectroscopy. Chem. Rev., 1986, 86: 1.

[4] Carr R, Evans N H, Parker D. Lanthanide complexes as chiral probes exploiting circularly polarized luminescence. Chem. Soc. Rev., 2012, 41: 7673.

[5] Zinna F, Di Bari L. Lanthanide Circularly Polarized Luminescence: Bases and Applications. Chirality, 2015, 27: 1.

[6] Muller G. Circularly Polarised Luminescence**.** In *Luminescence of Lanthanide Ions in Coordination Compounds and Nanomaterials*. Edited by de Bettencourt-Dias A. Hoboken: John Wiley & Sons, 2014. 77.

[7] Brittain H G. Circularly polarized luminescence studies of chiral lanthanide complexes. J. Coord. Chem., 1989, 20: 331.

[8] Muller G. Luminescent chiral lanthanide(III) complexes as potential molecular probes. Dalton Trans, 2009, 9692.

[9] Staszak K, Wieszczycka K, Marturano V, Tylkowski B. Lanthanides complexes - Chiral sensing of biomolecules. Coord. Chem. Rev., 2019, 397: 76.

[10] Frawley A T, Linford H V, Starck M, Pal R, Parker D. Enantioselective cellular localisation of europium(iii) coordination complexes. Chem Sci., 2018, 9: 1042.

[11] Frawley A T, Pal R, Parker D. Very bright, enantiopure europium(III) complexes allow time-gated chiral contrast imaging. Chem. Commun., 2016, 52: 13349.

[12] Bünzli J-C G. Lanthanide light for biology and medical diagnosis. J.Lumin., 2016, 170: 866.

[13] Zinna F, Giovanella U, Di Bari L. Highly Circularly Polarized Electroluminescence from a Chiral Europium Complex. Adv. Mater., 2015, 27: 1791.

[14] Brandt J R, Wang X, Yang Y, Campbell A J, Fuchter M J. Circularly Polarized Phosphorescent Electroluminescence with a High Dissymmetry Factor from PHOLEDs Based on a Platinahelicene. J. Am. Chem. Soc., 2016, 138: 9743.

[15] Zinna F, Pasini M, Galeotti F, Botta C, Di Bari L, Giovanella U. Design of Lanthanide-Based OLEDs with Remarkable Circularly Polarized Electroluminescence. Adv. Funct. Mater., 2017, 27: 1603719.

[16] Richardson F S. Selection rules for lanthanide optical activity. Inorg. Chem., 1980, 19: 2806.

[17] Kumar J, Nakashima T, Kawai T. Circularly Polarized Luminescence in Chiral Molecules and Supramolecular Assemblies. J. Phys. Chem. Lett., 2015, 6: 3445.

[18] Sánchez-Carnerero E M, Agarrabeitia A R, Moreno F, Maroto B L, Muller G, Ortiz M J, de la Moya S. Circularly Polarized Luminescence from Simple Organic Molecules. Chem. Eur. J., 2015, 21: 13488.

[19] Jiménez J R, Doistau B, Cruz C M, Besnard C, Cuerva J M, Campaña A G, Piguet C. Chiral Molecular Ruby $[Cr(dqp)_2]^{3+}$ with Long-Lived Circularly Polarized Luminescence. J. Am. Chem. Soc., 2019, 141: 13244.

[20] Dee C, Zinna F, Kitzmann W R, Pescitelli G, Heinze K, Di Bari L, Seitz M. Strong Circularly Polarized Luminescence of an Octahedral Chromium(III) Complex. Chem. Comm., 2019, 55: 13078.

[21] Lunkley J L, Shirotani D, Yamanari K, Kaizaki S, Muller G. Extraordinary Circularly Polarized Luminescence Activity Exhibited by Cesium Tetrakis(3-heptafluoro-butylryl-(+)-camphorato) Eu(III) Complexes in EtOH and $CHCl_3$ Solutions. J. Am. Chem. Soc., 2008, 130: 13814.

[22] Lunkley J L, Shirotani D, Yamanari K, Kaizaki S, Muller G. Chiroptical Spectra of a Series of Tetrakis((+)-3-heptafluorobutylyrylcamphorato)lanthanide(III) with an Encapsulated Alkali Metal Ion: Circularly Polarized Luminescence and Absolute Chiral Structures for the Eu(III) and Sm(III) Complexes. Inorg. Chem., 2011, 50: 12724.

[23] Di Pietro S, Di Bari L. The Structure of $MLn(hfbc)_4$ and a Key to High Circularly Polarized Luminescence. Inorg. Chem., 2012, 51: 12007.

[24] Dai L, Zhang J, Chen Y, MacKenzie L E, Pal R, Law, G-L. Synthesis of Water-Soluble Chiral DOTA Lanthanide Complexes with Predominantly Twisted Square Antiprism Isomers and Circularly Polarized Luminescence. Inorg. Chem., 2019, 58: 12506.

[25] Starck M, MacKenzie L E, Batsanov A S, Parker D, Pal R. Excitation modulation of Eu:BPEPC based complexes as low-energy reference standards for circularly polarised luminescence (CPL). Chem. Commun., 2019, 55: 14115.

[26] Kotova O, Comby S, Pandurangan K, Stomeo F, O'Brien J E, Feeney M, Peacock R D, McCoy C P, Gunnlaugsson T. The effect of the linker size in C_2-symmetrical chiral ligands on the self-assembly formation of luminescent triple-stranded di-metallic Eu(III) helicates in solution. Dalton Trans., 2018, 47: 12308.

[27] Okayasu Y, Yuasa J. Evaluation of circularly polarized luminescence in a chiral lanthanide ensemble. Mol. Syst. Des. Eng., 2018, 3: 66.

[28] Armelao L, Belli Dell'Amico D, Bellucci L, Bottaro G, Di Bari L, Labella L, Marchetti F, Samaritani S, Zinna F. Circularly Polarized Luminescence of Silica-Grafted Europium Chiral Derivatives Prepared through a Sequential Functionalization. Inorg. Chem., 2017, 56: 7010.

[29] Casanovas B, Zinna F, Di Bari L, Salah El Fallah M, Font-Bardía M, Vicente R. Circularly polarized luminescence on dinuclear Tb(III) and Eu(III) complexes with (S-) and (R-) 2-phenylpropionate. Dalton Trans., 2017, 46: 6349.

[30] Kono Y, Hara N, Shizuma M, Fujiki M, Imai Y. Complexes of $Eu(III)(hfa)_3$ with a planar chiral P(III) ligand (Phanephos): solvent-sensitive sign inversion of circularly polarized luminescence. Dalton Trans., 2017, 46: 5170.

[31] Leonzio M, Melchior A, Faura G, Tolazzi M, Zinna F, Di Bari L, Piccinelli F. Strongly Circularly Polarized Emission from Water-Soluble Eu(III)- and Tb(III)-Based Complexes: A Structural and Spectroscopic Study. Inorg. Chem., 2017, 56: 4413.

[32] Neil E R, Fox M A, Pal R, Parker D. Induced europium CPL for the selective signaling of phosphorylated amino acids and O-phosphorylated hexapeptides. Dalton Trans., 2016, 45: 8355.

[33] Dai L, Lo W-S, Coates I D, Pal R, Law G-L. New Class of Bright and Highly Stable Chiral Cyclen Europium Complexes for Circularly Polarized Luminescence Applications. Inorg. Chem., 2016, 55: 9065.

[34] Zinna F, Resta C, Abbate S, Castiglioni E, Longhi G, Mineo P, Di Bari L. Circularly polarized luminescence under near-UV excitation and structural elucidation of a Eu complex. Chem. Commun., 2015, 51: 11903.

[35] Evans N H, Carr R, Delbianco M, Pal R, Yufit D S, Parker D. Complete stereocontrol in the synthesis of macrocyclic lanthanide complexes: direct formation of enantiopure systems for circularly polarised luminescence applications. Dalton Trans. 2013, 42: 15610.

[36] Seitz M, Do K, Ingram A J, Moore E G, Muller G, Raymond K N. Circularly Polarized Luminescence in Enantiopure Europium and Terbium Complexes with Modular, All-Oxygen Donor Ligands. Inorg. Chem., 2009, 48: 8469.

[37] Bonsall S D, Houcheime M, Straus D A, Muller G. Optical isomers of N,N'-bis(1-phenylethyl)-2,6-pyridinedicarboxamide coordinated to europium(III) ions as reliable circularly polarized luminescence calibration standards. Chem. Commun., 2007, 35: 3676.

[38] Routledge J D, Jones M W, Faulkner S, Tropiano M. Kinetically Stable Lanthanide Complexes Displaying Exceptionally High Quantum Yields upon Long-Wavelength Excitation: Synthesis, Photophysical Properties, and Solution Speciation. Inorg. Chem., 2015, 54: 3337.

[39] Butler S J, Delbianco M, Lamarque L, McMahon B K, Neil E R, Pal R, Parker D, Walton J W, Zwier J M. EuroTracker dyes: design, synthesis, structure and photophysical properties of very bright europium complexes and their use in bioassays and cellular optical imaging. Dalton Trans., 2015, 44: 4791.

[40] Deiters E, Song B, Chauvin A-S, Vandevyver C D B, Gumy F, Bünzli J-C G. Luminescent Bimetallic Lanthanide Bioprobes for Cellular Imaging with Excitation in the Visible-Light Range. Chem. Eur. J., 2009, 15: 885.

[41] Pal R, Parker D. A single component ratiometric pH probe with long wavelength excitation of europium emission. Chem. Commun., 2007, 474.

[42] Yang C, Fu L-M, Wang Y, Zhang J-P, Wong W-T, Ai X-C, Qiao Y-F, Zou B-S, Gui L-L. A highly luminescent europium complex showing visible-light-sensitized red emission: direct observation of the singlet pathway. Angew. Chem., Int. Ed. Engl., 2004, 43: 5010.

[43] Dadabhoy A, Faulkner S, Sammes P G. Long wavelength sensitizers for europium(III) luminescence based on acridone derivatives. J. Chem. Soc., Perkin Trans.2, 2002, 348.

[44] Dadabhoy A, Faulkner S, Sammes P G. Small singlet–triplet energy gap of acridone enables longer wavelength sensitisation of europium(III) luminescence. J. Chem. Soc., Perkin Trans. 2, 2000, 2359.

[45] Lehn J-M, Roth C O. Synthesis and Properties of Sodium and Europium(III) Cryptates Incorporating the 2,2' Bipyridine 1,1'-Dioxide and 3,3'-Biisoquinoline 2,2'-Dioxide Units. Helv. Chim. Acta, 1991, 74: 572.

[46] Prodi L, Maestri M, Balzani V, Lehn J-M, Roth C. Luminescence properties of cryptate europium (III) complexes incorporating heterocyclic N-oxide groups. Chem. Phys. Lett., 1991, 180: 45.

[47] Dee C, Esteban-Gómez D, Platas-Iglesias C, Seitz M. Long Wavelength Excitation of Europium Luminescence in Extended, Carboline-Based Cryptates. Inorg. Chem., 2018, 57: 7390.

[48] Kreidt E, Dee C, Seitz M. Chiral Resolution of Lanthanoid Cryptates with Extreme Configurational Stability. Inorg. Chem., 2017, 56: 8752.

[49] Kreidt E, Arrico L, Zinna F, Di Bari L, Seitz M. Circularly Polarised Luminescence in Enantiopure Samarium and Europium Cryptates. Chem. Eur. J., 2018, 24: 13556.

[50] Güden-Silber T, Doffek C, Platas-Iglesias C, Seitz M. The first enantiopure lanthanoid cryptate. Dalton Trans., 2014, 43: 4238.

[51] Zinna F, Bruhn T, Guido C A, Ahrens J, Bröring M, Di Bari L, Pescitelli G. Circularly Polarized Luminescence from Axially Chiral BODIPY DYEmers: An Experimental and Computational Study. Chem. Eur. J., 2016, 22: 16089.

[52] Tao J, Perdew J P, Staroverov V N, Scuseria G E. Climbing the Density Functional Ladder: Nonempirical Meta-Generalized Gradient Approximation Designed for Molecules and Solids. Phys. Rev. Lett., 2016, 91: 146401.

[53] Frisch M J, Trucks G W, Schlegel H B, Scuseria G E, Robb M A, Cheeseman J R, Scalmani G, Barone V, Mennucci B, Petersson G A, et al. Gaussian 09, Revision D.01, Gaussian, Inc.: Wallingford CT, 2009.

[54] Nonat A, Esteban-Gómez D, Valencia L, Pérez-Lourido P, Barriada J L, Charbonnière L J, Platas-Iglesias C. The Role of Ligand to Metal Charge-Transfer States on the Luminescence of Europium Complexes with 18-Membered Macrocyclic Ligands. Dalton Trans., 2019, 48: 4035.

[55] Dolg M, Stoll H, Savin A, Preuss H. Energy-adjusted pseudopotentials for the rare earth elements. Theor. Chim. Acta, 1989, 75: 173.

[56] Stratmann R E, Scuseria G E, Frisch M J. An efficient implementation of time-dependent density-functional theory for the calculation of excitation energies of large molecules. J. Chem. Phys., 1998, 109: 8218.

[57] Bauernschmitt R, Ahlrichs R. Treatment of electronic excitations within the adiabatic approximation of time dependent density functional theory. Chem. Phys. Lett., 1996, 256: 454;

[58] Casida M E, Jamorski C, Casida K C, Salahub D R. Molecular excitation energies to high-lying bound states from time-dependent density-functional response theory: Characterization and correction of the time-dependent local density approximation ionization threshold. J. Chem. Phys., 1998, 108: 4439.

[59] Furche F, Ahlrichs R, Wachsmann C, Weber E, Sobanski A, Vögtle F, Grimme S. Circular Dichroism of Helicenes Investigated by Time-Dependent Density Functional Theory. J. Am. Chem. Soc., 2000, 122: 1717.

[60] Jang H, Kim N J, Heo J. Benchmarking Study on Time-Dependent Density Functional Theory Calculations of Electronic Circular Dichroism for Gas-Phase Molecules. Comput. Theor. Chem., 2018, 1125: 63.

[61] Dennington R, Keith T A, Millam J M. GaussView, Version 6, Semichem Inc., Shawnee Mission, KS, 2016.

[62] Pescitelli G, Bruhn T. Good Computational Practice in the Assignment of Absolute Configurations by TDDFT Calculations of ECD Spectra. Chirality, 2016, 28: 466.

[63] Tomasi J, Mennucci B, Cammi R. Quantum Mechanical Continuum Solvation Models. Chem. Rev., 2005, 105: 2999.

[64] Rappe A K, Casewit C J, Colwell K S, Goddard W A III, Skiff W M. UFF, a Full Periodic Table Force Field for Molecular Mechanics and Molecular Dynamics Simulations. J. Am. Chem. Soc., 1992, 114: 10024.

Lanthanide Sensitizers for Large Anti-Stokes Shift NIR-to-VIS Triplet-Triplet Annihilation Photon Upconversion

Natalia Kiseleva,[†] Pariya Nazari,[†] Carolin Dee,[‡] Dmitry Busko,[†] Bryce S. Richards,[†,▽] M. Seitz,[‡] Ian A. Howard,*[,†,▽] A. Turshatov*[,†]

[†]Institute of Microstructure Technology, Karlsruhe Institute of Technology, Hermann-von-Helmholtz-Platz 1, 76344 Eggenstein-Leopoldshafen, Germany

[‡]Institute of Inorganic Chemistry, University of Tübingen, Auf der Morgenstelle 18, 72076 Tübingen, Germany

[▽]Light Technology Institute, Karlsruhe Institute of Technology, Engesserstrasse 13, 76131 Karlsruhe, Germany

Supporting Information Placeholder

ABSTRACT: The upconversion of near-infrared (NIR) to visible (VIS) photons is of interest for display technologies and energy conversion. Although triplet-triplet annihilation (TTA) offers a mechanism for upconversion that works efficiently at low incident irradiance flux densities, current strategies for NIR-VIS upconversion based on TTA have fundamental limitations. Herein we report a strategy for NIR-VIS TTA based on lanthanide containing complexes to sensitize the upconversion. We demonstrate a β-diketonate complex of Yb^{3+} paired with rubrene that emits yellow (λ_{em} = 559 nm) under NIR excitation (λ_{exc} = 980 nm). This corresponds to an exceptional anti-Stokes shift of just less than 1 eV. Lanthanide complexes should unlock high performance NIR-VIS upconversion, of especial interest for 3D display technologies. Lanthanide sensitizers overcome the energy loss, reabsorption, and short-triplet lifetime that fundamentally limit porphyrin, nanocrystal, and direct S_0-T_1 sensitizers.

Triplet-triplet annihilation upconversion (TTA-UC) combines two low-energy photons into a single high-energy photon. TTA-UC operates under excitation from low-cost LED or laser sources (mW/cm^2 – W/cm^2 range)[1], and consequently is explored for a variety of applications.[2-6] A mixture of two molecules, a sensitizer and an emitter (Figure 1), is utilized for TTA-UC. Energy transfer (ET) from the sensitizer to the triplet state of the emitter, and TTA between two emitter molecules are the key elements of TTA-UC.[7] Typically, both the sensitizer and emitter have been organic molecules. This limited the ability of TTA-UC systems to upconvert NIR light, due to the limited number of appropriate organic sensitizers (and the energy loss during intersystem crossing from the singlet to triplet state in the sensitizer). Wu *et al.* made a significant step forward when they demonstrated that PbS nanocrystals could be used as a sensitizer.[8] Paired with rubrene as the emitter, the NIR light absorbed by the PbS nanocrystals could be re-emitted in the visible by rubrene, with energy transferring from the excited-state on the colloidal nanocrystal to the triplet state of the organic molecule. Unfortunately, the strong visible absorption of the PbS nanocrystals means that the much of the upconverted light is reabsorbed by the sensitizer.

Herein, we demonstrate a NIR-absorbing sensitizer for TTA-UC based on an Yb molecular complex (**Yb-L**, Figure 1). Coupled with a rubrene emitter, this novel sensitizer enables TTA-UC from the NIR (absorbing from 900 - 1000 nm, 980 nm peak) to the yellow (535 – 665 nm, emission peak at 559 nm). This corresponds to a very significant anti-Stokes shift of 0.95 eV (considering the 980 nm excitation and 559 nm emission peaks). Opposed to PbS, our approach avoids reabsorption of the upconverted light. Lanthanide-based sensitizer complexes should unlock NIR-VIS photon upconversion based on TTA with applications, for example, in 3D displays.

Yb^{3+} complexes were identified as a promising sensitizer candidates based on the following logic. Firstly, it is a known that energy transfer from a lanthanide ion to the triplet state on an organic molecule (and vice versa) is possible. The triplet state of an organic molecule can sensitize excited levels of lanthanide ions[9-10] or can induce the quenching of lanthanide luminescence due to back energy transfer.[11] With a single excited state ($^2F_{5/2}$), Yb^{3+} is the best choice of lanthanide to avoid back energy transfer from the emitter and/or reabsorption of the emitted photons. The lack of reabsorption is also important for mitigating the one weakness of lanthanides as a potential sensitizer.

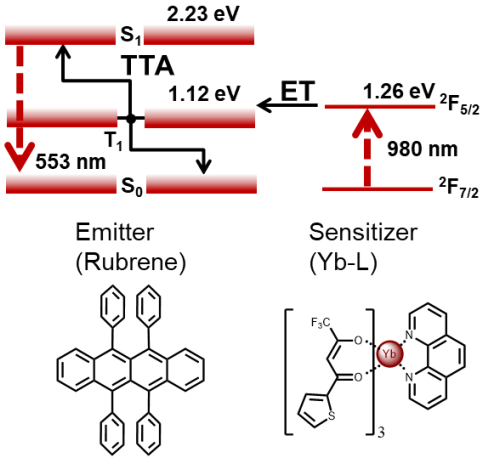

Figure 1. Scheme of TTA-UC with **Yb-L** as sensitizer and rubrene as emitter chemical structures of chromophores used for IR-to-yellow UC: **Yb-L** (sensitizer) and rubrene (emitter).

The absorption cross-section for the parity- and sometimes even spin-forbidden *f-f* transitions of trivalent rare earth ions is small. Yb^{3+}, the most efficient lanthanide absorber, has absorption cross-section of ~ 10^{-20} cm^2 (at 980 nm).[12] This cross-section is four orders of magnitude smaller than typical absorption cross-sections of organic sensitizers (~ 10^{-16} cm^2).[13] The lower triplet population density resulting from weaker absorption will detrimentally

increase the upconversion threshold. However, the negative impact of such a difference in absorption cross-section can be compensated by increasing the Yb^{3+} concentration in the UC system.

A typical TTA-UC system comprises a solution of an organic sensitizer with concentrations of ca. 10^{-5} M.[14] Consequently, a 0.1 M solution of Yb^{3+} would then exhibit a comparable optical density. We were able to achieve such high concentrations of Yb^{3+} in non-polar organic solvents via coordination of Yb^{3+} with non-polar organic ligands in order to achieve the high solubility required.[15-16] For this purpose, the first candidates are the well-known, neutral complexes with β-diketonate ligands.[17] One of the most suitable starting points is the known complex **Yb-L** with three anionic thenoyltrifluoroacetonate ligands and an additional neutral 1,10-phenanthroline unit to complete the eight-coordinate inner-sphere of the lanthanide. **Yb-L** is stable in solution, has high solubility in non-polar or moderately polar organic solvents, and exhibits relatively high quantum yield (QY) and long luminescence lifetimes (reported QY = 1.1 % and τ = 10 μs in toluene via UV excitation, e.g. λ_{exc} = 310 nm).[18-19]

Yb-centered excited states are highly susceptible to non-radiative deactivation by multiphonon relaxation via energy transfer to vibrational overtones of high-energy, highly anharmonic oscillators (mostly stretching modes of X-H moieties with X = O, N, C) in the vicinity of the metal. This problem can be alleviated by using deuterated solvents devoid of these moieties.[20] Considering both solubility of **Yb-L** and solvent availability, [D_8]-THF proved to be very suitable, enabling the preparation of 0.1 M solutions of **Yb-L** without any problems.

Given its success with PbS sensitizers, we hypothesized that rubrene with a triplet energy of 1.12 eV[21] would be a suitable quencher of the Yb^{3+}:$^2F_{5/2}$ state with energy of 1.26 eV.[22] The energy levels of the Yb^{3+} sensitizer along with the triplet and singlet energy levels on the rubrene emitter are presented in Figure 1.

Figure 2a demonstrates the absorption and emission spectra of the sensitizer (**Yb-L**) and the emitter (rubrene) in [D_8]-THF. The absorption maximum of the sensitizer is at 980 nm and it shows very little absorption at λ = 500-700 nm – the spectral range where emission of the rubrene is present. The UV absorption of the sensitizer is due to the ligands, and in no way disturbs the upconversion. The upconversion emission is shown in Figure 2b. Here, the red curve shows the observed upconversion emission spectrum after excitation at 980 nm at an excitation power density of 100 W/cm^2. The UC emission spectrum matches that of directly excited rubrene, the peak is slightly red-shifted in comparison to literature reports (made at lower rubrene concentrations) due to reabsorption by the rubrene itself at a concentration of 1mM. The black curve shows the excitation spectrum for the upconversion, monitoring the emission at 559 nm while the excitation wavelength is varied (and the excitation power density maintained at 100 W/cm^2). The excitation spectrum is narrower and shows sharper peaks than the absorption spectrum, as expected due to the nonlinear nature of the upconversion process. Lastly, Figure 2c presents a photograph taken with an exposure time of 30 ms of the yellow luminescence (that is easily visible with the naked eye). No optical filters were used on the camera.

Having established that lanthanide complexes are indeed very interesting as novel sensitizers for TTA-UC, we turned to examining the performance of this initial proof-of-concept system in more detail. Figure 3a plots the lifetime of the Yb^{3+}:$^2F_{5/2}$ level (monitored by its emission at 990 nm) in solutions without (black trace) and with (maroon trace) rubrene present in the solution. It is immediately apparent from the data that the quenching of the sensitizer lifetime is minimal, indicating that triplet energy transfer from the sensitizer to the emitter can be significantly improved in order to optimize the upconversion intensity (and lower the upconversion threshold) in these systems.

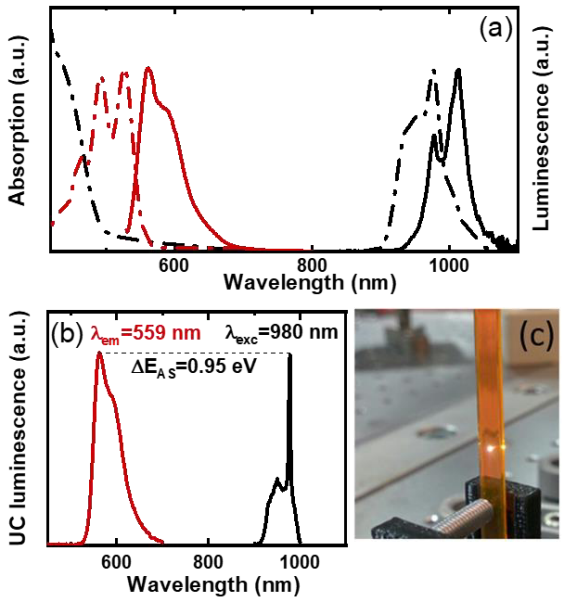

Figure 2. (a) Absorption (dashed lines) and emission (solid lines) spectra of **Yb-L** (black line) and rubrene (dark red lines). $C_{Yb\text{-}L}$ = 0.1 M, $C_{rubrene}$ = 1 mM; (b) UC luminescence of rubrene excited with a 980 nm laser (dark red line). Excitation spectrum of TTA-UC, laser intensity maintained at 100 W/cm^2 (black line). (c) Unfiltered photograph of UC luminescence (λ_{exc} = 980 nm, 300 W/cm^2).

Quantitatively, the efficiency of triplet energy transfer can be calculated with equation (1):

$$\eta_{ET} = 1 - \frac{\tau_{Yb-L}^{(R)}}{\tau_{Yb-L}} \quad (1)$$

where η_{ET} is the efficiency of energy transfer, $\tau_{Yb-L}^{(R)}$ is the lifetime of the Yb^{3+}:$^2F_{5/2}$ level in the presence of rubrene in solution, and τ_{Yb-L} is the lifetime of the Yb^{3+}:$^2F_{5/2}$ level without any rubrene present. Using equation (1), the efficiency of energy transfer is only 1.5 %. Significant increase in the efficiency of this transfer by improving the steric access of the emitter to the lanthanide in the sensitizer, and optimizing the energy levels is anticipated.

The lifetime of the UC luminescence is also shown in Figure 3a. The 55μs lifetime observed is significantly longer than lifetime of rubrene fluorescence in THF (8.1 ns)[23] and attests that TTA is indeed the mechanism for UC in our system.

Figure 3b displays the dependence of the UC luminescence on excitation intensity. In conventional TTA-UC, below the UC threshold the UC intensity is a quadratic function of excitation power density.[7] While above the threshold, the bimolecular TTA process starts to dominate over any other relaxation channels for the emitter triplet state and UC becomes linearly dependent on excitation intensity.[7] In our case, the slope remains 2 over the entire almost 4 orders of magnitude measured (Figure 3b). Thus, the current system is sub-threshold even at very high excitation power densities. This is not surprising, given the inverse relationship between the threshold and the rate of energy transfer from the sensitizer to the emitter, and the limited energy transfer observed above.[7] Given that here UC is always operating sub-threshold, the UC QY is also limited in this proof-of-concept system. The UC QY of approximately 0.005 % was measured at 300 W/cm^2 with 980 nm excitation in an integrating sphere.

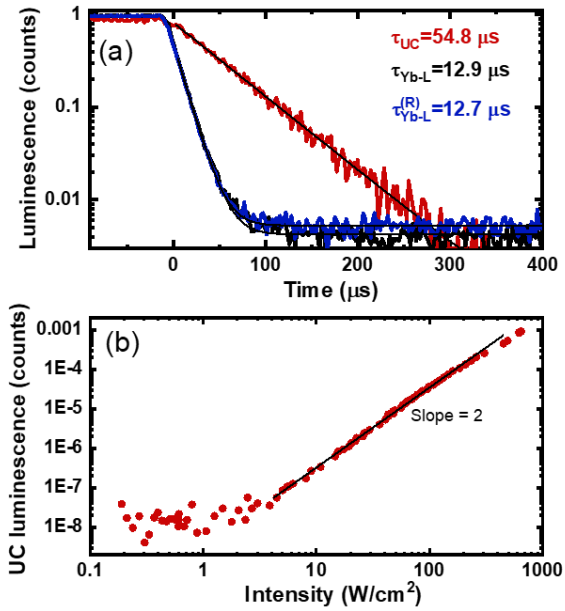

Figure 3. (a) Decays of **Yb-L** luminescence (λ_{em} = 990 nm) measured with (blue) and without rubrene (black) (λ_{exc}= 980 nm). Decay of UC (dark red) measured at λ_{em} = 559 nm (λ_{exc} = 980 nm); (b) UC intensity as function of excitation intensity ($C_{\mathbf{Yb\text{-}L}}$ = 0.1 M, $C_{rubrene}$ = 1 mM).

Optimization of the triplet energy transfer will be key to boosting efficiencies and lowering the UC thresholds, but as outlined below lanthanide sensitizers overcome the fundamental limitations of NIR sensitizers found to date.

A first example of NIR-to visible TTA-UC was demonstrated by Yakutkin *et al.* using a palladium tetraanthraporphyrin sensitizer. [24] Pd-TAP was excited with a 785 nm laser and yellow UC luminescence (emission maxima (λ_{em}) of 553 nm and amplitude of anti-Stokes shift (ΔE_{AS}) of 0.65 eV) was observed. The amplitude of anti-Stokes shift is directly related to energy losses (ΔE_L = 0.46 eV) due to internal conversion and intersystem crossing in the metallated porphyrin (Figure S1). Such systems that rely on singlet to triplet conversion after photon absorption will present significant reductions of the ΔE_{AS} that are avoided in lanthanide-based sensitizers. We do note that thermally-activated delayed-fluorescence (TADF) sensitizers can also reduce the loss in ΔE_{AS},[25] but, to date, this has not been demonstrated in the NIR.

As mentioned before, a limitation of the nanocrystal sensitization is the strong reabsorption of the upconverted light by the nanocrystal sensitizers. This means that only very thin layers of the sensitizer can be used, severely limiting the amount of incoming light that can be harvested (and therefore the brightness of the UC emission).[26] Lanthanide-based systems remove the parasitic absorption in the visible, and can therefore overcome the practical limitations for application of the NIR-to-VIS TTA-UC based on nanocrystal sensitizers.

The final competition is the elegant work presented by Amemori *et al*.[27] They demonstrated an osmium complex with a coupling between S_0 and T_1, allowing direct population of the triplet state after optical excitation. However, the triplet lifetime in such complexes is also necessarily short due to the strong coupling, meaning achieving energy transfer to the emitter is a challenge. By using solid-state nanoparticles to keep the sensitizer and rubrene emitter in close contact they demonstrated TTA-UC with parameters of λ_{exc} = 938 nm, ΔE_{AS} = 0.89 eV, I_{th} = 10 W/cm^2, QY_{UC} = 3.2 %. In a normal upconversion solution of this osmium complex sensitizer and emitter, the performance is much worse as a sensitizer-emitter encounter within the sensitizer lifetime is highly improbable. The three-order-of-magnitude-longer sensitizer lifetimes that we demonstrate for the Yb complexes are promising for enabling efficient TTA to be achieved in liquid-phase systems (wherein emitter aggregation can be easily avoided).

We have demonstrated that the ytterbium complex **Yb-L** can sensitize NIR-VIS TTA-UC. After NIR excitation (λ_{exc} = 980 nm), yellow light is emitted (λ_{em} = 559 nm) which is easily visible to the eye. The anti-Stokes shift is very large (ΔE_{AS} = 0.95 eV). Although the threshold and UC QY of this proof-of-concept need improvement through better design of sensitizer to emitter energy transfer, we demonstrate that lanthanide-based complexes exhibit high potential in comparison to their competitors as they uniquely combine the three desirable properties of: 1) no loss due to intersystem crossing and internal conversion, 2) no reabsorption of the upconverted light, and 3) long triplet lifetimes.

ASSOCIATED CONTENT

Supporting Information

The Supporting Information is available free of charge on the ACS Publications website.
Synthesis of **Yb-L**, **Yb-L** characterization data, experimental procedure for optical measurements, Supporting Figure (PDF)

AUTHORS INFORMATION

Corresponding Author

*E-mail: andrey.turshatov@kit.edu
*E-mail: ian.howard@kit.edu

ORCID

Bryce S. Richards:0000-0001-5469-048X
Michael Seitz:0000-0002-9313-2779
Ian A. Howard:0000-0002-7327-7356
Andrey Turshatov:0000-0002-8004-098X

Author Contributions

N.K and P.N. equally contributed to spectroscopic experiments. C.D. synthesized **Yb-L**. I.A.H. and A.T. developed the original concept and wrote the paper, and then D.B., B.S.R. and M.S. contributed to scoping and structuring the paper and provided additional guidance on experimental methods.

Notes

The authors declare no competing financial interests.

ACKNOWLEDGMENT

P.N., A.T., C.D., and M.S. acknowledge financial support of DFG (Research Grants TU487/2-1 and SE1448/6-1) within the Priority Program SPP 1928: COORNET. B.S.R, and A.T. acknowledge the Helmholtz Energy Materials Foundry (HEMF). N.K. acknowledges a DAAD scholarship.

REFERENCES

(1) Zhou, J.; Liu, Q.; Feng, W.; Sun, Y.; Li, F., Upconversion Luminescent Materials: Advances and Applications. *Chem. Rev.* **2015,** *115*, 395-465.
(2) Choi, D.; Nam, S. K.; Kim, K.; Moon, J. H., Enhanced Photoelectrochemical Water Splitting through Bismuth Vanadate with a Photon Upconversion Luminescent Reflector. *Angew. Chem., Int. Ed.* **2019,** *58*, 6891-6895.

(3) Yu, T.; Liu, Y.; Zeng, Y.; Chen, J.; Yang, G.; Li, Y. Triplet–Triplet Annihilation Upconversion for Photocatalytic Hydrogen Evolution. *Chem. - Eur. J.* **2019**, *25*, 16270-16276.
(4) Ravetz, B. D.; Pun, A. B.; Churchill, E. M.; Congreve, D. N.; Rovis, T.; Campos, L. M., Photoredox catalysis using infrared light via triplet fusion upconversion. *Nature* **2019,** *565*, 343-346.
(5) Gray, V.; Dzebo, D.; Abrahamsson, M.; Albinsson, B.; Moth-Poulsen, K., Triplet-triplet annihilation photon-upconversion: towards solar energy applications. *Phys. Chem. Chem. Phys.* **2014,** *16*, 10345-10352.
(6) Askes, S. H. C.; Pomp, W.; Hopkins, S. L.; Kros, A.; Wu, S.; Schmidt, T.; Bonnet, S., Imaging Upconverting Polymersomes in Cancer Cells: Biocompatible Antioxidants Brighten Triplet–Triplet Annihilation Upconversion. *Small* **2016,** *12*, 5579-5590.
(7) Monguzzi, A.; Tubino, R.; Hoseinkhani, S.; Campione, M.; Meinardi, F., Low power, non-coherent sensitized photon up-conversion: modelling and perspectives. *Phys. Chem. Chem. Phys.* **2012,** *14*, 4322-4332.
(8) Wu, M.; Congreve, D. N.; Wilson, M. W. B.; Jean, J.; Geva, N.; Welborn, M.; Van Voorhis, T.; Bulović, V.; Bawendi, M. G.; Baldo, M. A., Solid-state infrared-to-visible upconversion sensitized by colloidal nanocrystals. *Nat. Photonics* **2016,** *10*, 31-34.
(9) Moore, E. G.; Samuel, A. P. S.; Raymond, K. N., From Antenna to Assay: Lessons Learned in Lanthanide Luminescence. *Acc. Chem. Res.* **2009,** *42*, 542-552.
(10) de Sá, G. F.; Malta, O. L.; de Mello Donegá, C.; Simas, A. M.; Longo, R. L.; Santa-Cruz, P. A.; da Silva, E. F., Spectroscopic properties and design of highly luminescent lanthanide coordination complexes. *Coord. Chem. Rev.* **2000,** *196*, 165-195.
(11) Wang, Z.; Ananias, D.; Carné-Sánchez, A.; Brites, C. D. S.; Imaz, I.; Maspoch, D.; Rocha, J.; Carlos, L. D., Lanthanide–Organic Framework Nanothermometers Prepared by Spray-Drying. *Adv. Funct. Mater.* **2015,** *25*, 2824-2830.
(12) Strohhöfer, C.; Polman, A., Absorption and emission spectroscopy in Er^{3+}–Yb^{3+} doped aluminum oxide waveguides. *Opt. Mater.* **2003,** *21*, 705-712.
(13) Cheng, Y. Y.; Fückel, B.; MacQueen, R. W.; Khoury, T.; Clady, R. G. C. R.; Schulze, T. F.; Ekins-Daukes, N. J.; Crossley, M. J.; Stannowski, B.; Lips, K.; Schmidt, T. W., Improving the light-harvesting of amorphous silicon solar cells with photochemical upconversion. *Energy Environ. Sci.* **2012,** *5*, 6953-6959.
(14) Kiseleva, N.; Filatov, M. A.; Oldenburg, M.; Busko, D.; Jakoby, M.; Howard, I. A.; Richards, B. S.; Senge, M. O.; Borisov, S. M.; Turshatov, A., The Janus-faced chromophore: a donor–acceptor dyad with dual performance in photon up-conversion. *Chem. Commun.* **2018,** *54*, 1607-1610.
(15) Kruck, C.; Nazari, P.; Dee, C.; Richards, B. S.; Turshatov, A.; Seitz, M., Efficient Ytterbium Near-Infrared Luminophore Based on a Nondeuterated Ligand. *Inorg. Chem.* **2019,** *58*, 6959-6965.
(16) Davis, D.; Carrod, A. J.; Guo, Z.; Kariuki, B. M.; Zhang, Y.-Z.; Pikramenou, Z., Imidodiphosphonate Ligands for Enhanced Sensitization and Shielding of Visible and Near-Infrared Lanthanides. *Inorg. Chem.* **2019,** *58*, 13268-13275.
(17) Wang, K.-Z., β-Diketonate. In *Rare Earth Elements - Fundamentals and Applications*, Atwood, D. A., Ed. Jon Wiley & Sons: Chichester, 2012; pp 249-261.
(18) Meshkova, S. B.; Topilova, Z. M.; Bolshoy, D. V.; Beltyukova, S. V.; Tsvirko, M. P.; Venchikov, V. Y., Quantum efficiency of the luminescence of ytterbium(III) beta-diketonates. *Acta Phys Pol A* **1999,** *95*, 983-990.
(19) Doffek, C.; Seitz, M., The Radiative Lifetime in Near-IR-Luminescent Ytterbium Cryptates: The Key to Extremely High Quantum Yields. *Angew. Chem., Int. Ed.* **2015,** *54*, 9719-9721.
(20) Kreidt, E. K., C.; Seitz, M., Nonradiative Deactivation of Lanthanoid Luminescence by Multiphonon Relaxation in Molecular Complexes. In *Handbook on the Physics and Chemistry of Rare Earths*, Bünzli, J.-C. G.; Pecharsky, V. K., Eds.; Elsevier:: Amsterdam, 2018; Vol. 53, pp 35-79.
(21) Ma, L.; Zhang, K.; Kloc, C.; Sun, H.; Michel-Beyerle, M. E.; Gurzadyan, G. G., Singlet fission in rubrene single crystal: direct observation by femtosecond pump–probe spectroscopy. *Phys. Chem. Chem. Phys.* **2012,** *14*, 8307-8312.
(22) Huang, F.; Liu, X.; Ma, Y.; Kang, S.; Hu, L.; Chen, D., Origin of near to middle infrared luminescence and energy transfer process of Er^{3+}/Yb^{3+}co-doped fluorotellurite glasses under different excitations. *Sci. Rep.* **2015,** *5*, 8233.
(23) Mahajan, P. G.; Bhopate, D. P.; Kamble, A. A.; Dalavi, D. K.; Kolekar, G. B.; Patil, S. R., Selective sensing of Fe^{2+} ions in aqueous solution based on fluorescence quenching of SDS capped rubrene nanoparticles: application in pharmaceutical formulation. *Anal. Methods* **2015,** *7*, 7889-7898.
(24) Yakutkin, V.; Aleshchenkov, S.; Chernov, S.; Miteva, T.; Nelles, G.; Cheprakov, A.; Baluschev, S., Towards the IR Limit of the Triplet–Triplet Annihilation-Supported Up-Conversion: Tetraanthraporphyrin. *Chem. - Eur. J.* **2008,** *14*, 9846-9850.
(25) Wu, T. C.; Congreve, D. N.; Baldo, M. A., Solid state photon upconversion utilizing thermally activated delayed fluorescence molecules as triplet sensitizer. *Appl. Phys. Lett.* **2015,** *107*, 031103.
(26) Nienhaus, L.; Wu, M.; Geva, N.; Shepherd, J. J.; Wilson, M. W. B.; Bulović, V.; Van Voorhis, T.; Baldo, M. A.; Bawendi, M. G., Speed Limit for Triplet-Exciton Transfer in Solid-State PbS Nanocrystal-Sensitized Photon Upconversion. *ACS Nano* **2017,** *11*, 7848-7857.
(27) Amemori, S.; Sasaki, Y.; Yanai, N.; Kimizuka, N., Near-Infrared-to-Visible Photon Upconversion Sensitized by a Metal Complex with Spin-Forbidden yet Strong S_0–T_1 Absorption. *J. Am. Chem. Soc.* **2016,** *138*, 8702-8705.

TOC

Lanthanide Sensitizers for Large Anti-Stokes Shift NIR-to-VIS Triplet-Triplet Annihilation Photon Upconversion

Natalia Kiseleva,[†] Pariya Nazari,[†] Carolin Dee,[‡] Dmitry Busko,[†] Bryce S. Richards,[†,▽] M. Seitz,[‡] Ian A. Howard,*[,†,▽] A. Turshatov*[,†]

[†]Institute of Microstructure Technology, Karlsruhe Institute of Technology, Hermann-von-Helmholtz-Platz 1, 76344 Eggenstein-Leopoldshafen, Germany

[‡]Institute of Inorganic Chemistry, University of Tübingen, Auf der Morgenstelle 18, 72076 Tübingen, Germany

[▽]Light Technology Institute, Karlsruhe Institute of Technology, Engesserstrasse 13, 76131 Karlsruhe, Germany

Experimental Section

Chemicals

Rubrene (99.99 %), thenoyltrifluoroacetone, $YbCl_3 \cdot 6\ H_2O$ (99.9 % Yb), 1,10-phenanthroline, and deuterated tetrahydrofurane ([D_8]-THF, 99.5%D) were purchased in from Sigma-Aldrich (Merck). Ethanol for the synthesis of **Yb-L** was HPLC-grade.

Synthesis of Yb-L

Yb-L was synthesized according to a slightly altered literature procedure.[1]

In a round-bottom-flask, thenoyltrifluoroacetone (667 mg, 3.00 mmol, 3.0 equivs.) was suspended in EtOH (10 mL) and solid 1,10-phenanthroline (180 mg, 1.00 mmol, 1.0 equiv.) was added in portions. The mixture was heated to 75°C (bath temperature) until a clear solution was obtained. The solution was allowed to cool to 30°C (bath temperature) and an aqueous solution of NaOH (1 M, 3.00 mmol, 3.00 mL, 3.0 equivs.) was added dropwise. The solution was stirred at the same temperature for 30 minutes before a solution of $YbCl_3 \cdot 6\ H_2O$ (388 mg, 1.00 mmol, 1.0 equiv.) in water (7 mL) was added under efficient stirring. After complete addition, the mixture was heated back up to 60°C (bath temperature) and stirred at this temperature for 3.5 h. The suspension was allowed to cool to ambient temperature under stirring, the precipitate was collected on a Büchner funnel and washed with a minimum of ice-cold EtOH (ca. 1 mL). After drying the solid under reduced pressure for 5 h, the crude product was recrystallized from $CHCl_3$ (dissolve hot in a minimum of solvent, crystallization upon cooling to 4°C), collected on a Büchner funnel, washed with ice-cold $CHCl_3$ (ca. 1 mL), and dried in vacuo to yield the title compound as pale yellow solid (722 mg, 71 %). The analytical data were in agreement with previously reported data.[1-2]

^{1}H NMR (400 MHz, CD_2Cl_2): δ = 18.8 (s, 2 H), 18.1 (d, *J* = 6.3 Hz, 2 H), 13.1 (d, *J* = 6.5 Hz, 2H), 9.45 (s, 2 H), 6.67 (d, *J* = 5.0 Hz, 3 H), 5.46 (s, 3 H), 2.51 (s, 3 H), 11.2 (s, 3 H) ppm.

Sample preparation

The solutions of **Yb-L** (concentration 0.1 M) and rubrene (concentration 1 mM) in [D8]-THFTHF was prepared inside a N_2-filled glovebox (GS GLOVEBOX Systemtechnik GmbH) with concentration of oxygen 0.1 ppm. The solution was placed in 1 mm quartz cuvette (Hellma Analytics) and sealed inside the glovebox. The samples was stored in the glovebox between measurements.

Optical characterization

UV/VIS absorption spectra were recorded on a spectrophotometer (Lambda 950, PerkinElmer). The absorption spectra of all solutions were measured in a 1 mm quartz cuvette (Hellma Analytics) against the cuvette with THF as a reference. For photoluminescence (PL) of Yb^{3+}, the cuvette was excited with 980 nm continuous-wave (CW) laser diode (Thorlabs, L980P200) mounted on a temperature-controlled mount (Thorlabs, TCLDM9) and driven using a laser diode controller (Thorlabs, ITC4001). The Yb^{3+} PL was captured using a spectrometer (Avantes, AvaSpec - ULS2048 × 64TEC). The upconversion (UC) emission were excited with the 980 nm laser diode (Thorlabs, L980P200). The power of the beam and beam shape was measured with a powermeter (Thorlabs, PM320E) and beam profiler (Thorlabs, BP209 - IR/M), respectively. For characterisation of the intensity dependency of UC emission the laser beam was attenuated with motorized variable filter wheel (Thorlabs, NDC - 100C - 2). The UC excitation spectra was measured with earlier described experimental procedure.[3] Detailed description of measurements of PL lifetime and QY_{UC} have been also reported earlier.[4]

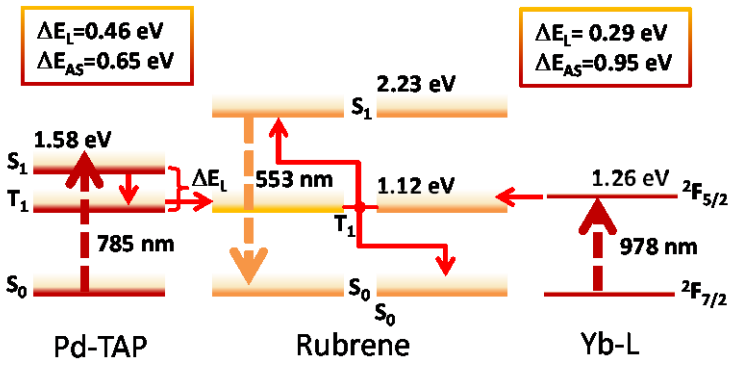

Figure S1. Scheme of TTA-UC with palladium tetraanthraporphyrin (Pd - TAP)[5] and Yb-L as sensitizer and rubrene as emitter.

The scheme displays the amplitude of anti-Stokes shift for both Pd-TPA (0.65 eV) and Yb-L (0.95 eV) sensitizers. The energy losses ($\Delta E_L = 0.46$ eV) due to internal conversion and intersystem crossing is much higher for Pd-TPA as compared with Yb-L (0.29 eV).

References

(1) Freund, C.; Porzio, W.; Giovanella, U.; Vignali, F.; Pasini, M.; Destri, S.; Mech, A.; Di Pietro, S.; Di Bari, L.; Mineo, P. Thiophene Based Europium β-Diketonate Complexes: Effect of the Ligand Structure on the Emission Quantum Yield *Inorg. Chem.* **2011**, *50*, 5417-5429.

(2) Doffek, C.; Seitz, M.; The Radiative Lifetime in Near-IR Luminescent Ytterbium Cryptates - The Key to Extremely High Quantum Yields. *Angew. Chem. Int. Ed.* **2015**, *54*, 9719-9721.

(3) Meijer, M. S.; Rojas-Gutierrez, P. A.; Busko, D.; Howard, I. A.; Frenzel, F.; Würth, C.; Resch-Genger, U.; Richards, B. S.; Turshatov, A.; Capobianco, J. A.; Bonnet, S. Absolute upconversion quantum yields of blue-emitting $LiYF_4:Yb^{3+},Tm^{3+}$ upconverting nanoparticles. *Phys. Chem. Chem. Phys.* **2018**, *20*, 22556-22562.

(4) Joseph, R. E.; Jiménez, C.; Hudry, D.; Gao, G.; Busko, D.; Biner, D.; Turshatov, A.; Krämer, K.; Richards, B. S.; Howard, I. A. Critical Power Density: A Metric To Compare the Excitation Power Density Dependence of Photon Upconversion in Different Inorganic Host Materials. *J. Phys. Chem. A* **2019**, *123*, 6799-6811

(5) Yakutkin, V.; Aleshchenkov, S.; Chernov, S.; Miteva, T.; Nelles, G.; Cheprakov, A.; Baluschev, S. Towards the IR Limit of the Triplet–Triplet Annihilation-Supported Up-Conversion: Tetraanthraporphyrin. *Chem. - Eur. J.* **2008**, *14*, 9846-9850.

CHEMIE IN UNSERER ZEIT
www.chiuz.de
DOI: 10.1002/ciuz.201900008

Die ChiuZ-Spargelstudie

Vom wohl- oder übelriechenden Spargelurin

KLAUS ROTH | SABINE STRELLER MIT

DANIEL APPEL, JOHANNES ASCHERL, ANJA BAUM, SEBASTIAN BESTGEN, RENÉ-CHRIS BRACHVOGEL, JULIA BUCHSBAUM, CAROLIN DEE, THOMAS JEREMIAS FEUERSTEIN, EMANUEL A. GLITSCHER, ANNA-BARBARA GREBHAHN, JANNICK GUSCHLBAUER, STEFAN HECHT, ANNA HEIB, CHRIS HEINTZ, GABRIELE HIERLMEIER, RONJA JORDAN, TOBIAS KLEIN, ULRICH KOCH, ANNIKA KOTTMANN, RUTH MARIA KRAMER, MATTHIAS M. KREJCA, GOSWINUS H.M. DE KRUIJFF, HANNES KÜHNLE, RALPH OTMAR KUSCHE, ANNA LECHNER, KLAUS LOCKE, PETER LUGER, ANNE MÄRKER, JULIA MÄRKER, SOPHIA MÄRKER, MARITA MEISSNER, ANGELA METZ, JULIAN MOEGLING, GREGOR NAGEL, CHRISTIAN NEIS, SASCHA OSSINGER, LORENZ PIETSCH, JULIA PÖPPINGHAUS, GABRIELE PÖPPINGHAUS, ANNELIE ROTH, ULRIKE SCHMITZ, FRANZ PETER SCHMITZ, MARKUS JULIAN SCHÖWE, LARA SCHULZ, ERIC SIEMES, SEBASTIAN SOBOTTKA, MANUEL STAPF, DANIEL JAMES TINDALL, ULRICH VOLLGRAF, CHRISTOPH WULF, DIANA ZELLER

Édouard Manet (1832–1883): Spargelbündel, 1810, (gemeinfrei)

Feinschmecker schwärmen vom feinen Aroma, Gesundheitsbewusste vom geringen Kaloriengehalt des Spargels und die Medien lobpreisen wie unglaublich gesund die weißen Stangen seien. Kurzum, Spargel wäre das ideale Gemüse, wenn, ja wenn nicht hinterher der eigene Urin so streng riechen würde. Eine Gruppe tapferer ChiuZ-Leser hat in Selbstversuchen erstmals eine fundierte Geruchsbewertung vorgenommen und dabei Bahnbrechendes aufgedeckt.

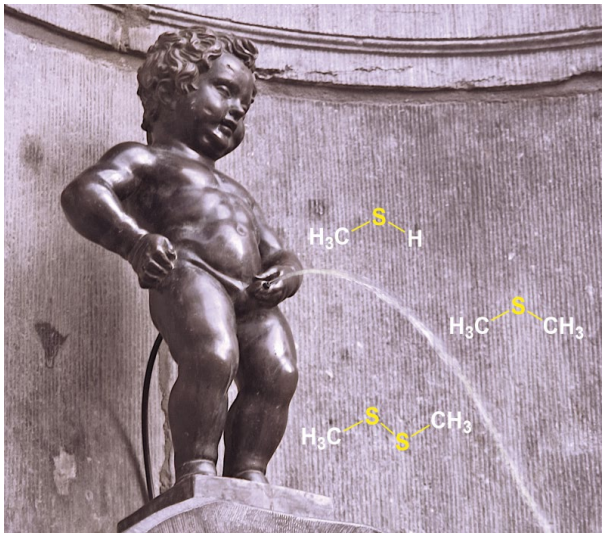

Im letzten Jahr waren der Spargelgenuss und seine Folgen unser Titelthema. Gleichzeitig hatten wir Sie aufgefordert, an unserer Umfrage zur Geruchsbewertung des Spargelurins teilzunehmen. Hier nun die Auswertung.

Vor einem Jahr wurden an dieser Stelle die historischen und chemischen Aspekte der Änderung des Uringeruchs nach Spargelgenuss ausführlich behandelt [1]. Spargel ist einzigartig, denn kein anderes Nahrungsmittel, ob roh, gekocht oder gebraten, verändert den Uringeruch so auffällig. Die geruchsbestimmenden Moleküle sind Methanthiol (***1***), Dimethylsulfid (***2***) und Dimethyldisulfid (***3***) (Abbildung 1), ein uns von Mundgeruch und Blähungen vertrautes Substanztrio. Die Verbindungen ***1–3*** tragen in geringem Maße auch zum normalen Uringeruch bei, allerdings ist deren Konzentration im Spargelurin um das Vielhundertfache höher [2].

Als biochemischer Ursprung des Spargeluringeruchs entpuppten sich die Asparagusinsäure (***4***) und ihr Methylester (***5***) (Abbildung 2). Beide Verbindungen wurden erst 1972 als Inhaltsstoffe des Spargels erkannt [3] und konnten bisher in keiner anderen Pflanze nachgewiesen werden. Die Konzentrationen beider Schwefelverbindungen erreichen in weißen Spargelstangen kurz vor dem Durchstoßen der Erdschicht ein Maximum und lassen mit Beginn der Photosynthese (Grünfärbung) und Verholzung rasch nach. Einen direkten Zusammenhang zwischen Wachstumsphase, Uringeruch und Wohlgeschmack erkannte bereits 1731 der Leibarzt von Queen Anne, John Arbuthnot (1667–1735): *„Spargel verleiht dem Urin einen stinkenden Geruch, besonders wenn er weiß gestochen wurde. … Wenn er älter ist und beginnt sich zu verzweigen, verliert er diese Eigenschaft, aber dann wird er nicht mehr so geschätzt.“*

Größere Mengen des stark riechenden, leicht flüchtigen Schwefeltrios ***1–3*** lassen sich weder in der wachsenden Pflanze, noch beim Lagern oder beim Kochen nachweisen. Die drei Verbindungen können demnach erst nach dem Spargelverzehr in unserem Körper entstanden sein. Mit jeder Spargelportion bauen wir einige Milligramm Aspara-

gusinsäure (*4*) und ihren Methylester (*5*) [4] zu ***1–3*** ab. Wie und wo dies geschieht, ist unbekannt, ja es ist nicht einmal sicher, ob wir diesen Abbau selbst vollbringen oder die in unserem Darm lebenden Symbionten [5].

Früher war man fest davon überzeugt, dass alle Menschen den charakteristischen Geruch erzeugen und auch riechen können. Neuere Studien weisen jedoch darauf hin, dass dies für einen wesentlichen Bevölkerungsteil *nicht* gilt. Eine aktuelle Studie aus dem Jahr 2016 belegt dies eindrucksvoll: Von 6900 Teilnehmern konnten nur 40 % den typischen Geruch in ihrem Spargelurin wahrnehmen, 60 % waren dazu *nicht* in der Lage [6]. Ob dies im Einzelfall an der mangelnden metabolischen Fähigkeit zur Erzeugung oder einer sensorischen Unempfindlichkeit gegenüber ***1–3*** lag, war nicht Gegenstand unserer Untersuchung. Die mögliche Vererbung dieser beiden Fähigkeiten war Gegenstand mehrerer Untersuchungen, wobei der selektive Ausfall der Geruchswahrnehmung (Anosmie) gegenüber ***1–3*** wahrscheinlich eine genetische Komponente hat [7].

Die ChiuZ-Spargelstudie

Über die Erzeugung und Wahrnehmung des Spargelurins und den dafür notwendigen metabolischen, sensorischen und genetischen Voraussetzungen liegen viele Studien vor [1]. Auch über die Geruchsqualität des Spargelurins wird in wissenschaftlichen Publikationen zahlreich, aber ausnahmslos genüsslich und anekdotisch in den Einleitungen berichtet. Dabei fällt auf, dass der Spargeluringeruch fast einhellig als stinkend und widerlich, also negativ bewertet wird (Abbildung 3). Die in der Belletristik gelegentlich auftauchende Gegenmeinungen werden als kuriose, fast abwegige Spinnereien abgetan. Wie groß eine Sehnsucht nach dem Geruch des Spargelurins werden kann, beschreibt zum Beispiel der mexikanische Literatur-Nobelpreisträger Gabriel García Márquez in seinem Roman „*Die Liebe in Zeiten der Cholera*“ am Beispiel des Protagonisten Dr. Juvenal Urbino: „*Auch wenn es nicht Spargelzeit war, musste man, koste es, was es wolle, welchen auftreiben, damit er sich an den Dämpfen seines duftenden Urins erfreuen konnte.*“

Es kann nur verwundern, warum bei einer jährlichen Erntemenge von 130 Millionen Kilogramm (Deutschland 2018) dieser ungewöhnlichen Nebenwirkung des Spargelessens keine wissenschaftliche Aufmerksamkeit geschenkt wurde. Eine beherzte Gruppe von ChiuZ-Lesern wollte nun endlich Licht in diese olfaktorische Finsternis bringen und in einer Pilotstudie klären, ob positive Geruchsempfindungen beim eigenen Spargelurin nur literarische Übertreibungen sind oder doch von einem größeren Bevölkerungsteil wahrgenommen werden.

Zur Gewinnung belastbarer Aussagen wurde für diese Studie ein Frageprotokoll entwickelt, bei dem zunächst die metabolischen und sensorischen Fähigkeiten der Testpersonen schrittweise abgefragt wurden:

1. Bitte beschreiben Sie mit drei Adjektiven den Geruch ihres normalen Urins.

ABB. 1 | DAS ANRÜCHIGE SCHWEFELTRIO IM SPARGELURIN

	Siedepunkt [°C]	Geruch	Geruchsschwelle [ppm]
CH_3-SH Methanthiol (*1*)	6	unangenehm stechend, nach verfaulendem Kohl	0,02 ppm
CH_3-S-CH_3 Dimethylsulfid (*2*)	37	unangenhem süßlich, kohlähnlich	0,29 ppm
CH_3-S-S-CH_3 Dimethyldisulfid (*3*)	110	unangenehm knoblauchähnlich	10 ppm

Hier sollte zunächst ergründet werden, ob die Teilnehmer ihren eigenen Urin differenziert bewerten konnten. In der Literatur gibt es Hinweise, dass 41 % der Menschen ihren eigenen Urin als geruchlos bezeichnen [8]. Bei unseren Teilnehmern dominierten zwar die Adjektive „normal“ und „geruchlos“, zusätzliche Angaben bewiesen jedoch, dass alle Teilnehmer sehr wohl eine deutlich feinere Differenzierung vornehmen können [9] (Abbildung 4).

2. Haben Sie nach Spargelverzehr jemals einen andersartigen Uringeruch wahrgenommen?
Diese Ja-Nein-Frage entschied, welche Teilnehmer eine verlässliche Geruchsbewertung vornehmen können. Hier hatten wir Glück, denn bis auf zwei Ausnahmen (1w/1m) konnten 58 Testpersonen (97 %) den Geruch von normalem und Spargelurin sicher unterscheiden und somit sowohl die Metaboliten **1–3** herstellen als auch wahrnehmen.

3. Genießen Sie ca. 300 g weißen Spargel und beschreiben Sie den Geruch Ihres Urins mit drei Adjektiven, den Sie zwei bis vier Stunden nach Verzehr gelassen haben.
Bei den 58 Teilnehmern dominierten die Adjektive „intensiv“, „schwefelig“, „stechend“, „süßlich“ und „streng“ (Abbildung 4).

ABB. 2

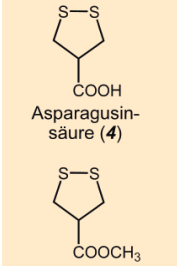

Der chemische Ursprung des Spargeluringeruchs

Abb. 3 ***Gegensätzliche sensorische Bewertungen von Spargelurin hatten Benjamin Franklin (1706–1790), links, und Marcel Proust (1871–1922), rechts.***

Abb. 4 ***Charakterisierung des Geruchs von eigenem Urin vor und nach Spargelgenuss. In diesen Wortwolken repräsentierten die Buchstabengrößen die Häufigkeit der von den Teilnehmern zur Beschreibung gewählten Adjektive. oben: normaler Urin, unten: Spargelurin***

ABB. 5 | OLFAKTORISCHE BEWERTUNG DES EIGENEN SPARGELURINS

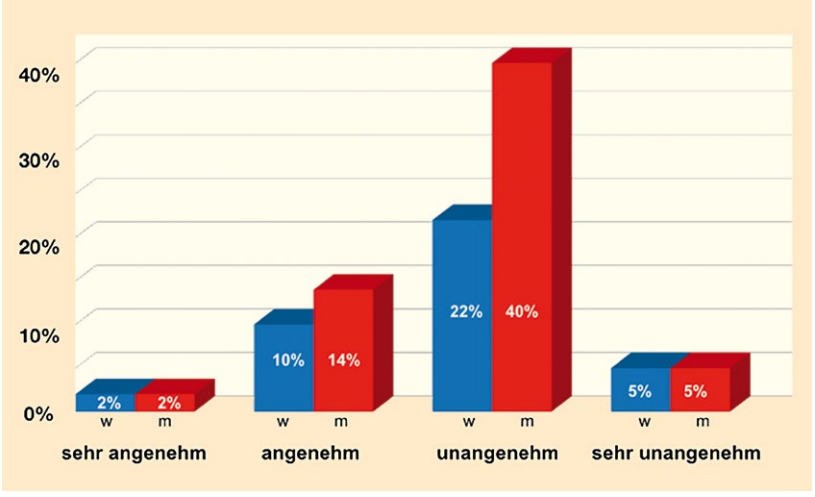

Die meisten der 60 Testpersonen bewerteten den Geruch von Spargelurin als „unangenehm" oder „sehr unangenehm". Zu unserer großen Überraschung empfanden aber über ein Viertel der Teilnehmer (28 %) diesen Geruch als „angenehm" oder „sehr angenehm", wobei kein signifikanter geschlechtsspezifischer Unterschied zu beobachten war (30 %w/ 26 %m).

4. Wie bewerten Sie den Geruch ihres eigenen Spargelurins, als sehr angenehm, angenehm, unangenehm oder als sehr unangenehm?

Dies war die wissenschaftliche Kernfrage unserer Studie und die Auswertung ergab ein überraschendes Bild (Abbildung 5).

Unabhängig vom Geschlecht bewerteten über ein Viertel der ChiuZ-Leser den Geruch ihres Spargelurins als „angenehm" oder „sehr angenehm". Diese sinnliche Freude am eigenen Spargelurin erlebt also ein wesentlicher Teil unserer Bevölkerung. Unter den Spargelkonsumenten gibt es demnach nicht nur „Stinker" und „Nichtstinker", sowie „Riecher" und „Nichtriecher", sondern auch „Angewiderte" und „Betörte".

Zusammenfassung

Die hier vorgelegte Pilotstudie gibt neue Einblicke in die Komplexität des Spargelgenusses. Wegen der eingeschränkten Möglichkeiten konnten nur Testpersonen aus einer begrenzten Bevölkerungsgruppe rekrutiert werden, den ChiuZ-Lesern. Auf dieser Basis ergeben sich die folgenden belastbaren Aussagen:

- ChiuZ-Leserinnen und -leser sind beim Spargelessen sowohl biochemisch als auch sinnlich äußerst sensibel. Nur zwei Teilnehmer (1/w; 1/m) konnten die Geruchsqualität ihres eigenen Spargelurins nicht bewerten. Ob diese zwei „Nicht-Riecher" oder „Nicht-Stinker" waren, konnte nicht entschieden werden. ChiuZ-Leserinnen und -leser sind demnach fast alle „Stinker" und „Riecher" des Spargelurins.
- 72 % aller Teilnehmer bewerteten den Geruch des eigenen Spargelurins als „unangenehm" oder „sehr unangenehm" und charakterisierten ihn vor allem als „schwefelig", „intensiv", „stechend", „streng", „beißend".
- Über 28 % der Teilnehmer empfanden ihren Spargelurin als „angenehm" oder „sehr angenehm" und bewerteten ihn bevorzugt mit „süßlich", „aromatisch", „würzig", „spargelig" und „angenehm".

Die in der wissenschaftlichen Literatur und im Alltag immer wieder kolportierte Behauptung, Spargelurin rieche unangenehm oder widerlich, ist in ihrer Allgemeinheit schlichtweg falsch. Wahrscheinlich trauen sich Andersempfindende aus falscher Scham nicht, auf ihren abweichenden Sinneseindruck deutlich hinzuweisen. Erst in dieser vertraulichen ChiuZ-Studie konnten sich die Testpersonen öffnen und so das vorherrschende Paradigma als unrichtig identifizieren. Diejenigen Feinschmecker, die mit ihrem angenehmen Uringeruch eine Verlängerung des Spargenusses erleben dürfen, sind also keineswegs eine absonderliche Randgruppe, sondern vielmehr olfaktorisch Privilegierte. Den ChiuZ-Lesern wird empfohlen, die Quintessenz dieser Studie beim nächsten Spargelessen der Familie oder den Freunden vorzustellen. Ein munteres und nimmer endendes Tischgespräch wird damit ausgelöst und mit Hilfe von Silvaner, Weißburgunder oder Grüner Veltliner wird dieses Spargelfestmahl für alle unvergesslich werden. Das garantieren die Autoren!

Danksagung

Wir danken Fabian Stollin, Berlin, für die Auswertung der Studie und allen Tapferen, die sich am Selbstversuch beteiligt und uns ihre sensorischen Eindrücke bereitwillig und offen mitgeteilt haben.

Die folgenden Testpersonen der ChiuZ-Studie haben bei der anschließenden Verlosung handsignierte Bücher aus dem Verlag Wiley-VCH gewonnen: Daniel Appel (Kiel), René-Chris Brachvogel (Nürnberg), Anna Heib (Saarbrücken), Ralph Kusche (Marburg), Christian Neis (Hamburg) und Sebastian Sobottka (Berlin).

Literatur und Anmerkungen

[1] S. Streller und K. Roth, *Chem. Unserer Zeit,* **2018**, *52*, 112.
[2] R.H. Waring et al., *Xenobiotica*, **1987**, *17*, 1363; S.C. Mitchell, R.H. Waring, D. Land, W.V. Thorpe, *Experientia*, **1987**, *43*, 382.
[3] H. Yanagawa *et al. Tetrahedron Lett.* **1972**, 2549.
[4] Entscheidend ist hier vor allem der Methylester (**5**). Seine Konzentration ist im rohen Spargel wesentlich höher als die der Asparagusinsäure (**4**) und weiterhin übersteht der Methylester (**5**) das Kochen unbeschadet, während **4** zerfällt. R. Tressl *et al., J. Agric. Food Chem.* **1977**, *25*, 459.
[5] In der DNA eines Menschen sind ca. 23.000 Gene kodiert, in der DNA seiner Darmflora jedoch über 3 Millionen.
[6] S.C. Markt et al., Brit. Med. J. **2016**, 355, i6071.
[7] S.C. Mitchell et al. *Experientia*, **1987**, *43*, 382; M.L. Pelchat et al., *Chem. Senses* **2011**, *43*, 382; Myths of Human Genetics, J.H. McDonald, **2011**, kostenfreies E-Book unter www.lulu.com/shop/john-mcdonald/myths-of-human-genetics/ebook/product-18739384.html
[8] M. Lison et al., *Brit. Med. J.* **1980**, 281, 1676.
[9] Für die Auswertung wurden ähnliche Begriffe zusammengefasst, z. B. „nach Spargelsuppe“ und „spargelsuppig“ oder „nach Kohl“ und „kohlartig“.

Die Autoren

Sabine Streller studierte nach der Ausbildung zur Chemielaborantin Chemie und Biologie an der Humboldt-Universität zu Berlin. Nach dem Referendariat war sie an einem Gymnasium tätig, bevor sie 2004 als wissenschaftliche Mitarbeiterin in die Abteilung Didaktik der Chemie der Freien Universität Berlin wechselte.
Klaus Roth von der Freien Universität Berlin ist ständiger Autor dieser Rubrik.
E-Mail: klaus.roth@fu-berlin.de

ALLES IST ERLEUCHTET – EUROPIUM IM KÄFIG

Die moderne Medizin ist auf der Suche nach intensiv leuchtenden (lumineszenten) Molekülen, die als Sonden in bildgebenden Verfahren eingesetzt werden können. Zu den möglichen Kandidaten gehören Verbindungen, die das Element Europium enthalten. Verbindungen dieser Art, die in lebenden Zellen eingesetzt werden könnten, kommen in der Natur aber nicht vor, sondern müssen erst im Labor hergestellt werden.

VON CAROLIN DEE

Der im Dunkeln leuchtende Sternenhimmel im Kinderzimmer, Knicklichter auf Partys oder Glühwürmchen an Sommerabenden – selbstleuchtende Stoffe faszinieren uns in vielen Bereichen des Lebens. Sie sind aber nicht nur schön anzusehen, sondern können auch praktische Aufgaben erfüllen und in technischen Anwendungen nützlich sein. Ein bekanntes Beispiel aus Krimis ist Luminol: Damit können Kriminaltechniker Blutspuren am Tatort sichtbar machen. Auch in der modernen Biologie und Medizin setzt man leuchtende Stoffe in bildgebenden Verfahren ein. Die mit ihrer Hilfe erstellten Bilder ermöglichen *nicht-invasive* (möglichst wenig in den Körper eindringende) Untersuchungen der Strukturen von Zellen und Organismen in Echtzeit und spielen mittlerweile eine wichtige Rolle in Diagnostik und Therapie.

Ein weniger bekannter Anwendungsbereich ist die Lumineszenz-Mikroskopie. Sie wird zur Untersuchung von Zellen verwendet. Hierbei wird ein leuchtendes Molekül als Sonde in die Zelle gebracht, mit dessen Hilfe z. B. Tumorzellen lokalisiert werden können. Das Bild kann dann unter einem Mikroskop aufgenommen werden. Abbildung 1 zeigt Gebärmutterhalskrebszellen, die mit zwei verschiedenen Metallkomplexen in grün und rot sichtbar gemacht wurden. Da die Leuchteigenschaft eines Moleküls, also seine Lumineszenz, eine zuverlässige Messgröße ist, ist der Bedarf an lumineszierenden Sonden für derartige Anwendungen hoch.

Lumineszenz

Wird ein Atom oder Molekül mit Energie, z. B. durch Licht, in einen angeregten Zustand versetzt (*Absorption*), kann es anschließend die aufgenommene bzw. absorbierte Energie wieder in Form von Licht (*Emission*) abgeben. Oder vereinfacht gesagt: Es wird zum Leuchten gebracht. Dieses Phänomen bezeichnet man als Lumineszenz. Eine Lumineszenzsonde kann in Zellen eingeschleust werden, um bestimmte Bereiche, z. B. Tumorzellen, sichtbar zu machen.

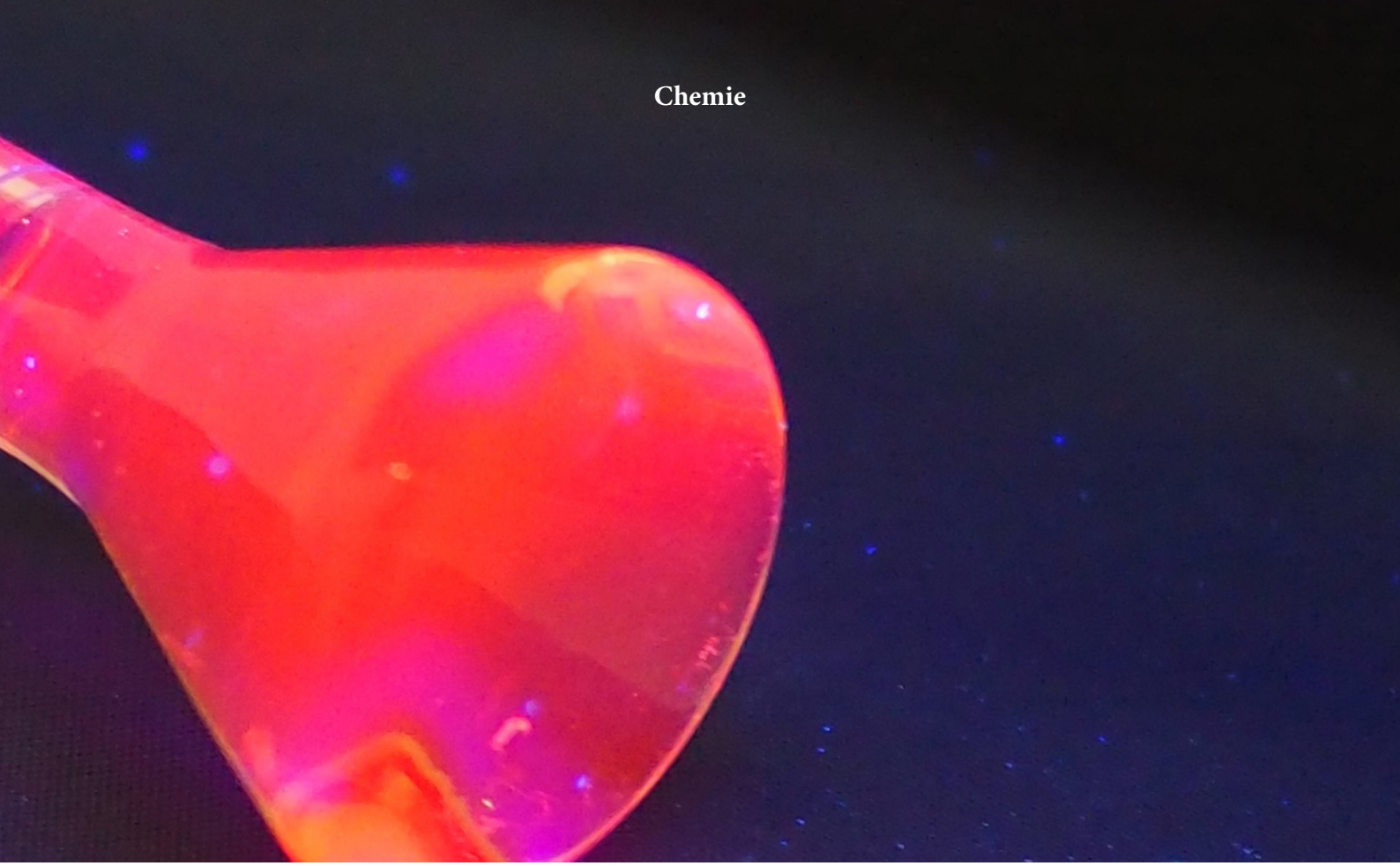

Titelbild: Rote Lumineszenz des neuen Europium-Carbolin-Cryptats in der Dunkelkammer (siehe Artikeltext).

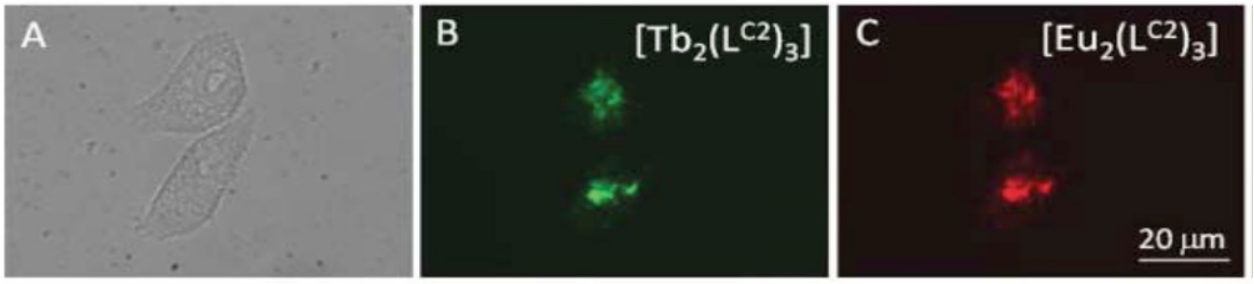

Abb. 1: Lichtmikroskop-Aufnahme (A) sowie Lumineszenzmikroskopie-Aufnahmen von Gebärmutterhalskrebszellen mit einer Terbiumsonde (Tb) in grün (B) und einer Europiumsonde (Eu) in rot (C).
(Bünzli et al, Org. Biomol. Chem. 2008, 6, 4125-4133: Reproduced by permission)

Für den Einsatz in biologischen Systemen gibt es hohe Anforderungen an die verwendeten Lumineszenzsonden:

1. Zunächst einmal dürfen sie *nicht giftig* sein. Dazu ist es besonders wichtig, dass sie chemisch sehr stabil sind und sich nicht in lebenden Systemen zu möglicherweise schädlichen Abbauprodukten zersetzen.

2. Hinzu kommt, dass sie *wasserlöslich* sein müssen, damit sie in biologischen Systemen erfolgreich eingesetzt werden können.

3. Eine besondere Herausforderung bildet die Anregung zur Lumineszenz mit *blauem Licht*, also z. B. mit dem Licht einer Glühbirne oder LED. Das hat damit zu tun, dass das bisherige Verfahren, die Lumineszenzsonden mit ultraviolettem Licht (UV-Licht) anzuregen, für lebende Zellen schädlich ist. Diese Gefahr ist auch aus dem Alltag bekannt: Zu langes und ungeschütztes Sonnenbaden schädigt die Haut nachhaltig.

STEIGERUNG DER LEUCHTKRAFT DURCH ZUSATZEMPFÄNGER

Lanthanoide wie Europium (Eu) oder Terbium (Tb) sind, wie oben bereits erwähnt, für Anwendungen als Lumineszenzsonden geeignet. Die durch einfaches Beleuchten erreichbare Leuchtkraft der Lanthanoide ist in den meisten Fällen bei weitem nicht ausreichend. Es ist daher notwendig, einen zusätzlichen Empfänger, also eine Hilfsantenne, mit dem Metall zu verknüpfen. Das heißt, man braucht Lanthanoidkomplexe, in denen das Lanthanoidzentrum von Molekülen (Liganden) umgeben ist und durch diese stabil festgehalten wird. Mit Licht kann nun der Ligand sehr leicht bzw. stark angeregt werden, wobei ein Teil dieser Energie auf das Lanthanoid übertragen wird und dessen Leuchtkraft deutlich verstärkt.

Lanthanoidkomplexe können mit verschiedenen Liganden dargestellt werden – zum Beispiel mit sogenannten Cryptaten. Das sind Liganden, die das Lanthanoid wie in einem Käfig einschließen. Diese käfigartigen Liganden haben viele vorteilhafte Eigenschaften. Unter anderem sind sie sehr stabil und zersetzen sich nicht. Ein großer Nachteil ist jedoch, dass sie mit UV-Strahlung angeregt werden müssen. Das ist ein großes Problem, wenn man sie in lebende Organismen einsetzen will.

MOLEKÜLDESIGN: VON DER IDEE ZUR SYNTHESE NEUER MOLEKÜLE

Jetzt kommt die Chemikerin ins Spiel. Ein Ziel meiner Forschungen war es, den Käfig so zu verändern, dass er mit sichtbarem Licht angeregt werden kann. Dabei sollten aber seine vorteilhaften Eigenschaften wie z. B. die hohe Stabilität

Lanthanoide

Lanthanoide sind Metalle, die auch unter dem Namen *Seltene Erden* bekannt sind. Als Lanthanoide werden die 15 chemischen Elemente von Lanthan (La) bis Lutetium (Lu) bezeichnet. Die Elemente eint, dass sie unter anderem faszinierende Lumineszenzeigenschaften besitzen. Sind sie in einem angeregten Zustand, indem sie z. B. mit Licht beleuchtet wurden, geben sie Licht einer ganz bestimmten Farbe (Wellenlänge) ab. Einige Farben können mit dem menschlichen Auge erfasst werden; so leuchtet Europium rot (Eu mit 610 nm Wellenlänge) und Terbium grün (Tb mit 540 nm).

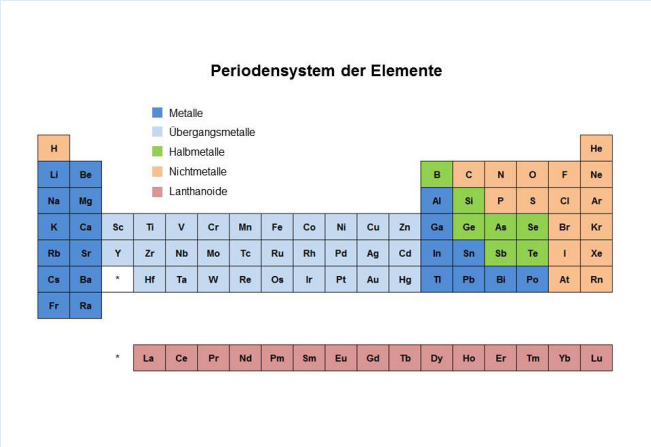

Abb. 2: Die Lanthanoide von Lanthan (La) bis Lutetium (Lu) im Periodensystem der Elemente.

Neben den bisher genannten Bereichen finden sich Elemente aus der Reihe der Lanthanoide auch in vielen technischen Anwendungen wie z. B. in Lasern, starken Magneten, Elektromotoren und Katalysatoren wieder.

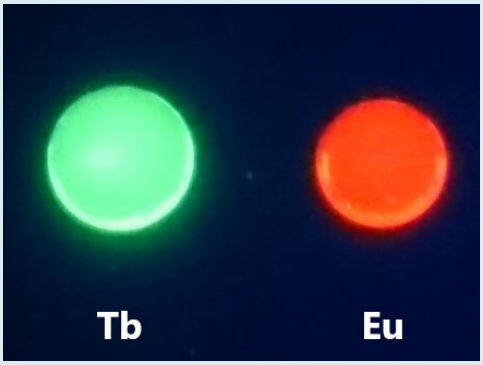

Abb. 3: Lumineszenz von Verbindungen, die Terbium (grün) und Europium (rot) enthalten.

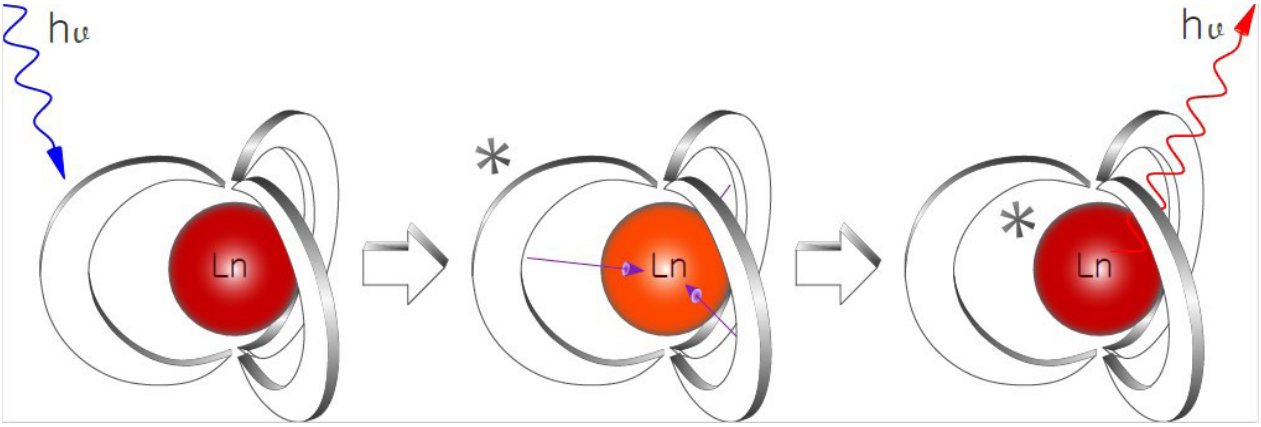

Abb. 4: Schematische Darstellung des Antenneneffekts: Der Ligand absorbiert Licht bzw. Energie (blaue Wellenlinie mit *hν*), wird dabei angeregt (Stern) und regt seinerseits dann das Lanthanoid an. Dieses kann die zusätzliche Energie nun in Form von Licht (rote Wellenlinie mit *hν*) wieder abgeben.

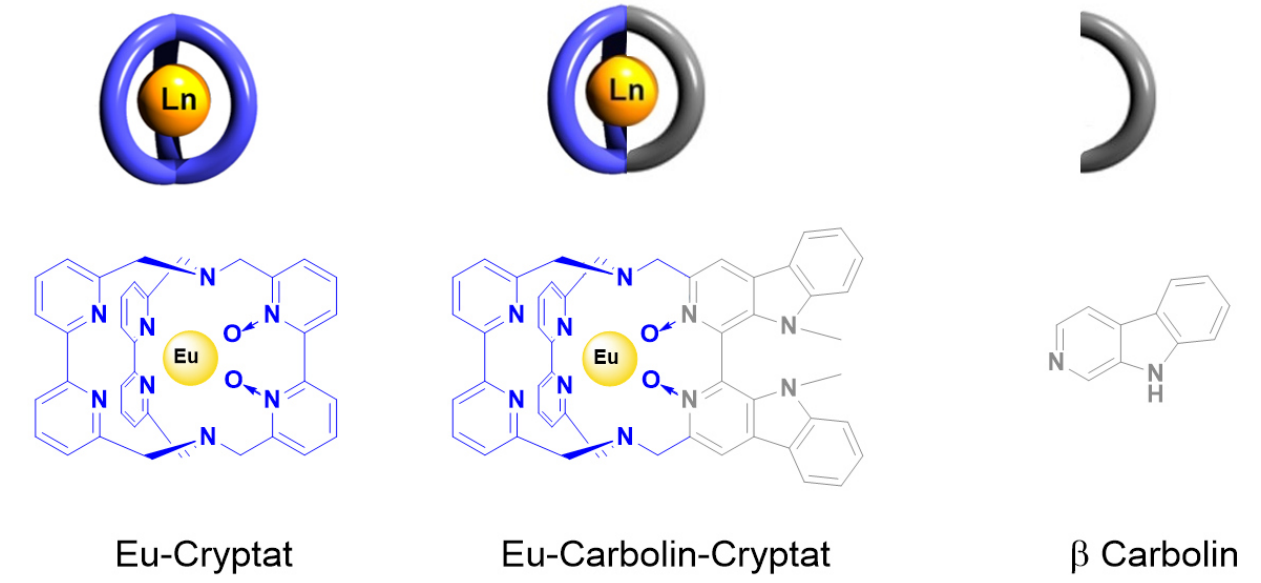

Abb. 5: Schematische Strukturen und Strukturformeln des ursprünglichen Eu-Cryptats (links), des neu entwickelten Eu-Carbolin-Cryptats (mitte) und des beta-Carbolins (rechts).

und Wasserlöslichkeit erhalten bleiben. Nach theoretischen Vorüberlegungen kamen wir zur folgenden praktischen Lösung des Problems: Der ursprüngliche Europium-Cryptat besteht aus drei Ligand-„Ärmchen" (siehe Abb. 5: links), wobei einer mit zwei zusätzlichen Sauerstoffatomen (Element O) für eine verbesserte Stabilität versehen wurde. In dieses erweiterte Ligand-„Ärmchen" wurden dann zwei beta-Carbolin Einheiten eingebaut. Die besonderen Absorptionseigenschaften dieses Moleküls, das in der Natur in der Steppenraute vorkommt, machen es ideal für den Einsatz als Ligand für Europium. So kann es sichtbares (blaues) Licht aufnehmen – eine Eigenschaft, die auch der damit hergestellte Europium-Carbolin-Cryptat übernimmt.

ZEIT FÜR MESSUNGEN AM LUMINESZENZ-SPEKTROMETER!

Intensive Lumineszenz kann der Mensch mit dem bloßen Auge sehen: Einfach einen Kolben mit einer Lösung des neuen Europium-Carbolin-Cryptats in eine Dunkelkammer legen und mit Licht einer Handlampe (ultraviolettes-blaues Licht) anregen.
Nach den theoretischen Überlegungen und der Synthese zur Herstellung des neuen Moleküls im Labor – auch kochen genannt –, standen nun physikalische Messungen und eine Datenanalyse an. Dabei stellte sich die Frage: Kann man den neuen Europium-Carbolin-Cryptat mit sichtbarem Licht zur Lumineszenz anregen? Wie stark leuchtet er? Für solche Messungen benötigt man ein Lumi-

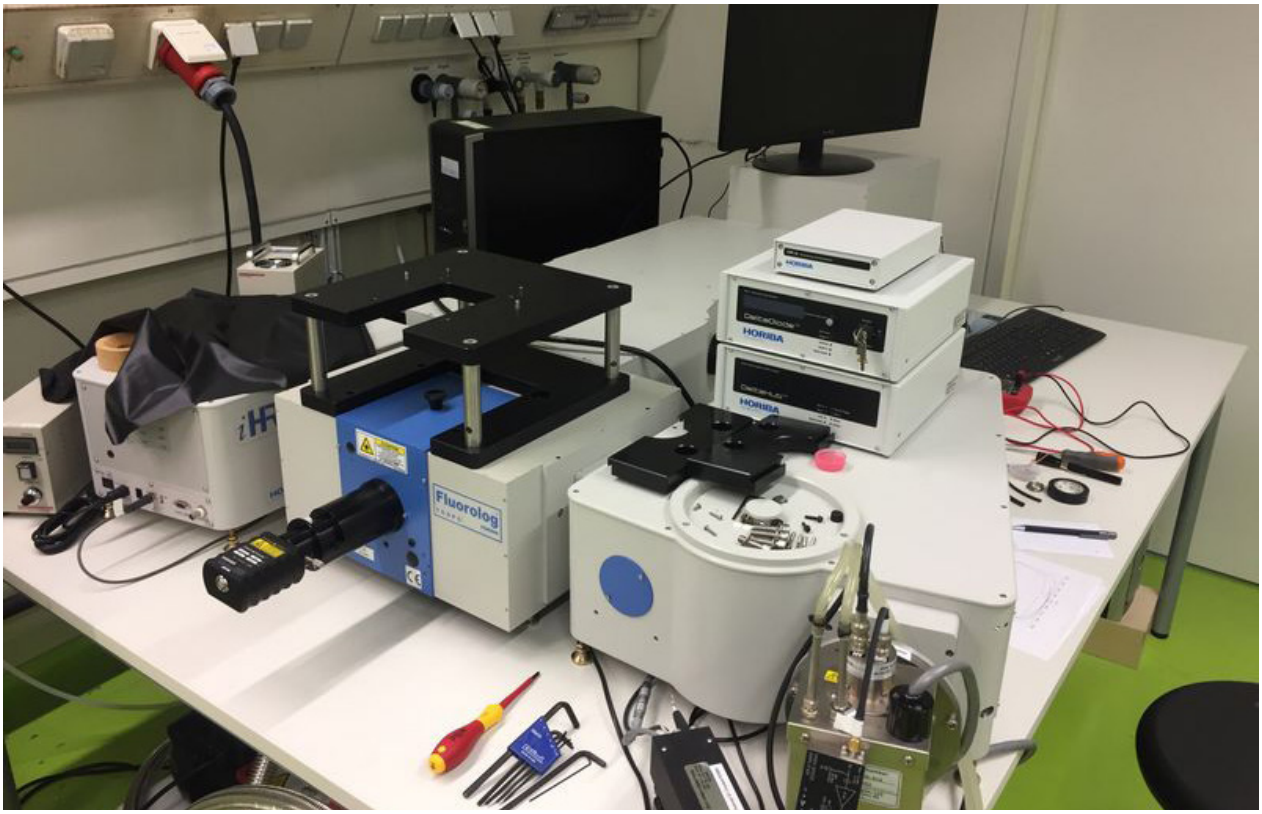

Abb. 6: Lumineszenzspektrometer im Institut für Anorganische Chemie in der Arbeitsgruppe von Prof. Seitz (Tübingen).

neszenzspektrometer (siehe Abb. 6). Hierbei wird die Probe in der Probenkammer mit Licht einer bestimmten Wellenlänge bzw. Farbe angeregt. Dadurch lumineszierd die Probe und gibt Licht mit verschiedenen Wellenlängen ab. Das Spektrometer fährt einen bestimmten Wellenlängen-Bereich ab und nimmt die Intensität des emittierten Lichts bei jeder einzelnen Wellenlänge auf. Regen wir unseren neuen Europium-Carbolin-Cryptat mit sichtbarem Licht an, welches eine geringere Energie hat als das bisher verwendete UV-Licht, können wir eine intensive Emission des abgegebenen roten Lichts von Europium messen.

VERSUCHE IN ZELLEN

Das Ziel, Europium mit sichtbarem Licht zur Lumineszenz anzuregen, konnte also mit dem neuen Käfig erreicht werden. Doch bevor die ersten Versuche in Zellen durchgeführt werden können, muss noch ein weiteres Problem gelöst werden: Europium liegt als dreifach positives Ion in dem Käfiggerüst vor. Damit ist es sehr hoch geladen und kann keine Zellwand durchdringen. Die nächste Aufgabe besteht also darin, die gesamte Ladung des Moleküls zu verkleinern. Dann erst können die Versuche in den Zellen beginnen. An dieser neuen Variation des Käfigs arbeiten wir bereits in unserem Labor.

LITERATUR

J.-C. G. Bünzli, Lanthanide Luminescence for Biomedical Analyses and Imaging, Chem. Rev. 2010, 110, 2729.

C. Dee, D. Esteban-Gomez, C. Platas-Iglesias, M. Seitz, Long Wavelength Excitation of Europium Luminescence in Extended, Carboline-Based Cryptates, Inorg. Chem. 2018, 57, 7390.

Carolin Dee studierte Chemie an der Universität Tübingen. Bereits in ihrer Masterarbeit beschäftigte sie sich mit dem Ligandendesign neuer Cryptate für die Anregung von Europium-Lumineszenz mit sichtbarem Licht. Diese Arbeit entstand unter der Leitung von Prof. Dr. Michael Seitz am Institut für Anorganische Chemie und wurde anschließend in ihrer Promotion fortgeführt.